Development of Stable, Active, and High-Throughput Experimentation Compatible Palladium Precatalysts

by

Jingjun Huang
B.Sc., University of Cincinnati, 2019
B.Sc., South China Normal University, 2019

A Dissertation Submitted for Fulfillment of the
Requirements for the Degree of

DOCTOR OF PHILOSOPHY

in the Department of Chemistry

Supervisory Committee

Development of Stable, Active, and High-Throughput Experimentation Compatible Palladium Precatalysts

by

Jingjun Huang
B.Sc., University of Cincinnati, 2019
B.Sc., South China Normal University, 2019

Supervisory Committee

Dr. David C. Leitch, Supervisor
Department of Chemistry

Dr. Violeta Iosub, Departmental Member
Department of Chemistry

Dr. Scott Mclndoe, Departmental Member
Department of Chemistry

Dr. David Goodlett, Outside Member
Department of Biochemistry and Microbiology

Abstract

Palladium-catalyzed cross-coupling has an approximately 50-year history, with seminal work in the 1970s leading to widespread use today, resulting in the 2010 Nobel Prize in Chemistry. The robustness of this chemistry, which enables constructions of C–C, C–H, C–N, C–O, and so on, has led to rapid growth and extensive applications of cross-coupling approaches in modern synthesis in the last decade. Alongside this, mechanistic studies of many Pd-catalyzed cross-coupling reactions are well-developed, with a wide range of catalytic systems established to maximize the reaction performance. Despite widespread acceptance of LPd^0 species as key intermediates in the catalytic cycle, new developments with Pd^0 precursors remain rare. Instead, Pd^{II} sources are the preferred precursor compounds; however, activation of these precatalysts involves reduction steps that can be complicated and challenging to elucidate.

The works presented here describe the development of a series of new Pd^0 precatalysts and one Pd^{II} precursor, which collectively resolve specific limitations of existing catalytic systems. The first palladium(0) precursor, ^{DMP}DAB–Pd–MAH, is an easily prepared, bench-stable, high-throughput screen compatible, and highly active precatalyst stabilized by an α-diimine ligand (*N*,*N'*-bis(2,6-dimethylphenyl)diazabutadiene, ^{DMP}DAB) and maleic anhydride (MAH). This precursor is an effective alternative to Pd_2dba_3•$CHCl_3$ (the most commonly used palladium(0) source) for *in situ* catalyst formation. Furthermore, single-component phosphine-ligated palladium(0) precursors derived from ^{DMP}DAB–Pd–MAH exhibit superior performance in both catalytic cross-coupling reactions and stereoselective asymmetric allylic alkylations. Finally, to address limitations identified for systems based on ^{DMP}DAB–Pd–MAH, we report a new palladium(II) precursor, ^{DMP}DAB–Pd–$(CH_2TMS)_2$, for oxidative addition complex generation, high-throughput experimentation, and preparative-scale synthesis. This system takes advantage of straightforward Pd^{II} to Pd^0 activation via reductive elimination of the alkyl ligands. Notably, ^{DMP}DAB–Pd–MAH is now commercially available at MilliporeSigma, and the other new precursors reported here are the subjects of filed patent applications. Thus, these new precursors have the potential for positive impact on

improving reaction performance in industry-scale syntheses for complex organic molecules, including pharmaceuticals and agrochemicals.

Table of Contents

List of Figures

List of Tables

List of Abbreviations

AAA ..... Asymmetric allylic alkylation
Ad ..... Adamantyl group
Ar ..... Aromatic ring
BSA ..... Bis(trimethylsilyl)acetamide
COD Cycloocta-1,5-diene
COSY ..... Correlated Spectroscopy
Cp ..... Cyclopentadienyl ligand
CPCM ..... Conductor-like polarizable continuum model
CPME ..... Cyclopentyl methyl ether
Cy ..... Cyclohexyl group
DAB ..... *N,N'*-diaryldiazabutadiene
DACH ..... Diaminocyclohexane
DAD ..... Diode array detectors
dba ..... Dibenzylideneacetone
DCM ..... Dichloromethane
DFT ..... Density functional theory
DMAP 4-Dimethylaminopyridine
DMF ..... Dimethylformamide
DMP ..... Dimethylphenyl
DNA ..... Deoxyribonucleic acid
DPP-4 ..... Dipeptidyl Peptidase-4
EDAC ..... 1-Ethyl-3-(3-dimethylaminopropyl)carbodiimide
ESI-HRMS ..... Electrospray ionization high-resolution mass spectrometry
Et ..... Ethyl group
G1 ..... Generation 1
G-protein ..... Guanine nucleotide-binding protein
HMBC ..... Heteronuclear Multiple Bond Correlation
HMDS ..... Bis(trimethylsilyl)amine
HRMS ..... High-resolution mass spectrometry
HTE ..... High-throughput experimentation

HTS ..... High-throughput screening
IPr..... 1,3-bis(2,6-diisopropylphenyl)imidazol-2-ylidene
L ..... Ligand
LCMS..... Liquid chromatography–mass spectrometry
M ..... Metal
MAH ..... Maleic anhydride
*n*Bu..... *n-butyl*
NHCs..... *N*-heterocyclic carbenes
NMR ..... Nuclear magnetic resonance
NOESY ..... Nuclear Overhauser Effect Spectroscopy
Nu..... Nucleophile
OAc ..... Acetoxy group
OACs..... Oxidative additive complexes
O*t*Bu ..... *tert*-butoxide
OTf ..... Trifluoromethanesulfonate
o-tol ..... *o*-tolyl group
Pd ..... Palladium
PEPPSI..... Pyridine enhanced precatalyst preparation, stabilization, and inhibition
Ph ..... Phenyl group
PHOX..... Phosphine-oxazoline
PNNP ..... Trost-type ligand with the loss of two amide protons
R ..... Organic Substituent
R&D..... Research and Development
R_3P ..... Tertiary phosphines
RB flask ..... Round bottom flask
spiro-MeOTAD..... 2,2’,7,7’-Tetrakis-di(*p*-methoxyphenylamino)-9,9’-spirobifluorene
TBME ..... Methyl *tert*-butyl ether
*t*Bu..... *tert*-butyl
THF ..... Tetrahydrofuran
TLC..... Thin layer chromatography
TMS ..... Trimethylsilyl group
TNF-α..... Tumor necrosis factor-α
TON ..... Turnover number

UPLC ..... Ultra-performance liquid chromatography
VT ..... Variable temperature
X ..... Halogen
XRD ..... X-ray diffraction

Acknowledgements

First of all, I would like to express my deep gratitude to my supervisor, Dr. David C. Leitch. Without his supervision, I would not have been able to complete my work within four years. What I have learned from him will benefit me forever. I really appreciate his patience, support, encouragement, and endless guidance during my Ph.D. study, enabling me to be a greater chemist. I also would like to thank the valuable time and encouragement from my supervisory committee: Dr. Violeta Iosub, Dr. Scott Mclndoe, and Dr. David Goodlett. I extend my heartfelt gratitude to Tyler Trefz, Ori Granot, and Christopher Barr for their guidance and help with the analytic techniques.

I am also indebted to everyone from the Leitch group. I have had an incredibly nice time working with all group members and gained valuable assistance from many of you. Though it is hard to list everyone individually, I would like to extend my sincere appreciation to the group members who have provided me with much assistance: Kushal Dhake, Nahiane Pipaon Fernandez, Jingru Lu, Greg Gaube, Kyla Woelk, Holly Celuszak, Ryan Watt, Hailey Gray, Mathias Burns, and Dr. Joseph Becica.

In addition, I greatly appreciate the impressive effort and help from all collaborators mentioned in the contribution parts. These projects would not have been accomplished efficiently and exceptionally without all your significant help.

Special thank goes to my family, my mom, my dad, my little brother, and my little sister, who has given me infinite love and support. I would not have enough courage to persist on this path without their support and encouragement. I really appreciate their unconditional understanding and tolerance when I lose my temper. A big thank you to my friends who made my life during this period much more colourful and happier: Angel, Yaxian, Yanqing, Tong, Bi. I am pretty thankful for having friends like you.

The last person that I always forget to thank and really would like to thank is myself. Thank you for always being hard-working, active, and persistent.

Chapter 1 Introduction

1.1 History of Palladium-Catalyzed Cross-Coupling

1.1.1 Importance of Palladium-Catalyzed Cross-Coupling

Cross-coupling is one of the most influential and reliable tools for the formation of carbon-carbon bonds and carbon-heteroatom bonds in chemistry.[1,2] It generally refers to metal-catalyzed transformations between carbon-based nucleophiles and organohalide electrophiles; this process involves the formation of new covalent bonds and loss of leaving groups. The discovery of cross-coupling can be dated back to the 1970s when Kochi reported the coupling between alkenyl halides and Grignard reagents in the presence of iron catalysts,[3] inspiring its later development. Over the last decade, the field of cross-coupling, encompassing various aspects such as catalytic mechanisms, reaction conditions, and substrate scope, has received increasing attention and experienced substantial investigation and progress. Palladium complexes became essential catalysts in traditional cross-coupling reactions of sp^2-hybridized aryl halide electrophiles on account of their excellent activity, functional group tolerance, and stability.[4] The 2010 Nobel Prize in Chemistry, awarded to Richard Frederick Heck, Ei-Ichi Negishi, and Akira Suzuki, is a milestone emphasizing the significance of palladium-catalyzed cross-coupling reactions. Even though other transition metals exhibited promising reactivity in new cross-coupling reactions,[5–8] palladium catalysts remain the most widely used, especially in large-scale applications.[9,10]

Palladium-catalyzed cross-coupling is significant in both academia and industry. It has been extensively applied to various areas, such as total synthesis, medicinal chemistry, agrochemistry, materials chemistry, and polymer chemistry,[11–16] as it enables the emergence of novel molecules and new synthetic strategies. For example, spiro-MeOTAD, an exemplar hole transport material for perovskite solar cells, and its derivatives are efficiently synthesized from the corresponding aryl bromide and secondary amines via Buchwald-Hartwig C–N coupling (Figure 1.1A).[16] Chung and co-workers at Merck Research Laboratories have applied Suzuki-Miyaura C–C coupling to the large-scale synthesis of MK-0913, a naphthyridinone-based p38 mitogen-activated protein kinase

inhibitor (Figure 1.1B).[17] This compound is an inhibitor of TNF-α release which could be potentially used in the treatment of rheumatoid arthritis, Crohn's disease, and psoriasis.[17] Forsyth and co-workers have reported a new one-pot preparation of a fungicide fenpropimorph (Figure 1.1C), an effective ingredient generally utilized to control the diseases of cereals, based on Heck C–C coupling.[18] In addition, a survey of the most commonly-used reactions in medicinal chemistry in 2014 reports that three palladium-catalyzed cross-coupling reactions, including Suzuki-Miyaura coupling, Sonogoshira coupling, and Buchwald-Hartwig coupling, are within the top 20 reactions (Figure 1.1D).[19]

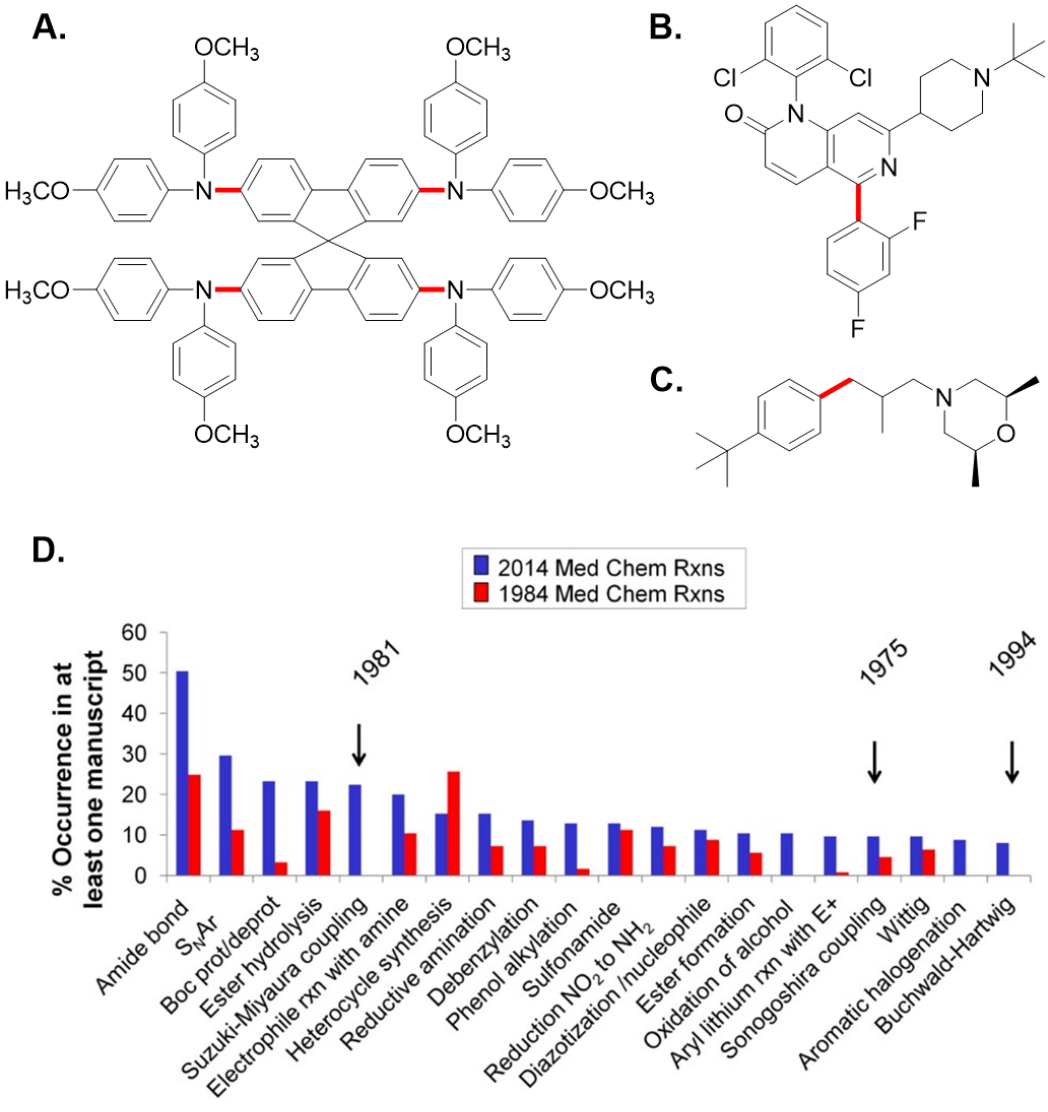

Figure 1.1. A-C: Molecules synthesized utilized Pd-catalyzed cross-coupling. **D:** Top-20 frequently used reactions in medicinal chemistry. The established years for three cross-couplings are indicated. **1.1D** is reprinted with permission from ref. 19. Copyright 2015 American Chemical Society.

1.1.2 Mechanism of Palladium-Catalyzed Cross-Coupling

Many investigations on the mechanism of typical palladium-catalyzed cross-coupling via either theoretical studies or experiments have been reported.[20–22] Generally, palladium-catalyzed cross-coupling proceeds through three essential steps involving oxidative addition, transmetallation, and reductive elimination (Figure 1.2). The active species LPd^0 reacts with ArX via oxidative addition to give a palladium(II) complex LPd(Ar)(X). This Pd^{II} complex then undergoes a transmetallation with the organometallic nucleophile (MNu) to give another Pd^{II} complex LPd(Ar)(Nu). A coupled product is finally obtained from the reductive elimination of ArNu, which also regenerates LPd^0. However, different cross-coupling reactions often have specific mechanistic differences. For instance, Buchwald-Hartwig C–N coupling involves amine coordination and deprotonation steps instead of a direct transmetallation.[23,24] As well, Suzuki-Miyaura C–C coupling and Miyaura borylation often undergo a salt metathesis step with an external base to replace Pd–X with Pd–OR before transmetallation occurs.[25]

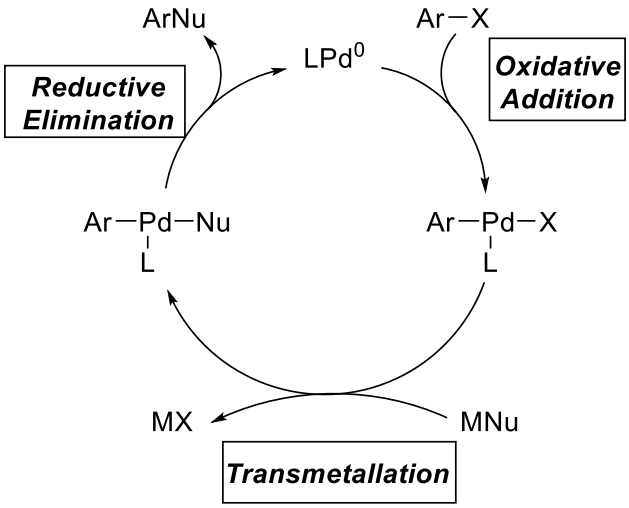

Figure 1.2. General mechanism for Pd-catalyzed cross-coupling.

1.1.3 Activation of Palladium Precatalysts

As shown above, a coordinatively unsaturated LPd^0 complex is generally regarded as the key catalytic intermediate required to initiate the catalytic cycle;[26–28] however, these complexes are extremely reactive, making isolation of these species challenging.[29–31]

Given the significance of palladium-catalyzed cross-coupling, a variety of palladium precursors, including Pd^{II}, Pd^{I}, and Pd^{0} complexes, have been developed. Different types of precursors are proposed to undergo different pathways to generate LPd^{0}, and it has been shown that the activation rate for these precursors can be highly influential to the reaction rate.[32–35] To generate the active species, palladium(II) and palladium(I) precatalysts have to undergo reduction to Pd^{0} with the help of external bases or ligands, and the reduction pathways can be challenging to elucidate (Figure 1.3). To be specific, activation of Buchwald palladacycles generally proceeds through deprotonation of the Pd-bound amine, releasing HX-base, followed by C–N reductive elimination to form LPd^{0} and indoline or carbazole as the by-product.[36] Similarly, three potential activation pathways have been reported for $[LPdX]_2$ dimers, giving different palladium-ligated species. Whether the resulting palladium species are catalytically active or not depends on the structures of the ligands used.[37,38] This type of dimeric palladium(I) sources can serve as a precursor to LPd^{0}, but it can also potentially act as a dinuclear catalyst in specific cases.[39,40] In contrast, palladium(0) complexes, such as Pd_2dba_3•solvent, the most widely-used palladium(0) precursor, can be activated via ligand displacement without further reduction.[41,42]

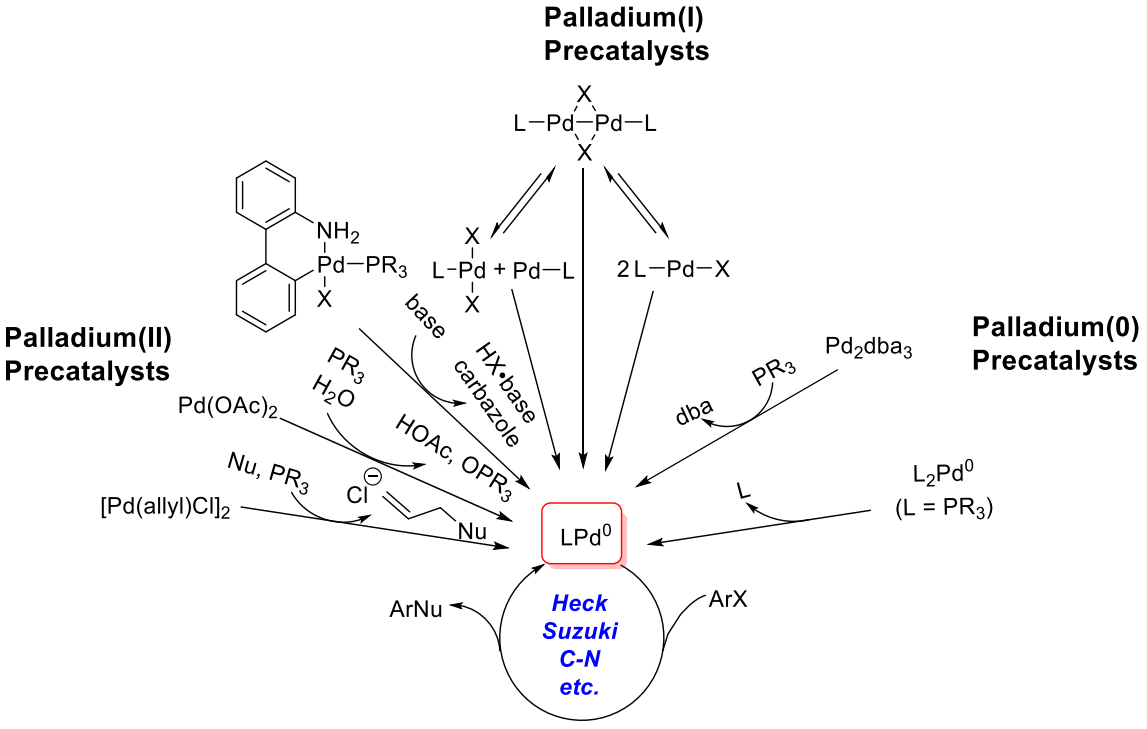

Figure 1.3. Simplified activation pathways of diverse palladium precatalysts.

1.2 Palladium Precatalysts

Due to the broad application of palladium-catalyzed cross-coupling and the relatively high cost of palladium catalysts, studies on generating active and efficient palladium precursors have attracted considerable attention. Over the last decade, numerous palladium precursors have been established for cross-coupling reactions, aiming to improve catalyst activation, substrate scope tolerance, as well as ligand compatibility. Existing palladium precatalysts could be classified into palladium(II), palladium(I), and palladium(0) precursors based on the formal oxidation state of the palladium centers. Palladium(II) precatalysts are the most common, due largely to their excellent stability and ease-of-use. While less common, palladium(0) precatalysts often result in outstanding activity. Compared to the other two types, palladium(I) precatalysts are much less common due to challenges in synthesis, relatively poor stability, and potentially complicated activation pathways. Among the various options, many are pre-formed complexes that already contain the required supporting ligand(s) (Figure 1.4). Some have a 1:1 palladium-to-ligand ratio, while others have two or more ligands per palladium. Generally, the former variety results in high catalytic reactivity with no need for further ligand dissociation; this also often avoids the need for excess ligands.[33,36,37,43–86] The latter variety, such as L_2Pd^0, is also prevalent in specific applications; however, a common issue is the potential for slow ligand dissociation to generate an LPd^0 active species.[71,87–90] Many pre-formed precatalysts are designed to have carefully selected reactive sites, as well as required ligands, which sidestep the ligand substitution step. This largely leads to their excellent catalytic performance in specific transformations.

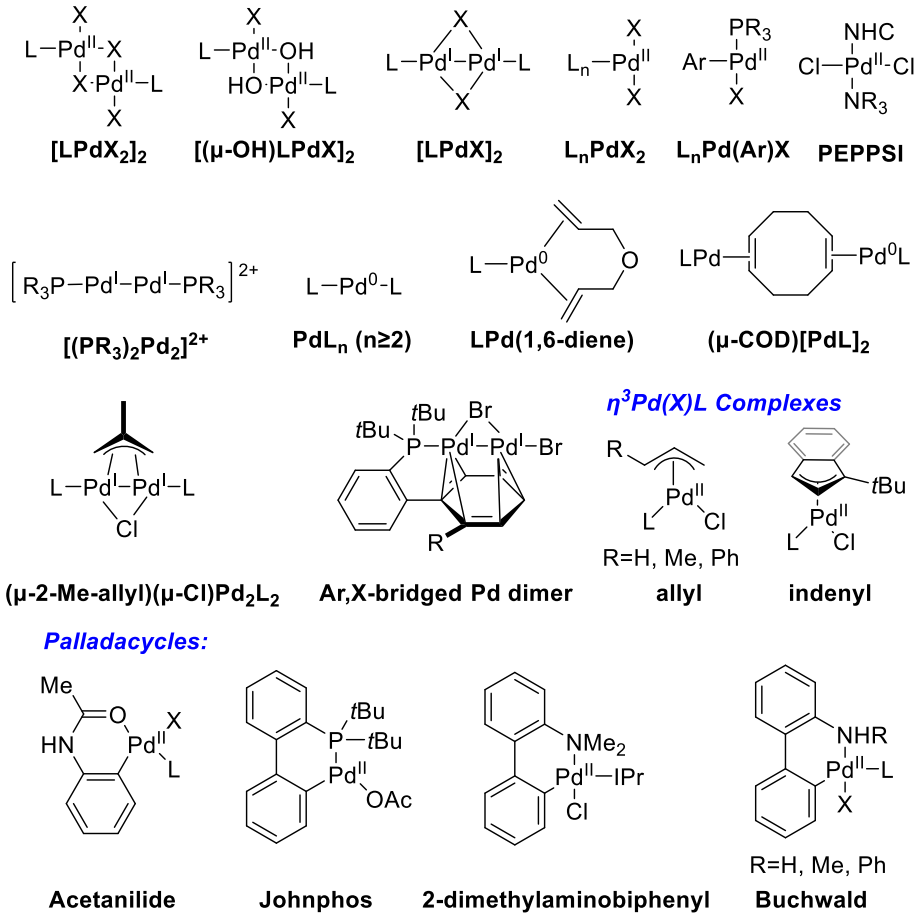

Figure 1.4. Selected single-component Pd precatalyst classes that have ancillary ligands already installed.

Supporting ligand identity is one of the most important factors in determining catalyst suitability and/or activity for a new cross-coupling reaction or new substrate combination.[91–95] Synthesizing pre-formed precatalysts with many different ligands requires a lot of synthetic effort, especially given that many potential ligands will not work for the reaction under investigation. Complementary to pre-ligated precatalysts, there are a number of Pd precursor compounds used to generate active species by adding supporting ligands separately, called *in situ* generated catalysts. The remainder of this chapter will mainly focus on the precursors used for *in situ* catalyst formation, which are frequently used for catalyst optimization and are compatible with high-throughput experimentation.

1.2.1 Pd^{II} Precatalysts and Precursors

Thus far, there are many more Pd^{II} precursors in use for cross-coupling than for the other two types (Pd^{I} and Pd^{0} precursors). Simple Pd^{II} sources such as halide and carboxylate salts have been the most common choice for forming *in situ* catalysts due to their long-term stability and generally lower cost (Figure 1.5A). However, the reduction pathways for catalyst activation using these sources are often more complicated than they appear. For example, $Pd(OAc)_2$, which is the most representative source in this class, potentially can generate LPd^0 (kinetically more active) and/or L_2Pd^0 (less active) as the catalyst, going either through base-mediated or nucleophile-mediated reduction.[96,97] During these catalyst activation processes, several side products may also form as impurities, depending on the reaction conditions.[96,98–100] Another weakness of these simple Pd sources is that their reactivity can diminish significantly when applied to more challenging cross-coupling reactions. All of these issues have led researchers to develop more advanced palladium(II) sources, which are designed specifically to avoid these problems.

Most state-of-the-art single-component Pd precatalysts for cross-coupling reactions can be categorized into four general classes: palladium allyl complexes, palladium indenyl complexes, the PEPPSI (pyridine enhanced precatalyst preparation, stabilization, and initiation) family of complexes, and Buchwald palladacycles (Figure 1.5B).[4] These precursors are more catalytic efficient than the simple-sources-plus-ligand, though they are generally more expensive/less available. In addition, while these precatalysts are generally best known as pre-ligated single-component complexes, all except for PEPPSI have corresponding precursor versions for *in situ* catalyst formation.

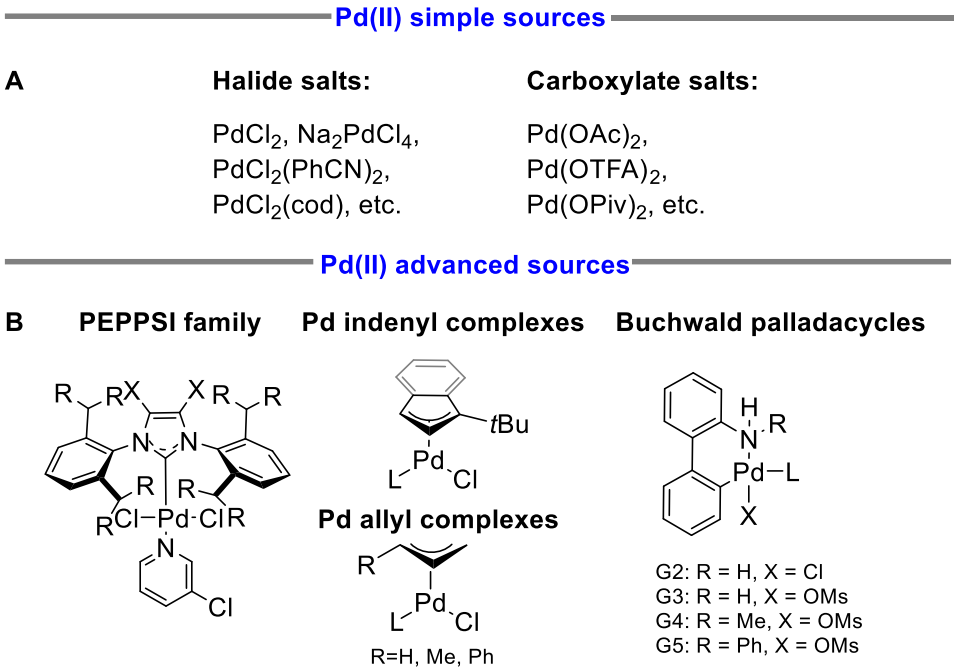

Figure 1.5. Common Pd^{II} sources for cross-coupling catalysis. (**A**) Simple Pd^{II} salts used for *in situ* catalyst formation. (**B**) State-of-the-art Pd^{II} precatalyst classes.

Organ and co-workers reported a new type of Pd^{II} precatalysts, (NHC)Pd(pyridine)Cl_2, easily prepared from $PdCl_2$, corresponding imidazolium salts, and pyridine in the presence of a base.[49] Handling free *N*-heterocyclic carbenes (NHCs), which are a complementary alternative to phosphine ligands in cross-coupling, usually requires experimental operation in a rigorous air/moisture free environment.[101,102] Alternatively, NHCs can be generated *in situ* from the corresponding imidazolium salt under strongly basic conditions. In contrast, the PEPPSI precatalysts are stable and easy-to-handle precursors that circumvent the stability issues and exhibit excellent activity. To date, a series of PEPPSI complexes have been developed by modifying the R and X groups on the NHCs, leading to enhanced activity in challenging reactions involving sterically hindered substrates. PEPPSI complexes are widely used as highly efficient precursors in a variety of cross-coupling reactions, especially in Suzuki-Miyaura, Buchwald-Hartwig, and Negishi couplings.[49,50,103–108] Nevertheless, the activation of these precursors necessitates the addition of external reductants, typically organometallic reagents, to initiate the reduction

from Pd^{II} to Pd^0.[50] In some cases, the reductants can be part of the cross-coupling, such as boronic acids and alcohols.

A diverse and highly active class of Pd^{II} precatalysts are based on substituted η^3-allyl and related ligands, which exploit the reactivity of coordinated allyl groups to facilitate the *in situ* generation of Pd^0 active species. Precatalysts containing cyclopentadiene and allyl groups, including CpPd(allyl) and CpPd(cinnamyl), are suitable precursors for producing Pd^0 species, though they typically form bisphosphine L_2Pd^0 instead of monoligated LPd^0 complexes (Figure 1.6A).[109,110] These Cp-based complexes readily react with phosphine ligands to produce palladium(0) species via reductive elimination, but the reduction outcome does depend on the ligand identity.[111]

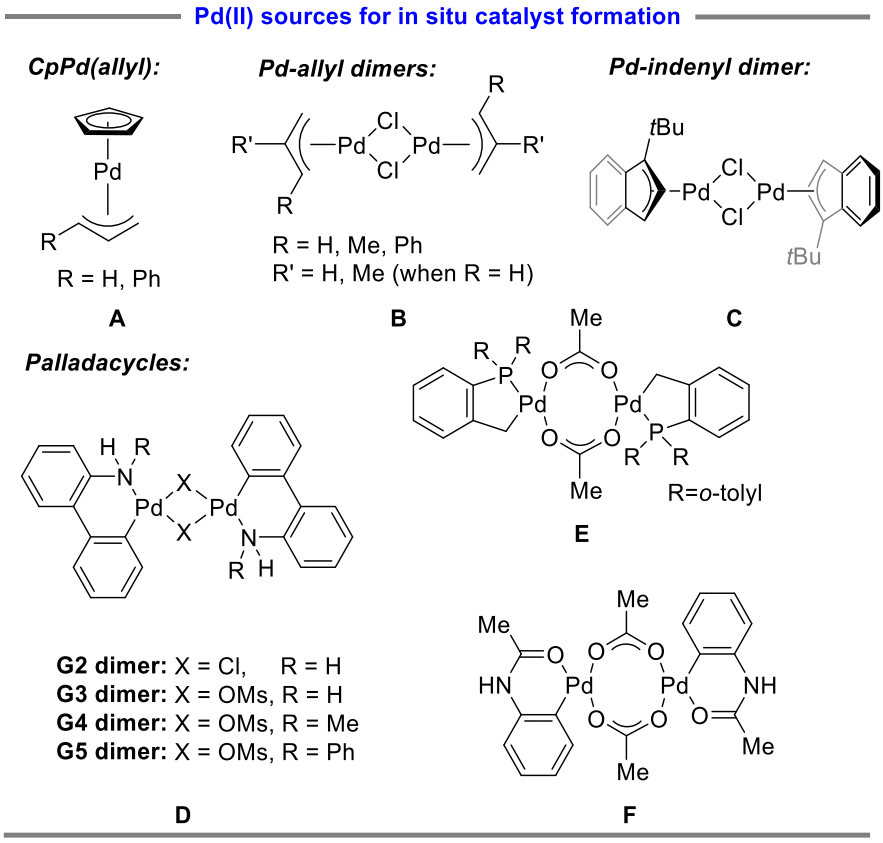

Figure 1.6. Common Pd^{II} sources for *in situ* catalyst formation.

Another type of allyl-based complexes, palladium allyl chloride-bridged dimers, are more compatible with diverse supporting ligands and are generally more efficient and

easy-to-use than cyclopentadienyl allyl palladium sources (Figure 1.6B).[112,113] These dimers are frequently used as precursors to (η^3-allyl)Pd(L)X complexes, which can be isolated or used to generate palladium(0) catalysts *in situ*.[33,54–56,114] Furthermore, the terminal position of the allyl ligand can be substituted with either a methyl or a phenyl group to improve the catalytic activity, and the corresponding crotyl or cinnamyl dimers exhibit remarkable activity in many challenging cross-coupling reactions.[33,54,114–119] However, there is a common drawback to these precursors that manifests during catalyst activation. An inactive and off-cycle palladium(I) dimer may occur via comproportionation from the LPd^0 active species and any remaining (η^3-allyl)Pd(L)X complex. While the cinnamyl source slightly alleviates this problem owing to faster activation than crotyl or allyl complexes, it does not completely prevent its occurrence.[56,57,120]

To avoid the formation of inactive Pd^I dimers via comproportionation, an improved precursor has been developed by Hazari and co-workers. This now commercially available indenyl-based palladium dimer (Figure 1.6C) can be combined with many supporting ligands to access single-component precatalysts of the type (η^3-1-*t*Bu-indenyl)Pd(Cl)(L), or used for *in situ* catalyst generation.[58] It is a superior precursor in a variety of challenging cross-coupling reactions, even with an extremely low catalyst loading.[58,113,121–123]

As described above, allyl-based palladium sources are clearly excellent precursors used for cross-coupling reactions; however, there is a general drawback that has been observed among these dimers during ligand metalation. It has been shown to be difficult for them to coordinate with very bulky ligands, including many biaryl phosphines, such as BrettPhos, *t*BuXPhos, and BippyPhos, that are proposed to be highly active for diverse cross-coupling reactions.[33,93,124,125] An external silver salt, such as AgOTf, is added to abstract the chloride ligand, opening a coordination site at Pd^{II} to accommodate these bulky ligands. This is obviously not ideal for *in situ* catalyst formation using large cone angle ligands.

Another attractive Pd precursor class is based on palladacycle structures, which includes the well-known Buchwald precatalysts. Palladacycles are palladium complexes stabilized by a chelating ligand, where at least one of the metal-ligand bonds is to an X-type carbon ligand.[126,127] The Buchwald precatalyst scaffold is based on an *N,C*-

palladacycle, and either chloride (G1 and G2) or mesylate (G3, G4 and G5) ligands. These have become one of the established benchmarks for palladium-catalyzed cross-coupling (Figure 1.6D). The corresponding Pd^{II} G2-G5 (generation 2-5) dimers, bridging through chloride or mesylate, can efficiently generate single-component complexes with ligands added,[65,67] and are suitable for *in situ* catalyst formation. The five generations are known to be superior precursors for a wide range of cross-coupling reactions compared to conventional palladium sources.[63–65,67,128–133] After ligand metalation, resulting monopalladium complexes are proposed to react with the base present to deprotonate the coordinated N–H ligand, followed by reductive elimination to generate an LPd^0 active species.[36] Thus, rather than activating through action of a reducing agent or nucleophile, these palladacycles are activated by base. Notably, an indoline (G1) or carbazole (G2-5) by-product is also generated in this process. The first two Buchwald precatalyst generations (G1-2) had difficulty in coordinating sterically hindered ligands; therefore, a weakly coordinating methanesulfonate ligand was installed instead of chlorine in the following generations.[65] Later generations G4 and G5 were established to alleviate inhibition caused by the carbazole by-product,[33,85] though they do still produce *N*-substituted carbazole by-products. In addition, the current Buchwald catalyst systems are not compatible with the aforementioned NHC ligands.

There are many other palladacycle precatalysts in addition to the Buchwald palladacycles. In one example, Beller and Herrmann reported an unprecedented catalytic activity for Heck reactions by an acetate-bridged palladacycle based on P(*o*-tol)$_3$ ligands (Figure 1.6E).[134,135] However, special exogenous salt, typically alkali metal salts and tetrabutylammonium bromide, are required to stabilize the catalyst, which makes this palladacycle less suitable for *in situ* catalyst generation. In addition, an acetanilide-derived palladacycle has been demonstrated to be a superior precursor among a variety of IPr-ligated palladacycles in challenging Suzuki-Miyaura couplings.[61,62] The mononuclear single-component complexes have been successfully isolated from the dimeric precursor complex with the addition of NHCs, though very high reaction temperatures are required (Figure 1.6F).[61] This dimeric acetate-bridged palladacycle is also suitable as a precursor for *in situ* catalyst formation.

1.2.2 Pd^{I} Precatalysts and Precursors

As stated above, the catalytic cycle for palladium-catalyzed cross-coupling generally involves Pd^{0} and Pd^{II} oxidation states, and therefore Pd^{I} precatalysts have attracted much less attention than the other two. Many palladium(I) precursors are stabilized by bridging ligands, such as arenes or halides; examples include $[LPdX]_2$ dimers, $L_2Pd_2(\mu\text{-allyl})(\mu\text{-X})$ dimers, and "Ar,X-bridged Pd dimers" (Figure 1.4). Several compounds within these classes are highly active precursors in specific cross-coupling reactions;[37,74,76,82,83,136–139] however, the development of these Pd^{I} systems is complicated by multiple possible reduction pathways, which can lead to lower activity and/or reproducibility issues. Notably, nearly all Pd^{I} complexes have ancillary ligands already bound, making them not suitable for *in situ* catalyst generation.

1.2.3 Pd^{0} Precatalysts and Precursors

Palladium(0) complexes are, in theory, ideal precursors for Pd-catalyzed cross-coupling, with Pd_2dba_3 exhibiting superior reactivity in many reactions. Since a key intermediate within the catalytic cycle is LPd^{0}, palladium(0) precursors do not need to be reduced during catalyst activation. While they have the potential to be superior precursors, investigations on palladium(0) precatalysts are relatively limited; this is mainly due to greater sensitivity to oxidation (e.g. by air) and instability toward the formation of Pd black (colloidal Pd metal).

Palladium(0) complexes, including L_nPd^{0} ($n \geq 2$), (1,6-diene)PdL, and $(\mu\text{-COD})[PdL]_2$, exhibit good catalytic activity in specific cases,[84,86,89,140,141] though the fact they already contain ancillary ligands limits their ability to form new catalysts *in situ* (Figure 1.7). In addition, there are other reasons for the more limited use of these palladium(0) sources in catalysis. Homoleptic palladium(0) sources, L_nPd^{0}, generally have reduced catalytic activity due to slow ligand dissociation to generate active monoligated LPd^{0}.[90] Challenging synthesis and handling is a common drawback for both (1,6-diene)PdL and $(\mu\text{-COD})[PdL]_2$ complexes due to the air-sensitivity of (1,6-diene)PdL and thermal instability of $(COD)Pd(CH_2TMS)_2$ (which is the precursor to $(\mu\text{-COD})[PdL]_2$).

In contrast, Pd_2dba_3•solvent (solvent = dba, $CHCl_3$, toluene) are widely used compounds in catalysis, and are the most practical among all palladium(0) sources. Various combinations of Pd_2dba_3 with diverse supporting ligands have been demonstrated to be robust in a wide range of cross-coupling reactions.[142–149] It is known that added ligands will partially or completely substitute the dibenzylideneacetone (dba) ligand(s) during activation;[42] however, dba can be hard to remove during purification because of its relatively poor solubility in several organic solvents, and even acts as a catalytic inhibitor in several cases.[41,150,151] Moreover, the poor solubility of Pd_2dba_3, its decomposition in the solid state or in solution, and reactivity discrepancies between different commercial batches or even different crystalline solvates are all significant drawbacks of Pd_2dba_3•solvent as reliable catalyst precursors.[152–154]

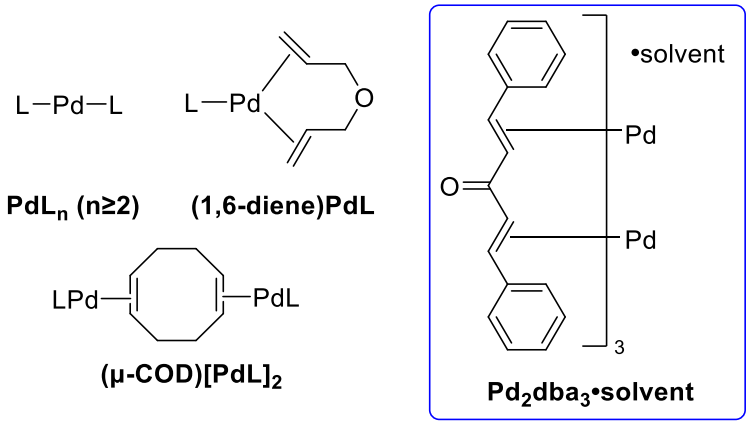

Figure 1.7. The most commonly used Pd^0 sources in catalysis.

1.3 Overview of High-Throughput Screening

In organopalladium catalysis, there is a huge number of factors to consider when discovering and optimizing reactions. Given that there are so many existing palladium precursors and supporting ligands, how does one determine the best catalytic system for the targeted cross-coupling reaction? Furthermore, how long will it take if one needs to optimize all of the relevant reaction factors? High-throughput screening (HTS) is one effective solution to this problem and is increasingly being used in synthetic chemistry.

High-throughput screening is an extremely powerful approach that utilizes automated instruments to carry out a large number of miniaturized experiments at the same

time. Compared to the conventional one-experiment-at-a-time method, microscale HTS substantially decreases the required amounts of materials, including solvents, substrates, and catalysts, thereby reducing the chemical waste production. Meanwhile, it effectively accelerates the exploration of multiple experimental factors simultaneously by parallel operation of a huge number of experiments. This leads to more efficient and economic optimization of reaction systems.

1.3.1 History of High-Throughput Screening

The origin of HTS can be traced back to the 1950s, when Takatsy developed a spiral loop that enabled transfer of 0.025- 0.2 mL of water for serial dilution with less than ± 2% error.[155] Since then, numerous technology advances in instrumentation and analysis have further enabled HTS approaches. These include sensitive spectroscopic detectors, automation and robotics for sample handling, instrument miniaturization, and data analysis software, all of which facilitate and accelerate the screening process.[156,157]

HTS is also historically associated with life science applications. Biological targets, including enzymes, hormones, DNA, G-protein coupled receptors, and nuclear receptors, were shown to compromise 88% of the targets studied by HTS in the 2010s.[158] Within this context, HTS has been well-developed and extensively implemented in biology and biotechnology research, including drug discovery,[159–161] functional genomics,[162–164] biomarker detection[165–167] and protein engineering.[168–171] For example, a large number of potential drug molecules can be efficiently screened using HTS for hit identification according to their biological activity against a target protein.[160] An amazing breakthrough is that screening of more than 100,000 compounds has become feasible since 2008.[158,161]

Compared to biology, HTS and miniaturization is much less exploited in synthetic chemistry laboratories, mainly due to the characteristics of our experiments. These are often heterogeneous reaction mixtures that must be heated and mixed thoroughly to obtain meaningful results. They also contain volatile solvents that require sealed reaction vessels to prevent evaporation. Chemical compatibility is another issue, where plastic consumables used in biology-based HTS are often unsuitable for reaction chemistry. There is also a

divide between industry and academia regarding HTS applications in chemistry laboratories. Sophisticated and expensive automated instruments built for HTS are rarely seen in academia, while chemistry R&D departments of many large chemical companies (e.g. pharmaceutical) conduct HTS routinely. This uneven development can be attributed to the high cost of equipment, as well as a lack of expertise with this approach in academic labs.

HTS has not been extensively implemented in industrial synthetic chemistry laboratories, typically pharmaceutical labs, until the 2000s. A representative example is the efficient optimization of unprecedented asymmetric hydrogenation toward the synthesis of Sitagliptin, a DPP-4 inhibitor for the therapy of type 2 diabetes (Figure 1.8A).[172] Asymmetric hydrogenation of an unprotected enamine was one of the proposed approaches to maximize the synthetic efficiency of Sitagliptin, but related literature remained sporadic at that time. In light of this situation, the utilization of HTS enabled hundreds of optimization screens to be accomplished within 3 months, leading to an efficient synthesis of Sitagliptin on a hundreds of kilograms scale within a short period. In addition to asymmetric hydrogenation, HTS also had a substantial effect on alkene polymerization in the 2000s due to the need of this transformation for extensive optimization of many reaction factors. An early application is the development of innovative catalysts for the generation of isotactic polypropylene at high temperatures (Figure 1.8B).[173] With the substantial assistance of HTS, a class of Hf-based non-metallocene olefin polymerization catalysts was established after efficient catalyst discovery and system optimization. The discovery of this catalyst class promoted the development of an industrial solution production of isotactic polypropylene based materials within 4 years. Afterwards, the rapid development and widespread applications of cross-coupling over the last 15 years make it surpass these two transformations and become the primary HTS application.[174]

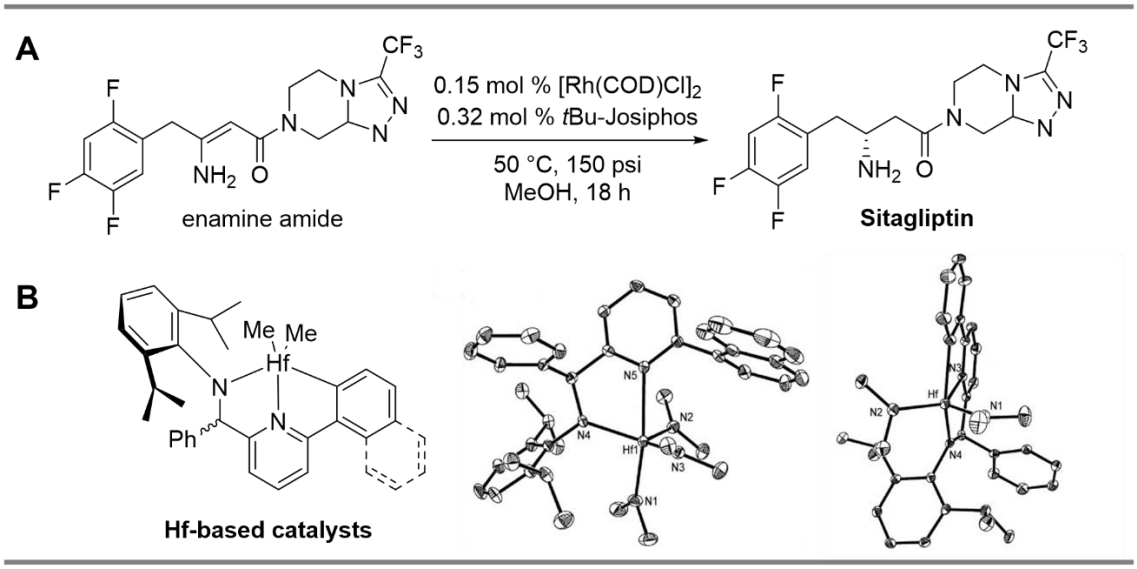

Figure 1.8. A: Synthesis of Sitagliptin via asymmetric hydrogenation. **B:** Innovative Hf-based catalysts for alkene polymerization. **1.8B** is reprinted with permission from ref. 173. Copyright 2006 WILEY-VCH Verlag GmbH & Co. KGaA, Weinheim.

By observing an increase in the need for HTS, the Merck Catalysis group started a collaboration on the development of HTS tools with Analytical Sales around 15 years ago.[175] One of the important collaborative achievements is the further miniaturization of 96-well reaction plates by reducing the size of reaction vials from 1 mL to 250 μL. Along with the evolution of HTS equipment, this powerful approach has been increasingly used in industrial laboratories over the last 15 years, with extended applications in different areas, such as catalysis, synthesis, and reaction discovery.

1.3.2 High-Throughput Screening in Catalysis

Though HTS in chemistry is not as mature as in biology studies, miniaturized experiments are now receiving more and more attention from chemists, with widespread applications in pharmaceutical chemistry.[176–179] This is particularly relevant to organopalladium chemistry and catalysis. Mennen and co-workers conducted a survey on the top ten reactions screened in pharmaceutical process chemistry, as well as predictions on what will be important in the future. The data reveals that cross-coupling reactions take

up a significant proportion (Figure 1.9);[178] specifically, Suzuki-Miyaura and Buchwald-Hartwig couplings are the top two reactions. This indicates a clear need for HTS in developing cross-coupling reactions for complex molecule synthesis.

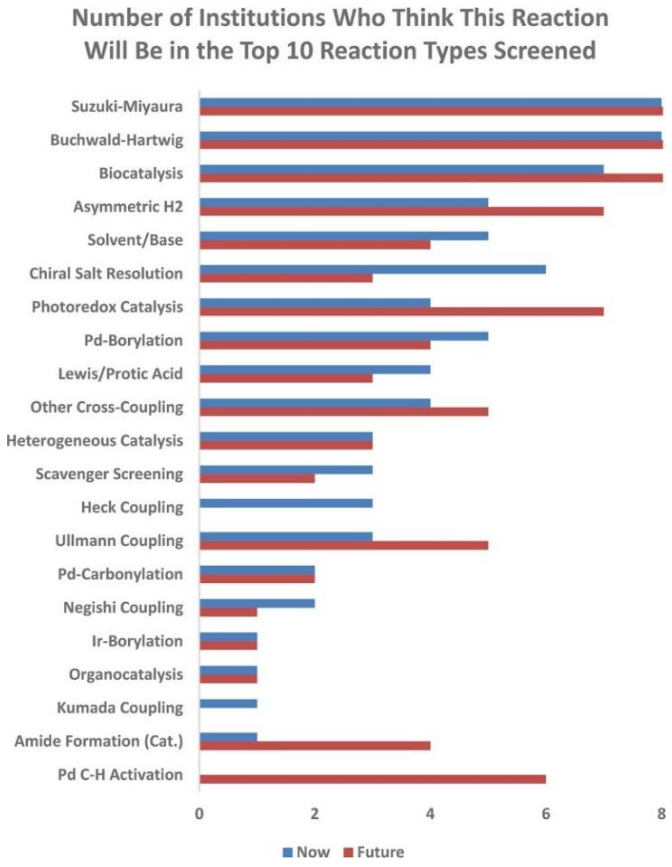

Figure 1.9. The most frequently screened reactions now (blue) and in the future (red) based on a survey of practitioners in pharmaceutical process chemistry. "Institutions" refers to large pharmaceutical process chemistry HTS groups. Reprinted with permission from ref. 179. Copyright 2019 American Chemical Society.

The efficiency and importance of HTS can be best explained by describing how it is performed. The workflow of a typical HTS experiment consists of five steps, including array design, experiment set-up, screen execution, result analysis, and data visualization (Figure 1.10). Becica and Leitch described three tiers of HTS capabilities, ranging from "essential" to "advanced" in terms of infrastructure.[174] The HTS techniques used in this thesis can be categorized as the "essential" class (common in academic applications). It is

also reasonable that "advanced" HTS is mostly applied in industrial R&D labs due to the high cost of acquiring, operating, and maintaining automated instruments.

Given that HTS is frequently used for screening cross-coupling reactions, there is a variety of screening approaches for different purposes. The applications of HTS in conjunction with cross-coupling can be classified as scope evaluation, new reaction discovery, and condition optimization.[174] These three categories can be differentiated based on the experimental design, which is the essential step in the HTS process. The design of a scope evaluation usually involves different functional group additives to evaluate the scope of a specific reaction.[180–182] In contrast, new reaction discovery always includes a large pool of potential substrates to look for any valuable unanticipated reactivity.[183–186] Lastly, optimization screening, as the most commonly-seen type, enables the parallel examination of multiple variables, such as solvents, temperatures, reaction time, catalysts, and bases.[187–193] HTS significantly improves the efficiency and the feasibility of optimizing a broad range of variables simultaneously.

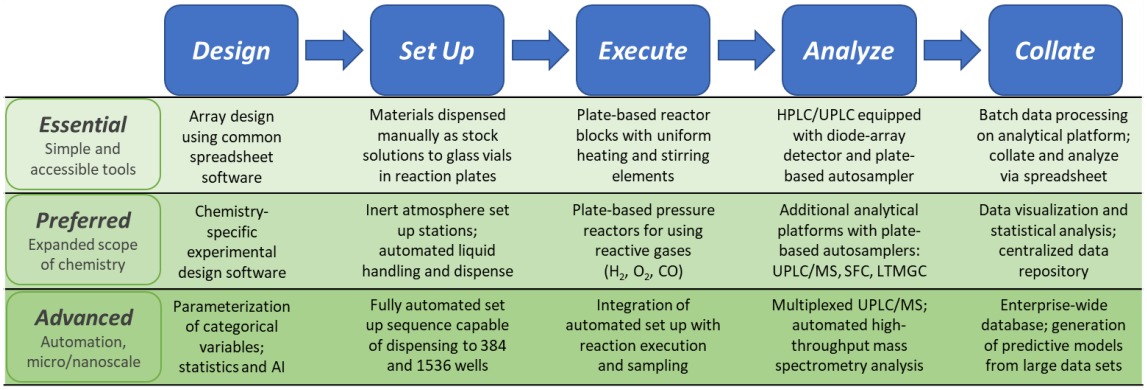

Figure 1.10. A general workflow of HTS in chemistry laboratories.
Reprinted with permission from ref. 174. Copyright 2022 Elsevier.

As an essential part of cross-coupling reactions, the catalytic system is an important factor that must be optimized when there is a new methodology or reaction. The power of HTS in catalysis has been demonstrated by its applications in a broad range of cross-coupling reactions, including C–C, C–B, C–N, C–O, and C–H bond formations.[187,191,194–205] In the previous sections, "precursors for *in situ* catalyst formation" has been highlighted and reviewed extensively because ligand identity is one of the most crucial factors in cross-

coupling reactions.[91–95,124,206] A subtle modification in the ligand structure can substantially change the reactivity, making it challenging to predict which ligand will be most suitable for a new reaction. There is no doubt that pre-ligated palladium precursors are beneficial in specific cases;[57,60–62] however, *in situ* catalyst formation (precursor + ligand) is strongly preferred in HTS due to the greater flexibility it affords. Another advantage of utilizing non-ligated palladium precursors in HTS catalyst evaluation is that unexpected activity may occur as a function of catalyst precursor: even for the same ligand, certain precursors may work well, while others fail completely.

A description of the general HTS workflow used in this thesis is given below (Figure 1.11). The HTS purpose is catalyst optimization, which will be further described in the next chapter. The array design is generated based on the researcher's experience and reported literature, and it is summarized and interpreted as a spreadsheet (Microsoft Excel). The design includes different palladium sources and supporting ligands to increase the possibility of obtaining anticipated hits. Next, reaction set-up involves the use of (for example) a 24-well plate, enabling the parallel evaluation of 24 reactions. These plates are aluminum reaction blocks containing 1 mL glass vials (wells) that contain magnetic stirbars and the reaction mixtures. These plates can be sealed with a screwed-down top to prevent solvent evaporation and avoid exposure to ambient atmosphere. HTS execution is assisted by a heat block / magnetic tumble stirrer, which is able to properly control the reaction time, temperatures, and achieve consistent mixing within each well. Sample analysis is achieved by either liquid chromatography–mass spectrometry (LCMS) or ultra-performance liquid chromatography (UPLC) using diode array UV/Vis detectors (DAD). Finally, the results are interpreted and visualized using the design spreadsheet.

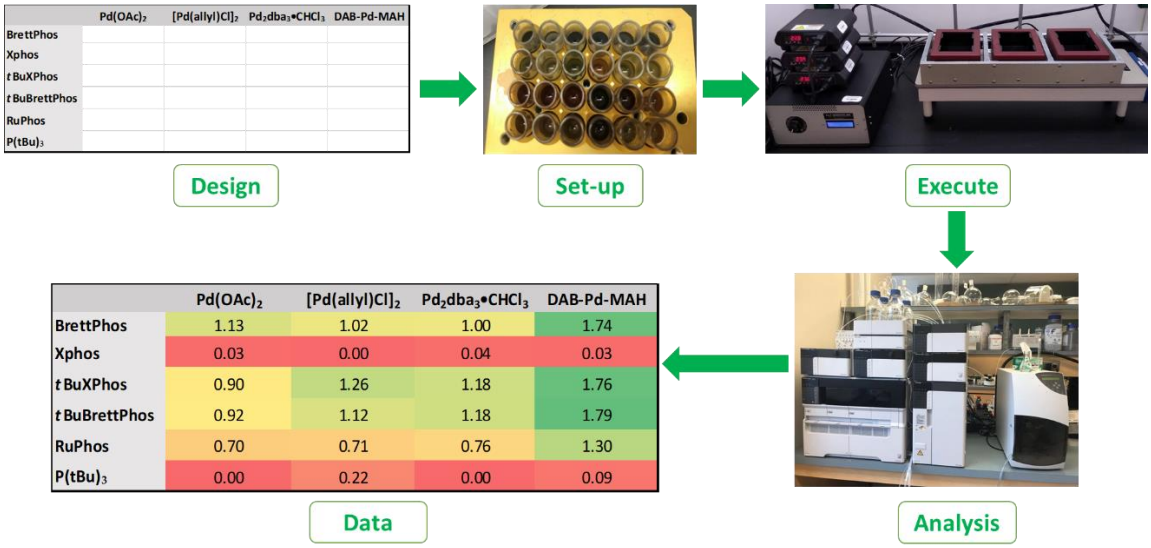

	$Pd(OAc)_2$	$[Pd(allyl)Cl]_2$	$Pd_2dba_3•CHCl_3$	DAB-Pd-MAH
BrettPhos	1.13	1.02	1.00	1.74
Xphos	0.03	0.00	0.04	0.03
t BuXPhos	0.90	1.26	1.18	1.76
t BuBrettPhos	0.92	1.12	1.18	1.79
RuPhos	0.70	0.71	0.76	1.30
$P(tBu)_3$	0.00	0.22	0.00	0.09

Figure 1.11. Workflow of HTS utilized in this thesis.

1.4 Thesis Objectives

As described above, a minor modification in the structure of either the ligands or palladium precursors can significantly change the corresponding catalytic reactivity. Similarly, a seemingly subtle advance in the catalytic system may contribute to a considerable improvement in industrial applications. Given the high cost of palladium and many supporting ligands, maximizing catalysis efficiency toward low catalyst loading, high functional group tolerance, and ease-of-use, is economically and practically beneficial when a synthesis is scaled up. As stated, cross-coupling reactions have extensive applications in industry and academia, and the palladium precursor plays a critical role in cross-coupling reactions. Within this context, the main objective of this thesis is to develop new palladium precursors for both *in situ* catalyst formation and as single-component precatalysts, addressing the drawbacks of existing palladium sources (Figure 1.12).

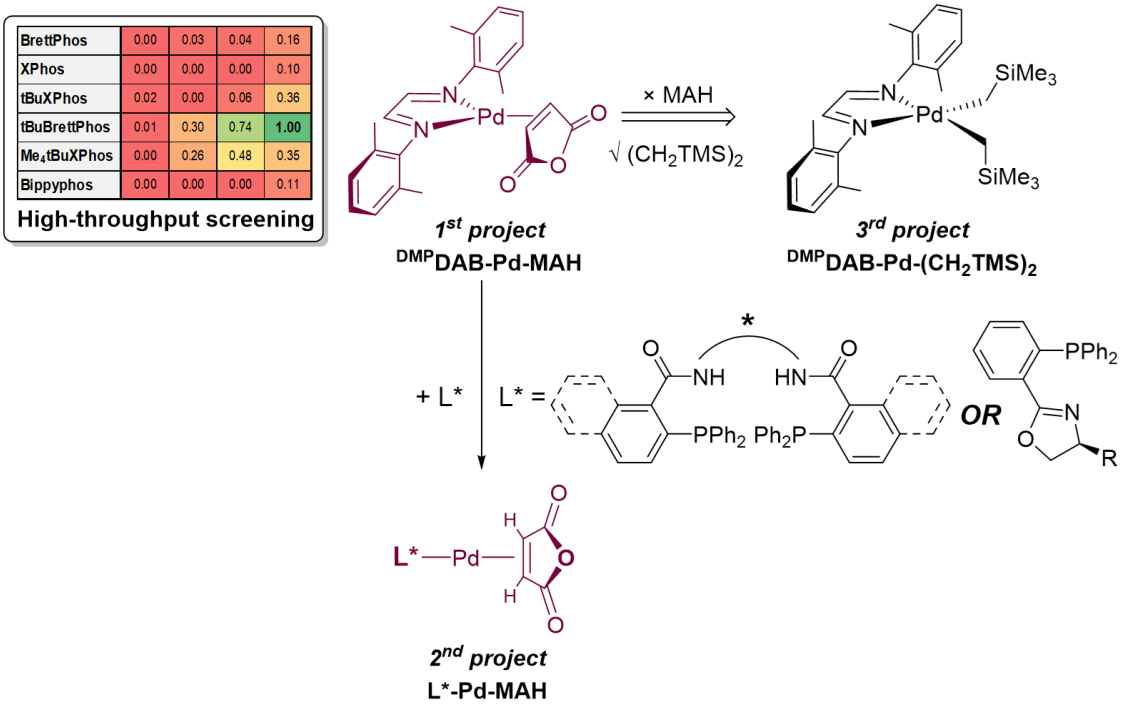

Figure 1.12. Summary of research projects in this thesis.

Based on the overview of the existing palladium precatalysts in palladium-catalyzed cross-coupling reactions, we first aimed to develop a new palladium(0) precatalyst (Chapter 2). This would enable the palladium catalyst to enter the catalytic cycle with no need for reduction. To be impactful, this new precursor would have to be more practical than Pd_2dba_3•solvent, in terms of stability, solubility, and activity. If this goal could be achieved, it would significantly influence the field. In the first project, a new palladium(0) precursor, ^{DMP}DAB–Pd–MAH, stabilized by a chelating *N*,*N*′-diaryldiazabutadiene (DAB) ligand and maleic anhydride (MAH), was prepared and evaluated. This precursor is an outstanding candidate for HTS because of its excellent stability, solubility, and rapid ligand displacement. Its superior activity in HTS comparisons with other common palladium sources and successful application in large-scale synthesis fulfill our initial goals for this project.

After obtaining many successful hits in relatively simple cross-coupling reactions, we turned our focus to more challenging reactions: asymmetric allylic alkylations (Chapter 3). The second project is a collaborative effort with the Arseniyadis group at Queen Mary

University of London. Our group focused on developing and characterizing new palladium complexes, and the Arseniyadis group applied the new complexes to various asymmetric allylic alkylations. As described in Section 1.2.1, single-component precatalysts can give superior reactivity than *in situ* generated catalysts. This is due in part to avoiding the need for ligand substitution during catalyst activation. Furthermore, pre-ligated complexes already have the ideal Pd-to-ligand ratio. Thus, six new chiral palladium(0) precursors have been successfully prepared from ^{DMP}DAB–Pd–MAH and corresponding chiral ligands commonly used in asymmetric allylic alkylations. This led to the first isolable and crystallographically characterized examples of palladium(0) complexes featuring the Trost ligands. The results we obtained through collaboration support that these chiral precursors are robust and promising catalytic systems for asymmetric allylic alkylations.

The last project (Chapter 4) focuses on a new, highly active palladium(II) precursor. While the strongly bound of maleic anhydride leads to great catalyst stability, it is a drawback in certain catalytic examples. The strong π back donation from the palladium(0) center to maleic anhydride leads to inefficient activation without strong bases or nucleophiles. Therefore, we sought to replace the maleic anhydride with two alkyl groups that can easily dissociate from the palladium center via reductive elimination. Even though it is a palladium(II) precursor, it can undergo direct reduction without the need for external reducing agents. This precursor is shown to be an excellent alternative for generating L–Pd–(X)Ar oxidative addition complexes, and to be an excellent catalyst precursor. The superior catalytic activity of ^{DMP}DAB–Pd–$(CH_2TMS)_2$ has been demonstrated by extensive comparison with other commonly-used palladium sources at low palladium loadings.

Chapter 5 summarizes the major achievements of each research project (Chapters 2-4), including the development of active precatalysts for Pd-catalyzed transformations, especially cross-coupling reactions, as well as the overall impacts on this field. In addition, future research plans derived from these projects are proposed. It includes further investigation on the activation pathway of MAH-based precatalysts, ongoing optimization of unprecedented reduction of [PNNP]Pd^{II}, extended catalytic evaluation of ^{DMP}DAB–Pd–$(CH_2TMS)_2$ on challenging transformations, and potential applications of diimine oxidative additive complexes (OACs), ^{DMP}DAB–Pd(X)–Ar.

1.5 References

(1) Campeau, L.-C.; Hazari, N. Cross-Coupling and Related Reactions: Connecting Past Success to the Development of New Reactions for the Future. *Organometallics* **2019**, *38* (1), 3–35. https://doi.org/10.1021/acs.organomet.8b00720.

(2) Johansson Seechurn, C. C. C.; Kitching, M. O.; Colacot, T. J.; Snieckus, V. Palladium-Catalyzed Cross-Coupling: A Historical Contextual Perspective to the 2010 Nobel Prize. *Angew. Chem. Int. Ed.* **2012**, *51* (21), 5062–5085. https://doi.org/10.1002/anie.201107017.

(3) Neumann, S. M.; Kochi, J. K. Synthesis of Olefins. Cross-Coupling of Alkenyl Halides and Grignard Reagents Catalyzed by Iron Complexes. *J. Org. Chem.* **1975**, *40* (5), 599–606. https://doi.org/10.1021/jo00893a013.

(4) Shaughnessy, K. H. Development of Palladium Precatalysts That Efficiently Generate LPd(0) Active Species. *Isr. J. Chem.* **2019**, *59*, 1–16. https://doi.org/10.1002/ijch.201900067.

(5) Mesganaw, T.; Garg, N. K. Ni- and Fe-Catalyzed Cross-Coupling Reactions of Phenol Derivatives. *Org. Process Res. Dev.* **2013**, *17* (1), 29–39. https://doi.org/10.1021/op300236f.

(6) Zhou, J. (Steve); Fu, G. C. Suzuki Cross-Couplings of Unactivated Secondary Alkyl Bromides and Iodides. *J. Am. Chem. Soc.* **2004**, *126* (5), 1340–1341. https://doi.org/10.1021/ja039889k.

(7) Kabir, M. S.; Lorenz, M.; Namjoshi, O. A.; Cook, J. M. First Application of An Efficient and Versatile Ligand for Copper-Catalyzed Cross-Coupling Reactions of Vinyl Halides with *N*-Heterocycles and Phenols. *Org. Lett.* **2010**, *12* (3), 464–467. https://doi.org/10.1021/ol9026446.

(8) Aleena, M. B.; Philip, R. M.; Anilkumar, G. Advances in Non-Palladium-Catalysed Stille Couplings. *Appl. Organomet. Chem.* **2021**, *35* (12), e6430. https://doi.org/10.1002/aoc.6430.

(9) Hazari, N.; Melvin, P. R.; Beromi, M. M. Well-Defined Nickel and Palladium Precatalysts for Cross-Coupling. *Nat. Rev. Chem.* **2017**, *1* (3), 1–16. https://doi.org/10.1038/s41570-017-0025.

(10) Colacot, T. *New Trends in Cross-Coupling: Theory and Applications*; Royal Society of Chemistry, 2014.

(11) Nicolaou, K. C.; Bulger, P. G.; Sarlah, D. Palladium-Catalyzed Cross-Coupling Reactions in Total Synthesis. *Angew. Chem. Int. Ed.* **2005**, *44* (29), 4442–4489. https://doi.org/10.1002/anie.200500368.

(12) Buskes, M. J.; Blanco, M.-J. Impact of Cross-Coupling Reactions in Drug Discovery and Development. *Molecules* **2020**, *25* (15), 3493. https://doi.org/10.3390/molecules25153493.

(13) Devendar, P.; Qu, R.-Y.; Kang, W.-M.; He, B.; Yang, G.-F. Palladium-Catalyzed Cross-Coupling Reactions: A Powerful Tool for the Synthesis of Agrochemicals. *J.*

Agric. Food Chem. **2018**, *66* (34), 8914–8934. https://doi.org/10.1021/acs.jafc.8b03792.

(14) Magano, J.; Dunetz, J. R. Large-Scale Applications of Transition Metal-Catalyzed Couplings for the Synthesis of Pharmaceuticals. *Chem. Rev.* **2011**, *111* (3), 2177–2250. https://doi.org/10.1021/cr100346g.

(15) Baker, M. A.; Tsai, C.-H.; Noonan, K. J. T. Diversifying Cross-Coupling Strategies, Catalysts and Monomers for the Controlled Synthesis of Conjugated Polymers. *Chem. – Eur. J.* **2018**, *24* (50), 13078–13088. https://doi.org/10.1002/chem.201706102.

(16) Stoessel, P.; Spreitzer, H.; Becker, H. Method for the Production of Arylamines. WO03037844A1, May 8, **2003**.

(17) Chung, J. Y. L. Development of a Practical Synthesis of Naphthyridone P38 MAP Kinase Inhibitor MK-0913. In *Transition Metal-Catalyzed Couplings in Process Chemistry*; John Wiley & Sons, Ltd, 2003; pp 39–56. https://doi.org/10.1002/9783527658909.ch04.

(18) Forsyth, S. A.; Gunaratne, H. Q. N.; Hardacre, C.; McKeown, A.; Rooney, D. W. One-Pot Multistep Synthetic Strategies for the Production of Fenpropimorph Using an Ionic Liquid Solvent. *Org. Process Res. Dev.* **2006**, *10* (1), 94–102. https://doi.org/10.1021/op050172m.

(19) Brown, D. G.; Boström, J. Analysis of Past and Present Synthetic Methodologies on Medicinal Chemistry: Where Have All the New Reactions Gone? *J. Med. Chem.* **2016**, *59* (10), 4443–4458. https://doi.org/10.1021/acs.jmedchem.5b01409.

(20) Xie, H.; Fan, T.; Lei, Q.; Fang, W. New Progress in Theoretical Studies on Palladium-Catalyzed C−C Bond-Forming Reaction Mechanisms. *Sci. China Chem.* **2016**, *59* (11), 1432–1447. https://doi.org/10.1007/s11426-016-0018-2.

(21) Amatore, C.; Jutand, A. Structural and Mechanistic Aspects of Palladium-Catalyzed Cross-Coupling. In *Handbook of Organopalladium Chemistry for Organic Synthesis*; John Wiley & Sons, Ltd, 2002; pp 943–972. https://doi.org/10.1002/0471212466.ch39.

(22) García-Melchor, M.; Braga, A. A. C.; Lledós, A.; Ujaque, G.; Maseras, F. Computational Perspective on Pd-Catalyzed C–C Cross-Coupling Reaction Mechanisms. *Acc. Chem. Res.* **2013**, *46* (11), 2626–2634. https://doi.org/10.1021/ar400080r.

(23) Jiang, L.; Buchwald, S. L. Palladium-Catalyzed Aromatic Carbon-Nitrogen Bond Formation. In *Metal-Catalyzed Cross-Coupling Reactions*; John Wiley & Sons, Ltd, 2004; pp 699–760. https://doi.org/10.1002/9783527619535.ch13.

(24) Thomas, G. T.; Janusson, E.; Zijlstra, H. S.; McIndoe, J. S. Step-by-Step Real Time Monitoring of a Catalytic Amination Reaction. *Chem. Commun.* **2019**, *55* (78), 11727–11730. https://doi.org/10.1039/C9CC05076K.

(25) Amatore, C.; Le Duc, G.; Jutand, A. Mechanism of Palladium-Catalyzed Suzuki–Miyaura Reactions: Multiple and Antagonistic Roles of Anionic “Bases” and Their

Countercations. *Chem. – Eur. J.* **2013**, *19* (31), 10082–10093. https://doi.org/10.1002/chem.201300177.

(26) Li, Z.; Fu, Y.; Guo, Q.-X.; Liu, L. Theoretical Study on Monoligated Pd-Catalyzed Cross-Coupling Reactions of Aryl Chlorides and Bromides. *Organometallics* **2008**, *27* (16), 4043–4049. https://doi.org/10.1021/om701065f.

(27) Hartwig, J. F.; Kawatsura, M.; Hauck, S. I.; Shaughnessy, K. H.; Alcazar-Roman, L. M. Room-Temperature Palladium-Catalyzed Amination of Aryl Bromides and Chlorides and Extended Scope of Aromatic C−N Bond Formation with a Commercial Ligand. *J. Org. Chem.* **1999**, *64* (15), 5575–5580. https://doi.org/10.1021/jo990408i.

(28) Kawatsura, M.; Hartwig, J. F. Simple, Highly Active Palladium Catalysts for Ketone and Malonate Arylation: Dissecting the Importance of Chelation and Steric Hindrance. *J. Am. Chem. Soc.* **1999**, *121* (7), 1473–1478. https://doi.org/10.1021/ja983378u.

(29) Christmann, U.; Vilar, R. Monoligated Palladium Species as Catalysts in Cross-Coupling Reactions. *Angew. Chem. Int. Ed.* **2005**, *44* (3), 366–374. https://doi.org/10.1002/anie.200461189.

(30) Ortiz, D.; Blug, M.; Le Goff, X.-F.; Le Floch, P.; Mézailles, N.; Maître, P. Mechanistic Investigation of the Generation of a Palladium(0) Catalyst from a Palladium(II) Allyl Complex: A Combined Experimental and DFT Study. *Organometallics* **2012**, *31* (17), 5975–5978. https://doi.org/10.1021/om300375b.

(31) Zheng, Q.; Liu, Y.; Chen, Q.; Hu, M.; Helmy, R.; Sherer, E. C.; Welch, C. J.; Chen, H. Capture of Reactive Monophosphine-Ligated Palladium(0) Intermediates by Mass Spectrometry. *J. Am. Chem. Soc.* **2015**, *137* (44), 14035–14038. https://doi.org/10.1021/jacs.5b08905.

(32) Hooper, M. W.; Utsunomiya, M.; Hartwig, J. F. Scope and Mechanism of Palladium-Catalyzed Amination of Five-Membered Heterocyclic Halides. *J. Org. Chem.* **2003**, *68* (7), 2861–2873. https://doi.org/10.1021/jo0266339.

(33) DeAngelis, A. J.; Gildner, P. G.; Chow, R.; Colacot, T. J. Generating Active "L-Pd(0)" via Neutral or Cationic π-Allylpalladium Complexes Featuring Biaryl/Bipyrazolylphosphines: Synthetic, Mechanistic, and Structure–Activity Studies in Challenging Cross-Coupling Reactions. *J. Org. Chem.* **2015**, *80* (13), 6794–6813. https://doi.org/10.1021/acs.joc.5b01005.

(34) Littke, A. F.; Fu, G. C. Palladium-Catalyzed Coupling Reactions of Aryl Chlorides. *Angew. Chem. Int. Ed.* **2002**, *41* (22), 4176–4211. https://doi.org/10.1002/1521-3773(20021115)41:22<4176::AID-ANIE4176>3.0.CO;2-U.

(35) Strieter, E. R.; Blackmond, D. G.; Buchwald, S. L. Insights into the Origin of High Activity and Stability of Catalysts Derived from Bulky, Electron-Rich Monophosphinobiaryl Ligands in the Pd-Catalyzed C−N Bond Formation. *J. Am. Chem. Soc.* **2003**, *125* (46), 13978–13980. https://doi.org/10.1021/ja037932y.

(36) Bruneau, A.; Roche, M.; Alami, M.; Messaoudi, S. 2-Aminobiphenyl Palladacycles: The "Most Powerful" Precatalysts in C–C and C–Heteroatom Cross-Couplings. *ACS Catal.* **2015**, *5* (2), 1386–1396. https://doi.org/10.1021/cs502011x.

(37) Stambuli, J. P.; Kuwano, R.; Hartwig, J. F. Unparalleled Rates for the Activation of Aryl Chlorides and Bromides: Coupling with Amines and Boronic Acids in Minutes at Room Temperature. *Angew. Chem. Int. Ed.* **2002**, *41* (24), 4746–4748. https://doi.org/10.1002/anie.200290036.

(38) Amatore, C.; Jutand, A. Anionic Pd(0) and Pd(II) Intermediates in Palladium-Catalyzed Heck and Cross-Coupling Reactions. *Acc. Chem. Res.* **2000**, *33* (5), 314–321. https://doi.org/10.1021/ar980063a.

(39) Jackman, K. M. K.; Liang, G.; Boyle, P. D.; Zimmerman, P. M.; Blacquiere, J. M. Changes in Ligand Coordination Mode Induce Bimetallic C–C Coupling Pathways. *Dalton Trans.* **2022**, *51* (10), 3977–3991. https://doi.org/10.1039/D2DT00322H.

(40) De, S.; Sivendran, N.; Maity, B.; Pirkl, N.; Koley, D.; Gooßen, L. J. Dinuclear Pd^{I} Catalysts in Equilibrium Isomerizations: Mechanistic Understanding, in Silico Casting, and Catalyst Development. *ACS Catal.* **2020**, *10* (8), 4517–4533. https://doi.org/10.1021/acscatal.9b05345.

(41) Amatore, C.; Jutand, A. Role of Dba in the Reactivity of Palladium(0) Complexes Generated in Situ from Mixtures of $Pd(dba)_2$ and Phosphines. *Coord. Chem. Rev.* **1998**, *178–180*, 511–528. https://doi.org/10.1016/S0010-8545(98)00073-3.

(42) Janusson, E.; Zijlstra, H. S.; Nguyen, P. P. T.; MacGillivray, L.; Martelino, J.; McIndoe, J. S. Real-Time Analysis of $Pd_2(dba)_3$ Activation by Phosphine Ligands. *Chem. Commun.* **2017**, *53* (5), 854–856. https://doi.org/10.1039/C6CC08824D.

(43) Viciu, M. S.; Kissling, R. M.; Stevens, E. D.; Nolan, S. P. An Air-Stable Palladium/N-Heterocyclic Carbene Complex and Its Reactivity in Aryl Amination. *Org. Lett.* **2002**, *4* (13), 2229–2231. https://doi.org/10.1021/ol0260831.

(44) Diebolt, O.; Braunstein, P.; Nolan, S. P.; Cazin, C. S. J. Room-Temperature Activation of Aryl Chlorides in Suzuki–Miyaura Coupling Using a $[Pd(\mu\text{-}Cl)Cl(NHC)]_2$ Complex (NHC = *N*-Heterocyclic Carbene). *Chem. Commun.* **2008**, No. 27, 3190–3192. https://doi.org/10.1039/B804695F.

(45) Tessin, U. I.; Bantreil, X.; Songis, O.; Cazin, C. S. J. Highly Active $[Pd(\mu\text{-}Cl)Cl(NHC)]_2$ Complexes in the Mizoroki–Heck Reaction. *Eur. J. Inorg. Chem.* **2013**, *2013* (12), 2007–2010. https://doi.org/10.1002/ejic.201300169.

(46) Barnett, K. L.; Howard, J. R.; Treager, C. J.; Shipley, A. T.; Stullich, R. M.; Qu, F.; Gerlach, D. L.; Shaughnessy, K. H. Air-Stable $[(R_3P)PdCl_2]_2$ Complexes of Neopentylphosphines as Cross-Coupling Precatalysts: Catalytic Application and Mechanism of Catalyst Activation and Deactivation. *Organometallics* **2018**, *37* (9), 1410–1424. https://doi.org/10.1021/acs.organomet.8b00082.

(47) Krause, S. B.; McAtee, J. R.; Yap, G. P. A.; Watson, D. A. A Bench-Stable, Single-Component Precatalyst for Silyl–Heck Reactions. *Org. Lett.* **2017**, *19* (20), 5641–5644. https://doi.org/10.1021/acs.orglett.7b02807.

(48) Ostrowska, S.; Lorkowski, J.; Kubicki, M.; Pietraszuk, C. [{Pd(μ-OH)Cl(IPr)}$_2$]—A Highly Efficient Precatalyst for Suzuki–Miyaura Coupling Also Able To Act under Base-Free Conditions. *ChemCatChem* **2016**, *8* (23), 3580–3583. https://doi.org/10.1002/cctc.201600998.

(49) O'Brien, C. J.; Kantchev, E. A. B.; Valente, C.; Hadei, N.; Chass, G. A.; Lough, A.; Hopkinson, A. C.; Organ, M. G. Easily Prepared Air- and Moisture-Stable Pd–NHC (NHC=*N*-Heterocyclic Carbene) Complexes: A Reliable, User-Friendly, Highly Active Palladium Precatalyst for the Suzuki–Miyaura Reaction. *Chem. – Eur. J.* **2006**, *12* (18), 4743–4748. https://doi.org/10.1002/chem.200600251.

(50) Nasielski, J.; Hadei, N.; Achonduh, G.; Kantchev, E. A. B.; O'Brien, C. J.; Lough, A.; Organ, M. G. Structure–Activity Relationship Analysis of Pd–PEPPSI Complexes in Cross-Couplings: A Close Inspection of the Catalytic Cycle and the Precatalyst Activation Model. *Chem. – Eur. J.* **2010**, *16* (35), 10844–10853. https://doi.org/10.1002/chem.201000138.

(51) Chen, M.-T.; Vicic, D. A.; Turner, M. L.; Navarro, O. (*N*-Heterocyclic Carbene)$PdCl_2$(TEA) Complexes: Studies on the Effect of the "Throw-Away" Ligand in Catalytic Activity. *Organometallics* **2011**, *30* (18), 5052–5056. https://doi.org/10.1021/om200699p.

(52) Farmer, J. L.; Pompeo, M.; Lough, A. J.; Organ, M. G. [(IPent)$PdCl_2$(morpholine)]: A Readily Activated Precatalyst for Room-Temperature, Additive-Free Carbon–Sulfur Coupling. *Chem. – Eur. J.* **2014**, *20* (48), 15790–15798. https://doi.org/10.1002/chem.201404705.

(53) Diebolt, O.; Jurčík, V.; Correa da Costa, R.; Braunstein, P.; Cavallo, L.; Nolan, S. P.; Slawin, A. M. Z.; Cazin, C. S. J. Mixed Phosphite/N-Heterocyclic Carbene Complexes: Synthesis, Characterization and Catalytic Studies. *Organometallics* **2010**, *29* (6), 1443–1450. https://doi.org/10.1021/om9011196.

(54) Viciu, M. S.; Germaneau, R. F.; Navarro-Fernandez, O.; Stevens, E. D.; Nolan, S. P. Activation and Reactivity of (NHC)Pd(allyl)Cl (NHC = *N*-Heterocyclic Carbene) Complexes in Cross-Coupling Reactions. *Organometallics* **2002**, *21* (25), 5470–5472. https://doi.org/10.1021/om020804i.

(55) Viciu, M. S.; Germaneau, R. F.; Nolan, S. P. Well-Defined, Air-Stable (NHC)Pd(allyl)Cl (NHC = *N*-Heterocyclic Carbene) Catalysts for the Arylation of Ketones. *Org. Lett.* **2002**, *4* (23), 4053–4056. https://doi.org/10.1021/ol026745m.

(56) Hill, L. L.; Crowell, J. L.; Tutwiler, S. L.; Massie, N. L.; Hines, C. C.; Griffin, S. T.; Rogers, R. D.; Shaughnessy, K. H.; Grasa, G. A.; Johansson Seechurn, C. C. C.; Li, H.; Colacot, T. J.; Chou, J.; Woltermann, C. J. Synthesis and X-Ray Structure Determination of Highly Active Pd(II), Pd(I), and Pd(0) Complexes of Di(tert-butyl)neopentylphosphine (DTBNpP) in the Arylation of Amines and Ketones. *J. Org. Chem.* **2010**, *75* (19), 6477–6488. https://doi.org/10.1021/jo101187q.

(57) Hruszkewycz, D. P.; Balcells, D.; Guard, L. M.; Hazari, N.; Tilset, M. Insight into the Efficiency of Cinnamyl-Supported Precatalysts for the Suzuki–Miyaura Reaction: Observation of Pd(I) Dimers with Bridging Allyl Ligands During

Catalysis. *J. Am. Chem. Soc.* **2014**, *136* (20), 7300–7316. https://doi.org/10.1021/ja412565c.

(58) Melvin, P. R.; Nova, A.; Balcells, D.; Dai, W.; Hazari, N.; Hruszkewycz, D. P.; Shah, H. P.; Tudge, M. T. Design of a Versatile and Improved Precatalyst Scaffold for Palladium-Catalyzed Cross-Coupling: $(\eta^3\text{-}1\text{-}^t\text{Bu-indenyl})_2(\mu\text{-Cl})_2\text{Pd}_2$. *ACS Catal.* **2015**, *5* (6), 3680–3688. https://doi.org/10.1021/acscatal.5b00878.

(59) Zim, D.; Buchwald, S. L. An Air and Thermally Stable One- Component Catalyst for the Amination of Aryl Chlorides. *Org. Lett.* **2003**, *5* (14), 2413–2415. https://doi.org/10.1021/ol034561h.

(60) Viciu, M. S.; Kelly, R. A.; Stevens, E. D.; Naud, F.; Studer, M.; Nolan, S. P. Synthesis, Characterization, and Catalytic Activity of *N*-Heterocyclic Carbene (NHC) Palladacycle Complexes. *Org. Lett.* **2003**, *5* (9), 1479–1482. https://doi.org/10.1021/ol034264c.

(61) Peh, G.-R.; Kantchev, E. A. B.; Er, J.-C.; Ying, J. Y. Rational Exploration of *N*-Heterocyclic Carbene (NHC) Palladacycle Diversity: A Highly Active and Versatile Precatalyst for Suzuki–Miyaura Coupling Reactions of Deactivated Aryl and Alkyl Substrates. *Chem. – Eur. J.* **2010**, *16* (13), 4010–4017. https://doi.org/10.1002/chem.200902842.

(62) Chen, L.; Ren, P.; Carrow, B. P. Tri(1-adamantyl)phosphine: Expanding the Boundary of Electron-Releasing Character Available to Organophosphorus Compounds. *J. Am. Chem. Soc.* **2016**, *138* (20), 6392–6395. https://doi.org/10.1021/jacs.6b03215.

(63) Biscoe, M. R.; Fors, B. P.; Buchwald, S. L. A New Class of Easily Activated Palladium Precatalysts for Facile C−N Cross-Coupling Reactions and the Low Temperature Oxidative Addition of Aryl Chlorides. *J. Am. Chem. Soc.* **2008**, *130* (21), 6686–6687. https://doi.org/10.1021/ja801137k.

(64) Kinzel, T.; Zhang, Y.; Buchwald, S. L. A New Palladium Precatalyst Allows for the Fast Suzuki−Miyaura Coupling Reactions of Unstable Polyfluorophenyl and 2-Heteroaryl Boronic Acids. *J. Am. Chem. Soc.* **2010**, *132* (40), 14073–14075. https://doi.org/10.1021/ja1073799.

(65) Bruno, N. C.; Tudge, M. T.; Buchwald, S. L. Design and Preparation of New Palladium Precatalysts for C–C and C–N Cross-Coupling Reactions. *Chem. Sci.* **2013**, *4* (3), 916–920. https://doi.org/10.1039/C2SC20903A.

(66) Lee, H. G.; Milner, P. J.; Buchwald, S. L. Pd-Catalyzed Nucleophilic Fluorination of Aryl Bromides. *J. Am. Chem. Soc.* **2014**, *136* (10), 3792–3795. https://doi.org/10.1021/ja5009739.

(67) Bruno, N. C.; Niljianskul, N.; Buchwald, S. L. *N*-Substituted 2-Aminobiphenylpalladium Methanesulfonate Precatalysts and Their Use in C–C and C–N Cross-Couplings. *J. Org. Chem.* **2014**, *79* (9), 4161–4166. https://doi.org/10.1021/jo500355k.

(68) Hu, H.; Qu, F.; Gerlach, D. L.; Shaughnessy, K. H. Mechanistic Study of the Role of Substrate Steric Effects and Aniline Inhibition on the

Bis(trineopentylphosphine)palladium(0)-Catalyzed Arylation of Aniline Derivatives. *ACS Catal.* **2017**, *7* (4), 2516–2527. https://doi.org/10.1021/acscatal.7b00024.

(69) Ingoglia, B. T.; Buchwald, S. L. Oxidative Addition Complexes as Precatalysts for Cross-Coupling Reactions Requiring Extremely Bulky Biarylphosphine Ligands. *Org. Lett.* **2017**, *19* (11), 2853–2856. https://doi.org/10.1021/acs.orglett.7b01082.

(70) Chen, L.; Francis, H.; Carrow, B. P. An "On-Cycle" Precatalyst Enables Room-Temperature Polyfluoroarylation Using Sensitive Boronic Acids. *ACS Catal.* **2018**, *8* (4), 2989–2994. https://doi.org/10.1021/acscatal.8b00341.

(71) Tang, S.-Q.; Bricard, J.; Schmitt, M.; Bihel, F. Fukuyama Cross-Coupling Approach to Isoprekinamycin: Discovery of the Highly Active and Bench-Stable Palladium Precatalyst POxAP. *Org. Lett.* **2019**, *21* (3), 844–848. https://doi.org/10.1021/acs.orglett.9b00031.

(72) Hazari, N.; Hruszkewycz, D. P. Dinuclear Pd^{I} Complexes with Bridging Allyl and Related Ligands. *Chem. Soc. Rev.* **2016**, *45* (10), 2871–2899. https://doi.org/10.1039/C5CS00537J.

(73) Hruszkewycz, D. P.; Guard, L. M.; Balcells, D.; Feldman, N.; Hazari, N.; Tilset, M. Effect of 2-Substituents on Allyl-Supported Precatalysts for the Suzuki–Miyaura Reaction: Relating Catalytic Efficiency to the Stability of Palladium(I) Bridging Allyl Dimers. *Organometallics* **2015**, *34* (1), 381–394. https://doi.org/10.1021/om501250y.

(74) Weissman, H.; Shimon, L. J. W.; Milstein, D. Unsaturated Pd(0), Pd(I), and Pd(II) Complexes of a New Methoxy-Substituted Benzyl Phosphine. Aryl−X (X = Cl, I) Oxidative Addition, C−O Cleavage, and Suzuki−Miyaura Coupling of Aryl Chlorides. *Organometallics* **2004**, *23* (16), 3931–3940. https://doi.org/10.1021/om0497588.

(75) Finke, A. D.; Elleby, E. C.; Boyd, M. J.; Weissman, H.; Moore, J. S. Zinc Chloride-Promoted Aryl Bromide−Alkyne Cross-Coupling Reactions at Room Temperature. *J. Org. Chem.* **2009**, *74* (22), 8897–8900. https://doi.org/10.1021/jo902015w.

(76) Denmark, S. E.; Baird, J. D. Palladium-Catalyzed Cross-Coupling Reactions of Heterocyclic Silanolates with Substituted Aryl Iodides and Bromides. *Org. Lett.* **2006**, *8* (4), 793–795. https://doi.org/10.1021/ol053165r.

(77) Vilar, R.; Mingos, D. M. P.; Cardin, C. J. Synthesis and Structural Characterisation of $[Pd_2(\mu\text{-}Br)_2(PBu^t_3)_2]$, an Example of a Palladium(I)–Palladium(I) Dimer. *J. Chem. Soc. Dalton Trans.* **1996**, No. 23, 4313–4314. https://doi.org/10.1039/DT9960004313.

(78) Durà-Vilà, V.; Mingos, D. M. P.; Vilar, R.; White, A. J. P.; Williams, D. J. Insertion of O_2 into a Pd(I)–Pd(I) Dimer and Subsequent C–O Bond Formation by Activation of a C–H Bond. *Chem. Commun.* **2000**, No. 16, 1525–1526. https://doi.org/10.1039/B004537N.

(79) Kalvet, I.; Magnin, G.; Schoenebeck, F. Rapid Room-Temperature, Chemoselective Csp^2 −Csp^2 Coupling of Poly(pseudo)halogenated Arenes Enabled by Palladium(I)

Catalysis in Air. *Angew. Chem. Int. Ed Engl.* **2017**, *56* (6), 1581–1585. https://doi.org/10.1002/anie.201609635.

(80) Pirkl, N.; Grosso, A. D.; Mallick, B.; Doppiu, A.; Gooßen, L. J. Dihalogen-Bridged NHC–Palladium(I) Dimers: Synthesis, Characterisation and Applications in Cross-Coupling Reactions. *Chem. Commun.* **2019**, *55* (36), 5275–5278. https://doi.org/10.1039/C9CC02239B.

(81) Christmann, U.; Vilar, R.; White, A. J. P.; Williams, D. J. Synthesis of Two Novel Dinuclear Palladium(I) Complexes and Studies of Their Catalytic Activity in Amination Reactions. *Chem. Commun.* **2004**, No. 11, 1294–1295. https://doi.org/10.1039/B402283A.

(82) Barder, T. E. Synthesis, Structural, and Electron Topographical Analyses of a Dialkylbiaryl Phosphine/Arene-Ligated Palladium(I) Dimer: Enhanced Reactivity in Suzuki−Miyaura Coupling Reactions. *J. Am. Chem. Soc.* **2006**, *128* (3), 898–904. https://doi.org/10.1021/ja0558995.

(83) Kirlikovali, K. O.; Cho, E.; Downard, T. J.; Grigoryan, L.; Han, Z.; Hong, S.; Jung, D.; Quintana, J. C.; Reynoso, V.; Ro, S.; Shen, Y.; Swartz, K.; Sahakyan, E. T.; Wixtrom, A. I.; Yoshida, B.; Rheingold, A. L.; Spokoyny, A. M. Buchwald–Hartwig Amination Using Pd(I) Dimer Precatalysts Supported by Biaryl Phosphine Ligands. *Dalton Trans.* **2018**, *47* (11), 3684–3688. https://doi.org/10.1039/C8DT00119G.

(84) Andreu, M. G.; Zapf, A.; Beller, M. Molecularly Defined Palladium(0) Monophosphine Complexes as Catalysts for Efficient Cross-Coupling of Aryl Chlorides and Phenylboronic Acid1. *Chem. Commun.* **2000**, No. 24, 2475–2476. https://doi.org/10.1039/B006791L.

(85) Lee, H. G.; Milner, P. J.; Buchwald, S. L. An Improved Catalyst System for the Pd-Catalyzed Fluorination of (Hetero)Aryl Triflates. *Org. Lett.* **2013**, *15* (21), 10.1021/ol402859k. https://doi.org/10.1021/ol402859k.

(86) Dennis, J. M.; White, N. A.; Liu, R. Y.; Buchwald, S. L. Breaking the Base Barrier: An Electron-Deficient Palladium Catalyst Enables the Use of a Common Soluble Base in C–N Coupling. *J. Am. Chem. Soc.* **2018**, *140* (13), 4721–4725. https://doi.org/10.1021/jacs.8b01696.

(87) Green, R. A.; Hartwig, J. F. Palladium-Catalyzed Amination of Aryl Chlorides and Bromides with Ammonium Salts. *Org. Lett.* **2014**, *16* (17), 4388–4391. https://doi.org/10.1021/ol501739g.

(88) Dai, C.; Fu, G. C. The First General Method for Palladium-Catalyzed Negishi Cross-Coupling of Aryl and Vinyl Chlorides: Use of Commercially Available Pd(P(*t*-Bu)$_3$)$_2$ as a Catalyst. *J. Am. Chem. Soc.* **2001**, *123* (12), 2719–2724. https://doi.org/10.1021/ja003954y.

(89) Arentsen, K.; Caddick, S.; Cloke, F. G. N. On the Efficiency of Two-Coordinate Palladium(0) *N*-Heterocyclic Carbene Complexes in Amination and Suzuki–Miyaura Reactions of Aryl Chlorides. *Tetrahedron* **2005**, *61* (41), 9710–9715. https://doi.org/10.1016/j.tet.2005.06.070.

(90) Littke, A. F.; Dai, C.; Fu, G. C. Versatile Catalysts for the Suzuki Cross-Coupling of Arylboronic Acids with Aryl and Vinyl Halides and Triflates under Mild Conditions. *J. Am. Chem. Soc.* **2000**, *122* (17), 4020–4028. https://doi.org/10.1021/ja0002058.

(91) Withbroe, G. J.; Singer, R. A.; Sieser, J. E. Streamlined Synthesis of the Bippyphos Family of Ligands and Cross-Coupling Applications. *Org. Process Res. Dev.* **2008**, *12* (3), 480–489. https://doi.org/10.1021/op7002858.

(92) Martin, R.; Buchwald, S. L. Palladium-Catalyzed Suzuki-Miyaura Cross-Coupling Reactions Employing Dialkylbiaryl Phosphine Ligands. *Acc. Chem. Res.* **2008**, *41* (11), 1461–1473. https://doi.org/10.1021/ar800036s.

(93) Surry, D. S.; Buchwald, S. L. Dialkylbiaryl Phosphines in Pd-Catalyzed Amination: A User's Guide. *Chem. Sci.* **2010**, *2* (1), 27–50. https://doi.org/10.1039/C0SC00331J.

(94) Lundgren, R. J.; Hesp, K. D.; Stradiotto, M. Design of New 'DalPhos' P,N-Ligands: Applications in Transition-Metal Catalysis. *Synlett* **2011**, *2011* (17), 2443–2458. https://doi.org/10.1055/s-0030-1260321.

(95) Lundgren, R. J.; Stradiotto, M. Addressing Challenges in Palladium-Catalyzed Cross-Coupling Reactions Through Ligand Design. *Chem. – Eur. J.* **2012**, *18* (32), 9758–9769. https://doi.org/10.1002/chem.201201195.

(96) Wei, C. S.; Davies, G. H. M.; Soltani, O.; Albrecht, J.; Gao, Q.; Pathirana, C.; Hsiao, Y.; Tummala, S.; Eastgate, M. D. The Impact of Palladium(II) Reduction Pathways on the Structure and Activity of Palladium(0) Catalysts. *Angew. Chem. Int. Ed.* **2013**, *52* (22), 5822–5826. https://doi.org/10.1002/anie.201210252.

(97) Amatore, C.; Carre, E.; Jutand, A.; M'Barki, M. A. Rates and Mechanism of the Formation of Zerovalent Palladium Complexes from Mixtures of $Pd(OAc)_2$ and Tertiary Phosphines and Their Reactivity in Oxidative Additions. *Organometallics* **1995**, *14* (4), 1818–1826. https://doi.org/10.1021/om00004a039.

(98) Fors, B. P.; Krattiger, P.; Strieter, E.; Buchwald, S. L. Water-Mediated Catalyst Preactivation: An Efficient Protocol for C−N Cross-Coupling Reactions. *Org. Lett.* **2008**, *10* (16), 3505–3508. https://doi.org/10.1021/ol801285g.

(99) Wagschal, S.; Perego, L. A.; Simon, A.; Franco-Espejo, A.; Tocqueville, C.; Albaneze-Walker, J.; Jutand, A.; Grimaud, L. Formation of XPhos-Ligated Palladium(0) Complexes and Reactivity in Oxidative Additions. *Chem. – Eur. J.* **2019**, *25* (28), 6980–6987. https://doi.org/10.1002/chem.201900451.

(100) Carole, W. A.; Colacot, T. J. Understanding Palladium Acetate from a User Perspective. *Chem. – Eur. J.* **2016**, *22* (23), 7686–7695. https://doi.org/10.1002/chem.201601450.

(101) Arduengo, A. J.; Krafczyk, R.; Schmutzler, R.; Craig, H. A.; Goerlich, J. R.; Marshall, W. J.; Unverzagt, M. Imidazolylidenes, Imidazolinylidenes and Imidazolidines. *Tetrahedron* **1999**, *55* (51), 14523–14534. https://doi.org/10.1016/S0040-4020(99)00927-8.

(102) Nair, V.; Bindu, S.; Sreekumar, V. *N*-Heterocyclic Carbenes: Reagents, Not Just Ligands! *Angew. Chem. Int. Ed.* **2004**, *43* (39), 5130–5135. https://doi.org/10.1002/anie.200301714.

(103) Organ, M. G.; Çalimsiz, S.; Sayah, M.; Hoi, K. H.; Lough, A. J. Pd-PEPPSI-IPent: An Active, Sterically Demanding Cross-Coupling Catalyst and Its Application in the Synthesis of Tetra-Ortho-Substituted Biaryls. *Angew. Chem. Int. Ed.* **2009**, *48* (13), 2383–2387. https://doi.org/10.1002/anie.200805661.

(104) Chartoire, A.; Frogneux, X.; Boreux, A.; Slawin, A. M. Z.; Nolan, S. P. [Pd(IPr*)(3-Cl-pyridinyl)Cl_2]: A Novel and Efficient PEPPSI Precatalyst. *Organometallics* **2012**, *31* (19), 6947–6951. https://doi.org/10.1021/om300725f.

(105) Pompeo, M.; Froese, R. D. J.; Hadei, N.; Organ, M. G. Pd-PEPPSI-IPentCl: A Highly Effective Catalyst for the Selective Cross-Coupling of Secondary Organozinc Reagents. *Angew. Chem. Int. Ed.* **2012**, *51* (45), 11354–11357. https://doi.org/10.1002/anie.201205747.

(106) Zhang, Y.; Lavigne, G.; César, V. Buchwald–Hartwig Amination of (Hetero)Aryl Tosylates Using a Well-Defined *N*-Heterocyclic Carbene/Palladium(II) Precatalyst. *J. Org. Chem.* **2015**, *80* (15), 7666–7673. https://doi.org/10.1021/acs.joc.5b01272.

(107) Lan, X.-B.; Li, Y.; Li, Y.-F.; Shen, D.-S.; Ke, Z.; Liu, F.-S. Flexible Steric Bulky Bis(Imino)acenaphthene (BIAN)-Supported *N*-Heterocyclic Carbene Palladium Precatalysts: Catalytic Application in Buchwald–Hartwig Amination in Air. *J. Org. Chem.* **2017**, *82* (6), 2914–2925. https://doi.org/10.1021/acs.joc.6b02867.

(108) Ouyang, J.-S.; Li, Y.-F.; Huang, F.-D.; Lu, D.-D.; Liu, F.-S. The Highly Efficient Suzuki–Miyaura Cross-Coupling of (Hetero)Aryl Chlorides and (Hetero)Arylboronic Acids Catalyzed by "Bulky-yet-Flexible" Palladium–PEPPSI Complexes in Air. *ChemCatChem* **2018**, *10* (2), 371–375. https://doi.org/10.1002/cctc.201701076.

(109) Mitchell, E. A.; Baird, M. C. Optimization of Procedures for the Syntheses of Bisphosphinepalladium(0) Precursors for Suzuki−Miyaura and Similar Cross-Coupling Catalysis: Identification of 3:1 Coordination Compounds in Catalyst Mixtures Containing Pd(0), PCy_3, and/or $PMeBu^t_2$. *Organometallics* **2007**, *26* (21), 5230–5238. https://doi.org/10.1021/om700580d.

(110) Norton, D. M.; Mitchell, E. A.; Botros, N. R.; Jessop, P. G.; Baird, M. C. A Superior Precursor for Palladium(0)-Based Cross-Coupling and Other Catalytic Reactions. *J. Org. Chem.* **2009**, *74* (17), 6674–6680. https://doi.org/10.1021/jo901121e.

(111) Borjian, S.; Baird, M. C. NMR Studies of the Species Present in Cross-Coupling Catalysis Systems Involving Pd(η^3-1-Ph-C_3H_4)(η^5-C_5H_5) and [Pd(η^3-1-Ph-C_3H_4)Cl]$_2$ Activated by PBu^t_3, XPhos, and Mor-Dalphos: Nonexistence of Pd(XPhos)$_n$ and Pd(Mor-Dalphos)$_n$ (n = 1, 2) at Moderate Temperatures. *Organometallics* **2014**, *33* (15), 3936–3940. https://doi.org/10.1021/om500618e.

(112) Alsabeh, P. G.; Lundgren, R. J.; McDonald, R.; Johansson Seechurn, C. C. C.; Colacot, T. J.; Stradiotto, M. An Examination of the Palladium/Mor-DalPhos Catalyst System in the Context of Selective Ammonia Monoarylation at Room

Temperature. *Chem. – Eur. J.* **2013**, *19* (6), 2131–2141. https://doi.org/10.1002/chem.201203640.

(113) Melvin, P. R.; Hazari, N.; Lant, H. M. C.; Peczak, I. L.; Shah, H. P. Comparison of the Catalytic Activity for the Suzuki–Miyaura Reaction of (η^5-Cp)Pd(IPr)Cl with (η^3-cinnamyl)Pd(IPr)(Cl) and (η^3-1-*t*-Bu-indenyl)Pd(IPr)(Cl). *Beilstein J. Org. Chem.* **2015**, *11* (1), 2476–2486. https://doi.org/10.3762/bjoc.11.269.

(114) Marion, N.; Navarro, O.; Mei, J.; Stevens, E. D.; Scott, N. M.; Nolan, S. P. Modified (NHC)Pd(allyl)Cl (NHC = *N*-Heterocyclic Carbene) Complexes for Room-Temperature Suzuki−Miyaura and Buchwald−Hartwig Reactions. *J. Am. Chem. Soc.* **2006**, *128* (12), 4101–4111. https://doi.org/10.1021/ja057704z.

(115) Lundgren, R. J.; Peters, B. D.; Alsabeh, P. G.; Stradiotto, M. A P,N-Ligand for Palladium-Catalyzed Ammonia Arylation: Coupling of Deactivated Aryl Chlorides, Chemoselective Arylations, and Room Temperature Reactions. *Angew. Chem. Int. Ed.* **2010**, *49* (24), 4071–4074. https://doi.org/10.1002/anie.201000526.

(116) Martin, A. R.; Chartoire, A.; Slawin, A. M. Z.; Nolan, S. P. Extending the Utility of [Pd(NHC)(cinnamyl)Cl] Precatalysts: Direct Arylation of Heterocycles. *Beilstein J. Org. Chem.* **2012**, *8* (1), 1637–1643. https://doi.org/10.3762/bjoc.8.187.

(117) Chartoire, A.; Frogneux, X.; Nolan, S. P. An Efficient Palladium-NHC (NHC=*N*-Heterocyclic Carbene) and Aryl Amination Pre-Catalyst: [Pd(IPr*)(cinnamyl)Cl]. *Adv. Synth. Catal.* **2012**, *354* (10), 1897–1901. https://doi.org/10.1002/adsc.201200207.

(118) Chartoire, A.; Lesieur, M.; Falivene, L.; Slawin, A. M. Z.; Cavallo, L.; Cazin, C. S. J.; Nolan, S. P. [Pd(IPr*)(cinnamyl)Cl]: An Efficient Pre-Catalyst for the Preparation of Tetra-*ortho*-substituted Biaryls by Suzuki–Miyaura Cross-Coupling. *Chem. – Eur. J.* **2012**, *18* (15), 4517–4521. https://doi.org/10.1002/chem.201104009.

(119) Steinsoultz, P.; Bailly, A.; Wagner, P.; Oliva, E.; Schmitt, M.; Grimaud, L.; Bihel, F. *In Situ* Formation of Cationic π-Allylpalladium Precatalysts in Alcoholic Solvents: Application to C–N Bond Formation. *ACS Catal.* **2022**, *12* (1), 560–567. https://doi.org/10.1021/acscatal.1c04641.

(120) Johansson Seechurn, C. C. C.; Parisel, S. L.; Colacot, T. J. Air-Stable Pd(R-allyl)LCl (L= Q-Phos, P(*t*-Bu)$_3$, Etc.) Systems for C–C/N Couplings: Insight into the Structure–Activity Relationship and Catalyst Activation Pathway. *J. Org. Chem.* **2011**, *76* (19), 7918–7932. https://doi.org/10.1021/jo2013324.

(121) Norman, J. P.; Larson, N. G.; Entz, E. D.; Neufeldt, S. R. Unconventional Site Selectivity in Palladium-Catalyzed Cross-Couplings of Dichloroheteroarenes under Ligand-Controlled and Ligand-Free Systems. *J. Org. Chem.* **2022**, *87* (11), 7414–7421. https://doi.org/10.1021/acs.joc.2c00665.

(122) Reeves, E. K.; Humke, J. N.; Neufeldt, S. R. *N*-Heterocyclic Carbene Ligand-Controlled Chemodivergent Suzuki–Miyaura Cross Coupling. *J. Org. Chem.* **2019**, *84* (18), 11799–11812. https://doi.org/10.1021/acs.joc.9b01692.

(123) Dardir, A. H.; Casademont-Reig, I.; Balcells, D.; Ellefsen, J. D.; Espinosa, M. R.; Hazari, N.; Smith, N. E. Synthesis of Triarylmethanes via Palladium-Catalyzed

Suzuki–Miyaura Reactions of Diarylmethyl Esters. *Organometallics* **2021**, *40* (14), 2332–2344. https://doi.org/10.1021/acs.organomet.1c00085.

(124) Ingoglia, B. T.; Wagen, C. C.; Buchwald, S. L. Biaryl Monophosphine Ligands in Palladium-Catalyzed C–N Coupling: An Updated User's Guide. *Tetrahedron* **2019**, *75* (32), 4199–4211. https://doi.org/10.1016/j.tet.2019.05.003.

(125) Crawford, S. M.; Lavery, C. B.; Stradiotto, M. BippyPhos: A Single Ligand With Unprecedented Scope in the Buchwald–Hartwig Amination of (Hetero)Aryl Chlorides. *Chem. – Eur. J.* **2013**, *19* (49), 16760–16771. https://doi.org/10.1002/chem.201302453.

(126) Dupont, J.; Consorti, C. S.; Spencer, J. The Potential of Palladacycles: More Than Just Precatalysts. *Chem. Rev.* **2005**, *105* (6), 2527–2572. https://doi.org/10.1021/cr030681r.

(127) Nájera, C. Oxime-Derived Palladacycles: Applications in Catalysis. *ChemCatChem* **2016**, *8* (11), 1865–1881. https://doi.org/10.1002/cctc.201600035.

(128) Cheung, C. W.; Buchwald, S. L. Mild and General Palladium-Catalyzed Synthesis of Methyl Aryl Ethers Enabled by the Use of a Palladacycle Precatalyst. *Org. Lett.* **2013**, *15* (15), 3998–4001. https://doi.org/10.1021/ol401796v.

(129) Yang, Y.; Oldenhuis, N. J.; Buchwald, S. L. Mild and General Conditions for Negishi Cross-Coupling Enabled by the Use of Palladacycle Precatalysts. *Angew. Chem. Int. Ed.* **2013**, *52* (2), 615–619. https://doi.org/10.1002/anie.201207750.

(130) Zhang, H.; Ruiz-Castillo, P.; Schuppe, A. W.; Buchwald, S. L. Improved Process for the Palladium-Catalyzed C–O Cross-Coupling of Secondary Alcohols. *Org. Lett.* **2020**, *22* (14), 5369–5374. https://doi.org/10.1021/acs.orglett.0c01668.

(131) Zhang, H.; Ruiz-Castillo, P.; Buchwald, S. L. Palladium-Catalyzed C–O Cross-Coupling of Primary Alcohols. *Org. Lett.* **2018**, *20* (6), 1580–1583. https://doi.org/10.1021/acs.orglett.8b00325.

(132) Friis, S. D.; Skrydstrup, T.; Buchwald, S. L. Mild Pd-Catalyzed Aminocarbonylation of (Hetero)Aryl Bromides with a Palladacycle Precatalyst. *Org. Lett.* **2014**, *16* (16), 4296–4299. https://doi.org/10.1021/ol502014b.

(133) Bhonde, V. R.; O'Neill, B. T.; Buchwald, S. L. An Improved System for the Aqueous Lipshutz–Negishi Cross-Coupling of Alkyl Halides with Aryl Electrophiles. *Angew. Chem.* **2016**, *128* (5), 1881–1885. https://doi.org/10.1002/ange.201509341.

(134) Herrmann, W. A.; Brossmer, C.; Öfele, K.; Reisinger, C.-P.; Priermeier, T.; Beller, M.; Fischer, H. Palladacycles as Structurally Defined Catalysts for the Heck Olefination of Chloro- and Bromoarenes. *Angew. Chem. Int. Ed. Engl.* **1995**, *34* (17), 1844–1848. https://doi.org/10.1002/anie.199518441.

(135) Herrmann, W. A.; Brossmer, C.; Reisinger, C.-P.; Riermeier, T. H.; Öfele, K.; Beller, M. Palladacycles: Efficient New Catalysts for the Heck Vinylation of Aryl Halides. *Chem. – Eur. J.* **1997**, *3* (8), 1357–1364. https://doi.org/10.1002/chem.19970030823.

(136) Christmann, U.; Pantazis, D. A.; Benet-Buchholz, J.; McGrady, J. E.; Maseras, F.; Vilar, R. Experimental and Theoretical Investigations of New Dinuclear Palladium

Complexes as Precatalysts for the Amination of Aryl Chlorides. *J. Am. Chem. Soc.* **2006**, *128* (19), 6376–6390. https://doi.org/10.1021/ja057825z.

(137) Elliott, E. L.; Ray, C. R.; Kraft, S.; Atkins, J. R.; Moore, J. S. Solid-Phase Synthesis of *m*-Phenylene Ethynylene Heterosequence Oligomers. *J. Org. Chem.* **2006**, *71* (14), 5282–5290. https://doi.org/10.1021/jo0607212.

(138) Prashad, M.; Mak, X. Y.; Liu, Y.; Repič, O. Palladium-Catalyzed Amination of Aryl Bromides with Hindered *N*-Alkyl-Substituted Anilines Using a Palladium(I) Tri-tert-butylphosphine Bromide Dimer. *J. Org. Chem.* **2003**, *68* (3), 1163–1164. https://doi.org/10.1021/jo020609d.

(139) Hama, T.; Hartwig, J. F. α-Arylation of Esters Catalyzed by the Pd(I) Dimer {[P(*t*-Bu)$_3$]PdBr}$_2$. *Org. Lett.* **2008**, *10* (8), 1545–1548. https://doi.org/10.1021/ol8002578.

(140) Lu, G.-P.; Voigtritter, K. R.; Cai, C.; Lipshutz, B. H. Ligand Effects on the Stereochemical Outcome of Suzuki–Miyaura Couplings. *J. Org. Chem.* **2012**, *77* (8), 3700–3703. https://doi.org/10.1021/jo300437t.

(141) Ichiishi, N.; Malapit, C. A.; Woźniak, Ł.; Sanford, M. S. Palladium- and Nickel-Catalyzed Decarbonylative C–S Coupling to Convert Thioesters to Thioethers. *Org. Lett.* **2018**, *20* (1), 44–47. https://doi.org/10.1021/acs.orglett.7b03305.

(142) Dasaradhan, C.; Nawaz Khan, F.-R. Pd_2dba_3/P(*t*-Bu)$_3$H.BF_4/Cy_2NMe Catalyzed Heck Coupling in Synthesis of 3-Alkenyl-*1H*-Isochromen-1-Ones. *Polycycl. Aromat. Compd.* **2022**, *42* (4), 1048–1060. https://doi.org/10.1080/10406638.2020.1764987.

(143) Lavery, C. B.; Rotta-Loria, N. L.; McDonald, R.; Stradiotto, M. Pd_2dba_3/Bippyphos: A Robust Catalyst System for the Hydroxylation of Aryl Halides with Broad Substrate Scope. *Adv. Synth. Catal.* **2013**, *355* (5), 981–987. https://doi.org/10.1002/adsc.201300088.

(144) Nandakumar, M. V.; Verkade, J. G. Pd_2dba_3/P(*i*-$BuNCH_2CH_2)_3N$: A Highly Efficient Catalyst for the One-Pot Synthesis of *trans*-4-*N*,*N*-Diarylaminostilbenes and *N*,*N*-Diarylaminostyrenes. *Tetrahedron* **2005**, *61* (41), 9775–9782. https://doi.org/10.1016/j.tet.2005.06.117.

(145) Horibe, H.; Fukuda, Y.; Kondo, K.; Okuno, H.; Murakami, Y.; Aoyama, T. Asymmetric Kumada–Corriu Cross-Coupling Reaction with $Pd_2(dba)_3$ and an *N*–Ar Axially Chiral Mimetic-Type Ligand Catalyst. *Tetrahedron* **2004**, *60* (47), 10701–10709. https://doi.org/10.1016/j.tet.2004.09.010.

(146) Wang, H. B.; Hu, Y.-L.; Li, D.-J. Facile and Efficient Suzuki–Miyaura Coupling Reaction of Aryl Halides Catalyzed by $Pd_2(dba)_3$ in Ionic Liquid/Supercritical Carbon Dioxide Biphasic System. *J. Mol. Liq.* **2016**, *218*, 429–433. https://doi.org/10.1016/j.molliq.2016.02.056.

(147) Old, D. W.; Wolfe, J. P.; Buchwald, S. L. A Highly Active Catalyst for Palladium-Catalyzed Cross-Coupling Reactions: Room-Temperature Suzuki Couplings and Amination of Unactivated Aryl Chlorides. *J. Am. Chem. Soc.* **1998**, *120* (37), 9722–9723. https://doi.org/10.1021/ja982250+.

(148) Wolfe, J. P.; Wagaw, S.; Buchwald, S. L. An Improved Catalyst System for Aromatic Carbon−Nitrogen Bond Formation: The Possible Involvement of Bis(Phosphine) Palladium Complexes as Key Intermediates. *J. Am. Chem. Soc.* **1996**, *118* (30), 7215–7216. https://doi.org/10.1021/ja9608306.

(149) Tanaka, M.; Hikawa, H.; Yokoyama, Y. Convenient Synthesis of Chiral Tryptophan Derivatives Using Negishi Cross-Coupling. *Tetrahedron* **2011**, *67* (33), 5897–5901. https://doi.org/10.1016/j.tet.2011.06.053.

(150) Fairlamb, I. J. S. π-Acidic Alkene Ligand Effects in Pd-Catalysed Cross-Coupling Processes: Exploiting the Interaction of Dibenzylidene Acetone (dba) and Related Ligands with Pd(0) and Pd(II). *Org. Biomol. Chem.* **2008**, *6* (20), 3645–3656. https://doi.org/10.1039/B811772A.

(151) Macé, Y.; Kapdi, A. R.; Fairlamb, I. J. S.; Jutand, A. Influence of the Dba Substitution on the Reactivity of Palladium(0) Complexes Generated from $Pd^0{}_2$(dba-*n,n'*-Z)$_3$ or Pd^0(dba-*n,n'*-Z)$_2$ and PPh_3 in Oxidative Addition with Iodobenzene. *Organometallics* **2006**, *25* (7), 1795–1800. https://doi.org/10.1021/om0510876.

(152) Zalesskiy, S. S.; Ananikov, V. P. $Pd_2(dba)_3$ as a Precursor of Soluble Metal Complexes and Nanoparticles: Determination of Palladium Active Species for Catalysis and Synthesis. *Organometallics* **2012**, *31* (6), 2302–2309. https://doi.org/10.1021/om201217r.

(153) Weber, P.; Biafora, A.; Doppiu, A.; Bongard, H.-J.; Kelm, H.; Gooßen, L. J. A Comparative Study of Dibenzylideneacetone Palladium Complexes in Catalysis. *Org. Process Res. Dev.* **2019**, *23* (7), 1462–1470. https://doi.org/10.1021/acs.oprd.9b00214.

(154) Yamamoto, T.; Ohta, T.; Ito, Y. Palladium-Catalyzed Addition of Arylboronic Acids to Aldehydes. *Org. Lett.* **2005**, *7* (19), 4153–4155. https://doi.org/10.1021/ol051501y.

(155) Takátsy, G. The Use of Spiral Loops in Serological and Virological Micro-Methods. *Acta Microbiol.* **1955**, *3* (1/2), 191–202.

(156) Pereira, D. A.; Williams, J. A. Origin and Evolution of High Throughput Screening. *Br. J. Pharmacol.* **2007**, *152* (1), 53–61. https://doi.org/10.1038/sj.bjp.0707373.

(157) Zeng, W.; Guo, L.; Xu, S.; Chen, J.; Zhou, J. High-Throughput Screening Technology in Industrial Biotechnology. *Trends Biotechnol.* **2020**, *38* (8), 888–906. https://doi.org/10.1016/j.tibtech.2020.01.001.

(158) E.a, M.; R, R.; R.r, B. High-Throughput Screening: The Hits and Leads of Drug Discovery- An Overview. *J. Appl. Pharm. Sci.* **2011**, *:* (Issue), 02–10.

(159) Lloyd, M. D. High-Throughput Screening for the Discovery of Enzyme Inhibitors. *J. Med. Chem.* **2020**, *63* (19), 10742–10772. https://doi.org/10.1021/acs.jmedchem.0c00523.

(160) Blay, V.; Tolani, B.; Ho, S. P.; Arkin, M. R. High-Throughput Screening: Today's Biochemical and Cell-Based Approaches. *Drug Discov. Today* **2020**, *25* (10), 1807–1821. https://doi.org/10.1016/j.drudis.2020.07.024.

(161) Szymański, P.; Markowicz, M.; Mikiciuk-Olasik, E. Adaptation of High-Throughput Screening in Drug Discovery—Toxicological Screening Tests. *Int. J. Mol. Sci.* **2011**, *13* (1), 427–452. https://doi.org/10.3390/ijms13010427.

(162) Potvin, E.; Lehoux, D. E.; Kukavica-Ibrulj, I.; Richard, K. L.; Sanschagrin, F.; Lau, G. W.; Levesque, R. C. In Vivo Functional Genomics of Pseudomonas Aeruginosa for High-Throughput Screening of New Virulence Factors and Antibacterial Targets. *Environ. Microbiol.* **2003**, *5* (12), 1294–1308. https://doi.org/10.1046/j.1462-2920.2003.00542.x.

(163) Friedman, A.; Perrimon, N. Genome-Wide High-Throughput Screens in Functional Genomics. *Curr. Opin. Genet. Dev.* **2004**, *14* (5), 470–476. https://doi.org/10.1016/j.gde.2004.07.010.

(164) Shalem, O.; Sanjana, N. E.; Zhang, F. High-Throughput Functional Genomics Using CRISPR–Cas9. *Nat. Rev. Genet.* **2015**, *16* (5), 299–311. https://doi.org/10.1038/nrg3899.

(165) Saini, J. S.; Corneo, B.; Miller, J. D.; Kiehl, T. R.; Wang, Q.; Boles, N. C.; Blenkinsop, T. A.; Stern, J. H.; Temple, S. Nicotinamide Ameliorates Disease Phenotypes in a Human IPSC Model of Age-Related Macular Degeneration. *Cell Stem Cell* **2017**, *20* (5), 635-647.e7. https://doi.org/10.1016/j.stem.2016.12.015.

(166) Pan, S.; Zhang, H.; Rush, J.; Eng, J.; Zhang, N.; Patterson, D.; Comb, M. J.; Aebersold, R. High Throughput Proteome Screening for Biomarker Detection *. *Mol. Cell. Proteomics* **2005**, *4* (2), 182–190. https://doi.org/10.1074/mcp.M400161-MCP200.

(167) Wilson, B. A. P.; Wang, H.; Nacev, B. A.; Mease, R. C.; Liu, J. O.; Pomper, M. G.; Isaacs, W. B. High-Throughput Screen Identifies Novel Inhibitors of Cancer Biomarker α-Methylacyl Coenzyme A Racemase (AMACR/P504S). *Mol. Cancer Ther.* **2011**, *10* (5), 825–838. https://doi.org/10.1158/1535-7163.MCT-10-0902.

(168) Kostallas, G.; Samuelson, P. Novel Fluorescence-Assisted Whole-Cell Assay for Engineering and Characterization of Proteases and Their Substrates. *Appl. Environ. Microbiol.* **2010**, *76* (22), 7500–7508. https://doi.org/10.1128/AEM.01558-10.

(169) Cheng, F.; Kardashliev, T.; Pitzler, C.; Shehzad, A.; Lue, H.; Bernhagen, J.; Zhu, L.; Schwaneberg, U. A Competitive Flow Cytometry Screening System for Directed Evolution of Therapeutic Enzyme. *ACS Synth. Biol.* **2015**, *4* (7), 768–775. https://doi.org/10.1021/sb500343g.

(170) Tu, R.; Martinez, R.; Prodanovic, R.; Klein, M.; Schwaneberg, U. A Flow Cytometry–Based Screening System for Directed Evolution of Proteases. *SLAS Discov.* **2011**, *16* (3), 285–294. https://doi.org/10.1177/1087057110396361.

(171) Pitzler, C.; Wirtz, G.; Vojcic, L.; Hiltl, S.; Böker, A.; Martinez, R.; Schwaneberg, U. A Fluorescent Hydrogel-Based Flow Cytometry High-Throughput Screening Platform for Hydrolytic Enzymes. *Chem. Biol.* **2014**, *21* (12), 1733–1742. https://doi.org/10.1016/j.chembiol.2014.10.018.

(172) Shultz, C. S.; Krska, S. W. Unlocking the Potential of Asymmetric Hydrogenation at Merck. *Acc. Chem. Res.* **2007**, *40* (12), 1320–1326. https://doi.org/10.1021/ar700141v.

(173) Boussie, T. R.; Diamond, G. M.; Goh, C.; Hall, K. A.; LaPointe, A. M.; Leclerc, M. K.; Murphy, V.; Shoemaker, J. A. W.; Turner, H.; Rosen, R. K.; Stevens, J. C.; Alfano, F.; Busico, V.; Cipullo, R.; Talarico, G. Nonconventional Catalysts for Isotactic Propene Polymerization in Solution Developed by Using High-Throughput-Screening Technologies. *Angew. Chem. Int. Ed.* **2006**, *45* (20), 3278–3283. https://doi.org/10.1002/anie.200600240.

(174) Leitch, D. C.; Becica, J. 13.12 - High-Throughput Experimentation in Organometallic Chemistry and Catalysis. In *Comprehensive Organometallic Chemistry IV*; Parkin, G., Meyer, K., O'hare, D., Eds.; Elsevier: Oxford, 2022; pp 502–555. https://doi.org/10.1016/B978-0-12-820206-7.00111-6.

(175) Emmert, M. H.; Christensen, M.; DiRocco, D. A.; Dreher, S. D.; Isom, D. C.; Isom, R.; Shevlin, M. Inventing and Building HTE Technology for End-Users: The Merck/Analytical Sales and Services Collaboration — An Interview. In *The Power of High-Throughput Experimentation: General Topics and Enabling Technologies for Synthesis and Catalysis (Volume 1)*; ACS Symposium Series; American Chemical Society, 2022; Vol. 1419, pp 87–104. https://doi.org/10.1021/bk-2022-1419.ch006.

(176) J. Welch, C. High Throughput Analysis Enables High Throughput Experimentation in Pharmaceutical Process Research. *React. Chem. Eng.* **2019**, *4* (11), 1895–1911. https://doi.org/10.1039/C9RE00234K.

(177) Cernak, T.; Dykstra, K. D.; Tyagarajan, S.; Vachal, P.; Krska, S. W. The Medicinal Chemist's Toolbox for Late Stage Functionalization of Drug-like Molecules. *Chem. Soc. Rev.* **2016**, *45* (3), 546–576. https://doi.org/10.1039/C5CS00628G.

(178) Mennen, S. M.; Alhambra, C.; Allen, C. L.; Barberis, M.; Berritt, S.; Brandt, T. A.; Campbell, A. D.; Castañón, J.; Cherney, A. H.; Christensen, M.; Damon, D. B.; Eugenio de Diego, J.; García-Cerrada, S.; García-Losada, P.; Haro, R.; Janey, J.; Leitch, D. C.; Li, L.; Liu, F.; Lobben, P. C.; MacMillan, D. W. C.; Magano, J.; McInturff, E.; Monfette, S.; Post, R. J.; Schultz, D.; Sitter, B. J.; Stevens, J. M.; Strambeanu, I. I.; Twilton, J.; Wang, K.; Zajac, M. A. The Evolution of High-Throughput Experimentation in Pharmaceutical Development and Perspectives on the Future. *Org. Process Res. Dev.* **2019**, *23* (6), 1213–1242. https://doi.org/10.1021/acs.oprd.9b00140.

(179) Leitch, D. C. High-Throughput Synthetic Chemistry in Academia: Case Studies in Overcoming Barriers through Industrial Collaborations and Accessible Tools. In *The Power of High-Throughput Experimentation: General Topics and Enabling Technologies for Synthesis and Catalysis (Volume 1)*; ACS Symposium Series; American Chemical Society, 2022; Vol. 1419, pp 35–57. https://doi.org/10.1021/bk-2022-1419.ch004.

(180) Richardson, J.; Ruble, J. C.; Love, E. A.; Berritt, S. A Method for Identifying and Developing Functional Group Tolerant Catalytic Reactions: Application to the

Buchwald–Hartwig Amination. *J. Org. Chem.* **2017**, *82* (7), 3741–3750. https://doi.org/10.1021/acs.joc.7b00201.

(181) Collins, K. D.; Glorius, F. Intermolecular Reaction Screening as a Tool for Reaction Evaluation. *Acc. Chem. Res.* **2015**, *48* (3), 619–627. https://doi.org/10.1021/ar500434f.

(182) Collins, K. D.; Glorius, F. A Robustness Screen for the Rapid Assessment of Chemical Reactions. *Nat. Chem.* **2013**, *5* (7), 597–601. https://doi.org/10.1038/nchem.1669.

(183) Robbins, D. W.; Hartwig, J. F. A Simple, Multidimensional Approach to High-Throughput Discovery of Catalytic Reactions. *Science* **2011**, *333* (6048), 1423–1427. https://doi.org/10.1126/science.1207922.

(184) McNally, A.; Prier, C. K.; MacMillan, D. W. C. Discovery of an α-Amino C–H Arylation Reaction Using the Strategy of Accelerated Serendipity. *Science* **2011**, *334* (6059), 1114–1117. https://doi.org/10.1126/science.1213920.

(185) Quinton, J.; Kolodych, S.; Chaumonet, M.; Bevilacqua, V.; Nevers, M.-C.; Volland, H.; Gabillet, S.; Thuéry, P.; Créminon, C.; Taran, F. Reaction Discovery by Using a Sandwich Immunoassay. *Angew. Chem. Int. Ed.* **2012**, *51* (25), 6144–6148. https://doi.org/10.1002/anie.201201451.

(186) Troshin, K.; Hartwig, J. F. Snap Deconvolution: An Informatics Approach to High-Throughput Discovery of Catalytic Reactions. *Science* **2017**, *357* (6347), 175–181. https://doi.org/10.1126/science.aan1568.

(187) Fordham, J. M.; Kollmus, P.; Cavegn, M.; Schneider, R.; Santagostino, M. A "Pool and Split" Approach to the Optimization of Challenging Pd-Catalyzed C–N Cross-Coupling Reactions. *J. Org. Chem.* **2022**, *87* (6), 4400–4414. https://doi.org/10.1021/acs.joc.2c00104.

(188) Allen, C. L.; Leitch, D. C.; Anson, M. S.; Zajac, M. A. The Power and Accessibility of High-Throughput Methods for Catalysis Research. *Nat. Catal.* **2019**, *2* (1), 2–4. https://doi.org/10.1038/s41929-018-0220-4.

(189) Wolf, E.; Richmond, E.; Moran, J. Identifying Lead Hits in Catalyst Discovery by Screening and Deconvoluting Complex Mixtures of Catalyst Components. *Chem. Sci.* **2015**, *6* (4), 2501–2505. https://doi.org/10.1039/C5SC00268K.

(190) Eom, M. S.; Noh, J.; Kim, H.-S.; Yoo, S.; Han, M. S.; Lee, S. High-Throughput Screening Protocol for the Coupling Reactions of Aryl Halides Using a Colorimetric Chemosensor for Halide Ions. *Org. Lett.* **2016**, *18* (8), 1720–1723. https://doi.org/10.1021/acs.orglett.6b00300.

(191) Schmink, J. R.; Tudge, M. T. Facile Preparation of Highly-Functionalized, Nitrogen-Bearing Diarylmethanes. *Tetrahedron Lett.* **2013**, *54* (1), 15–20. https://doi.org/10.1016/j.tetlet.2012.09.112.

(192) Larson, H.; Schultz, D.; Kalyani, D. Ni-Catalyzed C–H Arylation of Oxazoles and Benzoxazoles Using Pharmaceutically Relevant Aryl Chlorides and Bromides. *J. Org. Chem.* **2019**, *84* (20), 13092–13103. https://doi.org/10.1021/acs.joc.9b02094.

(193) McDougal, N. T.; Virgil, S. C.; Stoltz, B. M. High-Throughput Screening of the Asymmetric Decarboxylative Alkylation Reaction of Enolate-Stabilized Enol Carbonates. *Synlett* **2010**, *2010* (11), 1712–1716. https://doi.org/10.1055/s-0030-1258094.

(194) Pipaón Fernández, N.; Gaube, G.; Woelk, K. J.; Burns, M.; Hruszkewycz, D. P.; Leitch, D. C. Palladium-Catalyzed Direct C–H Alkenylation with Enol Pivalates Proceeds via Reversible C–O Oxidative Addition to Pd(0). *ACS Catal.* **2022**, *12* (12), 6997–7003. https://doi.org/10.1021/acscatal.2c01305.

(195) Gaube, G.; Fernandez, N. P.; Leitch, D. C. An Evaluation of Palladium-Based Catalysts for the Base-Free Borylation of Alkenyl Carboxylates. *New J. Chem.* **2021**, *45* (43), 20095–20098. https://doi.org/10.1039/D1NJ04008A.

(196) Becica, J.; Hruszkewycz, D. P.; Steves, J. E.; Elward, J. M.; Leitch, D. C.; Dobereiner, G. E. High-Throughput Discovery and Evaluation of a General Catalytic Method for N-Arylation of Weakly Nucleophilic Sulfonamides. *Org. Lett.* **2019**, *21* (22), 8981–8986. https://doi.org/10.1021/acs.orglett.9b03380.

(197) Cai, C.; Chung, J. Y. L.; McWilliams, J. C.; Sun, Y.; Shultz, C. S.; Palucki, M. From High-Throughput Catalyst Screening to Reaction Optimization: Detailed Investigation of Regioselective Suzuki Coupling of 1,6-Naphthyridone Dichloride. *Org. Process Res. Dev.* **2007**, *11* (3), 328–335. https://doi.org/10.1021/op060215e.

(198) Greshock, T. J.; Moore, K. P.; McClain, R. T.; Bellomo, A.; Chung, C. K.; Dreher, S. D.; Kutchukian, P. S.; Peng, Z.; Davies, I. W.; Vachal, P.; Ellwart, M.; Manolikakes, S. M.; Knochel, P.; Nantermet, P. G. Synthesis of Complex Druglike Molecules by the Use of Highly Functionalized Bench-Stable Organozinc Reagents. *Angew. Chem. Int. Ed.* **2016**, *55* (44), 13714–13718. https://doi.org/10.1002/anie.201604652.

(199) Zacuto, M. J.; Shultz, C. S.; Journet, M. Preparation of 4-Allylisoindoline via a Kumada Coupling with Allylmagnesium Chloride. *Org. Process Res. Dev.* **2011**, *15* (1), 158–161. https://doi.org/10.1021/op1002837.

(200) Murray, P. M.; Bower, J. F.; Cox, D. K.; Galbraith, E. K.; Parker, J. S.; Sweeney, J. B. A Robust First-Pass Protocol for the Heck–Mizoroki Reaction. *Org. Process Res. Dev.* **2013**, *17* (3), 397–405. https://doi.org/10.1021/op300364p.

(201) Annand, J. R.; Riehl, P. S.; Schultz, D. M.; Schindler, C. S. High-Throughput Approach toward the Development of a Mizoroki–Heck Reaction To Access Tricyclic Spirolactones. *J. Org. Chem.* **2020**, *85* (14), 9071–9079. https://doi.org/10.1021/acs.joc.0c00997.

(202) Kashani, S. K.; Jessiman, J. E.; Newman, S. G. Exploring Homogeneous Conditions for Mild Buchwald–Hartwig Amination in Batch and Flow. *Org. Process Res. Dev.* **2020**. https://doi.org/10.1021/acs.oprd.0c00018.

(203) Arrington, K.; Barcan, G. A.; Calandra, N. A.; Erickson, G. A.; Li, L.; Liu, L.; Nilson, M. G.; Strambeanu, I. I.; VanGelder, K. F.; Woodard, J. L.; Xie, S.; Allen, C. L.; Kowalski, J. A.; Leitch, D. C. Convergent Synthesis of the NS5B Inhibitor

GSK8175 Enabled by Transition Metal Catalysis. *J. Org. Chem.* **2019**, *84* (8), 4680–4694. https://doi.org/10.1021/acs.joc.8b02269.

(204) Briggs, J. R.; Hagen, H.; Julka, S.; Patton, J. T. Palladium-Catalyzed 1,3-Butadiene Telomerization with Methanol. Improved Catalyst Performance Using Bis-o-Methoxy Substituted Triarylphosphines. *J. Organomet. Chem.* **2011**, *696* (8), 1677–1686. https://doi.org/10.1016/j.jorganchem.2011.02.007.

(205) Coombs, J. R.; Green, R. A.; Roberts, F.; Simmons, E. M.; Stevens, J. M.; Wisniewski, S. R. Advances in Base-Metal Catalysis: Development of a Screening Platform for Nickel-Catalyzed Borylations of Aryl (Pseudo)halides with $B_2(OH)_4$. *Organometallics* **2019**, *38* (1), 157–166. https://doi.org/10.1021/acs.organomet.8b00307.

(206) Renom-Carrasco, M.; Lefort, L. Ligand Libraries for High Throughput Screening of Homogeneous Catalysts. *Chem. Soc. Rev.* **2018**, *47* (13), 5038–5060. https://doi.org/10.1039/C7CS00844A.

Chapter 2 ^{DMP}DAB–Pd–MAH: A Versatile Palladium(0) Source for Precatalyst Formation, Reaction Screening, and Preparative-Scale Synthesis

This chapter has been adapted from:

Huang, J.; Isaac, M.; Watt, R.; Becica, J.; Dennis, E.; Saidaminov, M. I.; Sabbers, W. A.; Leitch, D. C. ^{DMP}DAB–Pd–MAH: A Versatile Pd(0) Source for Precatalyst Formation, Reaction Screening, and Preparative-Scale Synthesis. *ACS Catal.* 2021, 11 (9), 5636-5646. DOI: 10.1021/acscatal.1c00288.

Contributions:

^{DMP}DAB–Pd–MAH was initially prepared by Ryan Watt. The synthesis of [phosphine]-Pd-MAH complexes (Figure 2.5) were conducted by Matthew Isaac, Dr. Joseph Becica and Prof. David C. Leitch. The synthesis of *spiro*-OMeTAD was conducted in collaboration with Emma Dennis (who assisted with screening and synthesis) and Prof. Makhsud I. Saidaminov (who co-supervised Emma). XRD data were collected and analyzed by William A. Sabbers (Temple University). All other experimental work was conducted by Jingjun Huang.

2.1 Abstract

In this chapter, we report an easily prepared and bench-stable mononuclear palladium(0) source stabilized by a chelating *N*,*N'*-diaryldiazabutadiene ligand and maleic anhydride: ^{DMP}DAB–Pd–MAH.[1] Diverse phosphine ligands, including bidentate phosphines and large-cone-angle biarylphosphines, can rapidly and completely displace the diazabutadiene ligand at room temperature to give air-stable palladium(0) phosphine complexes. ^{DMP}DAB–Pd–MAH itself is readily soluble and stable in several organic solvents, making it an ideal Pd source for *in situ* catalyst preparation during reaction screening as well as solution-dispensing to plate-based reaction arrays for high-throughput

experimentation. Evaluation of ^{DMP}DAB–Pd–MAH alongside other common Pd^0 and Pd^{II} sources in microscale reaction screens reveals that ^{DMP}DAB–Pd–MAH is superior at identifying hits across six different C–N, C–C, and C–O coupling reactions. ^{DMP}DAB–Pd–MAH, and the phosphine precatalysts derived therefrom, are also effective in preparative-scale cross-couplings at low Pd loadings.

2.2 Introduction

As stated in Chapter 1, palladium-catalyzed cross-coupling is a significant and extensively used method in modern synthetic chemistry.[2–10] Existing palladium(II) sources can have complicated, condition-dependent reduction pathways, potentially hindering the development of efficient reactions. In stark contrast, palladium(0) sources are capable of entering the catalytic cycle without the need for the reduction, but are much less developed. To be specific, Pd_2dba_3, the most commonly used palladium(0) precursor, can easily decompose through ligand dissociation to yield insoluble palladium nanoparticles and dissociated dba during the storage either in solution or solid state. These dissociated ligands are observed to inhibit catalysis in some cases.[11,12] In addition to the poor stability arising from the dba dissociation, Pd_2dba_3 suffers from low solubility, different catalytic activity when using different crystalline solvates,[13,14] as well as problems with reproducibility.[15] All of these features of Pd_2dba_3 are problematic from a solution-dosing standpoint in high-throughput screening, which is an increasingly important approach in modern synthetic chemistry. To address these drawbacks, it is crucial to have a more stable palladium(0) precursor that is soluble in many different solvents.

α-Diimines have been widely exploited as a versatile ligand for many transition metal catalysts, predominantly due to their easy preparation, conformational rigidity, decent stability, and high functional group tolerance in the resulting catalysts.[16–22] The chelating binding mode and electron delocalization through the N=C–C=N conjugated system contribute to the stability of this ligand when coordinating to a metal center. Substitution on the two nitrogen atoms also gives rise to a variety of possible structures, which can impart different steric and electronic properties.

Because of the above ligand features, a broad range of palladium complexes featuring α-diimine ligands have been developed. Several representative examples will be discussed here. Brookhart and co-workers introduced a class of cationic palladium(II) precatalysts containing the *N*,*N*′-substituted diazabutadiene moiety (Figure 2.1A).[23] The applications of this catalyst class in olefin polymerization are a significant milestone in the field.[21,24,25] With the success of the Brookhart-type catalysts, an array of α-diimine palladium complexes derived from these structures were established through modifying the nitrogen substituents,[26–32] the reactive ligands,[27,28] and the substituents on the diimine backbone.[33–36] DAB-coordinated palladium(II) catalysts are also used in olefin copolymerization with polar co-monomers,[26,32,34,37–39] and the dimerization of vinyl ethers.[40]

Contrary to their broad applications in polymerization, these complexes are much less prevalent in cross-coupling reactions. There are still some promising α-diimine-based systems for specific cross-coupling reactions, including C–H bond activation,[41–44] Suzuki-Miyaura coupling,[45] Mizoroki−Heck reactions,[46–48] and Sonagashira and Hiyama reactions.[49] Apart from the Brookhart-type catalysts, palladium complexes containing *cis*-fixed diimine ligands and conjugated dienes were established and used to catalyze the functionalization of alkynes (Figure 2.1B).[50,51] Another example, featuring a similar *cis*-fixed diimine scaffold on palladium(0) stabilized with olefins has been used as catalysts for C–C bond formations[52] and hydrogenations[53,54] (Figure 2.1C). Diimine–Pd–olefin complexes can be traced back to the first reported examples by Vrieze and co-workers. They prepared and characterized a series of *N*,*N*′-dialkyl diazabutadiene (DAB) Pd^0 compounds consisting of assorted 1,4-diazabutadienes and olefins (Figure 2.1D). They also disclosed efficient ligand displacement of the diimine ligands with triphenylphosphine, demonstrating that the DAB ligand is labile toward substitution.[55] In addition to these representative examples, there are a few other reported α-diimine-palladium(0)-olefin complexes.[56–59]

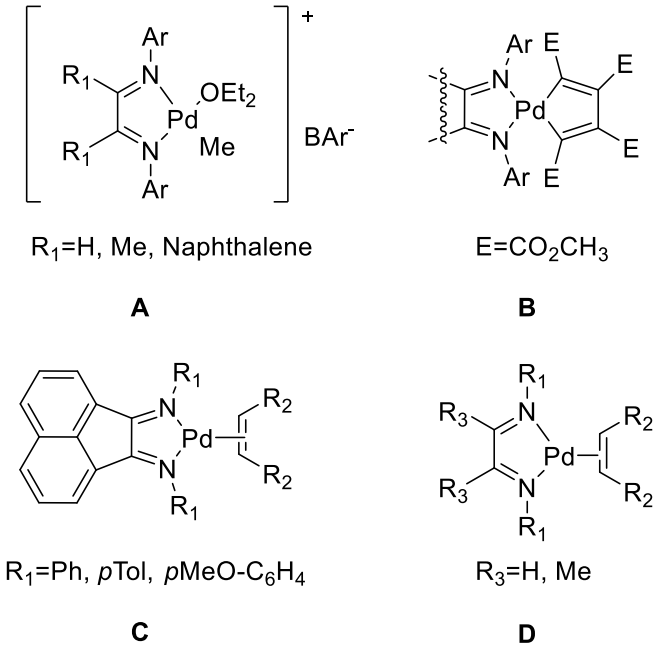

Figure 2.1. Representative classes of palladium complexes featuring α-diimine ligands.

Inspired by the work from Vrieze,[55] we designed our palladium(0) source ^{DMP}DAB–Pd–MAH (**2.1**, Figure 2.2) to feature an *N*,*N*′-diaryl DAB ligand and maleic anhydride (MAH). We expected this complex to be well stabilized by the chelating *N*,*N*′-diaryldiazabutadiene ligand and maleic anhydride, which is an electron-deficient alkene that engages in π-back donation from the electron-rich Pd^0 center.

Based on our evaluation, this Pd^0 complex offers several advantages over other palladium sources, including good solubility, solution stability, and efficient substitution of the *N*,*N*′-diaryldiazabutadiene ligand with a wide range of catalytically relevant phosphine ligands. We also report the preparation of 13 air-stable [phosphine]–Pd–MAH precatalysts by using complex **2.1** as a precursor. Through a series of microscale high-throughput screening experiments for C–N, C–O, and C–C coupling reactions, we demonstrate that ^{DMP}DAB–Pd–MAH is superior at identifying ligand hits when evaluated alongside other common palladium precursors. Finally, we show that catalysts derived from **2.1,** either generated *in situ* or preformed, are able to catalyze preparative-scale reactions at low palladium loadings, including a high-yielding synthetic application of the hole-transport material *spiro*-OMeTAD.[60]

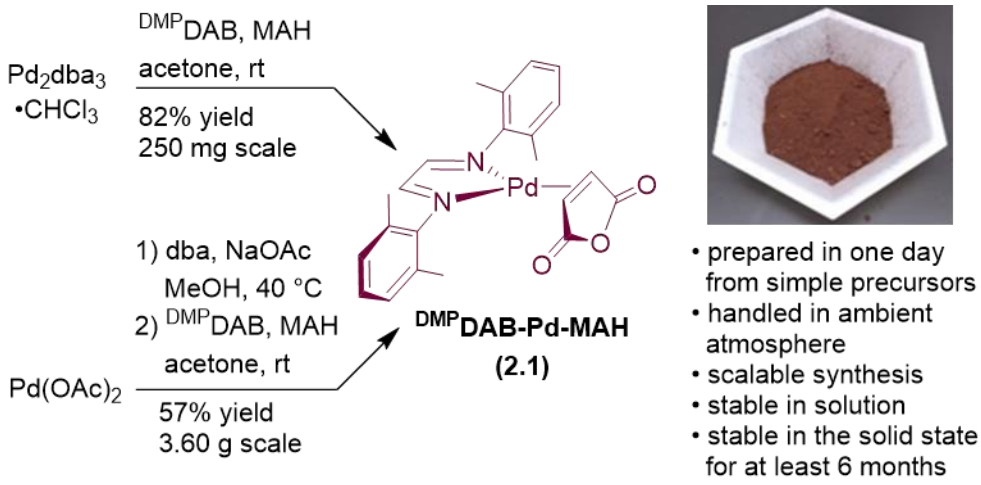

Figure 2.2. Synthesis of new Pd^0 source ^{DMP}DAB-Pd-MAH (**2.1**).

2.3 Result and Discussion

2.3.1 Structure and Properties of ^{DMP}DAB–Pd–MAH

Herein, we report a new and versatile palladium(0) precursor: ^{DMP}DAB–Pd–MAH (**2.1**, Figure 2.2) stabilized by an *N*,*N*′-diaryl DAB ligand and MAH. The *N*,*N*′-di-*tert*-butyl analogue of **2.1**, first prepared by Vrieze and co-workers, has been used as a starting material to generate new L–Pd^0–MAH complexes via substitution of the DAB with different supporting ligands.[61–70] For this precatalyst, we incorporated sterically demanding and less electron-donating 2,6-dimethylphenyl substituents at nitrogen (^{DMP}DAB) to favor rapid and complete ligand substitution with incoming phosphines during *in situ* catalyst formation. By adding ^{DMP}DAB and MAH to an acetone suspension of $Pd_2dba_3{\cdot}CHCl_3$ at room temperature in air, ^{DMP}DAB–Pd–MAH (**2.1**) can be isolated in 82% yield (Figure 2.2). We have also developed a telescoped synthesis of **2.1** from $Pd(OAc)_2$, giving a 57% isolated yield on a multigram scale. This synthetic pathway proceeds through crude "$Pd(dba)_2$" and can be conducted in one day. By using either method, complex **2.1** is isolated via simple precipitation in high purity with no need for recrystallization. Purity was determined by NMR spectroscopy and elemental analysis of the multigram batch.

Compound **2.1** is an air- and moisture-stable mononuclear Pd^0 complex that is soluble in a variety of organic solvents. Analysis by NMR spectroscopy generates simple

and easy-to-interpret spectra that are highly consistent with the given structure, providing an excellent method to assess purity quickly. This is in stark contrast to the solution behaviour of Pd_2dba_3. For Pd_2dba_3, the presence of multiple species and extensive magnetic inequivalence cause complicated NMR spectra,[15] and poor solubility gives rise to a low signal-to-noise ratio. We have also obtained the solid-state molecular structure of **2.1** via X-ray diffraction (Figure 2.3).

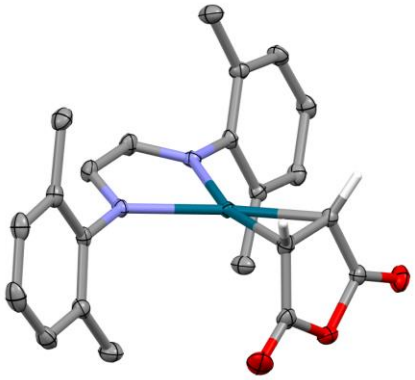

Figure 2.3. Solid-state molecular structure of complex **2.1**.

Atom colors: C: grey; N: light blue; O: red; Pd: green/blue. Thermal ellipsoids plotted at 50% probability. Hydrogen atoms omitted for clarity, except those on the maleic anhydride ligand. See the Supporting Information of reference 1 for metrical parameters and data collection details.[1]

Given the importance of reliability in both traditional and high-throughput reaction screenings, we assessed the stability of compound **2.1** over time in the solid state and in solution. This is to evaluate stability during long-term storage and manual or automated solution-dispensing, respectively. The compound is stable as a solid for at least six months at room temperature under an ambient atmosphere, with no noticeable change to the NMR spectra over this time. Previous studies of DAB–Pd^0–olefin complexes of this type describe rapid solution decomposition to metallic palladium,[55] which would significantly reduce its usefulness in solution-based-dispensing. We therefore monitored the stability of **2.1** in several organic solvents over 48 hours at room temperature under air by ^{1}H NMR spectroscopy (Figure 2.4).

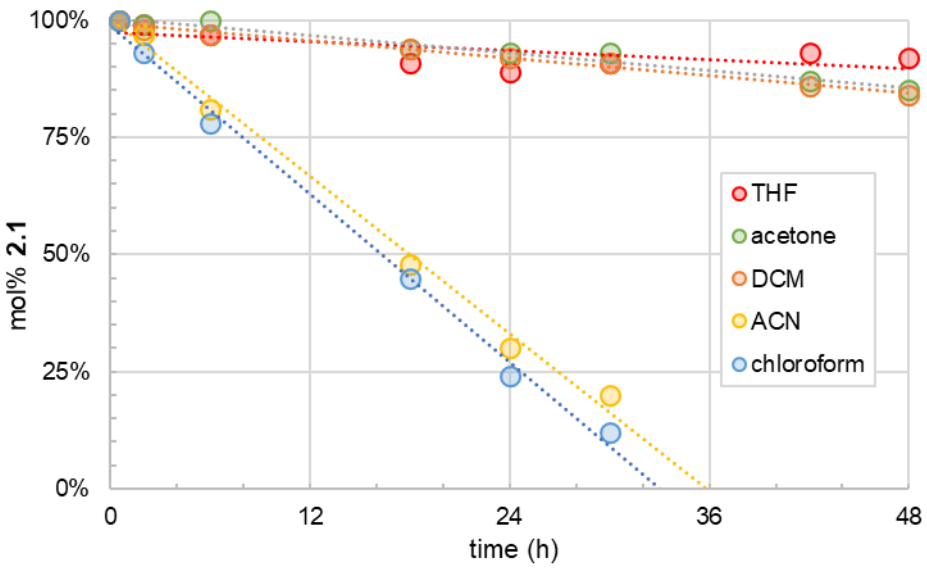

Figure 2.4. Solution stability of complex **2.1** at 20 mg/mL (0.043 M) initial concentration in five deuterated solvents (48 h, room temp., under air). Concentration determined using ^{1}H NMR spectroscopy (relative integration vs internal standard).

In both acetonitrile and chloroform, we observe rapid decomposition (around 3% **2.1** consumed per hour), with only 25–30% remaining after 24 hours. Fortunately, complex **2.1** is 10–20 times more stable in THF, acetone, and DCM, with decomposition rates 0.15–0.3% **2.1** consumed per hour. After 6 hours, a typical time needed for dispensing solutions to a screening plate, the amount of **2.1** remaining in these solvents is 97–100%. After 24 hours, the time length of an automated solution-dispensing protocol to multiple reaction plates, 89–93% of complex **2.1** still remains. Notably, no discernible by-products or formation of solids is observed during this process. Based on these data, we recommend working with **2.1** in freshly prepared THF or acetone solutions for dispensing to high-throughput experimentation (HTE) plates. Owing to the excellent air- and moisture-stability of **2.1**, solution preparation and dispensing can be performed using regular lab-grade solvents without the need for an inert-atmosphere glovebox.

2.3.2 Phosphine Metalation and Precatalyst Synthesis

Given the simple synthesis and high stability of **2.1**, we further studied its suitability as a precursor for *in situ* catalyst generation during reaction screening by HTE. Our key criteria is to have a rapid phosphine metalation to Pd^0 at room temperature to give a single and well-defined Pd species. This can ensure self-consistent results across a screening plate that do not depend on secondary factors such as catalyst activation. In a series of preliminary experiments, we mixed **2.1** with 2 equivalent of a variety of mono and bidentate phosphines in d_6-acetone to determine the extent of ligand substitution by ^{1}H and ^{31}P NMR spectroscopy. In each case, we observe the rapid and complete formation of one new ^{31}P-containing species at room temperature in the initial NMR spectra (15–60 min reaction time).

Based on these promising results, we prepared and isolated a series of 13 [phosphine]–Pd–MAH precatalysts (**2.2–2.14**) from a set of phosphine ligands that are commonly used in cross-coupling catalysis (Figure 2.5A). All of these syntheses are carried out at room temperature in THF in 1 hour, and the products are isolated by simple precipitation under an ambient atmosphere. The prepared compounds range from the known complex dppp–Pd–MAH (**2.2**) to those with large biaryl and bispyrazolyl ligands, including *t*BuBrettPhos (**2.11**), *t*BuBippyphos (**2.12**), Me_4*t*BuXPhos (**2.13**), and JackiePhos (**2.14**). Figure 2.5B contains solid-state molecular structures of five of these complexes, determined by single-crystal X-ray diffraction. The metrical parameters, data collection details, and full structures of these crystals are all filed in the Supporting Information of the published paper.[1]

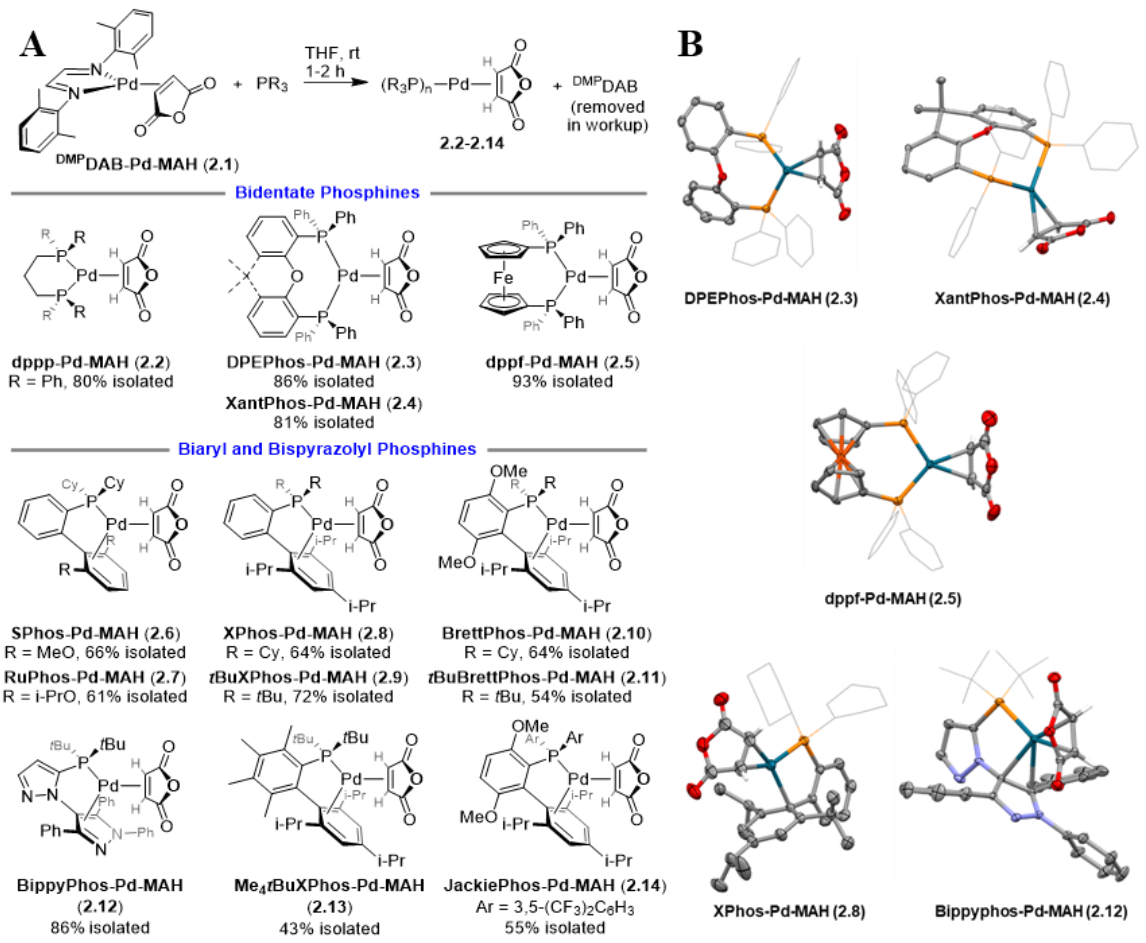

Figure 2.5. A: Synthesis and isolation of [phosphine]–Pd–MAH complexes **2.2**–**2.14** via ligand substitution at complex **2.1**; **B**: Solid-state molecular structures determined by single-crystal XRD of **2.3**, **2.4**, **2.5**, **2.8**, and **2.12**.

Atom colors: C, gray; N, light blue; O, red; P, orange; Pd, green/blue. Thermal ellipsoids plotted at 30% (**2.3**, **2.5**, **2.8**) or 50% (2.4, **2.12**) probability. Hydrogen atoms omitted for clarity, except those on the maleic anhydride ligand. Phosphine substituents (Ph, Cy, or *t*Bu) shown in wireframe for clarity; single conformation shown for disordered Cy ring in complex **2.8**. Solvent molecules in asymmetric unit omitted for clarity.

Table 2.1 contains key metrical parameters for the Pd–MAH fragments in complexes **2.1**, **2.3**-**2.5**, **2.8**, and **2.12** that were successfully recrystallized. By switching from the ^{DMP}DAB ancillary ligand to the various phosphines, the Pd–C bond lengths increase, while the C=C bond lengths and C–Pd–C angles decrease. This trend is consistent with what we expected: the Pd–alkene bonding is weaker when the more electron-donating phosphine ligands are present, though the metrical parameters are in a fairly narrow range for these phosphine complexes.

Table 2.1. Metrical parameters for Pd–MAH fragment from solid-state molecular structures.[a]

Complex	Pd–C_1 (Å)	Pd–C_2 (Å)	C1–C_2 (Å)	C_1–Pd–C_2 (°)
2.1	2.0868(13)	2.0556(14)	1.4315(18)	40.42(5)
2.3	2.104(4)	2.125(4)	1.396(6)	38.55(15)
2.4	2.141(3)	2.111(3)	1.420(4)	39.01(11)
2.5	2.140(16)	2.105(16)	1.39(2)	38.3(6)
2.8	2.135(3)[b]	2.077(3)[b]	1.406(6)	38.98(17)
2.12	2.133(3)[b]	2.081(3)[b]	1.422(4)	39.43(11)

[a]C_1 and C_2 are defined as the two alkene carbons in the MAH ligand. [b]For complexes **2.8** and **2.12**, C_1 is (approximately) trans to the phosphorus, while C_2 is cis-disposed; the longer C_1–Pd bond is due to trans influence.

To quantitatively assess the rates of ligand substitution with a representative subset of phosphines, we monitored the reaction progress over short reaction times by ^{1}H NMR spectroscopy in d_8-THF (Figure 2.6). With both DPEPhos and Bippyphos, we observe complete consumption of **2.1** along with the formation of the [phosphine]–Pd–MAH complex in less than 5 min at room temperature. Larger-cone-angle ligands, including *t*BuBrettPhos and Me$_4$*t*BuXPhos, have more than 98% conversion in less than 20 and 60 minutes, respectively. Notably, it is known that Me$_4$*t*BuXPhos requires elevated temperatures (>100 °C) to react with Pd_2dba_3 over similar timeframes.[71] In addition, *in situ* catalyst formation from this bulky ligand and palladium(II) precatalysts based on a palladacycle[72] or allyl[73] framework are reported to be challenging and potentially unreliable. Here, a simple pre-stir for around one hour at room temperature is sufficient to complete the metalation for this very sterically demanding ligand. We also tested the displacement of ^{DMP}DAB with the free DIPP NHC (*N*,*N*'-bis(2,6-diisopropylphenyl)imidazol-2-ylidene). Around 90% consumption of **2.1** was observed in only 5 minutes.

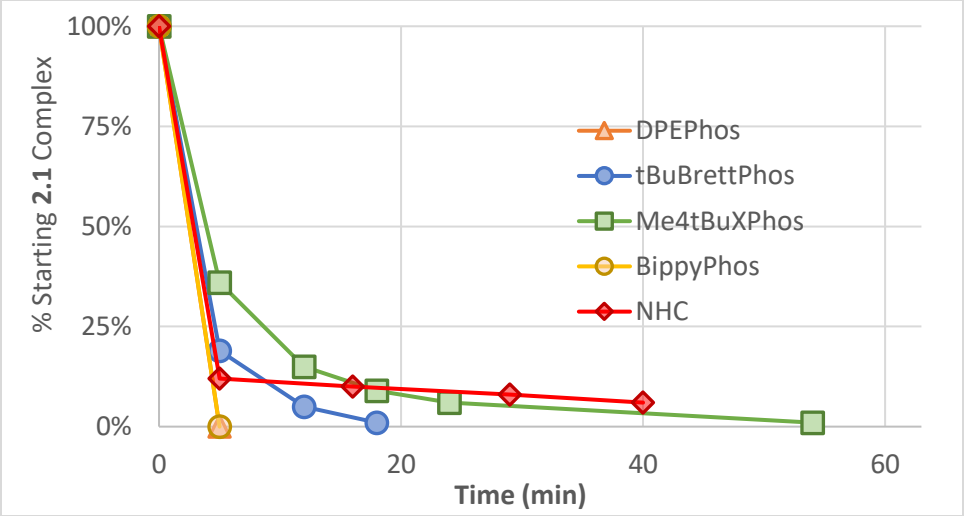

Figure 2.6. Comparison of ligand substitution reaction progress between ^{DMP}DAB–Pd–MAH (**2.1**) and several phosphines (P:Pd=2:1) or *N*,*N*′-bis(2,6-diisopropylphenyl)imidazol-2-ylidene and DPEPhos (1 equiv per Pd) to generate [ligand]–Pd–MAH complexes.

2.3.3 Applications in Screening and Preparative-Scale Synthesis

To assess the catalytic utility of complex **2.1** and the corresponding [phosphine]–Pd–MAH complexes, we have conducted a series of microscale high-throughput screens for several important cross-coupling reactions (Figure 2.7). Many properties of complex **2.1**, including solubility, stability, and rapid ligand displacement, make it attractive as a palladium precursor for microscale high-throughput screening. We therefore examined complex **2.1** alongside three of the most common palladium sources for *in situ* catalyst generation—$Pd(OAc)_2$, $[Pd(allyl)Cl]_2$, and freshly prepared/recrystallized[15] Pd_2dba_3•$CHCl_3$—in order to make fair comparisons.

Six microscale screens were designed to cover C–N, C–C, and C–O coupling reactions. These six reaction classes also do not involve substrates that can easily reduce palladium(II) to palladium(0) (such as arylboronic acids), even though reduction by other components, such as phosphine, amine, alcohol, etc., is possible. This indicates that a proper selection of palladium sources is essential to the success of an HTE screening. Each array was performed with 13 mol % Pd, where high catalyst loadings are typical and commonly seen in microscale HTE screening. The extent of the reaction was analyzed by

normalized HPLC peak area for the desired product versus the internal standard, which is scaled to a max ratio of 1.00 for values in Figure 2.7. In each of the six reactions, the identified hit(s) was(were) validated by conducting corresponding preparative scale syntheses (0.42–4.50 mmol of limiting reagent) at much lower catalyst loading (0.25–5 mol %) to obtain both solution and isolated yields.

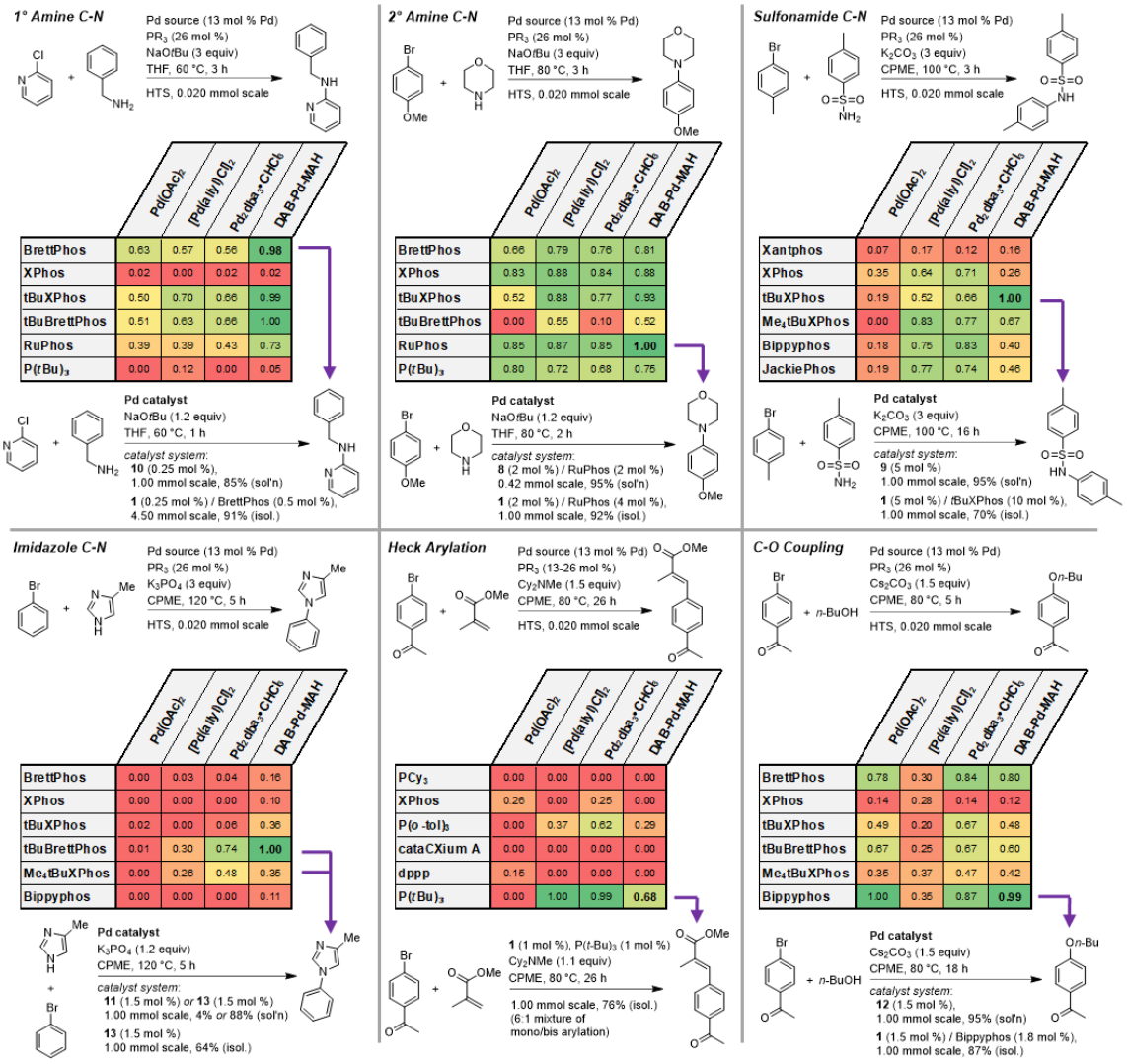

Figure 2.7. Microscale high-throughput screening results comparing four Pd sources for a series of Pd-catalyzed reactions including C–N coupling with several nucleophiles, Heck arylation, and C–O coupling.

Color gradient indicates normalized HPLC product peak area/internal standard peak area (red = 0; yellow = 0.50; green = 1.00; largest product/std area ratio normalized to 1.00). Low catalyst loading (≤2 mol % Pd) and/or preparative-scale (≥1 mmol) examples using either ^{DMP}DAB–Pd–MAH (**2.1**) or isolated [phosphine]–Pd–MAH precatalysts shown below each screening table. Solution yields determined by ^{1}H NMR spectroscopy vs internal standard (1,3,5-trimethoxybenzene).

Our evaluation began with a Buchwald–Hartwig amination using two different amines: primary (benzylamine) and secondary (morpholine) amines.[74–76] The identical six phosphine ligands, including BrettPhos, *t*BuBrettPhos, XPhos, tBuXPhos, RuPhos, and P(*t*Bu)$_3$, were tested in both reactions, and the reaction conditions were adapted from standard protocols for C–N coupling.[77,78] For the coupling between benzylamine and 2-chloropyridine, HPLC analysis reveals complex **2.1** as a superior precursor, giving the highest amount of desired product across several sets of conditions. Among the ligands screened, BrettPhos, *t*BuBrettPhos, and *t*BuXPhos were identified as the most active. It is known that BrettPhos can effectively catalyze the arylation of primary amines over secondary amines,[79–81] so this ligand was used for larger-scale validation. Using only 0.25 mol % of complex **2.10** as a single-component precatalyst gives an 85% solution yield of the secondary amine on 1.00 mmol scale, and the reaction extent was determined by ^{1}H NMR spectroscopy versus internal standard. By applying the *in situ* generated catalytic system from the combination of **2.1** (0.25 mol %) and BrettPhos (0.50 mol %), a 91% isolated yield (750 mg product) is obtained on 4.50 mmol scale.

For the coupling between morpholine and 4-bromoanisole, almost all palladium/ligand combinations give good yields of the product. However, the catalysts generated from Pd(OAc)$_2$/*t*BuXPhos, Pd(OAc)$_2$/*t*BuBrettPhos, and Pd$_2$dba$_3$•CHCl$_3$/ *t*BuBrettPhos perform relatively poorly, indicating inefficient precatalyst activation. Complex **2.1** is again comparable or superior to the other Pd sources in this screen, with **2.1**/RuPhos providing the highest amount of product.[79,81] In addition to the microscale screen, we also conducted larger-scale comparisons between BrettPhos and RuPhos, confirming the better catalytic activity of RuPhos for C–N couplings of secondary amines than BrettPhos (equation 2.1). Building on these results, we decided to use complex **2.8** (2 mol %) with added RuPhos (2 mol %) for preparative scale synthesis, giving 95% solution yield on 0.42 mmol scale. A combination of **2.1** (2 mol %) and RuPhos (4 mol %) gives 92% isolated yield of the desired product on 1.00 mmol scale.

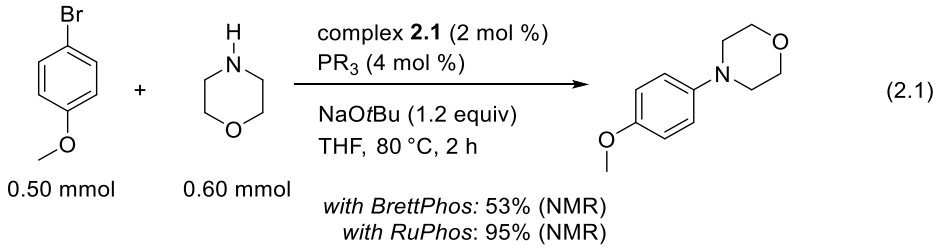

We also chose this reaction as the model to test the stability of these palladium sources when loaded into a screening plate and stored at room temperature under N_2 for 3 months. Another HTE screen was performed with these "old" palladium sources, with all other reaction conditions being the same (Figure 2.8). The reactivity trend is very consistent with that conducted with freshly-prepared precatalysts, except for $Pd(OAc)_2$. $Pd(OAc)_2$ gives a good amount of product with the combination of RuPhos, but no clear hits for all other ligand combinations. This comparison test again supports the reliability/stability of **2.1** at room temperature.

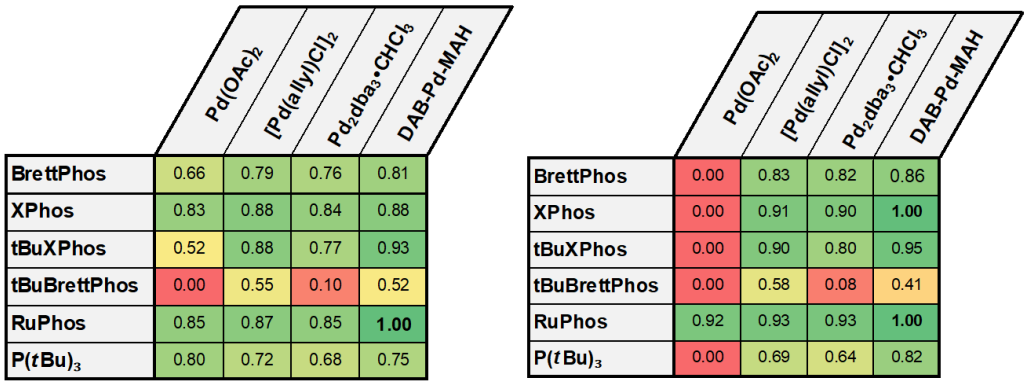

Figure 2.8. *Left*: screen results from freshly-prepared precursors (also in Figure 2.7). *Right*: screen results from the precursors stored at room temperature for three months.

In addition to C–N couplings with primary and secondary amines, we assessed complex **2.1** as a precursor for the more challenging arylation of sulfonamides[82–84] and imidazoles.[71] For the palladium-catalyzed synthesis of a representative *N*-arylsulfonamide, we evaluated several large-cone-angle ligands reported to be effective. These include bulky biarylphosphines, such as JackiePhos[85] and *t*BuXPhos,[82] as well as XantPhos[86] and Bippyphos.[83,87,88] Under the conditions used (excess K_2CO_3 and CPME solvent), adapted

from previously reported conditions,[83] $Pd(OAc)_2$ exhibited almost no activity, generating only low to modest amounts of product and no promising hits. The other three palladium sources performed much better, with the combination of **2.1** and *t*BuXPhos yielding the largest amount of *N*-arylsulfonamide product. Validation of this identified condition on 1.00 mmol scale revealed that 5 mol % of complex **2.9** gives a 95% solution yield, and the combination of **2.1** (5 mol %)/*t*BuXPhos (10 mol %) gives a 70% isolated yield after purification. To compare with other state-of-the-art palladium sources, we assessed **2.1**/*t*BuXPhos against $[Pd(crotyl)Cl]_2$ (**A**),[89] the Hazari indenyl dimer (**B**),[90] the Buchwald G4 dimer (**C**),[91] and acetanilide-derived acetate dimer (**D**)[92] in a shorter reaction time at 100 °C (eq 2.2). Under these conditions, **2.1** outperforms the other four palladium sources, achieving a 76% solution yield, which is determined by ^1H NMR spectroscopy versus internal standard.

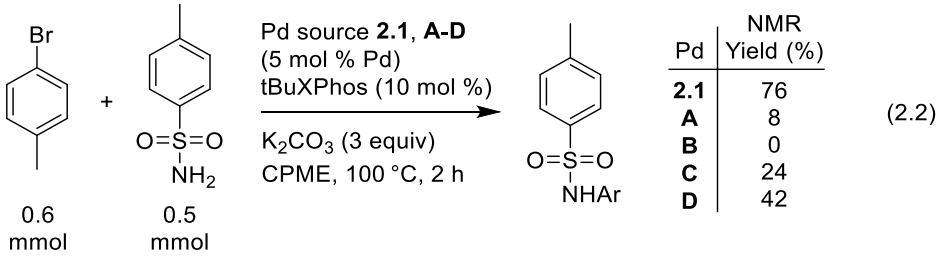

(2.2)

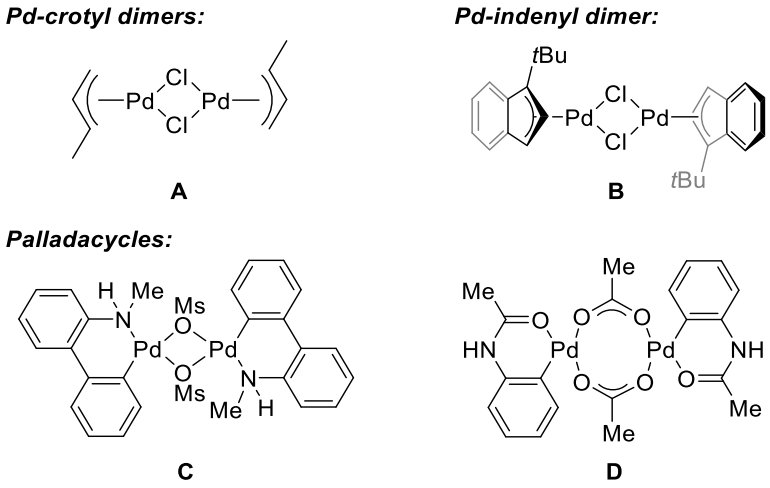

Another C–N coupling selected, palladium-catalyzed N^1-selective arylation of 4-methylimidazole, is known to be a challenging reaction.[71] For this reaction, we again chose a series of sterically demanding biaryl and bispyrazolyl phosphine ligands. Owing to the reported inhibitory effects of imidazole coordination on catalyst activation, we premixed

the palladium sources and ligands at room temperature for 1 h before adding the remaining reaction components. In contrast to the previously described screens and consistent with the aforementioned difficulties in carrying out this reaction,[71] very few catalytic systems give positive results. $Pd(OAc)_2$ and $[Pd(allyl)Cl]_2$ are almost inactive, giving nearly no to a low amount of product, though the latter does reveal possible hits with *t*BuBrettPhos and Me_4*t*BuXPhos. Compared with the former palladium(II) precursors, the two palladium(0) sources are more active, with *t*BuBrettPhos, *t*BuXPhos, and Me_4*t*BuXPhos identified as potentially effective under these conditions. To confirm these conditions, we conducted several microscale reactions on 0.02 mmol scale catalyzed by 13 mol % **2.1,** analyzed by ^{1}H NMR spectroscopy. For the combinations with *t*BuXPhos, *t*BuBrettPhos, and Me_4*t*BuXPhos, 28%, 96% and 29% solution yields are obtained respectively. Another reaction with *t*BuBrettPhos precatalyst **2.11** (13 mol %) as the precursor also gives high solution yield (91%) under these conditions.

Given the apparent superiority of *t*BuBrettPhos in the microscale reactions, we assessed precatalyst **2.11** (1.5 mol %) in a 1.00 mmol scale reaction. Unfortunately, only 4% solution yield of the *N*-arylimidazole is observed at this lower catalyst loading. This discrepancy with the screening results encouraged us to conduct a more thorough comparison of several palladium catalysts at low loadings (Table 2.2). All of the systems with either *t*BuXPhos or *t*BuBrettPhos failed to generate high amounts of products (entries 1–6). Using Me_4*t*BuXPhos and Pd_2dba_3•$CHCl_3$, the previously reported system,[82] gives only 40% solution yield when a 1:2 Pd-to-ligand ratio is used (entry 7). Notably, reducing the phosphine loading from 3.0 mol % to 1.8 mol % effectively shuts down the reaction (entry 8). This can potentially be attributed to the slow metalation of Me_4*t*BuXPhos using Pd_2dba_3•$CHCl_3$, as previously observed by Buchwald and co-workers,[82] resulting in the formation of inactive imidazolyl–Pd species. In contrast, catalytic system **2.1**/Me_4*t*BuXPhos is equally active at 1.8 mol % and 3 mol % ligand loading, even though solution yields are still modest (36–39%, entries 9–10). Comparison tests using $[Pd(crotyl)Cl]_2$ (**A**), the Buchwald G4 dimer (**C**) or acetanilide-derived acetate dimer (**D**) result in no reaction (entries 11, 13, 14). $[Pd(t$Bu-indenyl$)Cl]_2$ (**B**) is the only other precursor giving any product under these conditions (12%, entry 12).

Using the single-component Me$_4$*t*BuXPhos-ligated complex **2.13**, which has a perfect 1:1 Pd-to-ligand ratio, a much higher solution yield is obtained (88%), with a 64% isolated yield after column chromatography (entry 11). These results highlight the importance of validating high catalyst loading HTE hits on a preparative scale, where a change in reaction scale and catalyst loading can influence what the most active system is. In the present case, while *t*BuBrettPhos is a superior ligand at high Pd loading, reducing the catalyst concentration significantly reduces its effectiveness, likely due to a greater degree of inhibition by the imidazole substrate. In contrast, **2.1**/Me$_4$*t*BuXPhos initially appears modest, but the single-component system **2.13** ultimately proves to be superior at more reasonable Pd loading.

Table 2.2. Catalyst Comparison for Imidazole Arylation[a].

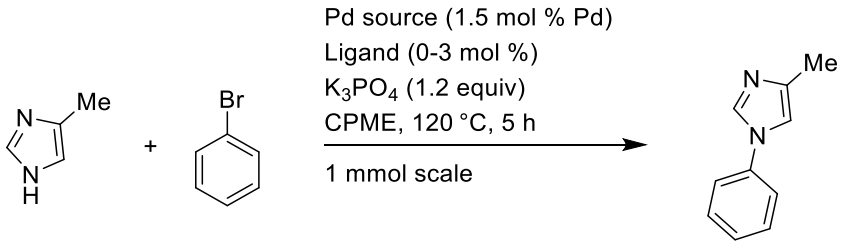

Entry	Pd source	Ligand (mol %)	Yield (%)[b]
1	**2.1**	*t*BuXPhos (3)	1
2	**2.1**	*t*BuXPhos (1.8)	1
3	**2.9**	n/a	4
4	Pd_2dba_3•$CHCl_3$	*t*BuBrettPhos (1.8)	6
5	**2.1**	*t*BuBrettPhos (1.8)	3
6	**2.11**	n/a	4
7	Pd_2dba_3•$CHCl_3$	Me$_4$*t*BuXPhos (3)	40
8	Pd_2dba_3•$CHCl_3$	Me$_4$*t*BuXPhos (1.8)	5
9	**2.1**	Me$_4$*t*BuXPhos (3)	39
10	**2.1**	Me$_4$*t*BuXPhos (1.8)	36
11	**A**	Me$_4$*t*BuXPhos (1.8)	1
12	**B**	Me$_4$*t*BuXPhos (1.8)	12
13	**C**	Me$_4$*t*BuXPhos (1.8)	0
14	**D**	Me$_4$*t*BuXPhos (1.8)	0
15	**2.13**	n/a	88, 64[c]

[a]Pd source and ligand were reacted for 1 h at room temperature before addition of other reaction components. [b]Determined by ^{1}H NMR spectroscopy versus internal standard (1,3,5-trimethoxybenzene). [c]Isolated yield of a separate experiment after chromatography.

We have also examined complex **2.1** as a precursor for Mizoroki–Heck arylation.[6,93,94] We selected six sterically hindered, electron-rich phosphine ligands known to be effective in Mizoroki–Heck couplings, and evaluated them using the conditions previously reported by Littke and Fu.[95,96] For the arylation of methyl methacrylate by *p*-bromoacetophenone, we first followed the reported literature to conduct our preliminary tests at room temperature,[97] but poor reactivity is obtained with complex **2.1** (0% NMR yield) and Pd_2dba_3•$CHCl_3$ (24% NMR yield). This prompted us to increase the reaction temperature for this screen to 80 °C. According to the screen results, few catalyst/ligand combinations are suitable. $Pd(OAc)_2$ gives inferior conversion for every ligand tested, while the other three palladium sources do generate some hits with P(*o*-tol)$_3$ and P(*t*Bu)$_3$. With P(*t*Bu)$_3$ as the ligand, the amount of product observed using **2.1** as the precursor is somewhat less than for $[Pd(allyl)Cl]_2$, and Pd_2dba_3•$CHCl_3$.

To further compare the activity of **2.1** and Pd_2dba_3•$CHCl_3$ under preparative-scale conditions, we tested both palladium sources at 1 mol % Pd loading for coupling at 80 °C (eq 2.3). Analysis of the reaction mixtures by ^{1}H NMR spectroscopy and LCMS revealed the presence of an over-reaction by-product, resulting from a second Mizoroki–Heck arylation (bis). While the two palladium sources have almost equal efficiency in generating the desired product (mono) (74% solution yield, determined by ^{1}H NMR spectroscopy versus internal standard), complex **2.1** gives slightly higher selectivity (mono:bis = 5.3:1 versus 3.5:1 with Pd_2dba_3•$CHCl_3$). Therefore, a preparative-scale synthesis was performed with 3 equiv of methyl methacrylate and 1 mol % **2.1**/P(*t*Bu)$_3$ to give a 6:1 mixture of the two products in 76% combined isolated yield. As previously stated in Section 2.2, α-diimine ligands have been used as supporting ligands in Heck reactions, and "ligand-free" reactivity is also possible.[98,99] We then tested each precursor in the absence of added phosphine with other reaction conditions as the same. No product is observed, ruling out the possibility of ligand-free reactivity.

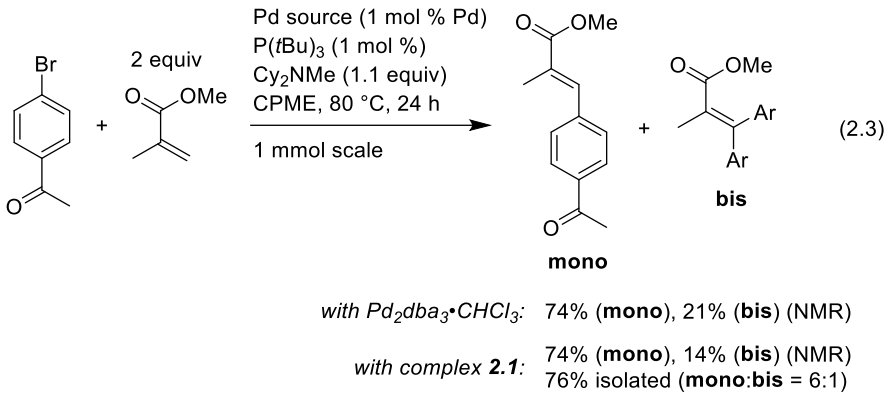

(2.3)

The sixth reaction we tested in microscale screening is C–O coupling, with a representative example using a primary alcohol (*n*BuOH) and an arylbromide (4-bromoacetophenone). Known to be a challenging transformation, previous work from the Buchwald group revealed several phosphine ligands as active,[100] while Beller and co-workers identified AdBippyphos as a superior ligand.[101] Our preliminary tests were conducted by adapting the former's conditions, with complex **2.1**, *t*BuBrettPhos, NaO*t*Bu at 80 °C. However, we observed poor reactivity under these conditions, and therefore turned our focus to the latter.

Due to the high cost and restricted availability of AdBippyPhos, we chose to evaluate a set of potential alternative ligands, including the parent Bippyphos, under analogous conditions.[100–102] While $Pd(OAc)_2$, Pd_2dba_3•$CHCl_3$, and complex **2.1** all generate hits for this reaction, with BrettPhos and Bippyphos giving the highest amount of desired product, $[Pd(allyl)Cl]_2$ exhibited poor catalytic activity in combination with all six ligands. Based on these small-scale results, $Pd(OAc)_2$/Bippyphos and **2.1**/Bippyphos are revealed to be the most promising catalytic systems. On a 1.00 mmol scale with 1.5 mol % Pd, using precatalyst **2.12** gives 95% solution yield, and the combination of **2.1** and Bippyphos (1.8 mol %) successfully gives 87% isolated yield. In addition, to compare **2.1** against palladium sources **A**–**D**, we conducted small-scale tests with lower Pd loading (0.5 mol %), lower temperature (60 °C), and shorter reaction time (30 min). As shown in eq 2.4, the combination of **2.1** and Bippyphos shows the second highest catalytic activity under these conditions, obtaining 30% NMR yield, when the isolated precatalyst **2.12** achieves the identical result. Only $[Pd(crotyl)Cl]_2$ (**A**) gives a higher though similar product yield (37%).

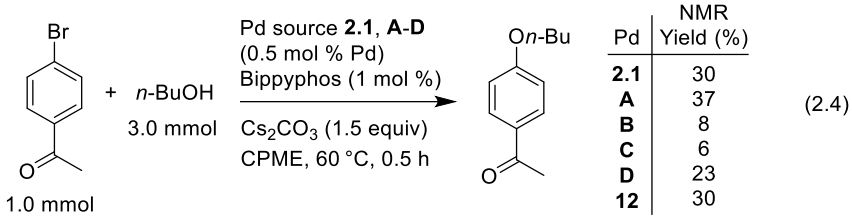

Pd	NMR Yield (%)
2.1	30
A	37
B	8
C	6
D	23
12	30

(2.4)

Finally, to demonstrate the utility of complex **2.1** as a precursor in an example optimization workflow, we explored the synthesis of *spiro*-OMeTAD, an organic hole-transport material used in perovskite-based solar cells,[60] through palladium-catalyzed C–N coupling (Figure 2.9). Six ligands, including several biaryl phosphines and XantPhos, were selected for microscale screening at high Pd loading and with excess diarylamine. XPhos, SPhos, RuPhos, and XantPhos showed good catalytic activity under these conditions with all palladium sources. To differentiate between these four ligands, we decreased the Pd loading from 13 to 5 mol % and analyzed the reaction mixtures by ^{1}H NMR spectroscopy. SPhos and RuPhos were identified as superior from these small-scale experiments, with SPhos giving a 94% solution yield using only 4.1 equiv of the diarylamine substrate. According to these results, we conducted a gram-scale synthetic procedure by using single-component precatalyst **2.6** and CPME as a higher boiling solvent. 81% isolated yield of pure *spiro*-OMeTAD is obtained after a simple silica plug chromatography and recrystallization from THF/MeOH. This procedure is higher yielding and operationally simpler than the reported synthesis,[103] which uses Pd_2dba_3/P(*t*Bu)$_3$ at high catalyst loading (8 mol % Pd, 45% isolated yield).

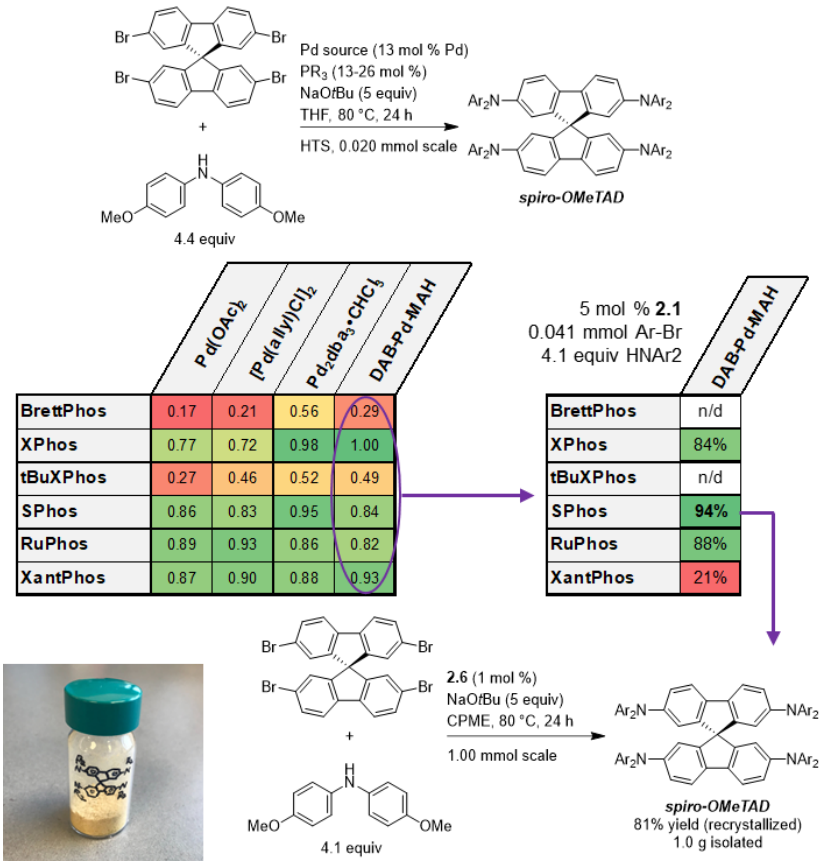

Figure 2.9. Reaction screening/optimization for the synthesis of spiro-OMeTAD via Pd-catalyzed C–N coupling. "HPLC" values indicate normalized HPLC product peak area/internal standard peak area; "NMR" percentages indicate solution yield determined by ^{1}H NMR spectroscopy versus internal standard. Internal standard is 1,3,5-trimethoxybenzene.

2.3.4 Reactivity Limitations and Activation Studies

While complex **2.1** shows superior or comparable catalytic activity in the preceding cross-coupling reactions, we also observed its poor activity in some specific reactions. One is Suzuki–Miyaura coupling, one of the most commonly-utilized couplings in the industry.[8] Our preliminary test starts with an example reaction of 2-chloro-5-methylpyridine and phenylboronic acid under standard biphasic reaction conditions,[73] analyzed by ^{1}H NMR spectroscopy. The combination of **2.1** and XPhos only gives 46% solution yield at 2 mol % Pd loading, while 86% solution yield is obtained with $Pd(OAc)_2$/XPhos (eq 2.5). In addition to 2-chloro-5-methylpyridine, we tested this coupling with a much more challenging and sterically hindered substrate—6-Chloro-N,9-bis(tetrahydro-2H-pyran-2-

yl)-9H-purin-2-amine. The poor activity was again found in this reaction (eq 2.6), indicating clear limitations of **2.1** in the Suzuki-Miyaura reaction.

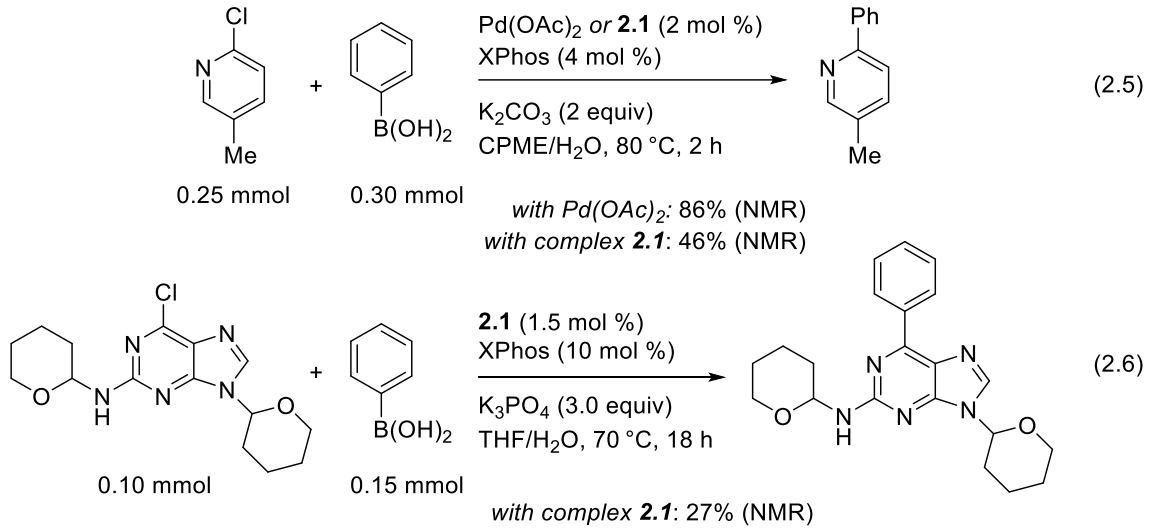

To understand and circumvent the inferior activity in Suzuki–Miyaura coupling, we further investigated the activation of **2.1**. We initially anticipated this complex to undergo a similar activation pathway as Pd_2dba_3•$CHCl_3$. Within the activation of Pd_2dba_3, the relatively labile olefin dissociates from the palladium center in the presence of other ligands, such as phosphines, and then generates oxidative addition complexes in combination with the halide coupling partners.[15] Thus, we investigated the potential formation of oxidative addition complexes from **2.1** using the C–N coupling of bromobenzene and morpholine as an example reaction. A series of control experiments were conducted with single-component precatalyst **2.8** and corresponding reactants on 0.01 mmol scale, monitored and analyzed by ^{31}P NMR spectroscopy versus internal standard (PPh_3 in C_6D_6) (Table 2.3). The majority of precatalyst **2.8** remains unchanged in the presence of ArBr and/or morpholine after 1 h (entries 1-3), while the previously reported oxidative addition complex[104] was detected when 1 equiv NaO*t*Bu was added (entry 5). Notably, only free XPhos was observed when excess NaO*t*Bu was added together with PhBr and **2.8** (entry 4). All of **2.8** is consumed and converted to unidentified phosphorus-containing species under conditions where all reagents are added (entries 6) or only NaO*t*Bu is added (entries 7 and 8). These reaction outcomes indicate that strong base is

required to activate [phosphine]–Pd–MAH complexes, though further study is needed to identify the new species observed in these experiments.

Table 2.3. Control Experiments for Catalyst Activation Investigations.

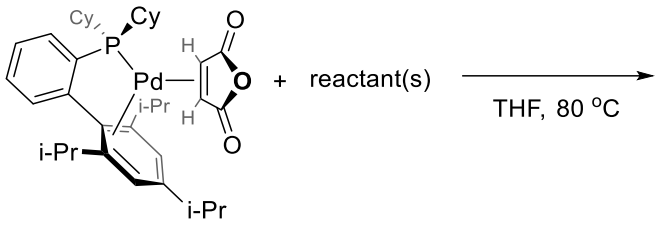

2.8
0.01 mmol

Entry	Reactant	PhBr	Morpholine	NaO*t*Bu	Outcome
1		√	–	–	Remaining **2.8**
2		√	√	–	96% **2.8** + 4% oxidative addition complex
3		–	√	–	Remaining **2.8**
4		√	–	10 equiv	100% XPhos
5		√	–	1 equiv	22% **2.8** + 42% oxidative addition complex +36% XPhos
6		√	√	10 equiv	38% XPhos + 62% unidentified substance at 59 ppm
7		–	–	10 equiv	4% XPhos + 88% and 8% unidentified substances at 29 ppm and 41.5 ppm
8		–	–	1 equiv	Unidentified substance at 31 ppm

Given that simple MAH dissociation is not likely to be the activation pathway, we chose the C–N coupling of benzylamine as a model system for further study using high Pd loading (13 mol % **2.10**). We also wanted to test whether free MAH is reactive under these conditions, and therefore also added 0.13 equivalent MAH instead of Pd catalyst to trace the fate of MAH (eq 2.7). LCMS analysis was conducted at time zero and at the end of the reactions to detect MAH-derived compounds as catalyst activation by-products. A species with an *m*/*z* value of 262 is observed in the reaction catalyzed by **2.10**. This is consistent with a combination of *tert*-butoxide, benzylamine, and MAH undergoing substitution reactions to generate amide compounds with molecular weights of 261 (Figure 2.10).

Notably, we do not observe this species in the absence of Pd. Based on these results, we propose that strong base and/or nucleophile can attack the coordinated MAH ligand, leading to a new olefin ligand that is less strongly bound to Pd^0. More research is needed to better understand this activation pathway to make catalysts using **2.1** more general.

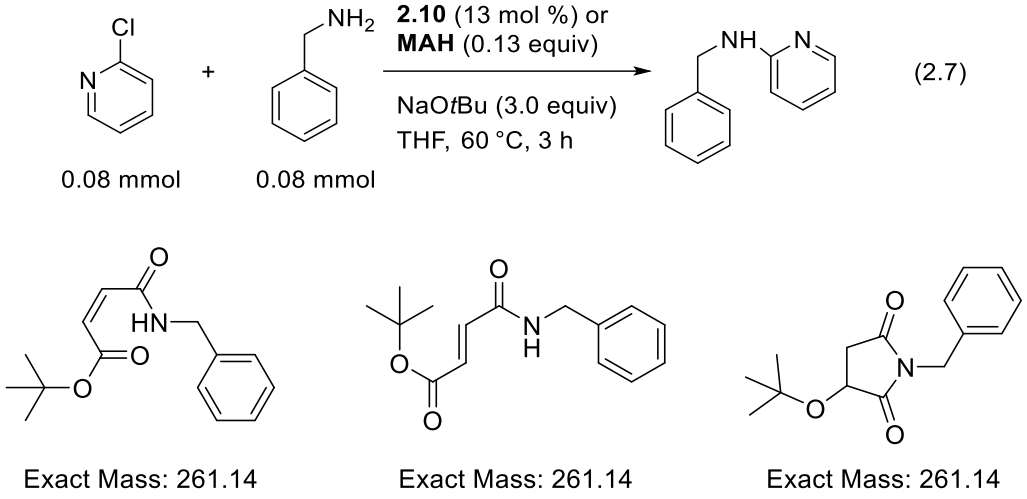

Figure 2.10. Possible intermediates formed with MAH.

Given the proposed activation, we hypothesized that complex **2.1** would be active in challenging cross-coupling reactions that proceed under harsh conditions, such as high temperatures and/or strong bases. We chose two challenging reactions, including the C–N coupling of indazole and direct arylation of benzothiazole, to test the activity of **2.1**, with analysis by ^{1}H NMR spectroscopy versus internal standard. No desired product is observed in the amination with **2.1** on 1.0 mmol scale, while the use of Pd_2dba_3•$CHCl_3$ achieved a measurable but still poor solution yield (35%) (eq 2.8). Similar to the amination, direct arylation was attempted using established reaction conditions,[105] however, no product was observed (eq 2.9). We do note that **2.1** was successfully used in screening studies for a related direct arylation reaction reported by our group.[105] Clearly, more work is needed to improve upon **2.1** and overcome the observed limitations for additional reaction classes.

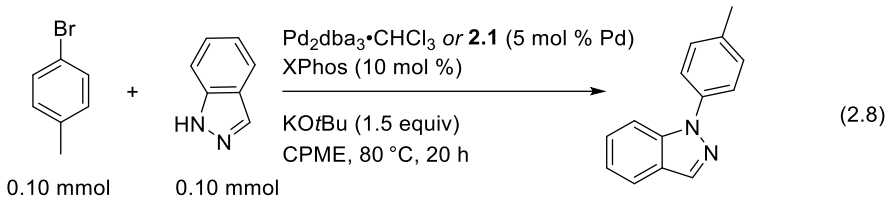

(2.8)

with Pd_2dba_3•$CHCl_3$: 35% (NMR)
*with complex **2.1***: 0% (NMR)

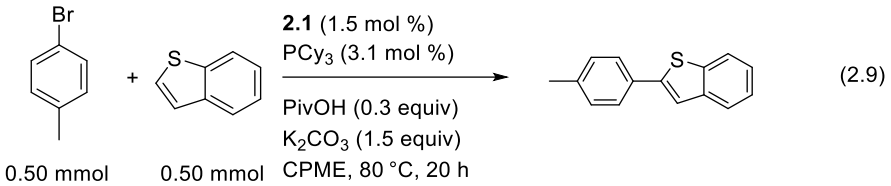

(2.9)

*with complex **2.1***: 0% (NMR)

2.4 Conclusions

In summary, we have developed a stable, easily prepared, and versatile palladium(0) complex as a reliable precursor for *in situ* cross-coupling catalyst preparation and as a platform for single-component precatalyst synthesis. Compared to other palladium sources commonly used for reaction screening, ^{DMP}DAB–Pd–MAH (**2.1**) offers distinct advantages, including good solubility in a variety of organic solvents, excellent solid-state and solution stability, and rapid ligand substitution of the chelating DAB with different phosphines relevant to cross-coupling, even with large cone angles. Furthermore, these rapid metalations with phosphines generate well-defined palladium(0) products that are easily isolated, providing a method to make new air-stable single-component palladium(0) precatalysts.

The evaluation of complex **2.1** against three other common palladium sources in microscale high-throughput screens demonstrates that **2.1** is excellent at identifying hits across six different reaction classes for C–N, C–C, and C–O formation. Notably, both $Pd(OAc)_2$ and $[Pd(allyl)Cl]_2$ are markedly inferior in multiple examples, including failure to clearly identify hits for primary sulfonamide arylation, imidazole arylation, Heck arylation, and C–O coupling with a primary alcohol. Preparative-scale reactions ($\geqslant$1 mmol substrate) with low Pd loading (0.25–5 mol %) are feasible using either catalysts generated

in situ from **2.1** and corresponding phosphines or with single-component precatalysts. Thus, complex **2.1** is a versatile Pd^0 source for cross-coupling reaction screening, optimization, and scale-up synthesis.

2.5 General Experimental Methods

2.5.1 Synthesis of ^{DMP}DAB–Pd–MAH (2.1)

Both of these procedures are carried out under ambient atmosphere.

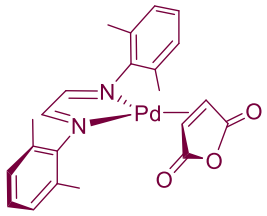

^{DMP}DAB-Pd-MAH (**2.1**)

From Pd_2dba_3•$CHCl_3$: A 250 mL round bottom flask containing a stirbar was charged with Pd_2dba_3•$CHCl_3$ (251.5 mg, 0.243 mmol), *N*, *N* ′-bis(2,6-dimethylphenyl)ethan-1,2-diimine (134.4 mg, 0.510 mmol, 2.1 equiv), and maleic anhydride (51.4 mg, 0.522 mmol, 2.15 equiv). Acetone (45 mL) was added to dissolve/suspend the components. The reaction mixture was stirred at room temperature for three hours, producing a dark purple/red homogeneous solution. The reaction solution was concentrated under vacuum to a volume of approximately 2 mL. TBME (40 mL) was added, and the solution was stirred for 15 minutes, producing a purple/red slurry. After the solid settled, the TBME was decanted, leaving a purple/red solid. The solid was dissolved in a minimum of acetone and filtered through Celite to remove palladium black. The Celite bed was thoroughly rinsed with acetone until the rinsings were colourless, and the combined filtrate was evaporated under vacuum. The resulting purple/red solid was washed with TBME (3 x 10 mL) and dried under vacuum to give compound **2.1** (187 mg, 82% yield).

From $Pd(OAc)_2$: A 1 L round bottom flask containing a stirbar was charged with dibenzylideneacetone (dba, 6.26 g, 26.7 mmol, 2 equiv) and sodium acetate (10.96 g, 133.6 mmol, 10 equiv). Methanol (250 mL) was added, and the mixture was stirred to ensure dissolution of the dba. With stirring, solid $Pd(OAc)_2$ (3.00 g, 13.4 mmol) was added through a powder funnel, which was rinsed with methanol (50 mL) to ensure quantitative transfer. The flask was immersed in an oil bath kept at 40-45 °C. The reaction mixture was stirred vigorously at this temperature for 3 hours. The flask was then cooled to room temperature. The resulting dark slurry was filtered through filter paper in a Buchner funnel to collect the crude "$Pd(dba)_2$" solid. The solid was washed successively with methanol (3 x 30 mL), water (3 x 30 mL), and acetone (2 x 10 mL). This solid was then transferred to a 1 L round bottom flask containing a stirbar, and slurried in acetone (300 mL). Solid *N*,*N*′-bis(2,6-dimethylphenyl)ethan-1,2-diimine (3.71 g, 14.0 mmol, 1.05 equiv) and maleic

anhydride (1.38 g, 14.0 mmol, 1.05 equiv) were added through a powder funnel, which was rinsed with acetone (100 mL) to ensure quantitative transfer. The reaction mixture was stirred at room temperature for 3 hours. The dark red solution was filtered through a bed of Celite using a medium porosity frit to remove palladium black. The Celite bed was thoroughly rinsed with acetone until the rinsings were colourless, and the combined filtrate was evaporated under vacuum. TBME (100 mL) was added, and the solid triturated in the flask. The purple/red solid was collected by suction filtration, and the filter cake was washed with TBME (6 x 10 mL, until rinsings were colourless) to completely remove dba. The solid was dried under vacuum to give compound **2.1** (3.60 g, 57% yield from $Pd(OAc)_2$).

^{1}H NMR: (300 MHz; d_6-acetone) δ 2.17 (s, 12H, 4 x Ar–CH_3), 3.44 (s, 2H, –C*H*=C*H*–), 6.99 (m, 6H, 6 x Ar–*H*), 8.42 (s, 2H, 2 x –C*H*=NAr).

^{13}C{^{1}H} NMR: (125 MHz; d_6-acetone) 17.3 (4 x Ar–*C*H$_3$), 42.1 (–*C*H=*C*H–), 126.2 (Ar), 128.2 (Ar), 149.0 (Ar), 165.2 (–N=*C*–*C*=N–), 171.0 (2 x *C*=O).

HRMS (ESI) of $[M + Na]^+$ (major isotopomer, sodium adduct): 491.05575 (calc'd); 491.05511 (found).

2.5.2 Synthesis of [phosphine]–Pd–MAH Complexes

Unless otherwise noted, the following general procedure was used to prepare all of the [phosphine]–Pd–MAH complexes. Starting materials were handled and weighed under inert dinitrogen atmosphere in the glovebox (due to oxygen-sensitivity of the phospines). A 20 mL vial or 50 mL round-bottom flask was charged with complex **2.1** (100.0 mg, 0.2133 mmol), the corresponding phosphine ligand (1.05 equiv, 0.2240 mmol), and a cross-shaped magnetic stirbar. Anhydrous, degassed THF (5-15 mL) was added, and the reaction mixture were stirred for 1-2 hours. During this time, the solution changes colour from an initial dark red/purple to yellow/orange; the exact final colour and the rate of colour change depends on the phosphine used. Note: after the 1-2 hours stirring, the solution can be opened to ambient atmosphere if desired.

The solvent was then removed *in vacuo* to give a yellow to orange residue. This residue was triturated with hexanes or diethyl ether (2-4 mL), followed by decantation of

the liquid phase (with or without centrifugation as required). This trituration/decantation process was repeated 2-5 more times to remove the ^{DMP}DAB by-product, as well as any excess phosphine. The solid was then dried *in vacuo* to give the product.

2.5.3 General Procedure for Microscale High-throughput Screens

The following general procedure was used to conduct all high-throughput screens in this thesis. The coupling of 2-chloropyridine and benzylamine is given here as an example.

Preparation of palladium sources:

Four different palladium precatalysts were dissolved in corresponding solvents with high solubility, respectively. Palladium acetate (21.0 mg, 0.0936 mmol) was dissolved in 1348 μL of dichloromethane. Allylpalladium(II) chloride dimer (17.1 mg, 0.0468 mmol) was dissolved in 2269 μL of acetone. Recrystallized Pd_2dba_3•$CHCl_3$ (48.4 mg, 0.0468 mmol) was dissolved in 1968 μL of tetrahydrofuran. 43.9 mg of ^{DMP}DAB–Pd–MAH (43.9 mg, 0.0936 mmol) was dissolved in 2235 μL of acetone. These palladium stock solutions were dispensed into a 96-well plate (24 wells for each palladium source). Specific amounts of corresponding palladium stock solutions were added to each well (40 uL for palladium acetate, 63.3 uL for allylpalladium chloride dimer, 56.3 uL Pd_2dba_3•$CHCl_3$, 63.3 uL ^{DMP}DAB–Pd–MAH. The solvents were then evaporated by Genevac, and the plate was stored in the glovebox for further use.

Preparation of phosphine ligands:

The Pd-to-L ratio is 2:1 for monodentate phosphines and 1:1 for bidentate phosphines. Inside the glovebox, 0.0624 mmol of each phosphine ligand (33.5 mg of BrettPhos, 29.7 mg of XPhos, 26.5 mg of *t*BuXPhos, 30.2 mg *t*BuBrettPhos, 29.1 mg of RuPhos, 29.2 μL of P(*t*Bu)3) was dissolved in anhydrous THF (600 μL), respectively. 100 μL of each ligand stock solution was weighed to obtain the density of each ligand solution. 0.0052 mmol of each ligand stock solution (51.5 μL of BrettPhos stock solution, 53.3 μL of XPhos stock solution, 51.9 μL of *t*BuXPhos stock solution, 51.7 μL of *t*BuBrettPhos stock solution, 51.5 μL of RuPhos stock solution and 52.4 μL of P(tBu)$_3$) was dispensed into designated wells.

Preparation of reaction stock solution:

A vial was charged with 2-chloropyridine (67.9 μL, 0.72 mmol), benzylamine (78.8 μL, 0.72 mmol), NaO-*t*Bu (207.6 mg, 2.16 mmol), 1,3,5-trimethoxybenzene (36.3 mg, 0.216 mmol), anhydrous THF (5.4 mL) and a stir bar. After being mixed well, 161.1 μL of this reaction stock solution was dispensed to each well. The top of the 24-well plate was screwed on, and the plate was stirred for 3 hours at 80 °C.

Analysis of 24-well reactions:

Once the reaction was stopped, 500 μL of acetonitrile was added to each well to dilute the reaction mixtures. 40 μL of each diluted reaction mixture was transferred to the corresponding HPLC vial, followed by the addition of 1 mL of acetonitrile for the diluting purpose. These samples were analyzed by the HPLC/UV-VIS detector.

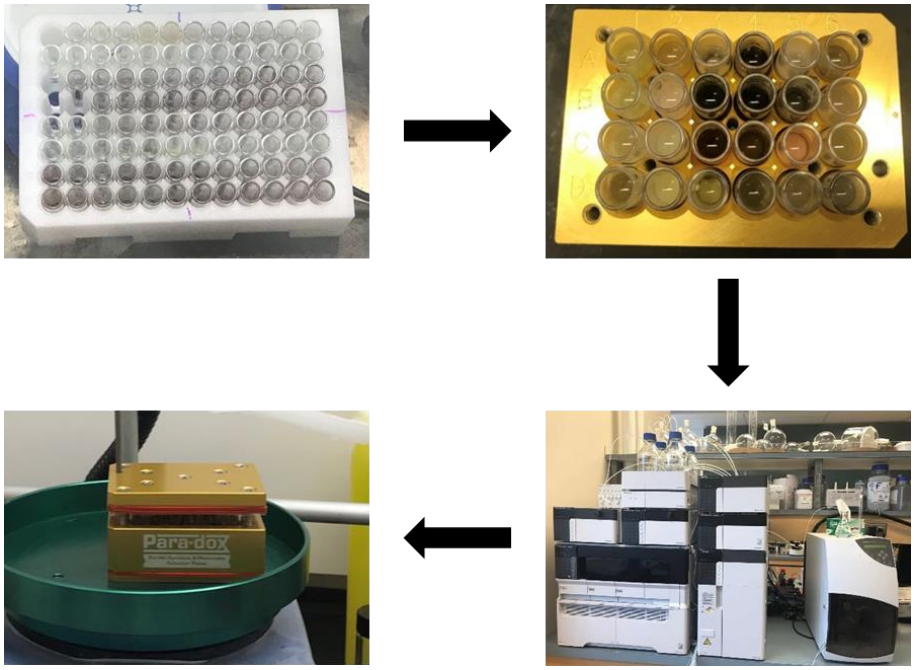

Figure 2.11. Flow chart of operating microscale high-throughput screens.

2.6 References

(1) Huang, J.; Isaac, M.; Watt, R.; Becica, J.; Dennis, E.; Saidaminov, M. I.; Sabbers, W. A.; Leitch, D. C. ^{DMP}DAB–Pd–MAH: A Versatile Pd(0) Source for Precatalyst Formation, Reaction Screening, and Preparative-Scale Synthesis. *ACS Catal.* **2021**, *11* (9), 5636–5646. https://doi.org/10.1021/acscatal.1c00288.

(2) Baker, M. A.; Tsai, C.-H.; Noonan, K. J. T. Diversifying Cross-Coupling Strategies, Catalysts and Monomers for the Controlled Synthesis of Conjugated Polymers. *Chem. – Eur. J.* **2018**, *24* (50), 13078–13088. https://doi.org/10.1002/chem.201706102.

(3) Johansson Seechurn, C. C. C.; Kitching, M. O.; Colacot, T. J.; Snieckus, V. Palladium-Catalyzed Cross-Coupling: A Historical Contextual Perspective to the 2010 Nobel Prize. *Angew. Chem. Int. Ed.* **2012**, *51* (21), 5062–5085. https://doi.org/10.1002/anie.201107017.

(4) Campeau, L.-C.; Hazari, N. Cross-Coupling and Related Reactions: Connecting Past Success to the Development of New Reactions for the Future. *Organometallics* **2019**, *38* (1), 3–35. https://doi.org/10.1021/acs.organomet.8b00720.

(5) Buchwald, S. L.; Hartwig, J. F. In Praise of Basic Research as a Vehicle to Practical Applications: Palladium-Catalyzed Coupling to Form Carbon-Nitrogen Bonds. *Isr. J. Chem.* **2020**, *60* (3–4), 177–179. https://doi.org/10.1002/ijch.201900167.

(6) Nicolaou, K. C.; Bulger, P. G.; Sarlah, D. Palladium-Catalyzed Cross-Coupling Reactions in Total Synthesis. *Angew. Chem. Int. Ed.* **2005**, *44* (29), 4442–4489. https://doi.org/10.1002/anie.200500368.

(7) Magano, J.; Dunetz, J. R. Large-Scale Applications of Transition Metal-Catalyzed Couplings for the Synthesis of Pharmaceuticals. *Chem. Rev.* **2011**, *111* (3), 2177–2250. https://doi.org/10.1021/cr100346g.

(8) Brown, D. G.; Boström, J. Analysis of Past and Present Synthetic Methodologies on Medicinal Chemistry: Where Have All the New Reactions Gone? *J. Med. Chem.* **2016**, *59* (10), 4443–4458. https://doi.org/10.1021/acs.jmedchem.5b01409.

(9) Ruiz-Castillo, P.; Buchwald, S. L. Applications of Palladium-Catalyzed C–N Cross-Coupling Reactions. *Chem. Rev.* **2016**, *116* (19), 12564–12649. https://doi.org/10.1021/acs.chemrev.6b00512.

(10) Devendar, P.; Qu, R.-Y.; Kang, W.-M.; He, B.; Yang, G.-F. Palladium-Catalyzed Cross-Coupling Reactions: A Powerful Tool for the Synthesis of Agrochemicals. *J. Agric. Food Chem.* **2018**, *66* (34), 8914–8934. https://doi.org/10.1021/acs.jafc.8b03792.

(11) Fairlamb, I. J. S. π-Acidic Alkene Ligand Effects in Pd-Catalysed Cross-Coupling Processes: Exploiting the Interaction of Dibenzylidene Acetone (dba) and Related Ligands with Pd(0) and Pd(II). *Org. Biomol. Chem.* **2008**, *6* (20), 3645–3656. https://doi.org/10.1039/B811772A.

(12) Amatore, C.; Jutand, A. Role of Dba in the Reactivity of Palladium(0) Complexes Generated *in Situ* from Mixtures of $Pd(dba)_2$ and Phosphines. *Coord. Chem. Rev.* **1998**, *178–180*, 511–528. https://doi.org/10.1016/S0010-8545(98)00073-3.

(13) Yamamoto, T.; Ohta, T.; Ito, Y. Palladium-Catalyzed Addition of Arylboronic Acids to Aldehydes. *Org. Lett.* **2005**, *7* (19), 4153–4155. https://doi.org/10.1021/ol051501y.

(14) Weber, P.; Biafora, A.; Doppiu, A.; Bongard, H.-J.; Kelm, H.; Gooßen, L. J. A Comparative Study of Dibenzylideneacetone Palladium Complexes in Catalysis. *Org. Process Res. Dev.* **2019**, *23* (7), 1462–1470. https://doi.org/10.1021/acs.oprd.9b00214.

(15) Zalesskiy, S. S.; Ananikov, V. P. $Pd_2(dba)_3$ as a Precursor of Soluble Metal Complexes and Nanoparticles: Determination of Palladium Active Species for Catalysis and Synthesis. *Organometallics* **2012**, *31* (6), 2302–2309. https://doi.org/10.1021/om201217r.

(16) Kovach, J.; Golisz, S. R.; Brennessel, W. W.; Jones, W. D. Iridium(I)– and Rhodium(I)–Olefin Complexes Containing an α-Diimine Supporting Ligand. *Organometallics* **2022**, *41* (22), 3167–3174. https://doi.org/10.1021/acs.organomet.2c00036.

(17) Nishiyama, H.; Ikeda, H.; Saito, T.; Kriegel, B.; Tsurugi, H.; Arnold, J.; Mashima, K. Structural and Electronic Noninnocence of α-Diimine Ligands on Niobium for Reductive C–Cl Bond Activation and Catalytic Radical Addition Reactions. *J. Am. Chem. Soc.* **2017**, *139* (18), 6494–6505. https://doi.org/10.1021/jacs.7b02710.

(18) Harding, D. A. J.; Hope, E. G.; Singh, K.; Solan, G. A. Cationic Rhodium(I) and Iridium(I) α-Diimine Complexes. *Polyhedron* **2012**, *33* (1), 360–366. https://doi.org/10.1016/j.poly.2011.11.058.

(19) Zarate, C.; Yang, H.; Bezdek, M. J.; Hesk, D.; Chirik, P. J. Ni(I)–X Complexes Bearing a Bulky α-Diimine Ligand: Synthesis, Structure, and Superior Catalytic Performance in the Hydrogen Isotope Exchange in Pharmaceuticals. *J. Am. Chem. Soc.* **2019**, *141* (12), 5034–5044. https://doi.org/10.1021/jacs.9b00939.

(20) Soshnikov, I. E.; Semikolenova, N. V.; Bryliakov, K. P.; Talsi, E. P. α-Diimine Ni-Catalyzed Ethylene Polymerizations: On the Role of Nickel(I) Intermediates. *Catalysts* **2021**, *11* (11), 1386. https://doi.org/10.3390/catal11111386.

(21) Wang, F.; Chen, C. A Continuing Legend: The Brookhart-Type α-Diimine Nickel and Palladium Catalysts. *Polym. Chem.* **2019**, *10* (19), 2354–2369. https://doi.org/10.1039/C9PY00226J.

(22) Biancalana, L.; Batchelor, L. K.; Funaioli, T.; Zacchini, S.; Bortoluzzi, M.; Pampaloni, G.; Dyson, P. J.; Marchetti, F. α-Diimines as Versatile, Derivatizable Ligands in Ruthenium(II) *p*-Cymene Anticancer Complexes. *Inorg. Chem.* **2018**, *57* (11), 6669–6685. https://doi.org/10.1021/acs.inorgchem.8b00882.

(23) Johnson, L. K.; Killian, C. M.; Brookhart, M. New Pd(II)- and Ni(II)-Based Catalysts for Polymerization of Ethylene and .Alpha.-Olefins. *J. Am. Chem. Soc.* **1995**, *117* (23), 6414–6415. https://doi.org/10.1021/ja00128a054.

(24) Ittel, S. D.; Johnson, L. K.; Brookhart, M. Late-Metal Catalysts for Ethylene Homo- and Copolymerization. *Chem. Rev.* **2000**, *100* (4), 1169–1204. https://doi.org/10.1021/cr9804644.

(25) Guo, L.; Chen, C. (α-Diimine)Palladium Catalyzed Ethylene Polymerization and (Co)Polymerization with Polar Comonomers. *Sci. China Chem.* **2015**, *58* (11), 1663–1673. https://doi.org/10.1007/s11426-015-5433-7.

(26) Xiao, Z.; Zheng, H.; Du, C.; Zhong, L.; Liao, H.; Gao, J.; Gao, H.; Wu, Q. Enhancement on Alternating Copolymerization of Carbon Monoxide and Styrene by Dibenzobarrelene-Based α-Diimine Palladium Catalysts. *Macromolecules* **2018**, *51* (22), 9110–9121. https://doi.org/10.1021/acs.macromol.8b01786.

(27) Carfagna, C.; Gatti, G.; Paoli, P.; Binotti, B.; Fini, F.; Passeri, A.; Rossi, P.; Gabriele, B. New Aryl α-Diimine Palladium(II) Catalysts in Stereocontrolled CO/Vinyl Arene Copolymerization. *Organometallics* **2014**, *33* (1), 129–144. https://doi.org/10.1021/om400887x.

(28) Dai, S.; Sui, X.; Chen, C. Highly Robust Palladium(II) α-Diimine Catalysts for Slow-Chain-Walking Polymerization of Ethylene and Copolymerization with Methyl Acrylate. *Angew. Chem. Int. Ed.* **2015**, *54* (34), 9948–9953. https://doi.org/10.1002/anie.201503708.

(29) Dai, S.; Chen, C. Direct Synthesis of Functionalized High-Molecular-Weight Polyethylene by Copolymerization of Ethylene with Polar Monomers. *Angew. Chem. Int. Ed.* **2016**, *55* (42), 13281–13285. https://doi.org/10.1002/anie.201607152.

(30) Zhai, F.; Jordan, R. F. Hydrogen Bonding Behavior of Amide-Functionalized α-Diimine Palladium Complexes. *Organometallics* **2014**, *33* (24), 7176–7192. https://doi.org/10.1021/om500978n.

(31) Sui, X.; Hong, C.; Pang, W.; Chen, C. Unsymmetrical α-Diimine Palladium Catalysts and Their Properties in Olefin (Co)Polymerization. *Mater. Chem. Front.* **2017**, *1* (5), 967–972. https://doi.org/10.1039/C6QM00235H.

(32) Tran, Q. H.; Wang, X.; Brookhart, M.; Daugulis, O. Cationic α-Diimine Nickel and Palladium Complexes Incorporating Phenanthrene Substituents: Highly Active Ethylene Polymerization Catalysts and Mechanistic Studies of Syn/Anti Isomerization. *Organometallics* **2020**, *39* (24), 4704–4716. https://doi.org/10.1021/acs.organomet.0c00696.

(33) Zou, W.; Chen, C. Influence of Backbone Substituents on the Ethylene (Co)Polymerization Properties of α-Diimine Pd(II) and Ni(II) Catalysts. *Organometallics* **2016**, *35* (11), 1794–1801. https://doi.org/10.1021/acs.organomet.6b00202.

(34) Zhong, S.; Tan, Y.; Zhong, L.; Gao, J.; Liao, H.; Jiang, L.; Gao, H.; Wu, Q. Precision Synthesis of Ethylene and Polar Monomer Copolymers by Palladium-Catalyzed Living Coordination Copolymerization. *Macromolecules* **2017**, *50* (15), 5661–5669. https://doi.org/10.1021/acs.macromol.7b01132.

(35) Huo, P.; Liu, W.; He, X.; Wei, Z.; Chen, Y. Substituent Effects and Activation Mechanism of Norbornene Polymerization Catalyzed by Three-Dimensional

Geometry α-Diimine Palladium Complexes. *Polym. Chem.* **2014**, *5* (4), 1210–1218. https://doi.org/10.1039/C3PY01092A.

(36) Wang, X.; Dong, B.; Yang, Q.; Liu, H.; Hu, Y.; Zhang, X. Boosting the Thermal Stability of α-Diimine Palladium Complexes in Norbornene Polymerization from Construction of Intraligand Hydrogen Bonding and Simultaneous Increasing Axial/Equatorial Bulkiness. *Inorg. Chem.* **2021**, *60* (4), 2347–2361. https://doi.org/10.1021/acs.inorgchem.0c03185.

(37) Shi, F.; Ren, X.; Wang, H.; Pu, M.; Liu, L.; Lei, M. Neutral Phosphine-Sulfonate Pd Complex-Catalyzed Copolymerization of 2-Methoxystyrene and Ethylene Polar Monomers: A DFT Mechanistic Study. *ACS Appl. Polym. Mater.* **2022**, *4* (8), 5901–5908. https://doi.org/10.1021/acsapm.2c00786.

(38) Cao, L.; Cai, Z.; Li, M. Synthesis and Characterization of Phosphinobenzenamine Palladium Complexes and Their Application in Ethylene Polymerization and Copolymerization with Polar Monomers. *Organometallics* **2022**, *41* (23), 3538–3545. https://doi.org/10.1021/acs.organomet.2c00389.

(39) Pan, H.; Zhu, L.; Li, J.; Zang, D.; Fu, Z.; Fan, Z. A Thermal Stable α-Diimine Palladium Catalyst for Copolymerization of Ethylene with Functionalized Olefins. *J. Mol. Catal. Chem.* **2014**, *390*, 76–82. https://doi.org/10.1016/j.molcata.2014.03.008.

(40) Chen, C.; Jordan, R. F. Palladium-Catalyzed Dimerization of Vinyl Ethers to Acetals. *J. Am. Chem. Soc.* **2010**, *132* (30), 10254–10255. https://doi.org/10.1021/ja104523y.

(41) Ouyang, J.-S.; Li, Y.-F.; Shen, D.-S.; Ke, Z.; Liu, F.-S. Bulky α-Diimine Palladium Complexes: Highly Efficient for Direct C–H Bond Arylation of Heteroarenes under Aerobic Conditions. *Dalton Trans.* **2016**, *45* (38), 14919–14927. https://doi.org/10.1039/C6DT02544G.

(42) Ackerman, L. J.; Sadighi, J. P.; Kurtz, D. M.; Labinger, J. A.; Bercaw, J. E. Arene C−H Bond Activation and Arene Oxidative Coupling by Cationic Palladium(II) Complexes. *Organometallics* **2003**, *22* (19), 3884–3890. https://doi.org/10.1021/om0303294.

(43) Williams, T. J.; Caffyn, A. J. M.; Hazari, N.; Oblad, P. F.; Labinger, J. A.; Bercaw, J. E. C−H Bond Activation by Air-Stable $[(\text{Diimine})M^{II}(M_2\text{-}OH)]_2^{2+}$ Dimers (M = Pd, Pt). *J. Am. Chem. Soc.* **2008**, *130* (8), 2418–2419. https://doi.org/10.1021/ja076740q.

(44) Hickman, A. J.; Sanford, M. S. Catalyst Control of Site Selectivity in the $Pd^{II}/^{IV}$-Catalyzed Direct Arylation of Naphthalene. *ACS Catal.* **2011**, *1* (3), 170–174. https://doi.org/10.1021/cs1001543.

(45) Grasa, G. A.; Hillier, A. C.; Nolan, S. P. Convenient and Efficient Suzuki−Miyaura Cross-Coupling Catalyzed by a Palladium/Diazabutadiene System. *Org. Lett.* **2001**, *3* (7), 1077–1080. https://doi.org/10.1021/ol015676t.

(46) Mino, T.; Shirae, Y.; Sasai, Y.; Sakamoto, M.; Fujita, T. Phosphine-Free Palladium Catalyzed Mizoroki−Heck Reaction Using Hydrazone as a Ligand. *J. Org. Chem.* **2006**, *71* (18), 6834–6839. https://doi.org/10.1021/jo0610006.

(47) Grasa, G. A.; Singh, R.; Stevens, E. D.; Nolan, S. P. Catalytic Activity of Pd(II) and Pd(II)/DAB-R Systems for the Heck Arylation of Olefins. *J. Organomet. Chem.* **2003**, *687* (2), 269–279. https://doi.org/10.1016/S0022-328X(03)00375-9.

(48) Gottumukkala, A. L.; Teichert, J. F.; Heijnen, D.; Eisink, N.; van Dijk, S.; Ferrer, C.; van den Hoogenband, A.; Minnaard, A. J. Pd-Diimine: A Highly Selective Catalyst System for the Base-Free Oxidative Heck Reaction. *J. Org. Chem.* **2011**, *76* (9), 3498–3501. https://doi.org/10.1021/jo101942f.

(49) Mino, T.; Shirae, Y.; Saito, T.; Sakamoto, M.; Fujita, T. Palladium-Catalyzed Sonogashira and Hiyama Reactions Using Phosphine-Free Hydrazone Ligands. *J. Org. Chem.* **2006**, *71* (25), 9499–9502. https://doi.org/10.1021/jo061734i.

(50) van Belzen, R.; Hoffmann, H.; Elsevier, C. J. Catalytic Three-Component Synthesis of Conjugated Dienes from Alkynes via Pd^0, Pd^{II}, and Pd^{IV} Intermediates Containing 1,2-Diimine. *Angew. Chem. Int. Ed. Engl.* **1997**, *36* (16), 1743–1745. https://doi.org/10.1002/anie.199717431.

(51) van Belzen, R.; Klein, R. A.; Kooijman, H.; Veldman, N.; Spek, A. L.; Elsevier, C. J. Stoichiometric and Catalytic Conversion of Alkynes to Conjugated (*Z,Z*)-Dienes and Cyclopentadienes via Palladacyclopentadienes and 1,3-Dienylpalladium(II) Halide and Triorganopalladium(IV) Halide Compounds Containing Chelating Nitrogen Ligands. *Organometallics* **1998**, *17* (9), 1812–1825. https://doi.org/10.1021/om970977l.

(52) Van Asselt, R.; Elsevier, C. J. New Palladium Complexes of Cis-Fixed Bidentate Nitrogen Ligands as Catalysts for Carbon-Carbon Bond Formation. *Organometallics* **1992**, *11* (6), 1999–2001. https://doi.org/10.1021/om00042a010.

(53) van Asselt, R.; Elsevier, C. J. Homogeneous Catalytic Hydrogenation of Alkenes by Zero-Valent Palladium Complexes of Cis-Fixed Dinitrogen Ligands. *J. Mol. Catal.* **1991**, *65* (3), L13–L19. https://doi.org/10.1016/0304-5102(91)85057-9.

(54) van Laren, M. W.; Elsevier, C. J. Selective Homogeneous Palladium(0)-Catalyzed Hydrogenation of Alkynes to (*Z*)-Alkenes. *Angew. Chem. Int. Ed.* **1999**, *38* (24), 3715–3717. https://doi.org/10.1002/(SICI)1521-3773(19991216)38:24<3715::AID-ANIE3715>3.0.CO;2-O.

(55) Cavell, K. J.; Stufkens, D. J.; Vrieze, K. 1,4-Diazabutadiene Olefin Complexes of Zerovalent Palladium: Preparation and Characterization. *Inorganica Chim. Acta* **1981**, *47*, 67–76. https://doi.org/10.1016/S0020-1693(00)89309-3.

(56) Crociani, B.; Bianca, F. D.; Uguagliati, P.; Canovese, L.; Berton, A. Phenylation of Cationic Allyl Palladium(II) Complexes by Tetraphenylborate. Synthesis of α-Diimine Olefin Palladium(0) Complexes and Mechanistic Aspects. *J. Chem. Soc. Dalton Trans.* **1991**, No. 1, 71–79. https://doi.org/10.1039/DT9910000071.

(57) Milani, B.; Anzilutti, A.; Vicentini, L.; Sessanta o Santi, A.; Zangrando, E.; Geremia, S.; Mestroni, G. Bis-Chelated Palladium(II) Complexes with Nitrogen-Donor Chelating Ligands Are Efficient Catalyst Precursors for the CO/Styrene Copolymerization Reaction. *Organometallics* **1997**, *16* (23), 5064–5075. https://doi.org/10.1021/om9703954.

(58) Klein, R. A.; Witte, P.; van Belzen, R.; Fraanje, J.; Goubitz, K.; Numan, M.; Schenk, H.; Ernsting, J. M.; Elsevier, C. J. Monodentate and Bridging Coordination of 3,3′-Annelated 2,2′-Bipyridines in Zerovalent Palladium- and Platinum-*p*-Quinone Complexes. *Eur. J. Inorg. Chem.* **1998**, *1998* (3), 319–330. https://doi.org/10.1002/(SICI)1099-0682(199803)1998:3<319::AID-EJIC319>3.0.CO;2-H.

(59) Popp, B. V.; Thorman, J. L.; Morales, C. M.; Landis, C. R.; Stahl, S. S. "Inverse-Electron-Demand" Ligand Substitution: Experimental and Computational Insights into Olefin Exchange at Palladium(0). *J. Am. Chem. Soc.* **2004**, *126* (45), 14832–14842. https://doi.org/10.1021/ja0459734.

(60) Hawash, Z.; Ono, L. K.; Qi, Y. Recent Advances in Spiro-MeOTAD Hole Transport Material and Its Applications in Organic–Inorganic Halide Perovskite Solar Cells. *Adv. Mater. Interfaces* **2018**, *5* (1), 1700623. https://doi.org/10.1002/admi.201700623.

(61) de Pater, Jeroen. J. M.; Maljaars, C. E. P.; de Wolf, E.; Lutz, M.; Spek, A. L.; Deelman, B.-J.; Elsevier, C. J.; van Koten, G. (Perfluoro)alkylsilyl-Substituted 2-[Bis(4-aryl)phosphino]pyridines: Synthesis and Comparison of Their Palladium Complexes in Methoxycarbonylation of Phenylacetylene in Regular Solvents and Supercritical CO_2. *Organometallics* **2005**, *24* (22), 5299–5310. https://doi.org/10.1021/om050479+.

(62) de Pater, J. J. M.; Tromp, D. S.; Tooke, D. M.; Spek, A. L.; Deelman, B.-J.; van Koten, G.; Elsevier, C. J. Palladium(0)-Alkene Bis(Triarylphosphine) Complexes as Catalyst Precursors for the Methoxycarbonylation of Styrene. *Organometallics* **2005**, *24* (26), 6411–6419. https://doi.org/10.1021/om0506419.

(63) Hauwert, P.; Boerleider, R.; Warsink, S.; Weigand, J. J.; Elsevier, C. J. Mechanism of Pd(NHC)-Catalyzed Transfer Hydrogenation of Alkynes. *J. Am. Chem. Soc.* **2010**, *132* (47), 16900–16910. https://doi.org/10.1021/ja1062407.

(64) Warsink, S.; Chang, I.-H.; Weigand, J. J.; Hauwert, P.; Chen, J.-T.; Elsevier, C. J. NHC Ligands with a Secondary Pyrimidyl Donor for Electron-Rich Palladium(0) Complexes. *Organometallics* **2010**, *29* (20), 4555–4561. https://doi.org/10.1021/om100670u.

(65) Lee, J.-Y.; Cheng, P.-Y.; Tsai, Y.-H.; Lin, G.-R.; Liu, S.-P.; Sie, M.-H.; Lee, H. M. Efficient Heck Reactions Catalyzed by Palladium(0) and -(II) Complexes Bearing N-Heterocyclic Carbene and Amide Functionalities. *Organometallics* **2010**, *29* (17), 3901–3911. https://doi.org/10.1021/om1006402.

(66) Warsink, S.; Bosman, S.; Weigand, J. J.; Elsevier, C. J. Rigid Pyridyl Substituted NHC Ligands, Their Pd(0) Complexes and Their Application in Selective Transfer Semihydrogenation of Alkynes. *Appl. Organomet. Chem.* **2011**, *25* (4), 276–282. https://doi.org/10.1002/aoc.1754.

(67) Nandi, D.; Jhou, Y.-M.; Lee, J.-Y.; Kuo, B.-C.; Liu, C.-Y.; Huang, P.-W.; Lee, H. M. Pd(0)-Catalyzed Decarboxylative Coupling and Tandem C–H Arylation/Decarboxylation for the Synthesis of Heteroaromatic Biaryls. *J. Org. Chem.* **2012**, *77* (20), 9384–9390. https://doi.org/10.1021/jo3015837.

(68) Sluijter, S. N.; Warsink, S.; Lutz, M.; Elsevier, C. J. Synthesis of Palladium(0) and -(II) Complexes with Chelating Bis(*N*-Heterocyclic Carbene) Ligands and Their Application in Semihydrogenation. *Dalton Trans.* **2013**, *42* (20), 7365–7372. https://doi.org/10.1039/C3DT32835J.

(69) Jhou, Y.-M.; Nandi, D.; Lee, J.-Y.; Tzeng, R.-J.; Lee, H. M. Palladium(0) Complexes of *N*-Heterocyclic Carbene Ligands with Dangling NMeCO Functionalities: Synthesis, Reactivity and Application in Mizoroki–Heck Reactions. *Polyhedron* **2015**, *100*, 28–35. https://doi.org/10.1016/j.poly.2015.07.027.

(70) Lee, J.-Y.; Shen, J.-S.; Tzeng, R.-J.; Lu, I.-C.; Lii, J.-H.; Hu, C.-H.; Lee, H. M. Well-Defined Palladium(0) Complexes Bearing N-Heterocyclic Carbene and Phosphine Moieties: Efficient Catalytic Applications in the Mizoroki–Heck Reaction and Direct C–H Functionalization. *Dalton Trans.* **2016**, *45* (25), 10375–10388. https://doi.org/10.1039/C6DT01323F.

(71) Ueda, S.; Su, M.; Buchwald, S. L. Completely N1-Selective Palladium-Catalyzed Arylation of Unsymmetric Imidazoles: Application to the Synthesis of Nilotinib. *J. Am. Chem. Soc.* **2012**, *134* (1), 700–706. https://doi.org/10.1021/ja2102373.

(72) Bruno, N. C.; Buchwald, S. L. Synthesis and Application of Palladium Precatalysts That Accommodate Extremely Bulky Di-*tert*-butylphosphino Biaryl Ligands. *Org. Lett.* **2013**, *15* (11), 2876–2879. https://doi.org/10.1021/ol401208t.

(73) DeAngelis, A. J.; Gildner, P. G.; Chow, R.; Colacot, T. J. Generating Active "L-Pd(0)" via Neutral or Cationic π-Allylpalladium Complexes Featuring Biaryl/Bipyrazolylphosphines: Synthetic, Mechanistic, and Structure–Activity Studies in Challenging Cross-Coupling Reactions. *J. Org. Chem.* **2015**, *80* (13), 6794–6813. https://doi.org/10.1021/acs.joc.5b01005.

(74) Ning, Z.; Tian, H. Triarylamine: A Promising Core Unit for Efficient Photovoltaic Materials. *Chem. Commun.* **2009**, No. 37, 5483–5495. https://doi.org/10.1039/B908802D.

(75) Horton, D. A.; Bourne, G. T.; Smythe, M. L. The Combinatorial Synthesis of Bicyclic Privileged Structures or Privileged Substructures. *Chem. Rev.* **2003**, *103* (3), 893–930. https://doi.org/10.1021/cr020033s.

(76) Eelkema, R.; Anderson, H. L. Synthesis of End-Functionalized Polyanilines. *Macromolecules* **2008**, *41* (24), 9930–9933. https://doi.org/10.1021/ma801697w.

(77) Bruno, N. C.; Tudge, M. T.; Buchwald, S. L. Design and Preparation of New Palladium Precatalysts for C–C and C–N Cross-Coupling Reactions. *Chem. Sci.* **2013**, *4* (3), 916–920. https://doi.org/10.1039/C2SC20903A.

(78) Maiti, D.; Fors, B. P.; Henderson, J. L.; Nakamura, Y.; Buchwald, S. L. Palladium-Catalyzed Coupling of Functionalized Primary and Secondary Amines with Aryl and Heteroaryl Halides: Two Ligands Suffice in Most Cases. *Chem. Sci.* **2010**, *2* (1), 57–68. https://doi.org/10.1039/C0SC00330A.

(79) Surry, D. S.; Buchwald, S. L. Dialkylbiaryl Phosphines in Pd-Catalyzed Amination: A User's Guide. *Chem. Sci.* **2010**, *2* (1), 27–50. https://doi.org/10.1039/C0SC00331J.

(80) Fors, B. P.; Watson, D. A.; Biscoe, M. R.; Buchwald, S. L. A Highly Active Catalyst for Pd-Catalyzed Amination Reactions: Cross-Coupling Reactions Using Aryl Mesylates and the Highly Selective Monoarylation of Primary Amines Using Aryl Chlorides. *J. Am. Chem. Soc.* **2008**, *130* (41), 13552–13554. https://doi.org/10.1021/ja8055358.

(81) Fors, B. P.; Davis, N. R.; Buchwald, S. L. An Efficient Process for Pd-Catalyzed C−N Cross-Coupling Reactions of Aryl Iodides: Insight Into Controlling Factors. *J. Am. Chem. Soc.* **2009**, *131* (16), 5766–5768. https://doi.org/10.1021/ja901414u.

(82) Rosen, B. R.; Ruble, J. C.; Beauchamp, T. J.; Navarro, A. Mild Pd-Catalyzed N-Arylation of Methanesulfonamide and Related Nucleophiles: Avoiding Potentially Genotoxic Reagents and Byproducts. *Org. Lett.* **2011**, *13* (10), 2564–2567. https://doi.org/10.1021/ol200660s.

(83) Becica, J.; Hruszkewycz, D. P.; Steves, J. E.; Elward, J. M.; Leitch, D. C.; Dobereiner, G. E. High-Throughput Discovery and Evaluation of a General Catalytic Method for N-Arylation of Weakly Nucleophilic Sulfonamides. *Org. Lett.* **2019**, *21* (22), 8981–8986. https://doi.org/10.1021/acs.orglett.9b03380.

(84) Laffoon, S. D.; Chan, V. S.; Fickes, M. G.; Kotecki, B.; Ickes, A. R.; Henle, J.; Napolitano, J. G.; Franczyk, T. S.; Dunn, T. B.; Barnes, D. M.; Haight, A. R.; Henry, R. F.; Shekhar, S. Pd-Catalyzed Cross-Coupling Reactions Promoted by Biaryl Phosphorinane Ligands. *ACS Catal.* **2019**, *9* (12), 11691–11708. https://doi.org/10.1021/acscatal.9b03012.

(85) Hicks, J. D.; Hyde, A. M.; Cuezva, A. M.; Buchwald, S. L. Pd-Catalyzed N-Arylation of Secondary Acyclic Amides: Catalyst Development, Scope, and Computational Study. *J. Am. Chem. Soc.* **2009**, *131* (46), 16720–16734. https://doi.org/10.1021/ja9044357.

(86) Yin, J.; Buchwald, S. L. Pd-Catalyzed Intermolecular Amidation of Aryl Halides: The Discovery That Xantphos Can Be Trans-Chelating in a Palladium Complex. *J. Am. Chem. Soc.* **2002**, *124* (21), 6043–6048. https://doi.org/10.1021/ja012610k.

(87) Withbroe, G. J.; Singer, R. A.; Sieser, J. E. Streamlined Synthesis of the Bippyphos Family of Ligands and Cross-Coupling Applications. *Org. Process Res. Dev.* **2008**, *12* (3), 480–489. https://doi.org/10.1021/op7002858.

(88) Singer, R. A.; Doré, M.; Sieser, J. E.; Berliner, M. A. Development of Nonproprietary Phosphine Ligands for the Pd-Catalyzed Amination Reaction. *Tetrahedron Lett.* **2006**, *47* (22), 3727–3731. https://doi.org/10.1016/j.tetlet.2006.03.132.

(89) Marion, N.; Navarro, O.; Mei, J.; Stevens, E. D.; Scott, N. M.; Nolan, S. P. Modified (NHC)Pd(allyl)Cl (NHC = *N*-Heterocyclic Carbene) Complexes for Room-Temperature Suzuki−Miyaura and Buchwald−Hartwig Reactions. *J. Am. Chem. Soc.* **2006**, *128* (12), 4101–4111. https://doi.org/10.1021/ja057704z.

(90) Melvin, P. R.; Nova, A.; Balcells, D.; Dai, W.; Hazari, N.; Hruszkewycz, D. P.; Shah, H. P.; Tudge, M. T. Design of a Versatile and Improved Precatalyst Scaffold for Palladium-Catalyzed Cross-Coupling: $(\eta^3\text{-}1\text{-}^t\text{Bu-indenyl})_2(\mu\text{-Cl})_2\text{Pd}_2$. *ACS Catal.* **2015**, *5* (6), 3680–3688. https://doi.org/10.1021/acscatal.5b00878.

(91) Bruno, N. C.; Niljianskul, N.; Buchwald, S. L. N-Substituted 2-Aminobiphenylpalladium Methanesulfonate Precatalysts and Their Use in C–C and C–N Cross-Couplings. *J. Org. Chem.* **2014**, *79* (9), 4161–4166. https://doi.org/10.1021/jo500355k.

(92) Peh, G.-R.; Kantchev, E. A. B.; Er, J.-C.; Ying, J. Y. Rational Exploration of *N*-Heterocyclic Carbene (NHC) Palladacycle Diversity: A Highly Active and Versatile Precatalyst for Suzuki–Miyaura Coupling Reactions of Deactivated Aryl and Alkyl Substrates. *Chem. – Eur. J.* **2010**, *16* (13), 4010–4017. https://doi.org/10.1002/chem.200902842.

(93) Dounay, A. B.; Overman, L. E. The Asymmetric Intramolecular Heck Reaction in Natural Product Total Synthesis. *Chem. Rev.* **2003**, *103* (8), 2945–2964. https://doi.org/10.1021/cr020039h.

(94) Beletskaya, I. P.; Cheprakov, A. V. The Heck Reaction as a Sharpening Stone of Palladium Catalysis. *Chem. Rev.* **2000**, *100* (8), 3009–3066. https://doi.org/10.1021/cr9903048.

(95) Murray, P. M.; Bower, J. F.; Cox, D. K.; Galbraith, E. K.; Parker, J. S.; Sweeney, J. B. A Robust First-Pass Protocol for the Heck–Mizoroki Reaction. *Org. Process Res. Dev.* **2013**, *17* (3), 397–405. https://doi.org/10.1021/op300364p.

(96) Littke, A. F.; Fu, G. C. Heck Reactions in the Presence of P(*t*-Bu)$_3$: Expanded Scope and Milder Reaction Conditions for the Coupling of Aryl Chlorides. *J. Org. Chem.* **1999**, *64* (1), 10–11. https://doi.org/10.1021/jo9820059.

(97) Littke, A. F.; Fu, G. C. A Versatile Catalyst for Heck Reactions of Aryl Chlorides and Aryl Bromides under Mild Conditions. *J. Am. Chem. Soc.* **2001**, *123* (29), 6989–7000. https://doi.org/10.1021/ja010988c.

(98) Amini, M.; Bagherzadeh, M.; Moradi-Shoeili, Z.; Boghaei, D. M. Pd(OAc)$_2$ without Added Ligand as an Active Catalyst for Mizoroki–Heck Reaction in Aqueous Media. *RSC Adv.* **2012**, *2* (32), 12091–12095. https://doi.org/10.1039/C2RA21459H.

(99) Yao, Q.; Kinney, E. P.; Yang, Z. Ligand-Free Heck Reaction: Pd(OAc)$_2$ as an Active Catalyst Revisited. *J. Org. Chem.* **2003**, *68* (19), 7528–7531. https://doi.org/10.1021/jo034646w.

(100) Zhang, H.; Ruiz-Castillo, P.; Buchwald, S. L. Palladium-Catalyzed C–O Cross-Coupling of Primary Alcohols. *Org. Lett.* **2018**, *20* (6), 1580–1583. https://doi.org/10.1021/acs.orglett.8b00325.

(101) Gowrisankar, S.; Sergeev, A. G.; Anbarasan, P.; Spannenberg, A.; Neumann, H.; Beller, M. A General and Efficient Catalyst for Palladium-Catalyzed C−O Coupling Reactions of Aryl Halides with Primary Alcohols. *J. Am. Chem. Soc.* **2010**, *132* (33), 11592–11598. https://doi.org/10.1021/ja103248d.

(102) Cheung, C. W.; Buchwald, S. L. Mild and General Palladium-Catalyzed Synthesis of Methyl Aryl Ethers Enabled by the Use of a Palladacycle Precatalyst. *Org. Lett.* **2013**, *15* (15), 3998–4001. https://doi.org/10.1021/ol401796v.

(103) Jeon, N. J.; Lee, H. G.; Kim, Y. C.; Seo, J.; Noh, J. H.; Lee, J.; Seok, S. I. *o*-Methoxy Substituents in Spiro-OMeTAD for Efficient Inorganic–Organic Hybrid Perovskite Solar Cells. *J. Am. Chem. Soc.* **2014**, *136* (22), 7837–7840. https://doi.org/10.1021/ja502824c.

(104) Shimomaki, K.; Murata, K.; Martin, R.; Iwasawa, N. Visible-Light-Driven Carboxylation of Aryl Halides by the Combined Use of Palladium and Photoredox Catalysts. *J. Am. Chem. Soc.* **2017**, *139* (28), 9467–9470. https://doi.org/10.1021/jacs.7b04838.

(105) Pipaón Fernández, N.; Gaube, G.; Woelk, K. J.; Burns, M.; Hruszkewycz, D. P.; Leitch, D. C. Palladium-Catalyzed Direct C–H Alkenylation with Enol Pivalates Proceeds via Reversible C–O Oxidative Addition to Pd(0). *ACS Catal.* **2022**, *12* (12), 6997–7003. https://doi.org/10.1021/acscatal.2c01305.

Chapter 3 Active, Selective, and Stable Single-Component Palladium(0) Precatalysts for Asymmetric Allylic Alkylation

This chapter has been adapted from:

Huang J.; Keenan T.; Richard F., Lu J.; Jenny S., Jean A.; Arseniyadis S.; Leitch D. C. Active, selective, and stable single-component precatalysts for asymmetric allylic alkylation. *ChemRxiv* **2023**, DOI: 10.26434/chemrxiv-2023-0xbh5

Contributions:

All experiments related to catalyst synthesis and characterization were conducted by Jingjun Huang. Catalytic evaluation of single-component precatalysts in asymmetric allylic alkylation reactions was accomplished by Thomas Keenan and Francois Richard (Queen Mary University of London, Arseniyadis lab). Computational analysis was performed by Jingru Lu (UVic, Leitch lab). Single crystal X-ray diffraction experiments and analysis were conducted by Sarah E. Jenny (Temple University, Dobereiner lab).

3.1 Abstract

In this chapter, we report six isolable, chiral palladium(0) single-component precatalysts for asymmetric allylic alkylation (AAA), a reaction type commonly applied to access chiral molecules in natural products and active pharmaceutical ingredients. The four Trost-type precatalysts in this work are the first characterized examples of stable and isolable Pd complexes with the diphosphines coordinated in the desired κ^2-P,P mode. All palladium(0) precatalysts reported here are indefinitely stable when stored under N_2 and can be easily handled as solids and even in solution without the need for an inert atmosphere or glovebox. Furthermore, catalytic evaluation involving 9 distinct AAA reactions by our collaborators (T. Keenan, F. Richard, S. Arseniyadis) reveals the superior

performance of these new precursors in terms of reactivity, selectivity, practicality, and the loading of both palladium and chiral ligand compared to other common *in situ* generated catalysts. We also report the application of these precatalysts in an unprecedented enantioselective allylation of hydantoins, which was optimized through a screening process. The resulting product is obtained in high isolated yield and enantioselectivity on preparative-scale with only 0.2 mol % catalyst loading (catalyst turnover number of 465). This reveals the power and compatibility of these new complexes in microscale high-throughput screening studies and preparative scale synthesis toward important chiral building blocks.

3.2 Introduction

A huge number of chiral molecules containing one or more stereogenic centers are the basis of many commercial compounds, such as drugs, agricultural products, and food additives. The properties and therapeutic activity can be significantly influenced by the chirality of these molecules; therefore, controlling stereochemistry during synthesis is critical.[1,2] Within this context, a variety of synthetic approaches have been developed for stereoselective bond construction. In general, this is challenging to achieve, and a predominant strategy is to apply asymmetric metal catalysts. Transition metal-catalyzed AAA, a set of powerful transformations enabling C–C, C–N, C–S, C–O, etc. bond formations, is able to efficiently and selectively build new stereocenters.[3] This is often a key strategy in the total synthesis of natural products.[4–11] In general, asymmetric allylation proceeds via nucleophile attack on a coordinated allyl ligand, with different enantiodiscrimination mechanisms dependent on the specific metal and nucleophile used. Importantly, this imparts great flexibility with reaction development and offers many opportunities to control the reactivity and selectivity of AAA. Notably, palladium complexes with chiral ligands take a dominant position as catalysts for this transformation,[7,12] though a few other transition metals are also used, such as iridium,[13–17] rhodium,[18–21] cobalt[22–24] and nickel.[25–27]

Similar to other Pd-catalyzed cross-coupling reactions, L_nPd^0 is viewed as an active species in the universally accepted mechanism of AAA reactions.[28] As stated in Chapter 1,

generating this active species is a critical step for these Pd-catalyzed transformations, wherein two general strategies are conventional. One is *in situ* catalyst formation, exemplified in Chapter 2 by the HTE evaluation with ^{DMP}DAB–Pd–MAH. Catalyst generation *in situ* undoubtedly provides several advantages, such as operational convenience and flexibility during optimization; thus, it is commonly employed in palladium-catalyzed AAA. However, *in situ* catalyst formation does often require extensive optimization, excess chiral ligand, and prolonged pretreatment/preheating of palladium source and ligand to ensure complete ligand substitution. If there is inefficient generation of active species, the yield and/or enantioselectivity of the reaction will suffer. This is a common issue with *in situ* catalyst formation in AAA reactions.

Notably, the major Pd sources generally used in this reaction are Pd_2dba_3 and Pd allyl dimers.[3,7,11,29] Drawbacks of the former have been illustrated in the previous two chapters, and the allyl by-product released during activation of the latter can potentially inhibit the reactivity. In stark contrast, another strategy—using single-component precatalysts containing chiral supporting ligands—effectively addresses these drawbacks and avoids using excess chiral ligands. This is important from an economic perspective, especially on larger scale, due to the high cost of most chiral ligands. Compared to *in situ* catalyst systems, only a few examples of AAA reactions using preformed precatalysts, are reported.[30–32]

Within this context, several isolable palladium complexes ligated with either phosphine-oxazoline PHOX-type ligands[30,33–42] or diphosphine Trost-type ligands[43,44] have been reported. These two ligand classes are most frequently used in AAA chemistry, giving high stereoselectivity for many reaction types. While there are several reported PHOX–Pd^0–olefin precatalysts (Figure 3.1A),[30,34,36–38] isolable Pd^0 precatalysts with Trost-type ligands have (to the best of our knowledge) never been reported. This is likely due to challenges with stability and isolation of these species, despite the fact that this ligand class has exceptional performance in a wide range of AAA reactions.[3,7,32]

A palladium(0) complex featuring the standard (*S,S*)-DACH-phenyl Trost ligand (**L1**) and coordinated dba, generated from Pd_2dba_3•$CHCl_3$ and **L1**, has been observed by NMR spectroscopy by Trost and co-workers.[45] However, the proposed (**L1**)Pd(dba)

species was not isolated due to its rapid oxidation when exposed to air, giving a tetracoordinate, catalytically inactive [PNNP]Pd^{II} complex (Figure 3.1B). Notably, this same Pd^{II} complex was isolated from an AAA reaction mixture by process chemists at Merck, using $[Pd(allyl)Cl]_2$/**L1** as the catalytic system.[46] In addition to palladium(0) complexes, Lloyd-Jones and co-workers reported the synthesis of Pd(allyl)(**L1**)][OTf], the only isolated single-component precatalyst with a Trost ligand as far as we know. This is prepared from **L1** and 1 equivalent of halide-free $[Pd(allyl)(MeCN)_2][OTf]$, though the structure was not able to be confirmed by XRD.[43] While this precatalyst induces high enantioselectivity and reactivity in AAA reactions, complicated solution-phase behaviour, including oligomerization, has been observed. Several factors impact the extent of oligomer formation, including concentration, solvent and counter anion.[44] By increasing the equivalents of $[Pd(allyl)(MeCN)_2][OTf]$ to 2, they obtained (**L1**)$Pd_2(allyl)_2(OTf)_2$, a catalytically active dipalladium complex (Figure 3.1C Left); however, this precatalyst produces racemic products in a kinetic resolution with (±)-cyclopent-2-en-1-yl pivalate and $[NaCH(CO_2Me)_2]$. This is likely due to the κ^2-P,O coordination mode, removing the active Pd centers from the chiral environment imparted by the desired κ^2-P,P mode bidentate mode. Similarly, a complex containing DACH-naphthyl Trost ligand (**L2**) coordinated via κ^2-P,O – (**L2**)$Pd_2(Ph–allyl–Ph)_2(BF_4)_2$ – has also been reported, though no data on its activity as a precatalyst was disclosed (Figure 3.1C Right).[47]

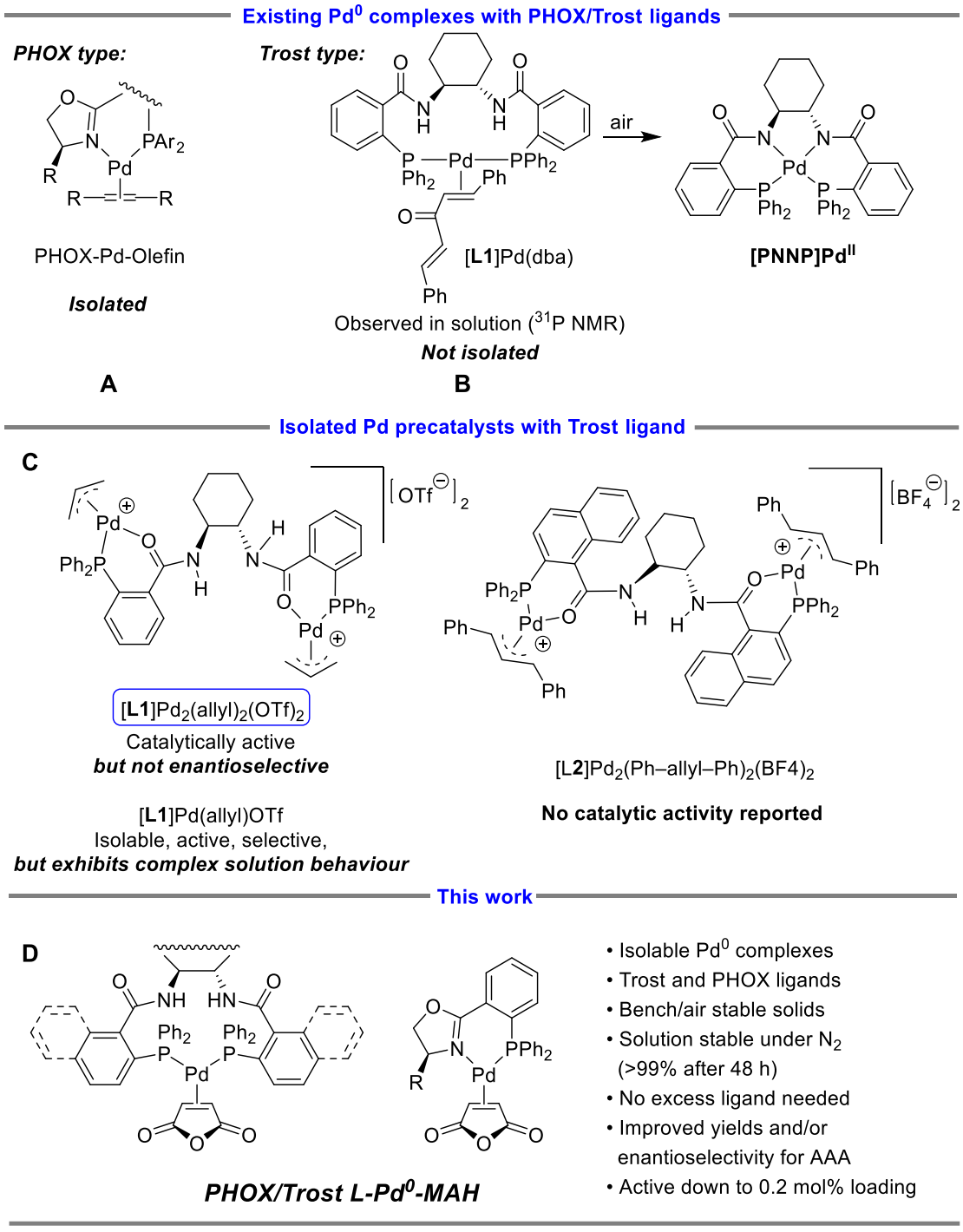

Figure 3.1. A: General structure of isolable PHOX-type Pd^0 complexes; **B: L1**–Pd–dba and decomposition by oxidation; **C:** The only reported isolable Pd precatalysts featuring a Trost-type ligand (*Left*) and a similar isolable Pd complex containing **L2** (*Right*); **D:** General structures for the new chiral Pd^0 single-component precatalysts in this work.

Given the promising preliminary activity and selectivity of ^{DMP}DAB–Pd–MAH over other common palladium sources in a AAA reaction key to a natural product total synthesis,[6] we collaborated with the Arseniyadis group from the Queen Mary University of London to develop new single-component palladium(0) precatalysts for this reaction type. Herein, we report six new, monomeric, and fully characterized palladium(0) single-component precatalysts generated via an efficient ligand substitution from ^{DMP}DAB–Pd–MAH with either Trost-type ligands or PHOX-type ligands (Figure 3.1D). Based on stability studies, all six complexes are fully stable for more than a year under N_2 storage, and are also easily handled without the use of a glovebox during experimental setup. This includes handling in solution under air without significant oxidation to [PNNP]Pd^{II}. The catalytic assessment of these complexes in 9 different palladium-catalyzed AAA processes by our collaborators reveals their superior catalytic activity and stereoselectivity over other common palladium sources, even at 0.2 mol % Pd loading.

3.3 Results and Discussion

3.3.1 Precatalyst Synthesis and XRD Characterization

The limited applications of single-component precatalysts in AAA reactions prompted us to develop new chiral palladium(0) precatalysts using our previously reported ^{DMP}DAB–Pd–MAH.[48] This palladium(0) precursor, discussed in Chapter 2, is able to easily generate [phosphine]–Pd–MAH complexes. Here, we assessed the metalation of a series of chiral bidentate ligands. In terms of ligand choice, four diphosphine Trost ligands (**L1-L4**) and two phosphine-oxazoline PHOX ligands (**L5-L6**) have been included (Figure 3.2), according to their prevalence in highly stereoselective AAA reactions.[49]

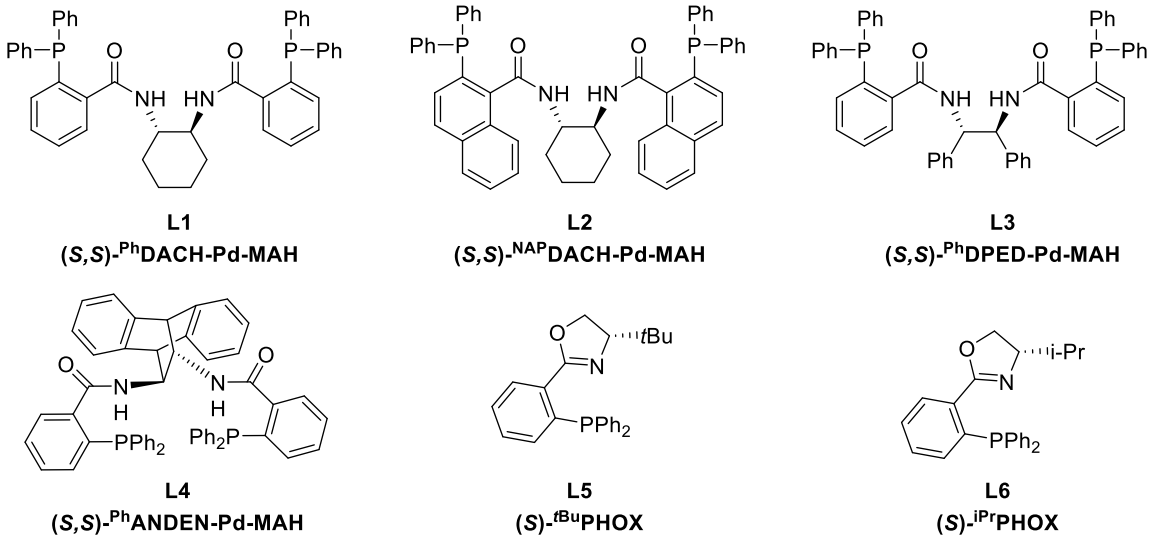

Figure 3.2. Chiral ligands used for the synthesis of single-component Pd^0 precataysts.

Preliminary investigations were conducted by monitoring the reactivity of ^{DMP}DAB–Pd–MAH with a slight excess of chiral ligand (1.05 equiv) at room temperature. Consumption of ^{DMP}DAB–Pd–MAH is observed in less than ten minutes by ^{1}H NMR spectroscopy, along with a visual colour change from purple/red to clear yellow. This reveals exceptionally rapid and efficient ligand displacement with all six ligands. Encouraged by these preliminary results, we then successfully isolated six stable palladium(0) precatalysts (**3.1**-**3.6**) via simple 1-to-1 combinations of ^{DMP}DAB–Pd–MAH and chiral ligands on preparative scale, followed by a simple trituration/decantation process to remove the ^{DMP}DAB by-product. Isolated yields for these complexes are between 63-90% (Figure 3.3). To the best of our knowledge, Pd^0 complexes **3.1**-**3.4** are the first isolable examples of well-defined, characterized, single-component palladium complexes featuring Trost-type ligands with the desired κ^2-P,P coordination mode. The feasibility of these isolations is likely due to easy removal of the ^{DMP}DAB by-product, and stabilization of Pd^0 arising from the strong synergestic bonding between MAH and the Pd^0 centre.

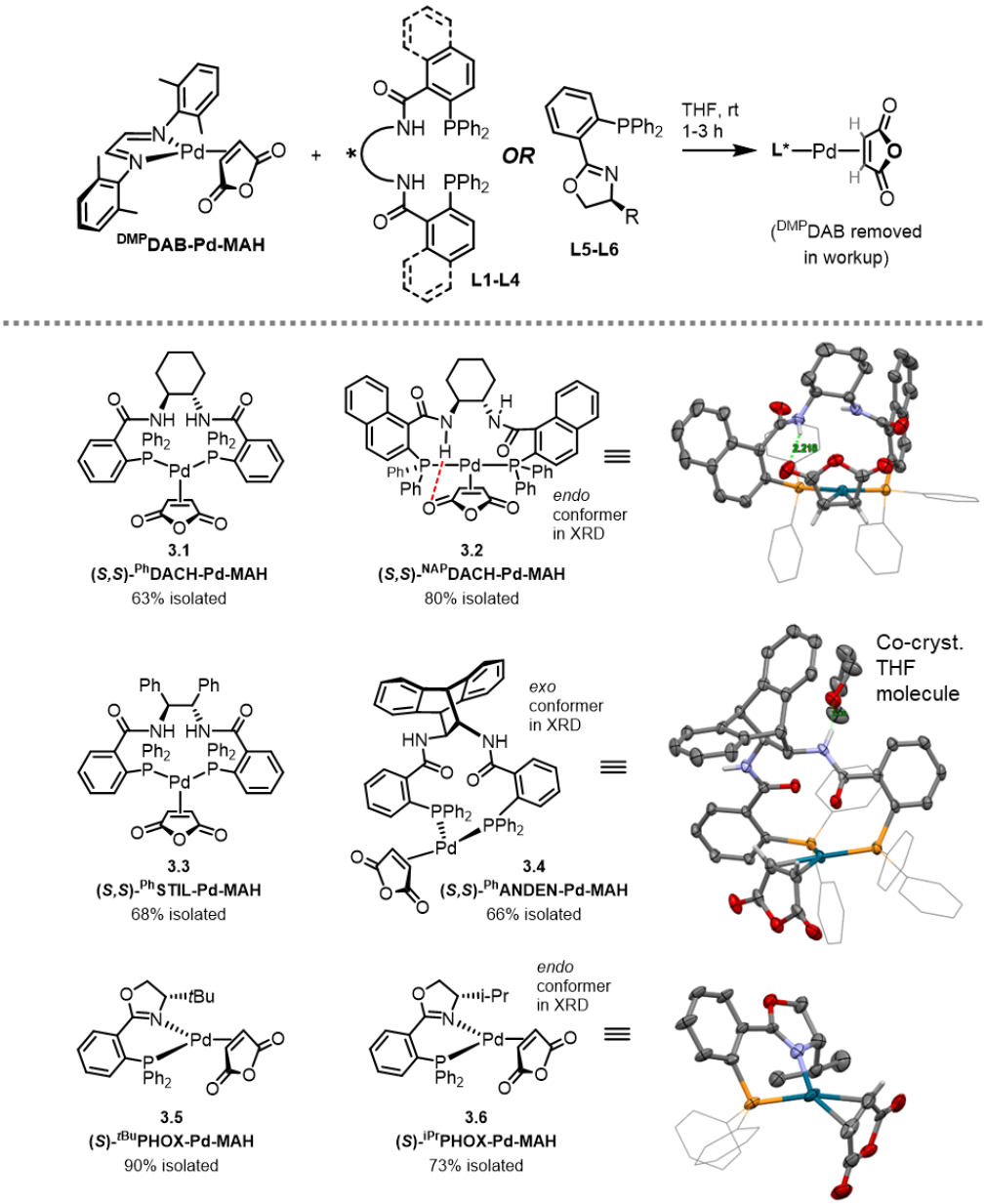

Figure 3.3. Synthesis of chiral Pd^0 precatalysts **3.1**-**3.6** via ligand substitution of ^{DMP}DAB–Pd–MAH. Solid-state molecular structures (X-ray diffraction, 50% probability ellipsoids, Ph groups on phosphorus shown in wireframe for clarity) shown for compounds **3.2**, **3.4**, and **3.6**; Intramolecular H-bond in **3.2** indicated with green dashed line, N–H---O distance = 2.22 Å.

We have successfully obtained solid-state molecular structures by single crystal X-ray crystallography for three complexes, including **3.2**, **3.4**, and **3.6** (Figure 3.3). The structures of **3.2** and **3.4** are the first solid-state molecular structures of monomeric single-

component Pd complexes based on the Trost-type ligand framework that retain intact N–H bonds in the ligand backbone. Notably, two distinct conformations are observed in the solid-state molecular structures of **3.2** and **3.4**. In complex **3.2**, the MAH ligand binds in an *endo* conformation, leading to close proximity between the carbonyl groups of MAH and the chiral tether of the ^{NAP}DACH ligand (**L2**). This results in an intramolecular hydrogen bond between the O of an MAH carbonyl group and an amide N–H in the chiral tether. A similar hydrogen-bonding interaction in related Pd systems has been proposed based on extensive studies by Lloyd-Jones and co-workers involving NMR spectroscopy, isotopic labelling, and computational studies.[50] One amide N–H in the chiral scaffold is directed toward a carbonyl group of an allylic ester substrate. The resulting hydrogen bond is proposed as a directing influence in the mechanism for inducing stereoselectivity in AAA reactions catalyzed by Pd systems with Trost-type ligands (Figure 3.4).

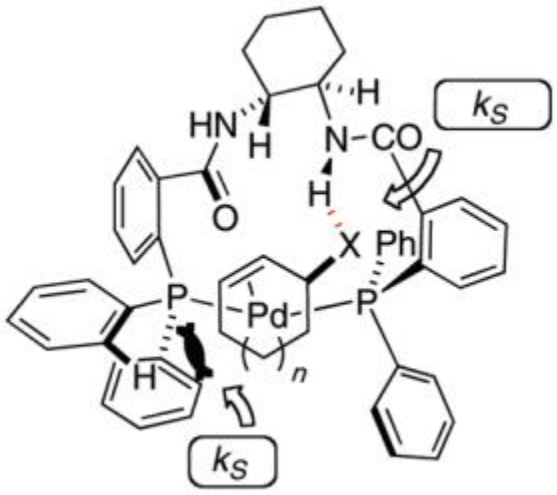

Figure 3.4. A reported hydrogen-bonding interaction between one N–H of **L1** and a substrate (X=OAc).

In contrast, the molecular structure of complex **3.4** adopts an *exo* conformation in the solid state, with the carbonyl groups of MAH pointing away from the chiral tether of the ligand. This prevents intramolecular hydrogen bonding between the N–H groups and the coordinated MAH. However, we do observe an intermolecular hydrogen bond between an amide N–H and a co-crystallized THF molecule (Figure 3.5A). This hints at solvent

playing a role in determining the preferred conformer (Section 3.3.2). During the X-ray crystallography analysis of complex **3.4**, crystals of a [PNNP]Pd^{II} oxidation by-product containing **L4** were also analyzed. These crystals were part of the same sample that contained **3.4**, indicating some degree of oxidative decomposition for complex **3.4** when exposed to air (Figure 3.5B). In addition to the Trost-type complexes, we also successfully obtained the solid-state molecular structure of complex **3.6**, which displays an *endo* conformation with respect to the MAH and the isopropyl groups of **L6**.

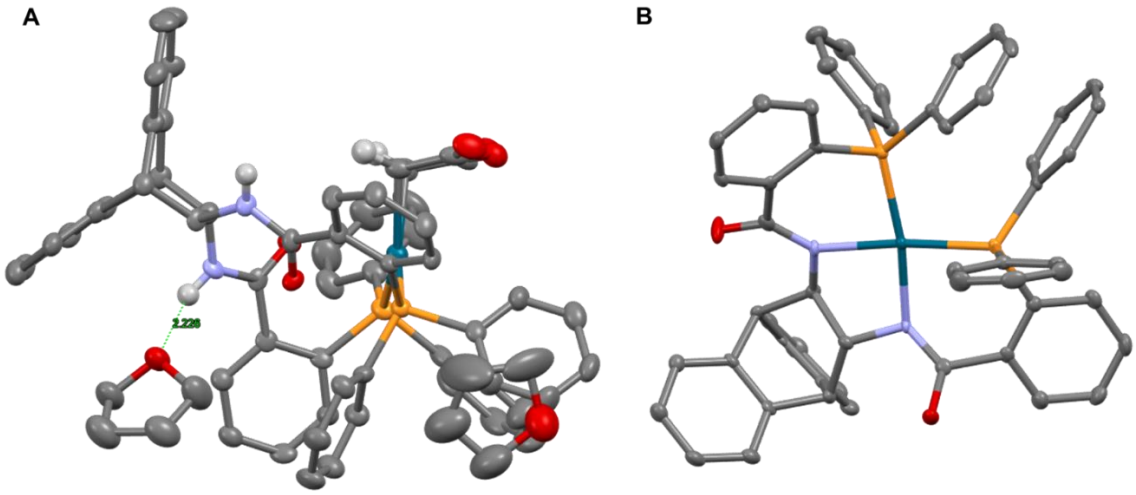

Figure 3.5. A: Expansion of the solid-state molecular structure of complex **3.4** with co-crystallized THF molecules. Intermolecular H-bond in **3.4** between amide N–H and THF molecule indicated with green dashed line, N–H---OTHF distance = 2.226 Å; **B**: Solid-state molecular structure of [PNNP]Pd^{II} oxidation by-product containing **L4 (**X-ray diffraction, 50% probability ellipsoids**)**.

3.3.2 Solution-State Characterization and Computational Studies

In addition to characterization of three complexes by single crystal X-ray crystallography, all six complexes (**3.1-3.6**) have been fully characterized by multinuclear NMR spectroscopy and high-resolution mass spectrometry (HRMS). Based on the data obtained from NMR spectroscopy, two distinct conformers – assigned as *endo* and *exo* – are observed in the solution for all six precatalysts. For complex **3.1**, two sets of phosphorus signals are observed by $^{31}P\{^{1}H\}$ NMR spectroscopy, with a 14:1 ratio between the major and minor species in d_8-THF, and a 55:45 ratio in d_2-DCM. Each signal set is a matching pair of doublets, which is characteristic of a bidentate κ^2-P,P coordination to Pd with two

inequivalent phosphines that couple to one another (Figure 3.6A). We assign these two species as the **3.1-*exo*** (major) and **3.1-*endo*** (minor) conformers; a detailed discussion of this assignment follows below.

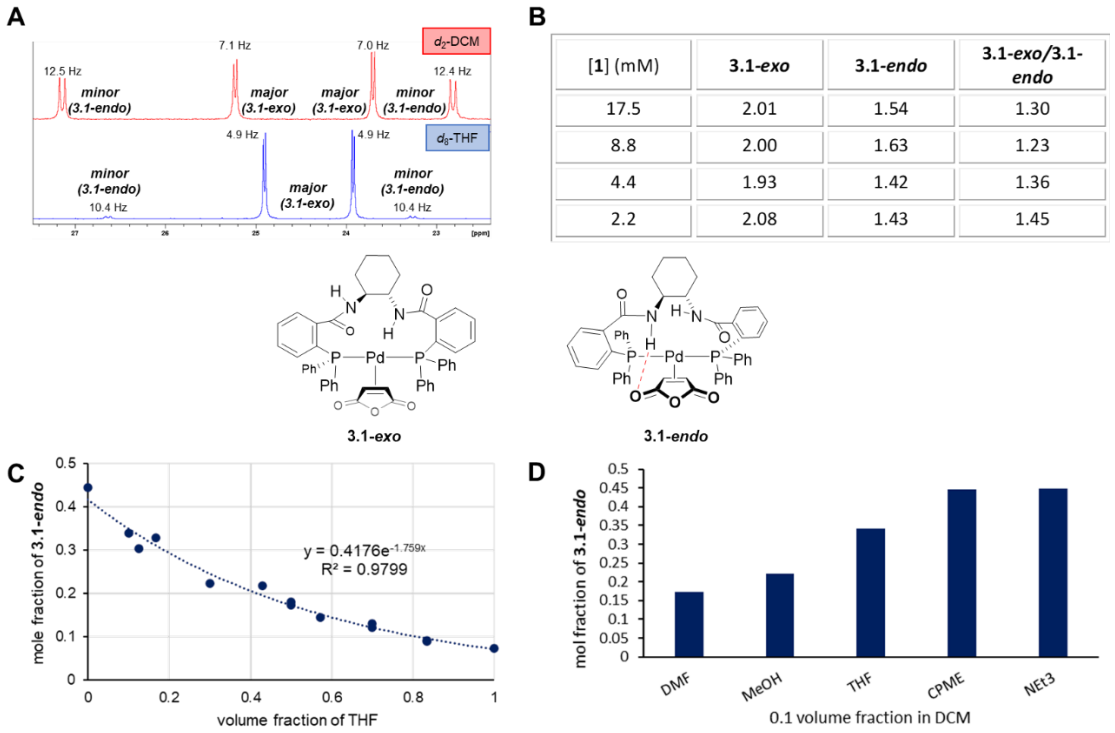

Figure 3.6. A: ^{31}P NMR spectra of complex **3.1** in d_2-DCM and d_8-THF, revealing two conformers (**3.1-*exo*** and **3.1-*endo***), with coupling constant values corresponding to $^3J_{P\text{-}P}$ coupling; **B**: Peak integrations and integration ratio of the two conformers in ^{31}P NMR spectra with sample concentration dilution in DCM; **C**: Mole fraction of minor conformer (**3.1-*endo***) versus volume fraction of THF in DCM, which follows an exponential correlation (equation and R^2 value given); **D**: Mol fraction of minor conformer (**3.1-*endo***) versus 10% various solvents in DCM.

While we failed to obtain a crystal structure of complex **3.1** after multiple recrystallization attempts, we conducted a series of solution studies to better understand the conformational behaviour of this complex. To begin with, we wanted to rule out dimerization/oligomerization as a possible explanation for observing multiple species. Monitoring the peak area ratio of the two signals by $^{31}P\{^1H\}$ NMR spectroscopy at different sample concentrations reveals no significant change (Figure 3.6B). This rules out the possibility of dimer/monomer equilibrium, as the amount of potential dimeric species should decrease with lower concentration.

Since the ratio of these two conformers is clearly dependent on solvent composition, we also investigated the relationship between conformer ratio and the ratio of DCM to THF. As the proportion of THF in the solvent mixture increases from 0% to 100% (v/v), the mol fraction of the minor conformer decreases smoothly from 0.44 to 0.07, following an exponential trend (Figure 3.6C). The two edge values at 0% THF and 100% THF are highly consistent with the independently observed ratios in d_2-DCM and d_8-THF. Furthermore, considering the strong solvent dependence of these two conformers and distinct solid-state molecular structures obtained for complexes **3.2** and **3.4**, we propose the two conformers observed in the solution of complex **3.1** to be analogous to the solid-state structures of **3.2** (minor, *endo*) and **3.4** (major, *exo*). With increasing volume fraction of THF, the *exo* conformer would be further stabilized by intermolecular hydrogen bonding to the solvent (as observed in the crystal structure of **3.4**).

To further test this hypothesis, a study of conformer ratio of complex **3.1** with varying polarity of co-solvents (90% DCM and 10% co-solvent, v/v) has been performed (Figure 3.6D). Compared to 10% THF (0.34 mol fraction **3.1-*endo***), mol fractions of the minor conformer in solvents with stronger hydrogen-bond accepting properties—DMF and methanol—are lower (0.17 and 0.22 respectively), while the addition of weakly hydrogen bond accepting solvents (CPME and NEt_3) result in identical conformer ratios to 100% DCM (0.45 mol fraction **3.1-*endo***). The decreasing amount of the minor conformer with better hydrogen bond accepting solvents supports the assignment of **3.1-*endo***, where the intramolecular hydrogen bonding is interrupted by stronger N–H hydrogen bonding to the polar (co-)solvent in **3.1-*exo***.

If hydrogen bonding involving a ligand N–H group is present, this should be evident in ^{1}H NMR spectroscopy of **3.1**. In d_8-THF, given the large proportion of the major conformer, the amide protons are assigned to peaks at 7.82 and 8.06 ppm, based on 2D COSY correlations with the methine cyclohexyl protons. With this in mind, one correlation between an amide N–H (7.82 ppm) and one vinyl proton on the coordinated MAH (4.08 ppm) is observed in the 2D NOESY NMR spectrum. This supports the assignment of an ***exo*** conformation as the major species in THF: in **3.1-*exo***, the carbonyl groups of coordinated MAH point away from the chiral tether (Figure 3.7A). We do not observe a

NOESY correlation for the second pair of N–H/C=C–H, though this consistent with the analogous structure of **3.4**: the two N–H bonds point in opposite directions, with one pointing away from the Pd center, while the other is directed toward the coordinated MAH. This would lead to only one N–H/C=C–H through-space NOESY correlation.

To further establish the conformer assignments, we have also analyzed 2D NMR spectra in d_2-DCM, where we see a 55:45 ratio of **3.1-*exo*** to **3.1-*endo***. Peak assignment for the N–H protons in d_2-DCM is more complicated than in d_8-THF due to the presence of both conformers and overlapping signals in the aromatic region of the ^{1}H NMR spectrum. The amide protons for each conformer are assigned based on their COSY correlations with methine protons on the cyclohexyl rings, enabling location of all four signals (Figure 3.7B). The N–H protons of the major **3.1-*exo*** conformer are assigned to the peaks at 6.14 ppm and 7.86 ppm, and those of the minor **3.1-*endo*** conformer are at 6.74 ppm and 7.09 ppm (overlapping with aromatic signals). The MAH vinyl protons are assigned based on correlations in the ^{1}H-^{31}P HMBC spectrum. Both conformers have an overlapping signal for one MAH proton at 4.45 ppm; however, there are two resolved signals for the second MAH proton at 4.02 ppm (major) and 3.97 ppm (minor)

Importantly, we observe only one through-space correlation between an N–H and an MAH proton in the ^{1}H-^{1}H NOESY spectrum of **3.1** in d_2-DCM. This is between the amide N–H at 6.14 ppm and the MAH C=C–H at 4.02 ppm, both of which correspond to the major conformer (Figure 3.7C). Since this through-space correlation is consistent with the geometry of **3.1-*exo***, this confirms our assignment of **3.1-*exo*** as the major conformer, and **3.1-*endo*** as the minor. In addition, we observe exchange correlations (same phase) between all four amide protons of **3.1-*exo*** and **3.1-*endo*** in the NOESY spectrum. This indicates that **3.1-*exo*** and **3.1-*endo*** interconvert in solution.

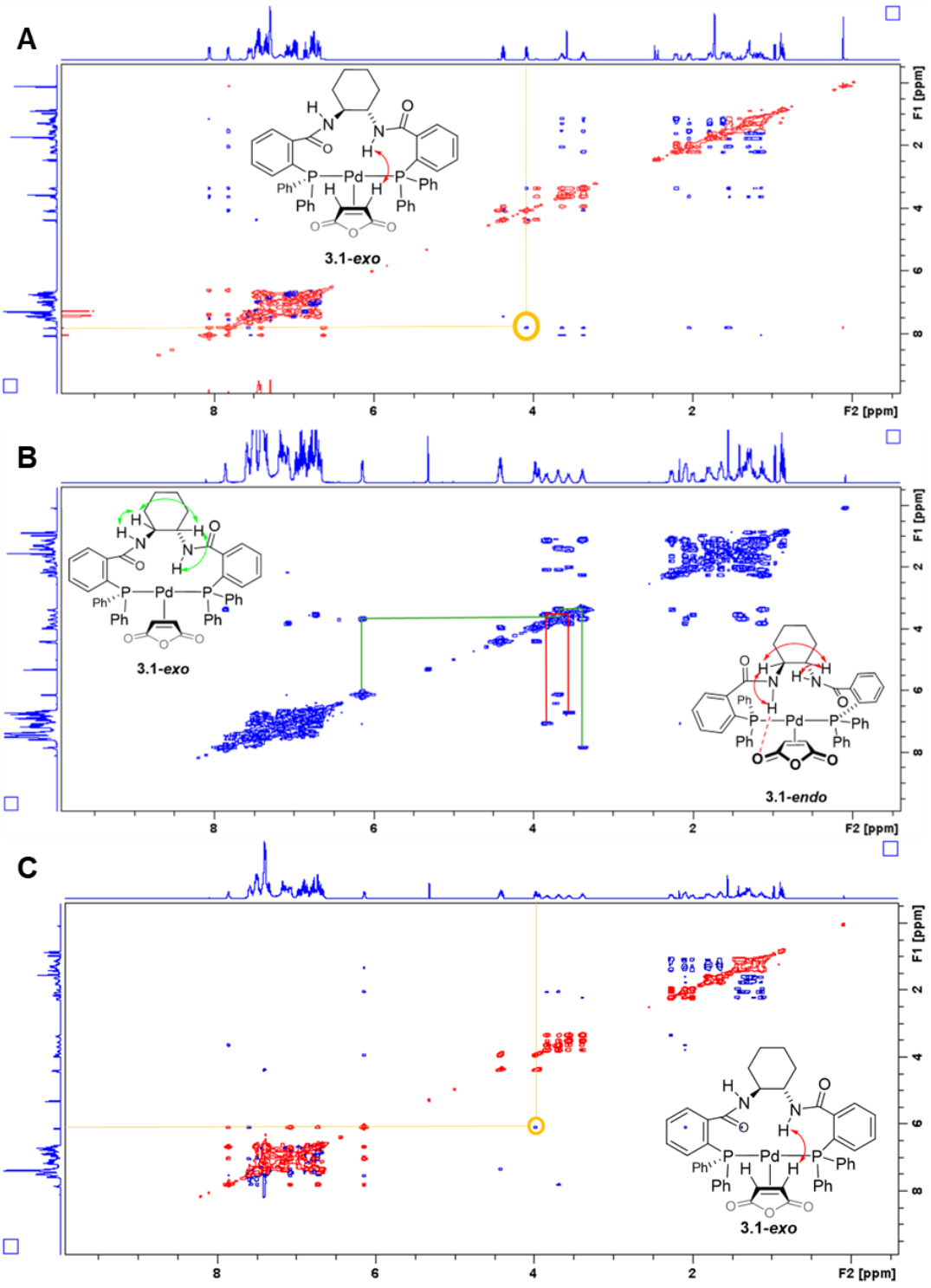

Figure 3.7. A: ^{1}H-^{1}H NOESY NMR spectrum of complex **3.1** in d_8-THF showing a correlation between an N–H of the chiral tether and MAH–H (circled in orange). **B**: ^{1}H-^{1}H COSY NMR spectrum of complex **3.1** in d_2-DCM. Pair matching is assisted by the correlations of the cyclohexyl protons of the same conformer highlighted in green/red (green: major conformer, red: minor conformer). **C**: ^{1}H-^{1}H NOESY NMR spectrum of **3.1** in d_2-DCM, revealing a correlation between N–H and MAH–H of the major conformer (circled in orange).

Relative to the chemical shift of N–H in the free ligand **L1** (6.37 ppm in a ^{1}H NMR spectrum in $CDCl_3$), the amide proton peaks of **3.1** generally shift downfield in both solvents. As a relatively polar solvent, THF can have increased intermolecular hydrogen-bonding interactions with amide protons of the major conformer, which would result in significantly deshielded N–H and higher chemical shifts. We do observe this, with the N–H signals at 7.82 and 8.06 ppm. In contrast, one of the N–H signals for **3.1-*exo*** in d_2-DCM is upfield shifted (6.14 ppm) relative to the free ligand. This is the N–H that is located within the chiral pocket, near the MAH ligand (based on NOESY correlations). The other N–H, which presumably points away from the Pd center and therefore is solvent accessible, is downfield shifted (7.86 ppm). For the minor **3.1-*endo*** conformer, both N–H signals are downfield shifted, though to a lesser extent (6.74 ppm and 7.09 ppm). One of these is presumably hydrogen bonding to an MAH carbonyl, and the other is solvent accessible, both of which would shift the signals downfield. While other factors may also contribute to the degree of N–H shielding, these relative chemical shifts are consistent with the proposed conformer structures.

Lastly, we performed DFT calculations to support these conformer assignments. This part was conducted by Jingru Lu, one of the co-authors of this project. CPCM implicit solvation models were used to calculate the relative electronic energies of **3.1-*exo*** and **3.1-*endo*** conformers (RI-B2PLYP-D3BJ/def2-TZVP//RI-BP86-D3BJ/def2-SVP, with def2-TZVP/C and def2/J auxiliary basis sets for the RI part, respectively) (Figure 3.8).[51] In gas phase calculations, both conformers exhibit an intramolecular hydrogen bond between the amides, and the **3.1-*endo*** conformer has an additional hydrogen bond between an amide N–H and the MAH, as observed in the solid-state molecular structure of **3.2**. This contributes to the **3.1-*endo*** conformer being 10.5 kJ mol^{-1} more stable than **3.1-*exo***. However, the energies calculated for **3.1-*exo*** and **3.1-*endo*** in implicit DCM solvent are very close, with **3.1-*exo*** only slightly more stable (0.5 kJ mol^{-1} difference). To compare energies in THF, we used both the CPCM implicit model and included one explicit THF molecule. In **3.1-*exo***, this THF hydrogen bonds to a ligand N–H, as observed in the solid-state molecular structure of **3.4**. This leads to **3.1-*exo*** being 6.3 kJ mol^{-1} more stable. These calculations support not only the assignment of **3.1-*exo*** as the major conformer in THF, but also exhibit the same solvent effect trend as our spectroscopic observations.

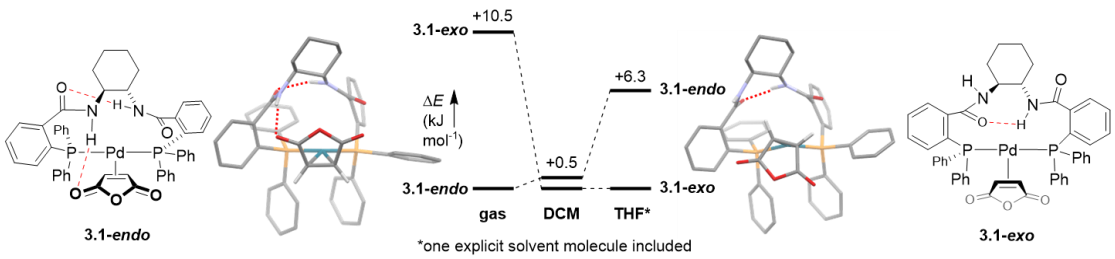

Figure 3.8. Calculated structures of **3.1-*endo*** and **3.1-*exo*** (gas phase geometry shown), with relative free energies in the gas phase, DCM, and THF (implicit solvation models; one explicit THF molecule included in THF-solvation calculations for both conformers).

An analogous study of the solution behaviour of **3.3** revealed that two conformers are also present. The $^{31}P\{^{1}H\}$ NMR spectrum of **3.3** in d_8-THF reveals a similar pattern of two sets of doublets to that of **3.1** (Figure 3.9A); however, an approximately 3:1 major-to-minor conformational ratio is observed, in contrast to the 14:1 ratio of **3.1** in the same solvent. This difference may be attributable to a greater degree of rotational freedom of the chiral linker in **L3**.[52] To confirm the structures of these two conformers, we conducted another comprehensive NMR spectroscopy characterization for this complex. MAH–H protons for each conformer are first assigned according to their long range P–H correlations with the phosphorus atoms of **L3** in the ^{1}H-^{31}P HMBC spectrum (Figure 3.9B). Then, the methine protons on the chiral tether were identified based on their chemical shifts (between 5.1-5.6 ppm). Based on the assignment of these C–H protons, we are able to assign the amide N–H protons based on through-bond correlations in the ^{1}H-^{1}H COSY spectrum (Figure 3.9C). All four amide protons are deshielded (>7.4 ppm), implying they are all engaged in some degree of hydrogen bonding.

Consistent with **3.1**, only one through-space correlation between an N–H (8.06 ppm) and an MAH–H (4.27 ppm) is observed in the ^{1}H-^{1}H NOESY spectrum. This correlation is between two signals corresponding to the major conformer, confirming that **3.3-*exo*** is the major conformer (Figure 3.9D). Moreover, we again observe exchange correlations between all four amide protons, confirming conformer interconversion in solution. In consideration of these NMR spectroscopy results and the similarity between **3.1** and **3.3**, we propose the major and minor conformers to be **3.3-*exo*** and **3.3-*endo***, respectively.

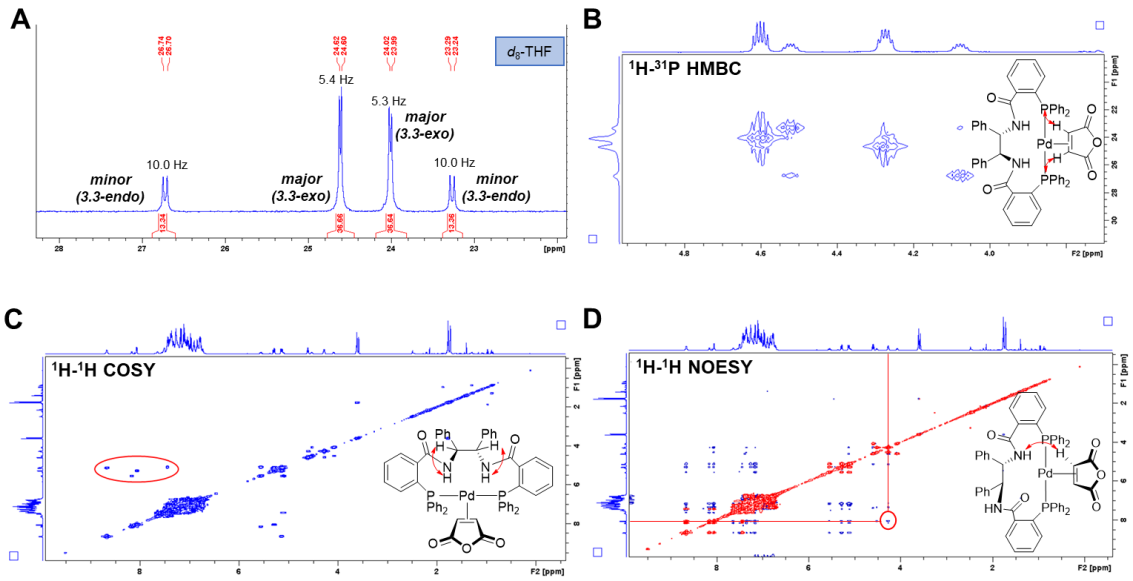

Figure 3.9. A: Expanded $^{31}P\{^1H\}$ NMR spectrum of **3.3** in d_8-THF. **B**: ^{1}H-^{31}P HMBC spectrum of **3.3** showing correlations between MAH–H and P. **C**: ^{1}H-^{1}H COSY spectrum of **3.3** with correlations circled between amide protons and linkage CH. **D**. ^{1}H-^{1}H NOESY spectrum of **3.3** showing a correlation between an N–H and MAH–H is observed in the major conformer (red circle).

As stated above, conformational interconversion is observed in the NOESY spectra of both **3.1** and **3.3**. This phenomenon is more apparent in complex **3.2,** which exhibits broad signals in all NMR spectra obtained at room temperature. Two broad signals at 23.2 and 22.8 ppm are observed in the $^{31}P\{^1H\}$ NMR spectrum with a 47:53 peak area ratio (Figure 3.10A). Amatore and co-workers have reported broad signals for a few **L2**-ligated Pd^{II} complexes, which they attributed to reversible ligand dissociation or oxidative addition ionization.[47] Given the low possibility of MAH dissociation and the absence of any exogenous ligands, we hypothesize that **3.2** undergoes reversible conformational exchange between ***endo*** and ***exo*** conformers.

To explore this hypothesis, we performed variable temperature (VT) NMR experiments by monitoring the ^{1}H and $^{31}P\{^1H\}$ NMR spectra of **3.2** in a solvent with a high boiling point (d_8-toluene) at both high and low temperatures. Data collected from $^{31}P\{^1H\}$ NMR spectra are more informative for conformational identification owing to considerably fewer signals relative to ^{1}H NMR spectra. The chemical shifts of **3.2** in VT experiments at room temperature slightly differ from those in Figure 3.10A (d_8-THF), due to use of a

different deuterated (d_8-toluene). As temperature increases from room temperature to 60 °C, the relatively tall peak becomes broader and shorter, and the two peaks begin to coalesce at the highest temperature investigated (Figure 3.10B); upon returning to room temperature, the spectrum regains the same features as the initial room temperature spectrum. This is consistent with our conformer exchange hypothesis, though due to instrument limitations we could not acquire spectra at higher temperatures.

In the low-temperature VT experiment, an increasing number of conformers is observed when decreasing the temperature from room temperature to -80 °C (Figure 3.10C). Based on the number of signals and peak integrations, at least three conformers are present at -80 °C, assuming each conformer would have two inequivalent phosphines (Figure 3.10D). Here we rule out the possibility of a monoligated bind mode with **L2** as proposed by Amatore and co-workers for a Pd^0 system, because all chemical shifts at -80 °C are significantly downfield from that of free **L2** (-12.7 ppm). The peak areas of these signals reveal that the three conformer pairs are peaks at 24.7 and 23.5 ppm, 23.3 and 22.0 ppm, and 20.3 and 13.9 ppm. Analogous to complex **3.1**, we assign the two pairs at higher chemical shifts to be **3.2-*endo*** and **3.2-*exo***, but the conformational structure of the new pair remains elusive. It is possible that an additional conformer exists due to restricted rotation within the macrocyclic chelate, imparted by the bulkier naphthyl linker units. As for the prior VT experiment, returning the sample to room temperature gives the same spectrum as that acquired before temperature variation.

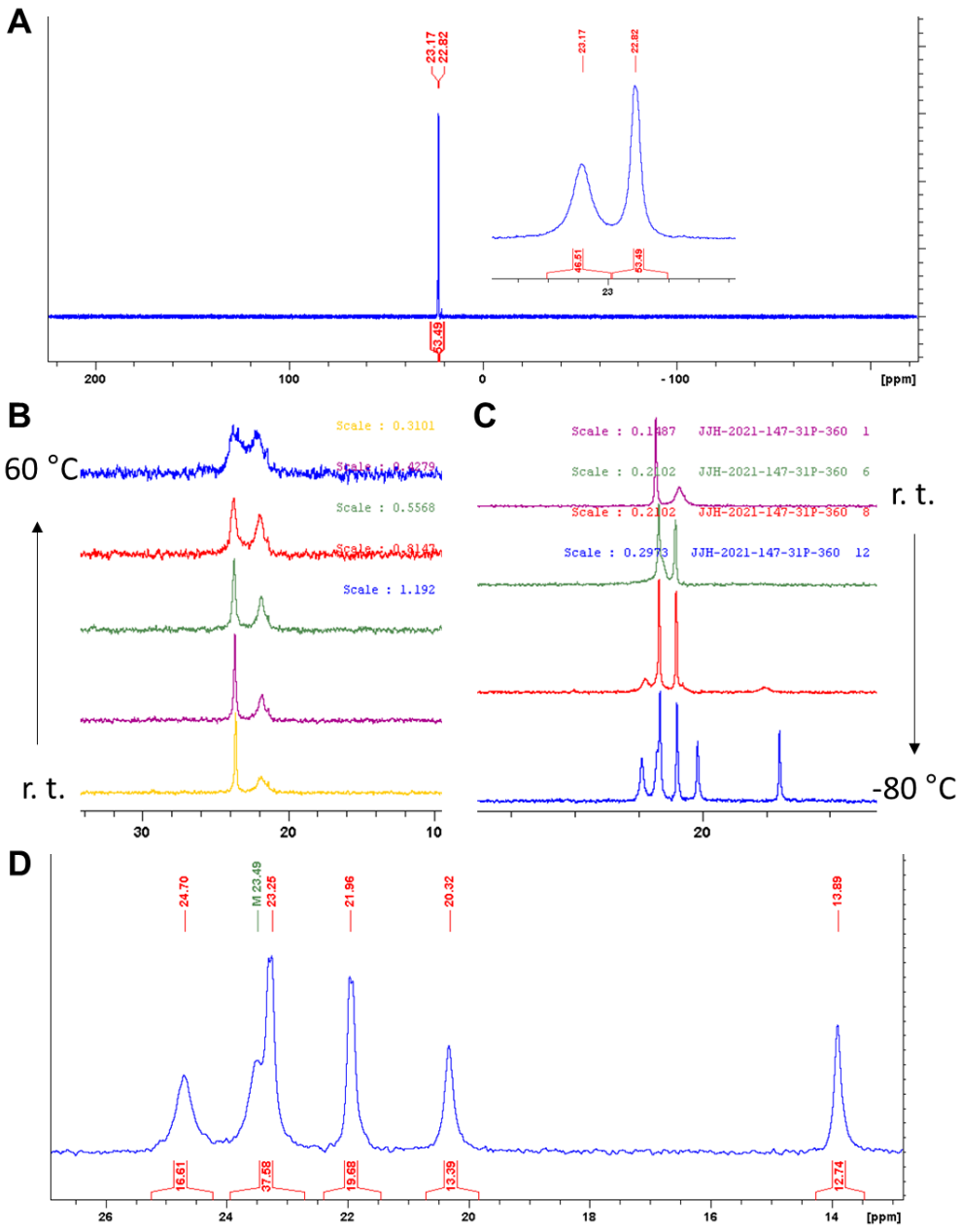

Figure 3.10. A: Expanded $^{31}P\{^{1}H\}$ NMR spectrum of **3.2** in d_8-THF. **B**: Selected $^{31}P\{^{1}H\}$ NMR spectra (d_8-Toluene) of **3.2** in a temperature-increasing VT experiment. **C**: Selected $^{31}P\{^{1}H\}$ NMR spectra (d_8-Toluene) of **3.2** in a temperature-decreasing VT experiment. **D**: Expansion of the $^{31}P\{^{1}H\}$ NMR spectrum of **3.2** obtained at -80 °C.

Notably, two distinct conformers are also detected in the PHOX-type complexes **3.5** and **3.6**, with nearly 1:1 ratios in the ^{1}H and $^{31}P\{^{1}H\}$ NMR spectra. This ratio is consistent in both d_2-DCM and d_8-THF. Here, we attribute this solvent-independent

solution behaviour to the presence of ***exo*** and ***endo*** conformers with respect to the relative orientation of the MAH anhydride unit and the alkyl group on the oxazoline. Based on the NMR data, there is no clear energetic preference for either of them,[30,37] though the solid-state molecular structure of **3.6** is ***endo*** (Figure 3.3). The presence of the ***exo*** conformer is also evident by the correlation between an MAH vinyl proton and a *tert*-butyl proton of **L5** in the 2D NOESY spectrum of complex **3.5** (Figure 3.11).

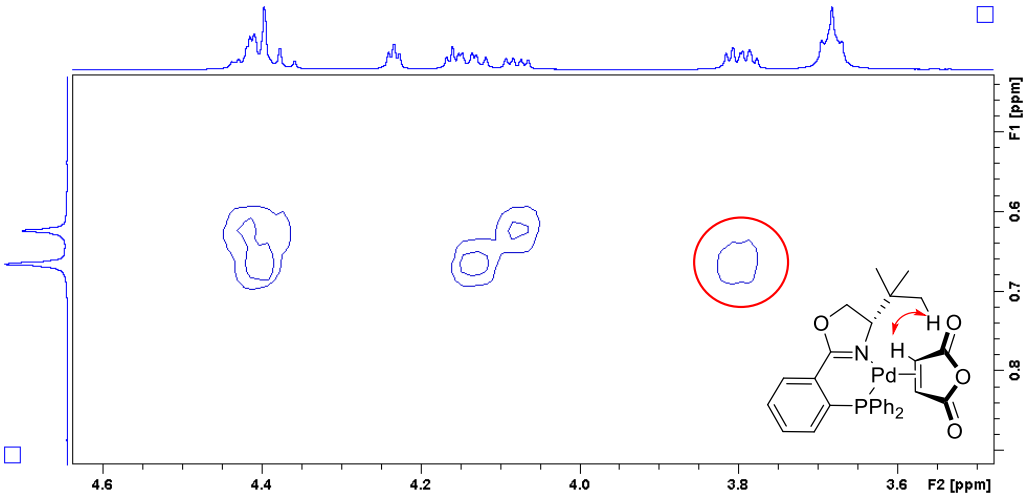

Figure 3.11. ^{1}H-^{1}H NOESY NMR spectrum of **3.5**. The correlation between MAH–H and CH_3 indicates the ***exo*** conformer is present.

3.3.3 Precatalyst Stability Evaluation

To evaluate the reliability and compatibility of these complexes as precursors for AAA reactions, we first needed to test their stability as solids and in solution. For Trost-type complexes, we took **3.1**, the precatalyst containing a representative ^{Ph}DACH Trost ligand (**L1**), as the model to evaluate the stability of this precatalyst class. As a solid, **3.1** is indefinitely stable as a solid when stored under N_2 at room temperature (2 years thus far). Furthermore, to assess its stability under an atmosphere of air, a small amount of complex **3.1** was exposed to the air for a few minutes, and subsequent ^{1}H and ^{31}P{^{1}H} NMR spectra were obtained after the sample was in a sealed vial for 1 week and 4 weeks. Less than 4% and 6% area of new signals were observed in ^{31}P{^{1}H} NMR spectra, respectively. This reveals reasonable stability of complex **3.1** as a solid in the air; certainly enough to

weigh/handle the solid precatalyst prior to experiments. For the PHOX-type complexes, **3.5** and **3.6** are very stable as solids under air, as the purification and isolation procedures were conducted on the bench.

In addition to solid-state stability, we also estimated solution stability of all six precatalysts in THF by monitoring concentrations over time by ^{31}P NMR spectroscopy (Figure 3.12A). With solutions prepared and stored in a glovebox, the concentrations remain unchanged over this period, revealing robust solution stability under N_2. The aforementioned [**L1**]Pd(dba) can be rapidly converted to [PNNP]Pd^{II} when exposed to the air, and we also observed the oxidation by-product [PNNP]Pd^{II} observed in complex **3.4**, prompting us to investigate the stability of Trost-type precatalysts under air. Thus, we also exposed a solution sample of **3.1** in THF to the air for a few seconds and monitored the concentrations of **3.1** over the same period. From acquired ^{31}P NMR spectra, there is only slow decomposition of **3.1**, with more than 80% remaining after 48 hours. We do observe the formation of [PNNP]Pd^{II}, which comprises the mass balance with respect to P-containing species.

To have a fair comparison with the reported [**L1**]Pd(dba), we also assessed its solution stability under air and N_2 (Figure 3.12B). Concentrations of [**L1**]Pd(dba) remain almost the same under N_2 during this period, while more than 50% of it decomposes after only 30 minutes, converting to by-product [PNNP]Pd^{II}. Notably, the conversion to [PNNP]Pd^{II} is complete within 18 hours. The odd concentration trend observed in the formation of [PNNP]Pd^{II} is due to its poor solubility in THF: the complex is observed to precipitate during this time. Overall, this evaluation means that precatalysts **3.1**-**3.6** can be handled and used without the need for a glovebox or inert atmosphere. In fact, all catalytic evaluations were carried out by weighing the precatalysts under air (Section 3.3.4).

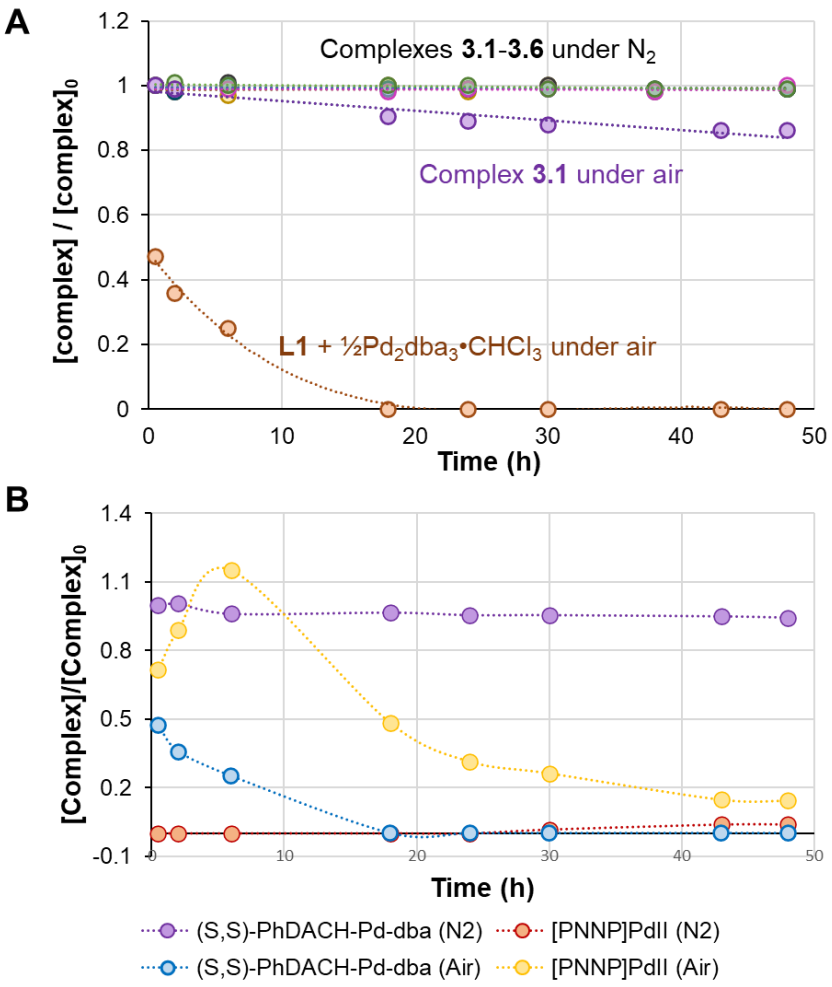

Figure 3.12. A: Concentration versus time plot for complexes **3.1**-**3.6** in THF under N_2 over 48 h, showing no decomposition over at least 48 h, as well as complex **3.1** and **L1** + $Pd_2(dba)_3$•$CHCl_3$ under air. **B:** Concentration versus time plot for **L1** + $Pd_2(dba)_3$•$CHCl_3$ in THF under N_2 and air over 48 h, showing the decomposition of [**L1**]Pd(dba) and formation of [PNNP]Pd^{II}.

3.3.4 Catalytic Evaluation in AAA Reactions

The catalytic evaluation of these precatalysts was performed by Thomas Keenan and Francois Richard at Queen Mary University of London. To demonstrate the potential of complexes **3.1**-**3.6**, we applied them to 9 distinct Pd-catalysed AAA reactions. The new precatalysts compared favourably with traditional catalytic systems, maintaining or improving enantioselectivity while enabling lower catalyst loadings in all cases (Figure 3.13). In addition, the single-component precatalysts **3.1**-**3.6** give perfect control of the Pd-

to-L ratio and circumvent the standard pretreatment protocols needed to ensure complete ligand metalation. We further demonstrate excellent reactivity at one of the lowest reported catalyst loadings for a Trost-type catalyst system. This was achieved in the unprecedented enantioselective allylation of a hydantoin derivative (Figure 3.14). The discovery and optimization of this new reaction were enabled by microscale array-based experiments, to which our precatalysts are ideally suited. Overall, the selectivity, activity, stability, and practicality of the single-component precatalysts make them powerful and attractive alternatives to established *in situ* procedures. As this work was completed by our collaborators, only three representative comparisons and the screening/optimization of the hydantoin allylation are included in this thesis.

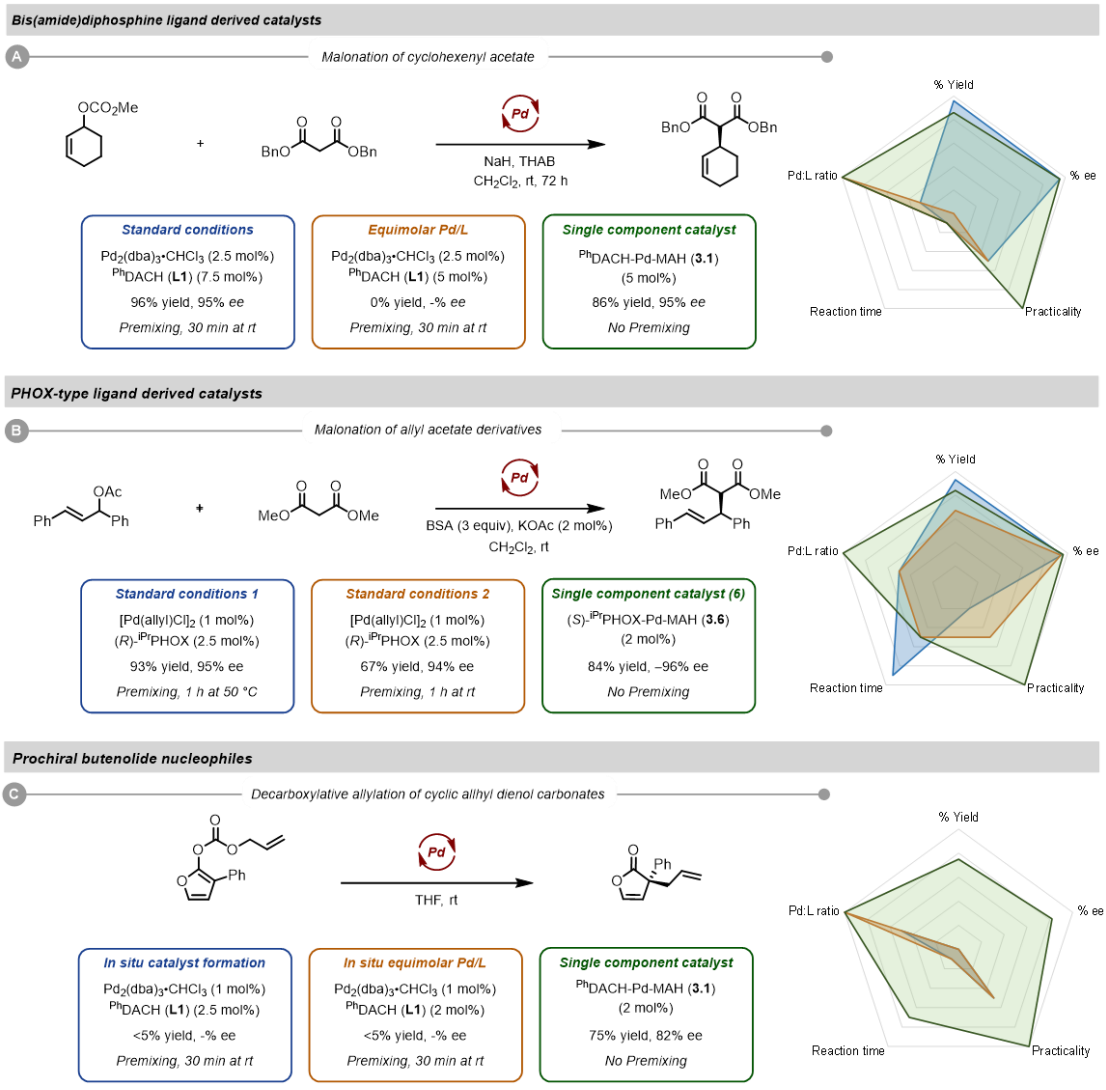

Figure 3.13. Representative examples of comparing our precatalysts to in situ systems for challenging AAA reactions.

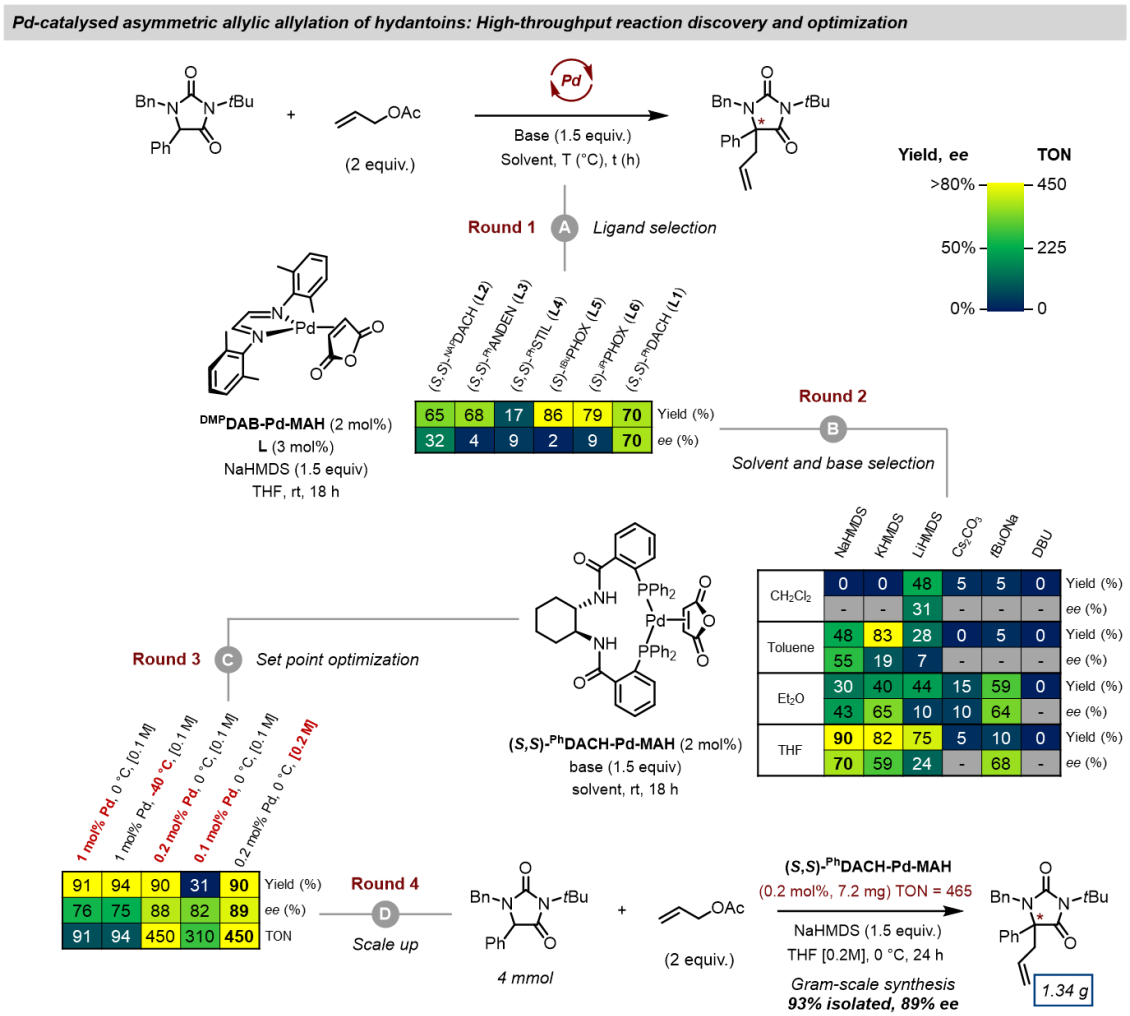

Figure 3.14. Application of MAH-based Pd precatalysts in reaction discovery and optimization for the asymmetric allylation of hydantoin derivative at low Pd loading.

Given the excellent performance of these precatalysts, it is important to understand the catalyst activation mechanism. A generally accepted catalytic cycle for Pd-catalyzed AAA reactions involves an oxidative addition step of LPd^0 active species, generating a cationic Pd^{II} η^3-allyl intermediate, followed by nucleophilic attack to the coordinated allyl.[28] Within this context, we first tested if our precatalysts can generate a cationic Pd^{II} η^3-allyl intermediate with only an allyl electrophile added. However, no consumption of **3.1** was observed after stirring with allyl acetate in THF at room temperature for 1 hour; the subsequent ^{31}P NMR spectrum also reveals that the concentration of complex **3.1** remains unchanged for additional 2 hours (Table 3.1, entry 1). This prompted us to

investigate the effects of other reaction components, such as bases and nucleophiles, on catalyst activation. In the catalytic reactions tested, carbon-based nucleophiles in several systems are generated by using either strong base (e.g. NaH) or soft enolization conditions (e.g. BSA/KOAc), with strong base being pre-mixed with the enolate precursor prior to other substrates, and BSA/KOAc being added along with all other reaction components. All tests were conducted in a similar manner by stirring mixtures at room temperature for 1 hour, followed by ^{31}P NMR spectroscopy analysis. We first examined the effect of these bases by mixing complex **3.1** with only KOAc or BSA with KOAc (Table 3.1, entries 2 and 3), where a catalytic amount of KOAc is often added to generate *N*-trimethylsilylacetamide and Me_3SiOAc.[53] Only 15% of **3.1** is consumed in BSA/KOAc system, with 0% consumption obtained in the one using only KOAc. Notably, **3.1** is completely consumed when only KO*t*Bu is added, which is similar to the outcome observed in the prior catalyst activation investigation of ^{DMP}DAB–Pd–MAH in Chapter 2 (Table 3.1, entry 4).

Table 3.1. Catalyst activation experiments of complex **3.1** with different reagents.

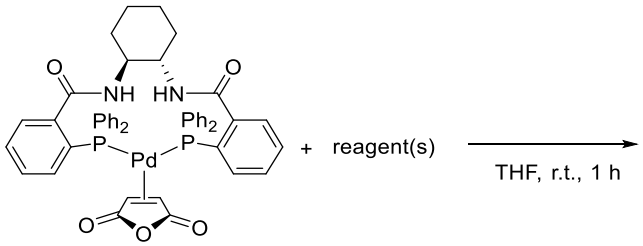

3.1
(*S,S*)-^{Ph}DACH-Pd-MAH

Entry	Reagent	Reagent	Reagent	Consumption of **3.1**
1	2 equiv allyl acetate	–	–	0%
2	2 equiv KOAc	–	–	0%
3	21 equiv BSA	3 equiv KOAc	–	15%
4	2 equiv KO*t*Bu	–	–	100%
5	21 equiv dimethyl malonate	21 equiv BSA	3 equiv KOAc	26%
6	20 equiv dimethyl malonate	20 equiv NaH	–	59%

For catalyst activation investigations with nucleophiles, we used NaH or BSA/KOAc to activate dimethyl malonate, a typical enolate precursor used in AAA reactions (Table 3.1, entries 5 and 6). Approximately 60% of **3.1** is consumed when deprotonating dimethyl malonate with NaH, while the one activated by BSA/KOAc has only 26% consumption. Based on these results, we propose that our precatalysts are most efficiently activated under strongly basic conditions, but further in-depth studies are still needed.

3.4 Conclusions

In sum, we have prepared and characterized a set of bench-stable, chiral palladium(0) precatalysts based on two important ligand classes used in Pd-catalysed AAA reactions. By utilizing the rapid ligand displacement reactivity of our ^{DMP}DAB–Pd–MAH precursor, palladium complexes with Trost-type and PHOX-type ligands can either be generated *in situ* or isolated as single-component precatalysts, providing effective systems for microscale HTE and preparative-scale synthesis. Furthermore, these single-component precatalysts are fully characterized by multinuclear NMR spectroscopy, HRMS and X-ray diffraction studies on three examples, revealing their conformations in solution and in the solid state. All six precatalysts can be utilized in AAA reactions without using a glovebox or inert atmosphere, and more importantly, our Trost-type complexes **3.1**-**3.4** do not suffer from rapid decomposition via oxidation in air.

We also assessed the potential of these precatalysts in multiple Pd-catalyzed AAA reactions. In all cases, our single-component precatalysts compared favourably with traditional catalytic systems, maintaining high enantioselectivity while enabling lower catalyst loadings. Furthermore, a gram-scale application of complex **3.1** in an unprecedented enantioselective allylation of a hydantoin derivative gave a large amount of selective product at the lowest reported catalyst loading. This overall catalytic evaluation demonstrates our precatalysts as excellent precursors for Pd-catalyzed AAA reactions. While preliminary studies indicate strong base is required for efficient catalyst activation, further investigations are needed to better understand these mechanisms under various reaction conditions, with the goal of further lowering the catalyst loading required.

3.5 General Experimental Methods

3.5.1 Synthesis of Single-Component Chiral Catalysts.

These reactions were set up in a glovebox under an inert nitrogen atmosphere due to the potential oxygen-sensitivity of the phosphine ligands. A representative procedure for the synthesis of **3.1** is given here, with specific procedures for all precatalysts given in Appendix A.

A 4 dram (~15 mL) vial was charged with ^{DMP}DAB–Pd–MAH (100.1 mg, 0.21 mmol), **L1** (147.2 mg, 0.21 mmol, 1.0 equiv), anhydrous inhibitor-free THF (4 mL) and a cross-shaped magnetic stir bar. The reaction mixture was stirred at room temperature for 1 h. The solvent was then removed *in vacuo* to give a yellow solid residue. This residue was mixed thoroughly with hexanes/diethyl ether (1:1), followed by decantation of the liquid phase (with or without centrifugation as required). This trituration/decantation process was repeated 5 more times to remove the ^{DMP}DAB by-product as well as any excess phosphine ligand. The solid was then dried in vacuo to give the corresponding single-component chiral catalyst **3.1** as a pale yellow solid (121.0 mg, 63% yield).

^{1}H NMR (500 MHz, THF-d_8) δ 8.06 (d, J = 5.6 Hz, 1H), 7.82 (d, J = 6.3 Hz, 1H), 7.59-6.65 (m, 28H), 4.38 (m, 1H), 4.08 (m, 1H), 3.64 (m, 1H), 3.37 (sept, J = 5.1 Hz, 1H), 2.21 (m, 1H), 2.05 (m, 1H), 1.79 (m, 1H), 1.65-1.53 (m, 2H), 1.33-1.24 (m, 1H), 1.12-1.24 (m, 2H).

^{13}C NMR (125 MHz, THF-d_8) δ 170.6, 170.3, 169.0, 168.0, 143.7, 139.7, 137.7, 136.1, 134.2, 133.9, 133.1, 132.5, 133.0, 129.6, 129.5$_4$, 129.4$_7$, 129.4, 129.3$_2$, 129.2$_8$, 129.0$_4$, 129.0$_0$, 128.7$_3$, 128.6$_9$, 128.6$_6$, 128.2, 128.0, 127.9, 127.8, 127.4, 127.3, 127.0, 126.9, 57.0, 52.4, 32.1, 31.2, 24.8, 23.7.

^{31}P NMR (200 MHz, THF-d_8) δ 24.9 (d, $^{2}J_{P\text{-}P}$ = 4.9 Hz), 23.9 (d, $^{2}J_{P\text{-}P}$ = 4.8 Hz).

Two conformers were observed when 3.1 was dissolved in CD_2Cl_2.

^{1}H NMR (500 MHz, CD_2Cl_2) δ *Major conformer*: 7.86 (d, J = 5.1 Hz, 1H), 7.60-6.65 (m, 56H, Ar–H), 6.14 (d, J = 6.1 Hz, 1H), 4.44-4.39 (m, 1H), 3.99-3.92 (m, 1H), 3.71-3.65 (m, 1H), 3.38 (septet, J = 5.2 Hz, 1H), 2.28-2.24 (m, 1H), 2.12-2.08 (m, 2H), 2.02-1.99 (m,

1H), 1.82-1.76 (m, 2H), 1.67-1.63 (m, 2H), 1.45-1.12 (m, 6H), 1.16-1.10 (m, 2H). *Minor conformer:* 7.60-6.65 (m, 56H, Ar–H), 4.44-4.39 (m, 1H), 3.99-3.92 (m, 1H), 3.87-3.80 (m, 1H), 3.59-3.52 (m, 1H), 2.28-2.24 (m, 1H), 2.12-2.08 (m, 2H), 2.02-1.99 (m, 1H), 1.82-1.76 (m, 2H), 1.67-1.63 (m, 2H), 1.45-1.12 (m, 6H), 1.16-1.10 (m, 2H).

^{31}P NMR (200 MHz, CD_2Cl_2) δ *Major conformer*: 24.5 (d, $^2J_{P\text{-}P}$ = 7.1 Hz), 23.0 (d, $^2J_{P\text{-}P}$ = 7.1 Hz). *Minor conformer:* 26.5 (d, $^2J_{P\text{-}P}$ = 12.0 Hz), 22.1 (d, $^2J_{P\text{-}P}$ = 11.9 Hz).

HRMS (ESI): m/z calc'd for $C_{48}H_{42}N_2O_5P_2Pd$, $[M + Na]^+$ (major isotopomer): 917.1496, found: 917.1510.

3.5.2 Catalytic reactions with single-component precatalysts.

These reactions were set up without use of a glovebox using standard air-free techniques involving nitrogen streams and balloons. As these experiments were carried out by our collaborators, only one representative procedure is given here. This is for the synthesis of 5-allyl-1-benzyl-3-(*tert*-butyl)-5-phenylimidazolidine-2,4-dione (Figure 3.14) using **3.1** as a single-component precatalyst. Specific procedures for all syntheses are given in the Supporting Information of reference 54.[54]

An oven-dried 50 mL round-bottom flask was charged with 1-benzyl-3-(*tert*-butyl)-5-phenylimidazolidine-2,4-dione (1.29 g, 4.00 mmol) and a teflon-coated stirbar. The flask was sealed with a rubber septum and placed under nitrogen atmosphere. THF (14 mL) was added, and the contents cooled to 0 °C. NaHMDS (1 M in THF, 6.00 mL, 6.00 mmol, 1.5 equiv) was added via syringe with stirring, and the mixture was stirred for 1 h at 0 °C. Compound **3.1** was then added as a solid (7.2 mg, 0.0080 mmol, 0.2 mol %), followed by allyl acetate via syringe (0.860 mL, 8.00 mmol, 2 equiv). The mixture was stirred at 0 °C for 24 h, after which time TLC analysis indicated complete conversion. The reaction was quenched with the addition of H_2O (50 mL), followed by extraction with CH_2Cl_2 (3 x 50 mL). The combined organic layers were then washed with 10% wt/wt aqueous citric acid (2 x 50 mL) and brine (50 mL). The organic phase was dried over $MgSO_4$, filtered, and the solvent removed under reduced pressure. The crude product was purified by column chromatography using silica gel and hexane/EtOAc eluent (100:0 to 80:20 v/v) to yield 5-allyl-1-benzyl-3-(*tert*-butyl)-5-phenylimidazolidine-2,4-dione (1.34

g, 93% yield 89% *ee*). Enantiopurity was measured by HPLC using a hexane/isopropanol mobile phase (isocratic 9:1 v/v, 1 mL/min) and a Daicel CHIRALPAK^{TM} IC column (250 x 4.6 mm; 5 μm; 35 °C).

3.6 References

(1) Maier, N. M.; Franco, P.; Lindner, W. Separation of Enantiomers: Needs, Challenges, Perspectives. *J. Chromatogr. A* **2001**, *906* (1), 3–33. https://doi.org/10.1016/S0021-9673(00)00532-X.

(2) Agranat, I.; Caner, H.; Caldwell, J. Putting Chirality to Work: The Strategy of Chiral Switches. *Nat. Rev. Drug Discov.* **2002**, *1* (10), 753–768. https://doi.org/10.1038/nrd915.

(3) Trost, B. M. Asymmetric Allylic Alkylation, an Enabling Methodology. *J. Org. Chem.* **2004**, *69* (18), 5813–5837. https://doi.org/10.1021/jo0491004.

(4) Liu, Y.; Du, H. Pd-Catalyzed Asymmetric Allylic Alkylations of 3-Substituted Indoles Using Chiral P/Olefin Ligands. *Org. Lett.* **2013**, *15* (4), 740–743. https://doi.org/10.1021/ol3032736.

(5) Trost, B. M.; Bai, Y.; Bai, W.-J.; Schultz, J. E. Enantioselective Divergent Synthesis of C19-Oxo Eburnane Alkaloids via Palladium-Catalyzed Asymmetric Allylic Alkylation of an N-Alkyl-α,β-Unsaturated Lactam. *J. Am. Chem. Soc.* **2019**, *141* (12), 4811–4814. https://doi.org/10.1021/jacs.9b00788.

(6) Richard, F.; Aubert, S.; Katsina, T.; Reinalda, L.; Palomas, D.; Crespo-Otero, R.; Huang, J.; Leitch, D. C.; Mateos, C.; Arseniyadis, S. Enantioselective Synthesis of γ-Butenolides through Pd-Catalysed C5-Selective Allylation of Siloxyfurans. *Nat. Synth.* **2022**, *1* (8), 641–648. https://doi.org/10.1038/s44160-022-00109-1.

(7) Pàmies, O.; Margalef, J.; Cañellas, S.; James, J.; Judge, E.; Guiry, P. J.; Moberg, C.; Bäckvall, J.-E.; Pfaltz, A.; Pericàs, M. A.; Diéguez, M. Recent Advances in Enantioselective Pd-Catalyzed Allylic Substitution: From Design to Applications. *Chem. Rev.* **2021**, *121* (8), 4373–4505. https://doi.org/10.1021/acs.chemrev.0c00736.

(8) Trost, B. M.; Horne, D. B.; Woltering, M. J. Palladium-Catalyzed DYKAT of Butadiene Monoepoxide: Enantioselective Total Synthesis of (+)-DMDP, (−)-Bulgecinine, and (+)-Broussonetine G. *Chem. – Eur. J.* **2006**, *12* (25), 6607–6620. https://doi.org/10.1002/chem.200600202.

(9) Robert A. Craig, I. I.; Roizen, J. L.; Smith, R. C.; Jones, A. C.; Virgil, S. C.; Stoltz, B. M. Enantioselective, Convergent Synthesis of the Ineleganolide Core by a Tandem Annulation Cascade. *Chem. Sci.* **2016**, *8* (1), 507–514. https://doi.org/10.1039/C6SC03347D.

(10) Mohammadkhani, L.; Heravi, M. M. Applications of Transition-Metal-Catalyzed Asymmetric Allylic Substitution in Total Synthesis of Natural Products: An Update. *Chem. Rec.* **2021**, *21* (1), 29–68. https://doi.org/10.1002/tcr.202000086.

(11) Trost, B. M. Pd Asymmetric Allylic Alkylation (AAA). A Powerful Synthetic Tool. *Chem. Pharm. Bull. (Tokyo)* **2002**, *50* (1), 1–14. https://doi.org/10.1248/cpb.50.1.

(12) Junk, L.; Kazmaier, U. The Allylic Alkylation of Ketone Enolates. *ChemistryOpen* **2020**, *9* (9), 929–952. https://doi.org/10.1002/open.202000175.

(13) Cheng, Q.; Tu, H.-F.; Zheng, C.; Qu, J.-P.; Helmchen, G.; You, S.-L. Iridium-Catalyzed Asymmetric Allylic Substitution Reactions. *Chem. Rev.* **2019**, *119* (3), 1855–1969. https://doi.org/10.1021/acs.chemrev.8b00506.

(14) He, H.; Zheng, X.-J.; Li, Y.; Dai, L.-X.; You, S.-L. Ir-Catalyzed Regio- and Enantioselective Decarboxylative Allylic Alkylations. *Org. Lett.* **2007**, *9* (21), 4339–4341. https://doi.org/10.1021/ol7019394.

(15) Chen, W.; Chen, M.; Hartwig, J. F. Diastereo- and Enantioselective Iridium-Catalyzed Allylation of Cyclic Ketone Enolates: Synergetic Effect of Ligands and Barium Enolates. *J. Am. Chem. Soc.* **2014**, *136* (45), 15825–15828. https://doi.org/10.1021/ja506500u.

(16) Graening, T.; Hartwig, J. F. Iridium-Catalyzed Regio- and Enantioselective Allylation of Ketone Enolates. *J. Am. Chem. Soc.* **2005**, *127* (49), 17192–17193. https://doi.org/10.1021/ja0566275.

(17) Jiang, X.; Chen, W.; Hartwig, J. F. Iridium-Catalyzed Diastereoselective and Enantioselective Allylic Substitutions with Acyclic α-Alkoxy Ketones. *Angew. Chem.* **2016**, *128* (19), 5913–5917. https://doi.org/10.1002/ange.201600235.

(18) Ashfeld, B. L.; Miller, K. A.; Smith, A. J.; Tran, K.; Martin, S. F. Features and Applications of $[Rh(CO)_2Cl]_2$-Catalyzed Alkylations of Unsymmetrical Allylic Substrates. *J. Org. Chem.* **2007**, *72* (24), 9018–9031. https://doi.org/10.1021/jo701290b.

(19) Thoke, M. B.; Kang, Q. Rhodium-Catalyzed Allylation Reactions. *Synthesis* **2019**, *51* (13), 2585–2631. https://doi.org/10.1055/s-0037-1611784.

(20) Tsuji, J.; Minami, I.; Shimizu, I. Allyation of Carbonucleophiles with Allylic Carbonates under Neutral Conditions Catalyzed by Rhodium Complexes. *Tetrahedron Lett.* **1984**, *25* (45), 5157–5160. https://doi.org/10.1016/S0040-4039(01)81551-3.

(21) Minami, I.; Shimizu, I.; Tsuji, J. Reactions of Allylic Carbonates Catalyzed by Palladium, Rhodium, Ruthenium, Molybdenum, and Nickel Complexes; Allylation of Carbonucleophiles and Decarboxylation- Dehydrogenation. *J. Organomet. Chem.* **1985**, *296* (1), 269–280. https://doi.org/10.1016/0022-328X(85)80354-5.

(22) Gosmini, C.; Bégouin, J.-M.; Moncomble, A. Cobalt-Catalyzed Cross-Coupling Reactions. *Chem. Commun.* **2008**, No. 28, 3221–3233. https://doi.org/10.1039/B805142A.

(23) Bhatia, B.; Reddy, M. M.; Iqbal, J. Cobalt (II) Catalysed Allylation of 1,3-Dicarbonyl Compounds with Allyl Acetates. *Tetrahedron Lett.* **1993**, *34* (39), 6301–6304. https://doi.org/10.1016/S0040-4039(00)73737-3.

(24) Gomes, P.; Gosmini, C.; Périchon, J. Cobalt-Catalyzed Direct Electrochemical Cross-Coupling between Aryl or Heteroaryl Halides and Allylic Acetates or Carbonates. *J. Org. Chem.* **2003**, *68* (3), 1142–1145. https://doi.org/10.1021/jo026421b.

(25) Yatsumonji, Y.; Ishida, Y.; Tsubouchi, A.; Takeda, T. Nickel(0) Triethyl Phosphite Complex-Catalyzed Allylic Substitution with Retention of Regio- and Stereochemistry. *Org. Lett.* **2007**, *9* (22), 4603–4606. https://doi.org/10.1021/ol702122d.

(26) Berkowitz, D. B.; Shen, W.; Maiti, G. In Situ Enzymatic Screening (ISES) of P,N-Ligands for Ni(0)-Mediated Asymmetric Intramolecular Allylic Amination. *Tetrahedron Asymmetry* **2004**, *15* (18), 2845–2851. https://doi.org/10.1016/j.tetasy.2004.06.052.

(27) Berkowitz, D. B.; Maiti, G. Following an ISES Lead: The First Examples of Asymmetric Ni(0)-Mediated Allylic Amination. *Org. Lett.* **2004**, *6* (16), 2661–2664. https://doi.org/10.1021/ol049159x.

(28) Evans, L. A.; Fey, N.; Harvey, J. N.; Hose, D.; Lloyd-Jones, G. C.; Murray, P.; Orpen, A. G.; Osborne, R.; Owen-Smith, G. J. J.; Purdie, M. Counterintuitive Kinetics in Tsuji-Trost Allylation: Ion-Pair Partitioning and Implications for Asymmetric Catalysis. *J. Am. Chem. Soc.* **2008**, *130* (44), 14471–14473. https://doi.org/10.1021/ja806278e.

(29) Trost, B. M.; Van Vranken, D. L. Asymmetric Transition Metal-Catalyzed Allylic Alkylations. *Chem. Rev.* **1996**, *96* (1), 395–422. https://doi.org/10.1021/cr9409804.

(30) Arthurs, R. A.; Hughes, D. L.; Richards, C. J. Planar Chiral Palladacycle Precatalysts for Asymmetric Synthesis. *Org. Biomol. Chem.* **2020**, *18* (28), 5466–5472. https://doi.org/10.1039/D0OB01331E.

(31) Masson-Makdissi, J.; Prieto, L.; Abel-Snape, X.; Lautens, M. Enantio- and Diastereodivergent Sequential Catalysis Featuring Two Transition-Metal-Catalyzed Asymmetric Reactions. *Angew. Chem. Int. Ed.* **2021**, *60* (31), 16932–16936. https://doi.org/10.1002/anie.202105800.

(32) Butt, N. A.; Zhang, W. Transition Metal-Catalyzed Allylic Substitution Reactions with Unactivated Allylic Substrates. *Chem. Soc. Rev.* **2015**, *44* (22), 7929–7967. https://doi.org/10.1039/C5CS00144G.

(33) Steinhagen, H.; Reggelin, M.; Helmchen, G. Palladium-Catalyzed Allylic Alkylation with Phosphinoaryldihydrooxazole Ligands: First Evidence and NMR Spectroscopic Structure Determination of a Primary Olefin–Pd^0 Complex. *Angew. Chem. Int. Ed. Engl.* **1997**, *36* (19), 2108–2110. https://doi.org/10.1002/anie.199721081.

(34) Selvakumar, K.; Valentini, M.; Wörle, M.; Pregosin, P. S.; Albinati, A. Palladium(0) Olefin Complexes and Enantioselective Allylic Amination/Alkylation with a P,N-Auxiliary. *Organometallics* **1999**, *18* (7), 1207–1215. https://doi.org/10.1021/om980920e.

(35) Helmchen, G.; Pfaltz, A. PhosphinooxazolinesA New Class of Versatile, Modular P,N-Ligands for Asymmetric Catalysis. *Acc. Chem. Res.* **2000**, *33* (6), 336–345. https://doi.org/10.1021/ar9900865.

(36) Zehnder, M.; Neuburger, M.; Schaffner, S.; Jufer, M.; Plattner, D. A. Synthesis, X-Ray Structures, NMR Studies and Density Functional Calculations of (η^2-Fumarodinitrile)palladium(0) Complexes Containing

Dihydro(phosphanylphenyl)oxazole Ligands. *Eur. J. Inorg. Chem.* **2002**, *2002* (6), 1511–1517. https://doi.org/10.1002/1099-0682(200206)2002:6<1511::AID-EJIC1511>3.0.CO;2-C.

(37) Dotta, P.; Magistrato, A.; Rothlisberger, U.; Pregosin, P. S.; Albinati, A. Dialkyl Effect on Enantioselectivity: π-Stacking as a Structural Feature in P,N Complexes of Palladium(II). *Organometallics* **2002**, *21* (14), 3033–3041. https://doi.org/10.1021/om020314q.

(38) Sherden, N. H.; Behenna, D. C.; Virgil, S. C.; Stoltz, B. M. Unusual Allylpalladium Carboxylate Complexes: Identification of the Resting State of Catalytic Enantioselective Decarboxylative Ketone Allylic Alkylation Reactions. *Angew. Chem. Int. Ed Engl.* **2009**, *48* (37), 6840–6843. https://doi.org/10.1002/anie.200902575.

(39) Schaffner, S.; Macko, L.; Neubufger, M.; Zehnder, M. Variants of Solid-State and Solution Structures of (η^3-Allyl)-{2-[2′-(diphenylphosphino)phenyl]-4,5-dihydrooxazole-P,N}palladium(II) Hexafluorophosphates and Tetraphenylborates. *Helv. Chim. Acta* **1997**, *80* (2), 463–471. https://doi.org/10.1002/hlca.19970800211.

(40) Sperrle, M.; Aeby, A.; Consiglio, G.; Pfaltz, A. Isotactic and Atactic Copolymerization of Styrene and Carbon Monoxide Using Cationic Palladium-Phosphino(dihydrooxazole) Complexes. Preliminary Communication. *Helv. Chim. Acta* **1996**, *79* (5), 1387–1392. https://doi.org/10.1002/hlca.19960790512.

(41) Hiroi, K.; Watanabe, K. Highly Enantioselective Palladium-Catalyzed Asymmetric Diels–Alder Reactions with Chiral Phosphino–Oxazoline Ligands. *Tetrahedron Asymmetry* **2002**, *13* (17), 1841–1843. https://doi.org/10.1016/S0957-4166(02)00484-6.

(42) Bélanger, É.; Pouliot, M.-F.; Courtemanche, M.-A.; Paquin, J.-F. Design, Synthesis, and Applications of Potential Substitutes of *t*-Bu-Phosphinooxazoline in Pd-Catalyzed Asymmetric Transformations and Their Use for the Improvement of the Enantioselectivity in the Pd-Catalyzed Allylation Reaction of Fluorinated Allyl Enol Carbonates. *J. Org. Chem.* **2012**, *77* (1), 317–331. https://doi.org/10.1021/jo2019653.

(43) Butts, C. P.; Crosby, J.; Lloyd-Jones, G. C.; Stephen, S. C. Robust and Catalytically Active Mono- and Bis-Pd-Complexes of the 'Trost Modular Ligand.' *Chem. Commun.* **1999**, No. 17, 1707–1708. https://doi.org/10.1039/A905851F.

(44) Racys, D. T.; Eastoe, J.; Norrby, P.-O.; Grillo, I.; Rogers, S. E.; Lloyd-Jones, G. C. Pd-η^3-C_6H_9 Complexes of the Trost Modular Ligand: High Nuclearity Columnar Aggregation Controlled by Concentration, Solvent and Counterion. *Chem. Sci.* **2015**, *6* (10), 5793–5801. https://doi.org/10.1039/C5SC01181G.

(45) Trost, B. M.; Breit, B.; Organ, M. G. On the Nature of the Asymmetric Induction in a Palladium Catalyzed Allylic Alkylation. *Tetrahedron Lett.* **1994**, *35* (32), 5817–5820. https://doi.org/10.1016/S0040-4039(00)78192-5.

(46) Campos, K. R.; Journet, M.; Lee, S.; Grabowski, E. J. J.; Tillyer, R. D. Asymmetric Synthesis of a Prostaglandin D_2 Receptor Antagonist. *J. Org. Chem.* **2005**, *70* (1), 268–274. https://doi.org/10.1021/jo048305+.

(47) Amatore, C.; Jutand, A.; Mensah, L.; Ricard, L. On the Formation of Pd(II) Complexes of Trost Modular Ligand Involving N–H Activation or P,O Coordination in Pd-Catalyzed Allylic Alkylations. *J. Organomet. Chem.* **2007**, *692* (7), 1457–1464. https://doi.org/10.1016/j.jorganchem.2006.11.039.

(48) Huang, J.; Isaac, M.; Watt, R.; Becica, J.; Dennis, E.; Saidaminov, M. I.; Sabbers, W. A.; Leitch, D. C. ^{DMP}DAB–Pd–MAH: A Versatile Pd(0) Source for Precatalyst Formation, Reaction Screening, and Preparative-Scale Synthesis. *ACS Catal.* **2021**, *11* (9), 5636–5646. https://doi.org/10.1021/acscatal.1c00288.

(49) Guerrero Rios, I.; Rosas-Hernandez, A.; Martin, E. Recent Advances in the Application of Chiral Phosphine Ligands in Pd-Catalysed Asymmetric Allylic Alkylation. *Molecules* **2011**, *16* (1), 970–1010. https://doi.org/10.3390/molecules16010970.

(50) Butts, C. P.; Filali, E.; Lloyd-Jones, G. C.; Norrby, P.-O.; Sale, D. A.; Schramm, Y. Structure-Based Rationale for Selectivity in the Asymmetric Allylic Alkylation of Cycloalkenyl Esters Employing the Trost 'Standard Ligand' (TSL): Isolation, Analysis and Alkylation of the Monomeric Form of the Cationic η^3-Cyclohexenyl Complex $[(\eta^3\text{-}c\text{-}C_6H_9)Pd(TSL)]+$. *J. Am. Chem. Soc.* **2009**, *131* (29), 9945–9957. https://doi.org/10.1021/ja8099757.

(51) Barone, V.; Cossi, M. Quantum Calculation of Molecular Energies and Energy Gradients in Solution by a Conductor Solvent Model. *J. Phys. Chem. A* **1998**, *102* (11), 1995–2001. https://doi.org/10.1021/jp9716997.

(52) Trost, B. M.; Van Vranken, D. L.; Bingel, C. A Modular Approach for Ligand Design for Asymmetric Allylic Alkylations via Enantioselective Palladium-Catalyzed Ionizations. *J. Am. Chem. Soc.* **1992**, *114* (24), 9327–9343. https://doi.org/10.1021/ja00050a013.

(53) Bourgeois, D.; Craig, D.; King, N. P.; Mountford, D. M. Synthesis of Homoallylic Sulfones through a Decarboxylative Claisen Rearrangement Reaction. *Angew. Chem. Int. Ed.* **2005**, *44* (4), 618–621. https://doi.org/10.1002/anie.200462023.

(54) Huang, J.; Keenan, T.; Richard, F.; Lu, J.; Jenny, S.; Jean, A.; Arseniyadis, S.; Leitch, D. Active, Selective, and Stable Single-Component Precatalysts for Asymmetric Allylic Alkylation. ChemRxiv May 3, 2023. https://doi.org/10.26434/chemrxiv-2023-0xbh5.

Chapter 4 ^{DMP}DAB–Pd–$(CH_2TMS)_2$: An Efficient Palladium(II) Precursor for Oxidative Addition Complex Formation, Reaction Screening, and Preparative-Scale Synthesis

Contributions:

^{DMP}DAB–Pd–$(CH_2TMS)_2$ was initially prepared by Dr. Joseph Becica. Large-scale isolation of this complex from COD–Pd–$(CH_2TMS)_2$ was accomplished by Jingjun Huang. The one-pot synthesis was conducted by Holly Celuszak, Dr. Binh Dang and Jingjun Huang. Ho. Single-crystal X-ray diffraction experiments and analysis were conducted by Sarah E. Jenny of Temple University. Holly Celuszak assisted with the catalytic evaluation of C-O coupling (Section 4.3.5, Figure 4.11Right and Table 4.4). All other experiments and analyses were accomplished by Jingjun Huang.

4.1 Abstract

Oxidative addition complexes (OACs) have a crucial role in Pd-catalyzed cross-coupling reactions. They are not only key intermediates of the catalytic cycle, but also can be used as powerful and robust precatalysts in challenging cross-couplings. The Pd^0 precursor ^{DMP}DAB–Pd–MAH failed in generating OACs, likely due to the unfavorable dissociation of MAH. Herein, we report a new, bench-stable, and versatile Pd^{II} source, ^{DMP}DAB–Pd–$(CH_2TMS)_2$, which is an excellent precursor for OAC formation and Pd-catalyzed cross-couplings. Using this precursor, Pd^0 formation is achieved without the formation of side products leading to inhibition. We also report the isolation of the previously reported XANTPhos–Pd–$(CH_2TMS)_2$, as well as 3 new OACs from ^{DMP}DAB–Pd–$(CH_2TMS)_2$; these OACs are characterized by multinuclear NMR spectroscopy, HRMS, and X-ray diffraction. A catalytic evaluation of ^{DMP}DAB–Pd–$(CH_2TMS)_2$ as a precursor in 3 distinct reaction classes also demonstrates the excellent activity of this new precursor, with a catalyst TON of 1880 obtained in a model Suzuki-Miyaura coupling.

4.2 Introduction

As stated in Chapter 1, a general catalytic mechanism for Pd-catalyzed cross-coupling has three essential steps—oxidative addition, transmetalation, and reductive elimination, wherein oxidative addition is often the rate- and/or selectivity-determining step.[1] As the intermediate generated in this essential step, OACs play a significant role in catalyst development research, such as mechanistic investigations,[2,3] reactivity and selectivity studies,[4,5] and catalyst deactivation studies.[6] Most importantly, these complexes have been exploited as robust and superior catalysts/precatalysts in specific cross-coupling reactions.[7–13] Buchwald and co-workers have incorporated sterically demanding biarylphosphine ligands in oxidative addition complexes (referred to Buchwald G6 precatalysts) and used them as precursors for a broad range of cross-coupling reactions (Figure 4.1A).[8,10] One remarkable example is that OACs exhibit superior catalytic activity over *in situ* generated catalysts in cross-couplings of structurally complex molecules, which offers substantial advantages in practical drug discovery (Figure 4.1B).[13] In addition, as an on-cycle species, OACs sidestep common issues observed for *in situ* generated catalysts, such as inefficient activation,[14,15] inactive off-cycle species generation,[16,17] and side products from activation acting as inhibitors.[18,19]

Our recently reported Pd^0 precursor[20]—^{DMP}DAB–Pd–MAH—failed to generate OACs in catalyst activation investigations. We attribute this to the unfavorable dissociation of MAH resulting from the strong bonding between MAH and Pd. Direct treatment of [phosphine]–Pd–MAH complexes with excess bromobenzene led to no observable reaction even at elevated temperatures. This limitation prompted us to develop a new precursor by replacing MAH with an easy-to-dissociate ligand, enabling a general activation pathway to generate OACs. Specifically, we sought to exploit C–C reductive elimination from a Pd^{II} precursor as a means to access reactive Pd^0 species that could then undergo oxidative addition.

Young and co-workers first reported a highly active dialkyl Pd precursor COD–Pd–$(CH_2TMS)_2$ (Figure 4.1C). The use of the trimethylsilyl group prevents β-H elimination as a potential decomposition pathway.[21] This complex is known to be thermally unstable, but is still widely used to generate phosphine dialkyl palladium complexes and a

wide range of OACs (Figure 4.1C). Furthermore, several palladium(0) dimers of the form [(μ-COD)Pd(L)]$_2$ derived from COD–Pd–(CH_2TMS)$_2$ have been demonstrated to be active precatalysts in challenging nucleophilic fluorinations as well as to generate the aforementioned OACs (Figure 4.1D).[13,19,22] However, the poor solubility, solution instability, and air sensitivity limit the broader application of these complexes.[19] To resolve stability problems, COD–Pd–($CH_2CMe_2C_6H_4$), an air-stable palladacycle first prepared by Cámpora (Figure 4.1E),[23] has been used as a precursor for OAC formation by Buchwald and co-workers.[24] In some specific cases, pre-heating and pre-mixing of COD–Pd–($CH_2CMe_2C_6H_4$) with ligands are required to generate [(μ-COD)Pd(L)]$_2$ in advance of the addition of aryl halides. Moreover, a common issue with dissociated COD is that it can act as an inhibitor in the catalytic cycle by competitive coordination of the alkene to Pd intermediates.[18] In light of the rapid diimine ligand displacement observed with our prior precursor ^{DMP}DAB–Pd–MAH, we decided to incorporate a diimine ligand to replace COD in dialkyl Pd complexes.

Inspired by the seminal work from Brookhart and co-workers, a considerable amount of α-diimine-containing palladium dialkyl complexes have been developed, mostly involving methyl ligands, for use in alkene polymerization.[25–32] In stark contrast, α-diimine palladium complexes containing –CH_2TMS as alkyl ligands are relatively limited. Cámpora and co-workers developed a range of dialkyl Pd and Ni complexes featuring various nitrogen-based ligands.[33] Notably, a Pd dimethyl complex featuring *N*,*N*'-bis(2,6-diisopropylphenyl)ethanediimine, was prepared and characterized; however, the corresponding bis-CH_2TMS complex could not be isolated or characterized due to incomplete ligand substitution and unsuccessful purification of the product out of this incomplete reaction mixture (Figure 4.1F).[33] The same paper featured three isolable palladium complexes containing –CH_2TMS ligands, with one containing an unsymmetric α-diimine (Figure 4.1G) and two based on bipyridyl and phenanthroline (Figure 4.1H).

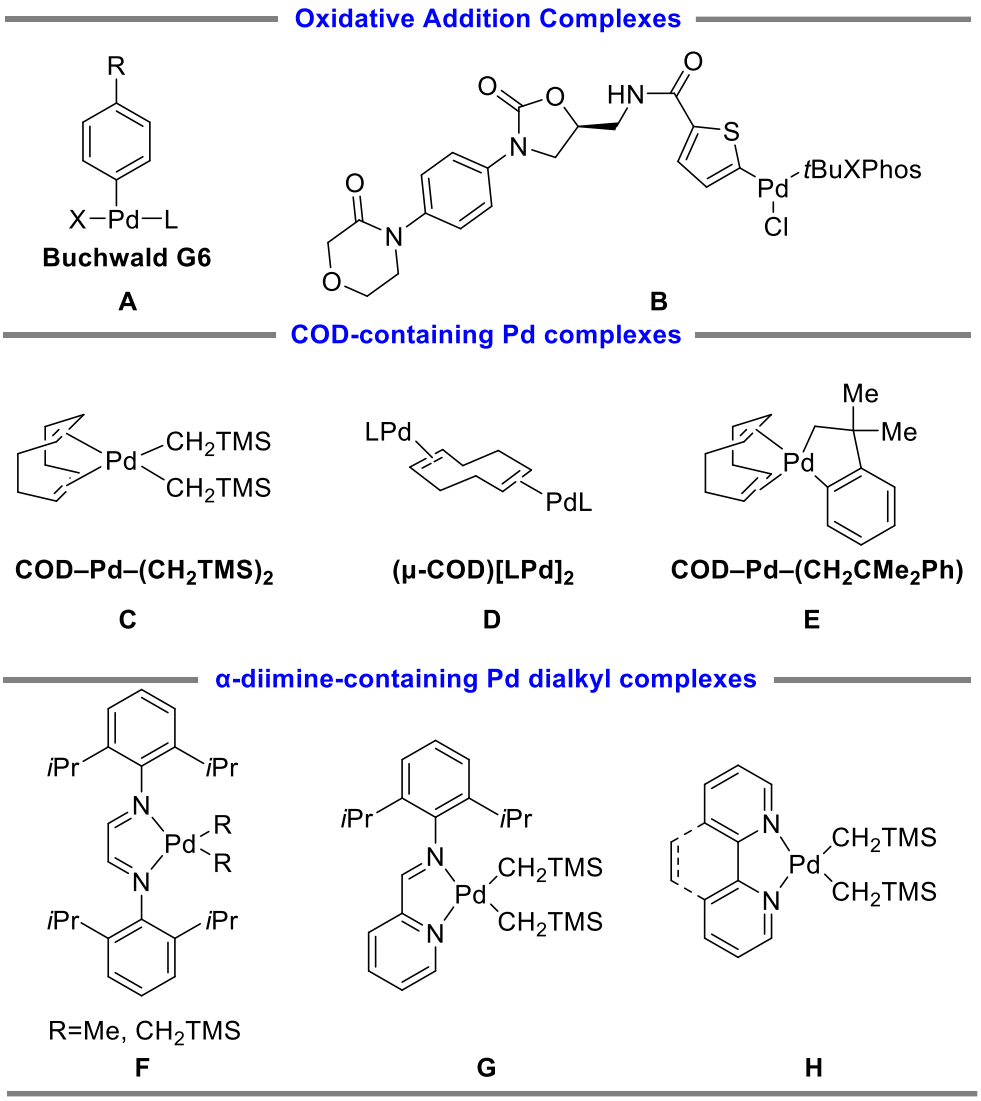

Figure 4.1. Representative OACs and dialkyl Pd complexes featuring either COD or α-diimine ligands.

Herein, we report a new, stable, active, and versatile palladium(II) precursor: ^{DMP}DAB−Pd– $(CH_2TMS)_2$ (Figure 4.2, **4.1**). This new complex, developed to improve on our prior palladium(0) precursor ^{DMP}DAB−Pd–MAH, offers several advantages, including excellent solubility and good stability in both solution and the solid state. This precursor is also effective for the direct formation of OACs. We report three OACs prepared and isolated from the combination of complex **4.1**, aryl halide, and phosphines, including bulky large-cone-angle bispyrazolyl ligands. We also report a new OAC containing the parent α-diimine ligand, as well as a simple synthesis of the known XANTPhos–Pd–$(CH_2TMS)_2$

complex. Thus, **4.1** provides an effective alternative method to generate OACs and phosphine dialkyl palladium complexes. Furthermore, a series of reaction screens in C–C and C–O cross-couplings at low Pd loading reveal the excellent activity of complex **4.1** when used for *in situ* catalyst generation.

4.3 Results and Discussion

4.3.1 Synthesis and Properties of ^{DMP}DAB–Pd–$(CH_2TMS)_2$

As described in Chapter 2, ^{DMP}DAB–Pd–MAH failed to generate OACs and exhibited poor reactivity in some specific cross-coupling reactions, likely due to strong Pd–MAH bonding. The focus of this Chapter is on the synthesis and applications of a new Pd^{II} precursor: ^{DMP}DAB–Pd–$(CH_2TMS)_2$ (**4.1**, Figure 4.2). This complex replaces the Pd^0–MAH unit with a Pd^{II}–dialkyl fragment, while retaining the *N,N'*-diaryl DAB ligand with 2,6-dimethylphenyl substituents at nitrogen (^{DMP}DAB). This replacement was done to take advantage of the C–C reductive elimination of the two alkyl ligands. Instead of simple alkyl ligands (e.g. methyl or ethyl), we chose the methyltrimethylsilyl ligand to avoid the formation of gaseous alkane products after reductive elimination, as well as avoiding β-H elimination. In addition, based on the favourable properties of ^{DMP}DAB as a stabilizing yet labile ligand mentioned in Chapter 2 and Chapter 3, this diimine is again employed to help alleviate potential thermal decomposition (as is observed with COD–Pd–$(CH_2TMS)_2$).

To first prepare the target complex **4.1**, we employed a simple ligand displacement from COD–Pd–$(CH_2TMS)_2$. In a nitrogen glovebox, simply mixing ^{DMP}DAB with commercially available COD–Pd–$(CH_2TMS)_2$ in THF at room temperature results in the formation of ^{DMP}DAB–Pd–$(CH_2TMS)_2$ (**4.1**) within 18 hours. A simple filtration through Celite and solvent evaporation gives 96% yield of the desired product as a dark purple crystalline solid (Figure 4.2)**.** Notably, we further investigated the efficiency of this ligand substitution by monitoring the consumption of COD–Pd–$(CH_2TMS)_2$ in d_8-THF after mixing with ^{DMP}DAB. It reveals that 70% conversion is achieved within 20 minutes and remains unchanged over 48 hours. Complete consumption observed after solvent evaporation under vacuum demonstrates that the removal of COD by-product helps to drive the substitution to completion. We also established a straightforward one-pot synthesis

from (COD)$PdCl_2$. This synthesis proceeds through (COD)$Pd(CH_2TMS)_2$ as a non-isolated intermediate, which is generated via alkylation of (COD)$PdCl_2$ with $TMSCH_2MgCl$. This is followed by ligand substitution with ^{DMP}DAB, solvent evaporation and celite filtrations (2 times) to give **4.1** in 82% isolated yield. Importantly, both synthetic pathways give highly pure **4.1**, which has been fully characterized by multinuclear NMR spectroscopy (see Appendix), HRMS, and single-crystal X-ray crystallography (Figure 4.2).

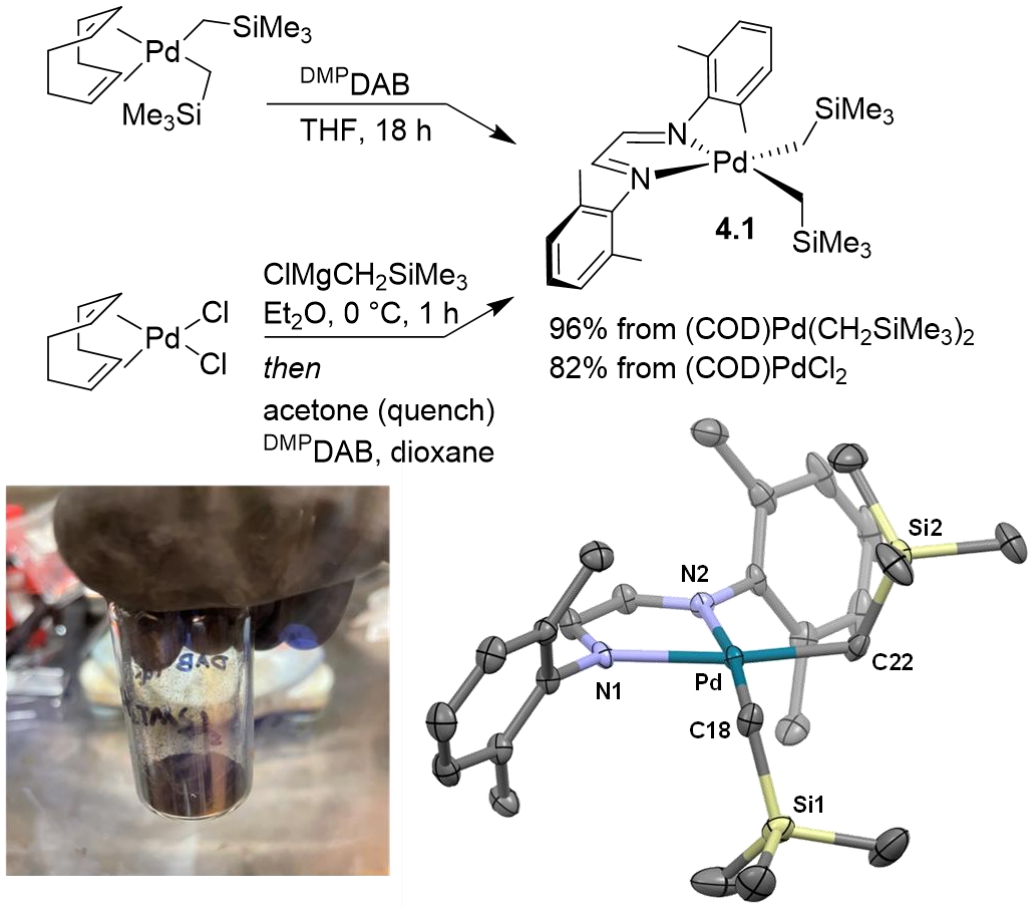

Figure 4.2. Two synthetic pathways of forming ^{DMP}DAB–Pd–$(CH_2TMS)_2$ (**4.1**). Solid-state molecular structure of **4.1**. Atom colours: C: grey; N: light blue; Si: pale yellow; Pd: blue. Thermal ellipsoids plotted at 50% probability. Hydrogen atoms omitted for clarity.

Given the poor stability of prior Pd dialkyl precursors,[21,33] we assessed the stability of **4.1** in the solid state and solution. As a solid, complex **4.1** is indefinitely stable for more than 1 year if stored under N_2 atmosphere at room temperature. Furthermore, no noticeable decomposition is observed if the solid is stored under an atmosphere of air for 1 week. To

assess the solution stability, we prepared a set of solutions of **4.1** in a variety of deuterated organic solvents, including benzene, THF, acetone, DCM, toluene, and chloroform, and held them at room temperature (Figure 4.3). In all cases, concentrations of **4.1** were monitored over 48 hours by ^{1}H NMR spectroscopy, with 1,3,5-trimethoxybenzene as an internal standard. Solutions were prepared under N_2, but then exposed to air after obtaining the first ^{1}H NMR spectra. During this period, more than 90% of **4.1** remains in most solvents, while a slightly increased rate of decomposition is detected in chloroform (84% of **4.1** remaining after 48 hours). Overall, complex **4.1** is stable in the solution and solid state under an atmosphere of air with great solubility.

In addition to **4.1**, we also examined the stability of COD–Pd–$(CH_2TMS)_2$. Surprisingly, given its documented thermal instability, we observed good stability of this complex in both solution and solid state under air, with 85% of COD–Pd–$(CH_2TMS)_2$ remaining in d_6-benzene within 48 hours. As a solid, only a small amount of $TMSCH_2CH_2TMS$ (the by-product of reductive elimination) is observed by ^{1}H NMR spectroscopy after 1 week; however, this sample rapidly decomposed once in solution, with a distinct colour change from pale yellow to dark gray. This is consistent with an autocatalytic-like decomposition, where trace Pd^0 could accelerate further decomposition.

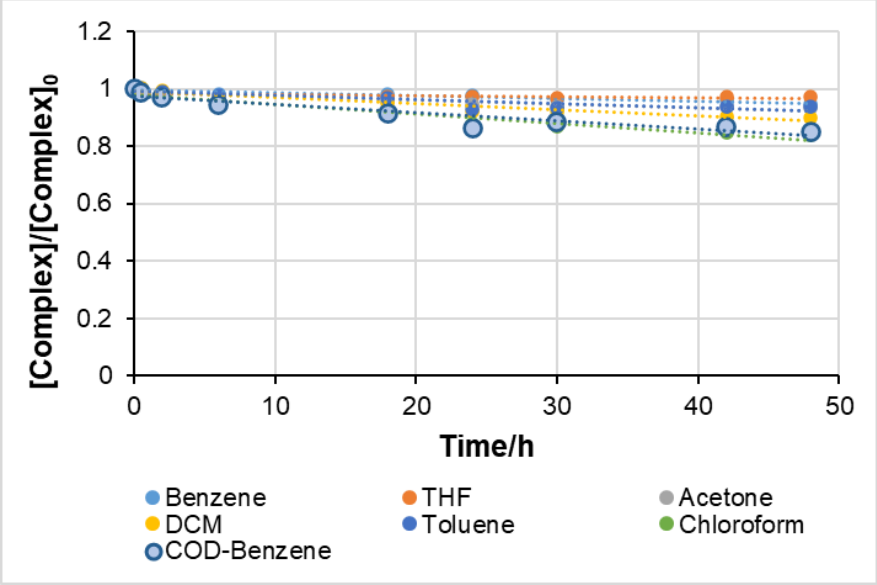

Figure 4.3. Solution stability plot of complex **4.1** (0.025 M) in six deuterated solvents (48 h, room temperature, under air) and COD–Pd–$(CH_2TMS)_2$ in d_6-benzene.

Concentration is determined using ^{1}H NMR spectroscopy (relative integration vs internal standard).

4.3.2 Ligand Substitution

One of the applications of COD–Pd–$(CH_2TMS)_2$ is to generate [phosphine]–Pd–(CH2TMS)$_2$ complexes.[21,34,35] These phosphine-ligated dialkyl complexes have been used as precursors for mechanistic studies,[35] cross-coupling reactions,[34] aminations of olefins,[36] generation of chiral Pd^{II} complexes for asymmetric catalysis,[37] and to access other [phosphine]-Pd^{II} derivatives where one or both alkyl group(s) are substituted.[38–41] To test if [phosphine]–Pd–$(CH_2TMS)_2$ can be formed from complex **4.1**, we conducted a series of ligand substitution experiments of **4.1** with a variety of phosphine ligands. As XANTPhos–Pd–$(CH_2TMS)_2$ (**4.2**) (previously prepared from COD–Pd–$(CH_2TMS)_2$) is known to be a good precursor for C–C and C–N couplings,[34] we first examined the reaction of **4.1** with 1 equivalent XANTPhos in THF at room temperature. The initially clear brown solution changes to a yellow suspension within 30 minutes. ^1H and ^{31}P NMR spectra of the reaction mixtures after simple solvent evaporation confirm the formation of complex **4.2** (^{31}P NMR δ 8.44 ppm), though around 5% (peak area) unknown component is also observed (Figure 4.4). Notably, we did not observe the presence of Pd(XANTPhos)$_2$[42] (0.8-3.4 ppm in THF) or unreacted XANTPhos (-17 ppm in $CDCl_3$). In stark contrast, the reported synthesis of **4.2** from COD–Pd–$(CH_2TMS)_2$ must be carried out under specific conditions to avoid the formation of Pd(XANTPhos)$_2$: in THF at room temperature, a mixture of COD–Pd–$(CH_2TMS)_2$ and XANTPhos gives Pd(XANTPhos)$_2$ as the only product.[34]

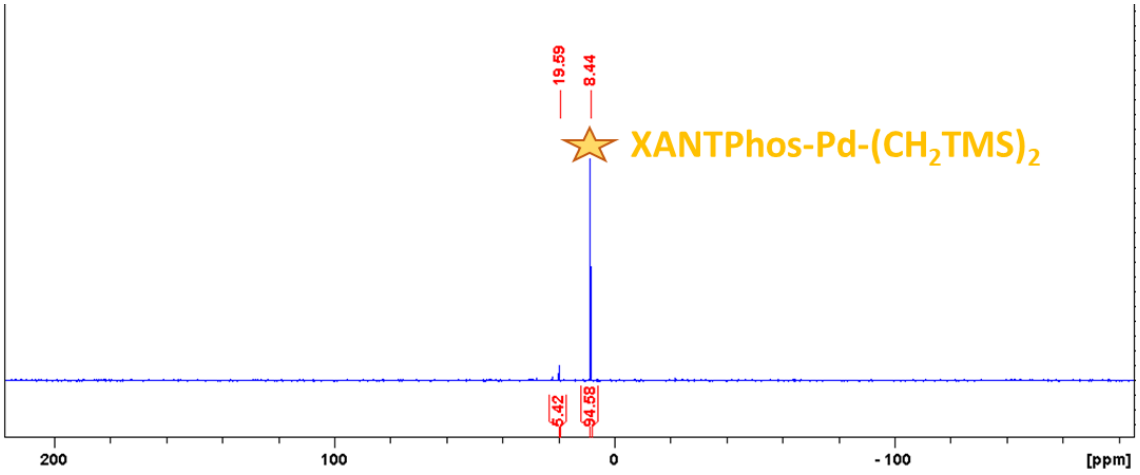

Figure 4.4. $^{31}P\{^1H\}$ NMR spectrum of the ligand substitution of **4.1** with XANTPhos in THF.

Following the small-scale metalation experiment, we sought to isolate **4.2** to ensure the ^{DMP}DAB by-product could be removed. Unfortunately, isolation of this complex was not successful when THF or acetonitrile was used as the reaction solvent. Complete removal of either THF or acetonitrile was difficult under vacuum at room temperature, and elevated temperatures are known to decompose complex **4.2**. Instead, we prepared **4.2** using diethyl ether, followed by a straightforward trituration/decantation with hexanes and diethyl ether to remove the by-product ^{DMP}DAB. This gives **4.2** in 68% yield (equation 4.1). Moreover, we performed the whole synthesis and isolated process under air at room temperature, while the reported synthesis requires an inert atmosphere and low temperature (likely owing to the assumed thermal sensitivity of COD–Pd–$(CH_2TMS)_2$). Overall, **4.1** is an efficient and operationally convenient precursor to access complex **4.2**; this also demonstrates that phosphine ligands can effectively displace ^{DMP}DAB from **4.1**.

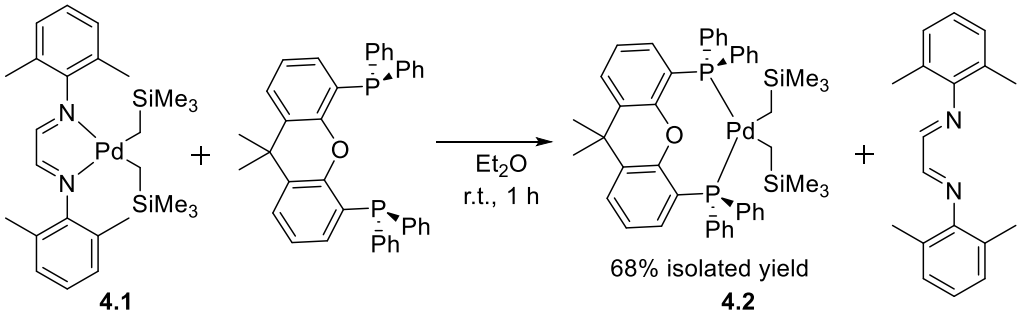

(4.1)

To further explore this chemistry, we examined the ligand substitution of **4.1** with a wide range of phosphine ligands, including bidentate, biaryl and bispyrazolyl phosphines. All tests were performed in a similar manner by mixing 0.01 mmol of **4.1** with 1 equivalent of phosphine in 0.6 mL THF for 1 h, followed by ^{31}P NMR spectroscopy using a capillary containing C_6D_6/PPh_3 as an internal standard (equation 4.2). Unfortunately, most of these experiments show only the free phosphines, or the absence of any peaks; the only new (minor) signals were observed in tests adding RuPhos and DPEPhos (Table 4.1). The new peak at 43 ppm in entry 1 is consistent with the RuPhos phosphine oxide based on the chemical shift,[43] while the tiny new peak detected with DPEPhos does belong to the expected DPEPhos–Pd–$(CH_2TMS)_2$ (Table 4.1, entry 8).[35] We attribute the inability to observe new Pd-based complexes to rapid reductive elimination of the alkyl groups from

any $LPd(CH_2TMS)_2$ generated, leading to the formation of unstabilized LPd^0, which will then decompose.

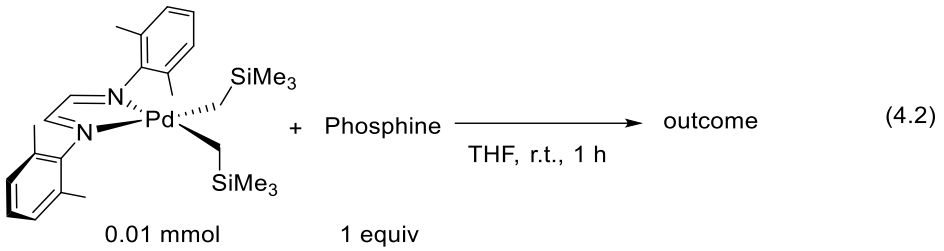

(4.2)

Table 4.1. Summarized qualitative outcomes of ligand substitution of complex **4.1** with different phosphine ligands.

Entry	Phosphine	Outcome
1	RuPhos	phosphine was consumed + a tiny peak at 43 ppm
2	*t*BuXPhos	phosphine remained
3	BrettPhos	phosphine remained
4	SPhos	phosphine was consumed
5	CPhos	phosphine was consumed[a]
6	BippyPhos	phosphine remained (small amount)[a]
7	*t*BuBrettPhos	phosphine remained (small amount)
8	DPEPhos	phosphine was consumed + a tiny peak at 10.6 ppm

[a]reaction time: 2 hours.

4.3.3 Oxidative Addition Complex Generation

While the observation of $LPd(CH_2TMS)_2$ for most phosphines was not successful, the outcomes of the aforementioned ligand displacement studies prompted us to explore trapping LPd^0 with Ar–Br to generate OACs. Specifically, we sought to use complex **4.1** to access OACs that ^{DMP}DAB–Pd–MAH failed in generating. Here, we report 3 OACs containing phosphines and 1 OAC still containing ^{DMP}DAB, with all complexes being characterized by multinuclear NMR spectroscopy, HRMS, and single-crystal X-ray crystallography.

OACs containing BippyPhos (**4.3**), AdBippyPhos (**4.4**), and XPhos (**4.5**), were synthesized by mixing **4.1** with 1 equivalent of the corresponding phosphine ligand and 2-

3 equivalents of 4-bromoacetophenone in CPME (or THF for complex **4.5**) at 50 °C for 2-24 hours under N_2 (Figure 4.5). Isolation of **4.3** and **4.4** is achieved by simply collecting the resulting precipitate by filtration, and washing with CPME or Et_2O, giving the OACs in 80% and 89% yields, respectively. Complex **4.5** is isolated by solvent evaporation, followed by trituration/decantation with Et_2O/hexanes to give 43% isolated yield for **4.3**. During these reactions, complete conversion of **4.1** to complexes **4.3** and **4.4** is apparent within 2 hours based on the distinct colour change from clear brown solutions to yellow suspensions. In contrast, in the synthesis of **4.5**, an orange precipitate formed within 4 hours, but the brown colour of the reaction solution was maintained; this reaction was thus left for 24 hours to ensure complete conversion, though *in situ* reaction progress monitoring was not performed to confirm.

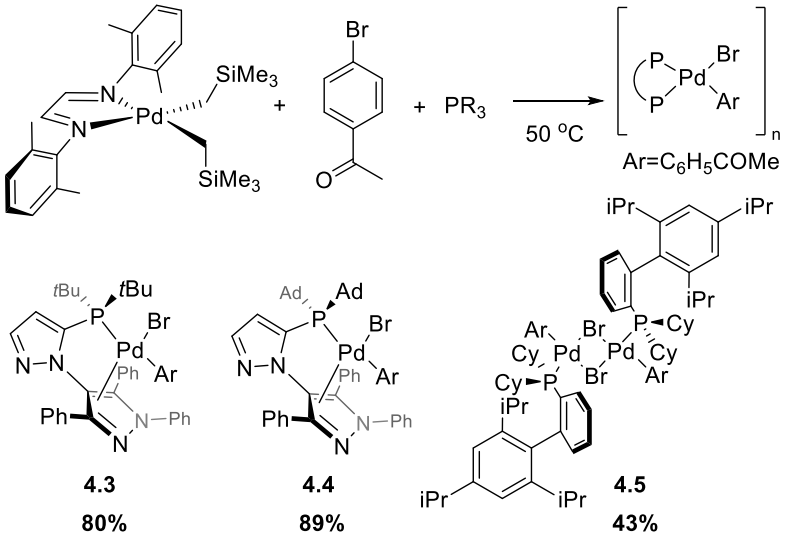

Figure 4.5. Synthesis and isolation of [[phosphine]–Pd(Br)-Ar]$_n$ complexes **4.3**-**4.5** via oxidative addition from complex **4.1**, phosphines, and 4-bromoacetophenone.

To the best of our knowledge, complex **4.4** is the first example of an isolated and characterized OAC based on AdBippyPhos. In light of the high cost of AdBippyPhos as a ligand, complex **4.4**, which contains the desired 1:1 L-to-Pd ratio, is an attractive single-component precatalyst. Moreover, only two OACs based on BippyPhos have been previously reported.[44,45] Importantly, our synthesis of **4.3** combines the advantages of the two reported synthetic pathways: high yield, short reaction time, operational convenience,

and readily removable by-products. In addition to solution phase characterization, we obtained solid-state molecular structures of **4.3** and **4.4,** with both being square planar about the Pd center (Figure 4.6). The BippyPhos/AdBippyPhos ligands are bidentate, with the pendant pyrazolyl group also coordinated to Pd through its π-system. This places the Ar and Br ligands *cis* to one another.

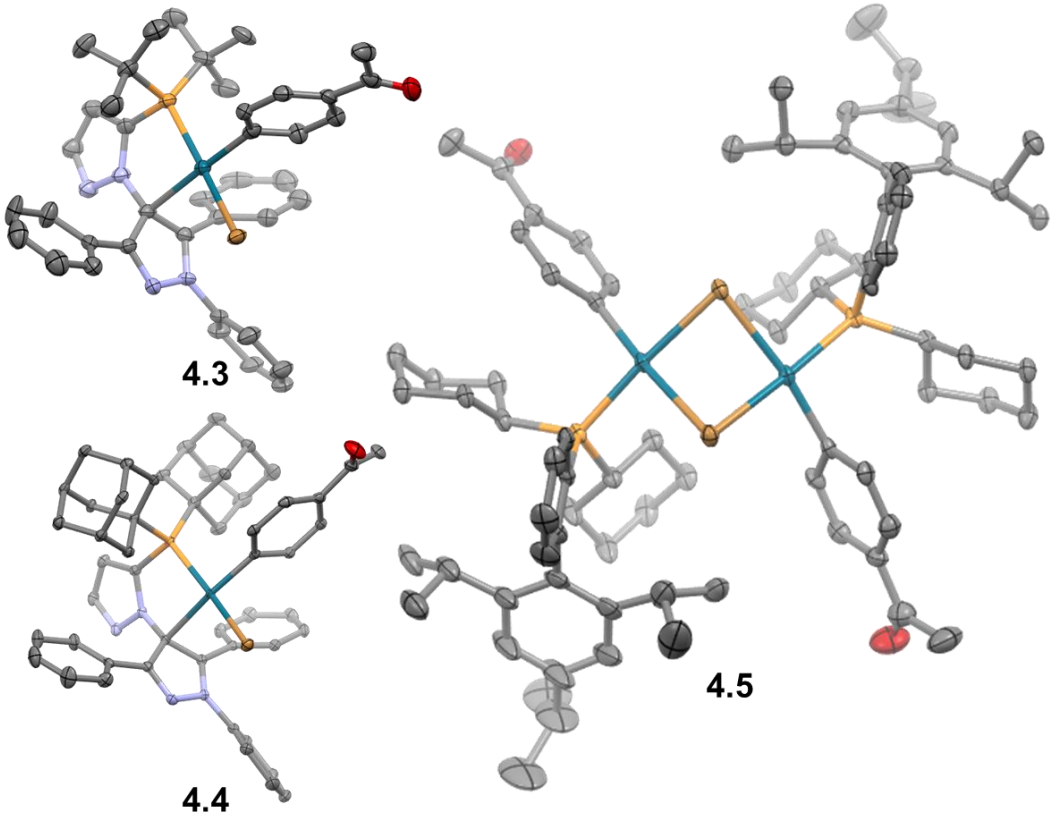

Figure 4.6. Solid-state molecular structures determined by single-crystal XRD of **4.3**, **4.4**, and **4.5**.
Atom colors: C, gray; N, light blue; O, red; P, bright orange; Br: dark yellow; Pd, blue. A disordered isopropyl group in XPhos of **4.5** over two orientations unshown for clarity. Thermal ellipsoids plotted at 50% probability. Hydrogen atoms omitted for clarity. Solvent molecules in asymmetric unit omitted for clarity.

While complexes **4.3** and **4.4** were characterized as monomers, complex **4.5** was revealed to be a bromide-bridged dimer in the solid state (Figure 4.6). Aïssa and co-workers also reported a dimeric solid-state structure for an XPhos-ligated OAC, while analysis by mass spectrometry revealed only the *m*/*z* of the corresponding monomer.[46] Conversely, we do observe the presence of the dimer in our ESI-HRMS data, based on the small intensity

m/*z* peak at 1481.54110. This is an excellent match to the calculated value for [XPhos–Pd–Ar](μ-Br)[XPhos–Pd–Ar]$^+$ (1481.53851), which corresponds to the loss of a Br anion from dimeric **4.5**. We also observe the corresponding *m*/*z* for the monomer [XPhos–Pd–Ar]$^+$ as the base peak (*m*/*z* = 701.31008, calculated value = 701.30981) (Figure 4.7). Though dimeric OACs are usually seen as off-cycle resting states during catalysts, their efficient catalytic activity as precatalysts has been revealed in some challenging cross-coupling reactions.[12,47]

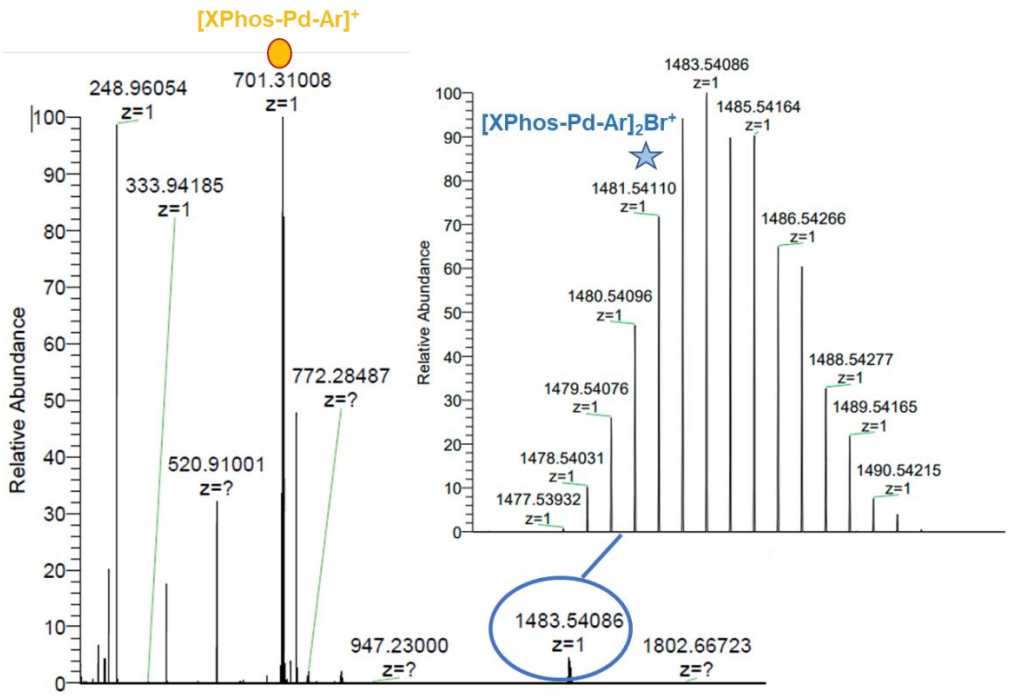

Figure 4.7. HRMS of isolated complex **4.5** showing the presence of monomeric and dimeric XPhos-ligated OACs.

Another OAC containing the parent ^{DMP}DAB diimine ligand was also prepared and fully characterized by NMR spectroscopy, HRMS, and single-crystal X-ray crystallography. During the attempted formation of an OAC containing the cataCXium® POMetB ligand, we observed the formation of a new Pd complex that did not contain any phosphine based on an absence of key signals in the ^{1}H NMR spectrum (and a complete lack of signals in the ^{31}P NMR spectrum). Instead, the NMR spectroscopic data was consistent with the structure ^{DMP}DAB–Pd(Ar)(Br) (**4.6**, Figure 4.8).

We first hypothesized that cataCXium® POMetB did not displace ^{DMP}DAB, and instead, C–C reductive elimination directly from **4.1** generated ^{DMP}DAB–Pd^{0}, which then underwent oxidative addition with 4-bromoacetophenone to give **4.6**. However, heating **4.1** with 4-bromoacetophenone in the absence of cataCXium® POMetB did not give **4.6**. We then reacted **4.1** with 1.2 equivalents of 4-bromoacetophenone and a catalytic amount (20 mol %) of cataCXium® POMetB. Stirring this mixture in TBME for 24 hours at room temperature resulted in an orange precipitate; subsequent isolation of this solid by filtration and trituration/decantation with TBME gave **4.6** in 62% isolated yield (Figure 4.8).

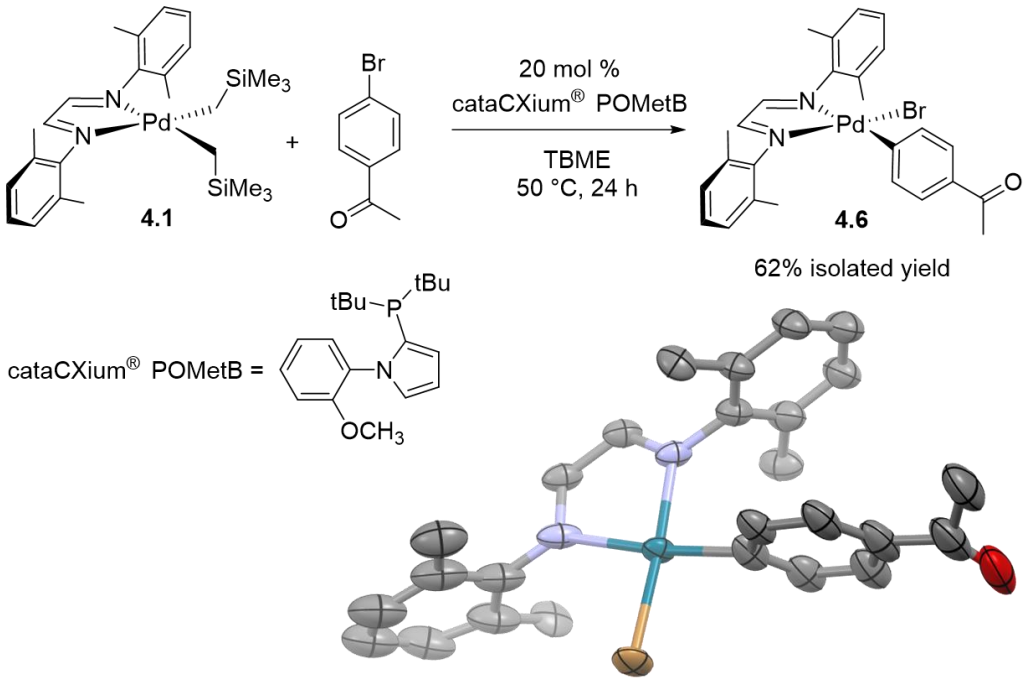

Figure 4.8. Synthesis of complex **4.6**, and its solid-state molecular structure determined by X-ray crystallography. Thermal ellipsoids plotted at 50% probability. Hydrogen atoms omitted for clarity. The structure is low resolution, and the molecule is disordered over two positions; only one is shown for clarity.

In addition to NMR spectroscopic characterization of **4.6**, we obtained confirmation of the molecular structure by X-ray diffraction. While the structure is low resolution, and further disordered over two orientations, the data does confirm the proposed connectivity and is consistent with solution phase characterization data. (Figure 4.8). Notably, the two dimethylphenyl groups on the DAB ligand are coplanar in this structure of **4.6**, while there

is a slight twisting between planes observed in the molecular structure of **4.1**; this is likely due to greater steric repulsion in **4.1** by the large –CH_2TMS ligands (Figure 4.2). Particularly, diimine-ligated palladium complexes are rarely used in cross-coupling. In one recent example, (diimine)Pd(Ar)(X) complexes are proposed as catalytic intermediates in a specific direct C–H arylation, and one example of an isolated diimine-ligated OAC was used as part of mechanistic studies in that case.[48]

Given the aforementioned results from ligand substitutions and oxidative additions, we propose the following general reaction pathway for the conversion of **4.1** to phosphine Pd dialkyl complexes (e.g. **4.2**), OACs **4.3**-**4.6**, as well as how **4.1** would undergo *in situ* activation in catalytic reactions (Figure 4.9). Generation of the active LPd^0 species proceeds through an $LPd(CH_2TMS)_2$ complex that is formed by ligand substitution of **4.1** with added phosphine; when L = XANTPhos, this complex can be isolated. Reductive elimination of the two alkyl groups then leads to the formation of LPd^0, which initiates the catalytic cycle of cross-coupling reactions. Oxidative addition of Ar–X then gives OACs, for which we have isolated 3 examples (**4.3**-**4.5**).

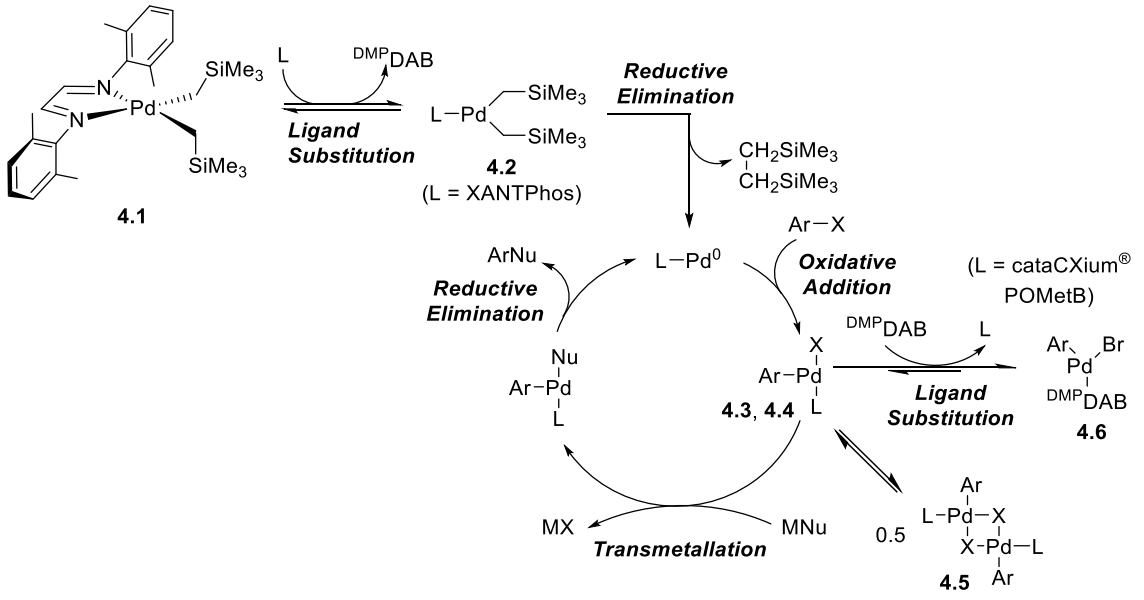

Figure 4.9. Proposed reaction pathways for conversion of complex **4.1** in the presence of phosphine and Ar–X substrates and formation of **4.6**.

Studies of the formation of **4.6**, specifically the null reaction of **4.1** with 4-bromoacetophenone, rule out an alternative pathway where reductive elimination and oxidative addition occur prior to phosphine displacement. Instead, for the generation of complex **4.6**, we hypothesize that the free ^{DMP}DAB displaces cataCXium® POMetB after oxidative addition. This would generate **4.6** and an equivalent of free cataCXium® POMetB, which can then react with **4.1** again. This double displacement explains why **4.6** is generated using only a catalytic amount of cataCXium® POMetB, though we do still observe **4.6** as the major product even with a full equivalent of cataCXium® POMetB. The thermodynamic preference for ^{DMP}DAB over cataCXium® POMetB can be partly explained by a more favourable hard-hard interaction between Pd^{II} and the chelating diimine; however, the fact that other phosphines in **4.3**-**4.5** are not displaced by ^{DMP}DAB means cataCXium® POMetB must also have weaker bonding to Pd^{II} than AdBippyPhos or XPhos.

4.3.4 Complex 4.1 as a Precatalyst in Suzuki Coupling

With the feasibility of *in situ* catalyst activation established from the studies of OAC formation, we then sought to assess the catalytic activity of **4.1** as a precursor for several cross-coupling reactions. First, we examined the Suzuki-Miyaura coupling of 2-chloro-5-methylpyridine with phenylboronic acid. In this specific reaction, we previously showed ^{DMP}DAB–Pd–MAH is an inferior precursor to $Pd(OAc)_2$ (Chapter 2, Section 2.3.4.[20] Our initial test of the new system was performed using 2 mol % **4.1** and 4 mol % XPhos under standard biphasic reaction conditions.[49] An 83% solution yield, determined by ^{1}H NMR spectroscopy versus internal standard (1,3,5-trimethoxybenzene), is obtained after stirring at 80 °C for 2 hours. This yield is comparable to the prior example with $Pd(OAc)_2$, and double that for ^{DMP}DAB–Pd–MAH under otherwise identical conditions (equation 4.3).

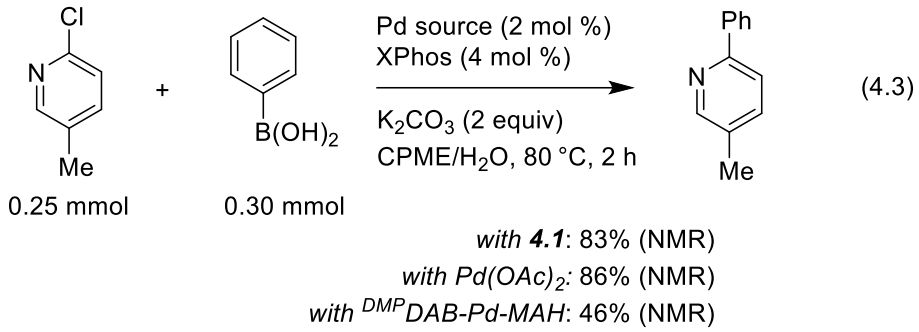

These results prompted us to evaluate these three precursors – **4.1**, $Pd(OAc)_2$, and ^{DMP}DAB–Pd–MAH – at ever lower catalyst loading (Table 4.2). This would enable a more in-depth comparison of the catalytic activity for these systems (expressed as turnover number, TON), and also reveal any activity cliffs/limits. In conjunction with lowering the Pd loading to 0.5 mol %, the initial reaction time was extended to 18 hours and the 2-chloro-5-methylpyridine concentration was increased from 0.25 M to 1.29 M; this was done to ensure sufficient conversion was observed and maintain a reasonable absolute [Pd]. Under these conditions, all three precursors gave high solution yields (entries 1-3). To further challenge these catalysts, the same reaction was performed at only 50 °C for 1.5 h. Complex **4.1** and $Pd(OAc)_2$ again gave comparable results (TON ~ 110), while ^{DMP}DAB–Pd–MAH exhibited a clear activity cliff, only giving 5% product (entries 4-6). With an even lower Pd loading of 0.1 mol % and a 5 h reaction time, complex **4.1** still gave a 59% NMR yield (TON = 590), while $Pd(OAc)_2$ exhibited its own activity cliff (16%, TON = 160) (entries 7-8). Further studies at 0.1 mol % **4.1** (entries 9-12) revealed that a 2:1 XPhos-to-Pd ratio at 50 °C for 24 h is optimal for yield (93%, entry 11).

To assess the limits of catalytic activity using **4.1** as a precursor, we continually decreased the catalyst loading to establish a maximum TON (Table 4.2, entries 13, 14, 16). Within 48 hours, a TON of 1880 is achieved using only 0.025 mol % **4.1** (47% yield, entry 14), while $Pd(OAc)_2$ / XPhos exhibits a nearly 3 times lower TON (680) under otherwise identical conditions (entry 15). These results show not only that complex **4.1** effectively overcomes the limitations of ^{DMP}DAB–Pd–MAH in this coupling, but that **4.1** significantly outperforms $Pd(OAc)_2$ for activity as an *in situ* catalyst precursor at low catalyst loading. These results compare well with other reported low catalyst loading systems for Suzuki-

Miyaura couplings with aryl chloride substrates, several of which require supported Pd catalysts, specific surfactant additives,[50] and/or highly activated substrates.

Table 4.2. Representative results of comparisons, optimization, and TON investigation for Suzuki-Miyaura coupling. All reactions used XPhos (2:1 L-to-Pd unless otherwise noted).

Entry	Pd source	Pd loading	Time/ h	Temp/ °C	NMR solution yield%	TON
1	**4.1**	0.5 mol %	18	80	100	200
2	$Pd(OAc)_2$	0.5 mol %	18	80	81	162
3	^{DMP}DAB-Pd-MAH	0.5 mol %	18	80	99	198
4	**4.1**	0.5 mol %	1.5	50	56	112
5	$Pd(OAc)_2$	0.5 mol %	1.5	50	54	108
6	^{DMP}DAB-Pd-MAH	0.5 mol %	1.5	50	5	10
7	**4.1**	0.1 mol %	5	50	59	590
8	$Pd(OAc)_2$	0.1 mol %	5	50	16	160
9	**4.1**	0.1 mol %	12	50	72	720
10[a]	**4.1**	0.1 mol %	12	50	69	690
11	**4.1**	0.1 mol %	24	50	93	930
12[a]	**4.1**	0.1 mol %	24	50	77	770
13	**4.1**	0.05 mol %	48	50	82	1640
14	**4.1**	0.025 mol %	48	50	47	1880
15	$Pd(OAc)_2$	0.025 mol %	48	50	17	680
16	**4.1**	0.0125 mol%	48	50	18	1440

[a]1:1 L-to-Pd ratio was applied.

By using the optimized conditions from entry 11 above, we performed this coupling on 3.0 mmol scale, obtaining a 66% isolated yield after a simple extraction work-up (equation 4.4).

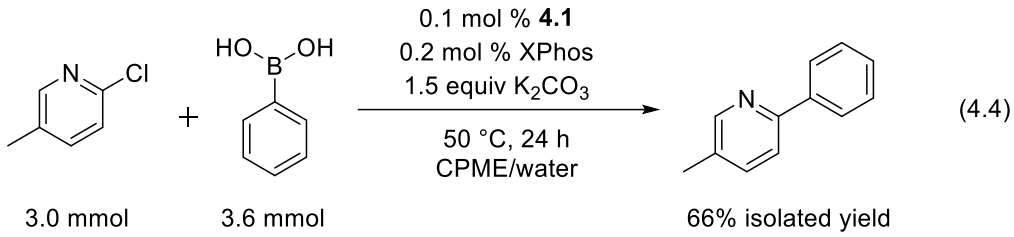

(4.4)

4.3.5 Complex 4.1 as a Precatalyst in Heck Coupling

In addition to the aforementioned Suzuki coupling, relatively poor catalytic activity is observed with ^{DMP}DAB–Pd–MAH in a model Heck reaction compared to other common Pd sources (Chapter 2, Section 2.3.3).[20] To evaluate the catalytic activity of **4.1** in a challenging Heck coupling of 4-chloroanisole (unactivated aryl chloride), we adapted reaction conditions as reported by Littke and Fu (equation 4.5).[51] By stirring 4-chloroanisole and 1.09 equivalents of methyl methacrylate in CPME at 120 °C for 18 hours, an 82% solution yield is obtained using 2.5 mol % **4.1** and 2.5 mol % P(*t*-Bu)$_3$, revealing promising activity of **4.1** in this challenging reaction (Table 4.3, entry 1).

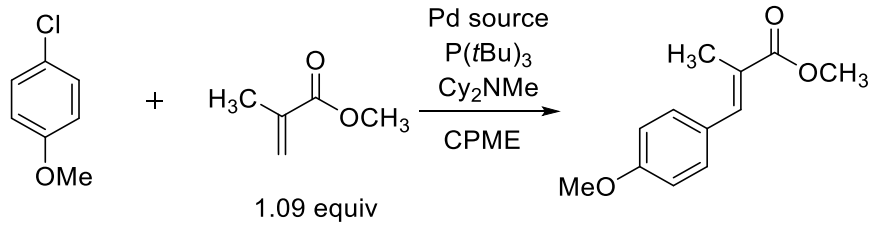

(4.5)

We then conducted two comparative experiments, using Pd_2da_3•$CHCl_3$ and $[Pd(allyl)Cl]_2$ as Pd sources under otherwise identical conditions, giving 38% and 62% NMR yields, respectively (Table 4.3, entries 2 and 3). Attempts to reduce the reaction temperature below 120 °C, including use of an alternative base or ligand, were not successful, giving only trace product in one case (entries 4-7). Maintaining a reaction temperature of 120 °C, we evaluated ever lower Pd loadings. At 1 mol % Pd, we obtained 56% NMR yield for **4.1** and observed ~20% lower NMR yield for the other two precursors (entries 8-10), again showing the superior activity **4.1**.

Table 4.3. Representative results of comparisons, optimization, and TON investigation for Heck coupling. P(*t*Bu)$_3$ was used as the phosphine ligand unless otherwise noted, with L-to-Pd ratios indicated.

Entry	Pd source	Pd mol %	Temp/°C	Time/ h	NMR solution yield%	Alternative additives	TON
1 [a]	**4.1**	2.5	120	18	82		32.8
2 [a]	Pd_2dba_3•$CHCl_3$	2.5	120	18	38		15.2
3 [a]	$[Pd(allyl)Cl]_2$	2.5	120	18	62		24.8
4[b]	**4.1**	2.0	100	18	0		
5[b]	**4.1**	2.0	100	18	0	Cs_2CO_3 instead of Cy_2NMe	
6[b]	**4.1**	1.6	110	18	0		
7[b]	**4.1**	2.0	110	18	5	MePhos instead of P(*t*Bu)$_3$	
8 [a]	**4.1**	1.0	120	18	56		56
9 [a]	Pd_2dba_3•$CHCl_3$	1.0	120	18	39		39
10 [a]	$[Pd(allyl)Cl]_2$	1.0	120	18	35		35
11 [a]	**4.1**	1.0	120	48	57		57
12[b]	**4.1**	1.0	120	48	87		87
13[b]	**4.1**	0.5	120	48	74		148
14[b]	**4.1**	0.25	120	48	42		168
15[b]	**4.1**	0.125	120	48	39		312
16[b]	**4.1**	0.08	120	48	28		350
17[b]	Pd_2dba_3•$CHCl_3$	0.08	120	48	14		175
18[b]	$[Pd(allyl)Cl]_2$	0.08	120	48	12		150
19[b]	**4.1**	0.04	120	48	7		175
20[b]	**4.1**	0.02	120	48	4		200

[a]1:1 L-to-Pd ratio was applied. [b]2:1 L-to-Pd ratio was utilized.

Next, we optimized the reaction conditions by prolonging reaction time, using a 2:1 L-to-Pd ratio, and testing lower catalyst loadings (entries 11-15). The highest solution yield (87%) is obtained by using 1 mol % **4.1** and 1:2 Pd-to-L ratio in 48 hours (Table 4.3, entry 12). A preparative-scale synthesis on 1.0 mmol under these conditions gives a 66% isolated yield (comparable to the reported 72%, which uses 3x more catalyst) (equation 4.6).[51] To further assess the maximum potential TON when using complex **4.1**, we continued decreasing the Pd loading to a limit of 0.02 mol%, where nearly no reactivity is observed

(entries 16, 19, 20). The highest TON (350) is achieved using 0.08 mol % **4.1** (entry 16), which is double the TON obtained using Pd_2da_3•$CHCl_3$ or $[Pd(allyl)Cl]_2$ under otherwise identical conditions (entries 17 and 18).

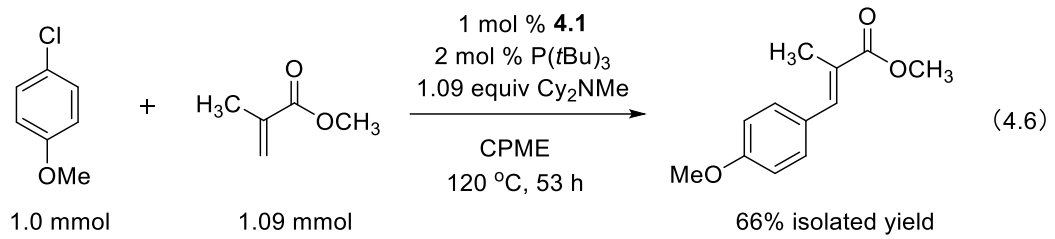

4.3.6 Complex 4.1 as a Precatalyst in C–O Coupling

Coupling of aryl halides and alcohols to form a C–O bond is generally challenging using Pd catalysis, requiring specific ligands to achieve high activity. As reported by Buchwald and co-workers, a series of C–O couplings can be conducted at mild temperatures using the *t*BuBrettPhos-based Buchwald G3 precatalyst for primary alcohols, and the AdCyBrettPhos-based G3 precatalyst for secondary alcohols.[52,53] In light of these results, our initial efforts focus on the assessment of **4.1** in C–O couplings under analogous reaction conditions (Figure 4.10). A preliminary test of coupling between 4-(4-bromophenyl)morpholine and 1-butanol gives excellent product yield (97%) at room temperature (Figure 4.10A), while using 2-chloro-4-methylpyridine gives only 44% yield (Figure 4.10B). The promising activity of **4.1**/*t*BuBrettPhos in these reactions prompted us to test this system for secondary alcohol coupling. Unfortunately, no product is generated under these conditions, though this is consistent with the literature report that AdCyBrettPhos is required for these secondary alcohol couplings.[53]

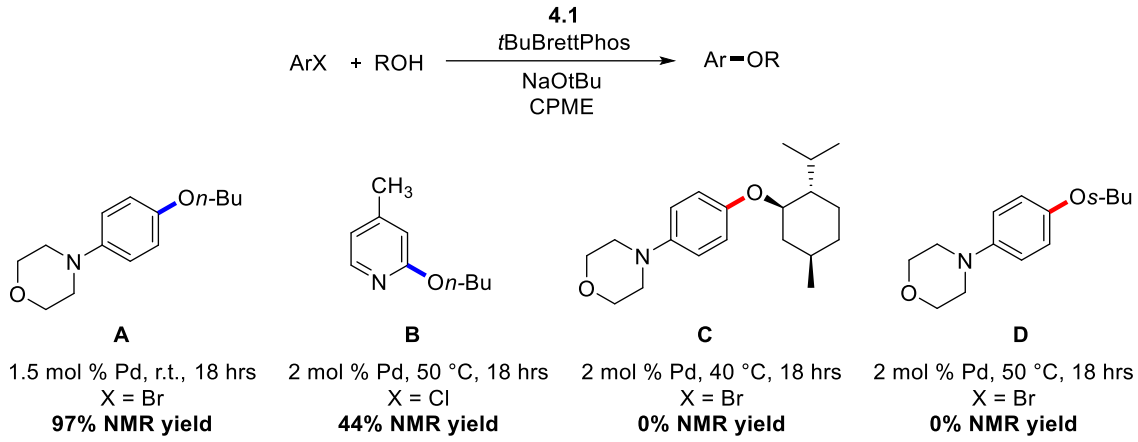

Figure 4.10. Preliminary tests using **4.1** in C–O couplings under conditions reported by Buchwald and co-workers.

To evaluate C–O coupling with a secondary alcohol, we adapted reaction conditions reported by Beller and co-workers,[54] using AdBippyPhos instead of AdCyBrettPhos. We examined the C–O coupling of 2-butanol and 4-bromoacetophenone, with 66% and 71% NMR yields being obtained for **4.1** and $[Pd(allyl)Cl]_2$ (equation 4.7). Notably, the good performance of $[Pd(allyl)Cl]_2$ in this reaction is inconsistent with the generally poor reactivity observed for $[Pd(allyl)Cl]_2$ in our prior studies for the coupling of 4-bromoacetophenone and *n*-butanol (Chapter 2, Section 2.3.3, and Figure 4.11, left).[20]

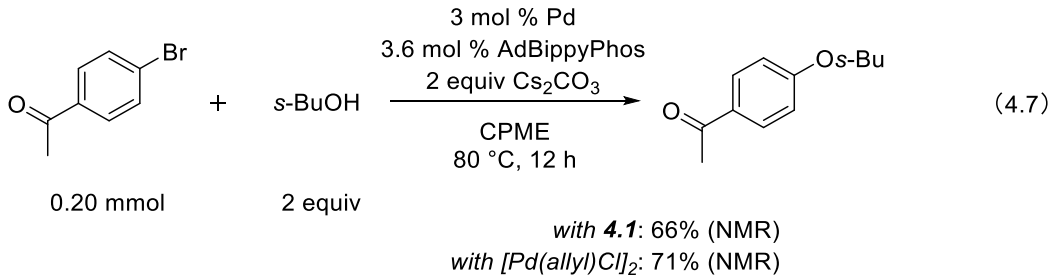

This apparent discrepancy prompted us to perform HTS on the 4-bromoacetophenone + *n*-butanol reaction. This would not only allow us to re-evaluate the prior results, but also to ensure an internally consistent and comprehensive comparison of **4.1** against ^{DMP}DAB–Pd–MAH and four other Pd sources for *in situ* catalyst formation (Figure 4.11, right). Given the generally poor reactivity of XPhos and Me$_4$*t*BuXPhos

observed initially, we omitted these ligands from the follow-up screen. To further accentuate differences in reactivity, we also conducted this follow-up screen at a lower reaction temperature (50 °C rather than 80 °C).

Compared to the prior screening results, we observe generally improved catalytic activity at 50 °C using only 1 equivalent of the base, though many of the trends remain consistent. BippyPhos is again a superior ligand with many Pd sources, giving high normalized product amounts when combined with ^{DMP}DAB–Pd–MAH, $Pd(OAc)_2$, and Pd_2da_3•$CHCl_3$; however, it again fails to give high activity when combined with $[Pd(allyl)Cl]_2$. Surprisingly, **4.1**/BippyPhos also performs poorly (confirmed with several repeat experiments). Generally, higher activity is observed with *t*BuBrettPhos in this screen compared to the previous screen (except with Pd_2da_3•$CHCl_3$, which is consistently poor in both). BrettPhos exhibits moderate to poor reactivity in all combinations at this lower temperature (failing with both $[Pd(allyl)Cl]_2$ and Pd_2dba_3•$CHCl_3$), whereas *t*BuXPhos exhibits improved performance.

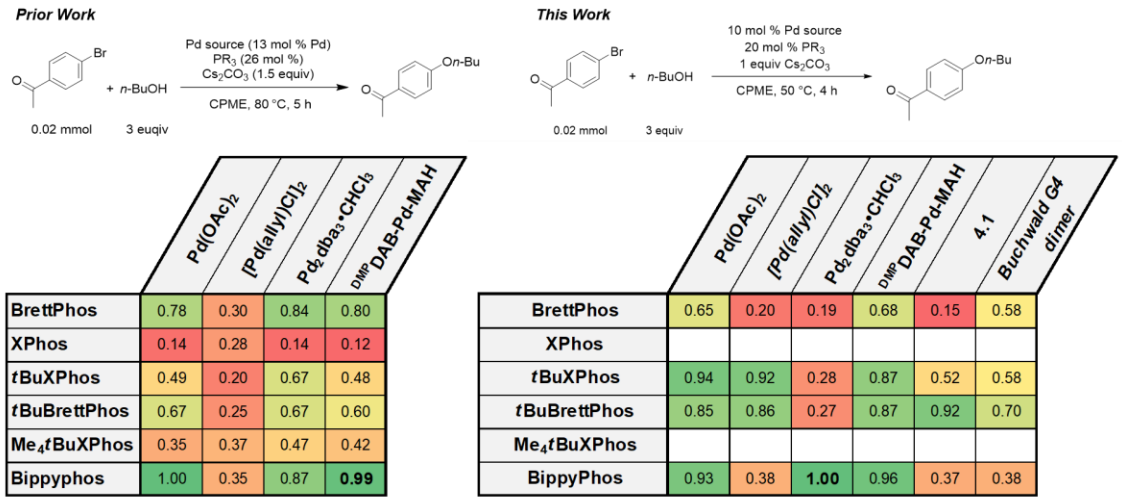

	$Pd(OAc)_2$	$[Pd(allyl)Cl]_2$	Pd_2dba_3•$CHCl_3$	^{DMP}DAB-Pd-MAH
BrettPhos	0.78	0.30	0.84	0.80
XPhos	0.14	0.28	0.14	0.12
*t*BuXPhos	0.49	0.20	0.67	0.48
*t*BuBrettPhos	0.67	0.25	0.67	0.60
Me_4*t*BuXPhos	0.35	0.37	0.47	0.42
Bippyphos	1.00	0.35	0.87	**0.99**

	$Pd(OAc)_2$	$[Pd(allyl)Cl]_2$	Pd_2dba_3•$CHCl_3$	^{DMP}DAB-Pd-MAH	4.1	Buchwald G4 dimer
BrettPhos	0.65	0.20	0.19	0.68	0.15	0.58
XPhos						
*t*BuXPhos	0.94	0.92	0.28	0.87	0.52	0.58
*t*BuBrettPhos	0.85	0.86	0.27	0.87	0.92	0.70
Me_4*t*BuXPhos						
BippyPhos	0.93	0.38	**1.00**	0.96	0.37	0.38

Figure 4.11. *Left*: HTE results of a C–O coupling of 4-bromoacetophenone and 1-butanol in our prior work. *Right*: HTE results of the same reaction in this work under milder conditions.

Color gradient indicates normalized HPLC product peak area/internal standard peak area (red = 0; yellow = 0.50; green = 1.00; largest product/std area ratio normalized to 1.00).

To confirm the reliability of these results, we used NMR spectroscopy to establish solution yields versus internal standard for several wells, and repeated many of these

reactions multiple times (e.g. **4.1**/BippyPhos). These repeat results are highly consistent with the trends observed from HTS, so we attribute the slight discrepancies between the earlier screen and the present one to the relatively high sensitivity of this coupling reaction to even slight modifications of reaction parameters.

From the HTS results, we further evaluated the 10 most promising on 0.43 mmol scale using only 1 mol % Pd loading and 1:2 Pd-to-L ratio for 5 hours (equation 4.8 and Table 4.4). At this 10-fold lower Pd loading, most of the catalytic systems yield poor to moderate amounts of product. Three systems stood out with solution yields ≥70%: **4.1**/*t*BuBrettPhos (90%), [Pd(allyl)Cl]$_2$/*t*BuBrettPhos (83%), and ^{DMP}DAB–Pd–MAH/*t*BuXPhos (70%) (entries 4, 7, and 8). Further comparing these three systems at only 1 hour reaction time reveals the same reactivity trend, with **4.1**/*t*BuBrettPhos being superior. Notably, there was only 1.1 equivalents of 1-butanol in these small-scale comparisons; generally, excess alcohol (2-3 equivalents) is used to prevent β-H elimination side reactions.

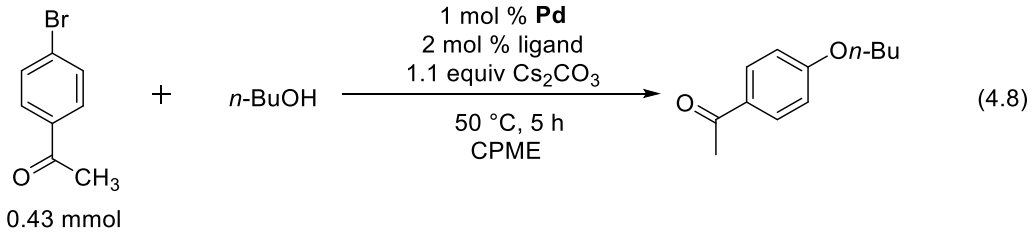

(4.8)

Table 4.4. Hit validation for 10 catalyst systems identified during HTS of C–O coupling.

Entry	Pd source	Pd loading	Phosphine (2 mol %)	NMR solution yield%
1	^{DMP}DAB–Pd–MAH	1 mol %	BippyPhos	53
2	Pd(OAc)$_2$	1 mol %	BippyPhos	53
3	Pd$_2$dba$_3$•CHCl$_3$	1 mol %	BippyPhos	48
4	**4.1**	1 mol %	*t*BuBrettPhos	90 (35 [a])
5	^{DMP}DAB–Pd–MAH	1 mol %	*t*BuBrettPhos	23
6	Pd(OAc)$_2$	1 mol %	*t*BuBrettPhos	26
7	[Pd(allyl)Cl]$_2$	1 mol %	*t*BuBrettPhos	83 (29[a])
8	^{DMP}DAB–Pd–MAH	1 mol %	*t*BuXPhos	70 (15[a])
9	Pd(OAc)$_2$	1 mol %	*t*BuXPhos	8
10	[Pd(allyl)Cl]$_2$	1 mol %	*t*BuXPhos	66

[a]Reaction time: 1 hour.

Given the superior performance of **4.1** and $[Pd(allyl)Cl]_2$ in combination with *t*BuBrettPhos, we conducted an in-depth comparison of these two precursors at low catalyst loading (Table 4.5). To optimize the reaction conditions, we continually reduced the catalyst loading until incomplete conversion was detected (Table 4.5, entries 1-9). Compared to the systems utilizing a 2:1 L-to-Pd ratio, 20-30% lower yields were observed using 1:1 L-to-Pd ratio, revealing the need for adding excess phosphine ligands. Complete conversion of 4-bromoacetophenone is only observed in entries 1 and 4, with the highest yields achieved under these two conditions. Though conditions in entry 1 give a slightly higher amount of product, the catalytic system in entry 4 gives significantly higher TON due to the lower loading. Therefore, conditions in entry 4 were translated into a large-scale synthesis on 1.01 mmol, giving 76% isolated yield after 24 hours (equation 4.9).

During TON assessment using **4.1**, we observe very little reactivity when the Pd loading is lower than 0.1 mol %. Accordingly, the highest TON (680 for **4.1** and 660 for $[Pd(allyl)Cl]_2$) in this coupling is obtained at 0.1 mol % Pd loading (entries 8 and 9) . Overall, our comparison also shows that **4.1** has comparable catalytic activity to $[Pd(allyl)Cl]_2$ at each Pd loading tested.

Table 4.5. Representative results of comparisons, optimization, and TON investigation for C–O coupling.

Entry	Pd source	Pd loading	*t*BuBrettPhos Loading mol%	Time/ h	NMR solution yield%	TON
1	**4.1**	0.5 mol %	1 mol %	18	92	184
2	**4.1**	0.2 mol %	0.2 mol %	18	72	360
3	$[Pd(allyl)Cl]_2$	0.2 mol %	0.2 mol %	18	60	300
4	**4.1**	0.2 mol %	0.4 mol %	18	84	420
5	$[Pd(allyl)Cl]_2$	0.2 mol %	0.4 mol %	18	81	405
6	**4.1**	0.1 mol %	0.1 mol %	18	38	380
7	$[Pd(allyl)Cl]_2$	0.1 mol %	0.1 mol %	18	46	460
8	**4.1**	0.1 mol %	0.2 mol %	18	68	680
9	$[Pd(allyl)Cl]_2$	0.1 mol %	0.2 mol %	18	66	660
10	**4.1**	0.05 mol %	0.1 mol %	48	17	340
11	$[Pd(allyl)Cl]_2$	0.05 mol %	0.1 mol %	48	21	420
12	**4.1**	0.025 mol %	0.05 mol %	48	5	200
13	**4.1**	0.0125 mol %	0.025 mol %	48	1	80

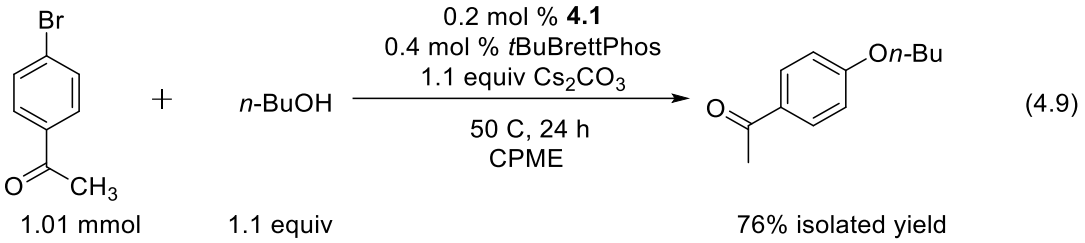

4.4 Conclusions

In summary, we developed a new, bench-stable, and active Pd^{II} dialkyl precursor (**4.1**) for OAC generation and cross-coupling reactions. This new precatalyst is thermally stable and can be handled in air without the need for a glovebox or inert atmosphere. It also exhibits good solution stability in a range of solvents over two days at room temperature under air, which is more than long enough to permit solution dispensing in many applications. Successful isolation of the known complex XANTPhos–Pd–$(CH_2TMS)_2$ as well as 3 OACs using **4.1** demonstrates that it is a good alternative to COD–Pd–$(CH_2TMS)_2$ in organometallic synthesis, as well as demonstrating how this precursor could undergo activation during *in situ* catalyst formation. Moreover, an extensive evaluation of catalytic performance in Suzuki-Miyaura, Heck, and C–O couplings demonstrates comparable or superior catalytic activity of **4.1** over common Pd sources, especially at low Pd loadings. A maximum TON of 1880 was obtained in a model Suzuki-Miyaura coupling reaction. Based on our assessment, complex **4.1** effectively addresses the issues of our prior precursor ^{DMP}DAB–Pd–MAH, including a straightforward activation pathway (via C–C reductive elimination), ability to generate OACs, and high activity in several reactions. Importantly, this precursor also overcomes the thermal stability problems of COD–Pd–$(CH_2TMS)_2$, and does not rely on stabilization by a potentially inhibiting electron-deficient alkene.

4.5 General Experimental Methods

Note: additional experimental details and images of relevant spectroscopic data are included in Appendix A.

4.5.1 Synthesis of ^{DMP}DAB–Pd–$(CH_2TMS)_2$ (4.1)

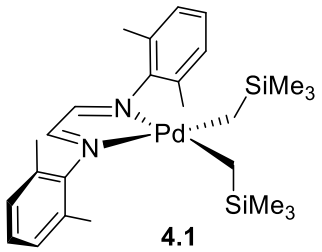

4.1

From (COD)Pd($CH_2TMS)_2$: In a glovebox under a dry, oxygen-free atmosphere of nitrogen gas, a 2-dram vial was charged with (1*E*,2*E*)-N^1,N^2-bis(2,6-dimethylphenyl)ethane-1,2-diimine (272.8 mg, 1.03 mmol) and cold THF (5 mL, stored in a -30 °C freezer before use) to prepare the imine ligand solution. A 4-dram vial was charged with (COD)Pd($CH_2TMS)_2$ (400 mg, 1.03 mmol) and cold THF (9 mL, stored in a -30 °C freezer before use) and a stirbar, followed by the dropwise addition of the cold imine ligand solution with stirring. The solution was stirred at room temperature for 22 hours. The resulting solution was then filtered through a Celite bed. The solvent and COD by-product were removed under vacuum to yield **4.1** as a dark brown/green solid (537.2 mg, 96%). No further purification was necessary.

From (COD)$PdCl_2$: In a glovebox under a dry, oxygen-free atmosphere of nitrogen, a 250 mL RB flask was charged with (COD)$PdCl_2$ (0.33 g, 1.17 mmol), anhydrous diethyl ether (4 mL), and a stirbar. The flask was sealed with a rubber septum and removed from the glovebox. Under a nitrogen stream, the suspension was cooled in an ice bath for 10 minutes. Then, with stirring, $TMSCH_2MgCl$ was added dropwise (1.0 M in diethyl ether, 2.0 mL, 2.0 mmol). The solution/slurry changed from a bright orange-yellow to dark grey-green. After stirring for an additional 15 minutes, the reaction was quenched with acetone (0.1 mL), followed by the addition of dioxane (1 mL). During this process, precipitation of dark coloured solids was observed. After opening the flask to air, ^{DMP}DAB (0.19 g, 0.89 mmol) was added to the reaction mixture, resulting in a colour change to dark brown. This mixture was stirred for 15 minutes at 0 °C. The resulting suspension was then filtered through a Celite bed, which was washed with diethyl ether (80 mL). Solvent evaporation under vacuum yielded a dark brown crude product, determined to be a mixture of **4.1** and residual ^{DMP}DAB. The residue was purified by silica gel column chromatography

(hexanes/ethyl acetate, 22:33 to 0:100) to yield a dark brown/green solid (0.23 g, 0.42 mmol, 42%).

^{1}H NMR: (500 MHz; benzene-d_6) δ 0.23 (s, 18 H, Si–CH_3), 0.44 (s, 4H, Pd–CH_2–Si), 2.17 (s, 12H, Ar–CH_3), 6.86 (s, 2H, NH), 6.96 (m, 6H, Ar–H).

^{13}C{^{1}H} NMR: (125 MHz; benzene-d_6) δ 0.32 (CH_2–Si), 4.10 (Si–CH_3), 18.82 (Ar–**C**H_3), 126.61 (Ar), 128.52 (Ar), 128.57 (Ar), 147.57 (Ar), 160.06 (–N=C–C=N–).

HRMS (ESI) of $C_{24}H_{34}N_3PdSi$, [^{DMP}DAB–Pd(MeCN)–(CH2TMS) + H]$^{+}$ (major isotopomer, proton adduct): 498.15513 (calc'd); 498.15530 (found). HRMS (ESI) of $C_{22}H_{31}N_2PdSi$, [M – CH_2TMS + H]$^{+}$ (second major isotopomer, proton adduct): 457.12859 (calc'd); 457.12877 (found).

4.5.2 Synthesis of XANTPhos–Pd–$(CH_2TMS)_2$ (4.2)

A 4-dram vial was charged with **4.1** (32.3 mg, 0.06 mmol), XANTPhos (32.7 mg, 0.06 mmol), diethyl ether (0.5 mL) and a stirbar. The mixture was stirred at room temperature for 1 hour, followed by solvent evaporation under vacuum. The crude product underwent trituratation/decantation with pentane/diethyl ether (1:1) until the wash solution was colorless (7 times). The solvent was evaporated under vacuum to give a pale-yellow solid (33.2 mg, 68%). The ^{1}H and ^{13}P{^{1}H} NMR spectra are consistent with the reported data.[34]

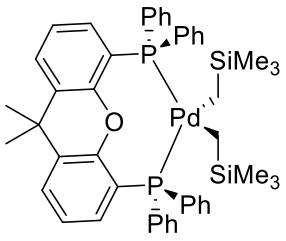

4.2

4.5.3 Synthesis of OACs

Synthesis of BippyPhos–Pd(Br)–(acetophenone) (4.3)

In a glovebox under a dry, oxygen-free atmosphere of nitrogen gas, a 1-dram vial was charged with 4-bromoacetophenone (24.9 mg, 0.13 mmol), **4.1** (21.9 mg, 0.04 mmol), BippyPhos (21.4 mg, 0.04 mmol), CPME (1 mL), and a stirbar. The mixture was stirred at 50 °C for 2 hours. The resulting precipitate was collected by vacuum filtration and washed with CPME (5 x 1 mL), followed by recrystallization using chloroform/CPME to give a pale-yellow solid (26.1 mg, 80%).

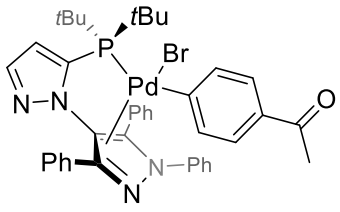

BippyPhos-Pd(Br)-acetophenone (4.3)
80% isolated yield

Crystals for X-ray diffraction were grown at room temperature from DCM/TBME (TBME as anti-solvent) by layering TBME on top of a concentrated solution of **4.3** in DCM.

^{1}H NMR: (500 MHz; $CDCl_3$) δ 0.74 (d, *J*=15.27 Hz, 9H, *t*Bu), 0.87 (d, *J*=15.21 Hz, 9H, *t*Bu), 2.47 (–CO–CH_3–), 6.69 (d, *J*=2.02 Hz, 1H, Ar–H), 7.16 (d, *J*=8.28 Hz 1H, =CH–), 7.19 (d, *J*=8.14 Hz, 1H, =CH–), 7.25-7.27 (m, 3H, Ar–H) 7.31-7.44 (m, 8H, Ar–H), 7.54-7.59 (m, 4H, Ar–H), 7.75-7.77 (m, 2H, Ar–H), 8.11 (d, *J*=2.06 Hz, 1H, Ar–H).

^{31}P{^{1}H} NMR: (202 MHz; $CDCl_3$) δ 32.11.

^{13}C{^{1}H} NMR: (125 MHz; $CDCl_3$) δ 26.43 (–CO–**C**H_3–), 29.14 (d, $^{2}J_{CP}$=5.00 Hz, *t*Bu CH_3), 29.54 (d, $^{2}J_{CP}$=5.09 Hz, *t*Bu CH_3), 37.20 (d, $^{1}J_{CP}$=13.59 Hz, *t*Bu C), 37.49 (d, $^{1}J_{CP}$=13.20 Hz, *t*Bu C), 115.64, 125.79, 126.08, 127.42, 128.09, 128.44, 128.49, 128.64, 128.85, 129.08, 129.50, 130.34, 131.01, 133.11, 138.22 (d, J_{CP}=2.48 Hz), 138.28 (d, J_{CP}=11.10 Hz), 139.21, 142.15, 142.42, 144.0 (d, J_{CP}=7.24 Hz), 144.88, 148.63, 153.56, 198.50 (C=O).

HRMS (ESI) of $C_{40}H_{42}N_4OPPd$, $[M - Br + H]^+$ (major isotopomer, proton adduct): 731.21256 (calc'd); 731.21259 (found).

Synthesis of AdBippyPhos–Pd(Br)–acetophenone (4.4)

In a glovebox under a dry, oxygen-free atmosphere of nitrogen gas, a 1-dram vial was charged with 4-bromoacetophenone (15.1 mg, 0.08 mmol), **4.1** (20.1 mg, 0.04 mmol), AdBippyPhos (24.4 mg, 0.04 mmol), CPME (1 mL), and a stirbar. The mixture was stirred at 50 °C for 4 hours, followed by solvent evaporation under vacuum. The crude product was triturated with diethyl ether, and the liquid phase was decanted. This trituration/decantation process was repeated until the wash solution became colourless (six times). Volatiles were removed under vacuum to give a pale-yellow powder (31.7 mg, 89%). Crystals for X-ray diffraction were grown at room temperature from DCM/diethyl ether (diethyl ether as anti-solvent) by layering diethyl ether on top of a concentrated solution of **4.4** in DCM.

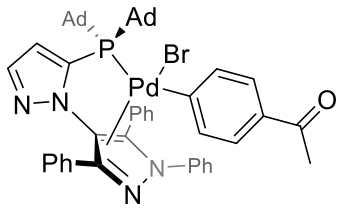

AdBippyPhos-Pd(Br)-acetophenone (4.4)
89% isolated yield

^{1}H NMR: (500 MHz; $CDCl_3$) δ 1.25-1.26 (m, 3H, Ad), 1.34-1.56 (m, 19H, Ad), 1.62 (m, 5H, Ad), 1.78 (m, 3H, Ad), 2.47 (s, 3H, –CO–CH_3), 6.67 (m, 1H, Ar–H), 7.25-7.45 (m, 13H, Ar–H and =CH–CH=), 7.55-7.60 (m, 4H, Ar–H), 7.76-7.78 (m, 2H, Ar–H), 8.13 (m, 1H, Ar–H).

^{31}P{^{1}H} NMR: (202 MHz; $CDCl_3$) δ 26.94.

^{13}C{^{1}H} NMR: (125 MHz; $CDCl_3$) δ 26.45 (CO–**C**H_3), 28.55 (t, $^{3}J_{CP}$=10.20 Hz, Ad), 35.95 (d, J_{CP}=5.06, Ad), 39.29 (Ad), 39.66 (Ad), 42.44 (t, $^{1}J_{CP}$=14.84 Hz, Ad), 42.55 (t, $^{1}J_{CP}$=14.33 Hz, Ad), 116.21, 125.55, 125.87, 127.42, 128.18, 128.43, 128.49, 128.64, 129.26, 129.41, 130.24, 130. 48, 131.07, 132.95, 138.83, 139.23, 140.05, 140.32, 143.87 (d, J=6.43 Hz), 144.50, 148.48, 153.56,198.55 (C=O)

HRMS (ESI) of $C_{52}H_{54}N_4OPPd$ $[M - Br + H]^+$ (major isotopomer, proton adduct): 887.30646 (calc'd); 887.30703 (found).

Synthesis of [XPhos–Pd(Br)–acetophenone]$_2$ (4.5)

In a glovebox under a dry, oxygen-free atmosphere of nitrogen gas, a 1-dram vial was charged with 4-bromoacetophenone (53.0 mg, 0.27 mmol), **4.1** (50.0 mg, 0.09 mmol), XPhos (43.6 mg, 0.09 mmol), THF (1 mL), and a stirbar. The mixture was stirred at 50 °C for 24 hours, followed by solvent evaporation under vacuum. The crude product underwent trituration/decantation with diethyl ether and hexanes at 0 °C. This trituration/decantation process was repeated until the wash solution became colourless (five times). Volatiles were removed under vacuum to give an orange solid (31.1 mg, 43%). Crystals for X-ray diffraction were grown at 0 °C from DCM/diethyl ether (diethyl ether as anti-solvent) by layering diethyl ether on top of a concentrated solution of **4.5** in DCM.

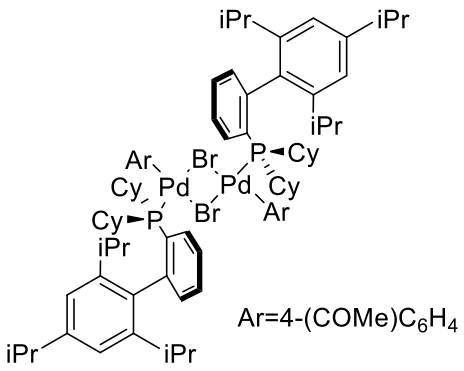

[XPhos–Pd(Br)–acetophenone]$_2$ (4.5)
42% isolated yield

^{1}H NMR: (500 MHz; $CDCl_3$) δ 0.60-0.72 (m, 2H, Cy–H), 0.90 (d, ^{3}J=6.65 Hz, –CH(C**H**$_3$)$_2$), 1.06-1.27 (m, 6H, Cy–H overlapped with hexanes residue), 1.39 (d, ^{3}J=6.95 Hz, –

CH(CH_3)$_2$), 1.58-1.74 (m, 14 H, Cy–H and –CH(CH_3)$_2$), 1.76-1.83 (m, 2H, Cy–H), 1.94 (br, 2H, Cy–H), 2.14-2.25 (m, 2H, Cy–H), 2.44 (sept, *J*=6.90 Hz, 2H, –*CH*(CH_3)$_2$), 2.50 (s, 3H, –CO–CH_3), 3.12 (sept, *J*=6.88 Hz, 1H, –*CH*(CH_3)$_2$), 6.84-6.90 (m, 1H, Ar–H), 7.14 (s, 2H, Ar–H), 7.23 (dd, J_1=1.64 Hz, J_2=8.40 Hz, Ar–H), 7.40-7.45 (m, 2H, Ar–H), 7.49 (d, *J*=8.01Hz, 2H, Ar–H), 7.63-7.69 (m, 1H, Ar–H).

$^{31}P\{^1H\}$ NMR: (202 MHz; $CDCl_3$) δ 26.55.

$^{13}C\{^1H\}$ NMR: (125 MHz; $CDCl_3$) δ 24.62 (Cy), 24.83 (Cy), 25.64 (Cy), 25.97 (Cy), 26.50 (–CO–CH_3), 27.30 (d, *J*=11.47 Hz, Cy), 27.61 (d, *J*=13.17 Hz, Cy), 27.84 (Cy), 28.52 (Cy), 31.67 (Cy), 34.36 (Cy), 35.32 (Cy), 35.53 (Cy), 125.01, 126.24, 127.08, 130.72 (d, *J*=1.74 Hz), 131.92, 133.09, 133.63, 133.72, 134.05, 137.19 (d, *J*=3.44 Hz), 146.82, 147.57, 149.83, 156.70, 198.79 (C=O)

HRMS (ESI) of $C_{41}H_{56}OPPd$, $[M/2 - Br + H]^+$ (major isotopomer, proton adduct): 701.30981 (calc'd); 701.31008 (found). HRMS (ESI) of $C_{82}H_{112}BrO_2P_2Pd_2$, $[M - Br + H]^+$ (minor isotopomer, proton adduct): 1481.53851 (calc'd); 1481.54110 (found).

Synthesis of ^{DMP}DAB–Pd(Br)–acetophenone (4.6)

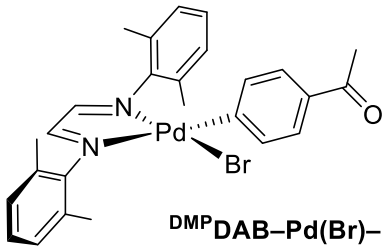

^{DMP}DAB–Pd(Br)–acetophenone (4.6)
62% isolated yield

In a glovebox under a dry, oxygen-free atmosphere of nitrogen gas, a 1-dram vial was charged with 4-bromoacetophenone (8.9 mg, 0.04 mmol), **4.1** (20.0 mg, 0.04 mmol), cataCXium® POMetB (2.4 mg, 0.08 mmol), TBME (0.5 mL), and a stirbar. The mixture was stirred at 50 °C for 24 hours. The resulting precipitate proceeded through trituration/decantation with TBME (4 times). A minimum amount of chloroform was added to redissolve all solids, and the resulting solution was dried over $MgSO_4$ and further dried under vacuum to give a yellow/orange solid (13.0 mg, 62%). Crystals for X-ray diffraction were grown at room temperature from DCM/diethyl ether (diethyl ether as anti-solvent) by layering diethyl ether on top of a concentrated solution of **4.6** in DCM.

^{1}H NMR: (500 MHz; CD_2Cl_2) δ 2.20 (s, 6H, Ar–*CH*$_3$), 2.34 (s, 3H, CO–CH_3), 2.36 (s, 6H, Ar–*CH*$_3$), 6.81-6.86 (m, 2H, Ar–H), 6.88-6.94 (m, 1H, Ar–H), 6.96-7.02 (m, 2H, Ar–H), 7.06-7.11 (m, 2H, Ar–H), 7.16 (m, 3H, Ar–H), 8.12 (s, 1H,), 8.18 (s, 1H, –N=C–H).

^{13}C{^{1}H} NMR: (125 MHz; CD_2Cl_2) δ 18.51 (Ar–*CH*$_3$), 18.95 (Ar–*CH*$_3$), 26.47 (CO–*CH*$_3$), 125.05, 127.54, 127.72, 128.28, 128.35, 128.66, 128.80, 133.08, 134.86, 146.46, 146.93, 155.74, 162.97 (–N=C–), 165.54 (–N=C–), 198.40 (C=O)

HRMS (ESI) of $C_{26}H_{27}BrN_2O_1Pd$, $[M + Na]^+$ (major isotopomer, sodium adduct): 591.02337 (calc'd); 591.02277 (found).

4.5.4 Catalytic Comparisons

Measurement procedures for low catalyst loading experiments:

If the amount of Pd sources/phosphine ligands required was >1.0 mg, solids were weighted using an analytical balance.

If the amount of Pd sources required was <1.0 mg, a stock solution of the corresponding Pd source was prepared at a suitable concentration. The required amount was then dispensed using a micropipette, and the solvent evaporated before adding additional components. Specific solvents used for preparing the Pd stock solutions: **4.1** in THF, $[Pd(allyl)Cl]_2$ in acetone, $Pd(OAc)_2$ in DCM, Pd_2dba_3•$CHCl_3$ in THF.

If the amount of phosphine ligands required was <1.0 mg, a stock solution of the corresponding ligand was prepared in CPME at a suitable concentration. The required amount was then dispensed using a micropipette.

Representative procedure for low catalyst loading reactions:

Suzuki-Miyaura coupling:

The following procedure corresponds to the reaction from Table 4.2, entry 14:

A stock solution of **4.1** in THF (2.3 mg/mL) was dispensed to a 1-dram vial (56.2 μL, 0.129 mg, 0.000237 mmol) containing a stirbar, followed by solvent evaporation under vacuum. The vial was then charged with 1,3,5-trimethoxybenzene (15.8 mg, 0.0939 mmol), phenylboronic acid (131.8 mg, 1.08 mmol), and K_2CO_3 (186.7, 1.35 mmol) under air. The vial was then brought into a nitrogen glovebox. A stock solution of XPhos in anhydrous CPME (2.4 mg/mL) was then dispensed to the reaction mixture (100.2 μL, 0.240 mg, 0.000504 mmol), followed by anhydrous CPME (0.6 mL), and 2-chloro-5-methylpyridine

(98.2 μL, 0.900 mmol). The vial was sealed with a cap containing a Teflon septum and removed from the glovebox. Degassed DI water (0.7 mL) was injected via syringe. The reaction mixture was stirred at 50 °C for 48 hours. The organic phase was transferred to a new 1-dram vial, followed by solvent evaporation and analysis by ^{1}H NMR spectroscopy.

Heck coupling:

The following procedure corresponds to the reaction from Table 4.3, entry 19:

A stock solution of **4.1** in THF (6.4 mg/mL) was dispensed to a 1-dram vial (56.1 μL, 0.362 mg, 0.000664 mmol) containing a stirbar, followed by solvent evaporation under vacuum. The vial was then charged with 1,3,5-trimethoxybenzene (12.7 mg, 0.0755 mmol), 4-chloroanisole (200 μL, 1.63 mmol) under air. The vial was then brought into a nitrogen glovebox. A stock solution of P(*t*Bu)$_3$ in anhydrous Toluene (5.3 mg/mL) was then dispensed to the reaction mixture (50.6 μL, 0.267 mg, 0.00132 mmol), followed by anhydrous CPME (0.9 mL), methyl methacrylate (190 μL, 1.78 mmol), and Cy_2NMe (380 μL, 1.78 mmol). The reaction mixture was stirred at 120 °C for 48 hours. The resulting solution underwent solvent evaporation and analysis by ^{1}H NMR spectroscopy.

C–O coupling:

The following procedure corresponds to the reaction from Table 4.5, entry 12:

A stock solution of **4.1** in THF (3.9 mg/mL) was dispensed to a 1-dram vial (56.2 μL, 0.221 mg, 0.000405 mmol) containing a stirbar, followed by solvent evaporation under vacuum. The vial was then charged with 1,3,5-trimethoxybenzene (17.1 mg, 0.102 mmol), 4-bromoacetophenone (300 mg, 1.51 mmol) under air. The vial was then brought into a nitrogen glovebox. A stock solution of *t*BuBrettPhos in anhydrous CPME (3.8 mg/mL) was then dispensed to the reaction mixture (100.4 μL, 0.381 mg, 0.000786 mmol), followed by Cs_2CO_3 (591.3 mg, 1.81 mmol), 1-butanol (151.7 μL, 1.66 mmol), anhydrous CPME (2.0 mL). The reaction mixture was stirred at 50 °C for 48 hours. The resulting solution underwent filtration to remove the base, followed by solvent evaporation and analysis by ^{1}H NMR spectroscopy.

4.6 References

(1) Reeves, E. K.; Entz, E. D.; Neufeldt, S. R. Chemodivergence between Electrophiles in Cross-Coupling Reactions. *Chem. – Eur. J.* **2021**, *27* (20), 6161–6177. https://doi.org/10.1002/chem.202004437.

(2) Maleckis, A.; Sanford, M. S. Catalytic Cycle for Palladium-Catalyzed Decarbonylative Trifluoromethylation Using Trifluoroacetic Esters as the CF_3 Source. *Organometallics* **2014**, *33* (10), 2653–2660. https://doi.org/10.1021/om500398z.

(3) Dennis, J. M.; White, N. A.; Liu, R. Y.; Buchwald, S. L. Pd-Catalyzed C–N Coupling Reactions Facilitated by Organic Bases: Mechanistic Investigation Leads to Enhanced Reactivity in the Arylation of Weakly Binding Amines. *ACS Catal.* **2019**, *9* (5), 3822–3830. https://doi.org/10.1021/acscatal.9b00981.

(4) Culkin, D. A.; Hartwig, J. F. Carbon−Carbon Bond-Forming Reductive Elimination from Arylpalladium Complexes Containing Functionalized Alkyl Groups. Influence of Ligand Steric and Electronic Properties on Structure, Stability, and Reactivity. *Organometallics* **2004**, *23* (14), 3398–3416. https://doi.org/10.1021/om049726k.

(5) Lu, J.; Donnecke, S.; Paci, I.; Leitch, D. C. A Reactivity Model for Oxidative Addition to Palladium Enables Quantitative Predictions for Catalytic Cross-Coupling Reactions. *Chem. Sci.* **2022**, *13* (12), 3477–3488. https://doi.org/10.1039/D2SC00174H.

(6) Widenhoefer, R. A.; Zhong, H. A.; Buchwald, S. L. Synthesis and Solution Structure of Palladium Tris(*o*-tolyl)phosphine Mono(Amine) Complexes. *Organometallics* **1996**, *15* (12), 2745–2754. https://doi.org/10.1021/om9509599.

(7) Vinogradova, E. V.; Zhang, C.; Spokoyny, A. M.; Pentelute, B. L.; Buchwald, S. L. Organometallic Palladium Reagents for Cysteine Bioconjugation. *Nature* **2015**, *526* (7575), 687–691. https://doi.org/10.1038/nature15739.

(8) Ingoglia, B. T.; Buchwald, S. L. Oxidative Addition Complexes as Precatalysts for Cross-Coupling Reactions Requiring Extremely Bulky Biarylphosphine Ligands. *Org. Lett.* **2017**, *19* (11), 2853–2856. https://doi.org/10.1021/acs.orglett.7b01082.

(9) Rojas, A. J.; Pentelute, B. L.; Buchwald, S. L. Water-Soluble Palladium Reagents for Cysteine S-Arylation under Ambient Aqueous Conditions. *Org. Lett.* **2017**, *19* (16), 4263–4266. https://doi.org/10.1021/acs.orglett.7b01911.

(10) Xu, J.; Liu, R. Y.; Yeung, C. S.; Buchwald, S. L. Monophosphine Ligands Promote Pd-Catalyzed C–S Cross-Coupling Reactions at Room Temperature with Soluble Bases. *ACS Catal.* **2019**, *9* (7), 6461–6466. https://doi.org/10.1021/acscatal.9b01913.

(11) Mallek, A. J.; Pentelute, B. L.; Buchwald, S. L. Selective N-Arylation of *p*-Aminophenylalanine in Unprotected Peptides with Organometallic Palladium Reagents. *Angew. Chem. Int. Ed.* **2021**, *60* (31), 16928–16931. https://doi.org/10.1002/anie.202104780.

(12) Hu, H.; Burlas, C. E.; Curley, S. J.; Gruchala, T.; Qu, F.; Shaughnessy, K. H. Effect of Aryl Ligand Identity on Catalytic Performance of Trineopentylphosphine Arylpalladium Complexes in N-Arylation Reactions. *Organometallics* **2020**, *39* (20), 3618–3627. https://doi.org/10.1021/acs.organomet.0c00140.

(13) Uehling, M. R.; King, R. P.; Krska, S. W.; Cernak, T.; Buchwald, S. L. Pharmaceutical Diversification via Palladium Oxidative Addition Complexes. *Science* **2019**, *363* (6425), 405–408. https://doi.org/10.1126/science.aac6153.

(14) Amatore, C.; Carre, E.; Jutand, A.; M'Barki, M. A. Rates and Mechanism of the Formation of Zerovalent Palladium Complexes from Mixtures of $Pd(OAc)_2$ and Tertiary Phosphines and Their Reactivity in Oxidative Additions. *Organometallics* **1995**, *14* (4), 1818–1826. https://doi.org/10.1021/om00004a039.

(15) Zalesskiy, S. S.; Ananikov, V. P. $Pd_2(dba)_3$ as a Precursor of Soluble Metal Complexes and Nanoparticles: Determination of Palladium Active Species for Catalysis and Synthesis. *Organometallics* **2012**, *31* (6), 2302–2309. https://doi.org/10.1021/om201217r.

(16) Hruszkewycz, D. P.; Balcells, D.; Guard, L. M.; Hazari, N.; Tilset, M. Insight into the Efficiency of Cinnamyl-Supported Precatalysts for the Suzuki–Miyaura Reaction: Observation of Pd(I) Dimers with Bridging Allyl Ligands During Catalysis. *J. Am. Chem. Soc.* **2014**, *136* (20), 7300–7316. https://doi.org/10.1021/ja412565c.

(17) Hruszkewycz, D. P.; Guard, L. M.; Balcells, D.; Feldman, N.; Hazari, N.; Tilset, M. Effect of 2-Substituents on Allyl-Supported Precatalysts for the Suzuki–Miyaura Reaction: Relating Catalytic Efficiency to the Stability of Palladium(I) Bridging Allyl Dimers. *Organometallics* **2015**, *34* (1), 381–394. https://doi.org/10.1021/om501250y.

(18) Fairlamb, I. J. S. π-Acidic Alkene Ligand Effects in Pd-Catalysed Cross-Coupling Processes: Exploiting the Interaction of Dibenzylidene Acetone (dba) and Related Ligands with Pd(0) and Pd(II). *Org. Biomol. Chem.* **2008**, *6* (20), 3645–3656. https://doi.org/10.1039/B811772A.

(19) Lee, H. G.; Milner, P. J.; Buchwald, S. L. An Improved Catalyst System for the Pd-Catalyzed Fluorination of (Hetero)Aryl Triflates. *Org. Lett.* **2013**, *15* (21), 5602–5605. https://doi.org/10.1021/ol402859k.

(20) Huang, J.; Isaac, M.; Watt, R.; Becica, J.; Dennis, E.; Saidaminov, M. I.; Sabbers, W. A.; Leitch, D. C. ^{DMP}DAB–Pd–MAH: A Versatile Pd(0) Source for Precatalyst Formation, Reaction Screening, and Preparative-Scale Synthesis. *ACS Catal.* **2021**, *11* (9), 5636–5646. https://doi.org/10.1021/acscatal.1c00288.

(21) Pan, Y.; Young, G. B. Syntheses and Spectroscopic Characteristics of Dialkylpalladium(II) Complexes; $PdR_2(COD)$ as Precursors for Derivatives with N- or P-Donor Ligands. *J. Organomet. Chem.* **1999**, *577* (2), 257–264. https://doi.org/10.1016/S0022-328X(98)01071-7.

(22) Lee, H. G.; Milner, P. J.; Buchwald, S. L. Pd-Catalyzed Nucleophilic Fluorination of Aryl Bromides. *J. Am. Chem. Soc.* **2014**, *136* (10), 3792–3795. https://doi.org/10.1021/ja5009739.

(23) Cámpora, J.; López, J. A.; Palma, P.; del Rio, D.; Carmona, E.; Valerga, P.; Graiff, C.; Tiripicchio, A. Synthesis and Insertion Reactions of the Cyclometalated Palladium−Alkyl Complexes $Pd(CH_2CMe_2\text{-}o\text{-}C_6H_4)L_2$. Observation of a Pentacoordinated Intermediate in the Insertion of SO_2. *Inorg. Chem.* **2001**, *40* (17), 4116–4126. https://doi.org/10.1021/ic010114r.

(24) King, R. P.; Krska, S. W.; Buchwald, S. L. A Neophyl Palladacycle as an Air- and Thermally Stable Precursor to Oxidative Addition Complexes. *Org. Lett.* **2021**, *23* (20), 7927–7932. https://doi.org/10.1021/acs.orglett.1c02307.

(25) Burns, C. T.; Jordan, R. F. Ethylene Dimerization by Cationic Palladium(II) Alkyl Complexes That Contain Bis(heterocycle)methane Ligands. *Organometallics* **2007**, *26* (27), 6726–6736. https://doi.org/10.1021/om700767r.

(26) Gorman, C. B.; Vest, R. W.; Palovich, T. U.; Serron, S. Preparation of Poly(cyanoacetylene) Using Late-Transition-Metal Catalysts. *Macromolecules* **1999**, *32* (13), 4157–4165. https://doi.org/10.1021/ma981773z.

(27) van Asselt, R.; Rijnberg, E.; Elsevier, C. J. Rigid Bidentate Nitrogen Ligands in Organometallic Chemistry and Homogeneous Catalysis. 7. Stabilization of High Oxidation States by Rigid Bidentate Nitrogen Ligands: Synthesis and Characterization of Diorgano- and Triorganopalladium(IV) and Cationic Triorganoplatinum(IV) Complexes. *Organometallics* **1994**, *13* (2), 706–720. https://doi.org/10.1021/om00014a049.

(28) Xu, H.; Hu, C. T.; Wang, X.; Diao, T. Structural Characterization of β-Agostic Bonds in Pd-Catalyzed Polymerization. *Organometallics* **2017**, *36* (21), 4099–4102. https://doi.org/10.1021/acs.organomet.7b00666.

(29) Allen, K. E.; Campos, J.; Daugulis, O.; Brookhart, M. Living Polymerization of Ethylene and Copolymerization of Ethylene/Methyl Acrylate Using "Sandwich" Diimine Palladium Catalysts. *ACS Catal.* **2015**, *5* (1), 456–464. https://doi.org/10.1021/cs5016029.

(30) Tempel, D. J.; Johnson, L. K.; Huff, R. L.; White, P. S.; Brookhart, M. Mechanistic Studies of Pd(II)−α-Diimine-Catalyzed Olefin Polymerizations1. *J. Am. Chem. Soc.* **2000**, *122* (28), 6686–6700. https://doi.org/10.1021/ja000893v.

(31) Shultz, L. H.; Brookhart, M. Measurement of the Barrier to β-Hydride Elimination in a β-Agostic Palladium−Ethyl Complex: A Model for the Energetics of Chain-Walking in $(\alpha\text{-Diimine})PdR^+$ Olefin Polymerization Catalysts. *Organometallics* **2001**, *20* (19), 3975–3982. https://doi.org/10.1021/om010197j.

(32) Shultz, L. H.; Tempel, D. J.; Brookhart, M. Palladium(II) β-Agostic Alkyl Cations and Alkyl Ethylene Complexes: Investigation of Polymer Chain Isomerization Mechanisms. *J. Am. Chem. Soc.* **2001**, *123* (47), 11539–11555. https://doi.org/10.1021/ja011055j.

(33) Cámpora, J.; del Mar Conejo, M.; Mereiter, K.; Palma, P.; Pérez, C.; Reyes, M. L.; Ruiz, C. Synthesis of Dialkyl, Diaryl and Metallacyclic Complexes of Ni and Pd Containing Pyridine, α-Diimines and Other Nitrogen Ligands: Crystal Structures of the Complexes Cis-NiR_2py_2 (R=benzyl, Mesityl). *J. Organomet. Chem.* **2003**, *683* (1), 220–239. https://doi.org/10.1016/S0022-328X(03)00691-0.

(34) Takahashi, R.; Kubota, K.; Ito, H. Air- and Moisture-Stable Xantphos-Ligated Palladium Dialkyl Complex as a Precatalyst for Cross-Coupling Reactions. *Chem. Commun.* **2020**, *56* (3), 407–410. https://doi.org/10.1039/C9CC06946A.

(35) Andersen, T. L.; Kramer, S.; Overgaard, J.; Skrydstrup, T. Evidence for Single-Electron Pathways in the Reaction between Palladium(II) Dialkyl Complexes and Alkyl Bromides under Thermal and Photoinduced Conditions. *Organometallics* **2017**, *36* (11), 2058–2066. https://doi.org/10.1021/acs.organomet.6b00893.

(36) Seligson, A. L.; Trogler, W. C. Protonolysis Approach to the Catalytic Amination of Olefins with Bis(phosphine)palladium(II) Dialkyls. *Organometallics* **1993**, *12* (3), 744–751. https://doi.org/10.1021/om00027a026.

(37) Cai, Y.; Shi, Y. Synthesis and X-Ray Characterization of Novel Palladium(II) Complexes with Tunable Chiral Anionic Counterions. *Dalton Trans.* **2013**, *42* (15), 5232–5236. https://doi.org/10.1039/C3DT00007A.

(38) Straub, B. F.; Rominger, F.; Hofmann, P. Diazoalkane Chemistry of Palladium: Synthesis of a Diphosphinomethanide Complex from Dimethyl Diazomalonate by N2 Loss and Proton Transfer. *Inorg. Chem. Commun.* **2000**, *3* (7), 358–360. https://doi.org/10.1016/S1387-7003(00)00098-8.

(39) Seligson, A. L.; Trogler, W. C. One-Electron Oxidative Cleavage of Palladium(II) Alkyl and Phenoxo Bonds. *J. Am. Chem. Soc.* **1992**, *114* (18), 7085–7089. https://doi.org/10.1021/ja00044a019.

(40) Stockland, R. A.; Anderson, G. K.; Rath, N. P. Reactions of $[PdX_2(dppm)]$ Complexes with Grignard Reagents. *Organometallics* **1997**, *16* (23), 5096–5101. https://doi.org/10.1021/om970376u.

(41) Marcone, J. E.; Moloy, K. G. Kinetic Study of Reductive Elimination from the Complexes (Diphosphine)Pd(R)(CN). *J. Am. Chem. Soc.* **1998**, *120* (33), 8527–8528. https://doi.org/10.1021/ja980762i.

(42) Klingensmith, L. M.; Strieter, E. R.; Barder, T. E.; Buchwald, S. L. New Insights into Xantphos/Pd-Catalyzed C−N Bond Forming Reactions: A Structural and Kinetic Study. *Organometallics* **2006**, *25* (1), 82–91. https://doi.org/10.1021/om050715g.

(43) Sotnik, S. O.; Mishchenko, A. M.; Rusanov, E. B.; Kozytskiy, A. V.; Gavrilenko, K. S.; Ryabukhin, S. V.; Volochnyuk, D. M.; Kolotilov, S. V. Third Generation Buchwald Precatalysts with XPhos and RuPhos: Multigram Scale Synthesis, Solvent-Dependent Isomerization of XPhos Pd G3 and Quality Control by ^{1}H- and ^{31}P-NMR Spectroscopy. *Molecules* **2021**, *26* (12), 3507. https://doi.org/10.3390/molecules26123507.

(44) Strotman, N. A.; Soumeillant, M. C.; Zhu, K.; Markwalter, C. E.; Wei, C. S.; Hsiao, Y.; Eastgate, M. D. Effects of Multiple Catalyst Deactivation Pathways and Continuous Ligand Recycling on the Kinetics of Pd-Catalyzed C–N Coupling Reactions. *J. Org. Chem.* **2019**, *84* (8), 4653–4660. https://doi.org/10.1021/acs.joc.8b02214.

(45) Mikus, M. S.; Sanchez, C.; Fridrich, C.; Larrow, J. F. Palladium Catalyzed C−O Coupling of Amino Alcohols for the Synthesis of Aryl Ethers. *Adv. Synth. Catal.* **2020**, *362* (2), 430–436. https://doi.org/10.1002/adsc.201901302.

(46) Janot, C.; Chagnoleau, J.-B.; Halcovitch, N. R.; Muir, J.; Aïssa, C. Palladium-Catalyzed Synthesis of α-Carbonyl- α′-(hetero)aryl Sulfoxonium Ylides: Scope and Insight into the Mechanism. *J. Org. Chem.* **2020**, *85* (2), 1126–1137. https://doi.org/10.1021/acs.joc.9b03032.

(47) Štěpnička, P.; Krupa, M.; Lamač, M.; Císařová, I. Trans-Spanning Ferrocene Amidodiphosphine Ligand: Synthesis, Palladium Complexes and Catalytic Use in Suzuki–Miyaura Cross-Coupling. *J. Organomet. Chem.* **2009**, *694* (18), 2987–2993. https://doi.org/10.1016/j.jorganchem.2009.04.039.

(48) Kim, J.; Hong, S. H. Ligand-Promoted Direct C–H Arylation of Simple Arenes: Evidence for a Cooperative Bimetallic Mechanism. *ACS Catal.* **2017**, *7* (5), 3336–3343. https://doi.org/10.1021/acscatal.7b00397.

(49) DeAngelis, A. J.; Gildner, P. G.; Chow, R.; Colacot, T. J. Generating Active "L-Pd(0)" via Neutral or Cationic π-Allylpalladium Complexes Featuring Biaryl/Bipyrazolylphosphines: Synthetic, Mechanistic, and Structure–Activity Studies in Challenging Cross-Coupling Reactions. *J. Org. Chem.* **2015**, *80* (13), 6794–6813. https://doi.org/10.1021/acs.joc.5b01005.

(50) Orecchia, P.; Petkova, D. S.; Goetz, R.; Rominger, F.; Hashmi, A. S. K.; Schaub, T. Pd-Catalysed Suzuki–Miyaura Cross-Coupling of Aryl Chlorides at Low Catalyst Loadings in Water for the Synthesis of Industrially Important Fungicides. *Green Chem.* **2021**, *23* (20), 8169–8180. https://doi.org/10.1039/D1GC02602J.

(51) Littke, A. F.; Fu, G. C. A Versatile Catalyst for Heck Reactions of Aryl Chlorides and Aryl Bromides under Mild Conditions. *J. Am. Chem. Soc.* **2001**, *123* (29), 6989–7000. https://doi.org/10.1021/ja010988c.

(52) Zhang, H.; Ruiz-Castillo, P.; Buchwald, S. L. Palladium-Catalyzed C–O Cross-Coupling of Primary Alcohols. *Org. Lett.* **2018**, *20* (6), 1580–1583. https://doi.org/10.1021/acs.orglett.8b00325.

(53) Zhang, H.; Ruiz-Castillo, P.; Schuppe, A. W.; Buchwald, S. L. Improved Process for the Palladium-Catalyzed C–O Cross-Coupling of Secondary Alcohols. *Org. Lett.* **2020**, *22* (14), 5369–5374. https://doi.org/10.1021/acs.orglett.0c01668.

(54) Gowrisankar, S.; Sergeev, A. G.; Anbarasan, P.; Spannenberg, A.; Neumann, H.; Beller, M. A General and Efficient Catalyst for Palladium-Catalyzed C−O Coupling Reactions of Aryl Halides with Primary Alcohols. *J. Am. Chem. Soc.* **2010**, *132* (33), 11592–11598. https://doi.org/10.1021/ja103248d.

Chapter 5 Conclusions and Future Work

5.1 Thesis Conclusions

This thesis, in brief, represents the development of active organometallic precatalysts for Pd-catalyzed cross-coupling reactions. Given the lack of an existing stable, robust, active Pd^0 precursor, Chapter 2 established ^{DMP}DAB–Pd–MAH as an air-stable monomeric Pd^0 source. This complex exhibits superior catalytic performance relative to other commonly used Pd sources in a range of commonly used cross-coupling reactions. Chapter 3 focused on establishing ^{DMP}DAB–Pd–MAH as a precursor beyond cross-coupling reactions. Asymmetric allylic alkylation, a stereoselective transformation for carbon-element bond formation, has thus far not seen widespread use of single-component precatalysts. We developed a series of chiral single-component Pd^0 precursors, L*–Pd–MAH, derived from ^{DMP}DAB–Pd–MAH. These new complexes are demonstrated to be exceptional precursors for AAA reactions, and are continuing to be used by our collaborators for natural product total synthesis. In addition to enabling catalysis, structural analysis of these complexes revealed conformational information about substrate binding, including direct observation of intramolecular hydrogen bonding. Finally, during our investigations of ^{DMP}DAB–Pd–MAH and L–Pd–MAH as precatalysts, we observed that catalyst activation generally requires a strong base and/or nucleophile. This prevents effective use of the MAH-based precatalysts in several reaction types, and prevents access to oxidative addition complexes directly from the Pd^0 complexes. This motivated the development of ^{DMP}DAB–Pd–$(CH_2TMS)_2$ as an alternative precursor, as described in Chapter 4. Based on our evaluation, ^{DMP}DAB–Pd–$(CH_2TMS)_2$ is a stable, versatile, active precursor for OAC generation, [phosphine]–Pd–dialkyl formation, reaction screening, and preparative-scale synthesis.

In summary, the overall goal of this project was to create new Pd-based precatalysts for a broad range of reactions, and to ensure these precatalysts have properties that make them compatible with high-throughput experimentation methods. The work presented in each research chapter demonstrates a continual improvement to the catalytic systems by addressing the existing limitations and expanding the scope of reactivity. From the perspective of short-term impacts, we have provided an effective Pd^0 alternative to

Pd_2dba_3•$CHCl_3$, as well as an active yet stable Pd^{II} dialkyl precursor with a straightforward reduction pathway. Our first precursor ^{DMP}DAB–Pd–MAH is now commercially available at MilliporeSigma, and the precursors reported in Chapters 3 and 4 are the subject of filed patent applications. These precursors can be easily accessed by other research groups and evaluated in a much wider range of reactions in the future, including academic research labs and large pharmaceutical high-throughput screening groups. The superior catalytic activity of our precursors at low Pd loading can also contribute to more efficient, user-friendly, and sustainable synthetic processes once utilized in industry.

"A journey of a thousand miles begins with a single step." This is a well-known old saying from one of my ancestors, Lao Zi. The development of optimal catalysts for synthesis is akin to the journey. It is not possible for us (or anyone else) to establish a perfect Pd precursor or catalytic system in the short term. By recognizing the key limitations of existing systems, and setting criteria for the desired features of an ideal system, we can overcome the drawbacks step by step to make the precursors better and more generally applicable in the field of cross-coupling and beyond. Every step we have made during this thesis research is meaningful, and I believe that we will achieve the goal of a universal precatalyst someday if we persist in improving.

5.2 Future Research Plans

5.2.1 Investigating the Activation Pathways of MAH-Based Precatalysts

As mentioned in Chapter 2 (Section 2.3.4), ^{DMP}DAB–Pd–MAH does not appear to follow an analogous catalyst activation to Pd_2dba_3•$CHCl_3$, and is instead likely activated by the strong base and/or nucleophile. Similarly, preliminary catalyst activation studies of single-component precursors L*–Pd–MAH (Chapter 3, Section 3.3.4) reveal the greatest extent of activation occurs with addition of the strong base or strong nucleophile. In addition, our collaborators have noted an apparent slow activation of our precatalysts in an AAA reaction under weakly basic conditions (equation 5.1). Specifically, slow reaction rates are observed for both single-component precatalyst and the catalyst generated *in situ* from ^{DMP}DAB–Pd–MAH/*i*Pr-PHOX ligand when soft enolization conditions are used (BSA/KOAc), though high isolated yield and enantiomeric excess are eventually obtained

in these two cases. We attribute this slow conversion to insufficient catalyst activation, due to the absence of either strong bases or nucleophiles.

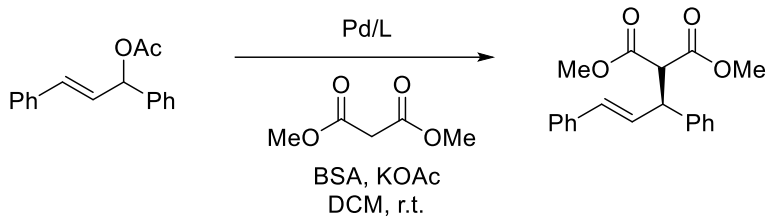

(5.1)

Pd	L	Pd:L	Time (h)	Isolated Yield (%)	ee (%)
Pd_2dba_3	(R)-*i*PrPHOX	1:1.25	1	80	95
^{DMP}DAB-Pd-MAH	(R)-*i*PrPHOX	1:1.25	24	81	97
(S)-*i*PrPHOX-Pd-MAH	-	1:1	24	84	-96

Based on the preliminary results, we hypothesize that strong bases assist the dissociation of MAH. Further investigation can focus on the impacts of bases and other additives on the rate and extent of catalyst activation of ^{DMP}DAB–Pd–MAH and phosphine complexes derived from it. The initial evaluation can start with the bases that have been utilized in our catalytic evaluations, with expanded and extensive base scope afterwards. It is critical to firmly establish the fate of MAH after activation to build on the preliminary LCMS data presented in Chapter 2.

Another direction is to evaluate the reactivity of different exogenous additives with ^{DMP}DAB–Pd–MAH. It is ideal to have an exogenous additive that promotes MAH dissociation without generating potential reactivity inhibitors during this process. This could include addition of mild reducing agents to reduce the C=C bond, or reactive dienes to promote a Diels-Alder cycloaddition with the MAH. Finally, alternative complexes with different electron-deficient alkenes, such as dimethylfumarate or acrylate derivatives, may have faster activation due to weaker Pd–alkene bonding; others in the Leitch lab are currently working on assessing these complexes. Overall, a better understanding of activation pathways is needed to maximize the catalytic efficiency of these precursors as well as give new directions to improve and expand their utility.

5.2.2 Pd Reduction for Catalyst Recycling

In Chapter 3, we observed slow formation of a side product – [PNNP]Pd^{II} – when exposing Trost-type L*–Pd–MAH precatalysts to the air. Though it is regarded as a catalytically inert complex in AAA chemistry, a similar [PNNP]Pd^{II} complex has shown promising activity in a common Suzuki-Miyaura coupling.[1] Given the high cost of Pd and the corresponding supporting ligands, such as the chiral Trost-type ligands and PHOX-type ligands used in Chapter 3, efficient recycling of these catalysts would be very beneficial. However, separating homogeneous catalysts (all Pd precursors mentioned in this thesis) from reaction mixtures can be challenging, especially in a form that is readily reusable.[2–4]

Since researchers at Merck Research Laboratories separated the [PNNP]Pd^{II} by-product from a large-scale AAA reaction catalyzed by $[Pd(allyl)Cl]_2$ and (*R*,*R*)-^{Ph}DACH Trost ligand,[5] we sought to convert this by-product back to catalytic active precursors. Since [PNNP]Pd^{II} forms via amide deprotonation of the chiral ligands, our Trost-type single-component precatalysts, in theory, can be reformed from [PNNP]Pd^{II} by adding MAH, electrons, and protons. With this hypothesis in mind, we tested this reduction with [PNNP]Pd^{II} (easily and efficiently isolated from Pd_2dba_3•$CHCl_3$ and (*S*,*S*)-^{Ph}DACH). We did observe reformation of our single-component precursor (*S*,*S*)-^{Ph}DACH–Pd–MAH under certain conditions (equation 5.2). To the best of our knowledge, this reduction strategy would represent the first example of recycling intact homogeneous palladium catalysts via reisolation and Pd reduction. Even though the reaction conditions are still being optimized, this unprecedented reduction strategy will ultimately have a significant impact on the field. It can be exploited as a new approach to recycle these Trost-type homogeneous Pd catalysts by separating [PNNP]Pd^{II} from reaction mixtures, reducing it back to active Pd precursor, and reusing the active precatalyst in a new reaction.

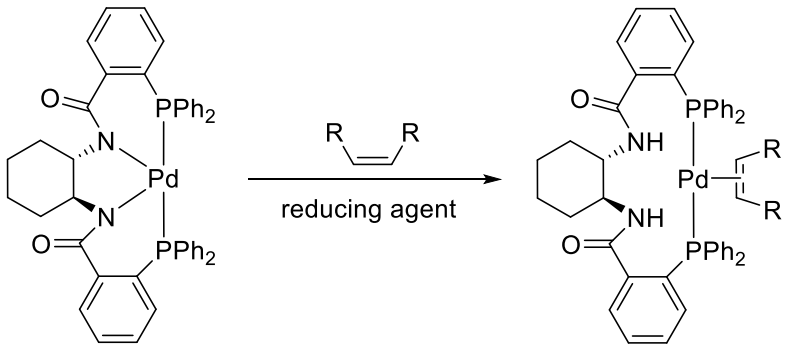

(5.2)

5.2.3 Expanding Catalytic Applications of ^{DMP}DAB–Pd–$(CH_2TMS)_2$

Though Chapter 4 contains extensive catalytic evaluation of ^{DMP}DAB–Pd–$(CH_2TMS)_2$, there are additional challenging cross-couplings that could be used to demonstrate its utility. Future work will focus on two specific reaction classes: challenging C–N couplings and AAA reactions.

Given the significant challenges to access the *N*,*N*-diarylsulfonamide motif,[6–8] we have conducted preliminary studies to evaluate ^{DMP}DAB–Pd–$(CH_2TMS)_2$ in a challenging C–N coupling of secondary sulfonamide. A significant decrease in reactivity has been previously observed with a 1:1 L-to-Pd at a low loading of $[Pd(crotyl)Cl]_2$, prompting us to evaluate whether our precursor can address this limitation.[8] Given the high cost of the reported ligand (AdBippyPhos), our preliminary experiments begin with the coupling of *N*-phenylmethanesulfonamide and 2-bromo-5-(trifluoromethyl)pyridine using 1:1 L-to-Pd ratio (equation 5.3).

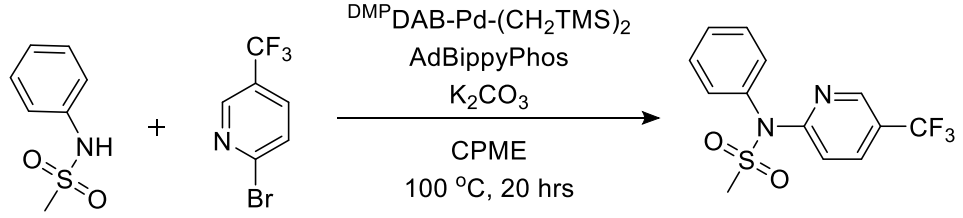

(5.3)

^{DMP}DAB-Pd-$(CH_2TMS)_2$: 48% (2 mol % Pd), 18% (1 mol % Pd)
$[Pd(allyl)Cl]_2$: 43% (2 mol % Pd), 16% (1 mol % Pd)

Under reported conditions, we obtained a 48% NMR yield with 2 mol % **4.1** and an 18 % NMR yield using 1 mol % **4.1**. Similar results are found in the catalytic systems using $[Pd(allyl)Cl]_2$, with 43% and 16% NMR yields obtained at 2 mol % and 1 mol % Pd loading. These yields, determined by ^{1}H NMR spectroscopy versus internal standard, are lower than anticipated and inconsistent with the analysis spectra. In all cases, no starting material is observed in ^{1}H NMR spectra, and the major peaks present are desired product and internal standard (Figure 5.1A). In light of the high sensitivity of ^{19}F NMR spectroscopy with increased signal-to-noise, we also used it to identify the presence of any remaining 2-bromo-5-(trifluoromethyl)pyridine or fluorine-containing side products.

Consistent with ^{1}H NMR spectra, the major signal in the ^{19}F NMR spectrum is the desired product, and no 2-bromo-5-(trifluoromethyl)pyridine is observed (Figure 5.1B). To confirm these results, reaction mixtures resulting from 2 mol % Pd loading were analyzed by LCMS. The major component (retention time at 3.69 minutes) has an *m*/*z* at 317, confirming the presence of the desired product (exact mass = 316). The second major component is the internal standard, while starting material is absent (Figure 5.1C). We attribute these discrepancies to the poor solubility of the desired product in $CDCl_3$, leading to inaccurate quantification by NMR spectroscopy.

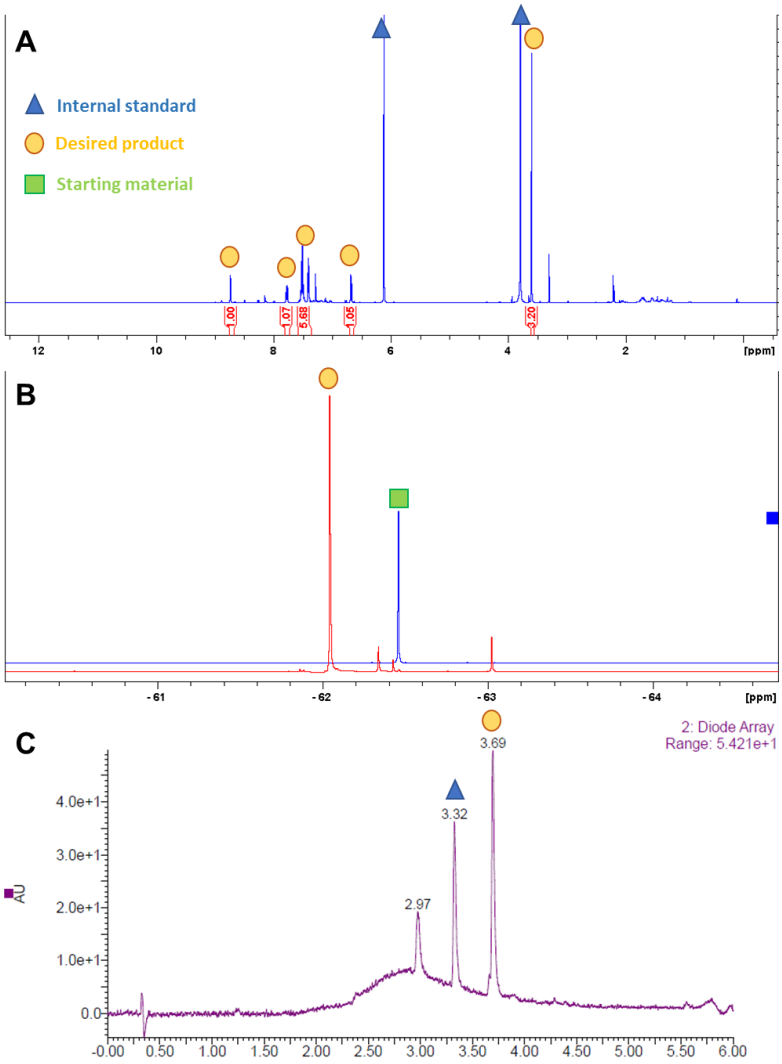

Figure 5.1. A: Representative ^{1}H NMR spectrum of the C-N coupling using 1 mol % ^{DMP}DAB–Pd–$(CH_2TMS)_2$. **B**: Representative ^{19}F NMR stacked spectra (blue: 2-Bromo-5-(trifluoromethyl)pyridine; pure red: the reaction mixtures catalyzed by 1 mol % ^{DMP}DAB–Pd–$(CH_2TMS)_2$). **C**: LCMS of the resulting solution using 2 mol % ^{DMP}DAB–Pd–$(CH_2TMS)_2$.

To examine this hypothesis, we repeated the experiment catalyzed by 1 mol % ^{DMP}DAB–Pd–$(CH_2TMS)_2$ without adding an internal standard. A work-up was performed by extracting the product with ethyl acetate and washing it with water, followed by concentration under vacuum. The crude product was dissolved in d_6-DMSO and analyzed by ^{1}H NMR spectroscopy. A 4:5 ratio is detected between the unreacted sulfonamide and desired product; however, 2-bromo-5-(trifluoromethyl)pyridine is again absent (Figure 5.2). This may be due to decomposition of the Ar–Br via nucleophilic aromatic substitution with hydroxide. This would generate a pyridone by-product, which may be water-soluble and lost during the work-up. Prior observations in sulfonamide coupling revealed competitive formation of phenols from Ar–X electrophiles, requiring the addition of molecular sieves as a drying agent to reaction mixtures. Further investigations could use a less activated aryl halide substrate and/or addition of a drying agent.

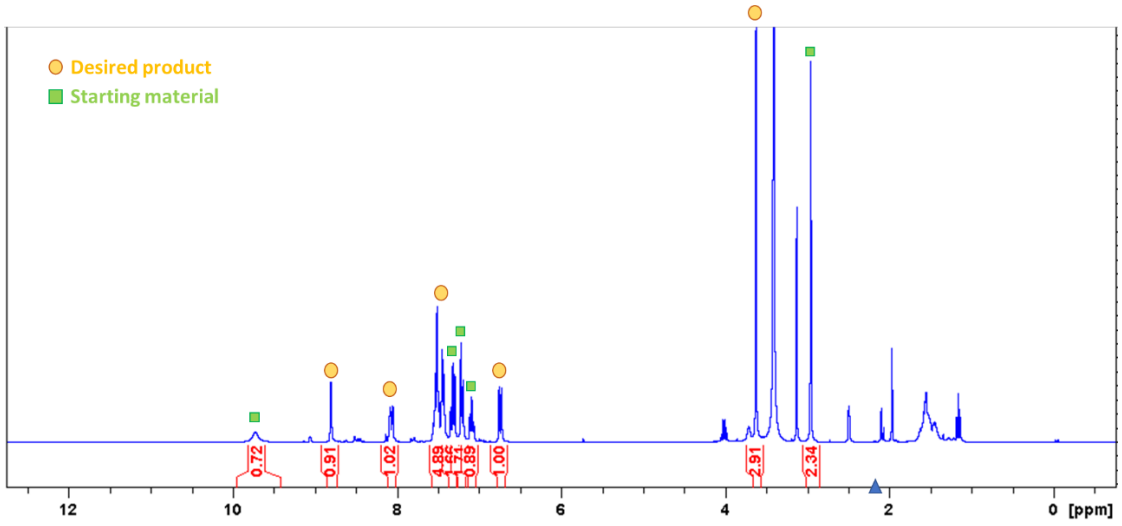

Figure 5.2. ^{1}H NMR spectrum (d_6-DMSO) of the repeated C-N coupling catalyzed by 1 mol % ^{DMP}DAB–Pd–$(CH_2TMS)_2$. The peaks for unreacted sulfonamide and desired product are indicated.

Another reaction class being evaluated is Pd-catalyzed AAA, where the use of ^{DMP}DAB–Pd–$(CH_2TMS)_2$ may overcome the slow activation observed for our Pd^0 single-component (equation 5.1). As an easily activated precursor, we hypothesize that ^{DMP}DAB–Pd–$(CH_2TMS)_2$ will show superior activity in this chemistry without the need for strong bases/nucleophiles. In addition, $[Pd(allyl)Cl]_2$ has exhibited exceptional and comparable

activity with ^{DMP}DAB–Pd–$(CH_2TMS)_2$ in our catalytic evaluation of C–O coupling (Section 4.3.4). However, the chloride ligand of the precursor may inhibit the reactivity of AAA reactions due to the requirement for cationic Pd intermediates. Thus, further work can focus on extensive activity comparisons between ^{DMP}DAB–Pd–$(CH_2TMS)_2$ and $[Pd(allyl)Cl]_2$ in this reaction.

5.2.4 Further Applications of Diimine–Pd(Br)–Ar

As discussed in Chapter 4, we have prepared and isolated a diimine–Pd(X)–Ar complex from ^{DMP}DAB–Pd–$(CH_2TMS)_2$. As far as we know, the use of diimine-ligated OACs as catalytic precursors for cross-coupling reactions remains unexplored. Given the promising activity of α-diimine ligands exhibited as supporting ligands in a range of cross-coupling reactions,[9–13] we can exploit this diimine OAC to be a precatalyst similar to the catalytic application of phosphine ligated OACs. Specifically, α-diimine–Pd(X)–Ar has been proposed as an intermediate in the catalytic cycle of benzene C–H arylation; future work could evaluate derivatives of our diimine OAC in this coupling by adapting and improving upon the reported conditions (equation 5.4).[14]

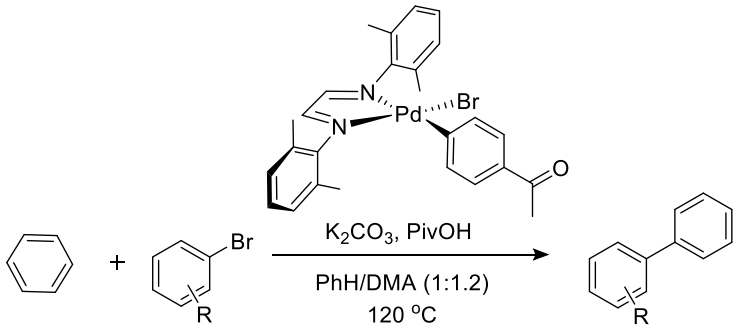

(5.4)

In addition, it is essential to compare the activity of this OAC with that of *in situ* generated catalysts to establish the importance of isolating diimine OACs. Other couplings, such as Suzuki-Miyaura, Heck, and Sonagashira couplings, can also be evaluated in consideration of the reported activity of α-diimine in these reactions. Another direction of future work is to investigate the ligand impact on the formation of this OAC type. We were able to isolate [phosphine]–Pd(Br)–Ar with three phosphine ligands, but diimine–Pd(Br)–

Ar was only obtained in the reaction with cataCXium® POMetB. Further evaluation of the ligand effect on generating diimine–Pd(Br)–Ar complexes, including with other diimines, will help us to understand the ligand binding mode and preparation of these OACs.

5.3 References

(1) Chahen, L.; Karmazin-Brelot, L.; Süss-Fink, G. Double HCl Elimination and Configuration Change in the Square-Planar Palladium Complex Trans-[{($Ph_2PC_6H_4CONH)_2C_6H_4$}$PdCl_2$] under Suzuki Conditions: Isolation and Molecular Structure of Cis-[{($Ph_2PC_6H_4CON)_2C_6H_4$}Pd]. *Inorg. Chem. Commun.* **2006**, *9* (12), 1151–1154. https://doi.org/10.1016/j.inoche.2006.07.007.

(2) Gürsel, I. V.; Noël, T.; Wang, Q.; Hessel, V. Separation/Recycling Methods for Homogeneous Transition Metal Catalysts in Continuous Flow. *Green Chem.* **2015**, *17* (4), 2012–2026. https://doi.org/10.1039/C4GC02160F.

(3) Cole-Hamilton, D. J. Homogeneous Catalysis--New Approaches to Catalyst Separation, Recovery, and Recycling. *Science* **2003**, *299* (5613), 1702–1706. https://doi.org/10.1126/science.1081881.

(4) Dioumaev, V. K.; Bullock, R. M. A Recyclable Catalyst That Precipitates at the End of the Reaction. *Nature* **2003**, *424* (6948), 530–532. https://doi.org/10.1038/nature01856.

(5) Campos, K. R.; Journet, M.; Lee, S.; Grabowski, E. J. J.; Tillyer, R. D. Asymmetric Synthesis of a Prostaglandin D_2 Receptor Antagonist. *J. Org. Chem.* **2005**, *70* (1), 268–274. https://doi.org/10.1021/jo048305+.

(6) Hicks, J. D.; Hyde, A. M.; Cuezva, A. M.; Buchwald, S. L. Pd-Catalyzed N-Arylation of Secondary Acyclic Amides: Catalyst Development, Scope, and Computational Study. *J. Am. Chem. Soc.* **2009**, *131* (46), 16720–16734. https://doi.org/10.1021/ja9044357.

(7) Wu, Y.-J.; Zhang, Y.; Good, A. C.; Burton, C. R.; Toyn, J. H.; Albright, C. F.; Macor, J. E.; Thompson, L. A. Synthesis and SAR of Hydroxyethylamine Based Phenylcarboxyamides as Inhibitors of BACE. *Bioorg. Med. Chem. Lett.* **2009**, *19* (10), 2654–2660. https://doi.org/10.1016/j.bmcl.2009.03.144.

(8) Becica, J.; Hruszkewycz, D. P.; Steves, J. E.; Elward, J. M.; Leitch, D. C.; Dobereiner, G. E. High-Throughput Discovery and Evaluation of a General Catalytic Method for N-Arylation of Weakly Nucleophilic Sulfonamides. *Org. Lett.* **2019**, *21* (22), 8981–8986. https://doi.org/10.1021/acs.orglett.9b03380.

(9) Ouyang, J.-S.; Li, Y.-F.; Shen, D.-S.; Ke, Z.; Liu, F.-S. Bulky α-Diimine Palladium Complexes: Highly Efficient for Direct C–H Bond Arylation of Heteroarenes under Aerobic Conditions. *Dalton Trans.* **2016**, *45* (38), 14919–14927. https://doi.org/10.1039/C6DT02544G.

(10) Hickman, A. J.; Sanford, M. S. Catalyst Control of Site Selectivity in the $Pd^{II/IV}$-Catalyzed Direct Arylation of Naphthalene. *ACS Catal.* **2011**, *1* (3), 170–174. https://doi.org/10.1021/cs1001543.

(11) Grasa, G. A.; Hillier, A. C.; Nolan, S. P. Convenient and Efficient Suzuki−Miyaura Cross-Coupling Catalyzed by a Palladium/Diazabutadiene System. *Org. Lett.* **2001**, *3* (7), 1077–1080. https://doi.org/10.1021/ol015676t.

(12) Grasa, G. A.; Singh, R.; Stevens, E. D.; Nolan, S. P. Catalytic Activity of Pd(II) and Pd(II)/DAB-R Systems for the Heck Arylation of Olefins. *J. Organomet. Chem.* **2003**, *687* (2), 269–279. https://doi.org/10.1016/S0022-328X(03)00375-9.

(13) Mino, T.; Shirae, Y.; Saito, T.; Sakamoto, M.; Fujita, T. Palladium-Catalyzed Sonogashira and Hiyama Reactions Using Phosphine-Free Hydrazone Ligands. *J. Org. Chem.* **2006**, *71* (25), 9499–9502. https://doi.org/10.1021/jo061734i.

(14) Kim, J.; Hong, S. H. Ligand-Promoted Direct C–H Arylation of Simple Arenes: Evidence for a Cooperative Bimetallic Mechanism. *ACS Catal.* **2017**, *7* (5), 3336–3343. https://doi.org/10.1021/acscatal.7b00397.

Appendices

Appendix A: Additional Experimental Details

General Considerations

Materials. All solvents and common organic reagents were purchased from commercial suppliers and used without further purification. All palladium sources (except Pd_2dba_3•$CHCl_3$) were purchased from Strem Chemicals and used as received. Pd_2dba_3•$CHCl_3$ was prepared according to the method of Zalesskiy and Ananikov.[1] *N*,*N*′-bis(2,6-dimethylphenyl)ethan-1,2-diimine was prepared using a reported procedure.[2] (*S*,*S*)-^{Ph}STIL (**L3**),[1] (*S*,*S*)-^{Ph}ANDEN (**L4**),[2] and (*S*)-$^{t\text{Bu}}$PHOX (**L5**)[3] were prepared following literature procedures (adapted procedures for **L3** and **L5** are given below). All other phosphine ligands were purchased from Strem Chemicals and used as received. Anhydrous solvents (SureSeal) were purchased from MilliporeSigma and used as received.

Techniques. All air-free manipulations were performed under a dry nitrogen atmosphere using an MBraun glovebox. High-throughput experimentation was performed using 1 mL capacity glass shell vials in sealable aluminum reaction blocks purchased from Analytical Sales. Heating/stirring was achieved using rare-earth magnetic tumble stirrers acquired from V&P Scientific.

Analysis and Spectroscopy. All NMR spectra were acquired on either a Bruker AVANCE 300 MHz spectrometer or a Bruker AVANCE Neo 500 MHz spectrometer. All ^{1}H and ^{13}C NMR chemical shifts are calibrated to residual protio-solvents and all ^{31}P NMR chemical shifts are calibrated to external standards. All NMR spectroscopic data is processed using Bruker TopSpin 4.07.

UPLC analysis was performed using a Shimadzu Nexera X2 instrument consisting of an autosampler, binary pumps, degassing unit, column oven with a diode-array UV/Vis detector. A Raptor ARC-18 column (100 × 2.1 mm, particle size 1.8 μm) and a Waters CORTECS® UPLC® T3 column (2.1 × 30 mm, particle size 1.6 μm) were used. The eluent used is the mixture of two mobile phases. Water with 0.05% trifluoroacetic acid (TFA) was set to be the mobile phase A, and acetonitrile with 0.05% TFA was set to be the mobile phase B. The gradient profiles, flow rates and injection volumes used for analysis are shown in Section III. The assignments to the key peaks are based on the retention times of isolated compounds and starting materials using the same separation method. All solvents used were HPLC grade.

LCMS analysis was performed using a Waters Acquity class H UPLC system which consists of a quaternary pump, a Sampler Manager-Flow Through Needle, columns selection module with an oven compartment, a photodiode array detector, and a QDa Mass Spectrometer. An ACQUITY UPLC® BEH C18 column (2.1 × 50 mm, particle size 1.7 μm) was used for the analysis of C-O coupling. The solvent mixture consists of solvent A which was water with 0.4% formic acid (FA) and solvent B was set to be acetonitrile with 0.4% FA. The detailed separation methods are also included in Section III. The assignments to the key peaks are also based on the retention times of the isolated product and starting materials using the same separation method. Masslynx was used to process the data. All solvents used were LC-MS grade.

High-resolution electrospray ionization mass spectrometric analysis was performed using a Thermo Scientific Ultimate 3000 ESI-Orbitrap Exactive Plus.

Ligand Substitution Evaluation of 2.1

The ligand substitution reaction progress for four phosphines and one NHC reacting with complex **2.1** at room temperature was followed by ^{1}H NMR spectroscopy using the following procedure. Inside a nitrogen glovebox, a 1.8 mL HPLC vial was charged with ligand (0.0134 mmol for DPEPhos and DIPP-NHC; 0.0271 mmol for monodentate phosphines) and d_8-THF (0.2 mL). The vial was sealed with an aluminum crimp cap containing a PTFE-lined rubber septum and removed from the glovebox. An NMR tube was charged with ^{DMP}DAB–Pd–MAH (**2.1**, 6.3 mg, 0.0134 mmol) and 1,3,5-trimethoxybenzene (~0.0134 mmol) with a total d_8-THF volume of 0.5 mL, and the tube capped with a screw-cap containing a septum. An initial ^{1}H NMR spectrum was obtained to lock and shim on the sample, and to establish the relative integration between the signals for the starting Pd complex and the internal standard. The solution of phosphine was then added to the NMR tube via syringe, and ^{1}H NMR spectra were taken at regular intervals to monitor the reaction progress (Figure A1).

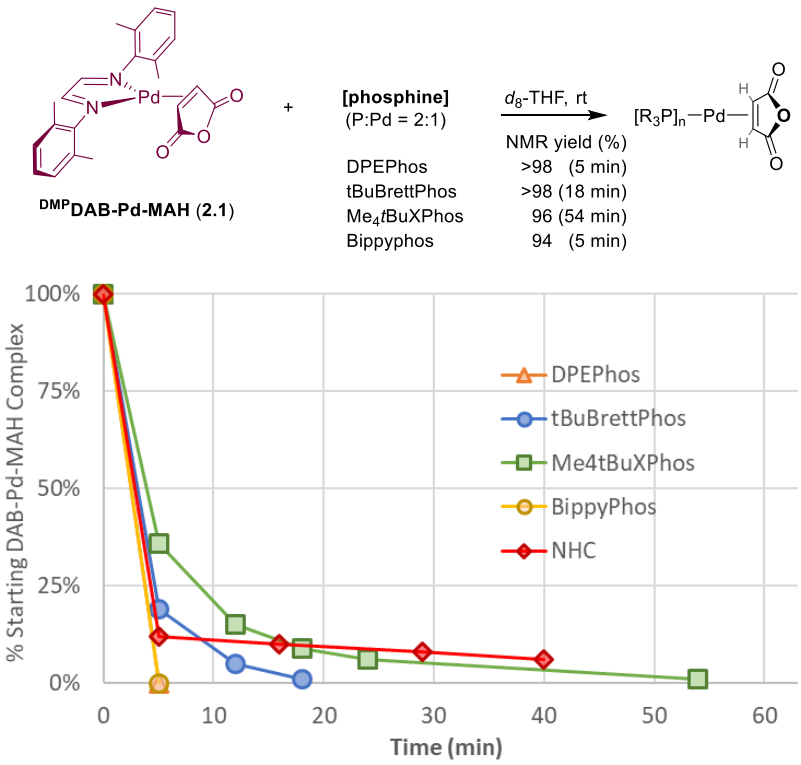

Figure A1. Comparison of ligand substitution reaction progress between ^{DMP}DAB–Pd–MAH (**2.1**) and several phosphines (P:Pd = 2) or *N*,*N*′-bis(2,6-diisopropylphenyl)imidazol-2-ylidene (DIPP-NHC, 1 equiv per Pd) to generate [ligand]–Pd–MAH complexes. Both DPEPhos and Bippyphos result in >95% substitution in less than 5 minutes. NMR yields determined by relative integration of product signals to 1,3,5-trimethoxybenzene internal standard. For DIPP-NHC, while immediate ligand substitution is apparent (~90% conversion of **2.1** in 5 min), the ^{1}H NMR spectra indicate the presence of multiple species (Figure A8).

Preparative-Scale Synthesis Using ^{DMP}DAB–Pd–MAH

N-Benzylpyridin-2-amine

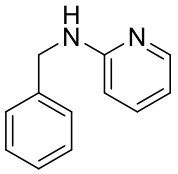

A 4-dram vial was charged with 2-chloropyridine (426 μL, 4.50 mmol), benzylamine (590 μL, 5.40 mmol), NaO*t*-Bu (519 mg, 5.40 mmol), **2.1** (5.3 mg, 0.0113 mmol), BrettPhos (12.1 mg, 0.0225 mmol), and 9 mL of THF. The mixture was stirred at 60 °C for 1 h. Ethyl acetate was added to dilute the reaction mixture, and the diluted mixture was washed three times with water, dried over Mg_2SO_4 anhydrous and concentrated in the rotary evaporator. Finally, the crude product was dried in the vacuo to give 755 mg (4.10 mmol, 91%) product as a light yellow solid. Spectroscopic data is consistent with reported values.[4]

4-(4-Methoxyphenyl)morpholine

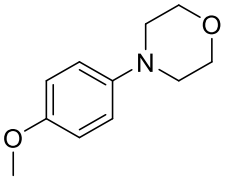

A 4-dram vial was charged with 4-bromoanisole (128 μL, 1.00 mmol), morpholine (106 μL, 1.20 mmol), NaO*t*Bu (116 mg, 1.20 mmol), **2.1** (9.4 mg, 0.02 mmol), RuPhos (18.7 mg, 0.04 mmol), and 2 mL of THF. The mixture was stirred at 80 °C for 2 h. Ethyl acetate was added to dilute the reaction mixture, and the diluted mixture was washed three times with water, dried over Mg_2SO_4 anhydrous and concentrated in the vacuo overnight to give 155.1 mg (0.92 mmol, 92%) product as a yellow solid. Spectroscopic data is consistent with reported values.[5]

N-(4-Methylphenyl)-4-methylbenzenesulfonamide

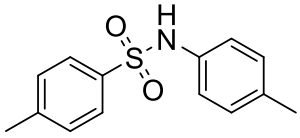

A 4-dram vial was charged with 4-bromotoluene (205 mg, 1.20 mmol), p-toluenesulfonamide (172 mg, 1.00 mmol), K_2CO_3 (415 mg, 3.00 mmol), **2.1** (23.4 mg, 0.05 mmol), *t*BuXPhos (42.5 mg, 0.10 mmol), and 4 mL of CPME. The mixture was stirred at 100 °C for 16 h. Ethyl acetate was added to dilute the reaction mixture, and the diluted mixture was washed three times with water, dried over $MgSO_4$ anhydrous and concentrated in the Genevac. The crude product was purified via a silica plug (DCM/TBME, 20:1) and dried over the Na_2SO_4 to give 183.7 mg (0.70 mmol, 70%) sulfate product as a pale yellow powder. Spectroscopic data is consistent with reported values.[6]

4-Methyl-1-phenyl-1*H*-imidazole

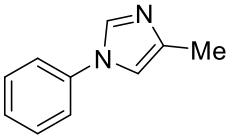

A 4-dram vial was charged with bromobenzene (106 μL, 1.00 mmol), 4-methylimidazole (99 mg, 1.20 mmol), K_3PO_4 (425 mg, 2.00 mmol), **2.13** (10.3 mg, 0.015 mmol), and 1 mL of CPME. The mixture was stirred at 120 °C for 5 h. The mixture was extracted by DCM and concentrated *in vacuo*. The crude product was purified via flash chromatography (ethyl acetate/hexane, 1:1) to give 101.1 mg (0.64 mmol, 64%) product as a pale yellow solid. Spectroscopic data is consistent with reported values.[7]

(*E*)-3-(4-Acetylphenyl)-2-methyl Acrylic Acid Methyl Ester

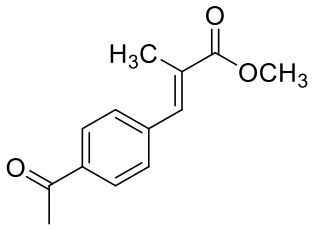

A 4-dram vial was charged with 4-bromoacetophenone (185 mg, 0.93 mmol), methyl methacrylate (300 μL, 2.78 mmol), Cy_2NMe (220 μL, 1.03 mmol), **2.1** (4.5 mg, 0.0095 mmol), P(*t*Bu)$_3$ (4.5 μL, 0.0095 mmol) and 0.84 mL of CPME. The mixture was stirred at 80 °C for 26 h. The mixture was extracted by DCM and washed by 1M HCl and water, followed by the drying over the $MgSO_4$. The filtrate was concentrated to give 142.5 mg (0.65 mmol, 76%) product as a light brown solid. Spectroscopic data is consistent with reported values.[8] ^{1}H NMR spectroscopy (Figure A17) and LCMS (Figure A157) reveals the presence of the bis(arylated) side product (15% by ^{1}H NMR relative integration).

1-(4-*n*-Butoxyphenyl)ethanone

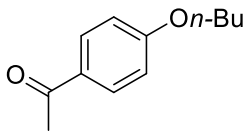

A 4-dram vial was charged with 4-bromoacetophenone (199 mg, 1.00 mmol), butyl alcohol (275 μL, 3.00 mmol), Cs_2CO_3 (489 mg, 1.50 mmol), **2.1** (4.7 mg, 0.01 mmol), *t*BuBippyPhos (10.1 mg, 0.02 mmol), and 1.8 mL of CPME. The mixture was stirred at 80 °C for 18 h. The mixture was extracted by ethyl acetate and washed three times with water. The rag layer was combined with the aqueous phase and extracted by the ethyl acetate two additional times. The organic layers were dried over Mg_2SO_4 and concentrated to give 168.2 mg (0.87 mmol, 87%) product as a brown liquid. Spectroscopic data is consistent with reported values.[9]

2,2',7,7'-Tetrakis-di(*p*-methoxyphenylamino)-9,9'-spirobifluorene (*spiro*-OMeTAD)

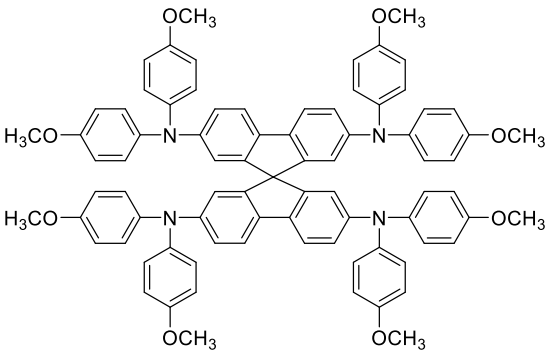

A 4-dram vial was charged with 2,2',7,7'-tetrabromo-9,9'-spirobifluorene (632 mg, 1.00 mmol), 4,4'-dimethoxydiphenylamine (940 mg, 4.10 mmol), NaO*t*Bu (480.5 mg, 5.00 mmol), **2.6** (6.2 mg, 0.01 mmol), and 10 mL of THF. The mixture was stirred at 80 °C for 24 h. The solvent was evaporated *in vacuo*. The residue was dissolved in minimal toluene, and passed through a silica plug (toluene:TBME, 20:1 eluent). The resulting solution was concentrated to give an orange solid. The solid was dissolved in 5 mL of THF, followed by the addition of 30 mL of methanol (anti-solvent) to crystallize the product. Pale yellow solid: 994.4 mg (0.81 mmol, 81% yield). Spectroscopic data is consistent with reported values.[10] NOTE: Initial purification attempts using standard flash column chromatography (hexanes/ethyl acetate eluent; material loaded as a DCM solution) resulted in low recovered yields due to suspected decomposition of the product (formation of multiple new colored species).

Synthesis of (*S*,*S*)-^{NAP}DACH–Pd–MAH (3.2) – The entire procedure was performed in a glovebox under a dry, oxygen-free atmosphere of nitrogen gas. A 4-dram vial was charged with of ^{DMP}DAB–Pd–MAH (100.1 mg, 0.21 mmol), (*S*,*S*)-DACH-naphthyl Trost ligand (168.7 mg, 0.21 mmol), and 5 mL of THF. The solution was stirred for one hour. THF was evaporated under vacuum followed by trituration/decantation with a 1:1 hexane/Et_2O solution until the washings were colourless (6 times). Residual solvents from the trituration/decantation were removed under vacuum, and the solid was dried under vacuum overnight to give a pale-yellow powder (169.6 mg, 80%). The product was recrystallized from pentane/THF.

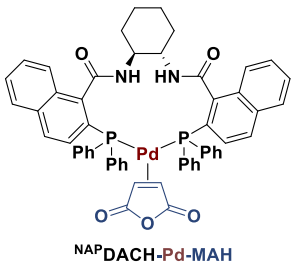

VT NMR Spectroscopy of 3.2

Procedure: VT NMR experiments were conducted at elevated temperatures: **3.2** (8 mg, 0.0089 mmol) was dissolved in 0.6 mL toluene-d_8. A series of ^{31}P NMR & ^{1}H NMR spectra were obtained at 26 °C, 32 °C, 40 °C, 50 °C, 60 °C.

A second set of VT experiments was performed at low temperatures: **3.2** (10 mg, 0.011 mmol) was dissolved in 0.6 mL toluene-d_8. A series of ^{31}P NMR and ^{1}H NMR spectra were obtained at 25 °C, 20 °C, 10 °C, 0 °C, –10 °C, –20 °C, –30 °C, –40 °C, –50 °C, –60 °C, –70 °C, –80 °C.

(For NMR spectra, see Figures A54 – A57 in Appendix B)

Synthesis of (*S*,*S*)-^{Ph}STIL (L3) – To a CH_2Cl_2 (42 mL) solution of DMAP (68 mg, 0.56 mmol), 2-(diphenylphosphanyl)benzoic acid (3.81 g, 12.4 mmol) and EDAC (2.1 g, 13.6 mmol) was added (1*S*,2*S*)-(−)-1,2-diphenylethylenediamine (1.2 g, 5.7 mmol), and the mixture stirred at rt overnight. Et_2O (80 mL) was added, and the organic phase was washed sequentially with 10% HCl (3 × 80 mL), water (1 × 80 mL), saturated aqueous $NaHCO_3$ (2 × 80 mL), 1 M NaOH (1 × 80 mL) and a saturated aqueous solution of brine (1 × 80 mL). The organic layer was dried over anhydrous $MgSO_4$, filtered, and the solvent removed under reduced pressure. The residue was purified by flash column chromatography over silica gel eluting with a hexanes/EtOAc gradient. The resulting white solid was re-dissolved in THF and dried with CaH_2 under N_2. The mixture was filtered, and the solvent removed under reduced pressure to recover the title compound (895 mg, 20%) as a white solid. This synthetic method is adapted from a reported procedure, and the NMR data are consistent with the reported values.[1]

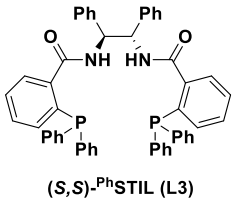

Synthesis of (*S*,*S*)-^{Ph}STIL–Pd–MAH (3.3) – The entire procedure was performed under an inert atmosphere. A 4-dram vial was charged with of ^{DMP}DAB–Pd–MAH (100 mg, 0.21 mmol), (*S*,*S*)-diphenyl Trost ligand (168.5 mg, 0.21 mmol) and 6 mL of anhydrous, inhibitor-free THF. The reaction mixtures were stirred for 3 h at rt. The solution was filtered through a pad of Celite© and the solvent evaporated under reduced pressure. The crude residue was then triturated/decanted six times with hexane until the washing was colourless. Residual solvents from the trituration/decantation were removed under vacuum and the desired product was precipitated from THF/hexane (1:4, 5 mL). The product was finally dried under vacuum to give a tan solid (146.2 mg, 68%).

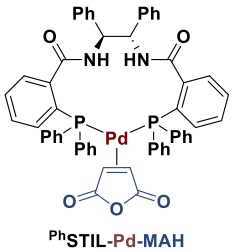

^{Ph}STIL-Pd-MAH

(*S*,*S*)-^{Ph}ANDEN–Pd–MAH (3.4) – The entire procedure was performed under an inert atmosphere. A 4-dram vial was charged with ^{DMP}DAB–Pd–MAH (70 mg, 0.18 mmol), (*S*,*S*)-ANDEN Trost ligand (121 mg, 0.15 mmol) and 9 mL of anhydrous THF. The solution was stirred for 1 h at rt. THF was evaporated under reduced pressure and the crude residue was triturated/decanted with hexane/Et_2O (1:1) until the washings were colourless (6 times). The product was dried under vacuum to give a light green solid (128.0 mg, 66%). The product was recrystallized from TBME/THF.

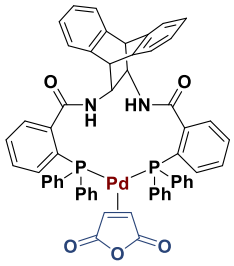

^{Ph}ANDEN-Pd-MAH

Synthesis of (*S*)-^{tBu}PHOX (L5) was synthesized in three steps using adaptations to the reported procedure.[3] This includes the synthesis of 2-diphenylphosphino-benzonitrile, (+)-{(4*S*)-4-*tert*-butyl-4,5-dihydro-2-[2'-(diphenylphosphino)phenyl]oxazole}zinc(II) dichloride, and the desired (*S*)-^{tBu}PHOX ligand.

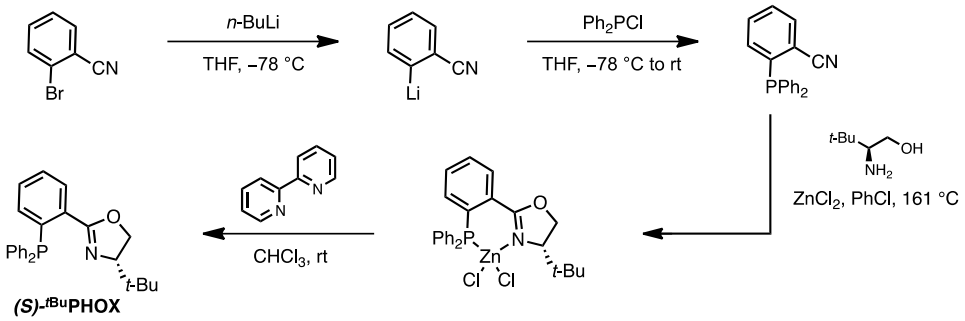

(*S*)-^{tBu}PHOX

To a solution of 2-bromobenzonitrile (2.73 g, 15 mmol) in THF (30 mL) at –78 °C, was added *n*-BuLi (2.5 M in hexanes, 6 mL, 15 mmol), and the reaction stirred for 1 h. A solution of chlorodiphenylphosphine (2.83 mL, 15 mmol) in THF (5 mL) was then added, and the reaction was stirred for a further 1 h at –78 °C, before being allowed to warm to rt and stirred at that temperature for 1 h. Et_2O (80 mL) was added, and the organic layer was washed with water (70 mL) and a saturated aqueous solution of brine (70 mL). The organic layer was dried over $MgSO_4$, filtered and the solvent removed under reduced pressure. The residue was purified by recrystallization from hot methanol to recover 2-diphenylphosphino-benzonitrile (1.39 g, 32%) as a white solid.

To a solution of 2-diphenylphosphino-benzonitrile (820 mg, 2.85 mmol) in chlorobenzene (12 mL) under a N_2 atmospher was added $ZnCl_2$ (499 mg, 3.66 mmol) and L-*tert*-leucinol (423 mg, 3.61 mmol), and the reaction heated at 160 °C for 4.5 days. The reaction was passed through a pad of silica and washed with EtOAc (600 mL) and the solvent removed under reduced pressure. The residue was purified by recrystallisation from chloroform/TBME to recover (+)-{(4*S*)-4-*tert*-butyl-4,5-dihydro-2-[2'-(diphenyl phosphino)phenyl]oxazole}zinc(II) (317 mg, 21%) as a white solid.

To a solution of (+)-{(4*S*)-4-*tert*-butyl-4,5-dihydro-2-[2'-(diphenylphosphino)phenyl] oxazole}zinc(II) (221 mg, 0.42 mmol) in $CHCl_3$ (4 mL) was added 2,2'-bypiridine (65 mg, 0.42 mmol) and the reaction was stirred at rt for 4 h. The crude reaction mixture was passed through a pad of silica and washed with $CHCl_3$ (50 mL), and the solvent was removed under reduced pressure to recover the (*S*)-$^{t\text{Bu}}$PHOX (**L5**) (140 mg, 86%) as a colorless and oily product. The NMR data are consistent with the literature.[4]

Synthesis of (*S*)-$^{t\text{Bu}}$PHOX–Pd–MAH (3.5) – The entire procedure was performed open to air. A 4-dram vial was charged with $^{\text{DMP}}$DAB–Pd–MAH (167 mg, 0.36 mmol), (*S*)-$^{t\text{Bu}}$PHOX (140 mg, 0.36 mmol), and 8 mL of THF. The solution was stirred at rt for 3 h. The reaction mixture was then filtered through a pad of Celite© followed by solvent evaporation. The crude product then underwent trituration/ decantation with hexane until the washing was colorless (8 times). The product was filtered and dried overnight to give a light brown solid (192 mg, 90%).

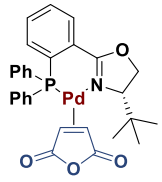

$^{t\text{Bu}}$PHOX-Pd-MAH

Synthesis of (*S*)-$^{i\text{Pr}}$PHOX–Pd–MAH (3.6) – The entire synthetic procedure was performed in a glovebox under a dry, oxygen-free atmosphere of nitrogen. A 4-dram vial was charged with of $^{\text{DMP}}$DAB–Pd–MAH (125 mg, 0.27 mmol), (*S*)-*i*PrPHOX ligand (100 mg, 0.27 mmol), and 5 mL of THF. The reaction mixture was stirred at rt for 1 h and then filtered through a pad of Celite©. The THF was evaporated and the crude residue was triturated/decanted with hexane/Et_2O (1:1) until the washings were colourless (8 times). Residual solvents from the trituration/decantation were removed under vacuum and the product was dried overnight to give a light green solid (113 mg, 73%). The product was recrystallized from pentane/THF. Two conformers were observed in DCM.

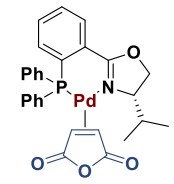

$^{i\text{Pr}}$PHOX-Pd-MAH

In Situ Metalation Analysis for Complexes 3.1-3.6

The following is a general procedure, with **L1** as representative: the sample preparation was performed in a glovebox under a dry, oxygen-free atmosphere of nitrogen gas following the procedure shown below. A sealed NMR tube was charged with a reference solution of $^{\text{DMP}}$DAB–Pd–MAH (6.3 mg, 0.0134 mmol), 1,3,5-trimethoxybenzene (2.3 mg, 0.0134 mmol) in 0.5 mL THF-d_8. Another 1-dram vial was charged with (*S*,*S*)-$^{\text{Ph}}$DACH (**L1**) (11.1 mg, 0.0161 mmol) and 0.2 mL THF-d_8 to prepare a stock solution. The initial ^{1}H NMR spectrum (500 MHz, THF-d_8) was obtained for the freshly prepared reference

solution. Subsequent ^{1}H NMR and $^{31}P\{^{1}H\}$ NMR spectra were obtained immediately after mixing with the **L1** stock solution. (For NMR spectra, see Figure A108 – A113 in Appendix B)

Solution Stability of Precatalysts 3.1-3.6

The following is a general procedure, with complex **3.1** as representative: an NMR sample was prepared from a solution of complex **3.1** (17.3 mg, 0.019 mmol) in 0.7 mL anhydrous THF. A sealed glass capillary containing PPh_3 in C_6D_6 was used as an internal standard. The initial ^{31}P NMR spectrum was obtained after 30 min (500 MHz). Subsequent ^{31}P NMR spectra were obtained at 2, 6, 18, 24, 30, 38, and 48 h. (For NMR spectra, see Figure A114 – A119 in Appendix B)

Table A1. Solution stability of six chiral Pd complexes over 48 h. The concentrations of complexes in THF over 48 h are normalized against the t = 30 min concentration to assess the stability.

[complex]/[complex]$_{30min}$

Time/h	3.1	3.2	3.3	3.4	3.3	3.6
0.5	1.00	1.00	1.00	1.00	1.00	1.00
2	0.99	0.98	0.98	0.98	1.01	0.99
6	0.99	0.97	1	1.01	1	0.99
18	1	1	0.99	0.99	1	0.98
24	0.99	0.98	0.99	0.99	1	0.99
30	1	1	0.99	1	0.99	0.99
38	0.99	0.99	0.99	0.98	0.99	0.98
48	0.99	0.99	0.99	0.99	0.99	1

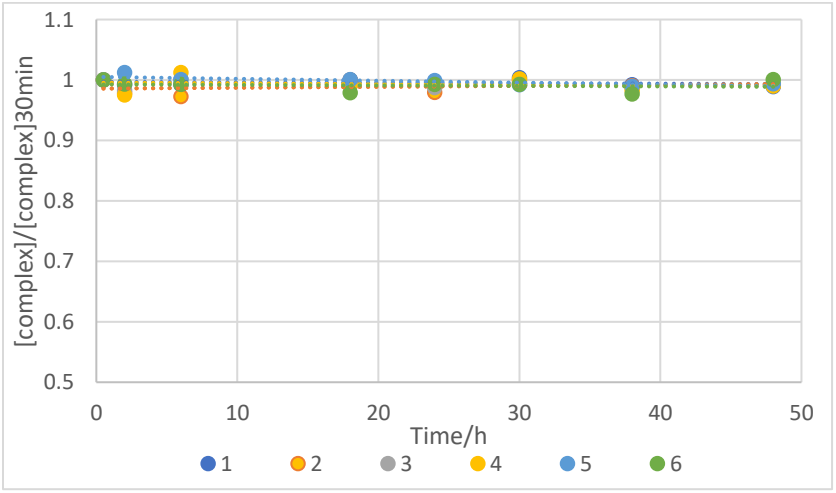

Figure A2. Plot of normalized [L*–Pd–MAH] in THF over 48 h at rt.

Stability of (*S*,*S*)-^{Ph}DACH–Pd–MAH (3.1) in air

An NMR sample was prepared from a solution of (*S*,*S*)-^{Ph}DACH–Pd–MAH (**3.1**) (14.9 mg, 0.017 mmol) in 0.6 mL THF. A sealed glass capillary containing PPh_3 in C_6D_6 was used as an internal standard. The initial ^{31}P NMR spectrum was obtained after 30 min. The NMR sample was exposed to the air once the initial ^{31}P NMR spectrum was obtained. Subsequent ^{31}P NMR spectra were recorded at 2, 18, 24, 30, 43, and 48 h. (For NMR spectra, see Figure A120 in Appendix B)

Table A2. Solution stability of **3.1** after exposure to air.
Normalized [**3.1**] and by-product formation in THF over 48 h to assess the stability.

Time/h	[3.1]/[3.1]$_{30min}$	[(PNNP)Pd^{II}]/[3.1]$_{30min}$
0.5	1.00	0.016
2	0.99	0.026
18	0.90	0.058
24	0.89	0.066
30	0.88	0.077
43	0.86	0.092
48	0.86	0.11

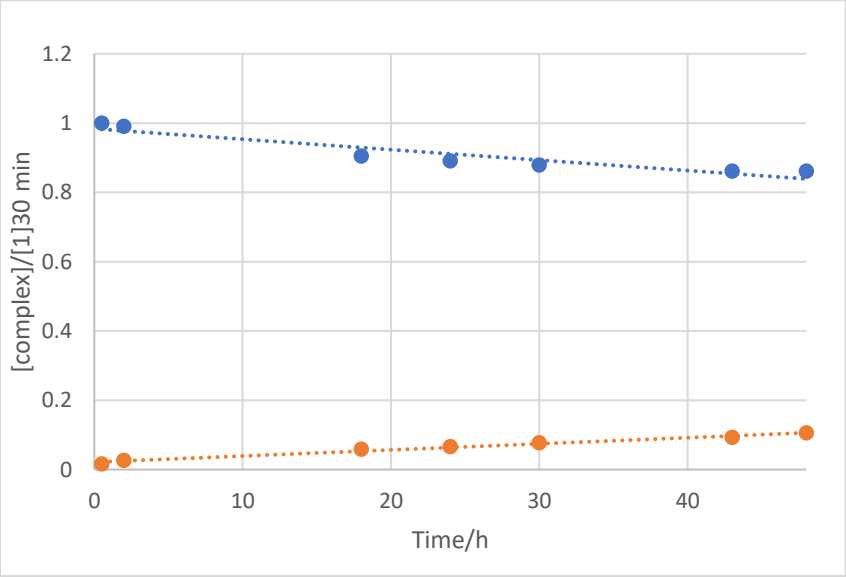

Figure A3. Plot of normalized [**3.1**] (blue) and [(PNNP)Pd^{II}] (orange) after exposure to air over 48 h at rt.

Stability of (*S*,*S*)-^{Ph}DACH–Pd–dba in N_2 and air

Pd_2dba_3•$CHCl_3$ (12.9 mg, 0.0125 mmol), (*S*,*S*)-^{Ph}DACH (**L1**) (16.8 mg, 0.0243 mmol), and 1.2 mL THF were added to a 1-dram vial under N_2 atmosphere. The mixtures were stirred at rt for one hour. The solution was evenly split into two portions and transferred to two different sealed NMR tubes with sealed glass capillaries containing PPh_3 in C_6D_6 as internal standards. The initial ^{31}P NMR spectrum was obtained for each solution after 30 min (200 MHz). One solution was exposed to the air after the initial ^{31}P NMR spectrum was obtained. Subsequent ^{31}P NMR spectra were obtained at 2, 6, 18, 24, 30, 43, and 48 h. (For NMR spectra, see Figure A121 – A122 in Appendix B)

Table A3. Solution stability of phenyl Trost ligand–Pd–dba in the air and N_2. Normalized [**(*S*,*S*)-^{Ph}DACH-Pd-dba**] and [PNNP]Pd^{II} in THF over 48 h.

Time/h	(*S*,*S*)-^{Ph}DACH–Pd–dba (N_2)	[PNNP]Pd^{II} (N_2)	(*S*,*S*)-^{Ph}DACH–Pd–dba (air)	[PNNP]Pd^{II} (air)
0.5	1.00	0.00	0.47	0.71
2	1.01	0.00	0.36	0.89
6	0.96	0.00	0.25	1.15
18	0.97	0.00	0.00	0.48
24	0.96	0.00	0.00	0.31
30	0.96	0.016	0.00	0.26
43	0.95	0.038	0.00	0.15
48	0.94	0.039	0.00	0.14

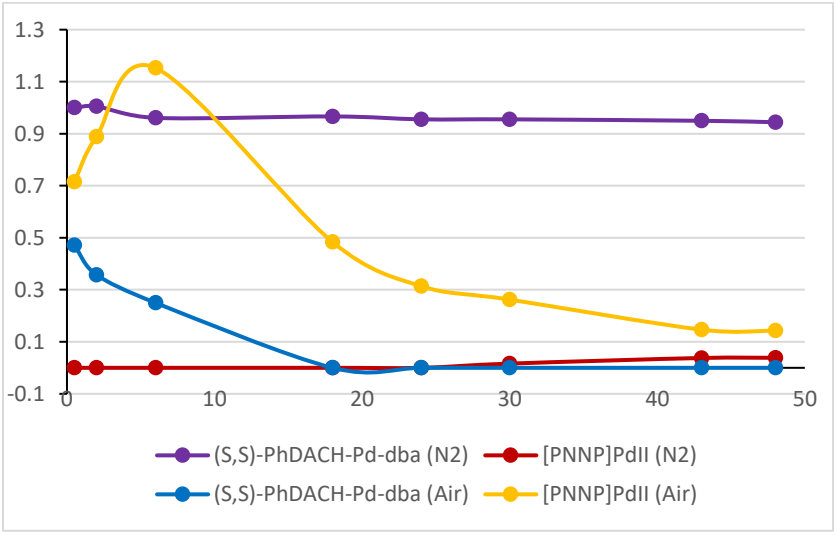

Figure A4. Plot of normalized [**(*S*,*S*)-^{Ph}DACH–Pd–dba**] and [[PNNP]Pd^{II}] in THF over 48 h at rt in the air and N_2. The decrease in [PNNP]Pd^{II} over time is due to precipitation of this poorly soluble complex.

Investigation of Complex 3.1 Conformer Ratios

Spectroscopic Studies

Two species are observed in the NMR spectra of (*S*,*S*)-^{Ph}DACH–Pd–MAH (**3.1**), with a closer ratio between the two species in DCM-d_2 than in THF-d_8. To establish these two species as conformers, as proposed in the main text, a series of studies was performed.

Concentration effects: A 1-dram vial was charged with (*S*,*S*)-^{Ph}DACH–Pd–MAH (**3.1**) (19 mg, 0.021 mmol) and 1.2 mL DCM under N_2. Half of the solution was transferred to a sealed NMR tube, and a capillary consisting of PPh_3 in C_6D_6 was used as an internal standard. An initial ^{31}P spectrum was obtained. The other half of the solution was diluted with 0.6 mL DCM. The analysis/dilution process was repeated to give the results shown in Table S4, revealing no change to the ratio of the two species in solution (ruling out a potential monomer/dimer equilibrium).

Table A4. Relative peak areas for two conformers of **3.1** in $^{31}P\{^1H\}$ NMR spectra at different concentrations.

[**3.1**] (mM)	major conformer	minor conformer	major/minor ratio
17.5	2.007	1.541	1.303
8.8	2.000	1.627	1.229
4.4	1.933	1.419	1.362
2.2	2.075	1.434	1.447

Solvent composition effects:

An NMR sample was prepared from a solution of (*S*,*S*)-^{Ph}DACH–Pd–MAH (**3.1**) (19.9 mg, 0.022 mmol) in 0.3 mL THF and 0.3 mL DCM under N_2 atmosphere. A sealed glass capillary containing PPh_3 in C_6D_6 was used as an internal standard. After the initial ^{31}P NMR spectrum was obtained, different amounts of THF were subsequently added to adjust the DCM/THF ratio to 3:4, 3:7, 1:5, 1:7, and 1:9. ^{31}P NMR spectra were obtained at each ratio.

A second experiment was performed in a similar way, with different amounts of DCM added to adjust the DCM/THF ratio to 4:3, 7:3, 5:1, and 7:1. ^{31}P NMR spectra were obtained at each ratio.

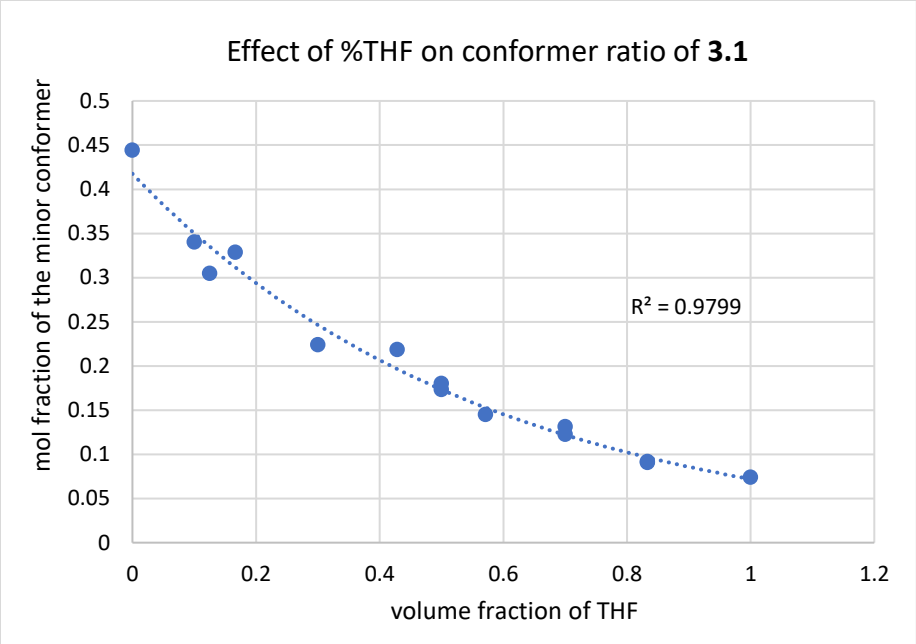

Figure A5. Plot of mol fraction of minor conformer at different THF/DCM ratios. Mol fraction of minor conformer is determined by the peak area ratio between its ^{31}P NMR signal and the total peak area for both conformer signals.

Co-solvent identity effects:

An NMR sample was prepared from a solution of (*S*,*S*)-^{Ph}DACH–Pd–MAH (**3.1**) (10 mg, 0.011 mmol) in 0.9 mL of DCM and 0.1 mL THF. A sealed glass capillary containing PPh_3 in C_6D_6 was used as an internal standard. Similarly, other samples were prepared using 0.1 mL MeOH, DMF, CPME, and NEt_3 instead of THF, with 0.9 mL of DCM. ^{31}P NMR spectra were obtained for each solution.

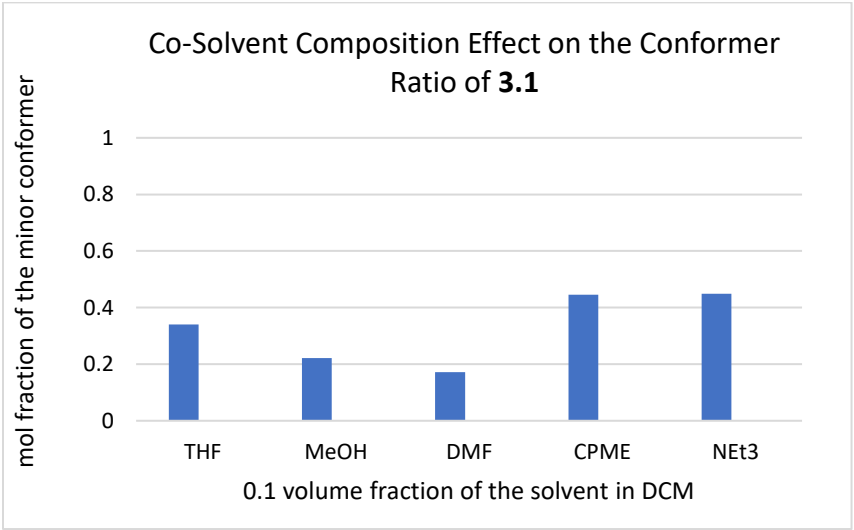

Figure A6. Conformer ratio changes of **3.1** in DCM mixed with five different co-solvents.

General Procedure for Catalyst Activation Studies

In the glovebox, a 1-dram vial was added ^{DMP}DAB–Pd–MAH (5.6 mg, 0.012 mmol), (*S,S*)-phenyl Trost ligand (8.3 mg, 0.012 mmol), 0.6 mL THF, and corresponding additives. The mixtures were stirred at room temperature for one hour. The reaction solution was then transferred to an NMR tube with a capillary consisting of PPh_3 in C_6D_6. ^{31}P NMR (200 MHz) spectrum was obtained, and the same capillary was used in all activation tests.

Additives and corresponding %consumption of complex **3.1** are listed below.

Table A5. Additives of activation tests and the corresponding %consumption of **3.1**.

Additives	Consumption of **3.1**
2 equiv. KO*t*Bu	100%
2 equiv. KOAc	0%
21 equiv. BSA + 3 equiv. KOAc	15%
1.3 equiv. 1,3-diphenylisobenzofuran	2%
20 equiv. dimethyl malonate + 20 equiv. NaH	59%
21 equiv. dimethyl malonate + 21 equiv. NaH + 26 equiv. BSA	73%
21 equiv. dimethyl malonate + 21 equiv. BSA + 3 equiv. KOAc	26%

Preparative-Scale Synthesis Using ^{DMP}DAB–Pd–$(CH_2TMS)_2$ (4.1)

5-Methyl-2-phenylpyridine

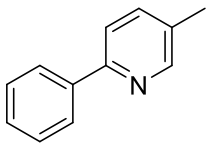

Under air, a 4-dram vial was added **4.1** (1.8 mg, 0.003 mmol), XPhos (2.9 mg, 0.006 mg), K_2CO_3 (621.9 mg,), phenylboronic acid (439.7 mg,), 4-chloroanisole (327.4 μL, 1 mmol) and a stir bar. 2.2 m CPME was added to the mixtures under N_2, followed by 2.2 mL DI water injection. The reaction mixtures were stirred at 50 °C for 24 hours. 10 mL ethyl acetate was added to dilute the resulting solution, and the organic phase was washed with DI water (1 x 10 mL). The aqueous phase was then washed with ethyl acetate (3 x 10 mL) to extract product residue. The combined organic phase was concentrated under vacuum, and the crude product was redissolved in 10 mL TBME and washed with 1M NaOH (2 x 10 mL). The organic layer was dried over $MgSO_4$, followed by filtration and solvent evaporation, to yield white-light gray solids (337.5 mg, 66%). The NMR spectrum is consistent with the reported data.[11]

(*E*)-3-(4-Methoxyphenyl)-2-methyl Acrylic Acid Methyl Ester

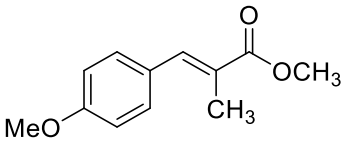

A 1-dram vial was added **4.1** (5.6 mg, 0.01 mmol) and 4-chloroanisole (116.5 μL, 0.95 mmol) under air. The vial was then added P(*t*Bu)$_3$ (9.4 μL, 0.02 mmol, 50 wt% in toluene), 0.58 mL CPME, methyl methacrylate (116.6 μL, 1.09 mmol), Cy_2NMe (233 μL, 1.09 mmol) in a glovebox under a dry, oxygen-free atmosphere of nitrogen gas. The mixtures were stirred at 120 °C for 53 hours. 10 mL diethyl ether was added to dilute the resulting solution, followed by washing with 1M HCl (1 x 8 mL), DI water (1 x 8 mL), and brine (1 x 8 mL). The organic layer was dried over $MgSO_4$, followed by filtration and solvent evaporation, to yield brown liquid (137.2 mg, 66%). The NMR spectrum is consistent with the reported data.[8]

1-(4-*n*-Butoxyphenyl)ethenone

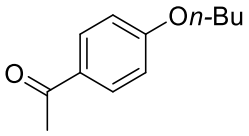

In the air, a 1-dram vial was added 4-bromoacetophenone (201 mg, 1.01 mmol), **4.1** (1.1 mg, 0.002 mmol). The following chemicals were added in a glovebox under a dry, oxygen-free atmosphere of nitrogen gas. *t*BuBrettPhos (2.2 mg, 0.0045 mmol), Cs_2CO_3 (380 mg, 1.17 mmol), 1.5 mL CPME, and 1-butanol (102 μL, 1.11 mmol) were added to the 1-dram vial. The mixtures were stirred at 50 °C for 24 hours. 8 mL ethyl acetate was added to dilute the resulting solution, followed by washing with DI water (1 x 8 mL), 1M NaOH (1 x 5 mL), DI water (2 x 5 mL), and brine (1 x 5 mL). The organic layer was dried over $MgSO_4$, followed by filtration and solvent evaporation to yield brown liquid (147.4 mg, 76%). The NMR spectrum is consistent with the reported data.[9]

Catalytic Comparison for ^{DMP}DAB–Pd–$(CH_2TMS)_2$

Measurement for low loading catalyst

If the amount of Pd sources/phosphine ligands required was >1.0 mg, solids were weighed using an analytical balance.

If the amount of Pd sources required was <1.0 mg, a stock solution of the corresponding Pd source was prepared at a suitable concentration. The required amount was then dispensed using a micropipette, and the solvent evaporated before adding additional components. Specific solvents used for preparing the Pd stock solutions: **4.1** in THF, $[Pd(allyl)Cl]_2$ in acetone, $Pd(OAc)_2$ in DCM, Pd_2dba_3•$CHCl_3$ in THF.

If the amount of phosphine ligands required was <1.0 mg, a stock solution of the corresponding ligand was prepared in CPME at a suitable concentration. The required amount was then dispensed using a micropipette.

General procedure for Suzuki-Miyaura coupling:

Procedure for entry 16 in Table A6 is given here.

A stock solution of **4.1** in THF (2.3 mg/mL) was dispensed to a 1-dram vial (56.2 μL, 0.129 mg, 0.000237 mmol) containing a stirbar, followed by solvent evaporation under vacuum. The vial was then charged with 1,3,5-trimethoxybenzene (15.8 mg, 0.0939 mmol), phenylboronic acid (131.8 mg, 1.08 mmol), and K_2CO_3 (186.7, 1.35 mmol) under air. The vial was then brought into a nitrogen glovebox. A stock solution of XPhos in anhydrous CPME (2.4 mg/mL) was then dispensed to the reaction mixture (100.2 μL, 0.240 mg, 0.000504 mmol), followed by anhydrous CPME (0.6 mL), and 2-chloro-5-methylpyridine (98.2 μL, 0.900 mmol). The vial was sealed with a cap containing a Teflon septum and removed from the glovebox. Degassed DI water (0.7 mL) was injected via syringe. The reaction mixture was stirred at 50 °C for 48 hours. The organic phase was transferred to a new 1-dram vial, followed by solvent evaporation and analysis by ^{1}H NMR spectroscopy.

Preparation of stock solutions:

Palladium stock solution was prepared from **4.1** (1.3 mg, 0.0024 mmol) and 560.4 μL THF. 56.2 μL palladium stock solution was dispensed to a 1-dram vial, followed by solvent evaporation under vacuum to have solid **4.1** (0.129 mg, 0.000237 mmol) in the designated vial.

XPhos stock solution was prepared from XPhos (1.2 mg, 0.0025 mmol) and 500 μL anhydrous CPME. 100.2 μL stock solution containing XPhos (0.240 mg, 0.000504 mmol) was dispensed to the reaction vial.

Table A6. Summarized results of fair comparisons, optimization, and TON investigation for the Suzuki-Miyaura coupling.

Entry	Pd source	Pd loading/ mol %	Time/ h	Tem/ °C	NMR solution yield%	TON
1	**4.1**	0.5	18	80	100	200
2	$Pd(OAc)_2$	0.5	18	80	81	162
3	^{DMP}DAB–Pd–MAH	0.5	18	80	99	198
4	**4.1**	0.5	1.5	50	56	112
5	$Pd(OAc)_2$	0.5	1.5	50	54	108
6	^{DMP}DAB–Pd–MAH	0.5	1.5	50	5	10
7	**4.1**	0.5	4	50	87	174
8	$Pd(OAc)_2$	0.5	4	50	78	156
9	**4.1**	0.1	5	50	59	590
10	$Pd(OAc)_2$	0.1	5	50	16	160
11	**4.1**	0.1	12	50	72	720
12[a]	**4.1**	0.1	12	50	69	690
13	**4.1**	0.1	24	50	93	930
14[a]	**4.1**	0.1	24	50	77	770
15	**4.1**	0.05	48	50	82	1640
16	**4.1**	0.025	48	50	47	1880
17	**4.1**	0.0125	48	50	18	1440
18	$Pd(OAc)_2$	0.025	48	50	17	680

[a]1:1 L-to-Pd ratio was applied.

General procedure for Heck coupling:

Procedure for entry 17 in Table A7 is given here.

A stock solution of **4.1** in THF (6.4 mg/mL) was dispensed to a 1-dram vial (56.1 μL, 0.362 mg, 0.000664 mmol) containing a stirbar, followed by solvent evaporation under vacuum. The vial was then charged with 1,3,5-trimethoxybenzene (12.7 mg, 0.0755 mmol), 4-chloroanisole (200 μL, 1.63 mmol) under air. The vial was then brought into a nitrogen glovebox. A stock solution of P(*t*Bu)$_3$ in anhydrous Toluene (5.3 mg/mL) was then dispensed to the reaction mixture (50.6 μL, 0.267 mg, 0.00132 mmol), followed by anhydrous CPME (0.9 mL), methyl methacrylate (190 μL, 1.78 mmol), and Cy_2NMe (380 μL, 1.78 mmol). The reaction mixture was stirred at 120 °C for 48 hours. The resulting solution underwent solvent evaporation and analysis by ^{1}H NMR spectroscopy.

Preparation of stock solutions:

Palladium stock solution was prepared from **4.1** (1.8 mg, 0.0033 mmol) and 278.9 μL THF. 56.1 μL palladium stock solution was dispensed to a 1-dram vial, followed by solvent evaporation under vacuum to have solid **4.1** (0.362 mg, 0.000664 mmol) in the designated vial.

P(*t*Bu)$_3$ stock solution was prepared from P(*t*Bu)$_3$ (50 wt% in toluene, 3.05 μL, 0.0065 mmol) and 250 μL anhydrous Toluene. 50.6 μL stock solution containing P(*t*Bu)$_3$ (0.267 mg, 0.00132 mmol) was dispensed to the reaction vial.

Table A7. Summarized results of fair comparisons, optimization, and TON investigation for the Heck coupling.

Entry	Pd source	Pd loadin/ mol %	Temp/°C	Time/ h	NMR solution yield%	Alternative additives	TON
1 [a]	**4.1**	2.5	120	18	82		32.8
2 [a]	Pd_2dba_3•CHC_3	2.5	120	18	38		15.2
3 [a]	$[Pd(allyl)Cl]_2$	2.5	120	18	62		24.8
4[b]	**4.1**	2.0	100	18	0		
5[b]	**4.1**	2.0	100	18	0	Cs_2CO_3 instead of Cy_2NMe	
6[b]	**4.1**	1.6	110	18	0		
7[b]	**4.1**	2.0	110	18	5	MePhos instead of P(*t*Bu)$_3$	
8 [a]	**4.1**	1.0	120	18	56		56
9 [a]	$[Pd(allyl)Cl]_2$	1.0	120	18	35		35
10 [a]	Pd_2dba_3•CHC_3	1.0	120	18	39		39
11 [a]	**4.1**	1.0	120	48	57		57
12[b]	**4.1**	1.0	120	48	87		87
13[b]	**4.1**	0.5	120	48	74		148
14[b]	**4.1**	0.25	120	48	42		168
15[b]	**4.1**	0.125	120	48	39		312
16[b]	**4.1**	0.08	120	48	28		350
17[b]	**4.1**	0.04	120	48	7		175
18[b]	**4.1**	0.02	120	48	4		200
19[b]	$[Pd(allyl)Cl]_2$	0.08	120	48	12		150
20[b]	Pd_2dba_3•CHC_3	0.08	120	48	14		175

[a]1:1 L-to-Pd ratio was applied. [b]2:1 L-to-Pd ratio was utilized.

General procedure for C–O coupling:

Procedure for entry 23 in Table A8 is given here.

A stock solution of **4.1** in THF (3.9 mg/mL) was dispensed to a 1-dram vial (56.2 μL, 0.221 mg, 0.000405 mmol) containing a stirbar, followed by solvent evaporation under vacuum. The vial was then charged with 1,3,5-trimethoxybenzene (17.1 mg, 0.102 mmol), 4-bromoacetophenone (300 mg, 1.51 mmol) under air. The vial was then brought into a nitrogen glovebox. A stock solution of *t*BuBrettPhos in anhydrous CPME (3.8 mg/mL) was then dispensed to the reaction mixture (100.4 μL, 0.381 mg, 0.000786 mmol), followed by Cs_2CO_3 (591.3 mg, 1.81 mmol), 1-butanol (151.7 μL, 1.66 mmol), anhydrous CPME (2.0 mL). The reaction mixture was stirred at 50 °C for 48 hours. The resulting solution underwent filtration to remove the base, followed by solvent evaporation and analysis by ^{1}H NMR spectroscopy.

Preparation of stock solutions:

Palladium stock solution was prepared from **4.1** (1.1 mg, 0.0033 mmol) and 279.7 μL THF. 56.2 μL palladium stock solution was dispensed to a 1-dram vial, followed by solvent evaporation under vacuum to have solid **4.1** (0.221 mg, 0.000405 mmol) in the designated vial.

tBuBrettPhos stock solution was prepared from *t*BuBrettPhos (1.9 mg, 0.0039 mmol) and 500 μL anhydrous Toluene. 100.4 μL stock solution containing *t*BuBrettPhos (0.381 mg, 0.000786 mmol) was dispensed to the reaction vial.

Table A8. Summarized results of fair comparisons, optimization, and TON investigation for the C-O coupling.

Entry	Pd source	Pd loading	*t*BuBrettPhos Loading	Time/ h	NMR solution yield%	TO N
1	^{DMP}DAB–Pd–MAH	1 mol %	2 mol % BippyPhos	5	53	53
2	$Pd(OAc)_2$	1 mol %	2 mol % BippyPhos	5	53	53
3	Pd_2dba_3•$CHCl_3$	1 mol %	2 mol % BippyPhos	5	48	48
4	**4.1**	1 mol %	2 mol % *t*BuBrettPhos	5	90 (35 [a])	90
5	^{DMP}DAB–Pd–MAH	1 mol %	2 mol % *t*BuBrettPhos	5	23	23
6	$Pd(OAc)_2$	1 mol %	2 mol % *t*BuBrettPhos	5	26	26
7	$[Pd(allyl)Cl_2$	1 mol %	2 mol % *t*BuBrettPhos	5	83 (29[a])	83
8	^{DMP}DAB–Pd–MAH	1 mol %	2 mol % *t*BuXPhos	5	70 (15[a])	70
9	$Pd(OAc)_2$	1 mol %	2 mol % *t*BuXPhos	5	8	8
10	$[Pd(allyl)Cl_2$	1 mol %	2 mol % *t*BuXPhos	5	66	66
11	**4.1**	0.5 mol %	1 mol % *t*BuBrettPhos	18	92	184

12	**4.1**	0.2 mol %	0.2 mol % *t*BuBrettPhos	18	72	360
13	[Pd(allyl)Cl_2	0.2 mol %	0.2 mol % *t*BuBrettPhos	18	60	300
14	**4.1**	0.2 mol %	0.4 mol % *t*BuBrettPhos	5	54	270
15	[Pd(allyl)Cl_2	0.2 mol %	0.4 mol % *t*BuBrettPhos	5	42	210
16	**4.1**	0.1 mol %	0.1 mol % *t*BuBrettPhos	18	38	380
17	[Pd(allyl)Cl]$_2$	0.1 mol %	0.1 mol % *t*BuBrettPhos	18	46	460
18	**4.1**	0.1 mol %	0.2 mol % *t*BuBrettPhos	18	68	680
19	[Pd(allyl)Cl]$_2$	0.1 mol %	0.2 mol % *t*BuBrettPhos	18	66	660
20	**4.1**	0.2 mol %	0.4 mol % *t*BuBrettPhos	18	84	420
21	[Pd(allyl)Cl]$_2$	0.2 mol %	0.4 mol % *t*BuBrettPhos	18	81	405
22	**4.1**	0.05 mol %	0.1 mol % *t*BuBrettPhos	48	17	340
23	**4.1**	0.025 mol %	0.05 mol % *t*BuBrettPhos	48	5	200
24	**4.1**	0.0125 mol %	0.025 mol % *t*BuBrettPhos	48	1	80
25	[Pd(allyl)Cl_2	0.05 mol %	0.1 mol % *t*BuBrettPhos	48	21	420

[a]Reaction time: 1 hour.

General Procedure for Ligand Substitution Investigation

A representative procedure with RuPhos is given here.

In a glovebox under a dry, oxygen-free atmosphere of nitrogen gas, a 1-dram vial was added **4.1** (6.2 mg, 0.011 mmol), RuPhos (5.2 mg, 0.011 mmol), and 0.6 mL anhydrous THF. The mixtures were stirred at room temperature for 1 h, and analyzed by ^{31}P NMR spectroscopy with a capillary consisting of C_6D_6/PPh_3 as the internal standard. The outcomes obtained from the ^{31}P NMR spectra are summarized in the following table.

Table A9. Summarized outcomes of ligand substitution of complex **4.1** with different phosphine ligands.

Entry	Phosphine	Outcomes
1	RuPhos	phosphine was consumed + a tiny peak at 43 ppm
2	*t*BuXPhos	phosphine remained
3	BrettPhos	phosphine remained
4	SPhos	phosphine was consumed
5	CPhos	phosphine was consumed[a]
6	BippyPhos	phosphine remained (small amount)[a]
7	*t*BuBrettPhos	phosphine remained (small amount)
8	DPEPhos	phosphine was consumed + a tiny peak at 10.6 ppm

[a]reaction time: 2 hours.

Appendix B: NMR Characterization Data and Spectra

^{DMP}DAB–Pd–MAH (2.1)

^{1}H NMR: (300 MHz; d_6-acetone) δ 2.17 (s, 12H, 4 x Ar–C**H**$_3$), 3.44 (s, 2H, –CH=CH–), 6.99 (m, 6H, 6 x Ar–H), 8.42 (s, 2H, 2 x –C**H**=NAr).

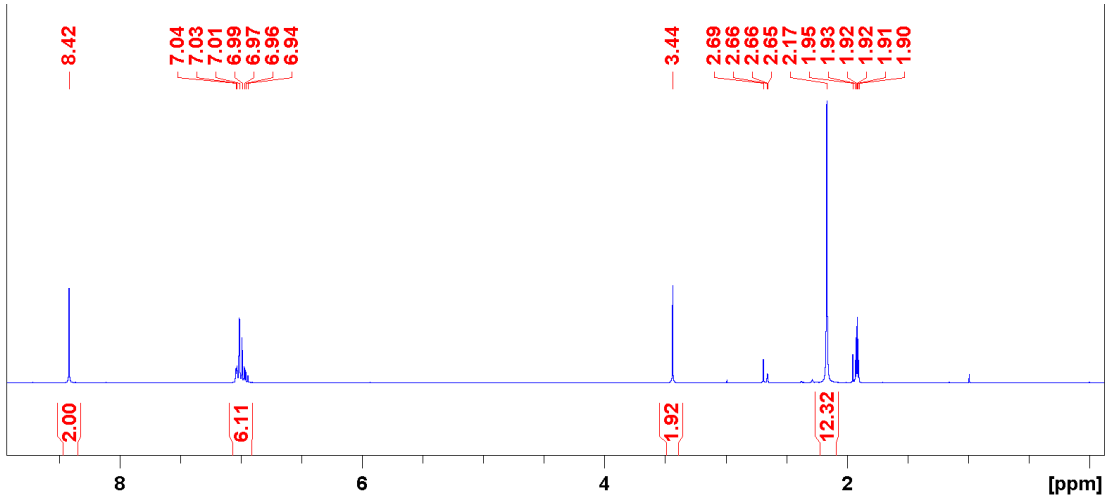

Figure A7. ^{1}H NMR spectrum (300 MHz; d_6-acetone) of **2.1**. Quintet at 1.92 ppm is d_5-acetone; singlet at 1.95 ppm is acetone; 1:1:1 triplet at 2.65 ppm is HDO; singlet at 2.69 ppm is H_2O.

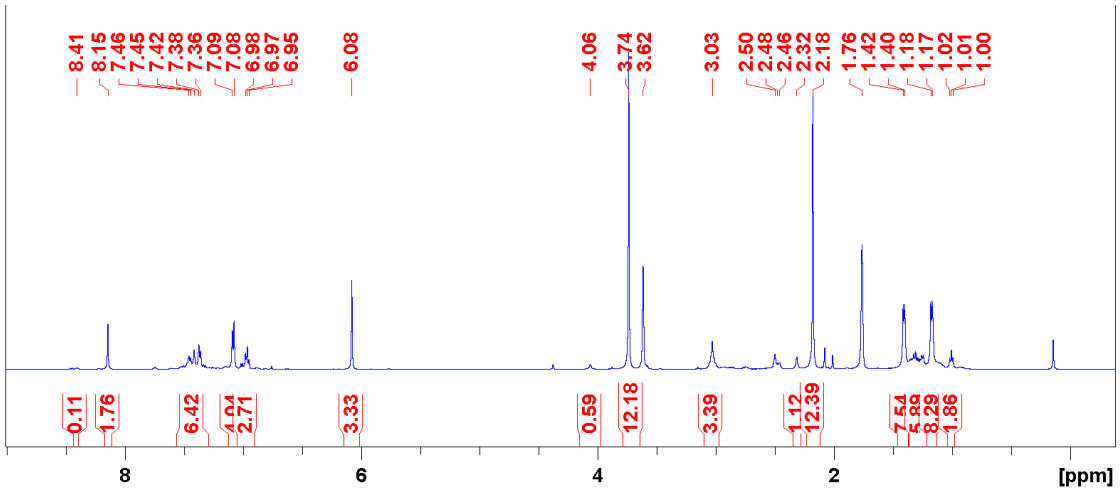

Figure A8. ^{1}H NMR spectrum of the reaction between **2.1** and DIPP-NHC (1 equiv).

N-benzylpyridin-2-amine

^{1}H NMR (300 MHz, $CDCl_3$): δ 8.11 (d, *J* = 4.0 Hz, 1H), 7.38 (m, 5H), 7.27 (m, 1H), 6.59 (m, 1H), 6.38 (d, *J* = 8.4 Hz, 1H), 4.92 (br, 1H), 4.51 (d, *J* = 5.8 Hz, 2H). **^{13}C NMR (75 MHz, $CDCl_3$): δ** 158.7, 148.2, 139.2, 137.5, 128.6, 127.4, 127.2, 113.1, 106.8, 46.3.

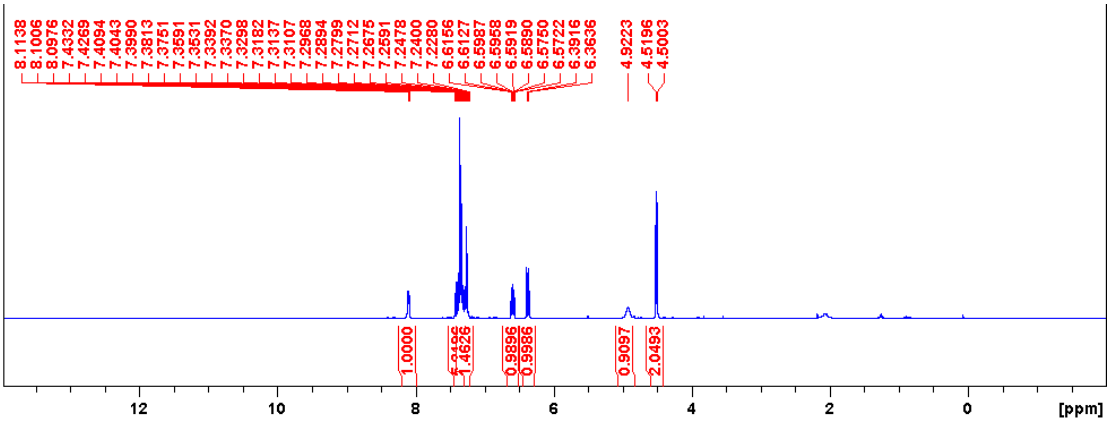

Figure A9. ^{1}H NMR spectrum (300 MHz; $CDCl_3$) of *N*-benzylpyridin-2-amine

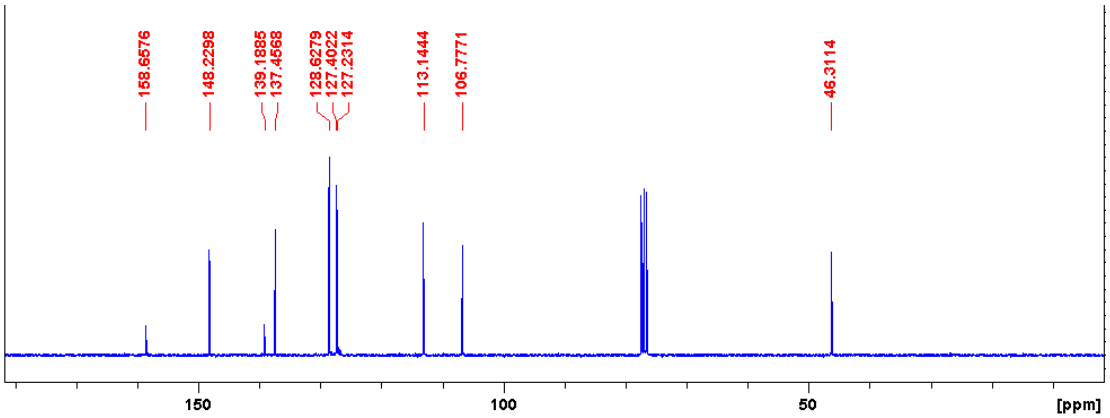

Figure A10. ^{13}C{^{1}H} NMR spectrum (75 MHz; $CDCl_3$) of *N*-benzylpyridin-2-amine

4-(4-methoxyphenyl)morpholine

^{1}H NMR (300 MHz, $CDCl_3$): δ 6.87 (m, 4H), 3.84 (appt, *J* = 4.8 Hz, 4H), 3.77 (s, 3H), 3.04 (appt, *J* = 4.8 Hz, 4H). **^{13}C NMR (75 MHz, $CDCl_3$):** δ 154.0, 145.6, 117.8, 114.5, 67.0, 55.5, 50.8.

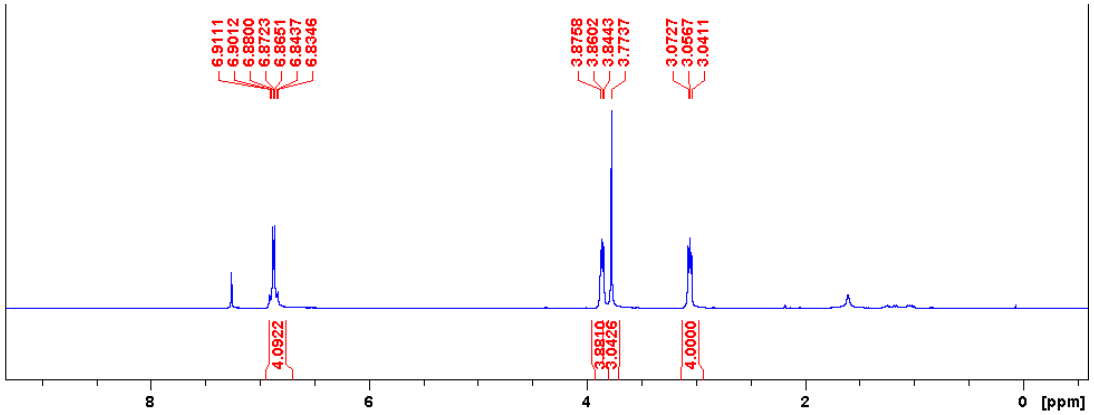

Figure A11. ^{1}H NMR spectrum (300 MHz; $CDCl_3$) of 4-(4-methoxyphenyl)morpholine

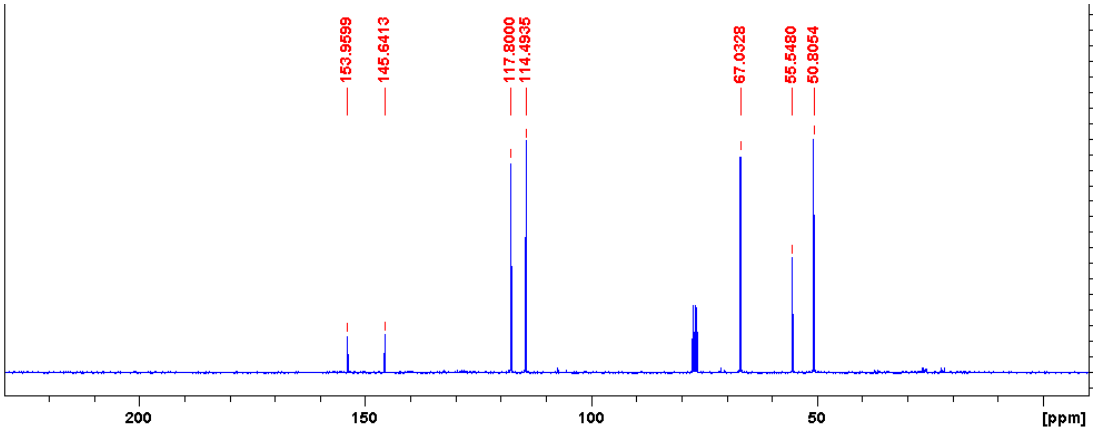

Figure A12. ^{13}C{^{1}H} NMR spectrum (75 MHz; $CDCl_3$) of 4-(4-methoxyphenyl)morpholine

***N*-(4-methylphenyl)-4-methylbenzenesulfonamide**

^{1}H NMR (300 MHz, $CDCl_3$): δ 2.27 (s, 3H), 2.40 (s, 3H), 6.31 (br, 1H), 6.91 (d, *J* = 8.4 Hz, 2H), 7.04 (d, *J* = 8.3 Hz, 2H), 7.21 (d, *J* = 8.0 Hz, 2H), 7.61 (d, *J* = 8.3 Hz, 2H); **^{13}C NMR (75 MHz, $CDCl_3$): δ** 143.7, 136.0, 135.0, 134.0, 129.6, 127.3, 122.0, 21.5, 20.8.

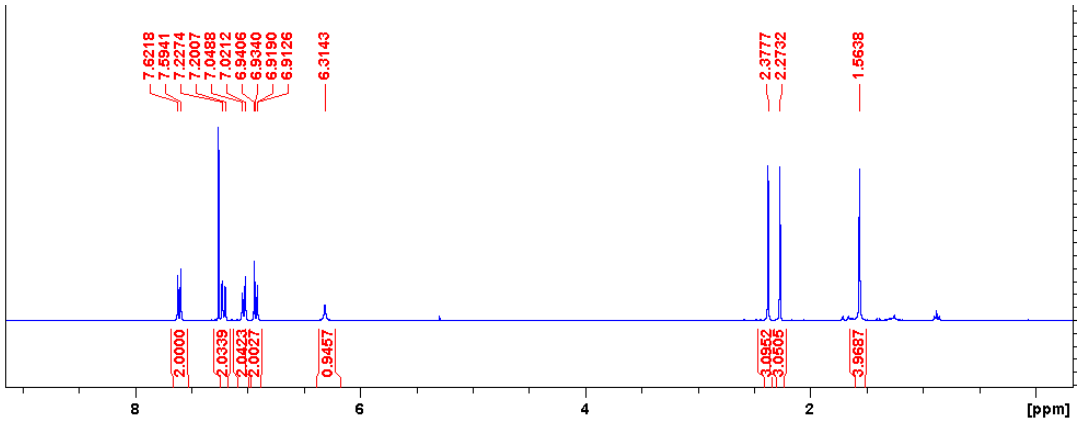

Figure A13. ^{1}H NMR spectrum (300 MHz; $CDCl_3$) of *N*-(4-methylphenyl)-4-methylbenzenesulfonamide

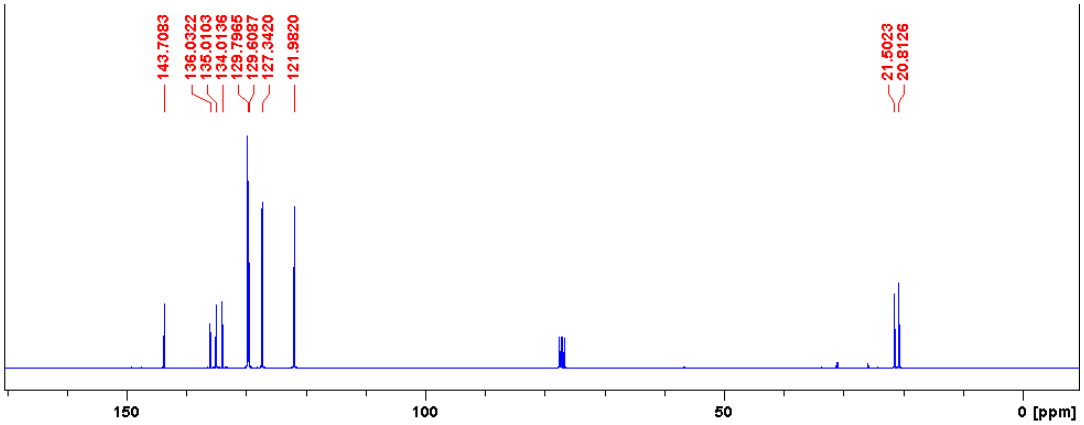

Figure A14. ^{13}C{^{1}H} NMR spectrum (75 MHz; $CDCl_3$) of *N*-(4-methylphenyl)-4-methylbenzenesulfonamide

4-methyl-1-phenyl-1*H*-imidazole

^{1}H NMR (300 MHz, $CDCl_3$): δ 7.76 (d, *J* = 1.6 Hz, 1H), 7.49-7.44 (m, 2H), 7.37-7.31 (m, 3H), 7.01 (s, 1H), 2.30 (s, 3H); **^{13}C NMR (75 MHz, $CDCl_3$): δ** 139.5, 137.4, 134.5, 129.8, 127.0, 121.0, 114.5, 13.7.

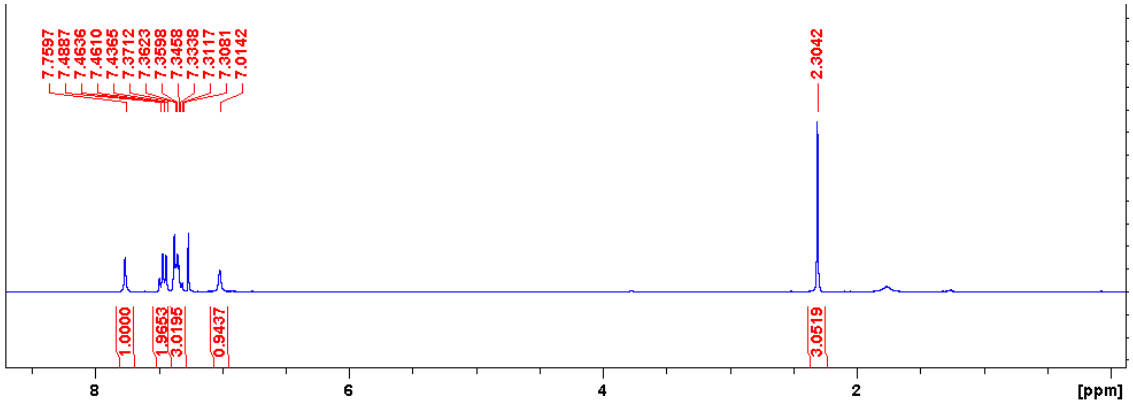

Figure A15. ^{1}H NMR spectrum (300 MHz; $CDCl_3$) of 4-methyl-1-phenyl-1*H*-imidazole

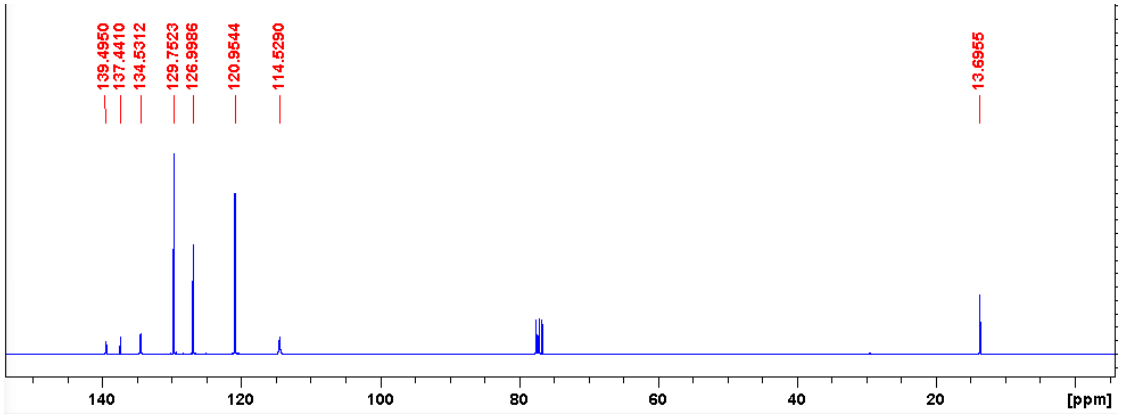

Figure A16. ^{13}C{^{1}H} NMR spectrum (75 MHz; $CDCl_3$) of 4-methyl-1-phenyl-1*H*-imidazole

(*E*)-3-(4-acetylphenyl)-2-methyl acrylic acid methyl ester

^{1}H NMR (300 MHz, $CDCl_3$): δ 7.98 (d, *J* = 8.4 Hz, 2H), 7.70 (apparent s, 1H), 7.46 (d, *J* = 8.3 Hz, 2H), 3.83 (s, 3H), 2.62 (s, 3H), 2.12 (d, *J* = 1.5 Hz, 3H). **^{13}C NMR (75 MHz, $CDCl_3$): δ** 197.3, 168.6, 140.4, 137.5, 136.3, 130.3, 129.6, 128.3, 52.2, 26.6, 14.1.

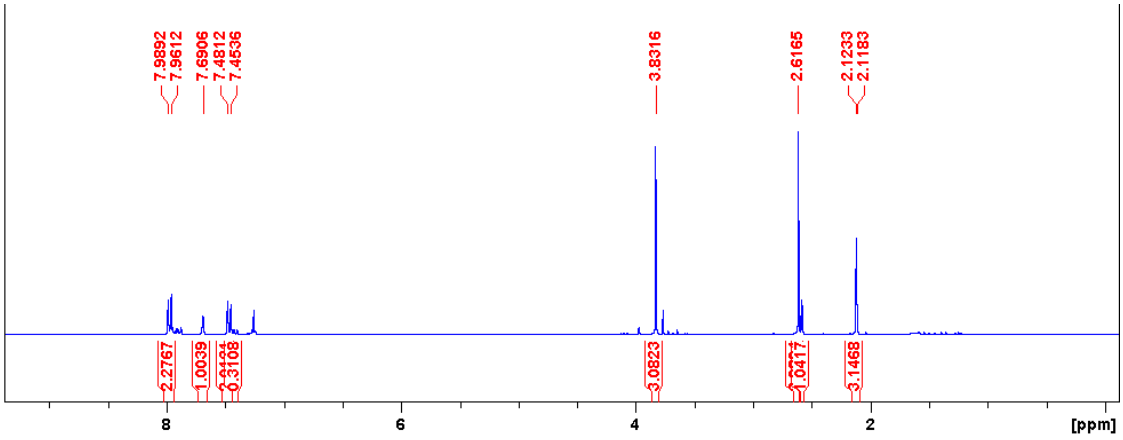

Figure A17. ^{1}H NMR spectrum (300 MHz; $CDCl_3$) of (*E*)-3-(4-acetylphenyl)-2-methyl acrylic acid methyl ester

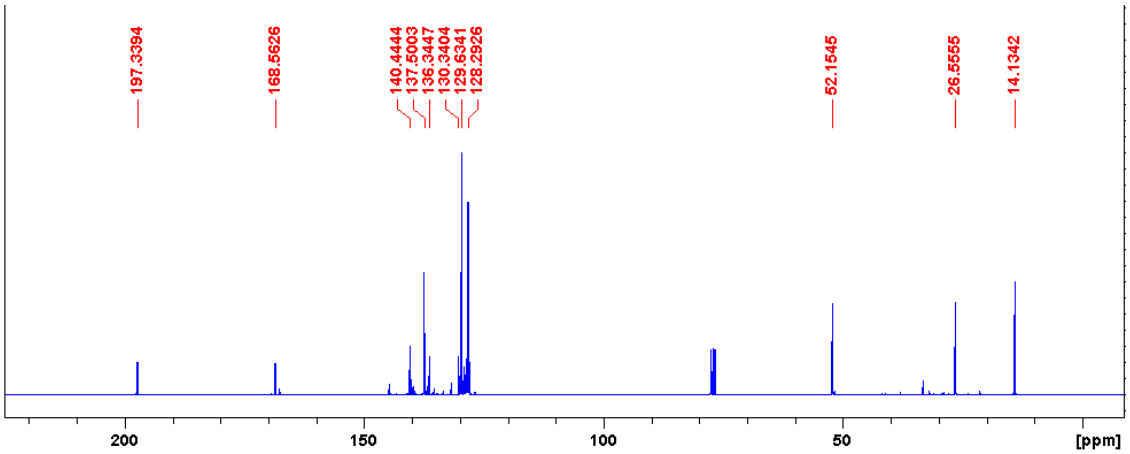

Figure A18. ^{13}C{^{1}H} NMR spectrum (75 MHz; $CDCl_3$) of (*E*)-3-(4-acetylphenyl)-2-methyl acrylic acid methyl ester

1-(4-*n*-Butoxyphenyl)ethanone

^{1}H NMR (300 MHz, $CDCl_3$): δ 7.92 (m, 2H), 6.91 (m, 2H), 4.02 (t, *J* = 6.5 Hz, 2H), 2.55 (s, 3H), 1.78 (m, 2H), 1.50 (m, 2H), 0.98 (t, *J* = 7.03 Hz, 3H). **^{13}C NMR (75 MHz, $CDCl_3$): δ** 196.8, 163.1, 130.5, 130.0, 114.1, 67.9, 31.1, 26.3, 19.2, 13.8.

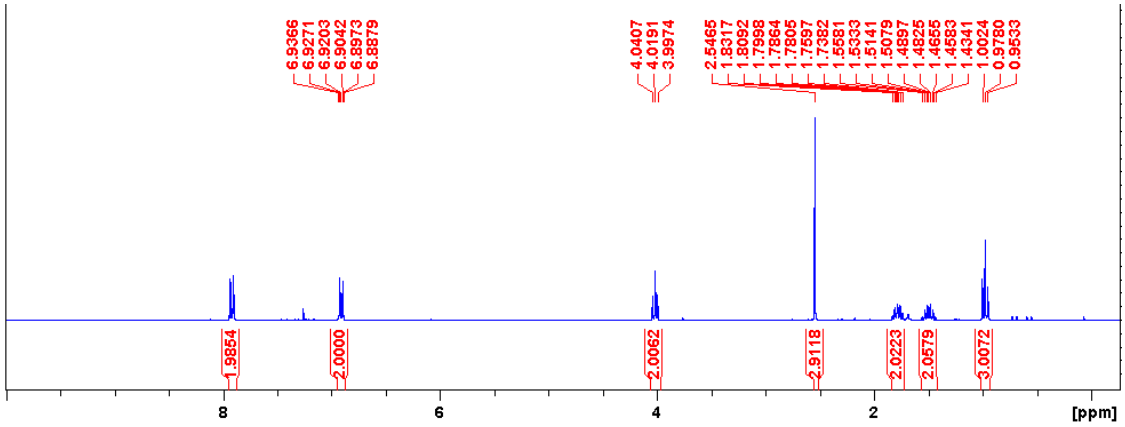

Figure A19. ^{1}H NMR spectrum (300 MHz; $CDCl_3$) of 1-(4-*n*-Butoxyphenyl)ethanone

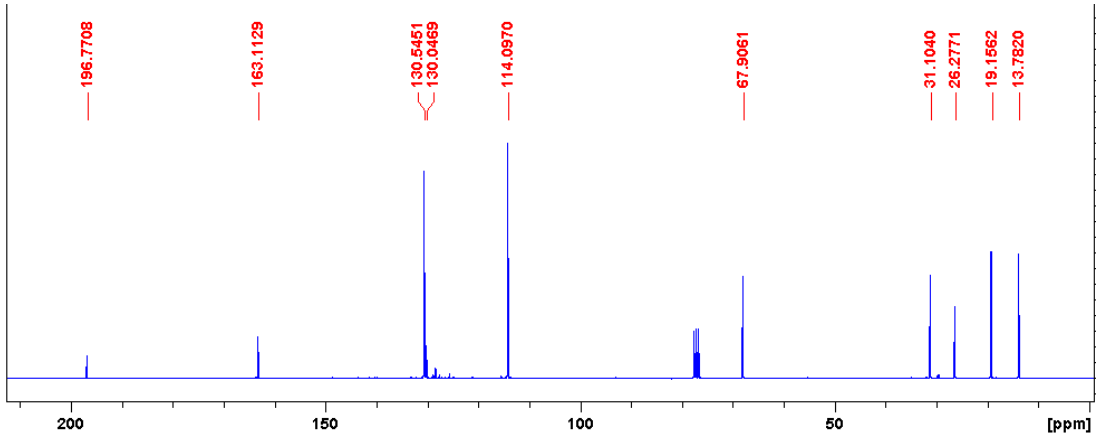

Figure A20. ^{13}C{^{1}H} NMR spectrum (75 MHz; $CDCl_3$) of 1-(4-*n*-Butoxyphenyl)ethanone

spiro-OMeTAD

^{1}H NMR (500 MHz, d^{6}-DMSO): δ 3.72 (s, 24 H, 8 x –OCH_3), 6.19 (d, 4H, *J* = 2.0 Hz), 6.70 (dd, 4H, *J* = 2.0, 8.4 Hz), 6.84 (m, 32H, Ar–H), 7.48 (d, 4H, *J* = 8.4 Hz). **^{13}C NMR (125 MHz, d^{6}-DMSO): δ** 155.7, 149.9, 147.7, 140.9, 134.4, 126.0, 121.4, 120.7, 116.2, 116.1, 65.4, 55.7.

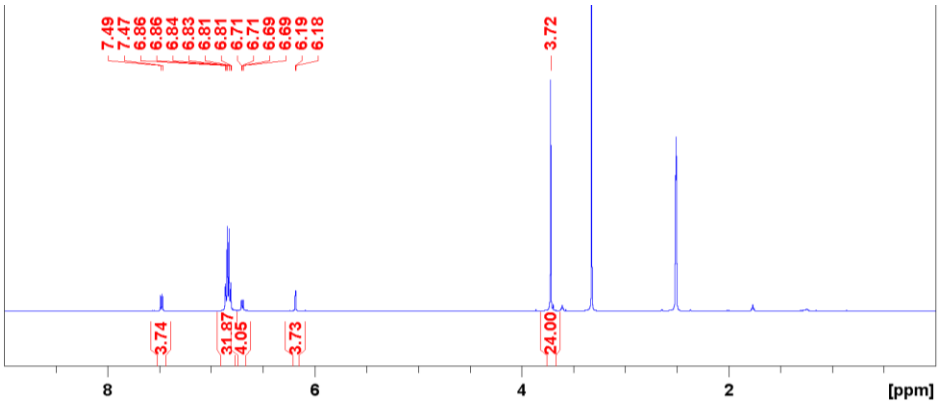

Figure A21. ^{1}H NMR spectrum (500 MHz; d^{6}-DMSO) of *spiro*-OMeTAD

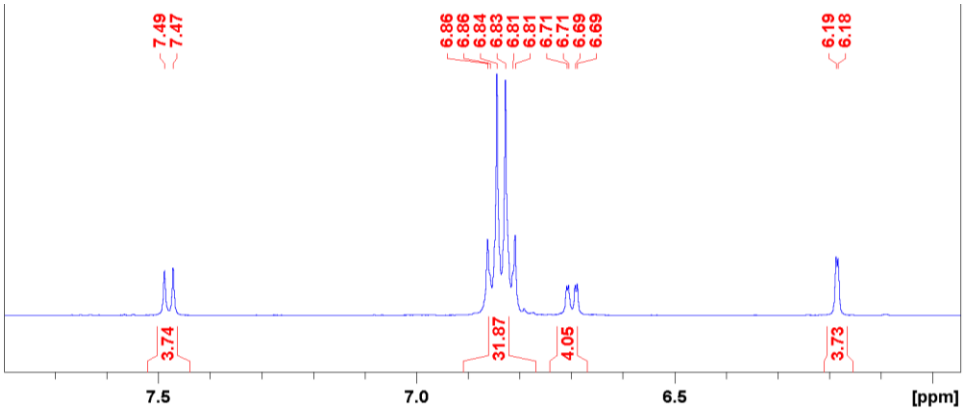

Figure A22. ^{1}H NMR spectrum (500 MHz; d^{6}-DMSO) of *spiro*-OMeTAD. Expansion of aromatic region.

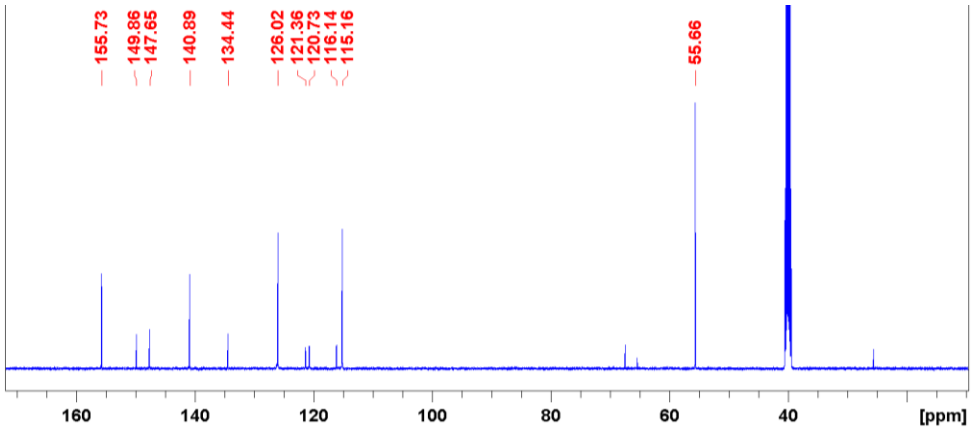

Figure A23. ^{13}C{^{1}H} NMR spectrum (125 MHz; d^{6}-DMSO) of *spiro*-OMeTAD. Signals at 26.0 and 67.5 ppm are trace residual THF from the recrystallization.

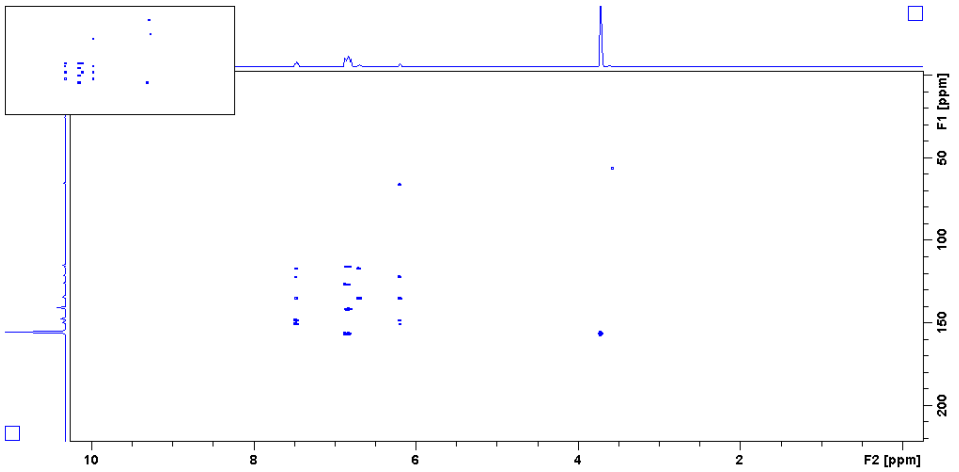

Figure A24. ^{1}H-^{13}C HMBC NMR spectrum (500 MHz and 125 MHz; d^{6}-DMSO) of *spiro*-OMeTAD.

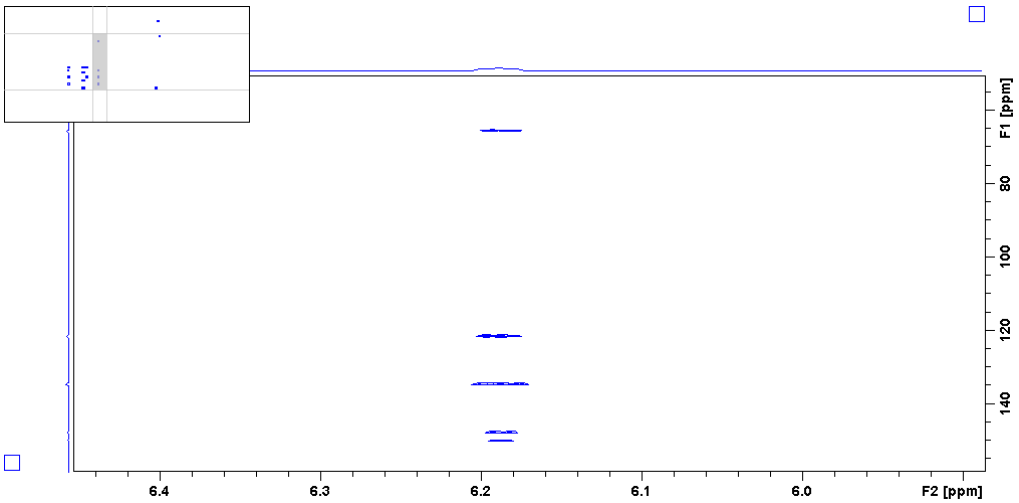

Figure A25. Expansion of ^{1}H-^{13}C HMBC NMR spectrum (500 MHz and 125 MHz; d^{6}-DMSO) of *spiro*-OMeTAD. Signal at 65.4 is confirmed as the central *spiro*-carbon (quaternary).

(*S*,*S*)-^{Ph}DACH–Pd–MAH (3.1)

^{1}H NMR (500 MHz, THF-*d*$_8$) δ 8.06 (d, *J* = 5.6 Hz, 1H), 7.82 (d, *J* = 6.3 Hz, 1H), 6.65-7.59 (m, 28H), 4.38 (m, 1H), 4.08 (m, 1H), 3.64 (m, 1H), 3.37 (sept, *J* = 5.1 Hz, 1H), 2.21 (m, 1H), 2.05 (m, 1H), 1.79 (m, 1H), 1.53-1.65 (m, 2H), 1.24-1.33 (m, 1H), 1.12-1.24 (m, 2H).

^{13}C NMR (125 MHz, THF-*d*$_8$) δ 170.6, 170.3, 169.0, 168.0, 143.7, 139.7, 137.7, 136.1, 134.2, 133.9, 133.1, 132.5, 133.0, 129.6, 129.5$_4$, 129.4$_7$, 129.4, 129.3$_2$, 129.2$_8$, 129.0$_4$, 129.0$_0$, 128.7$_3$, 128.6$_9$, 128.6$_6$, 128.2, 128.0, 127.9, 127.8, 127.4, 127.3, 127.0, 126.9, 57.0, 52.4, 32.1, 31.2, 24.8, 23.7.

^{31}P NMR (200 MHz, THF-*d*$_8$) δ 24.9 (d, $^{2}J_{P\text{-}P}$ = 4.9 Hz), 23.9 (d, $^{2}J_{P\text{-}P}$ = 4.8 Hz).

Two conformers were observed when **3.1** was dissolved in CD_2Cl_2.

^{1}H NMR (500 MHz, CD_2Cl_2) δ *Major conformer*: 7.86 (d, *J* = 5.1 Hz, 1H), 7.60-6.65 (m, 56H, Ar–H), 6.14 (d, *J* = 6.1 Hz, 1H), 4.44-4.39 (m, 1H), 3.99-3.92 (m, 1H), 3.71-3.65 (m, 1H), 3.38 (septet, *J* = 5.2 Hz, 1H), 2.28-2.24 (m, 1H), 2.12-2.08 (m, 2H), 2.02-1.99 (m, 1H), 1.82-1.76 (m, 2H), 1.67-1.63 (m, 2H), 1.45-1.12 (m, 6H), 1.16-1.10 (m, 2H). *Minor conformer:* 7.60-6.65 (m, 56H, Ar–H), 4.44-4.39 (m, 1H), 3.99-3.92 (m, 1H), 3.87-3.80 (m, 1H), 3.59-3.52 (m, 1H), 2.28-2.24 (m, 1H), 2.12-2.08 (m, 2H), 2.02-1.99 (m, 1H), 1.82-1.76 (m, 2H), 1.67-1.63 (m, 2H), 1.45-1.12 (m, 6H), 1.16-1.10 (m, 2H).

^{31}P NMR (200 MHz, CD_2Cl_2) δ *Major conformer*: 24.5 (d, $^{2}J_{P\text{-}P}$ = 7.1 Hz), 23.0 (d, $^{2}J_{P\text{-}P}$ = 7.1 Hz). *Minor conformer:* 26.5 (d, $^{2}J_{P\text{-}P}$ = 12.0 Hz), 22.1 (d, $^{2}J_{P\text{-}P}$ = 11.9 Hz).

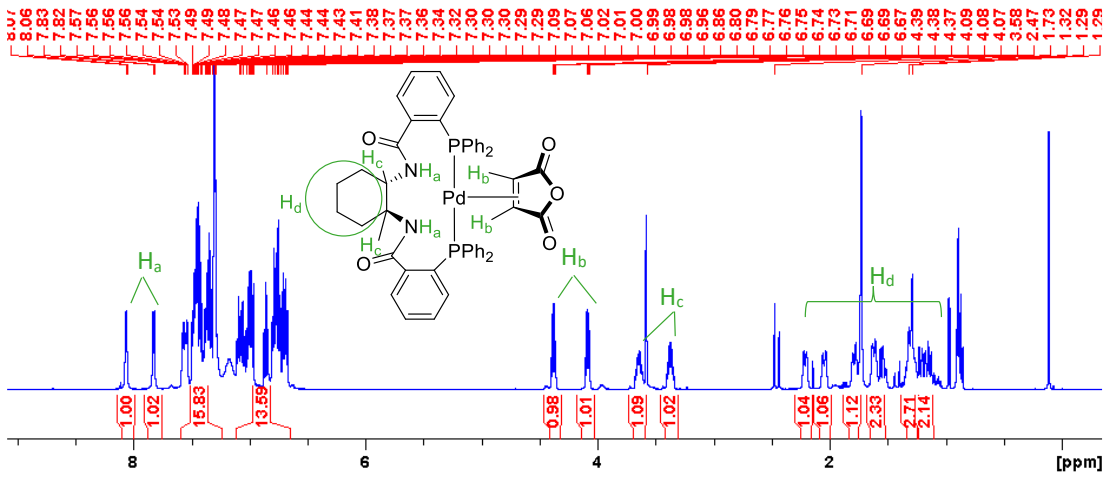

Figure A26. ^{1}H NMR spectrum (500 MHz, THF-*d*$_8$) of **3.1**. Key proton signals are assigned. The singlets at 2.47 ppm and 2.43 ppm are H_2O and HDO. Multiplet at 0.85-0.90 ppm is hexanes. Singlets at 1.73 ppm and 3.58 ppm are THF-d$_8$ residual signals.

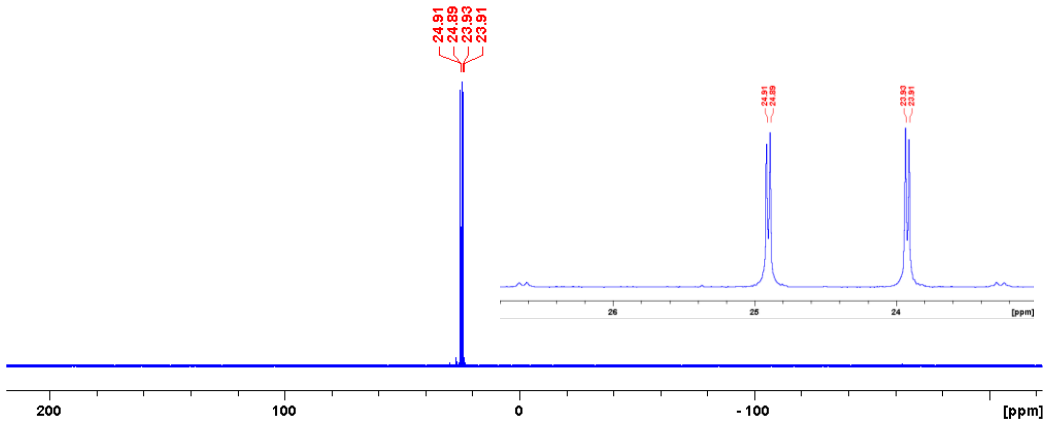

Figure A27. $^{31}P\{^{1}H\}$ NMR spectrum (200 MHz, THF-d_8) of **3.1**.

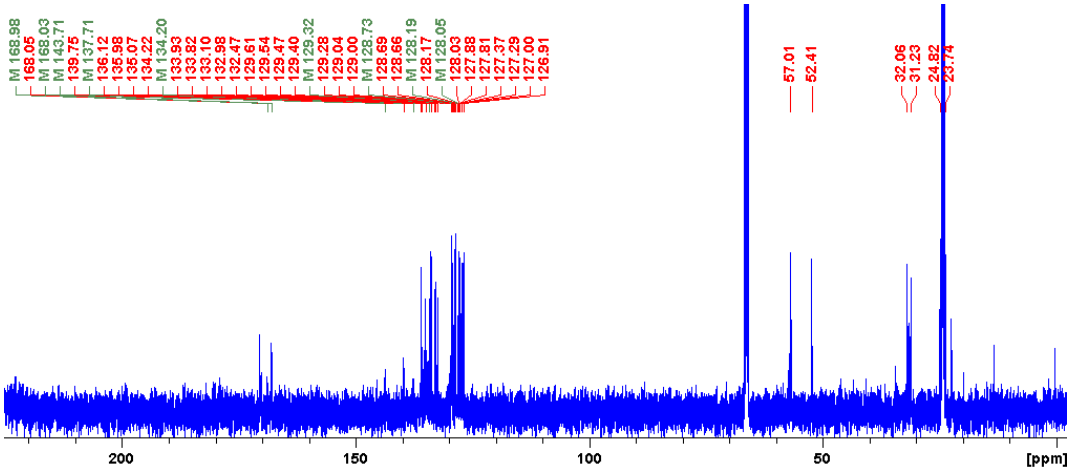

Figure A28. $^{13}C\{^{1}H\}$ NMR spectrum (125 MHz, THF-d_8) of **3.1** (Green labels are manually-picked peaks).

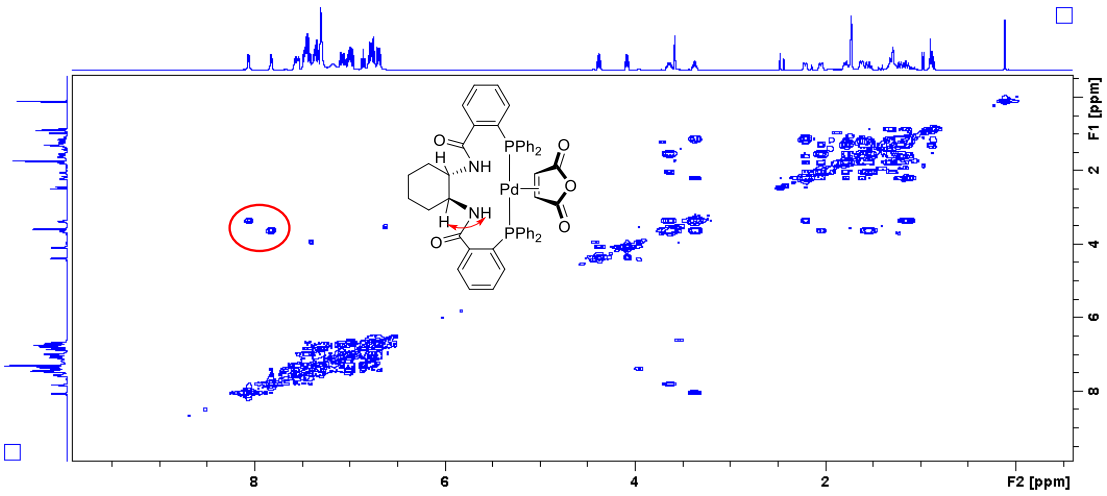

Figure A29. ^{1}H-^{1}H COSY NMR spectrum of **3.1**. Confirmation of NH protons.

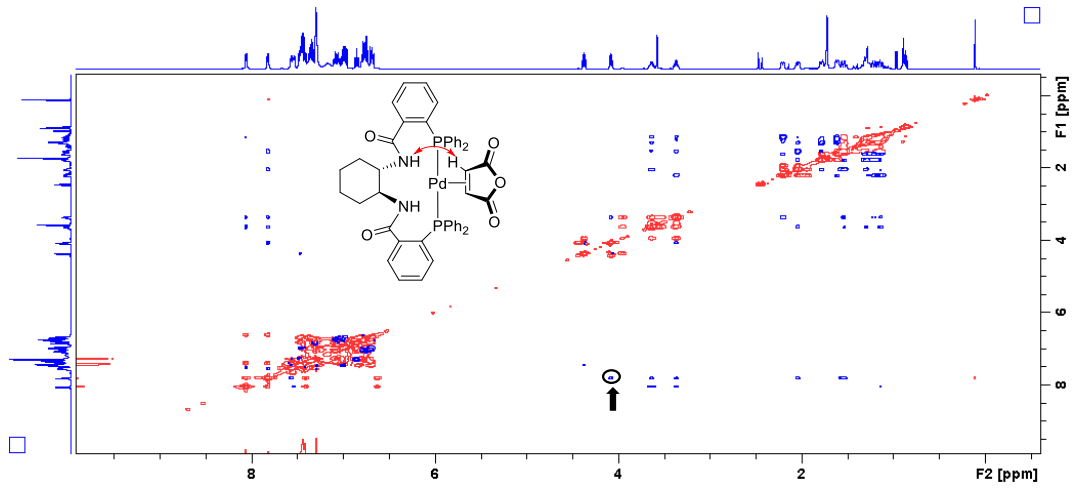

Figure A30. ^{1}H-^{1}H NOESY NMR spectrum of **3.1**. The only correlation between NH and MAH–H indicates the conformer without hydrogen bonding.

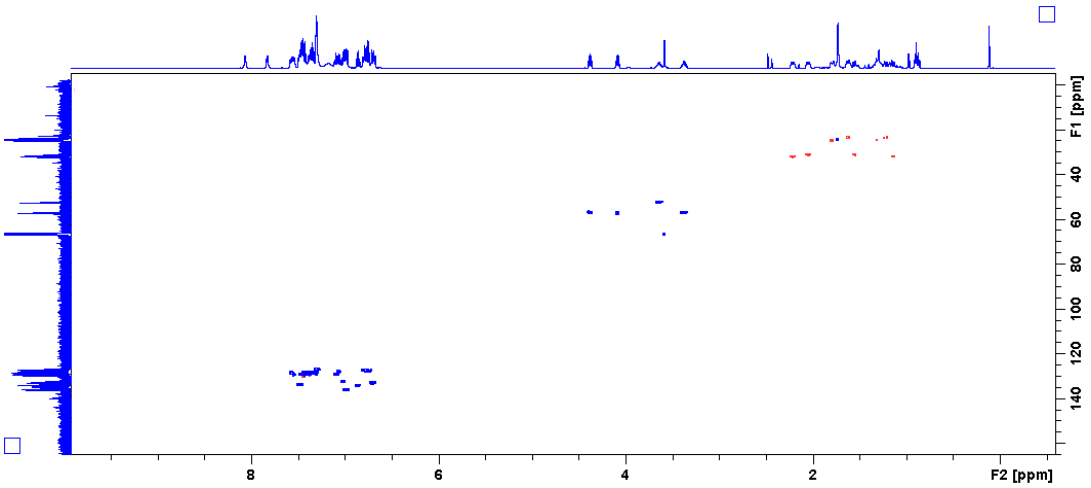

Figure A31. ^{1}H-^{13}C HSQC NMR spectrum of **3.1**.

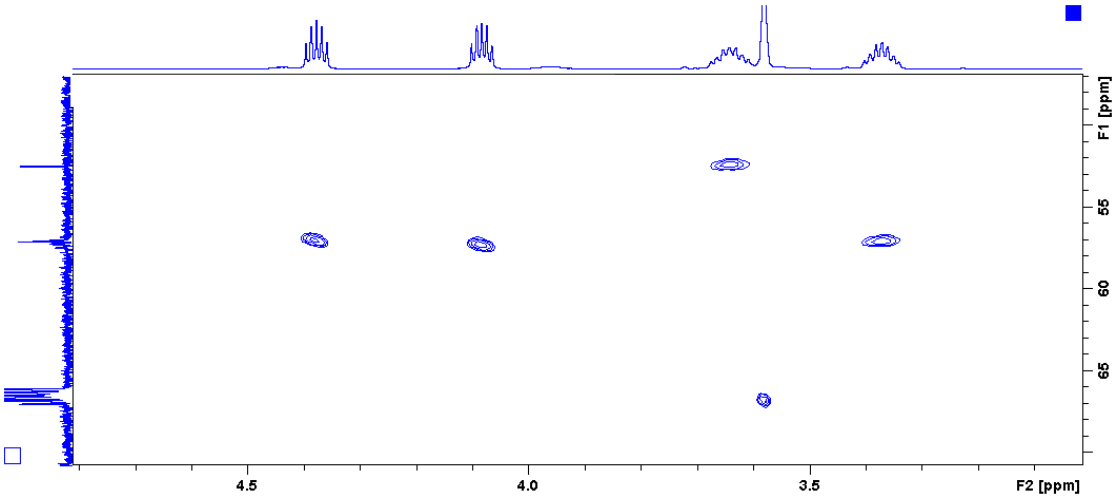

Figure A32. ^{1}H-^{13}C HSQC NMR spectrum of **3.1**. Expansion of overlapped carbon peaks at 57.01 ppm.

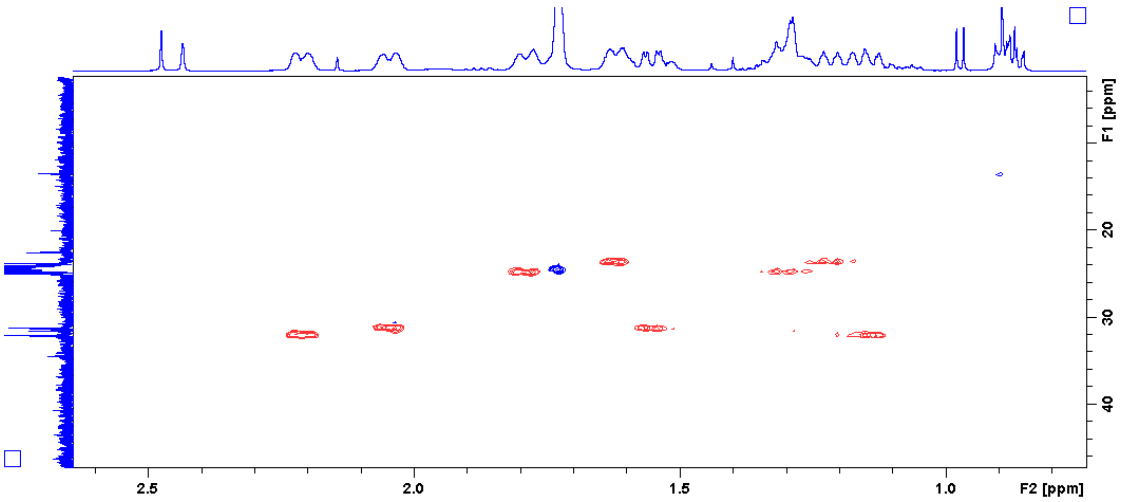

Figure A33. ^{1}H-^{13}C HSQC NMR spectrum expansion of **3.1**. Confirmation of cyclohexyl protons.

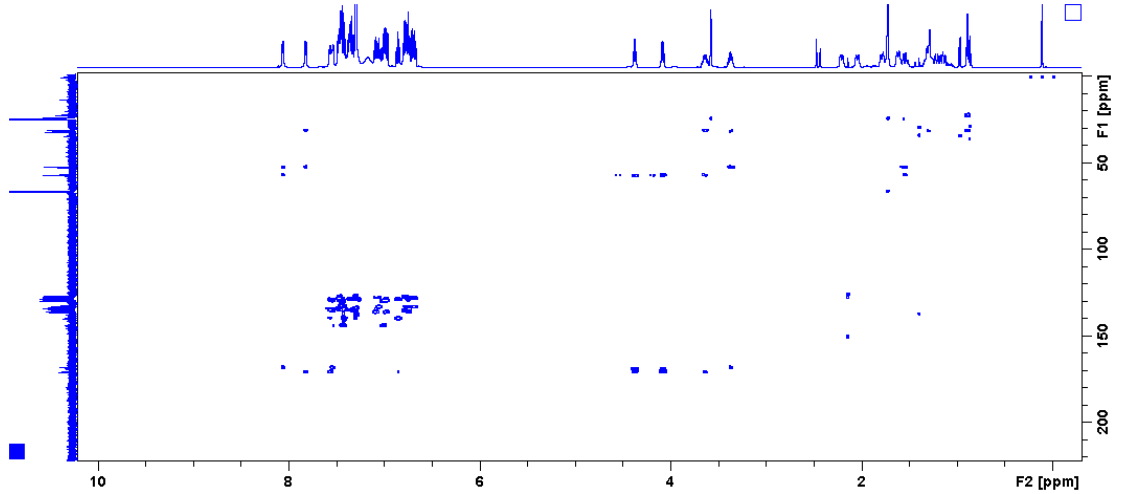

Figure A34. ^{1}H-^{13}C HMBC NMR spectrum of **3.1**.

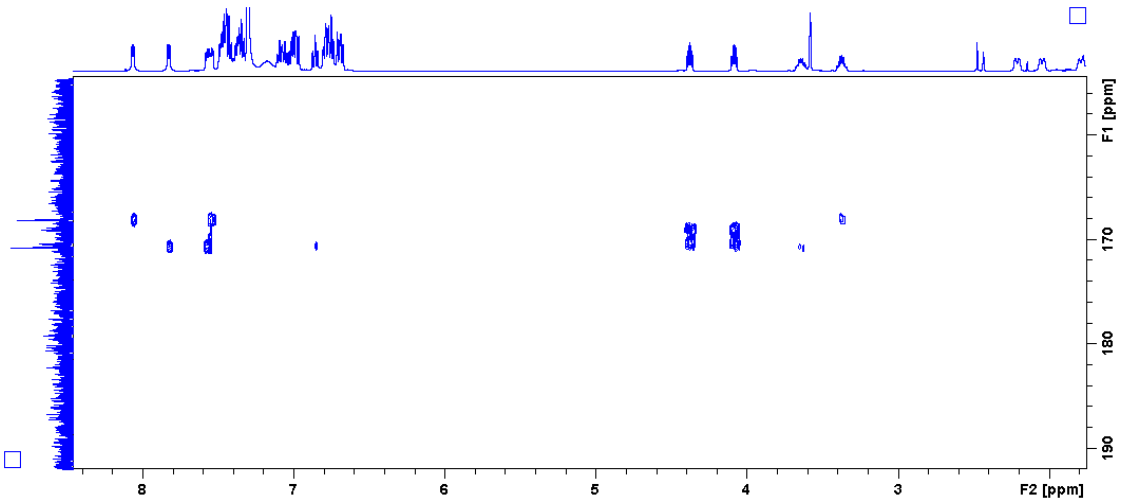

Figure A35. ^{1}H-^{13}C HMBC NMR spectrum expansion of **3.1**. Identification of the carbonyl groups of MAH.

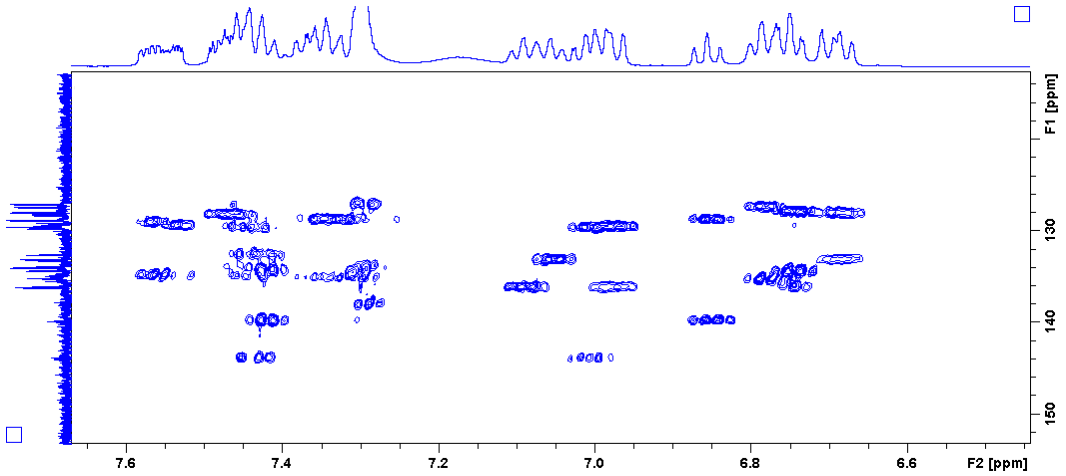

Figure A36. ^{1}H-^{13}C HMBC NMR spectrum of **3.1**. Aliphatic region expansion. Compensation of carbon determination by ^{1}H-^{13}C HSQC NMR spectrum.

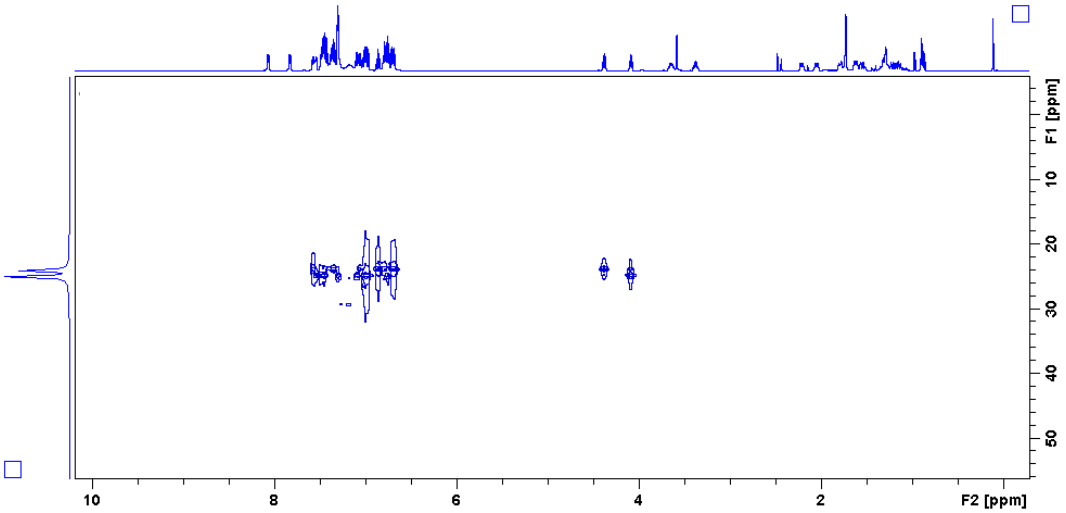

Figure A37. ^{1}H-^{31}P HMBC NMR spectrum of **3.1**.

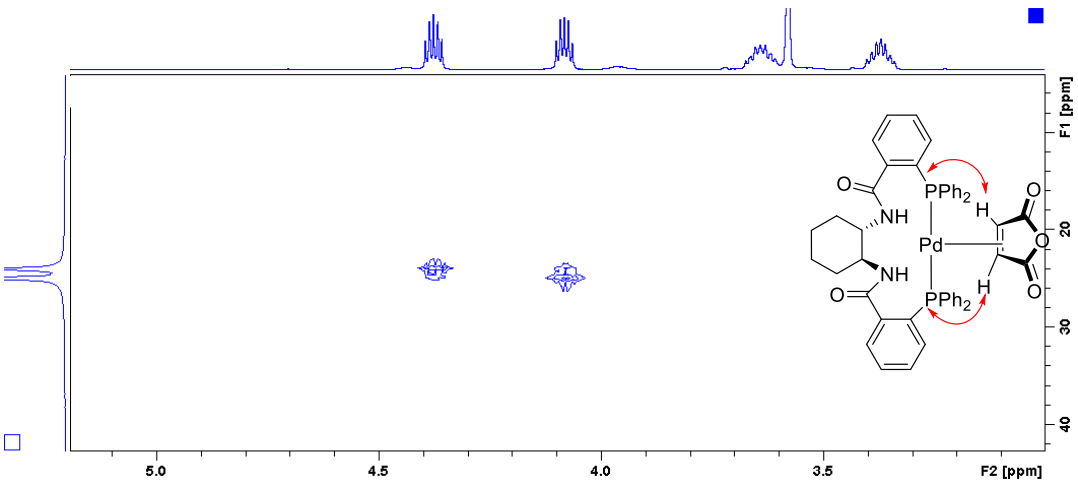

Figure A38. ^{1}H-^{31}P HMBC NMR spectrum expansion of **3.1**.
Correlations between MAH protons and the two P atoms are observed.

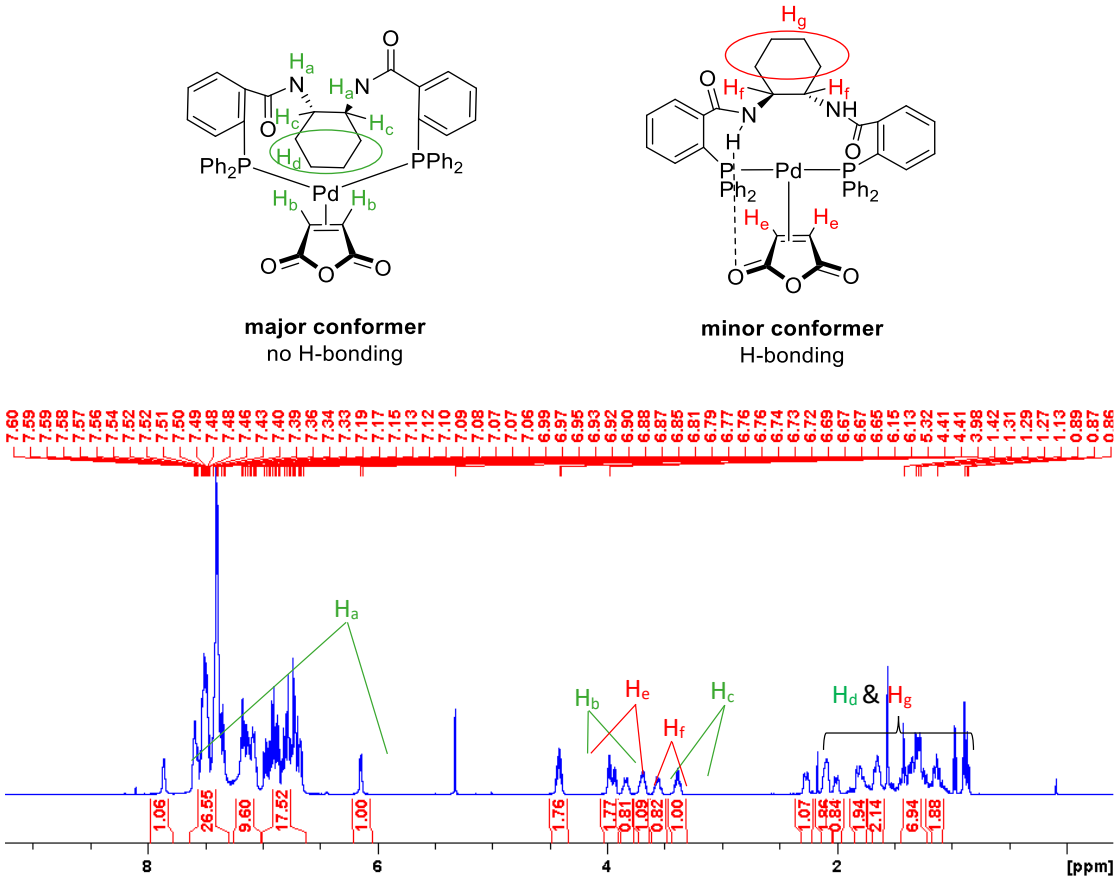

Figure A39. ^{1}H NMR spectrum (500 MHz, CD_2Cl_2) of **3.1**. Singlet at 5.32 ppm is the CD_2Cl_2 residual signal. Multiplet from 0.84 to 0.90 ppm is the signal of hexanes.

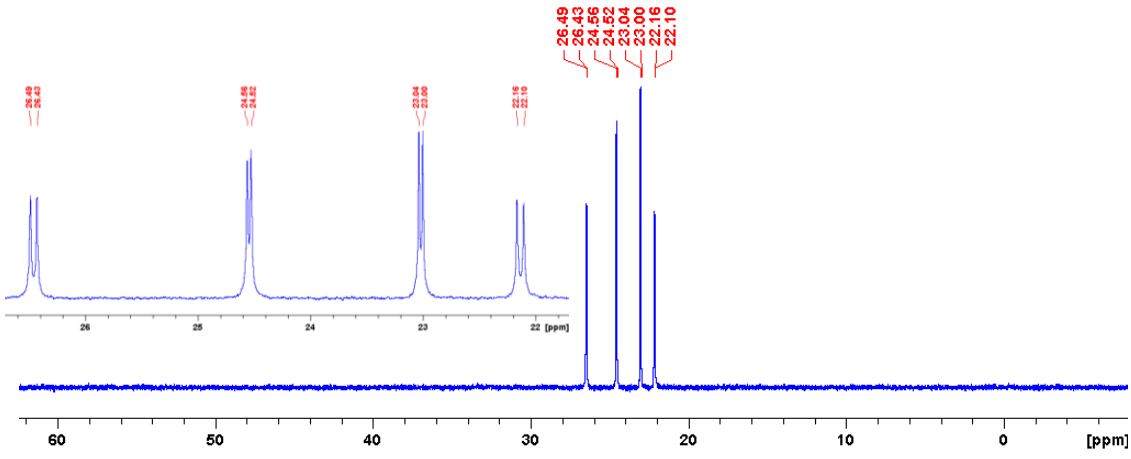

Figure A40. $^{31}P\{^{1}H\}$ NMR spectrum (200 MHz, CD_2Cl_2) of **3.1**.

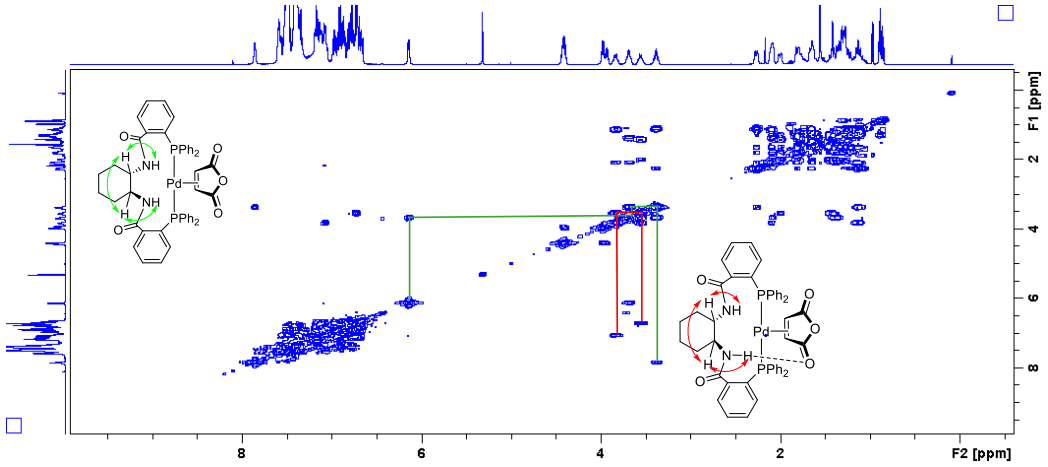

Figure A41. ^{1}H-^{1}H COSY spectrum (CD_2Cl_2) of **3.1**. NH identification of major conformer and minor conformer (green: major conformer, red: minor conformer).

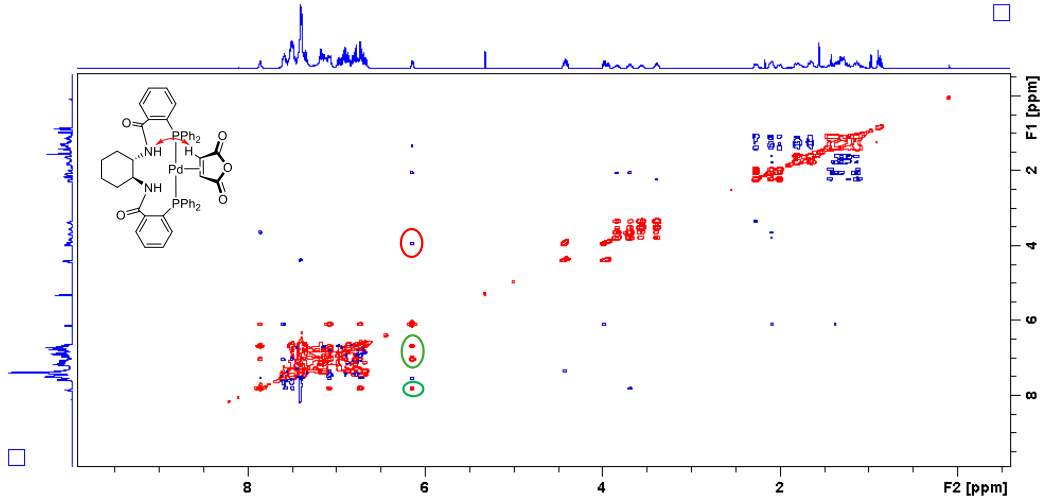

Figure A42. ^{1}H-^{1}H NOESY spectrum (CD_2Cl_2) of **3.1**. The correlation between MAH and NH indicates that the major conformer has no hydrogen bond (red circle). Proton exchanges between these two conformers are observed (green circle).

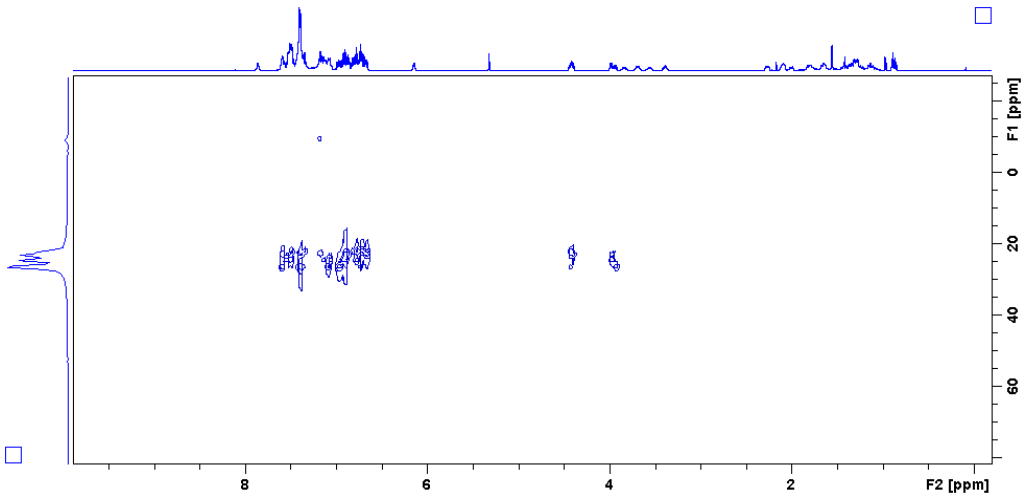

Figure A43. ^{1}H-^{31}P HMBC spectrum (CD_2Cl_2) of **3.1**.

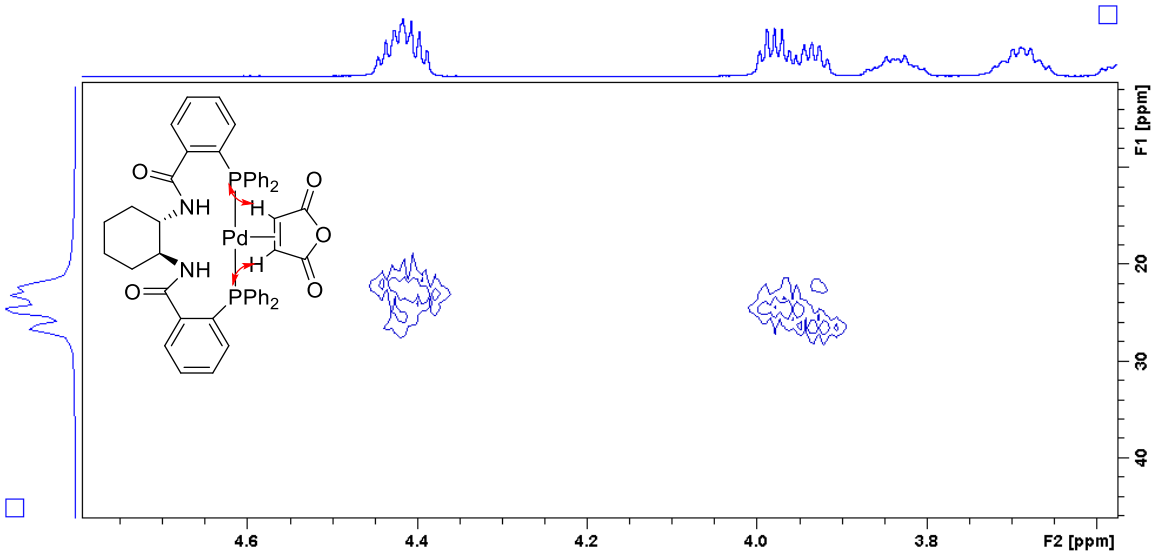

Figure A44. ^{1}H-^{31}P HMBC NMR spectrum expansion (CD_2Cl_2) of **3.1**. Correlations between MAH protons and P atoms are observed.

(*S*,*S*)-^{NAP}DACH–Pd–MAH (3.2)

^{1}H NMR (500 MHz, THF-*d*$_8$) δ 8.22 (br s, 2H), 6.76-7.91 (m, 32H), 4.57 (br s), 4.39 (s, 1H), 3.95 (sept, 1H), 3.57 (s, 1H), 2.92 (br s, 1H), 2.18 (br s, 1H), 1.75-1.84 (m, 2H), 1.28-1.57 (m, 4H).

^{13}C NMR (125 MHz, THF-*d*$_8$) δ 171.0, 170.6, 168.0, 136.6, 136.5, 136.3, 136.0, 135.7, 135.5, 135.2, 135.1, 135.0, 134.9, 134.8, 134.6, 134.5, 133.6 (d, *J* = 4.34 Hz), 133.4 (d, *J* = 3.52 Hz), 132.3, 132.2, 132.1$_3$, 132.0$_7$, 130.6, 130.3, 130.0 (d, *J* = 1.75 Hz), 129.7 (d, *J* = 4.41 Hz), 129.6, 129.1, 129.0, 128.9, 128.8, 128.3, 128.2 (d, *J* = 2.61 Hz), 128.1, 127.9, 127.8, 127.7, 126.7, 126.5, 59.4, 57.0, 54.3, 54.1, 32.6, 32.2, 25.8, 24.9.

^{31}P NMR (200 MHz, THF-*d*$_8$) δ 23.2, 22.8.

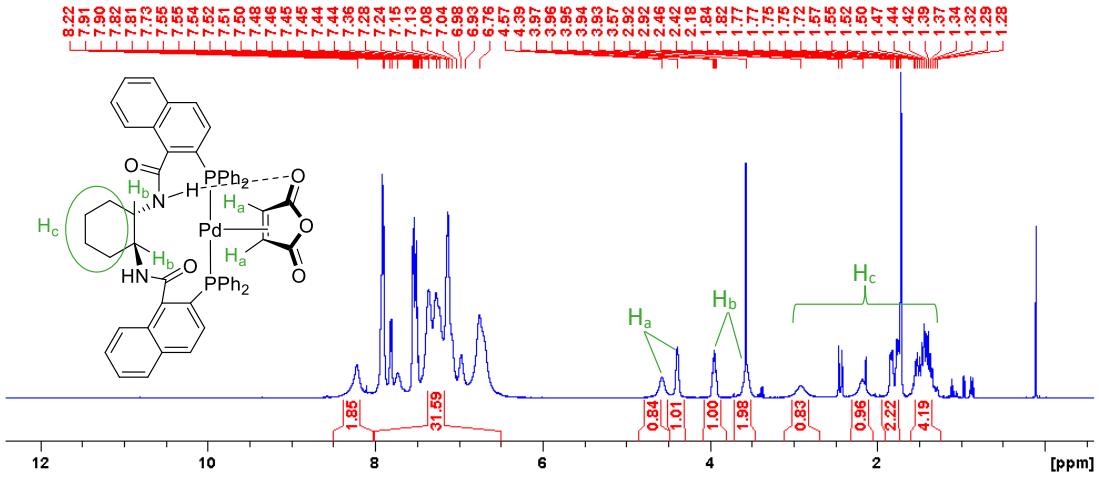

Figure A45. ^{1}H NMR spectrum (500 MHz, THF-*d*$_8$) of **3.2**. Key proton signals are assigned. Singlets at 1.72 and 3.57 ppm are deuterated THF residual signals. Singlets at 2.42 ppm and 2.46 ppm are HDO and H_2O.

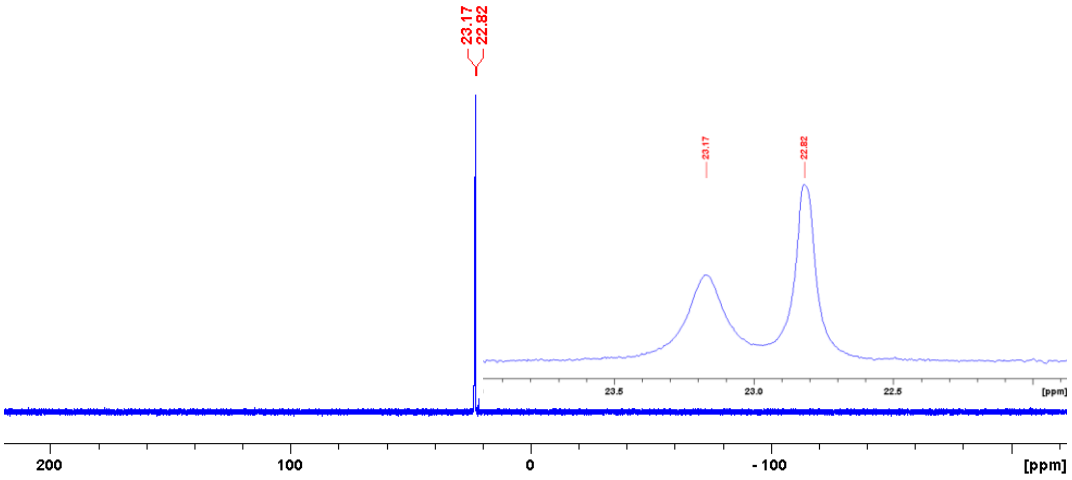

Figure A46. $^{31}P\{^{1}H\}$ NMR spectrum (200 MHz, THF-d_8) of **3.2**.

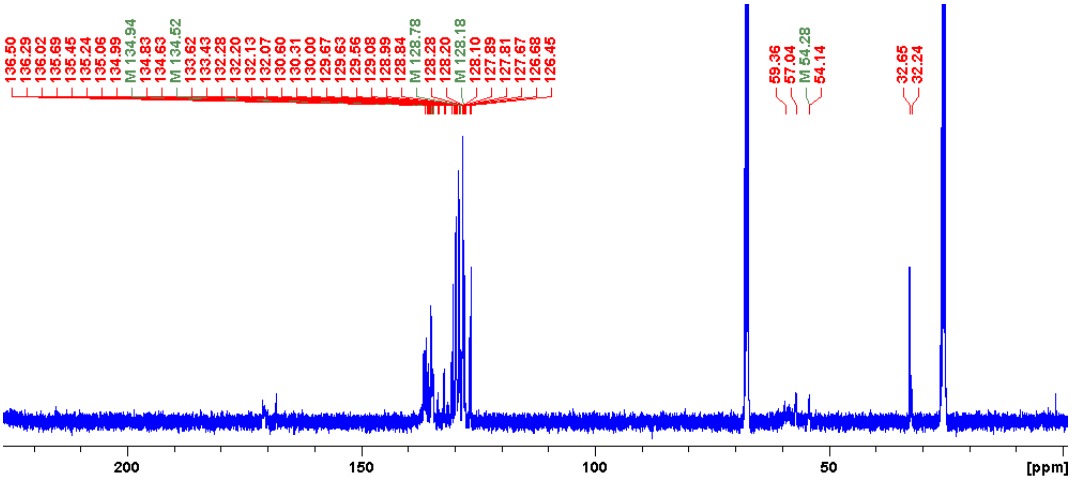

Figure A47. $^{13}C\{^{1}H\}$ NMR spectrum (125 MHz, THF-d_8) of **3.2**.

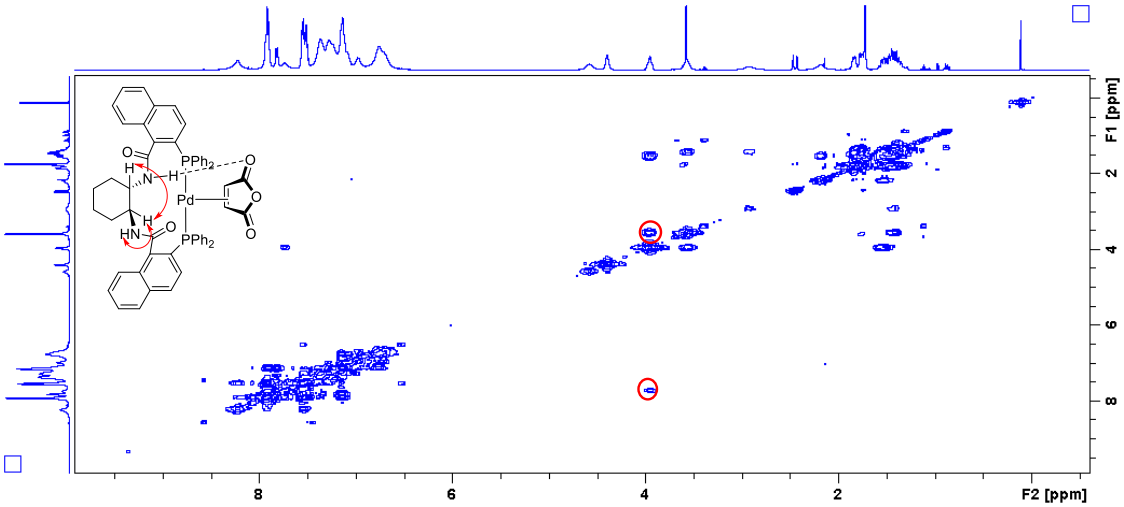

Figure A48. ^{1}H-^{1}H COSY NMR spectrum of **3.2**. Correlation between two CH protons indicates one CH overlaps with the peak of THF. The correlation between CH and NH also indicates that the NH protons are in the aliphatic region.

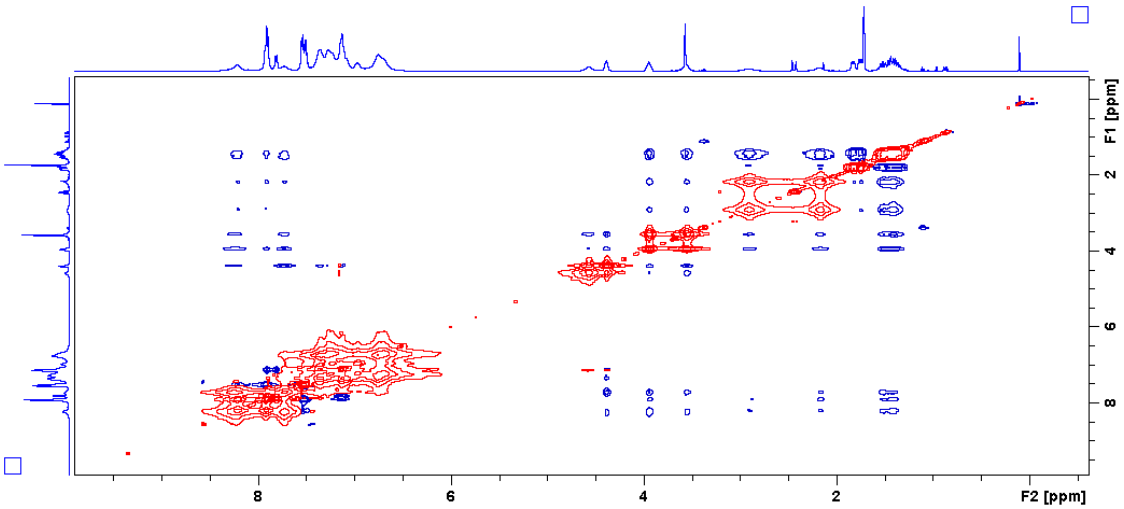

Figure A49. ^{1}H-^{1}H NOESY NMR spectrum of **3.2**. Proton exchanges are observed between the two conformers.

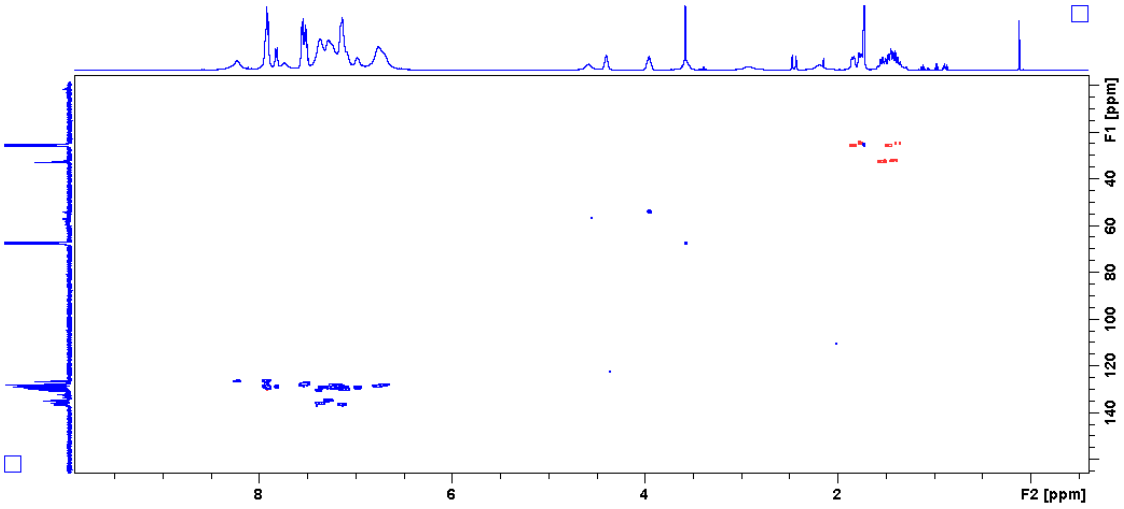

Figure A50. ^{1}H-^{13}C HSQC NMR spectrum of **3.2**.

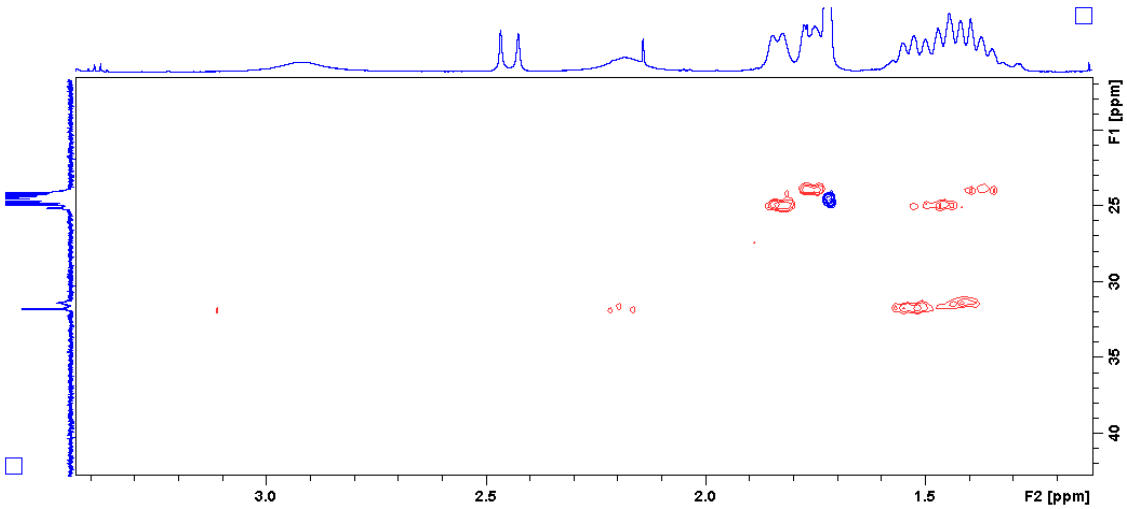

Figure A51. ^{1}H-^{13}C HSQC NMR spectrum of **3.2**. Cyclohexyl region expansion. Two cyclohexyl carbons overlap with the solvent peaks.

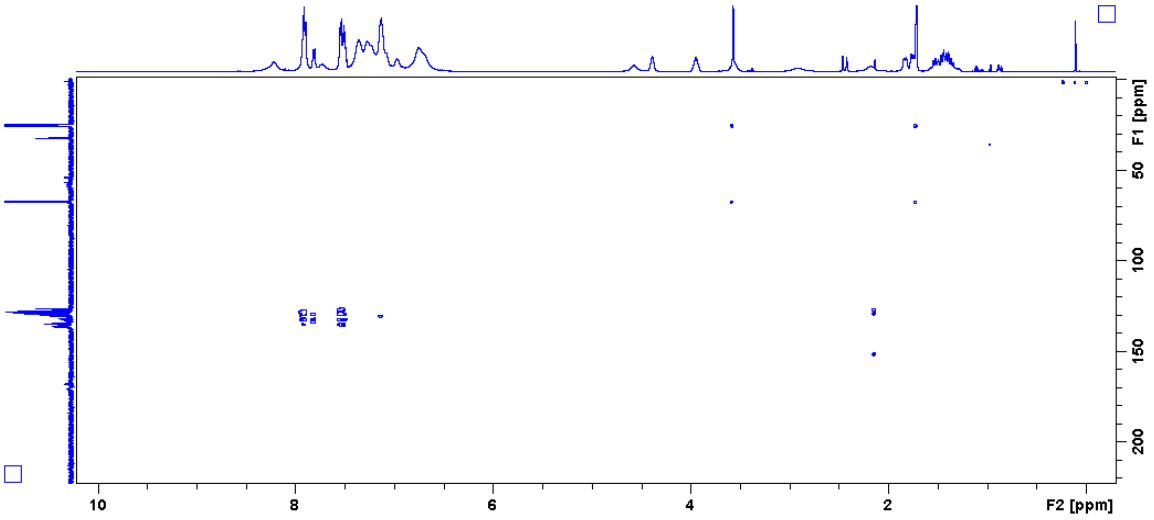

Figure A52. ^{1}H-^{13}C HMBC NMR spectrum of **3.2**.

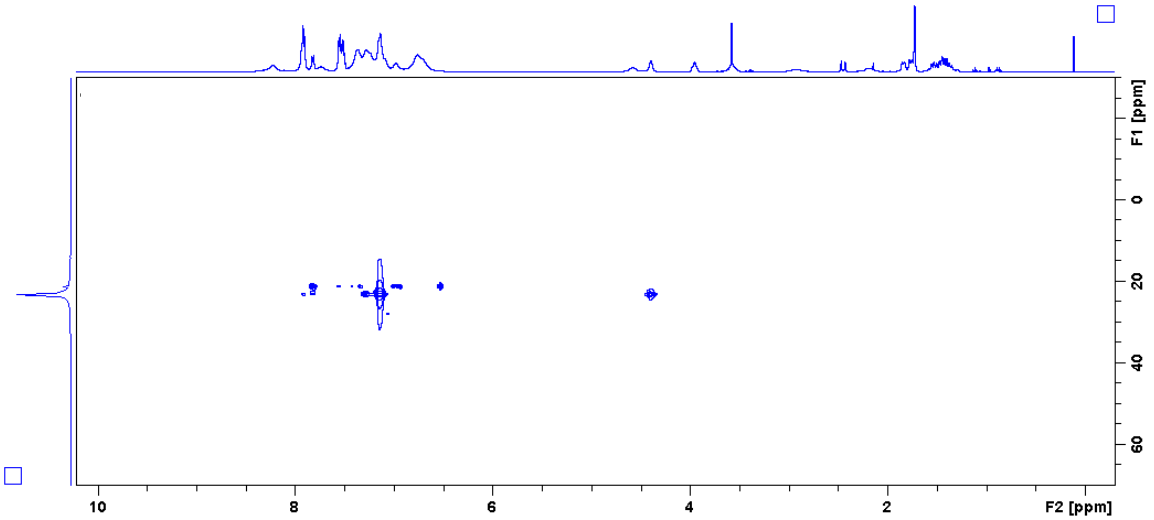

Figure A53. ^{1}H-^{31}P HMBC NMR spectrum of **3.2**.

VT NMR Spectroscopy of 3.2

Procedure: VT NMR experiments were conducted at elevated temperatures: **3.2** (8 mg, 0.0089 mmol) was dissolved in 0.6 mL toluene-d_8. A series of ^{31}P NMR & ^{1}H NMR spectra were obtained at 26 °C, 32 °C, 40 °C, 50 °C, 60 °C.

A second set of VT experiments was performed at low temperatures: **3.2** (10 mg, 0.011 mmol) was dissolved in 0.6 mL toluene-d_8. A series of ^{31}P NMR and ^{1}H NMR spectra were obtained at 25 °C, 20 °C, 10 °C, 0 °C, –10 °C, –20 °C, –30 °C, –40 °C, –50 °C, –60 °C, –70 °C, –80 °C

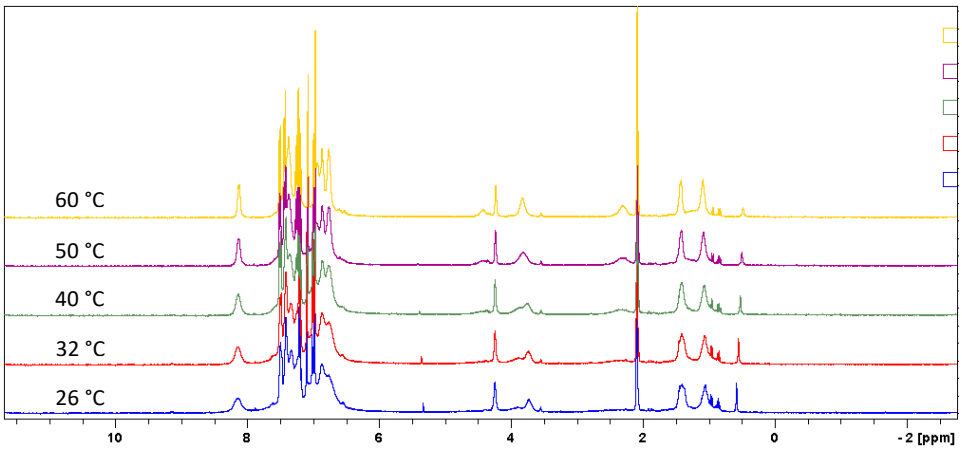

Figure A54. ^{1}H NMR spectra (360 MHz, toluene-d_8) at high temperatures of **3.2**. Temperatures of the spectra increase from the bottom, 26 °C, to the top, 60 °C.

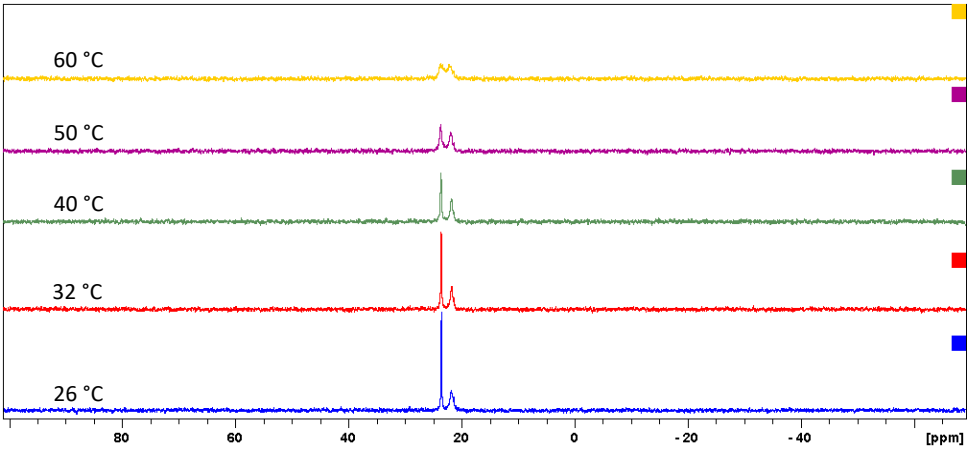

Figure A55. ^{31}P{^{1}H} NMR spectra (145 MHz, toluene-d_8) at high temperatures of **3.2**. Temperatures of the spectra increase from the bottom, 26 °C, to the top, 60 °C.

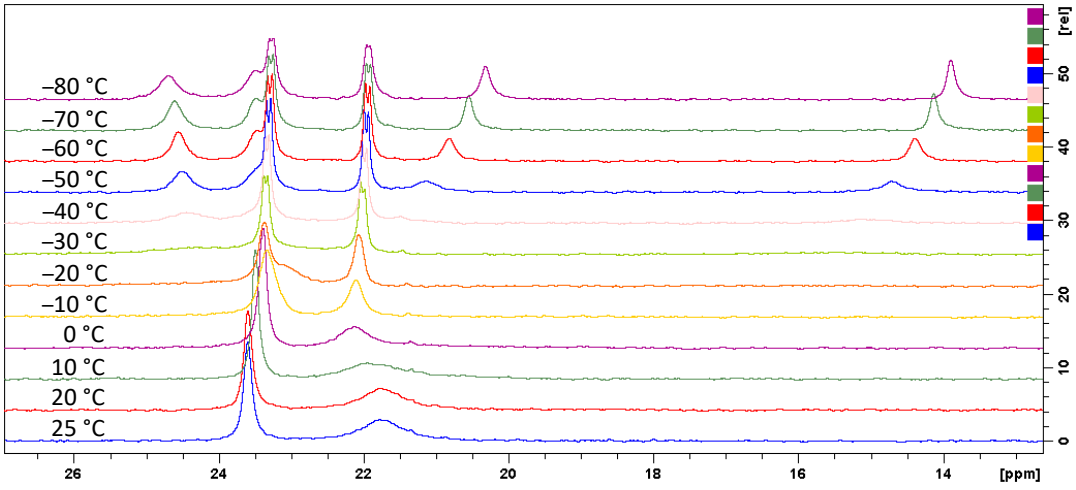

Figure A56. ^{31}P{^{1}H} NMR spectra (145 MHz, toluene-d_8) at high temperatures of **3.2**. Expansion of product peaks. Temperatures of the spectra decrease from bottom, 25 °C, to top, –80 °C. No signal detected beyond this range.

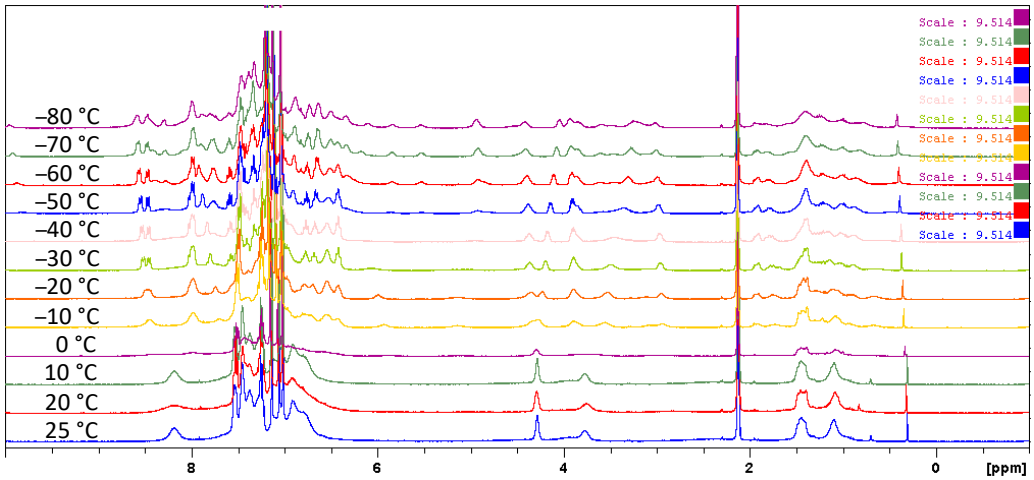

Figure A57. ^{1}H NMR spectra (360 MHz, toluene-d_8) at high temperatures of **3.2**. Temperatures of the spectra decrease from bottom, 25 °C, to top, –80 °C.

(*S*,*S*)-^{Ph}STIL (L3)

^{1}H NMR (300 MHz, $CDCl_3$) δ 7.49-7.53 (m, 2H), 6.92-7.21 (m, 32H), 6.76-6.80 (m, 6H), 5.24 (dd, 2H).

^{31}P NMR (121 MHz, $CDCl_3$) δ –10.15.

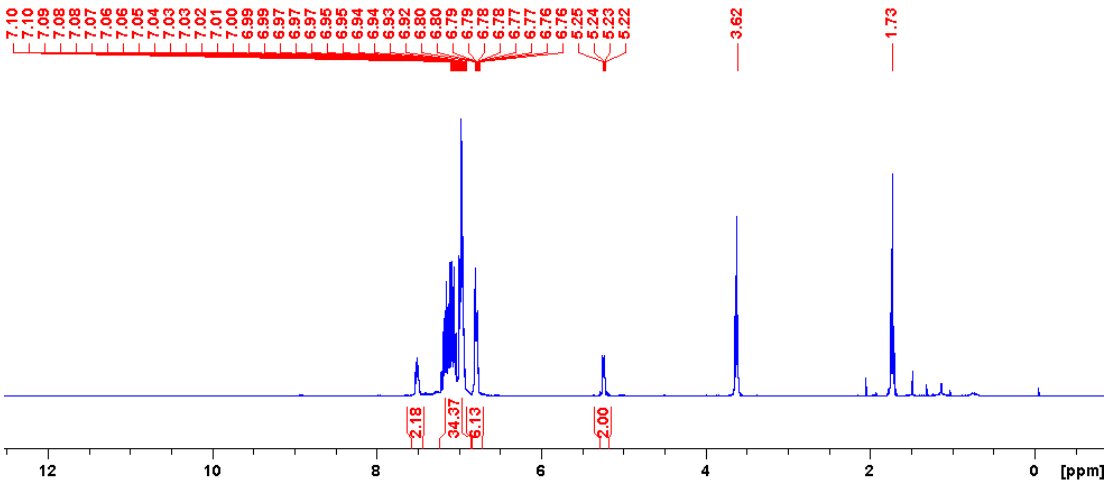

Figure A58. ^{1}H NMR spectrum (300 MHz, $CDCl_3$) of (*S*,*S*)-^{Ph}STIL (**L3**). Multiplets at 1.73 and 3.62 are regular THF residues.

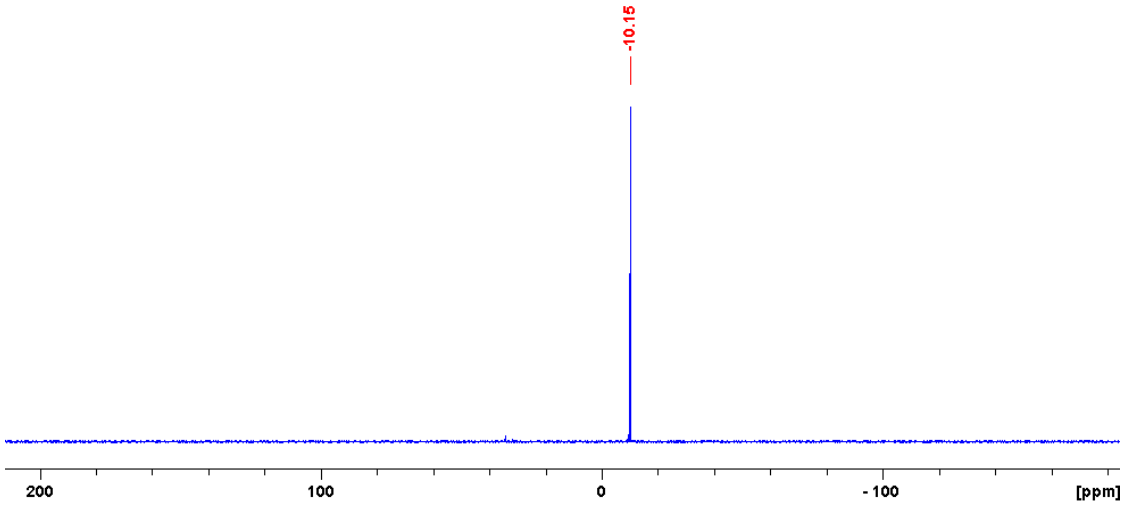

Figure A59. $^{31}P\{^{1}H\}$ NMR spectrum (121 MHz, $CDCl_3$) of (*S*,*S*)-^{Ph}STIL (**L3**).

(*S*,*S*)-^{Ph}STIL–Pd–MAH (3.3)

^{1}H NMR (500 MHz, THF-*d*$_8$) δ *Minor conformer:* 8.16 (d, 1H), 6.71-7.66 (m, 38H), 5.55 (m, 1H), 5.11 (m, 1H), 4.52 (m, 1H), 4.08 (m, 1H). *Major conformer:* 8.66 (d, 1H), 8.06 (d, 1H), 6.71-7.66 (m, 38H), 5.28 (m, 1H), 5.13 (m, 1H), 4.60 (m, 1H), 4.27 (m, 1H).

^{13}C NMR (125 MHz, THF-*d*$_8$) δ 170.8 (d, $^{3}J_{C\text{-}P}$ = 2.7 Hz), 170.2 (d, $^{3}J_{C\text{-}P}$ = 3.5 Hz), 169.1 (d, $^{3}J_{C\text{-}P}$ = 4.4 Hz), 167.8 (d, $^{3}J_{C\text{-}P}$ = 3.5 Hz), 143.3, 143.1, 141.5, 141.2, 139.2, 139.1, 139.0, 137.8, 137.7, 137.6, 137.4, 137.3, 136.2, 136.1, 136.0, 135.8$_3$, 135.8$_0$, 135.6, 135.5, 135.3, 135.2, 135.1$_4$, 135.0$_8$, 135.0$_4$, 135.0$_1$, 134.9, 134.8$_3$, 134.7$_9$, 134.6, 134.4, 134.2, 134.0, 133.9, 133.8, 133.7, 133.6, 133.5, 133.2, 133.1, 132.6, 130.8 (d, *J* = 1.8 Hz), 129.7$_2$, 129.6$_8$, 129.6, 129.5$_3$, 129.4$_6$, 129.4, 129.3 (d, *J* = 2.7 Hz), 129.2$_2$, 129.1$_7$, 128.9$_1$, 128.8$_7$, 128.7$_4$, 128.6$_9$, 128.5$_2$, 128.5$_0$, 128.3, 128.2, 128.1$_3$, 128.0$_9$, 128.0$_0$, 127.9$_7$, 127.9, 127.7, 127.6, 127.5$_1$, 127.4$_8$, 127.4$_4$, 127.3$_9$, 127.3, 127.1, 127.0, 126.9, 126.8, 126.4, 62.0, 61.1, 59.9, 59.5, 57.7 (dd, $^{2}J_{C\text{-}P1}$ = 4.4 Hz, $^{2}J_{C\text{-}P2}$ = 24.7 Hz), 57.2 (dd, $^{2}J_{C\text{-}P1}$ = 3.5 Hz, $^{2}J_{C\text{-}P2}$ = 24.7 Hz), 57.1 (dd, $^{2}J_{C\text{-}P1}$ = 3.5 Hz, $^{2}J_{C\text{-}P2}$ = 24.7 Hz), 54.6 (dd, $^{2}J_{C\text{-}P}$ = 26.4 Hz, the other coupling constant could not be determined due to low signal-to-noise ratio), 53.8 (dd, $^{2}J_{C\text{-}P}$ = 24.7 Hz, C=C, another coupling constant was not able to be determined due to low signal-to-noise ratio).

^{31}P NMR (200 MHz, THF-*d*$_8$) δ 26.7 (d, $^{2}J_{P\text{-}P}$ = 9.9 Hz, *minor conformer*), 24.6 (d, $^{2}J_{P\text{-}P}$ = 5.4 Hz, *major conformer*), 24.0 (d, $^{2}J_{P\text{-}P}$ = 5.3 Hz, *major conformer*), 23.3 (d, $^{2}J_{P\text{-}P}$ = 10.1 Hz, *minor conformer*).

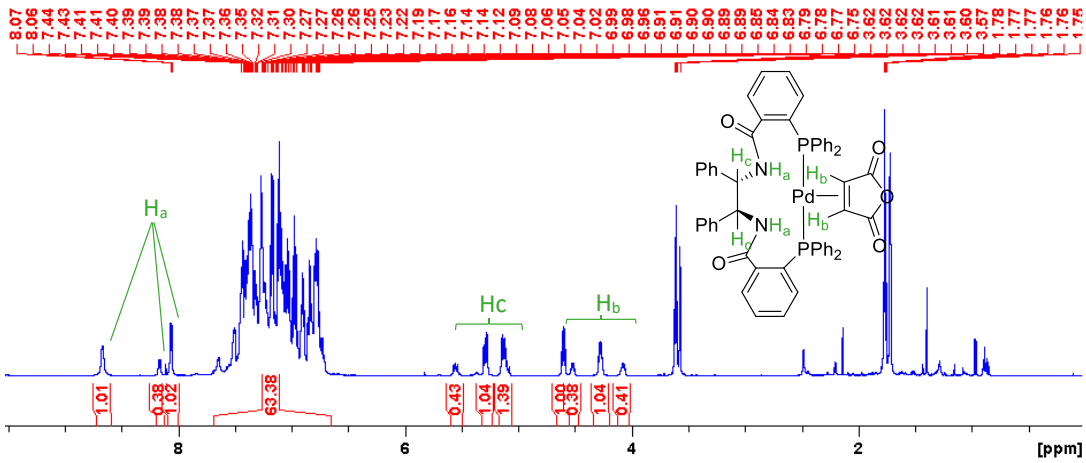

Figure A60. ^{1}H NMR spectrum (500 MHz, THF-d_8) of **3.3**. Key proton signals are assigned. Singlets at 1.72 and 3.57 ppm are deuterated THF residual signals. Multiplets at 1.77 and 3.61 ppm are protio THF. Singlet at 2.48 ppm is water. Multiplets at 0.89 and 1.28 ppm are hexanes.

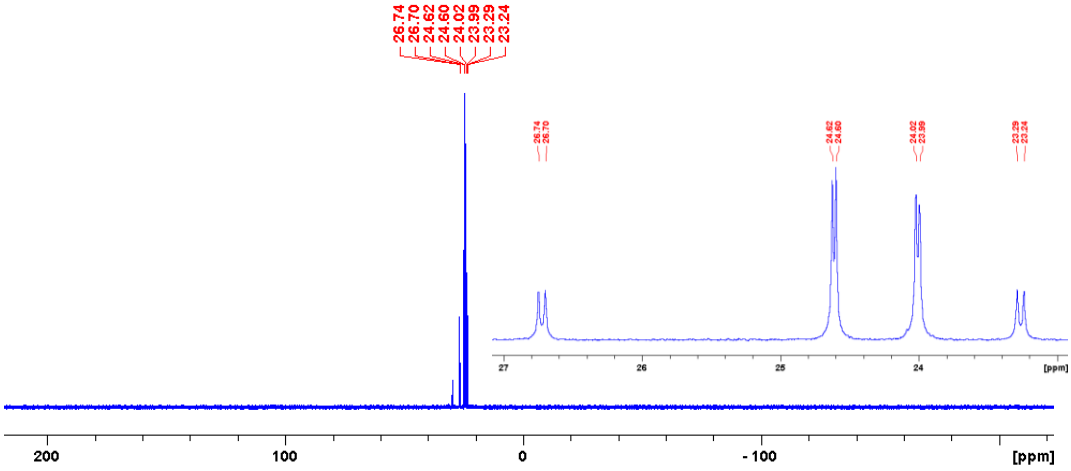

Figure A61. ^{31}P{^{1}H} NMR spectrum (200 MHz, THF-d_8) of **3.3**.

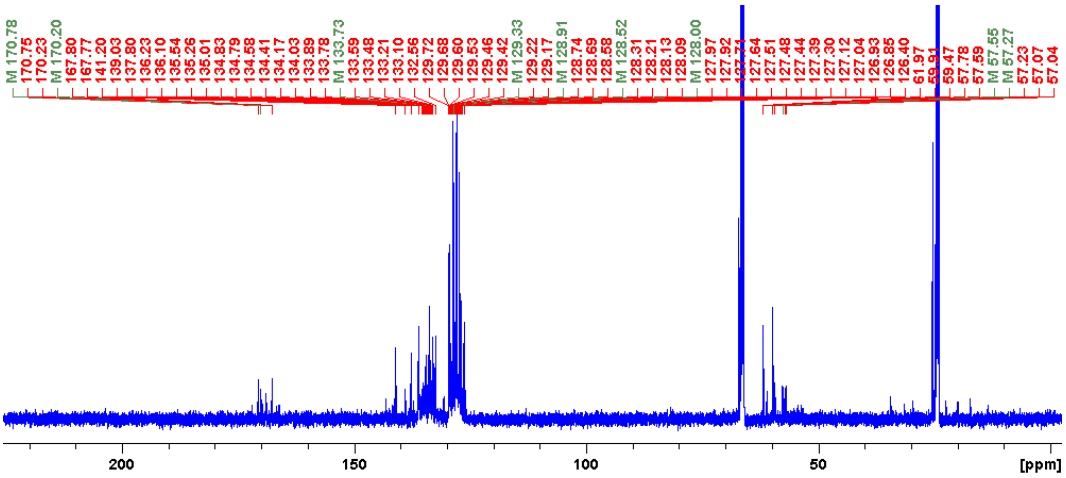

Figure A62. ^{13}C{^{1}H} NMR spectrum (125 MHz, THF-d_8) of **3.3** (Green labels are manually-picked peaks in multiplets).

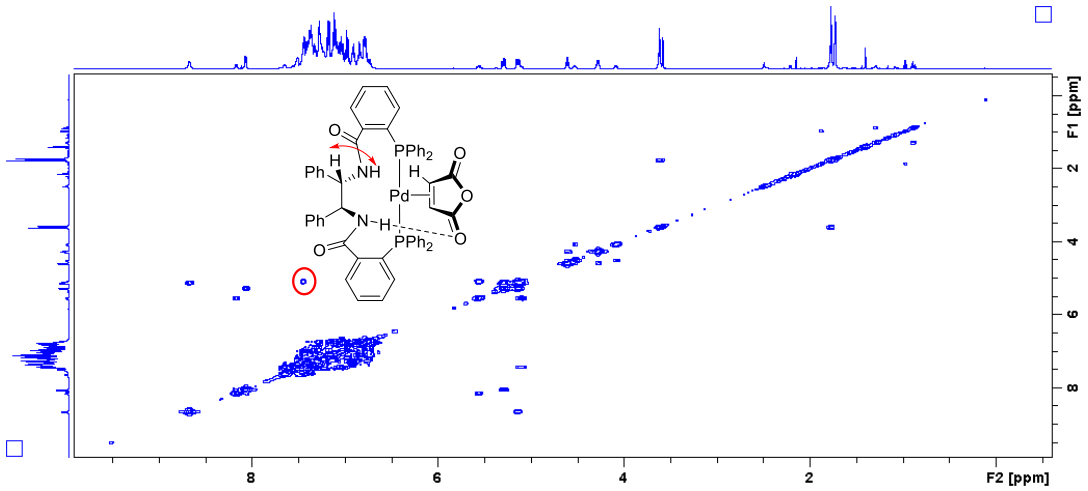

Figure A63. ^{1}H-^{1}H COSY NMR spectrum of **3.3**. One NH of the minor conformer (at 7.44 ppm) hides in the aliphatic region, indicated by the correlation between NH and CH.

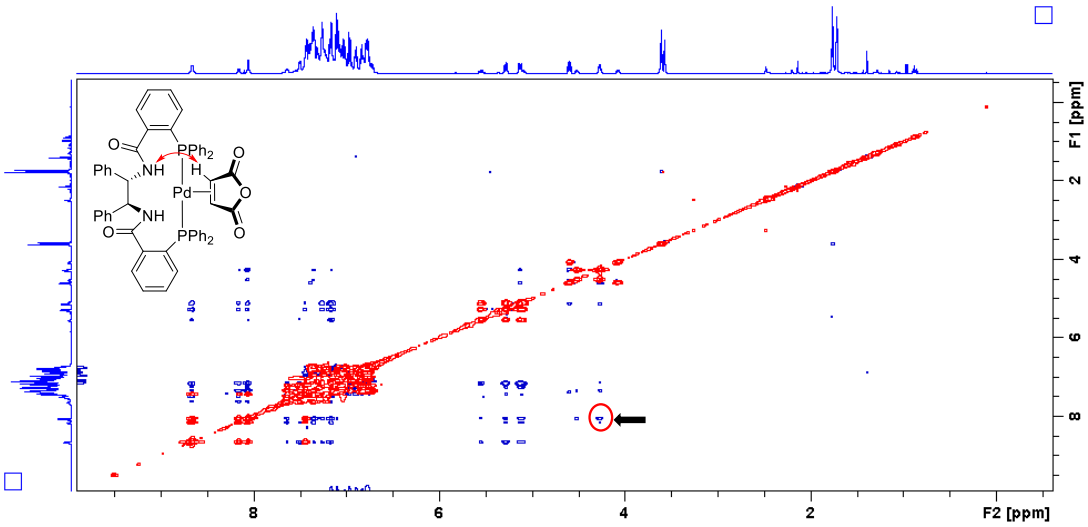

Figure A64. ^{1}H-^{1}H NOESY NMR spectrum of **3.3**. The correlation between NH and MAH-H of the major conformer indicates the conformational structure without hydrogen bonding.

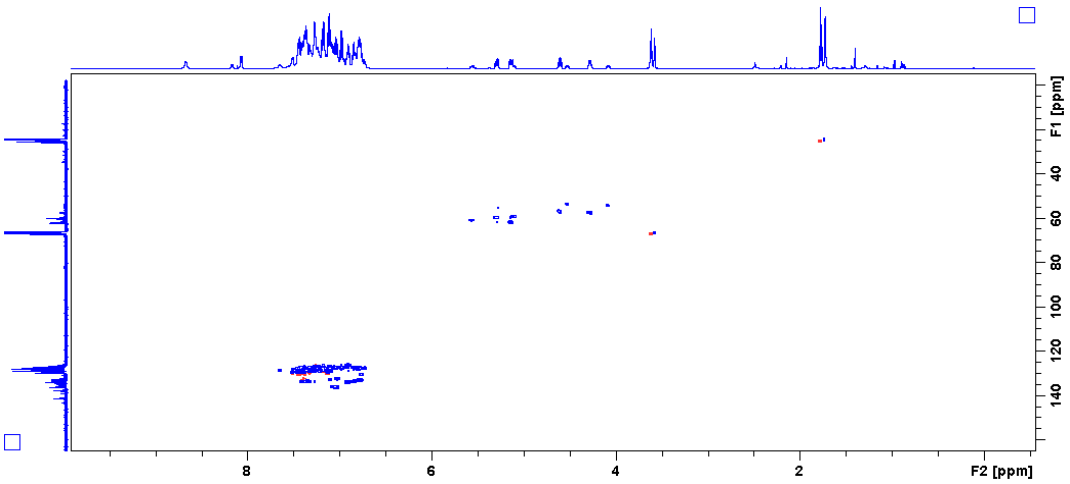

Figure A65. ^{1}H-^{13}C HSQC NMR spectrum of **3.3**.

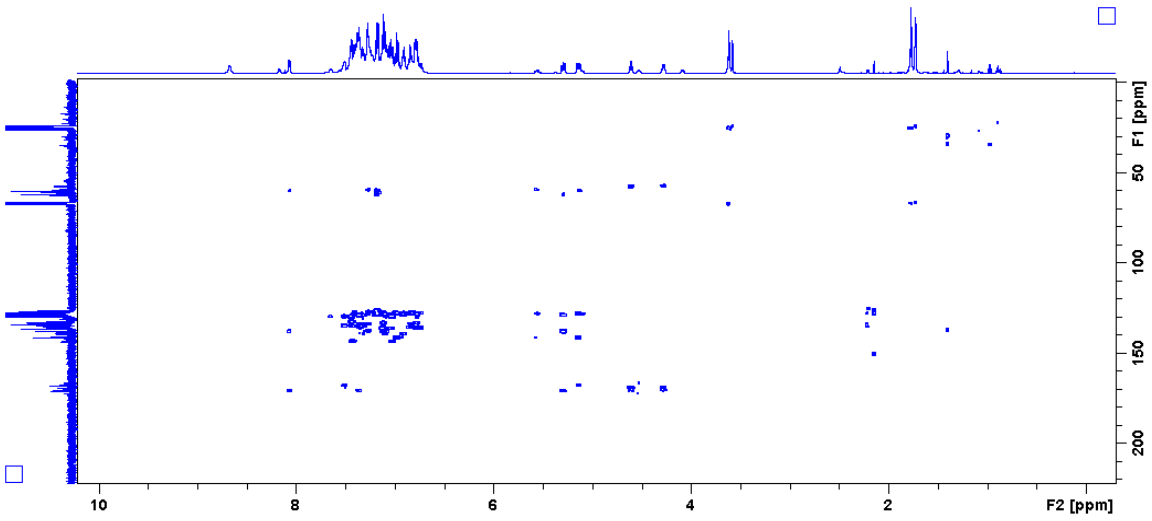

Figure A66. ^{1}H-^{13}C HMBC NMR spectrum of **3.3**.

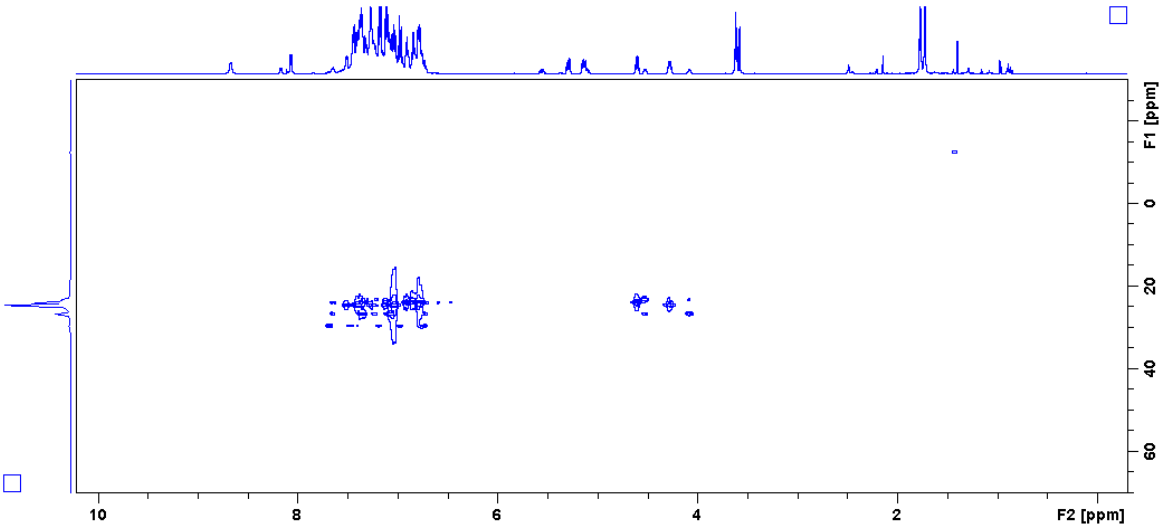

Figure A67. ^{1}H-^{31}P HMBC NMR spectrum of **3.3**.

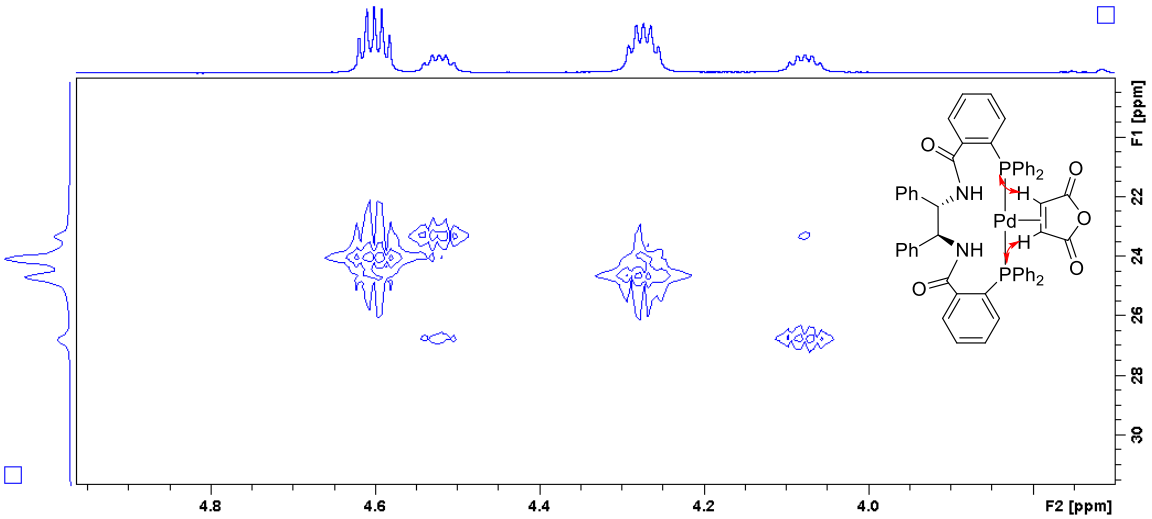

Figure A68. ^{1}H-^{31}P HMBC NMR spectrum expansion of **3.3**. The correlation between P and MAH-H.

(*S*,*S*)-^{Ph}ANDEN–Pd–MAH (3.4)

^{1}H NMR (500 MHz, THF-d_8) δ 7.80 (dd, J = 7.6 Hz, J = 2.5 Hz, 1H), 7.57 (dd, J = 7.4 Hz, J = 1.9 Hz, 1H), 7.48-6.70 (m, 36H), 4.48 (m, 1H), 4.28 (dd, 2H), 3.80 (m, 1H), 3.70 (m, 1H), 3.04 (m, 1H).

^{13}C NMR (125 MHz, THF-d_8) δ 170.3 (d, $^{3}J_{C\text{-}P}$ = 3.5 Hz), 169.0, 168.3 (d, $^{3}J_{C\text{-}P}$ = 3.5 Hz), 143.0, 142.7, 140.0, 138.4, 136.7, 136.6, 136.5, 136.3$_3$, 136.3$_1$ (d, J = 3.5 Hz), 135.7, 135.6, 134.4, 133.2, 133.1, 133.0, 132.2, 132.1, 129.7 (d, J = 5.3 Hz), 129.6, 129.1 (d, J = 3.51 Hz), 128.5, 128.3$_1$, 128.2$_5$, 128.2, 127.0 (d, J = 3.5 Hz), 127.9 (d, J = 3.5 Hz), 127.8, 127.5, 127.4, 127.3, 127.2, 127.1, 126.4, 126.0, 125.9, 125.8, 125.7, 125.6, 124.0, 123.3, 60.0, 60.0, 57.0, 56.7, 56.6, 50.0, 48.4.

^{31}P NMR (200 MHz, THF-d_8) δ 27.6 (m).

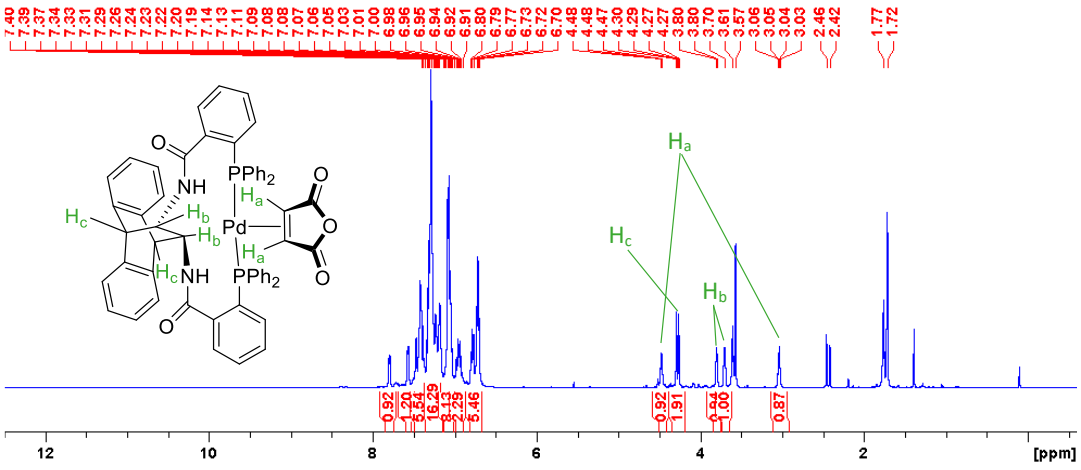

Figure A69. ^{1}H NMR spectrum (500 MHz, THF-d_8) of **3.4**. Multiplets at 1.77 and 3.61 ppm are regular THF. Singlets at 2.46 ppm and 2.42 ppm are H_2O and HDO.

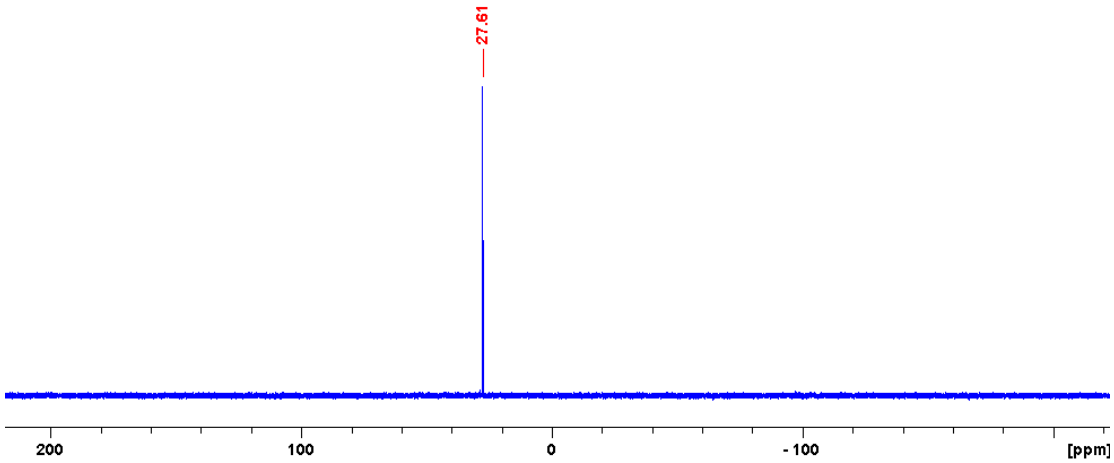

Figure A70. ^{31}P{^{1}H} NMR spectrum (200 MHz, THF-d_8) of **3.4**.

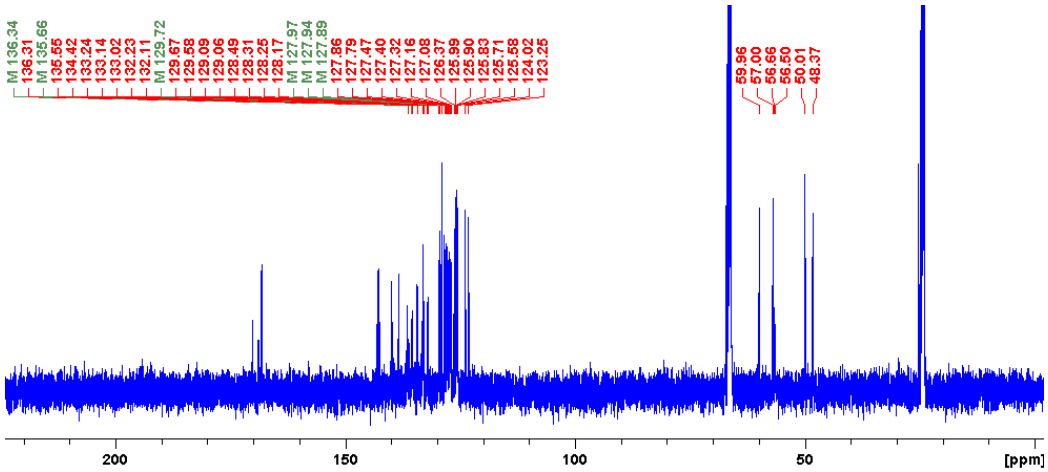

Figure A71. $^{13}C\{^{1}H\}$ NMR spectrum (125 MHz, THF-d_8) of **3.4** (Green labels are the manually-picked peaks in multiplets).

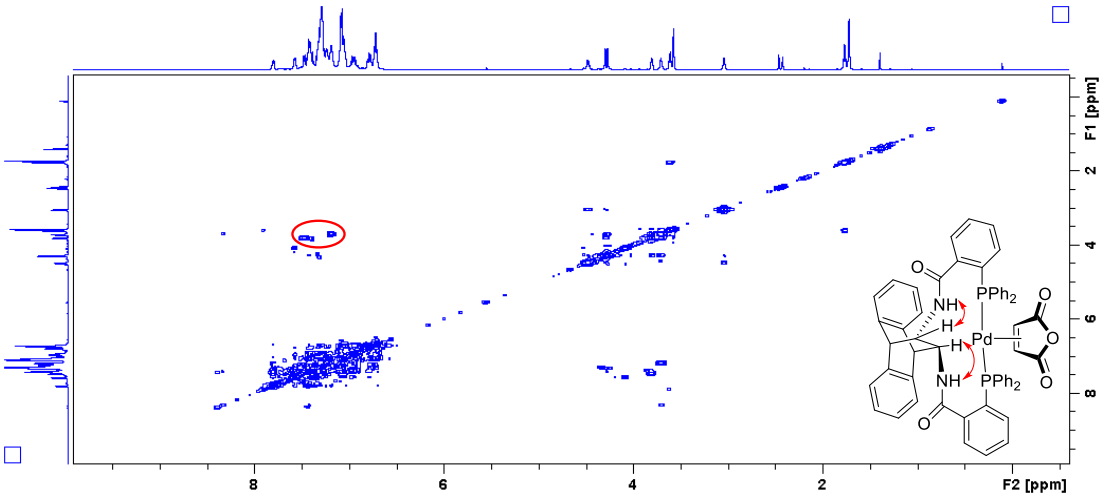

Figure A72. ^{1}H-^{1}H COSY NMR spectrum of **3.4**. Determination of two NH protons (at 7.19 ppm and 7.47 ppm) according to the correlations between CH and NH.

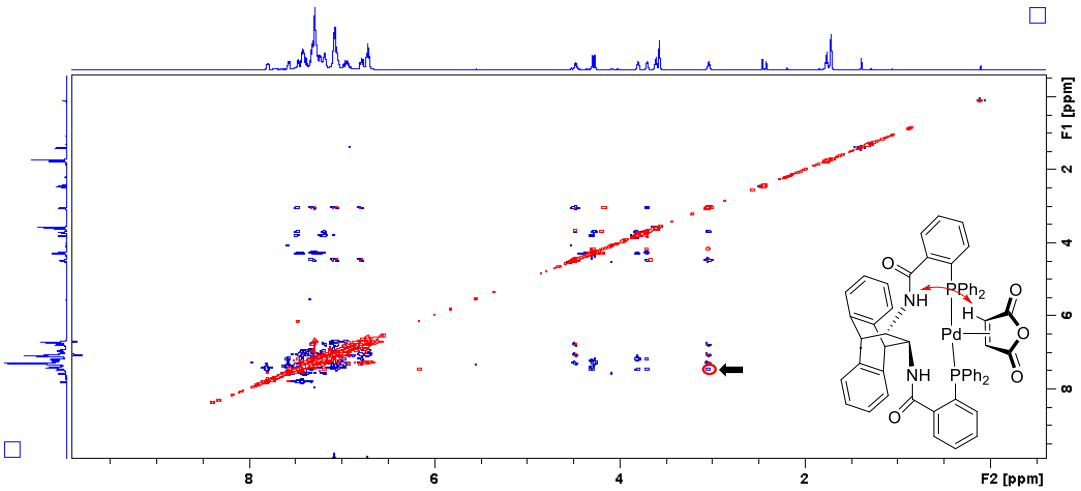

Figure A73. ^{1}H-^{1}H NOESY NMR spectrum of **3.4**. The correlation between one NH and one MAH–H indicates it is the conformer without hydrogen bonding.

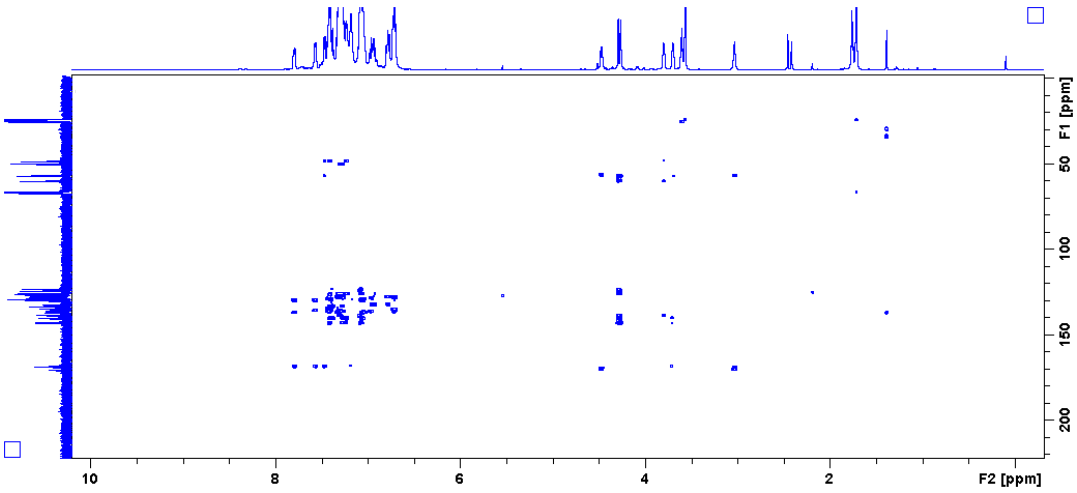

Figure A74. ^{1}H-^{13}C HMBC NMR spectrum of **3.4**.

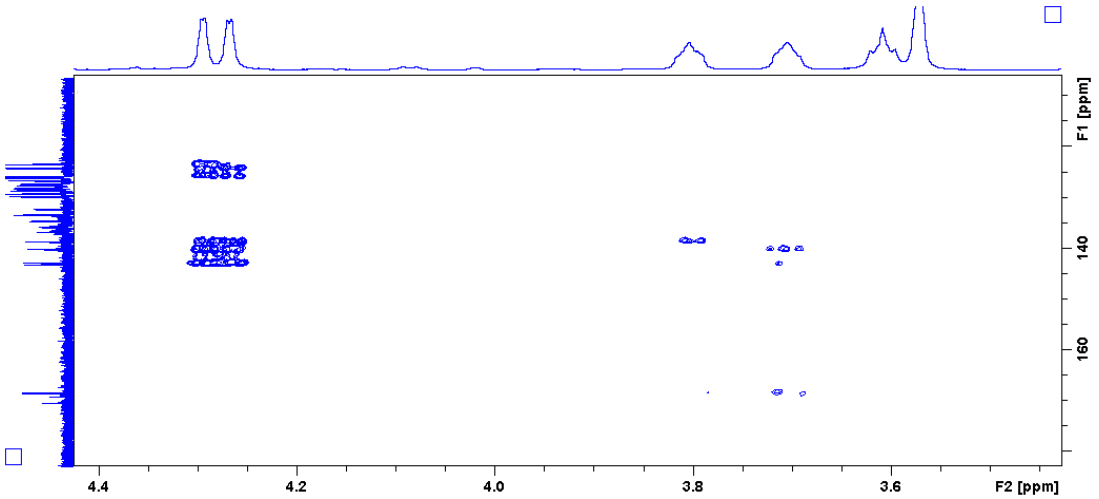

Figure A75. ^{1}H-^{13}C HMBC NMR spectrum expansion of **3.4**. Differentiation of 4 × CH (C**H**–NH has weaker correlations with Ar–H but stronger correlations with C=O than the other two CH).

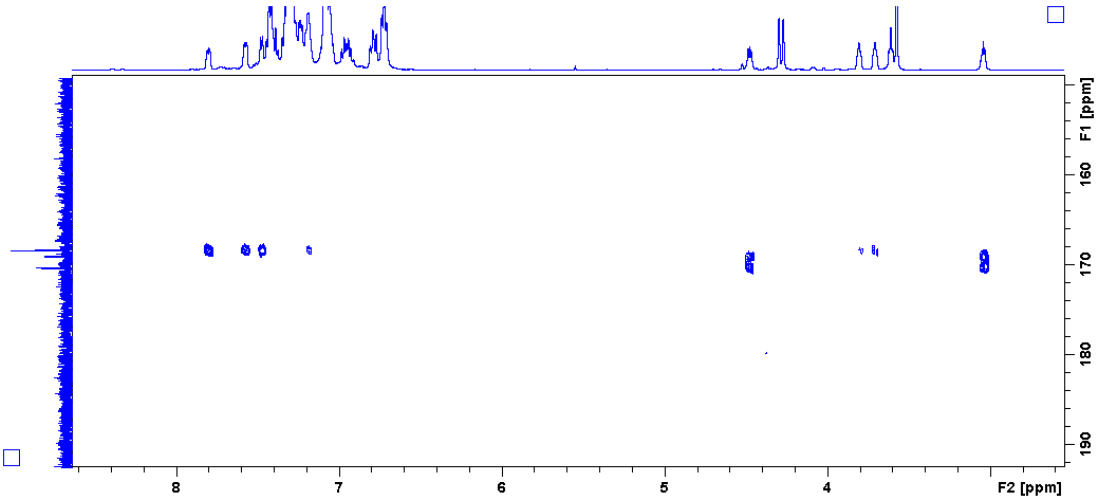

Figure A76. ^{1}H-^{13}C HMBC NMR spectrum expansion of **3.4**. Differentiation between NH–CO and C=O of MAH.

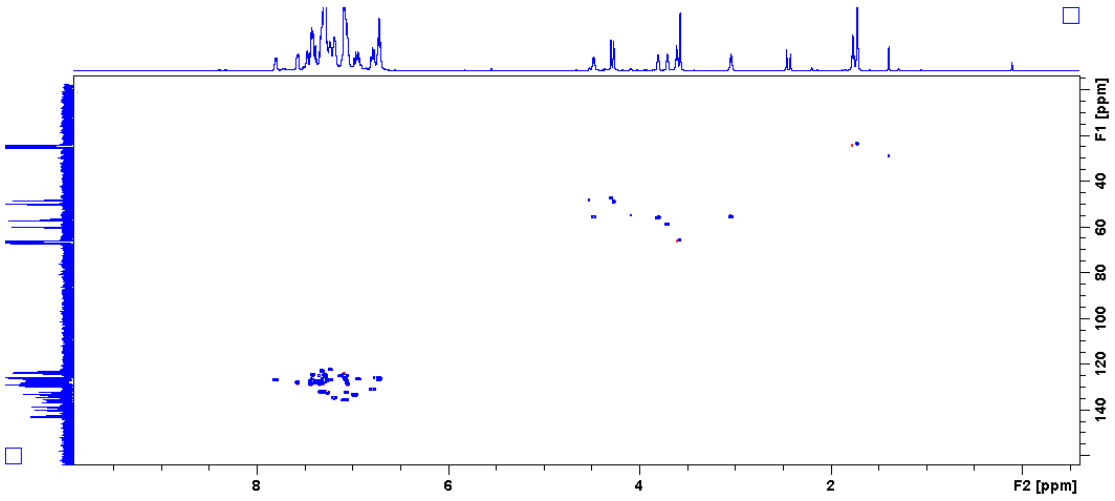

Figure A77. ^{1}H-^{13}C HSQC NMR spectrum of **3.4**.

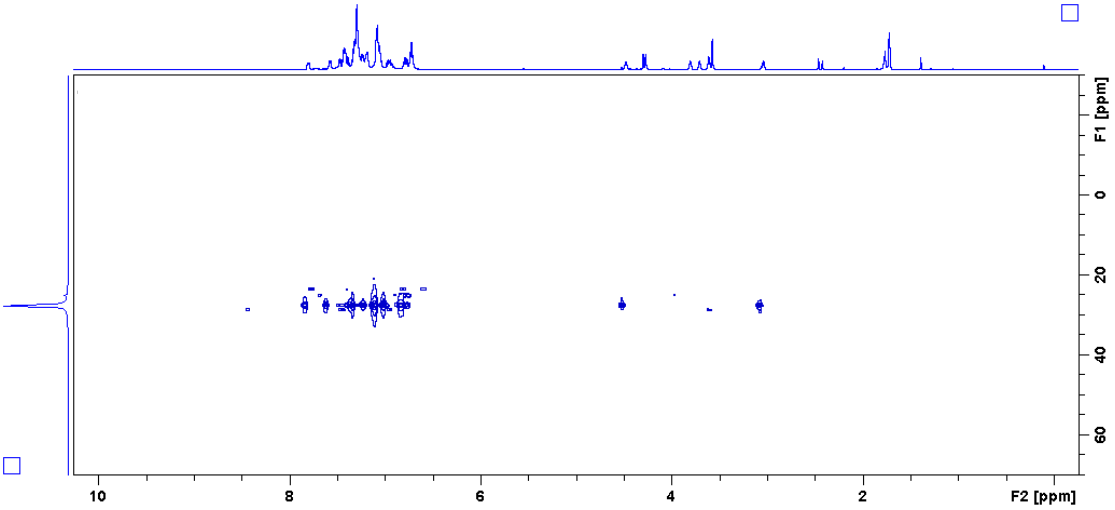

Figure A78. ^{1}H-^{31}P HMBC NMR spectrum of **3.4**.

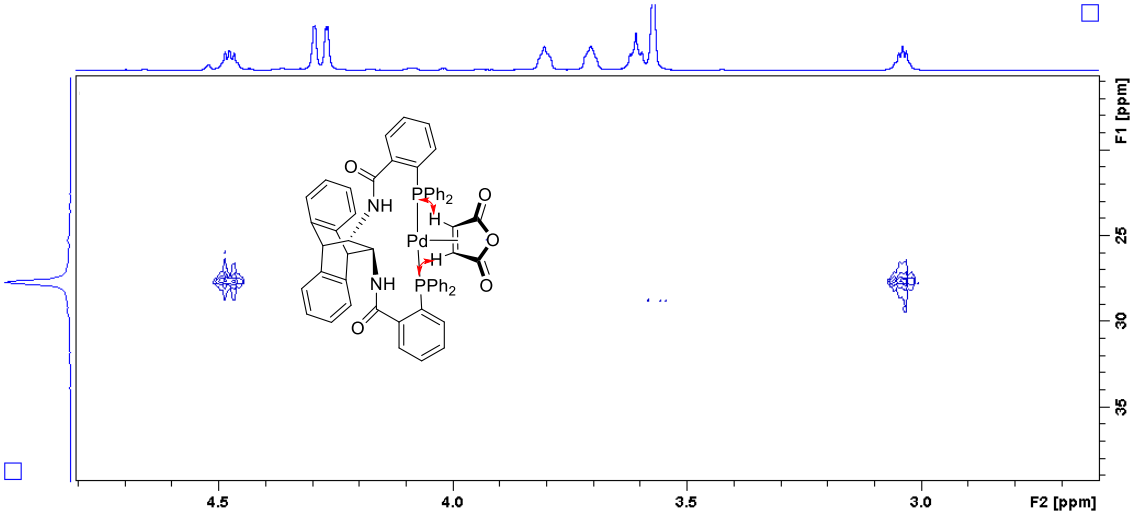

Figure A79. ^{1}H-^{31}P HMBC NMR spectrum expansion of **3.4**. Identification of MAH–H.

(*S*)-$^{t\text{Bu}}$PHOX (L5)

^{1}H NMR (300 MHz, CD_2Cl_2) δ 7.90 (m, 1H), 7.38-7.17 (m, 12H), 6.90 (m, 1H), 4.13 (dd, 1H), 4.02 (t, 1H), 3.85 (dd, 1H), 0.76 (s, 9H).

^{31}P NMR (121 MHz, CD_2Cl_2) δ –7.03

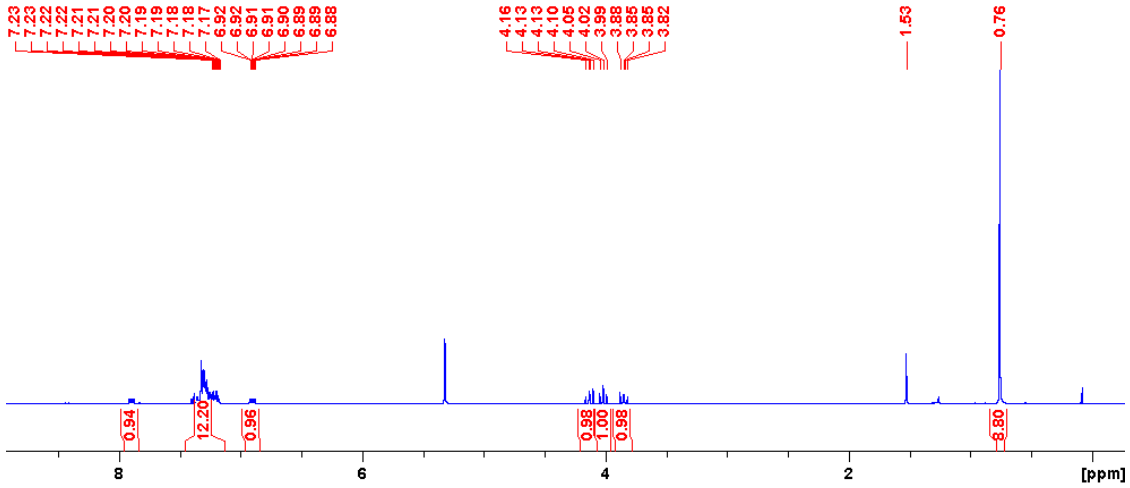

Figure A80. ^{1}H NMR spectrum (300 MHz, CD_2Cl_2) of (*S*)-$^{t\text{Bu}}$PHOX (**L5**).

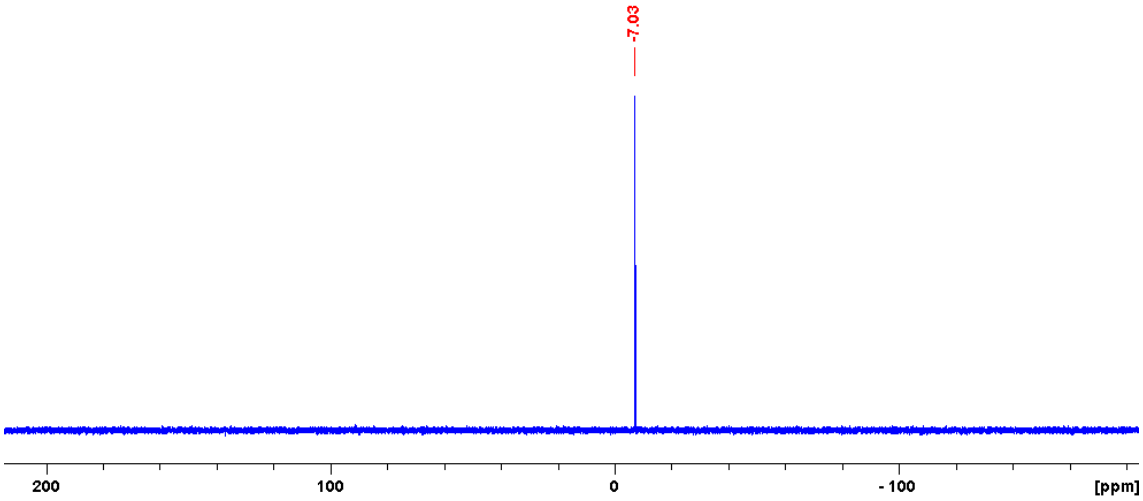

Figure A81. ^{31}P{^{1}H} NMR spectrum (121 MHz, CD_2Cl_2) of (*S*)-$^{t\text{Bu}}$PHOX (**L5**).

(*S*)-$^{t\text{Bu}}$PHOX–Pd–MAH (3.5)

^{1}H NMR (500 MHz, CD_2Cl_2): *Minor conformer* **δ** 8.18-8.15 (m, 1H), 7.56-7.17 (m, 12H), 6.98-6.92 (m, 1H), 4.44-4.36 (m, 2H), 4.17-4.12 (m, 1H), 4.07 (dd, *J* = 9.3, 4.3 Hz, 1H), 3.78-3.81 (m, 1H), 0.62 (s, 9H). *Major conformer* **δ** 8.18-8.15 (m, 1H), 7.56-7.17 (m, 12H), 6.98-6.92 (m, 1H), 4.44-4.36 (m, 2H), 4.23 (t, 1H), 4.17-4.12 (m, 1H), 3.81-3.78 (m, 1H), 0.66 (s, 9H).

^{13}C NMR (125 MHz, CD_2Cl_2) δ 173.0, 172.9, 171.8 (d, $^{3}J_{C\text{-}P}$ = 5.3 Hz), 171.4 (d, $^{3}J_{C\text{-}P}$ = 5.3 Hz), 164.6, 164.0, 134.6, 134.5, 134.4, 134.3, 134.1, 133.8, 133.7, 133.6, 133.5, 132.7, 132.6$_3$, 132.5$_6$ (d, *J* = 1.8 Hz), 132.4$_8$ (d, *J* = 3.5 Hz), 132.4$_3$, 132.4$_0$, 132,3$_7$, 130.9 (d, *J* = 1.8 Hz), 130.8 (d, *J* = 1.8 Hz), 130.6 (d, *J* = 1.8 Hz), 130.5, 130.4$_9$ (d, *J* = 2.6 Hz), 130.4, 129.1, 129.0 (m), 128.9 (d, *J* = 2.6 Hz), 128.8, 128.7, 80.2 (d, $^{3}J_{C\text{-}P}$ = 1.8 Hz), 79.9 (d, $^{3}J_{C\text{-}P}$ = 1.7 Hz), 68.9, 68.8, 48.5 (d, $^{2}J_{C\text{-}P}$ = 32.6 Hz), 47.2, 46.6$_9$ (d, $^{2}J_{C\text{-}P}$ = 33.5 Hz), 45.7$_3$, 34.4, 25.3, 24.5.

^{31}P NMR (200 MHz, CD_2Cl_2) δ 22.29 (*major conformer*), 23.12 (*minor conformer*).

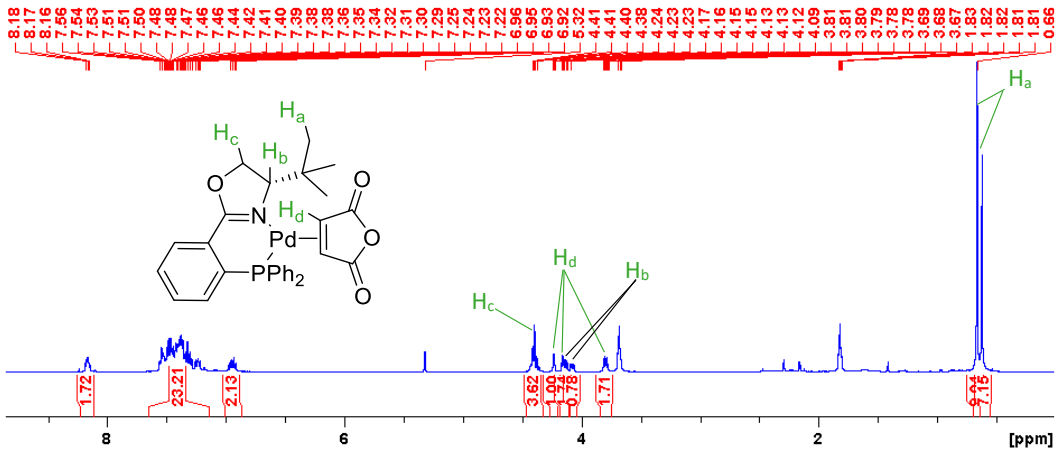

Figure A82. ^{1}H NMR spectrum (500 MHz, CD_2Cl_2) of **3.5**. Two conformers (MAH up and down) are observed, and key proton signals are assigned. Singlet at 5.32 ppm is CD_2Cl_2 residual signal. Multiplets at 1.82 and 3.68 ppm are THF.

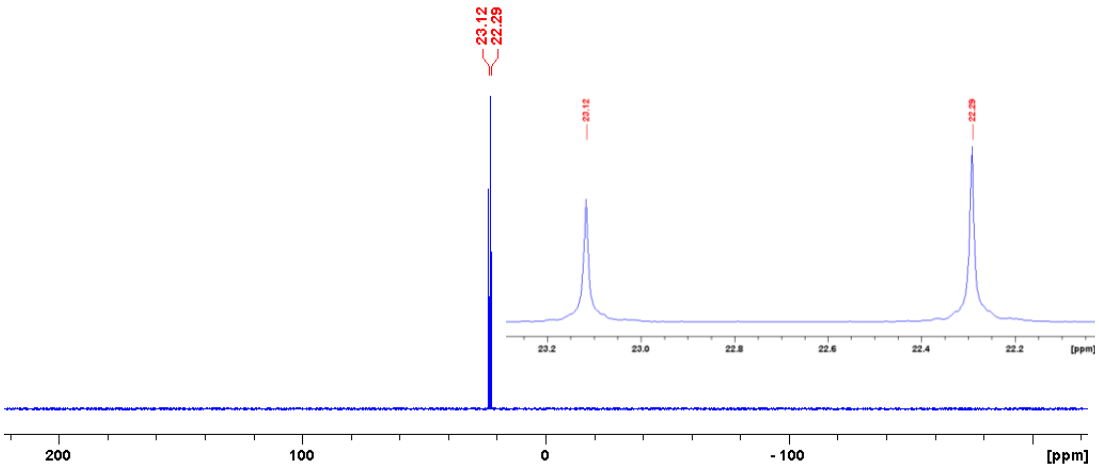

Figure A83. ^{31}P{^{1}H} NMR spectrum (200 MHz, CD_2Cl_2) of **3.5**. Two conformers are observed.

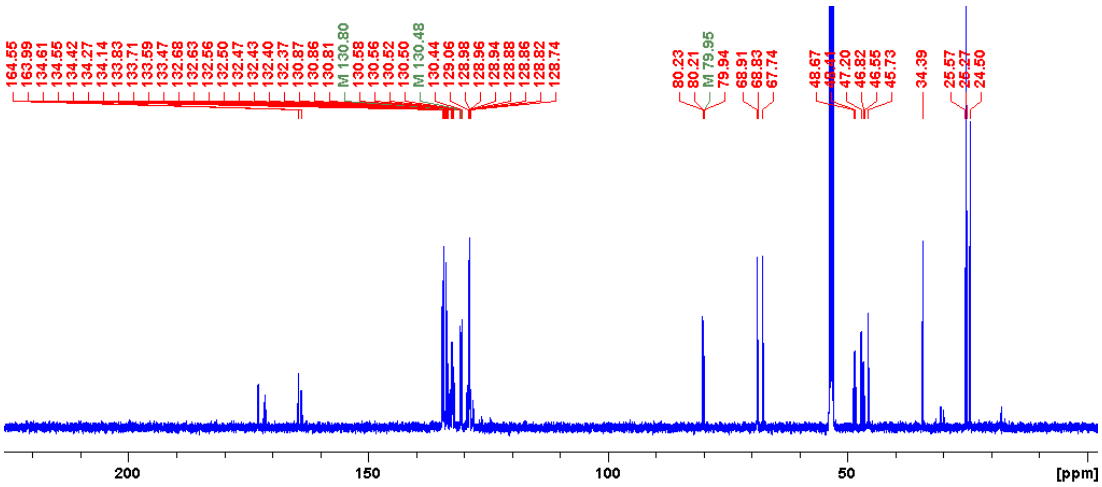

Figure A84. $^{13}C\{^{1}H\}$ NMR spectrum (125 MHz, CD_2Cl_2) of **3.5** (Green labels are the manually-picked peaks).

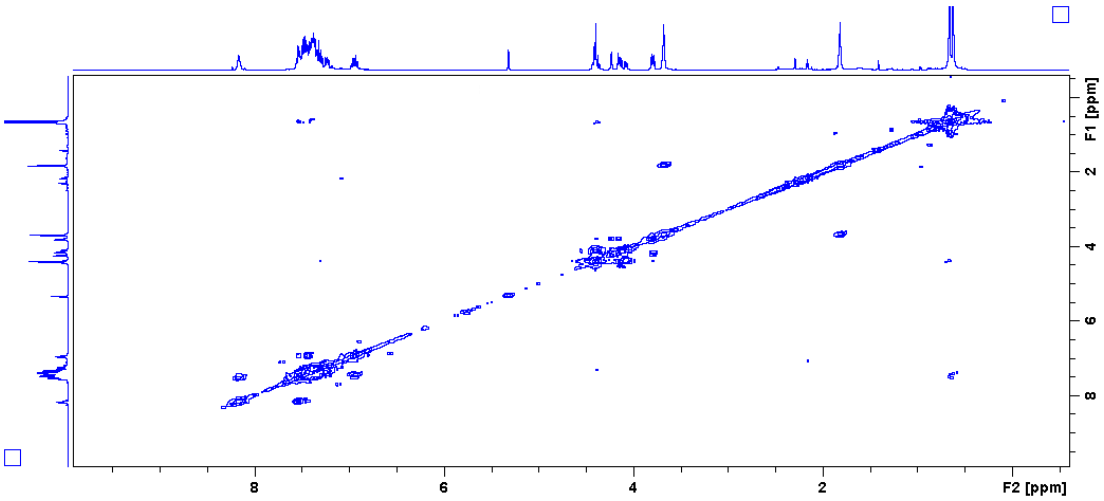

Figure A85. ^{1}H-^{1}H COSY NMR spectrum of **3.5**.

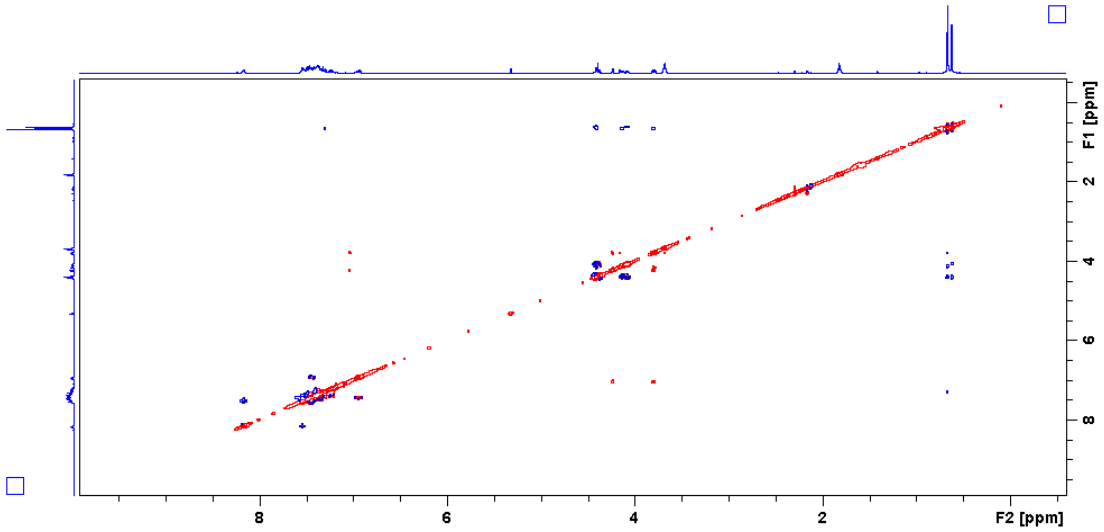

Figure A86. ^{1}H-^{1}H NOESY NMR spectrum of **3.5**.

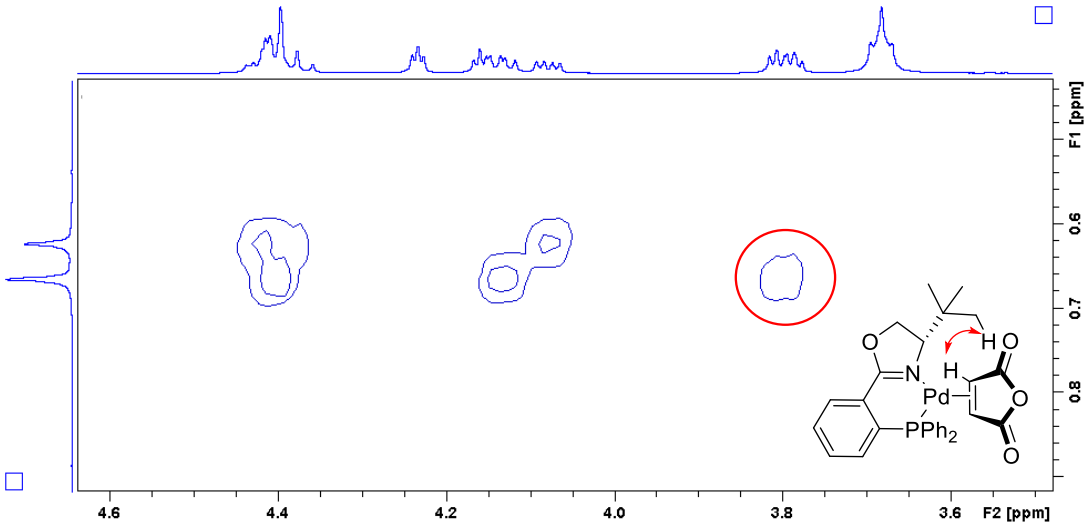

Figure A87. ^{1}H-^{1}H NOESY NMR spectrum of **3.5**. The correlation between MAH–H and CH_3 indicates that the major conformer has MAH and *tert*-butyl group *exo* to one another.

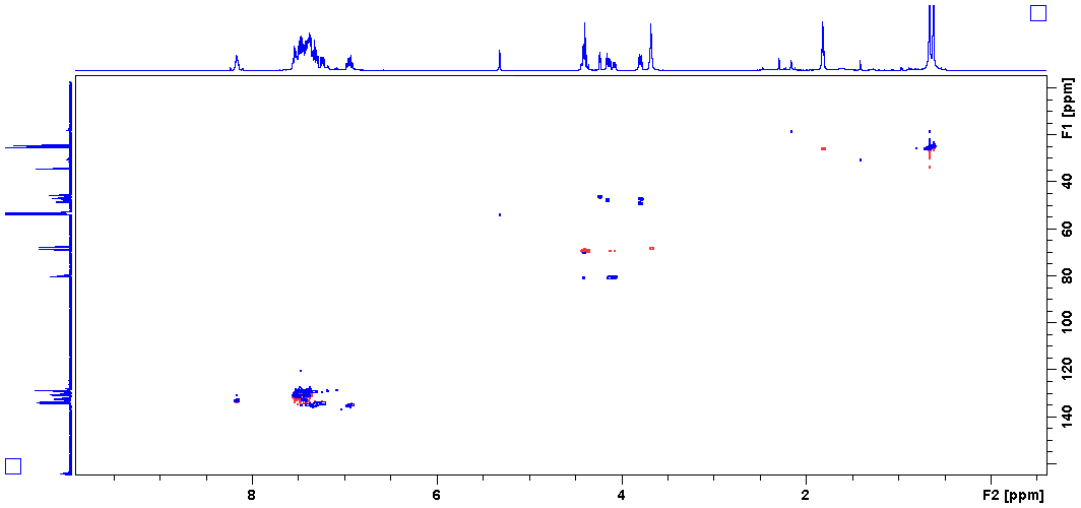

Figure A88. ^{1}H-^{13}C HSQC NMR spectrum of **3.5**.

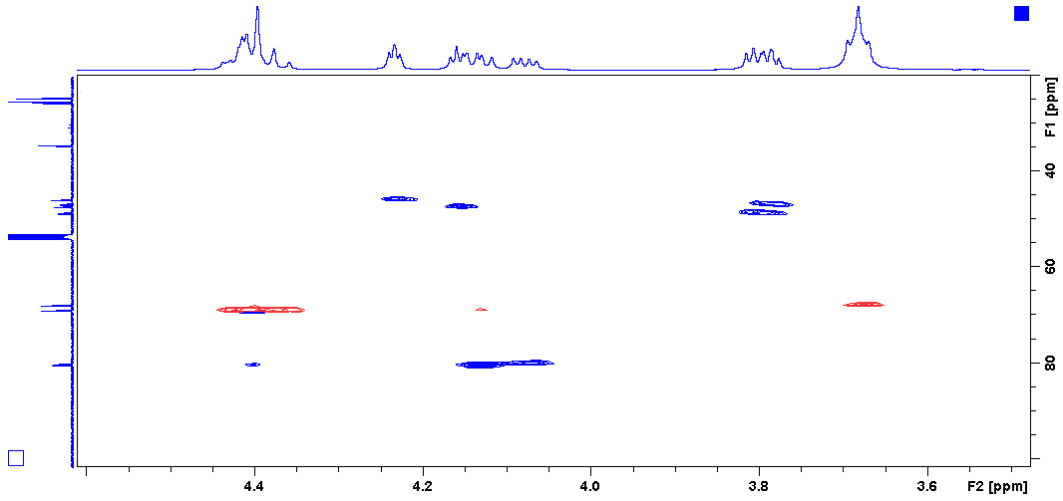

Figure A89. ^{1}H-^{13}C HSQC NMR spectrum expansion of **3.5**. Differentiation of CH_2 and CH.

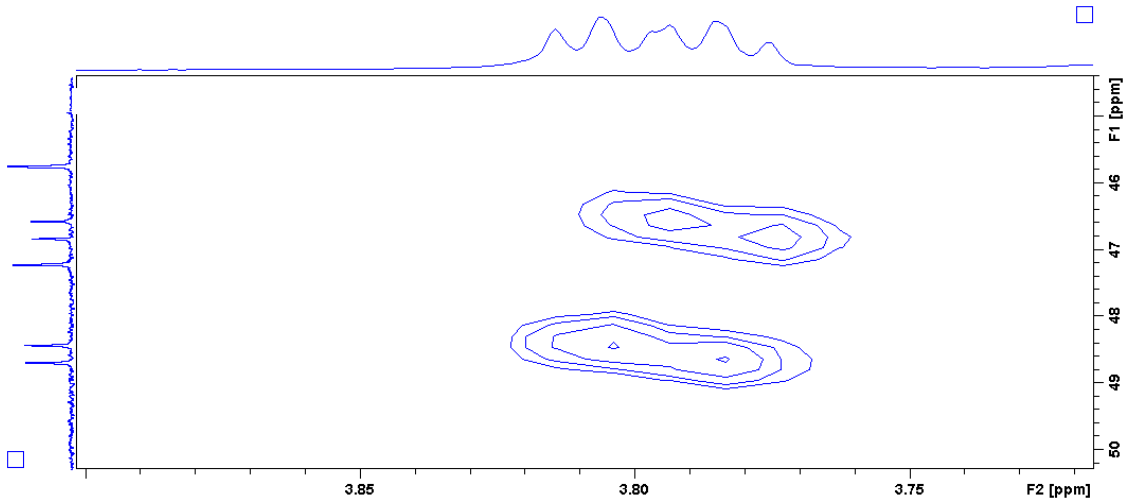

Figure A90. ^{1}H-^{13}C HSQC NMR spectrum expansion of **3.5**. C–H correlations of the two alkene carbons of MAH.

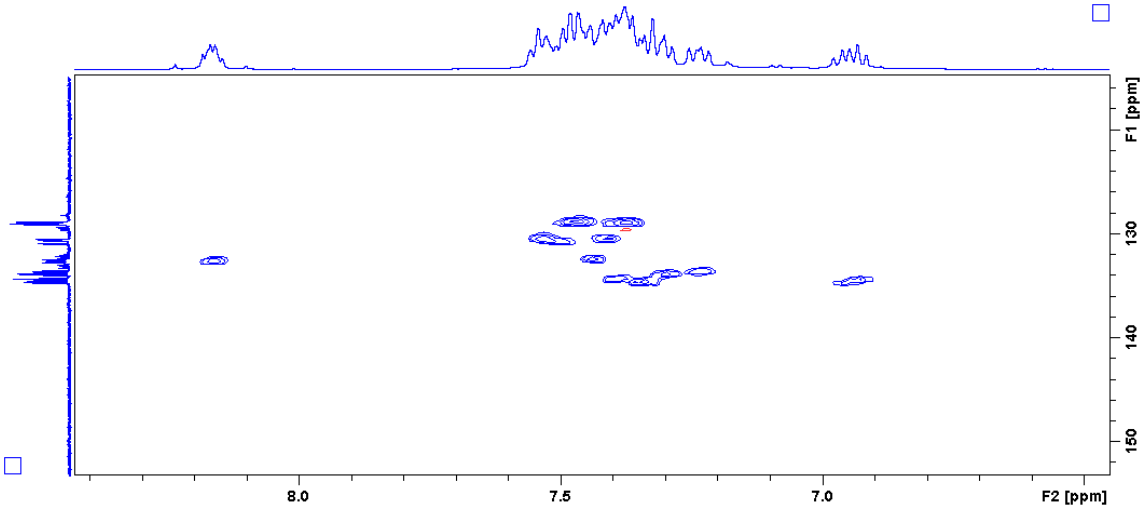

Figure A91. ^{1}H-^{13}C HSQC NMR spectrum of **3.5**. Aliphatic region expansion.

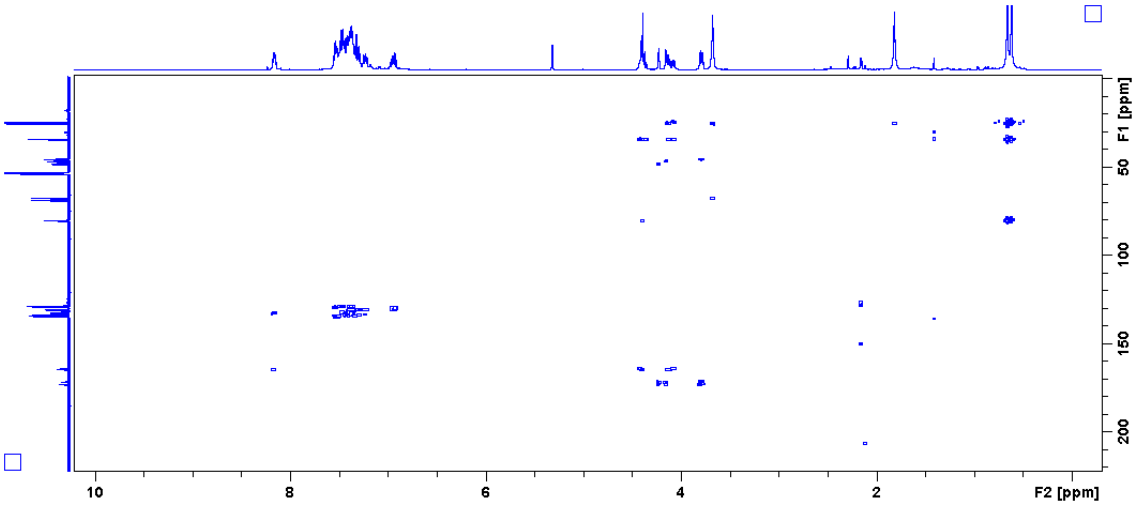

Figure A92. ^{1}H-^{13}C HMBC NMR spectrum of **3.5**.

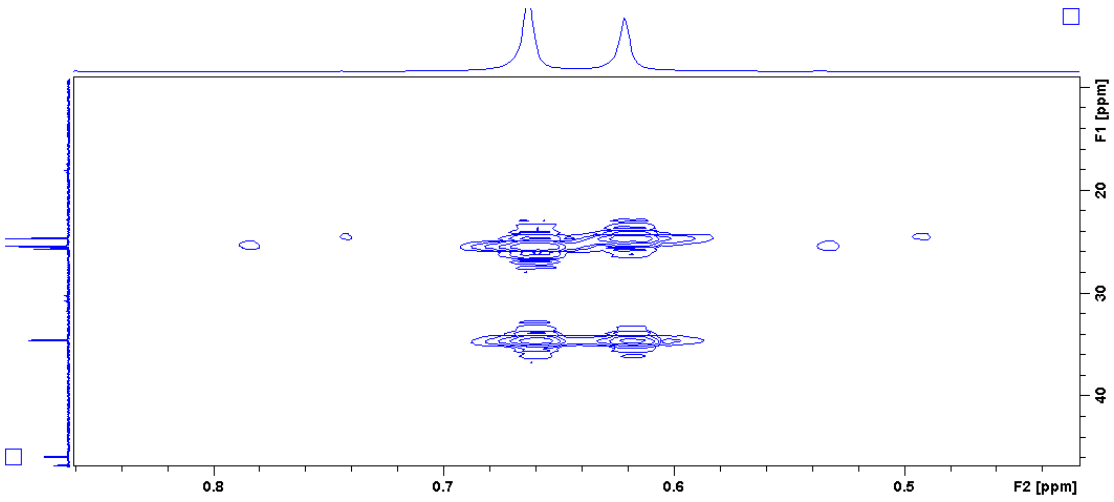

Figure A93. ^{1}H-^{13}C HMBC NMR spectrum expansion of **3.5**. Assignment of $C(CH_3)_3$.

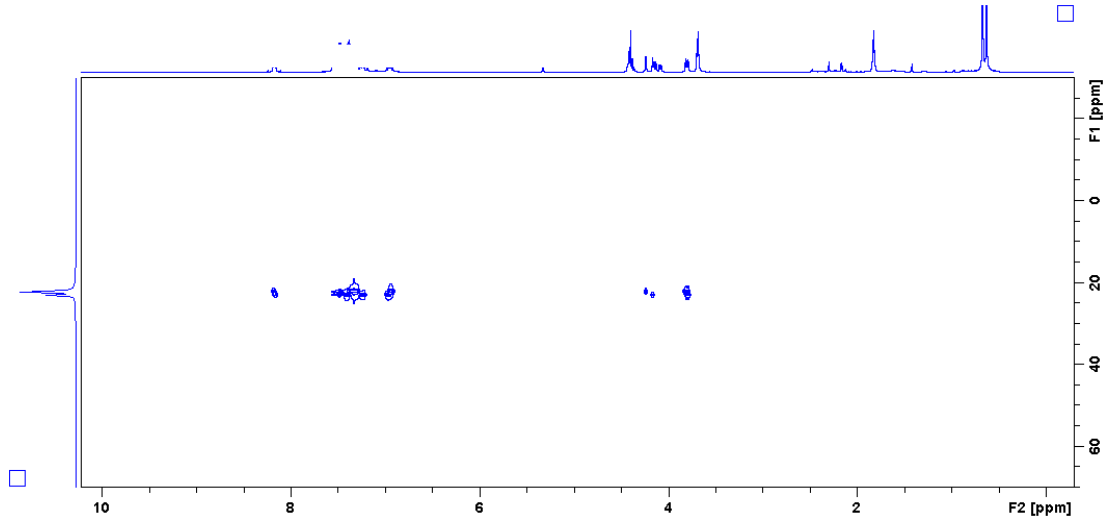

Figure A94. ^{1}H-^{31}P HMBC NMR spectrum expansion of **3.5**.

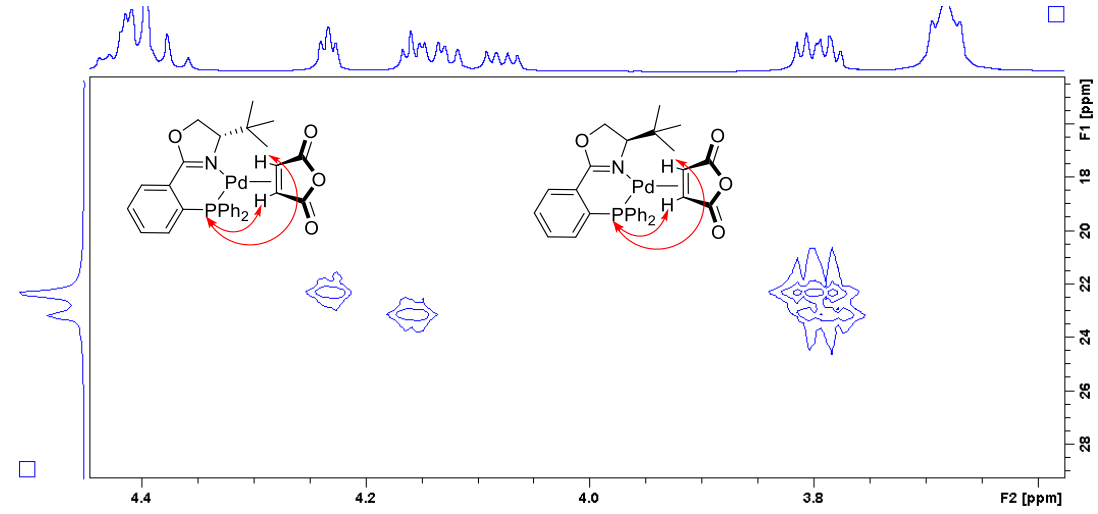

Figure A95. ^{1}H-^{31}P HMBC NMR spectrum expansion of **3.5**. The correlations between P and MAH–H are observed.

(*S*)-^{iPr}PHOX–Pd–MAH (3.6)

^{1}H NMR (500 MHz, CD_2Cl_2): *minor conformer* **δ** 8.08-8.13 (m, 1H), 7.23-7.56 (m, 12H), 7.01-7.05 (m, 1H), 4.27-4.40 (m, 3H), 4.11 (m, 1H), 3.82 (m, 1H), 2.09 (m, 1H), 0.83 (d, J = 6.8 Hz, 3H), 0.21 (d, J = 6.8 Hz, 3H). *Major conformer* **δ** 8.08-8.13 (m, 1H), 7.23-7.56 (m, 12H), 7.01-7.05 (m, 1H), 4.27-4.40 (m, 3H), 4.15 (m, 1H), 3.91 (m, 1H), 2.31 (m, 1H), 0.87 (m, 3H), 0.38 (d, J = 6.8 Hz, 3H).

^{13}C NMR (125 MHz, CD_2Cl_2): major **δ** 172.8, 172.6, 171.9 (d, $^{3}J_{C\text{-}P}$ = 5.3 Hz), 171.4 (d, $^{3}J_{C\text{-}P}$ = 6.2 Hz), 163.7, 163.3, 134.5, 134.1 (d, $J_{C\text{-}P}$ = 5.3 Hz), 134.0 (d, $J_{C\text{-}P}$ = 3.5 Hz), 133.9, 133.8, 133.6, 133.5, 132.3, 132.2$_3$, 132.2$_2$, 132.2$_0$, 132.0$_9$, 132.0$_6$, 132.0$_4$, 132.0$_1$, 130.8 (d, $J_{C\text{-}P}$ = 1.7 Hz), 130.7 (d, $J_{C\text{-}P}$ = 1.7 Hz), 130.6 (d, $J_{C\text{-}P}$ = 1.8 Hz), 130.5$_3$ (d, $J_{C\text{-}P}$ = 1.8 Hz), 130.4$_9$, 129.1, 129.0, 128.9$_3$ (d, $J_{C\text{-}P}$ = 3.6 Hz), 128.8$_7$ (d, $J_{C\text{-}P}$ = 1.8 Hz), 128.8$_5$, 128.8$_0$, 75.6 (d, $^{4}J_{C\text{-}P}$ = 1.8 Hz), 75.5, 67.7$_6$, 67.7$_5$, 47.1, 46.8 (d, $^{2}J_{C\text{-}P}$ = 4.3 Hz), 46.3, 46.0 (d, $^{2}J_{C\text{-}P}$ = 5.4 Hz), 31.0, 30.8, 18.4, 13.9, 13.3.

^{31}P NMR (200 MHz, CD_2Cl_2) δ 21.68 (major conformer), 22.29 (minor conformer).

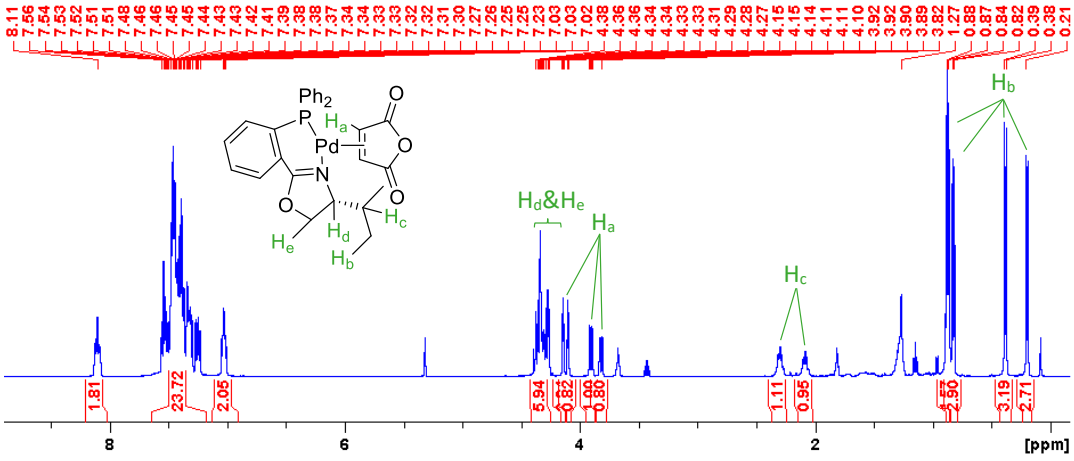

Figure A96. ^{1}H NMR spectrum (500 MHz, CD_2Cl_2) of **3.6**. Two conformers (MAH *endo* and *exo*) are observed, and key proton signals are assigned. Triplet at 1.15 ppm and quartet at 3.43 ppm are diethyl ether. Multiplets at 1.82 and 3.68 ppm are THF. Multiplets at 0.88 (overlapped with one CH_3 peak) and 1.27 are hexanes.

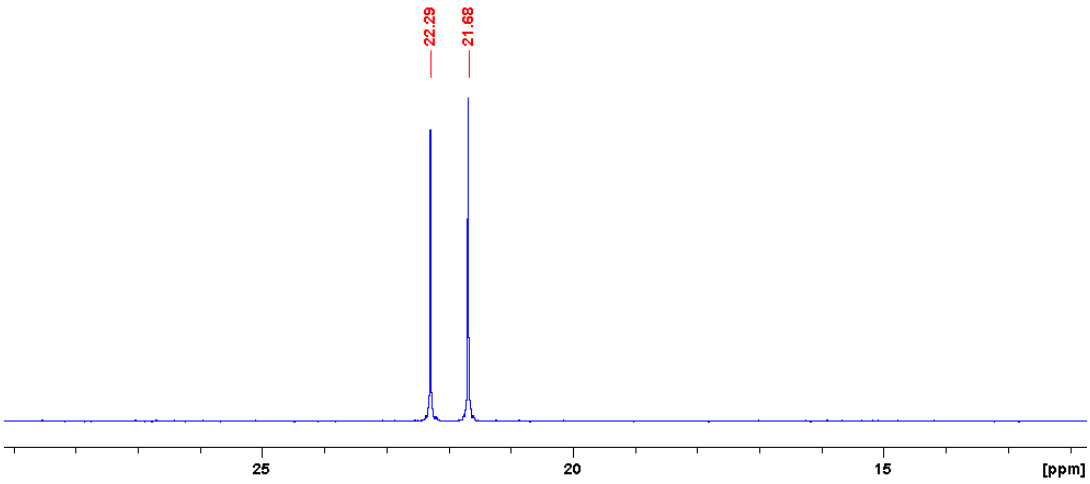

Figure A97. ^{31}P{^{1}H} NMR spectrum (200 MHz, CD_2Cl_2) of **3.6**. Two conformers are observed.

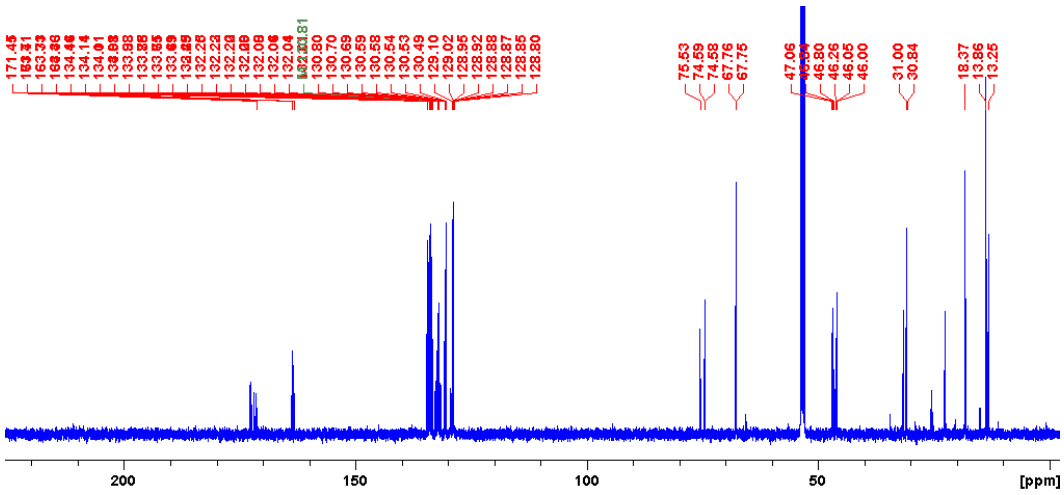

Figure A98. $^{13}C\{^{1}H\}$ NMR spectrum (125 MHz, CD_2Cl_2) of **3.6** (Green label is the manually-picked peak in a doublet).

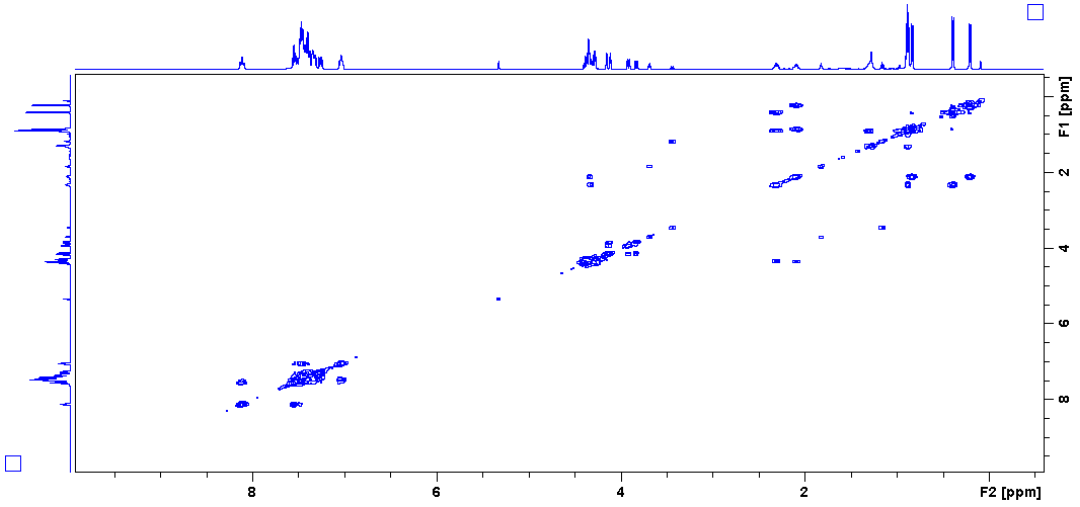

Figure A99. ^{1}H-^{1}H COSY NMR spectrum of **3.6**.

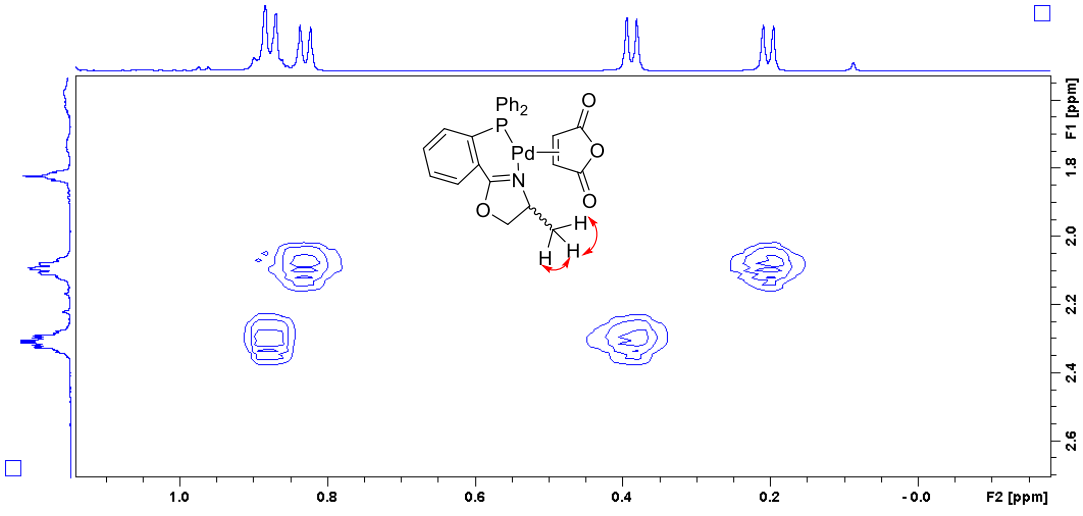

Figure A100. ^{1}H-^{1}H COSY NMR spectrum expansion of **3.6**. CH_3 assignment for corresponding conformers.

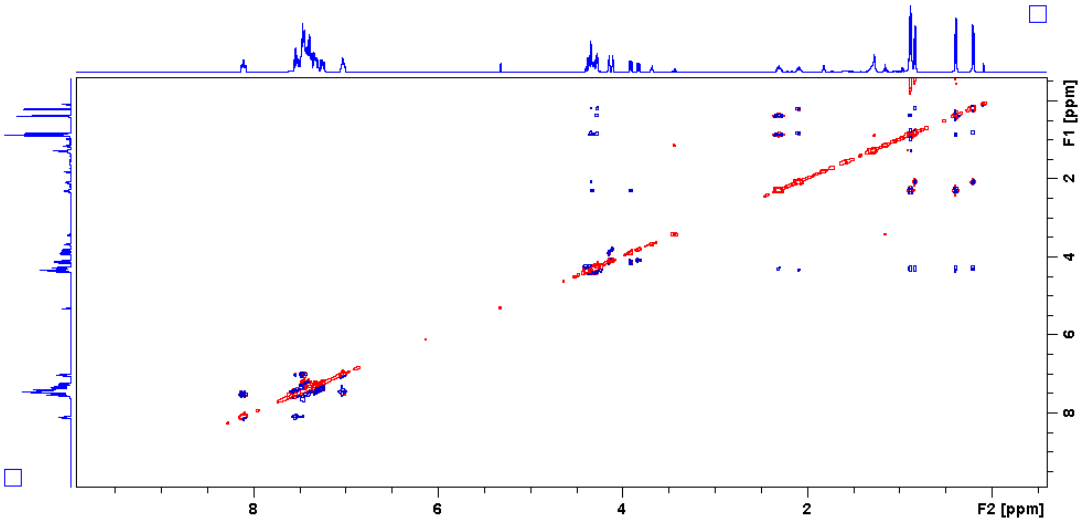

Figure A101. ^{1}H-^{1}H NOESY NMR spectrum of **3.6**.

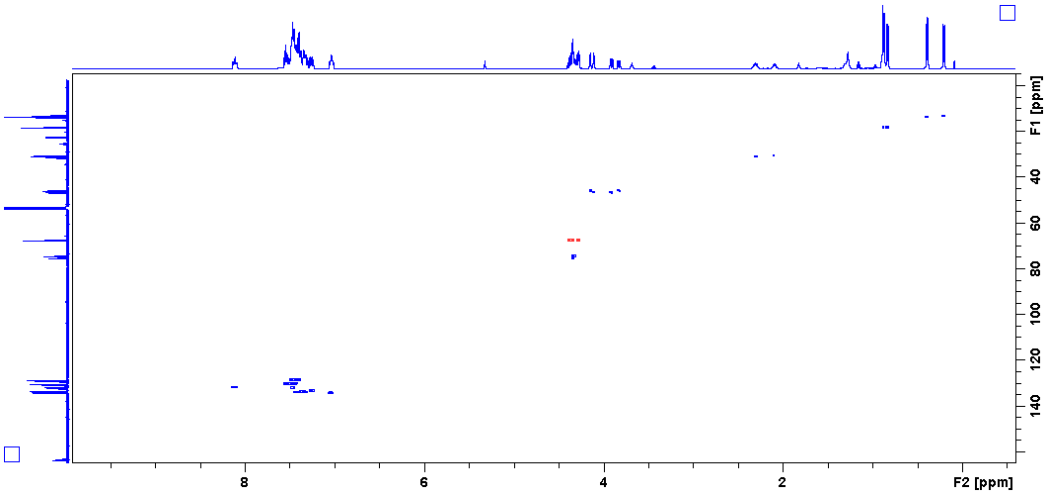

Figure A102. ^{1}H-^{13}C HSQC NMR spectrum of **3.6**.

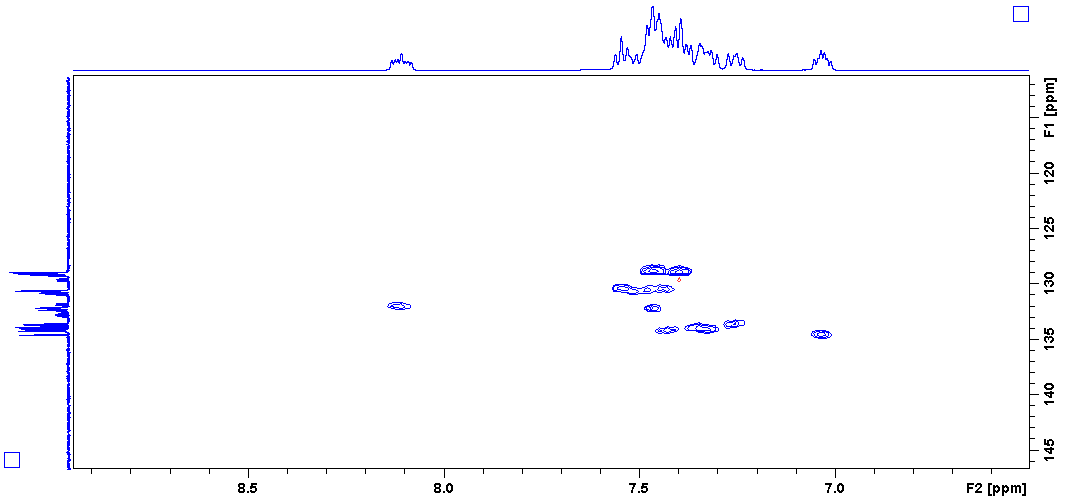

Figure A103. ^{1}H-^{13}C HSQC NMR spectrum of **3.6**. Expansion of the aliphatic region.

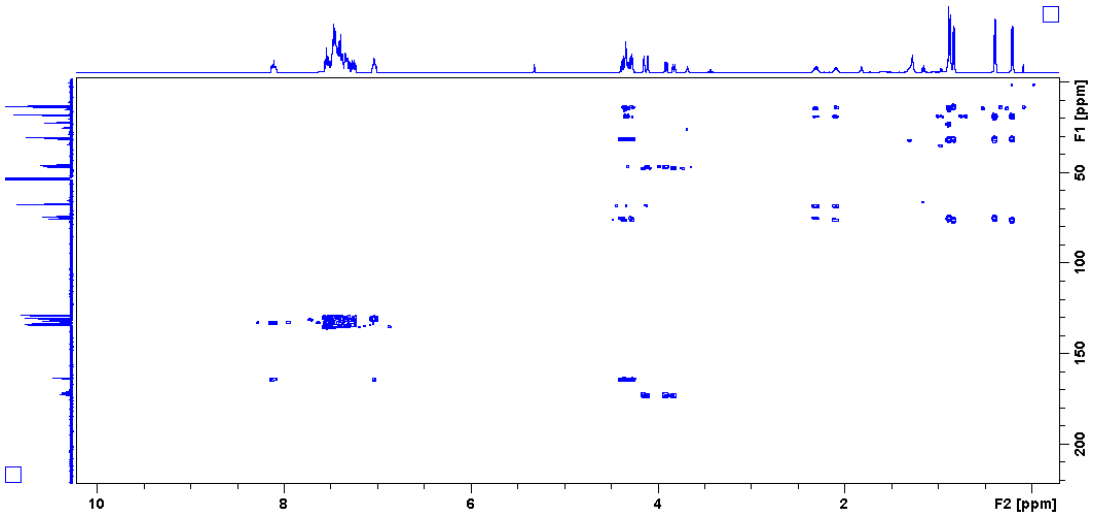

Figure A104. ^{1}H-^{13}C HMBC NMR spectrum of **3.6**.

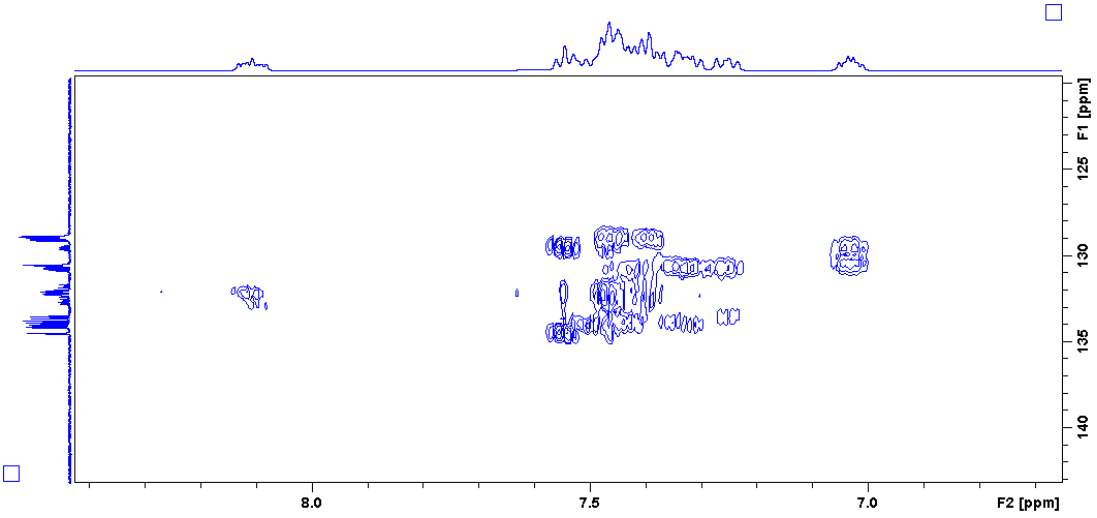

Figure A105. ^{1}H-^{13}C HMBC NMR spectrum of **3.6**. Expansion of aliphatic region.

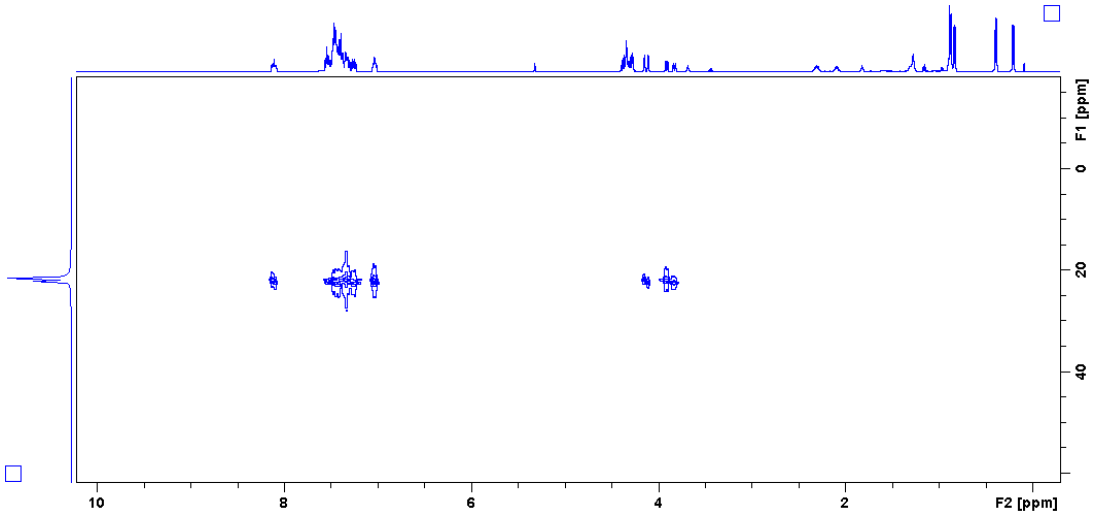

Figure A106. ^{1}H-^{31}P HMBC NMR spectrum of **3.6**.

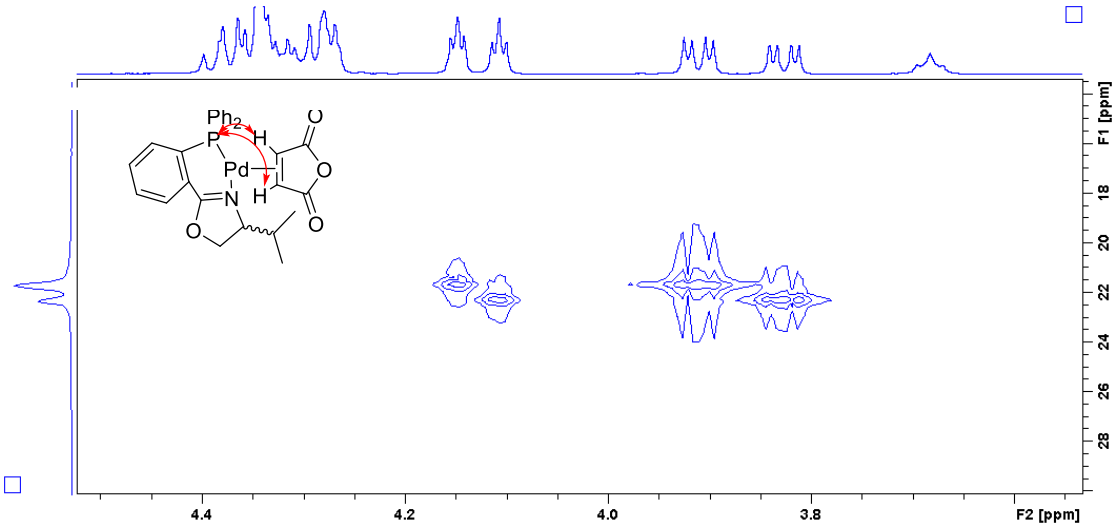

Figure A107. ^{1}H-^{31}P HMBC NMR spectrum expansion of **3.6**. The correlations between P and MAH–H.

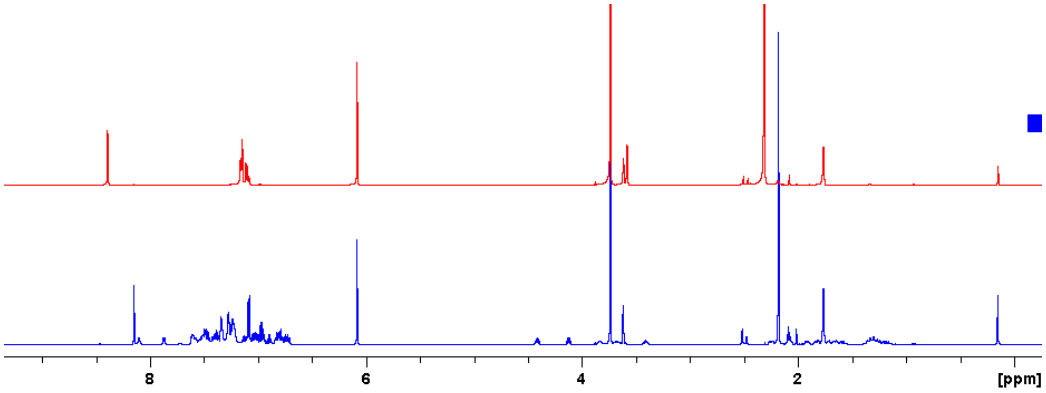

Figure A108. ^{1}H NMR spectra (500 MHz, THF-d_8) of the metalation test for **3.1**. Singlets at 3.74 and 6.08 ppm are 1,3,5-trimethoxybenzene. Red: initial spectrum of ^{DMP}DAB–Pd–MAH. Blue: spectrum obtained after mixing with **L1** stock solution, indicating complete consumption of ^{DMP}DAB–Pd–MAH.

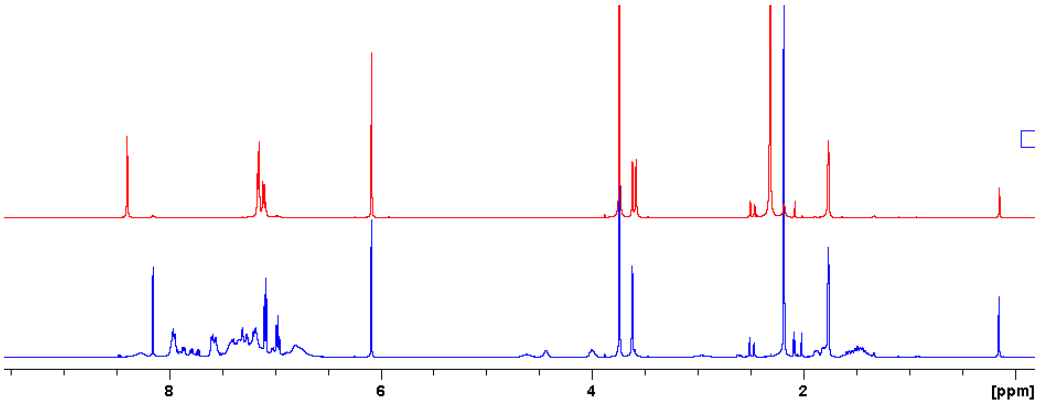

Figure A109. ^{1}H NMR spectra (500 MHz, THF-d_8) of the metalation test for **3.2**. Singlets at 3.74 and 6.08 ppm are 1,3,5-trimethoxybenzene. Red: initial spectrum consisting of ^{DMP}DAB–Pd–MAH. Blue: spectrum obtained after mixing with **L2** stock solution.

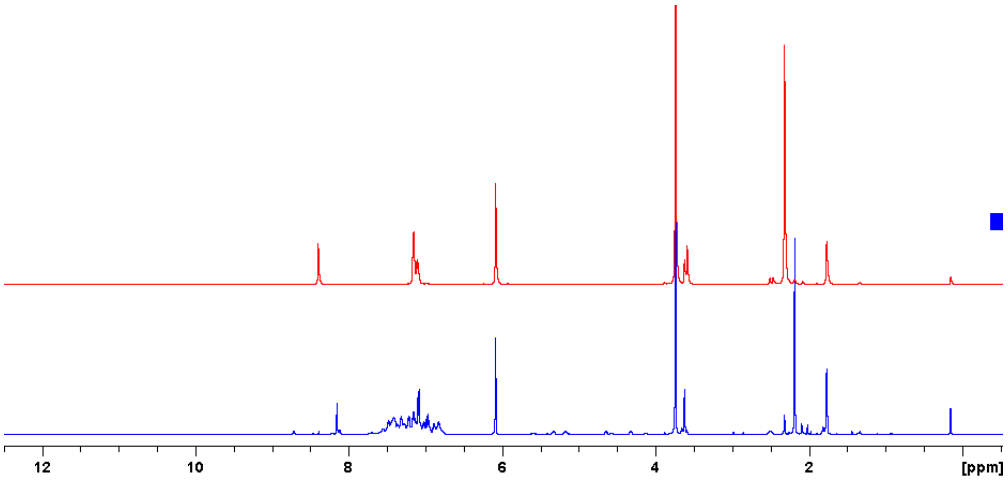

Figure A110. ^{1}H NMR spectra (500 MHz, THF-d_8) of the metalation test for **3.3**. Singlets at 3.74 and 6.08 ppm are 1,3,5-trimethoxybenzene. Red: initial spectrum consisting of ^{DMP}DAB–Pd–MAH and 1,3,5-trimethoxybenzene. Blue: spectrum obtained after mixing with **L3** stock solution

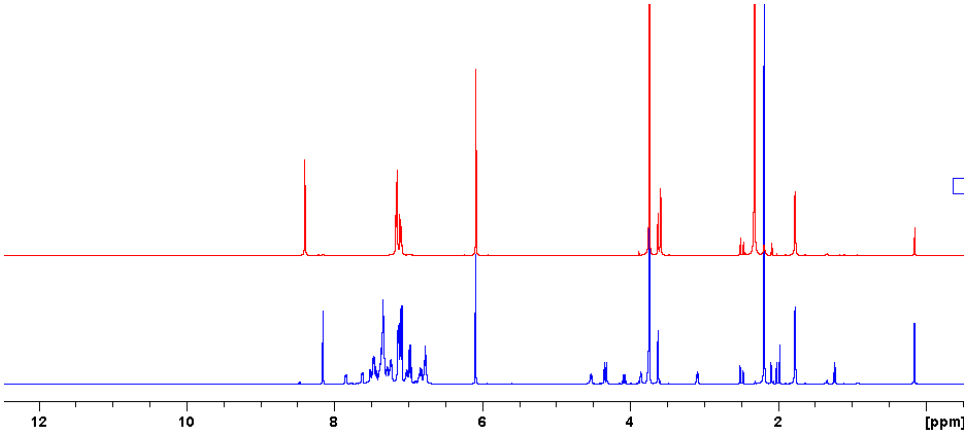

Figure A111. ^{1}H NMR spectra (500 MHz, THF-d_8) of the metalation test for **3.4**. Singlets at 3.74 and 6.08 ppm are 1,3,5-trimethoxybenzene. Red: initial spectrum consisting of ^{DMP}DAB–Pd–MAH and 1,3,5-trimethoxybenzene. Blue: spectrum obtained after mixing with **L4** stock solution.

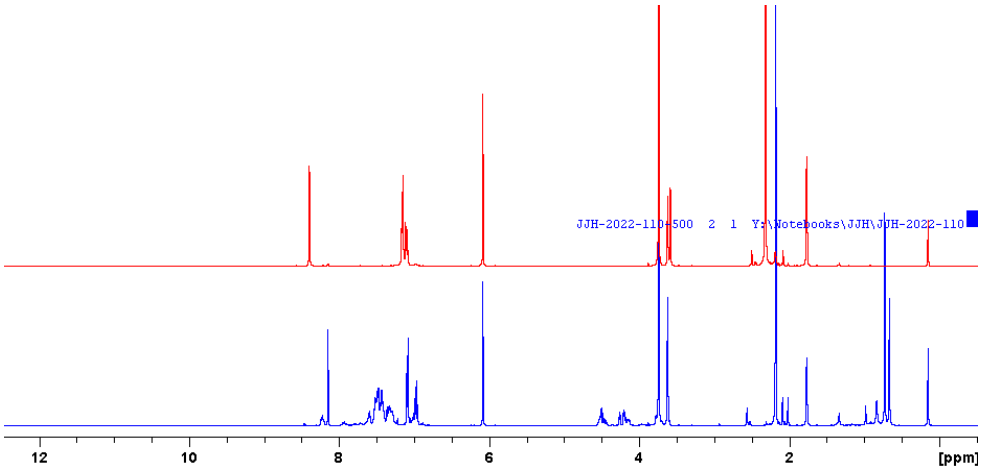

Figure A112. ^{1}H NMR spectra (500 MHz, THF-d_8) of the metalation test for **3.5**. Singlets at 3.74 and 6.08 ppm are 1,3,5-trimethoxybenzene. Red: initial spectrum consisting of ^{DMP}DAB–Pd–MAH and 1,3,5-trimethoxybenzene. Blue: spectrum obtained after mixing with **L5** stock solution.

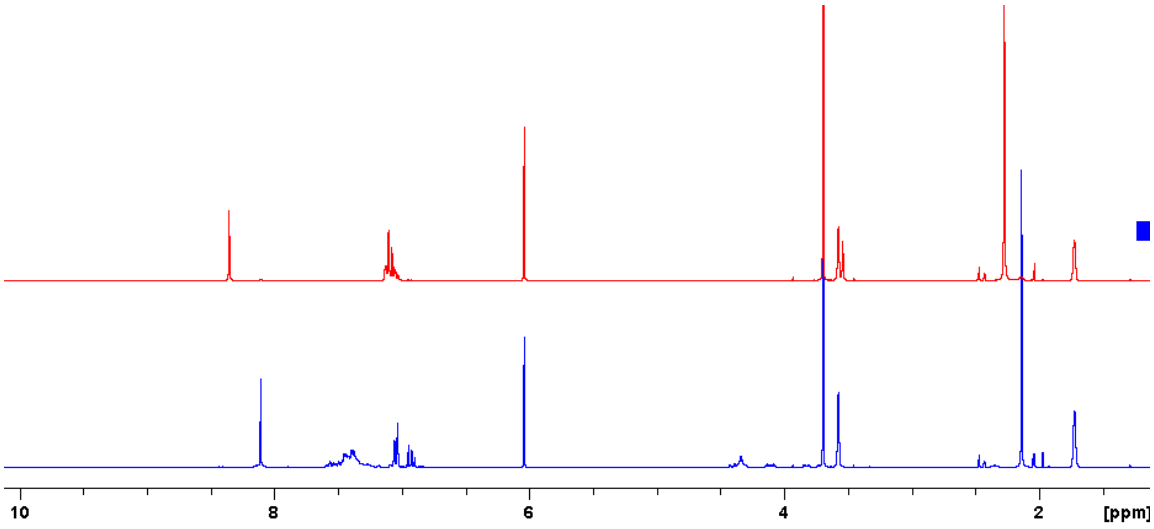

Figure A113. ^{1}H NMR spectra (500 MHz, THF-d_8) of the metalation test for **3.6**. Singlets at 3.74 and 6.08 ppm are 1,3,5-trimethoxybenzene. Red: initial spectrum consisting of ^{DMP}DAB–Pd–MAH and 1,3,5-trimethoxybenzene. Blue: spectrum obtained after mixing with **L6** stock solution.

Solution Stability Stack Plots for Complexes 3.1-3.6

(*S*,*S*)-^{Ph}DACH–Pd–MAH (3.1) (17.3 mg in 0.7 mL THF)

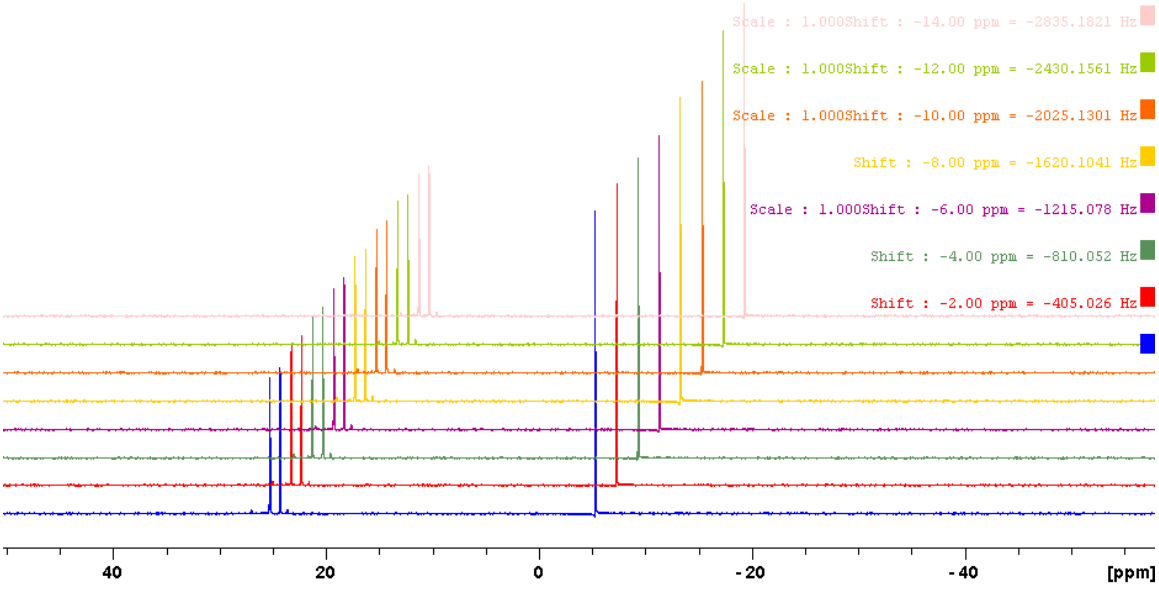

Figure A114. ^{31}P{^{1}H} NMR spectra (200 MHz) stack plots for solution stability of **3.1** with time increasing from the front (30 min) to the back (48 h). Key signals are the peaks of the major conformer (24.24 ppm and 25.20 ppm) and PPh_3 internal standard (–5.36 ppm).

(*S*,*S*)-^{NAP}DACH–Pd–MAH (3.2) (20.6 mg in 0.7 mL THF)

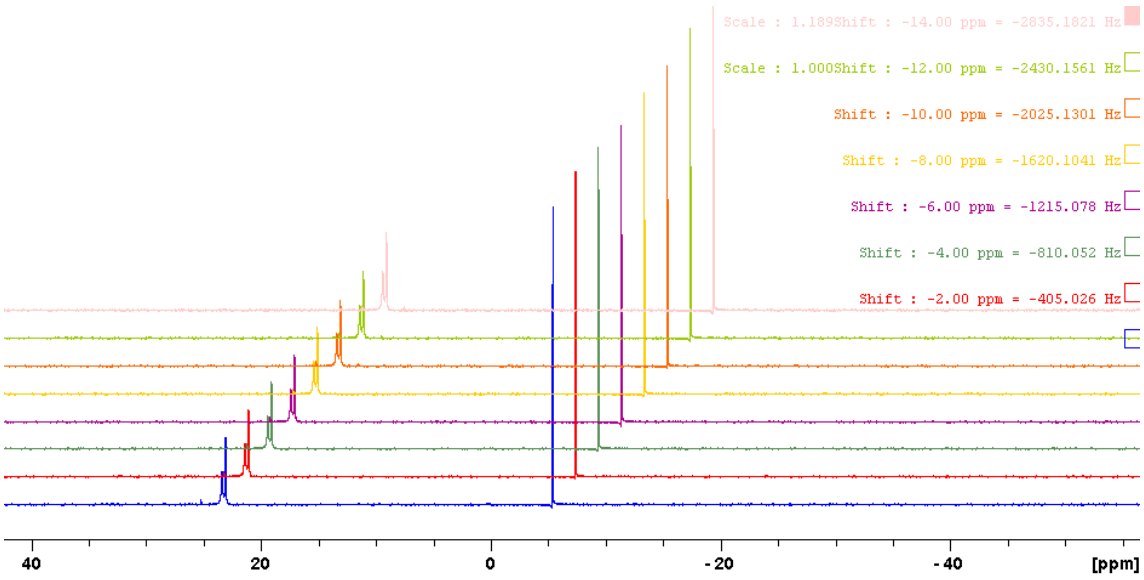

Figure A115. $^{31}P\{^{1}H\}$ NMR spectra (200 MHz) stack plots for solution stability of **3.2** with time increasing from the front (30 min) to the back (48 h). Key signals are the product peaks (23.12 ppm and 23.43 ppm) and the peak of PPh_3 internal standard (–5.36 ppm).

(*S*,*S*)-^{Ph}STIL–Pd–MAH (3.3) (19.6 mg, 0.7 mL THF)

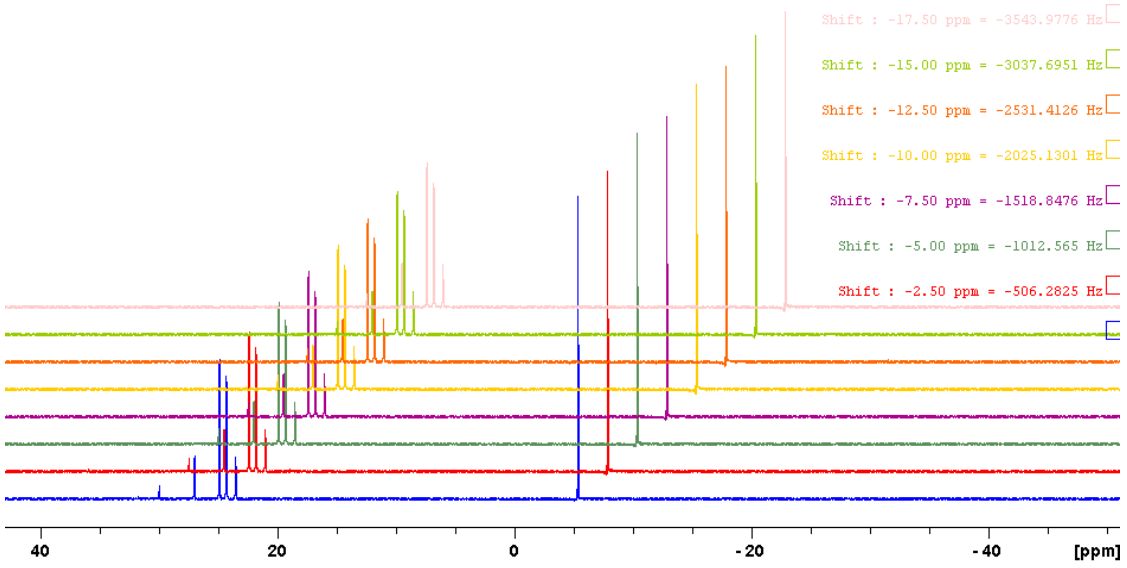

Figure A116. $^{31}P\{^{1}H\}$ NMR spectra (200 MHz) stack plots for solution stability of **3.3** with time increasing from the front (30 min) to the back (48 h). Key signals are the peaks of minor conformer (23.52 ppm and 27.00 ppm), major conformer (24.29 ppm and 24.89 ppm) and PPh_3 internal standard (–5.36 ppm).

(*S*,*S*)-^{Ph}ANDEN–Pd–MAH (3.4) (12.6 mg in 0.7 mL THF)

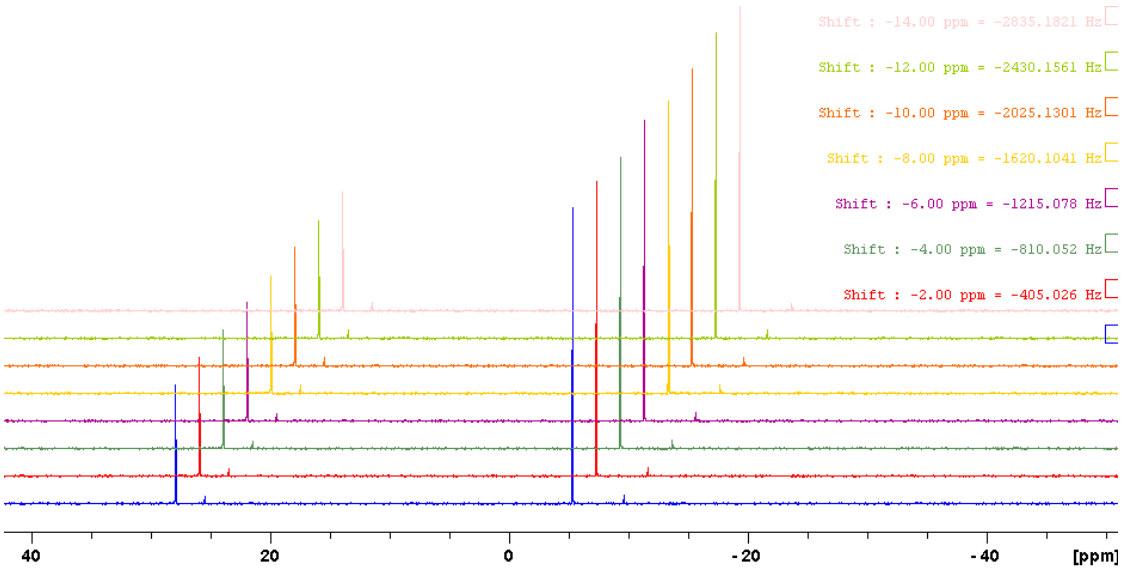

Figure A117. $^{31}P\{^{1}H\}$ NMR spectra (200 MHz) stack plots for solution stability of **3.4** with time increasing from the front (30 min) to the back (48 h). Key signals are the product peak (27.93 ppm) and the peak of PPh_3 internal standard (–5.36 ppm).

(*S*)-$^{t\text{Bu}}$PHOX–Pd–MAH (3.5) (33.2 mg, 0.6 mL THF)

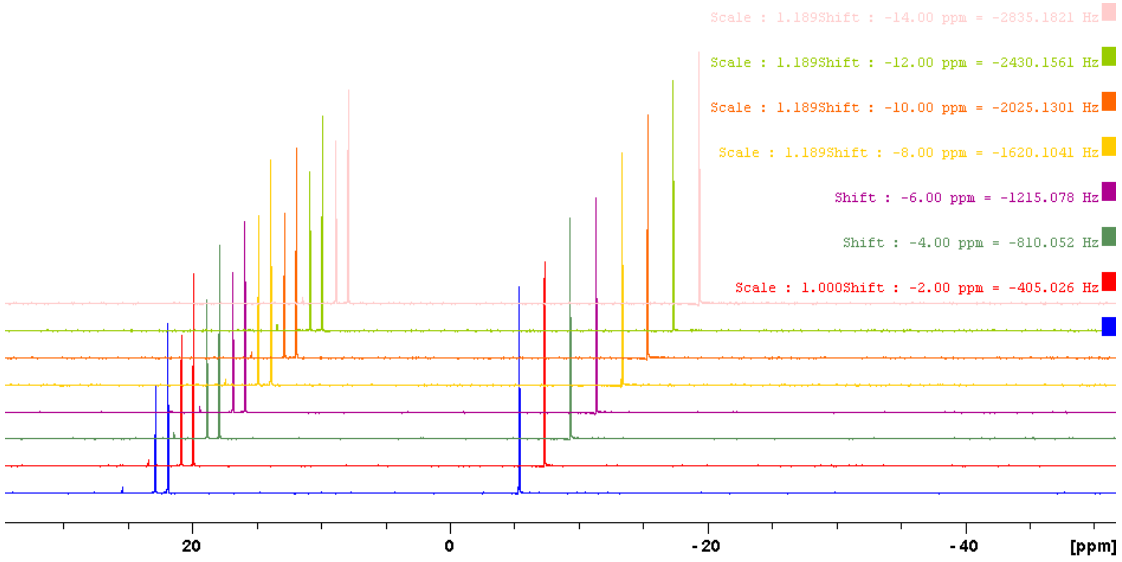

Figure A118. $^{31}P\{^{1}H\}$ NMR spectra (200 MHz) stack plots for solution stability of **3.5** with time increasing from the front (30 min) to the back (48 h). Key signals are the peaks of minor conformer (22.83 ppm), major conformer (21.88 ppm) and PPh_3 internal standard (–5.36 ppm).

(*S*)-$^{i\mathrm{Pr}}$PHOX–Pd–MAH (3.6) (11.8 mg, 0.6 mL THF)

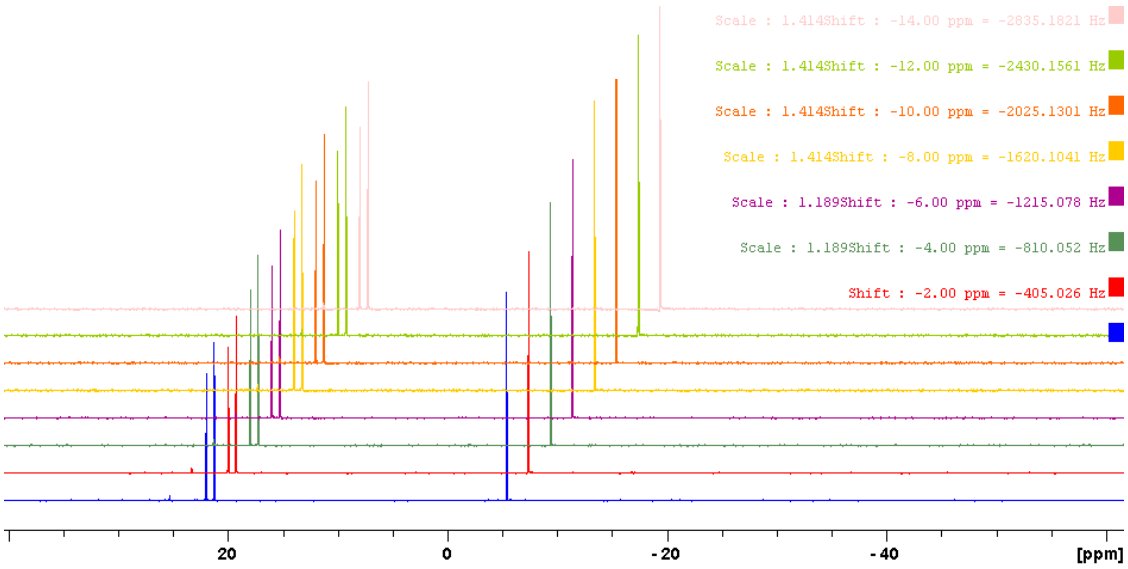

Figure A119. $^{31}P\{^{1}H\}$ NMR spectra (200 MHz) stack plots for solution stability of **3.6** with time increasing from the front (30 min) to the back (48 h). Key signals are the peaks of minor conformer (21.99 ppm), major conformer (21.25 ppm) and PPh_3 internal standard (–5.36 ppm).

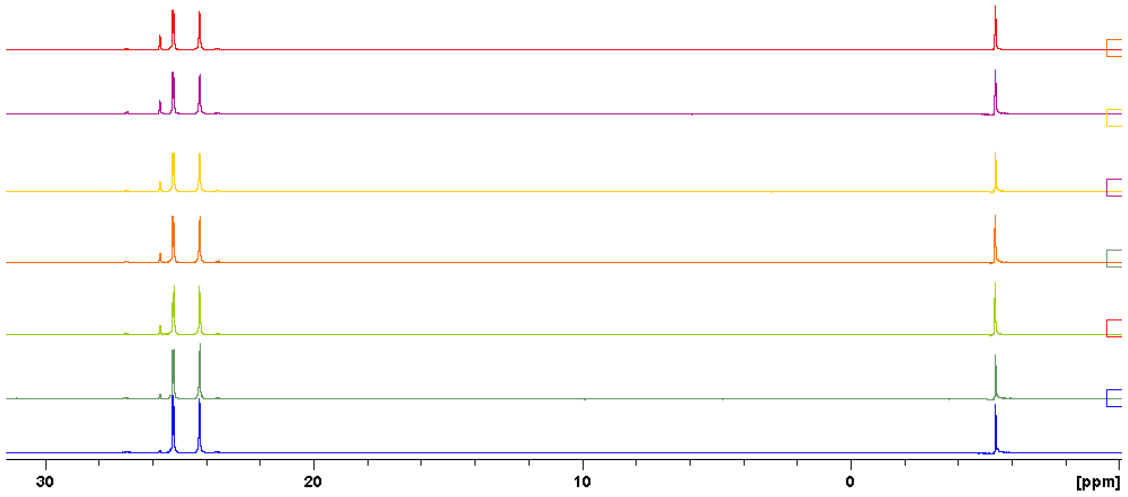

Figure A120. $^{31}P\{^{1}H\}$ NMR spectra (200 MHz) stack plots for solution stability of **3.1** in the air with time increasing from the front (30 min) to the back (48 h). Key signals are the peaks of major conformer (24.26 ppm and 25.23 ppm), oxidized by-product (25.73 ppm) and PPh_3 internal standard (–5.36 ppm).

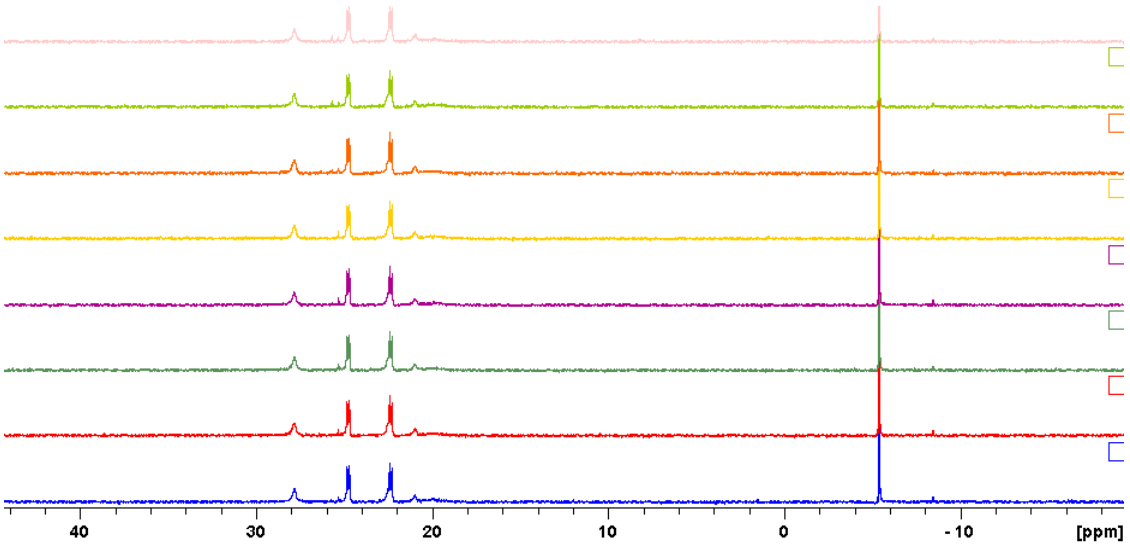

Figure A121. $^{31}P\{^{1}H\}$ NMR spectra (121 MHz) stack plots for solution stability of **(*S*,*S*)-^{Ph}DACH–Pd–dba** in N_2 with time increasing from the front (30 min) to the back (48 h). Key signals are the major product peaks (24.77 ppm and 22.35 ppm), [PNNP]Pd^{II} peak (25.69 ppm), and the peak of PPh_3 internal standard (–5.40 ppm).

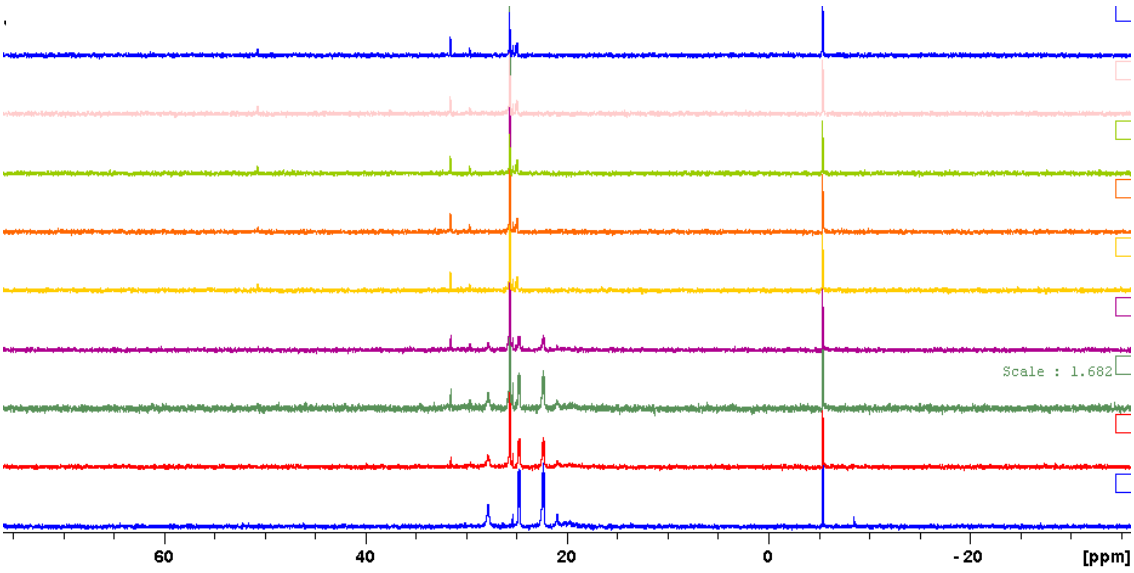

Figure A122. $^{31}P\{^{1}H\}$ NMR spectra (121 MHz) stack plots for solution stability of **(*S*,*S*)-^{Ph}DACH–Pd–dba** in the air with time increasing from the front (30 min) to the back (48 h). Key signals are the major product peaks (24.75 ppm and 22.32 ppm), [PNNP]Pd^{II} peak (25.68 ppm), and the peak of PPh_3 internal standard (–5.36 ppm).

^{DMP}DAB–Pd–($CH_2TMS)_2$ (4.1)

^{1}H NMR: (500 MHz; benzene-d_6) δ 0.23 (s, 18 H, Si–CH_3), 0.44 (s, 4H, Pd–CH_2–Si), 2.17 (s, 12H, Ar–CH_3), 6.86 (s, 2H, NH), 6.96 (m, 6H, Ar–H).

^{13}C{^{1}H} NMR: (125 MHz; benzene-d_6) δ 0.32 (CH_2–Si), 4.10 (Si–CH_3), 18.82 (Ar–**C**H_3), 126.61 (Ar), 128.52 (Ar), 128.57 (Ar), 147.57 (Ar), 160.06 (–N=C–C=N–).

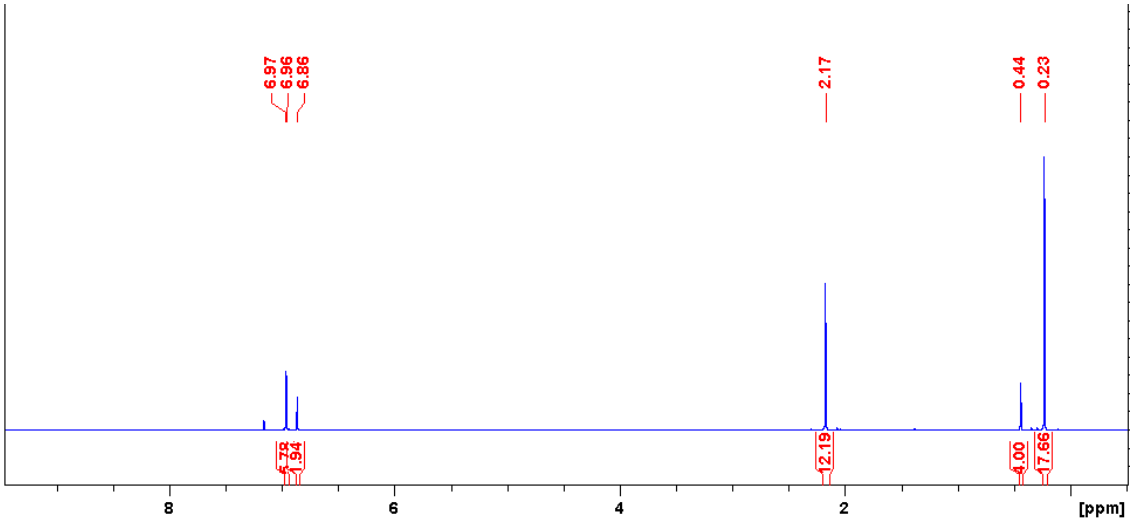

Figure A123. ^{1}H NMR spectrum (500 MHz; benzene-d_6) of **4.1**.

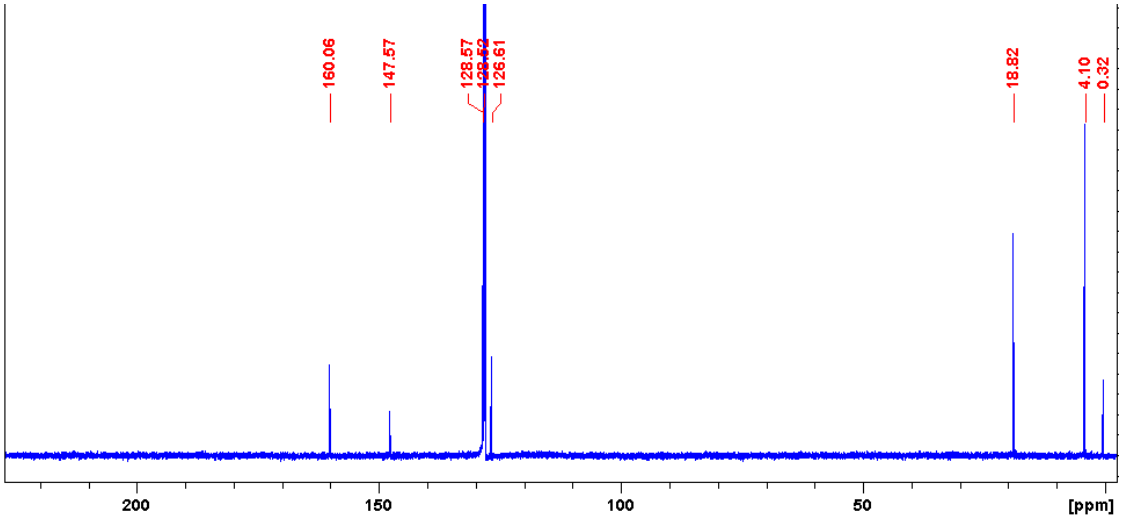

Figure A124. ^{13}C{^{1}H} NMR spectrum (125 MHz; benzene-d_6) of **4.1**.

Synthesis of XANTPhos–Pd–(CH_2TMS)$_2$ (4.2)

^{1}H NMR: (500 MHz; $CDCl_3$) δ -0.33 (s, 18H, Si–CH_3), 0.37-0.52 (m, 4H, Pd–CH_2–Si), 1.68 (s, 6H, CH_3–C–CH_3), 6.91-7.42 (m, 24H, Ar–H, overlapped with NMR solvent peak); 7.50 (dd, J_1=1.59 Hz, J_2=7.32 Hz, Ar–H)

^{31}P{^{1}H} NMR: (202 MHz; $CDCl_3$) δ 8.42

(Consistent with the reported NMR data[12])

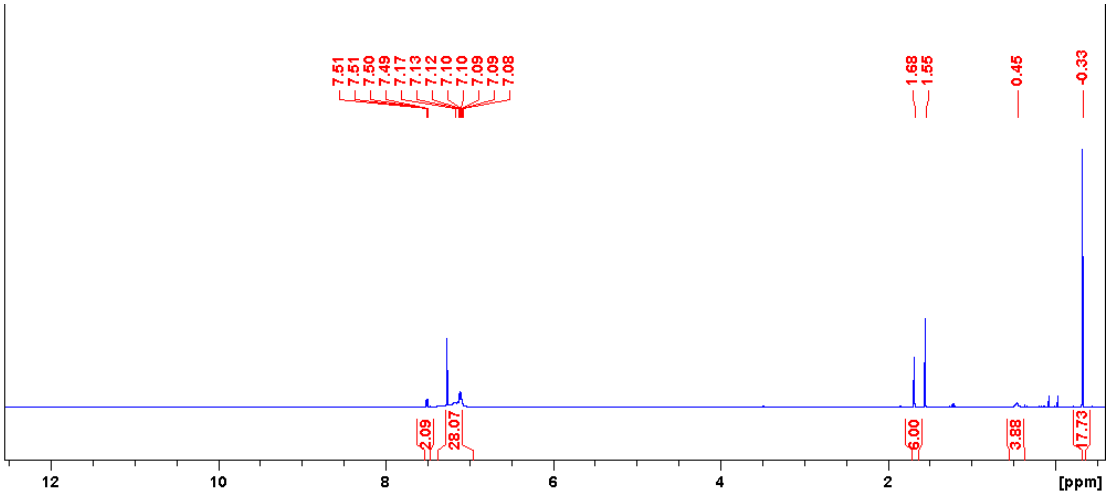

Figure A125. ^{1}H NMR spectrum (500 MHz; $CDCl_3$) of **4.2**. Singlet at 1.55 ppm is the water residue.

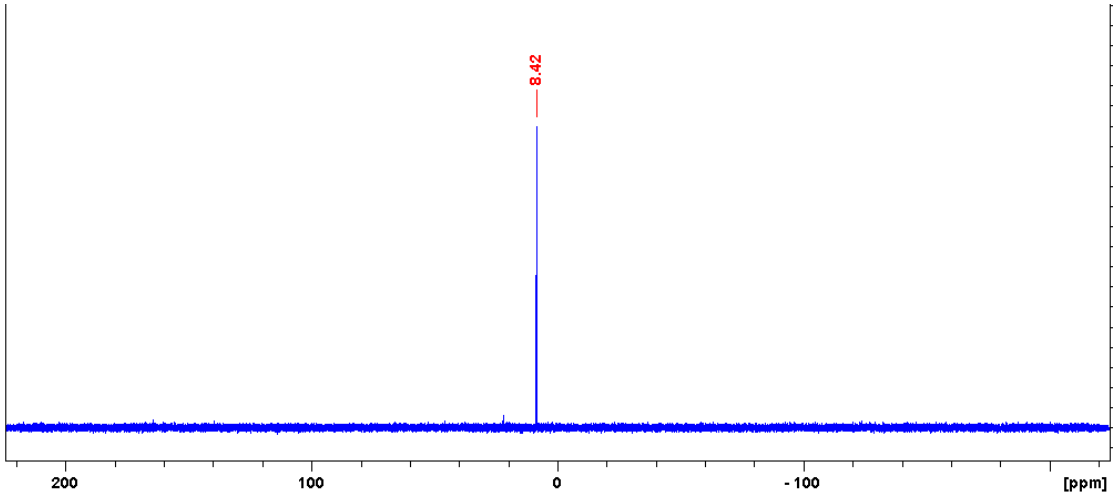

Figure A126. ^{31}P{^{1}H} NMR spectrum (202 MHz; $CDCl_3$) of **4.2**.

BippyPhos–Pd(Br)–(acetophenone) (4.3)

^{1}H NMR: (500 MHz; $CDCl_3$) δ 0.74 (d, *J*=15.27 Hz, 9H, *t*Bu), 0.87 (d, *J*=15.21 Hz, 9H, *t*Bu), 2.47 (–CO–CH_3–), 6.69 (d, *J*=2.02 Hz, 1H, Ar–H), 7.16 (d, *J*=8.28 Hz 1H, =CH–), 7.19 (d, *J*=8.14 Hz, 1H, =CH–), 7.25-7.27 (m, 3H, Ar–H) 7.31-7.44 (m, 8H, Ar–H), 7.54-7.59 (m, 4H, Ar–H), 7.75-7.77 (m, 2H, Ar–H), 8.11 (d, *J*=2.06 Hz, 1H, Ar–H).

^{31}P{^{1}H} NMR: (202 MHz; $CDCl_3$) δ 32.11.

^{13}C{^{1}H} NMR: (125 MHz; $CDCl_3$) δ 26.43 (–CO–**C**H_3–), 29.14 (d, $^{2}J_{CP}$=5.00 Hz, *t*Bu CH_3), 29.54 (d, $^{2}J_{CP}$=5.09 Hz, *t*Bu CH_3), 37.20 (d, $^{1}J_{CP}$=13.59 Hz, *t*Bu C), 37.49 (d, $^{1}J_{CP}$=13.20 Hz, *t*Bu C), 115.64, 125.79, 126.08, 127.42, 128.09, 128.44, 128.49, 128.64, 128.85, 129.08, 129.50, 130.34, 131.01, 133.11, 138.22 (d, J_{CP}=2.48 Hz), 138.28 (d, J_{CP}=11.10 Hz), 139.21, 142.15, 142.42, 144.0 (d, J_{CP}=7.24 Hz), 144.88, 148.63, 153.56, 198.50 (C=O).

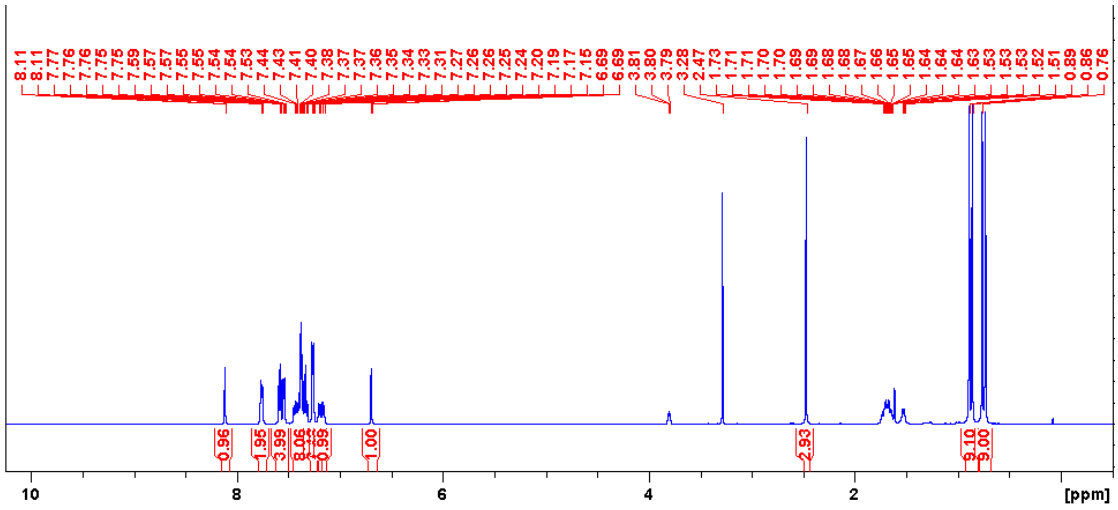

Figure A127. ^{1}H NMR spectrum (500 MHz; $CDCl_3$) of **4.3**. Multiplets at 1.51-1.53 ppm, 1.63-1.74 ppm, singlet at 3.28 ppm, and 3.78-3.82 ppm are the peaks of CPME. CPME is not removed even after prolonged drying under vacuum.

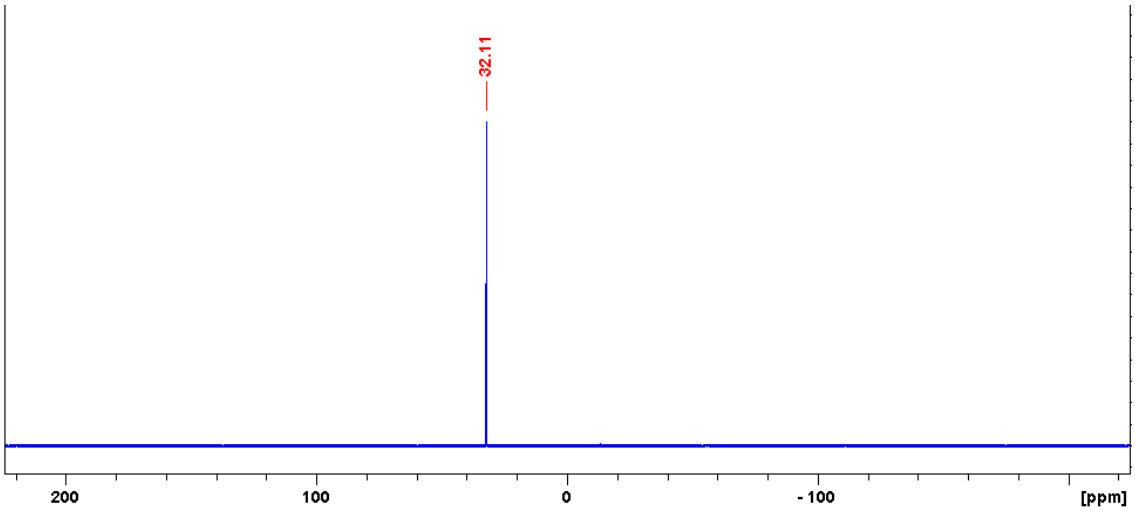

Figure A128. ^{31}P{^{1}H} NMR spectrum (202 MHz; $CDCl_3$) of **4.3**.

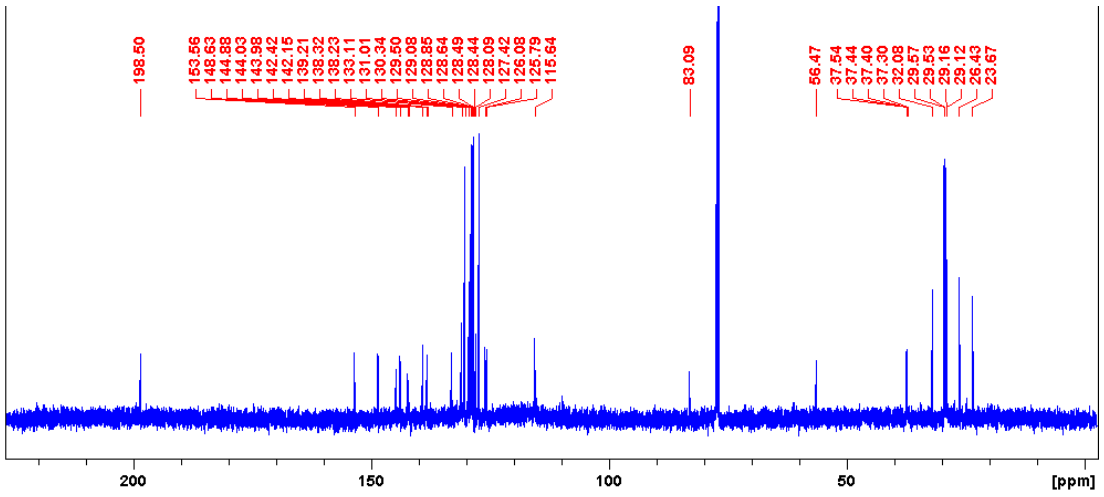

Figure A129. $^{13}C\{^{1}H\}$ NMR spectrum (125 MHz; $CDCl_3$) of **4.3**. Singlets at 23.67, 32.08, 56.47, 83.09 ppm are the peaks of CPME residue.

Synthesis of AdBippyPhos–Pd(Br)–acetophenone (4.4)

^{1}H NMR: (500 MHz; $CDCl_3$) δ 1.25-1.26 (m, 3H, Ad), 1.34-1.56 (m, 19H, Ad), 1.62 (m, 5H, Ad), 1.78 (m, 3H, Ad), 2.47 (s, 3H, –CO–CH_3), 6.67 (m, 1H, Ar–H), 7.25-7.45 (m, 13H, Ar–H and =CH–CH=), 7.55-7.60 (m, 4H, Ar–H), 7.76-7.78 (m, 2H, Ar–H), 8.13 (m, 1H, Ar–H).

$^{31}P\{^{1}H\}$ NMR: (202 MHz; $CDCl_3$) δ 26.94.

$^{13}C\{^{1}H\}$ NMR: (125 MHz; $CDCl_3$) δ 26.45 (CO–**C**H_3), 28.55 (t, $^{3}J_{CP}$=10.20 Hz, Ad), 35.95 (d, J_{CP}=5.06, Ad), 39.29 (Ad), 39.66 (Ad), 42.44 (t, $^{1}J_{CP}$=14.84 Hz, Ad), 42.55 (t, $^{1}J_{CP}$=14.33 Hz, Ad), 116.21, 125.55, 125.87, 127.42, 128.18, 128.43, 128.49, 128.64, 129.26, 129.41, 130.24, 130. 48, 131.07, 132.95, 138.83, 139.23, 140.05, 140.32, 143.87 (d, J=6.43 Hz), 144.50, 148.48, 153.56,198.55 (C=O)

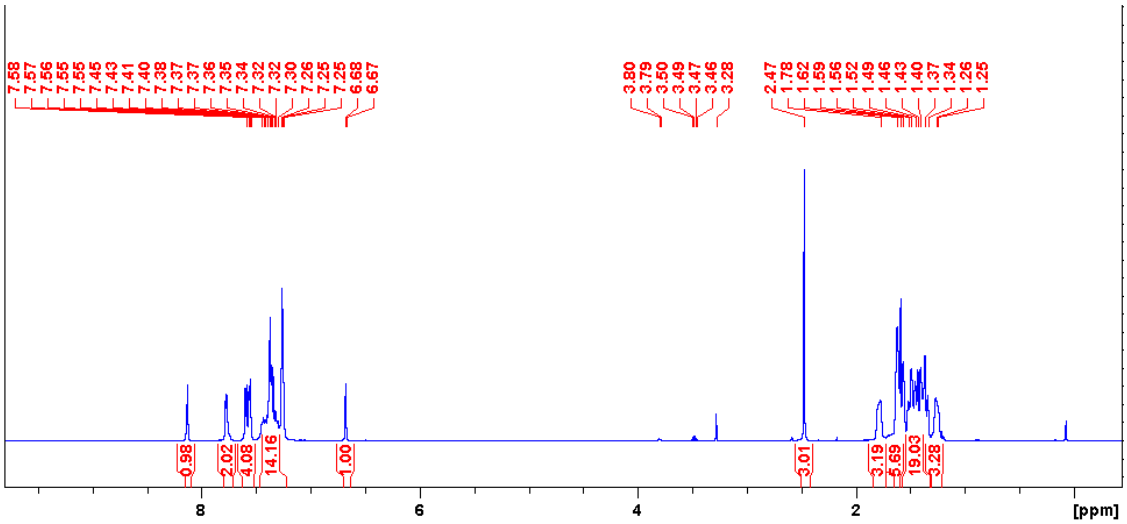

Figure A130. ^{1}H NMR spectrum (500 MHz, $CDCl_3$) of **4.4**. Singlet at 3.28 ppm and multiplets at 3.79-3.80 ppm are the peaks of CPME residue. The Quartet at 3.46-3.50 ppm is one of the peaks of diethyl ether.

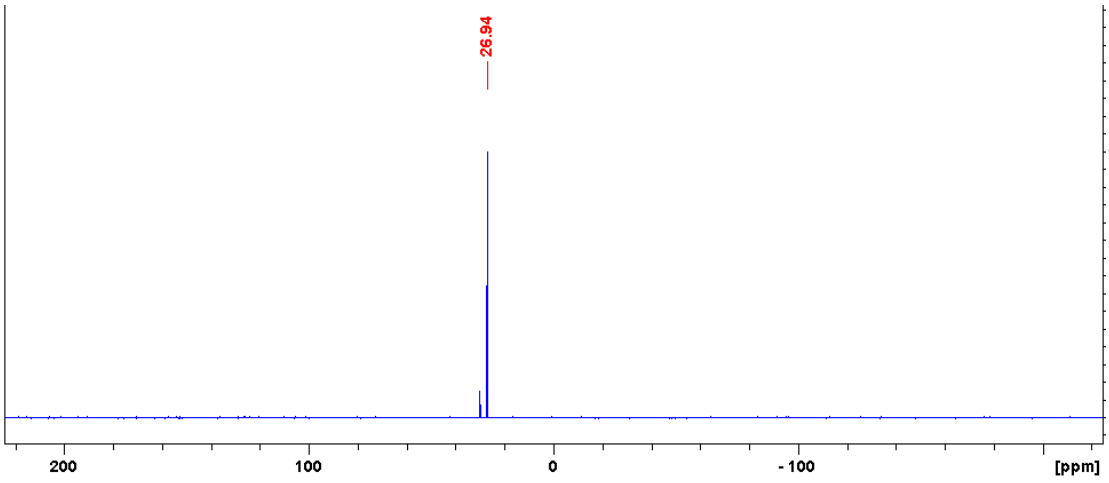

Figure A131. $^{31}P\{^{1}H\}$ NMR spectrum (202 MHz, $CDCl_3$) of **4.4**.

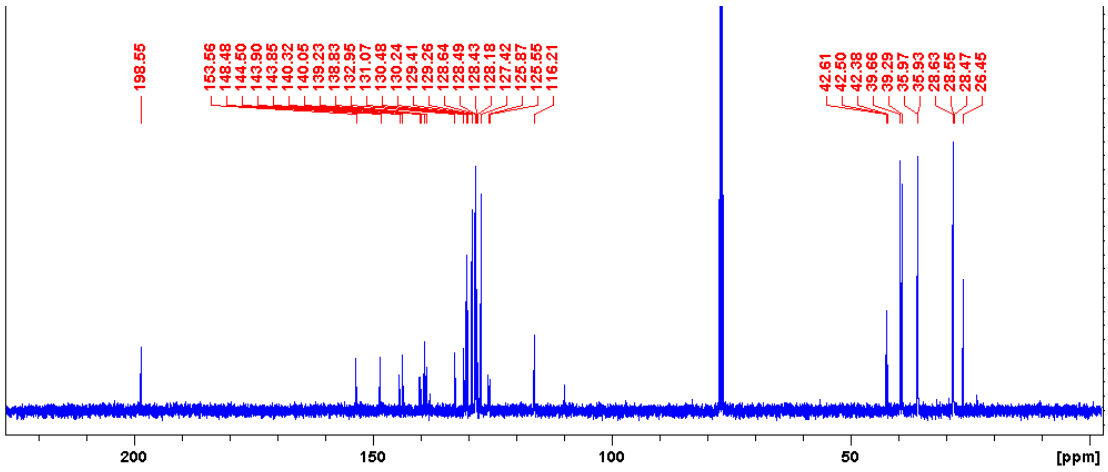

Figure A132. $^{13}C\{^{1}H\}$ NMR spectrum (125 MHz, $CDCl_3$) of **4.4.**

Synthesis of [XPhos–Pd(Br)–acetophenone]$_2$ (4.5)

^{1}H NMR: (500 MHz; $CDCl_3$) δ 0.60-0.72 (m, 2H, Cy–H), 0.90 (d, ^{3}J=6.65 Hz, –CH(C**H**$_3$)$_2$), 1.06-1.27 (m, 6H, Cy–H overlapped with hexanes residue), 1.39 (d, ^{3}J=6.95 Hz, –CH(C**H**$_3$)$_2$), 1.58-1.74 (m, 14 H, Cy–H and –CH(C**H**$_3$)$_2$), 1.76-1.83 (m, 2H, Cy–H), 1.94 (br, 2H, Cy–H), 2.14-2.25 (m, 2H, Cy–H), 2.44 (sept, J=6.90 Hz, 2H, –C**H**(CH$_3$)$_2$), 2.50 (s, 3H, –CO–CH$_3$), 3.12 (sept, J=6.88 Hz, 1H, –C**H**(CH$_3$)$_2$), 6.84-6.90 (m, 1H, Ar–H), 7.14 (s, 2H, Ar–H), 7.23 (dd, J_1=1.64 Hz, J_2=8.40 Hz, Ar–H), 7.40-7.45 (m, 2H, Ar–H), 7.49 (d, J=8.01Hz, 2H, Ar–H), 7.63-7.69 (m, 1H, Ar–H).

^{31}P{^{1}H} NMR: (202 MHz; $CDCl_3$) δ 26.55.

^{13}C{^{1}H} NMR: (125 MHz; $CDCl_3$) δ 24.62 (Cy), 24.83 (Cy), 25.64 (Cy), 25.97 (Cy), 26.50 (–CO–CH$_3$), 27.30 (d, J=11.47 Hz, Cy), 27.61 (d, J=13.17 Hz, Cy), 27.84 (Cy), 28.52 (Cy), 31.67 (Cy), 34.36 (Cy), 35.32 (Cy), 35.53 (Cy), 125.01, 126.24, 127.08, 130.72 (d, J=1.74 Hz), 131.92, 133.09, 133.63, 133.72, 134.05, 137.19 (d, J=3.44 Hz), 146.82, 147.57, 149.83, 156.70, 198.79 (C=O)

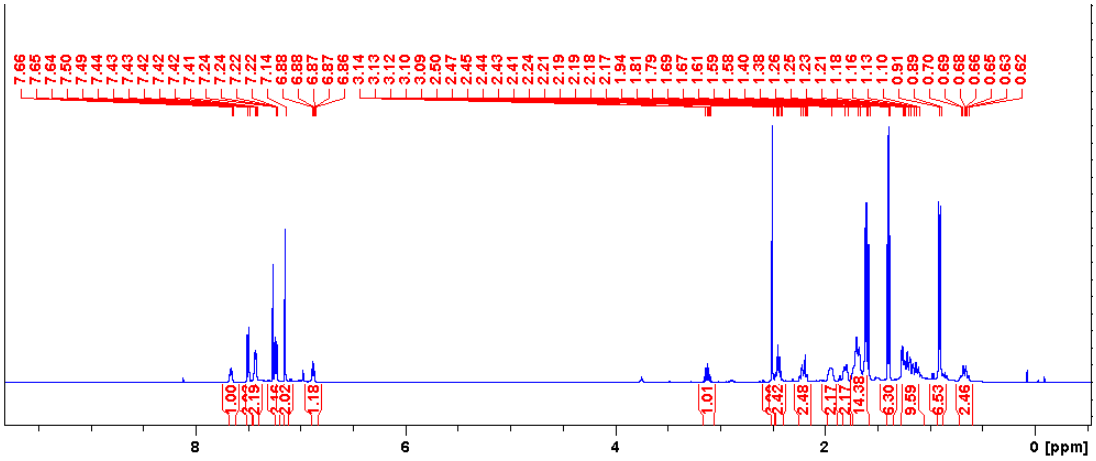

Figure A133. ^{1}H NMR spectrum (500 MHz, $CDCl_3$) of **4.5**.

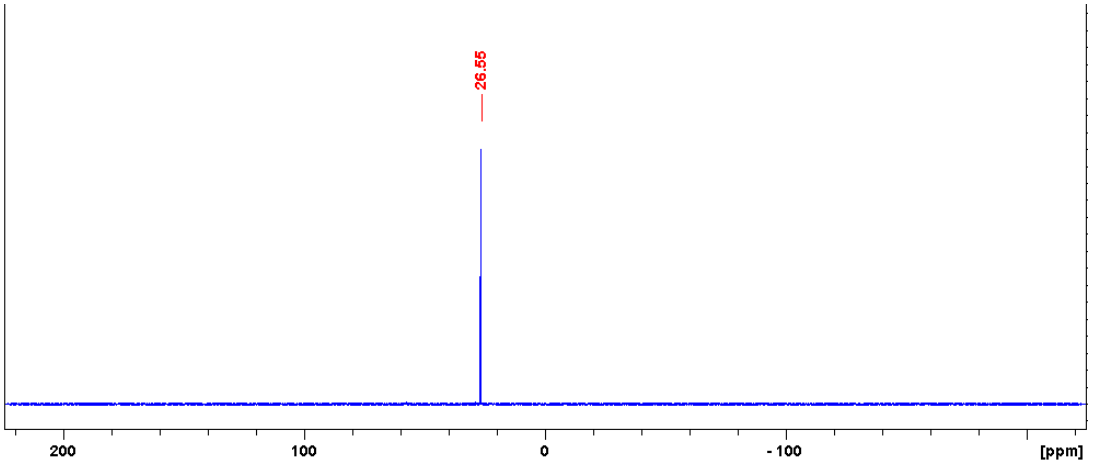

Figure A134. $^{31}P\{^{1}H\}$ NMR spectrum (202 MHz, $CDCl_3$) of **4.5**.

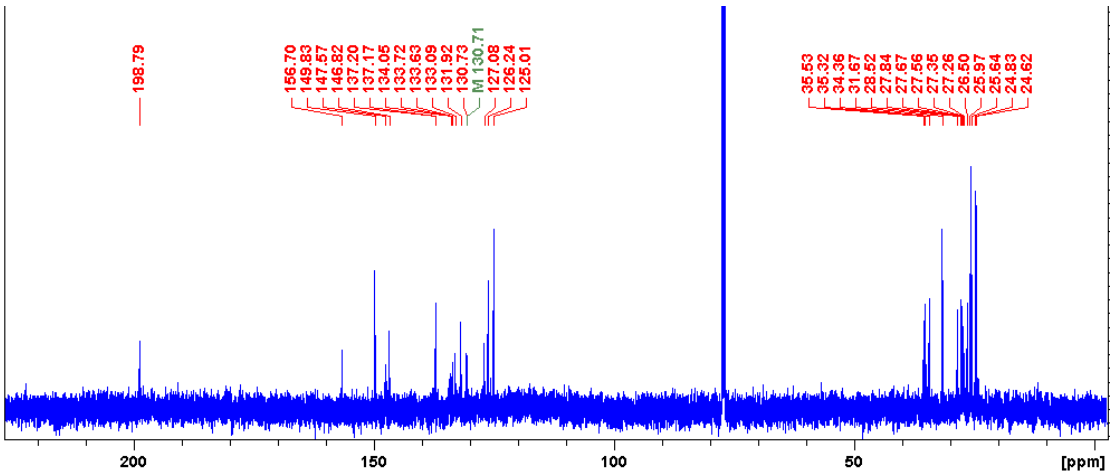

Figure A135. $^{13}C\{^{1}H\}$ NMR spectrum (125 MHz, $CDCl_3$) of **4.5**.

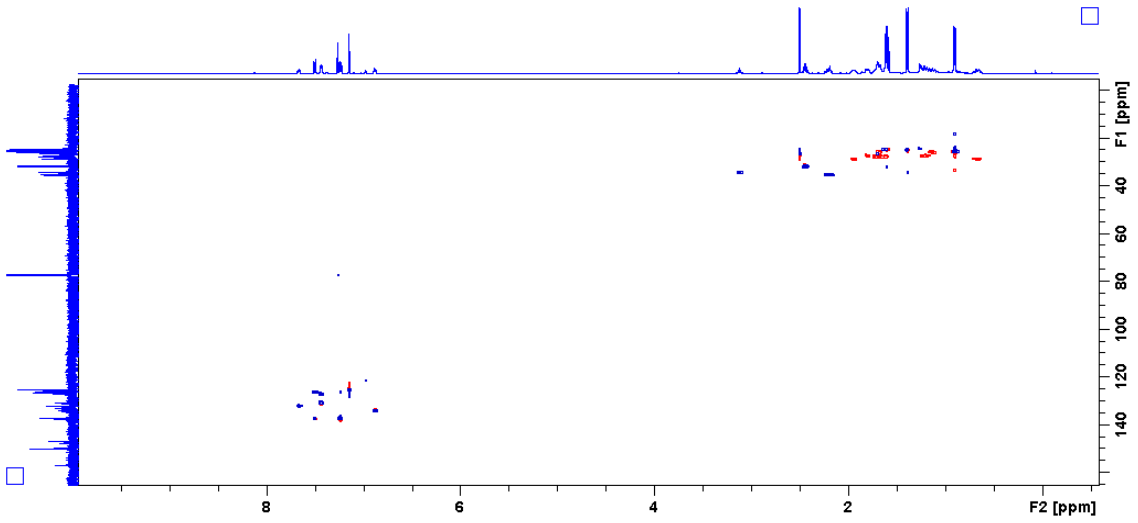

Figure A136. ^{1}H-^{13}C HSQC NMR spectrum of **4.5**.

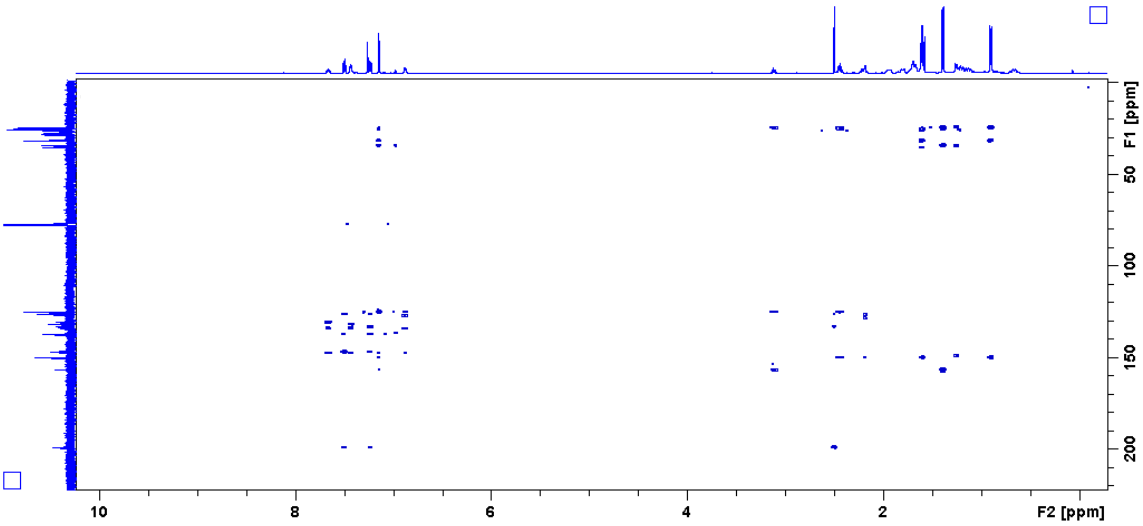

Figure A137. ^{1}H-^{13}C HMBC NMR spectrum of **4.5**.

^{DMP}DAB–Pd(Br)–acetophenone (4.6)

^{1}H NMR: (500 MHz; CD_2Cl_2) δ 2.20 (s, 6H, Ar–C**H**$_3$), 2.34 (s, 3H, CO–CH_3), 2.36 (s, 6H, Ar–C**H**$_3$), 6.81-6.86 (m, 2H, Ar–H), 6.88-6.94 (m, 1H, Ar–H), 6.96-7.02 (m, 2H, Ar–H), 7.06-7.11 (m, 2H, Ar–H), 7.16 (m, 3H, Ar–H), 8.12 (s, 1H,), 8.18 (s, 1H, –N=C–H).

^{13}C{^{1}H} NMR: (125 MHz; CD_2Cl_2) δ 18.51 (Ar–**C**H_3), 18.95 (Ar–**C**H_3), 26.47 (CO–**C**H_3), 125.05, 127.54, 127.72, 128.28, 128.35, 128.66, 128.80, 133.08, 134.86, 146.46, 146.93, 155.74, 162.97 (–N=C–), 165.54 (–N=C–), 198.40 (C=O)

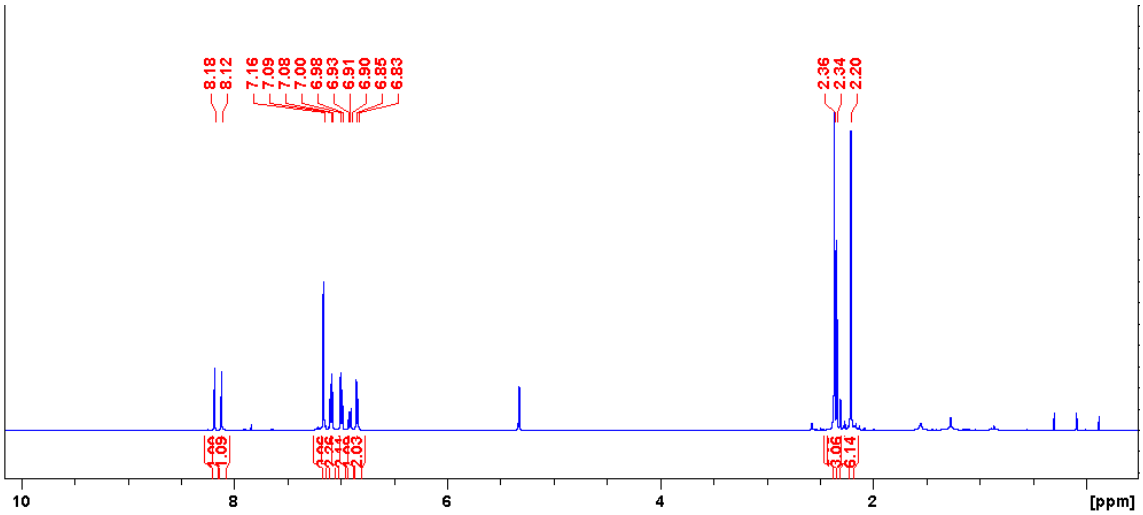

Figure A138. ^{1}H NMR spectrum (500 MHz, CD_2Cl_2) of **4.6.**

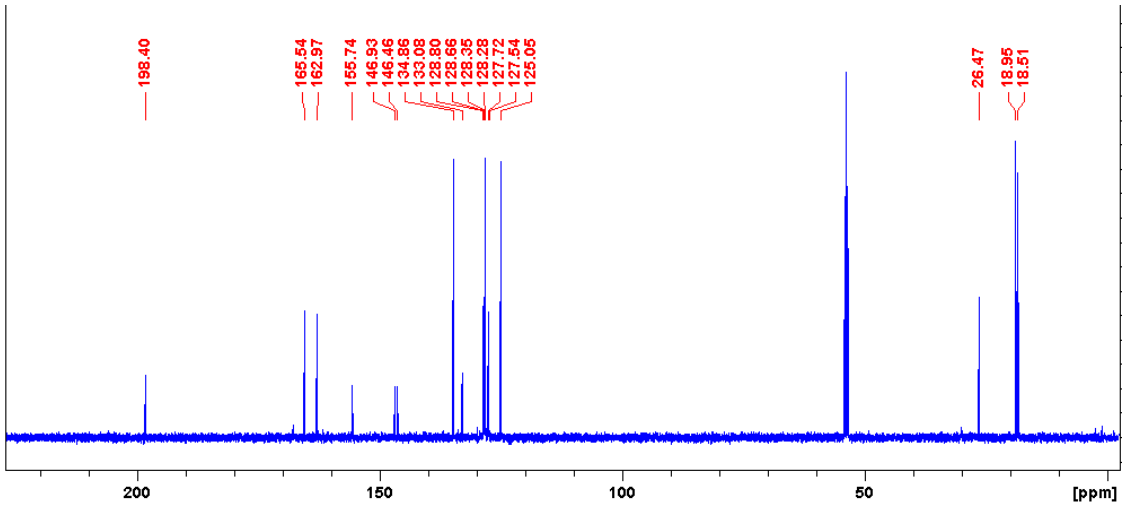

Figure A139. ^{13}C{^{1}H} NMR spectrum (125 MHz, CD_2Cl_2) of **4.6.**

5-Methyl-2-phenylpyridine

^{1}H NMR: (300 MHz; $CDCl_3$) δ 2.37 (s, 3H), 7.34-7.51 (m, 3H), 7.52-7.58 (dd, *J*=8.08, 1.79 Hz, 1H), 7.62 (d, *J*=8.08 Hz, 1H), 7.91-8.00 (m, 2H), 8.52 (s, 1H).

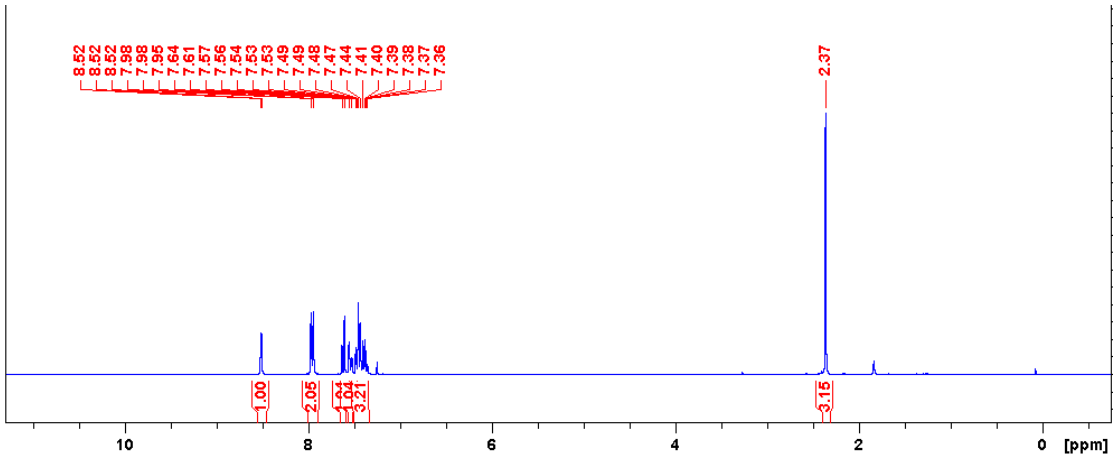

Figure A140. ^{1}H NMR spectrum {300 MHz; $CDCl_3$} of 5-methyl-2-phenylpyridine.

(*E*)-3-(4-Methoxyphenyl)-2-methyl Acrylic Acid Methyl Ester

^{1}H NMR: (500 MHz; $CDCl_3$) δ 2.13 (d, *J*=1.17 Hz, 3H), 3.80 (s, 3H), 3.82 (s, 3H), 6.91 (d, *J*=8.76 Hz, 2H), 7.37 (d, *J*=8.76 Hz, 2H), 7.64 (s, 1H).

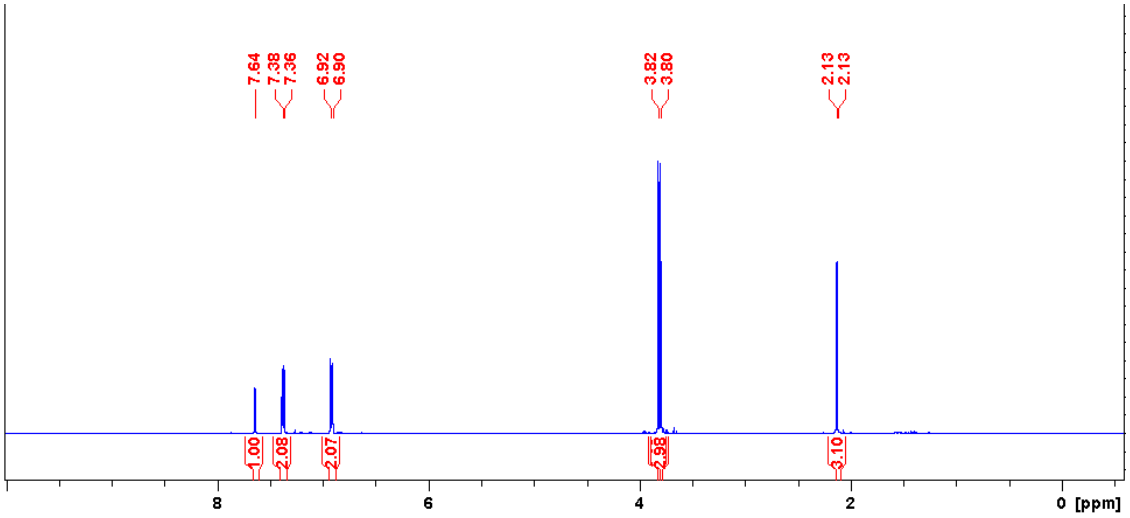

Figure A141. ^{1}H NMR spectrum {500 MHz; $CDCl_3$} of (*E*)-3-(4-Methoxyphenyl)-2-methyl Acrylic Acid Methyl Ester.

1-(4-*n*-Butoxyphenyl)ethenone

^{1}H NMR: (300 MHz; $CDCl_3$) δ 0.96 (t, *J*=7.34 Hz, 3H), 1.40-1.55 (m, 2H), 1.70-1.82 (m, 2H), 2.53 (s, 3H), 4.00 (t, *J*=6.55 Hz, 2H), 6.85-6.93 (m, 2H), 7.86-7.93 (m, 2H).

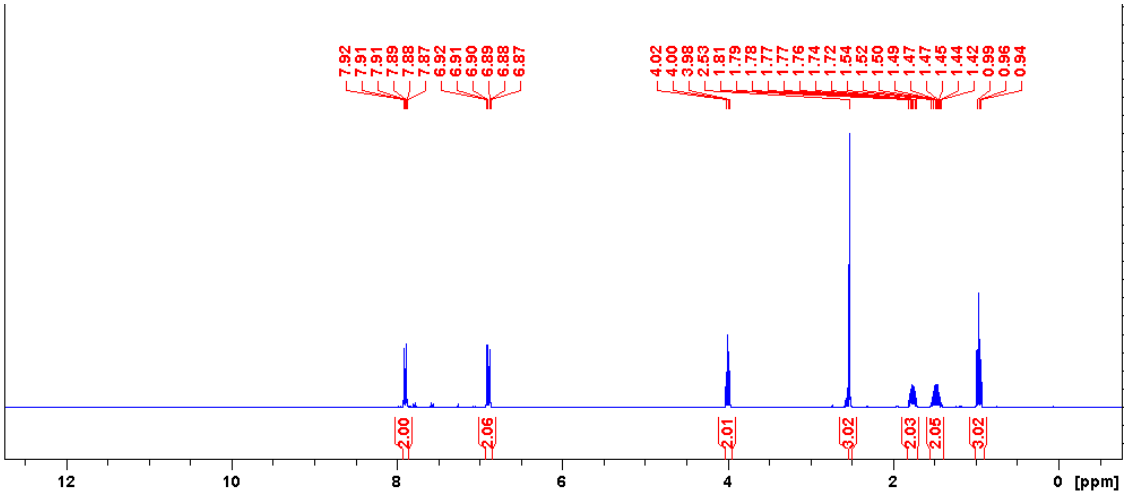

Figure A142. ^{1}H NMR spectrum {300 MHz; $CDCl_3$} of 1-(4-*n*-Butoxyphenyl)ethenone.

Appendix C: UPLC and LCMS Data and Spectra

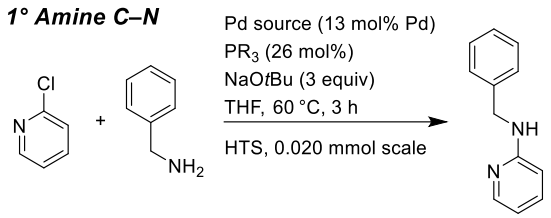

Table A10. UPLC gradient profile in primary amine C–N coupling.

Time (min)	Mobile Phase B (ACN) %	Flow Rate (mL/min)	Injection Volume (µL)
0.01	15	0.8	5
0.01-3.5	15-85		
3.5-3.6	85-15		
3.6-4.5	15		

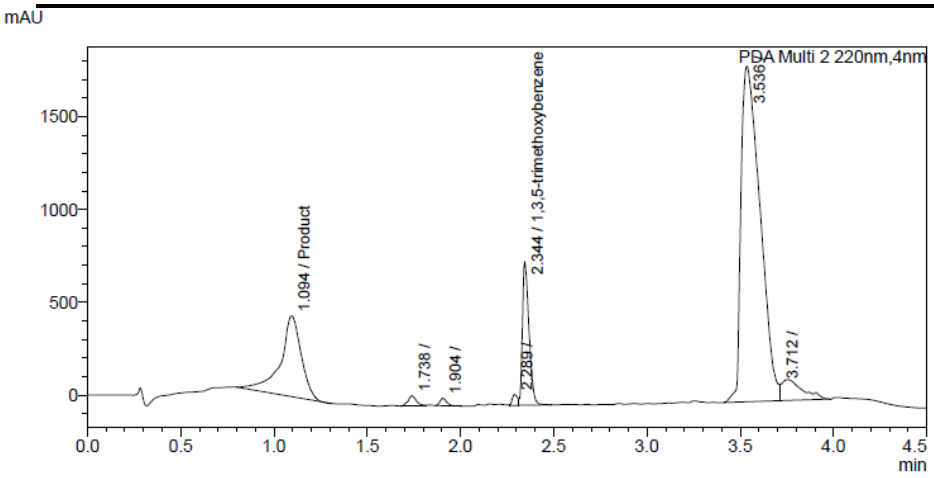

Figure A143. Representative UPLC trace for primary C–N coupling (^{DMP}DAB–Pd-–MAH/*t*BuBrettPhos)

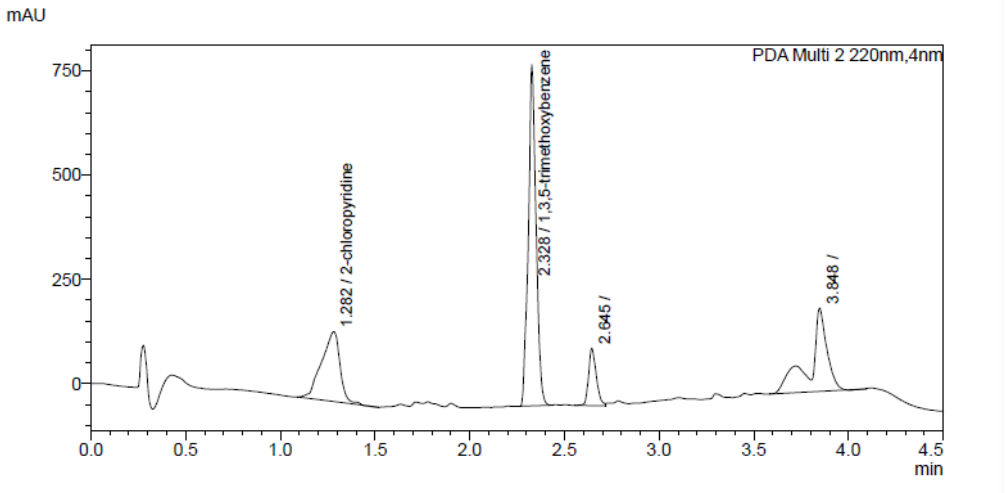

Figure A144. Representative UPLC trace for primary C–N coupling (Pd_2dba_3•$CHCl_3$/P(*t*Bu)$_3$)

Table A11. HPLC peak areas for the screen of the primary amine C–N coupling.

Peak Area				
		2-chloropyridine	N-Benzylpyridin-2-amine	1,3,5-trimethoxybenzene
$Pd(OAc)_2$	BrettPhos	0	3385492	2997690
	Xphos	0	76787	2453649
	*t*BuXPhos	0	2377402	2655255
	*t*BuBrettPhos	0	2307905	2515666
	RuPhos	0	1733149	2461734
	P(*t*Bu)3	1105874	0	2325394
$[Pd(allyl)Cl]_2$	BrettPhos	0	2370577	2334463
	Xphos	0	0	2271905
	*t*BuXPhos	0	3082567	2454643
	*t*BuBrettPhos	0	2729767	2434876
	RuPhos	0	1669756	2367546
	P(*t*Bu)3	673521	496436	2286357
Pd_2dba_3•$CHCl_3$	BrettPhos	0	3312089	3317989
	Xphos	0	81863	2288290
	*t*BuXPhos	0	2837787	2404427
	*t*BuBrettPhos	0	2952075	2509544
	RuPhos	0	1799661	2353881
	P(*t*Bu)3	1125019	0	2336137
^{DMP}DAB–Pd–MAH	BrettPhos	0	3447511	1976975
	Xphos	0	67808	2158353
	*t*BuXPhos	0	3283754	1861477
	*t*BuBrettPhos	0	3397940	1900147
	RuPhos	0	3072338	2358024
	P(*t*Bu)3	1019157	185338	1952504

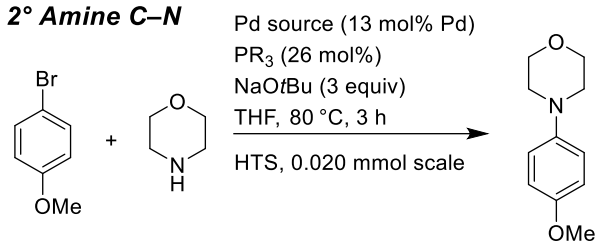

Table A12. UPLC gradient profile in secondary C–N coupling.

Time (min)	Mobile Phase B (ACN) %	Flow Rate (mL/min)	Injection Volume (µL)
0.01	2	0.8	5
0.01-4	2-98		
4-4.1	98-2		
4.1-4.5	2		

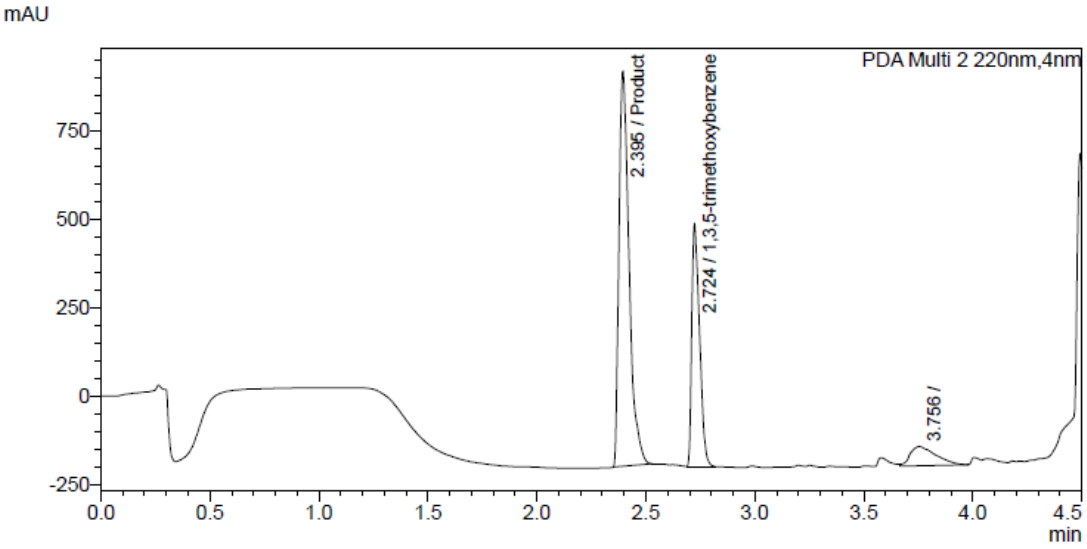

Figure A145. Representative UPLC trace for secondary C–N coupling (^{DMP}DAB–Pd–MAH/RuPhos)

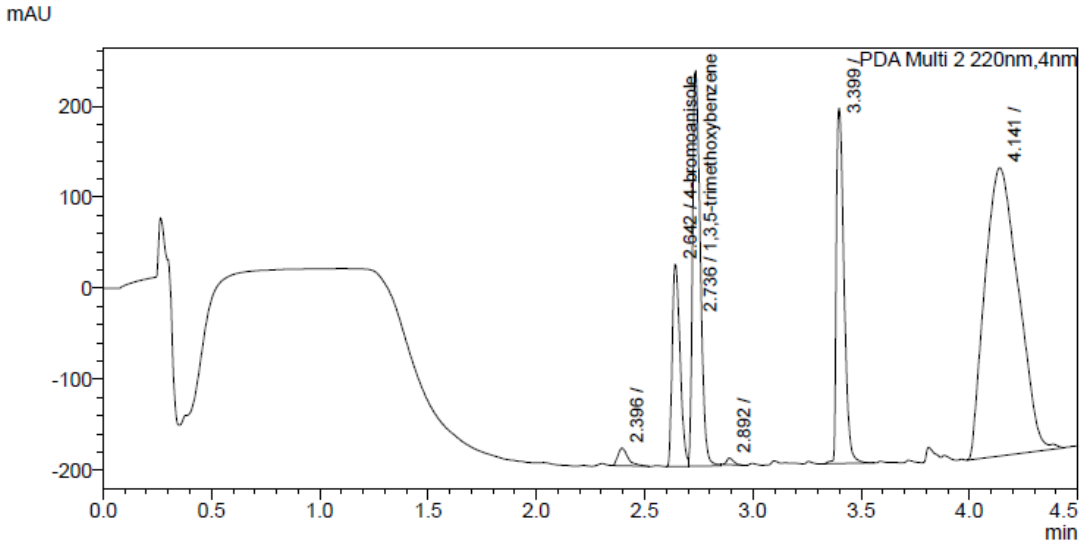

Figure A146. Representative UPLC trace for secondary C–N coupling ($Pd(OAc)_2$/*t*BuBrettPhos)

Table A13. HPLC peak areas for the screen of the secondary C–N coupling.

Peak Area				
		4-bromoanisole	4-(4-Methoxyphenyl)morpholine	1,3,5-trimethoxybenzene
$Pd(OAc)_2$	BrettPhos	252879	1621663	1155080
	Xphos	48764	2135289	1217403
	*t*BuXPhos	325613	1327837	1202379
	*t*BuBrettPhos	563476	0	1079231
	RuPhos	0	2239831	1248760
	P(*t*Bu)3	33578	2218340	1310637
$[Pd(allyl)Cl_2$	BrettPhos	154978	1962981	1170919
	Xphos	41485	2099868	1125205
	*t*BuXPhos	26394	2124637	1144206
	*t*BuBrettPhos	276407	1414466	1205944
	RuPhos	25981	2369094	1279222
	P(*t*Bu)3	58704	1741241	1143075
$Pd_2dba_3•CHCl_3$	BrettPhos	194292	1983567	1231454
	Xphos	81890	2597186	1461177
	*t*BuXPhos	76280	2335810	1430355
	*t*BuBrettPhos	515913	255223	1233285
	RuPhos	54649	2354111	1304103
	P(*t*Bu)3	143585	2551969	1763992
^{DMP}DAB–Pd–MAH	BrettPhos	232626	3141942	1836385
	Xphos	133078	2406601	1295819
	*t*BuXPhos	38335	3353916	1696089
	*t*BuBrettPhos	0	1887528	1698093
	RuPhos	0	3602097	1698681
	P(*t*Bu)3	62502	2763901	1727788

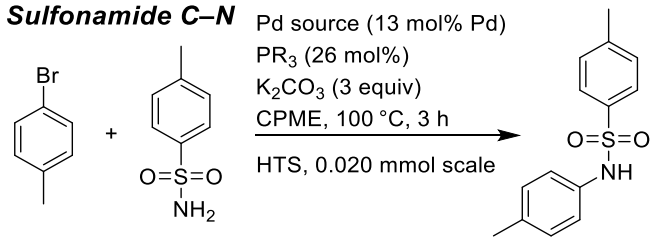

Table A14. UPLC gradient profile in sulfonamide C–N coupling.

Time (min)	Mobile Phase B (ACN) %	Flow Rate (mL/min)	Injection Volume (µL)
0.1	2	1.3	5
0.1-2	2-98		
2-2.1	98-2		
2.1-2.5	2		

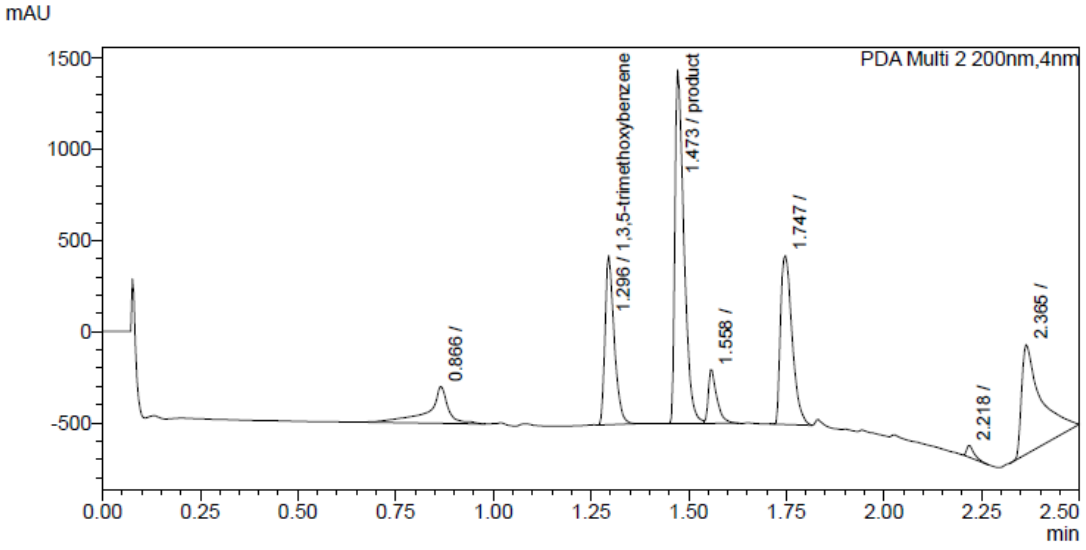

Figure A147. Representative UPLC trace for sulfonamide C–N coupling (^{DMP}DAB–Pd–MAH/*t*BuXPhos)

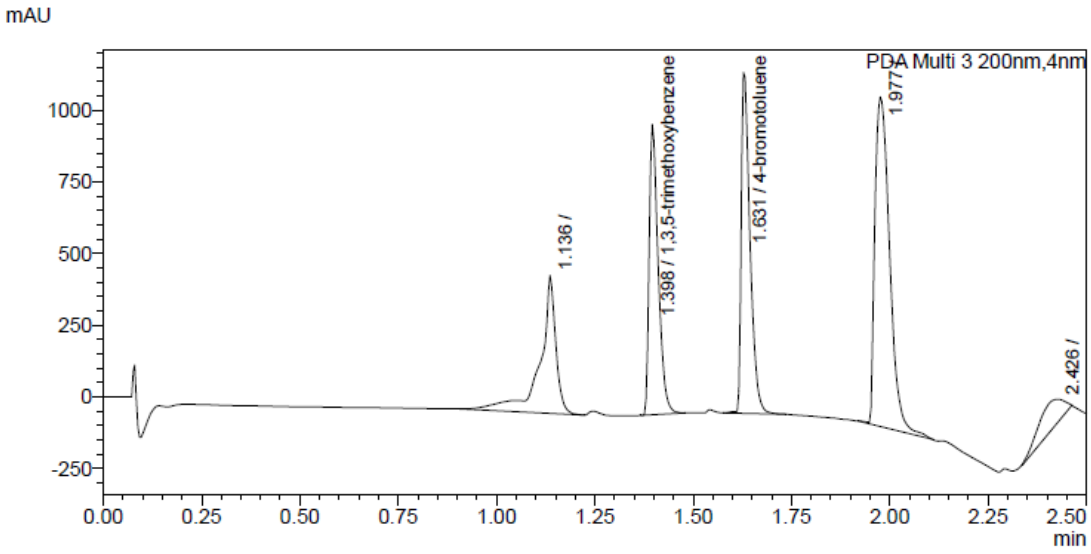

Figure A148. Representative UPLC trace for sulfonamide C–N coupling ($Pd(OAc)_2$/Me_4*t*BuXPhos)

Table A15. HPLC peak areas for the screen of the sulfonamide C–N coupling.

Peak Area				
		4-bromotoluene	N-(4-Methylphenyl)-4-methylbenzenesulfonamide	1,3,5-trimethoxybenzene
$Pd(OAc)_2$	XantPhos	828182	286064	1855238
	Xphos	1401321	1248346	1709830
	*t*BuXPhos	1713058	661591	1674885
	Me_4*t*BuXPhos	1842639	0	1612624
	BippyPhos	1894665	635097	1699286
	JackiePhos	1690195*	678312	1715822
$[Pd(allyl)Cl_2$	XantPhos	1490106*	690288	1899480
	Xphos	652314	2282165	1715642
	*t*BuXPhos	632700	1865855	1714584
	Me_4*t*BuXPhos	0	2955988	1715342
	BippyPhos	0	2735683	1759315
	JackiePhos	0	2769710	1738446
Pd_2dba_3•$CHCl_3$	XantPhos	1498090	461837	1906187
	Xphos	704468	2497133	1682254
	*t*BuXPhos	953414	2324289	1703807
	Me_4*t*BuXPhos	482981	2589245	1615176
	BippyPhos	149533*	2941408	1712223
	JackiePhos	0	2581352	1683564
^{DMP}DAB–Pd–MAH	XantPhos	1527896	670644	2020114
	Xphos	1629389	993276	1805830
	*t*BuXPhos	0	3130626	1505343
	Me_4*t*BuXPhos	1000338	2362555	1691062
	BippyPhos	1484447	1467249	1753619
	JackiePhos	1544264	1423967	1499409

*: The peak overlaps with other peaks

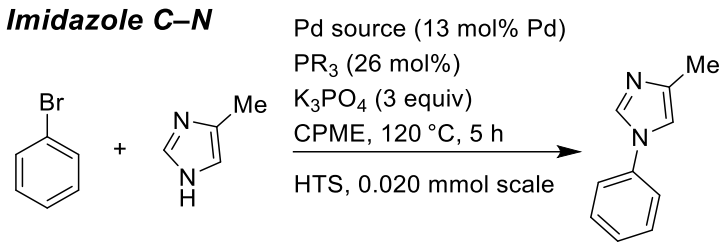

Table A16. UPLC gradient profile in imidazole C–N coupling.

Time (min)	Mobile Phase B (ACN) %	Flow Rate (mL/min)	Injection Volume (µL)
0.01	2	0.8	10
0.01-8	2-70		
8.0-10	70		
10-10.1	70-2		
10.1-12	2		

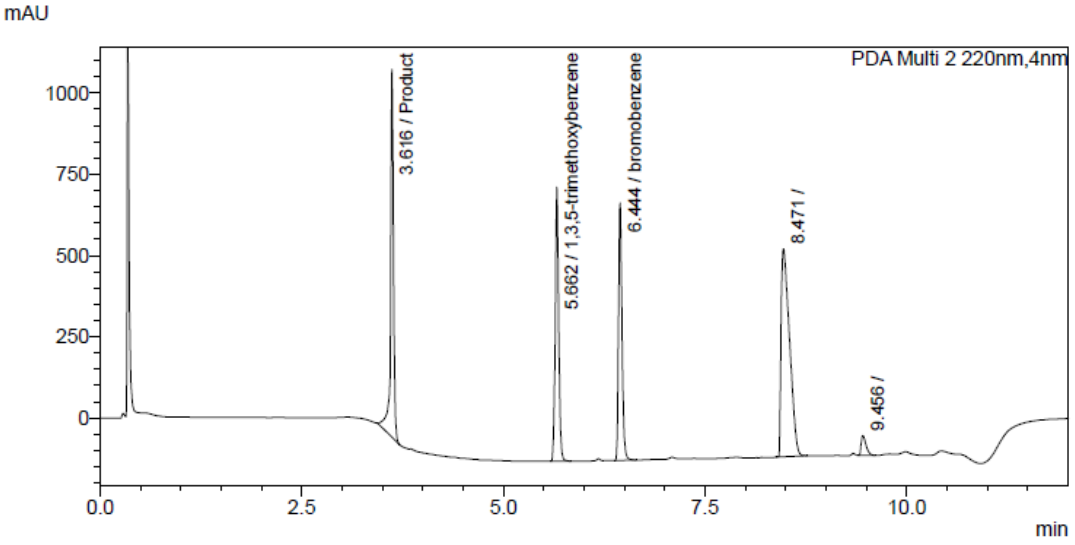

Figure A149. Representative UPLC trace for imidazole C–N coupling ([DMP]DAB–Pd–MAH/*t*BuBrettPhos)

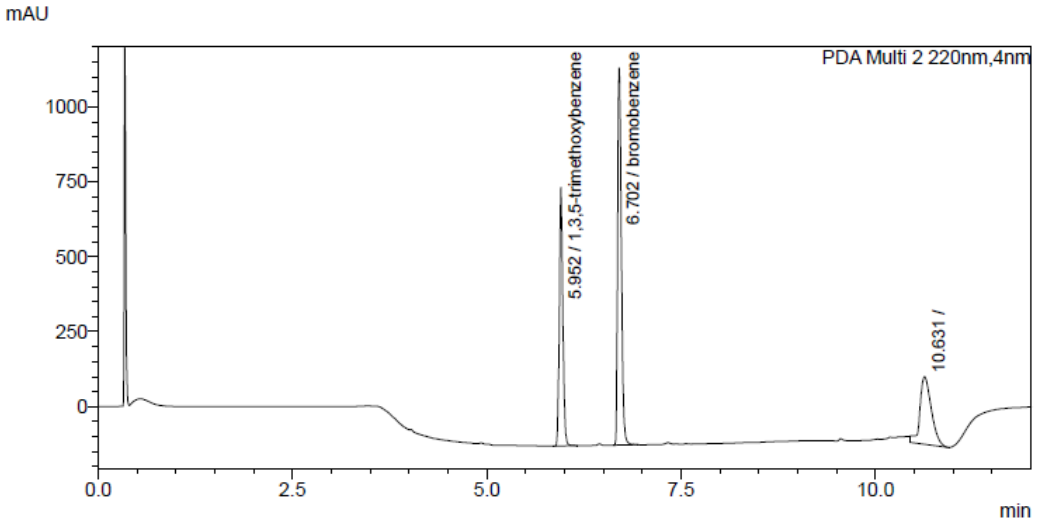

Figure A150. Representative UPLC trace for imidazole C–N coupling ([Pd(allyl)Cl]$_2$/XPhos)

Table A17. HPLC peak areas for the screen of the imidazole C–N coupling.

Peak Area				
		bromobenzene	4-methyl-1-phenyl-1H-imidazole	1,3,5-trimethoxybenzene
$Pd(OAc)_2$	BrettPhos	4902673	0	2908775
	Xphos	4571225	0	2693832
	*t*BuXPhos	4308077	50036	2570979
	*t*BuBrettPhos	4373545	25038	2669042
	Me$_4$*t*BuXPhos	4417449	0	2600933
	BippyPhos	4631296	0	2800852
$[Pd(allyl)Cl]_2$	BrettPhos	4125483	90172	2707002
	Xphos	4220220	0	2700361
	*t*BuXPhos	1439335	0	3221589
	*t*BuBrettPhos	2972207	1298343	3756382
	Me$_4$*t*BuXPhos	3519533	780383	2561988
	BippyPhos	4251645	0	2604595
Pd_2dba_3•$CHCl_3$	BrettPhos	4190279	119157	2736082
	Xphos	4025391	0	2568351
	*t*BuXPhos	3323695	178714	2536932
	*t*BuBrettPhos	2108103	2218445	2611913
	Me$_4$*t*BuXPhos	2792228	1376263	2514431
	BippyPhos	1248583	0	4432359
^{DMP}DAB–Pd–MAH	BrettPhos	4364954	488724	2711391
	Xphos	4129583	300332	2514790
	*t*BuXPhos	3361859	1031999	2484008
	*t*BuBrettPhos	2354270	2844027	2472766
	Me$_4$*t*BuXPhos	3796109	1193196	2944526
	BippyPhos	4106500	327324	2504938

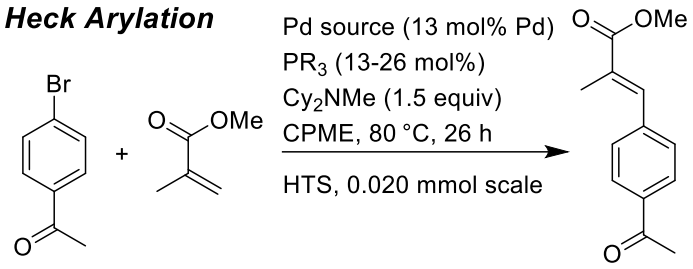

Table A18. UPLC gradient profile in Heck arylation.

Time (min)	Mobile Phase B (ACN) %	Flow Rate (mL/min)	Injection Volume (µL)
0.01	2	0.8	4
0.01-10	2-60		
10-10.1	60-2		
10.1-12.5	2		

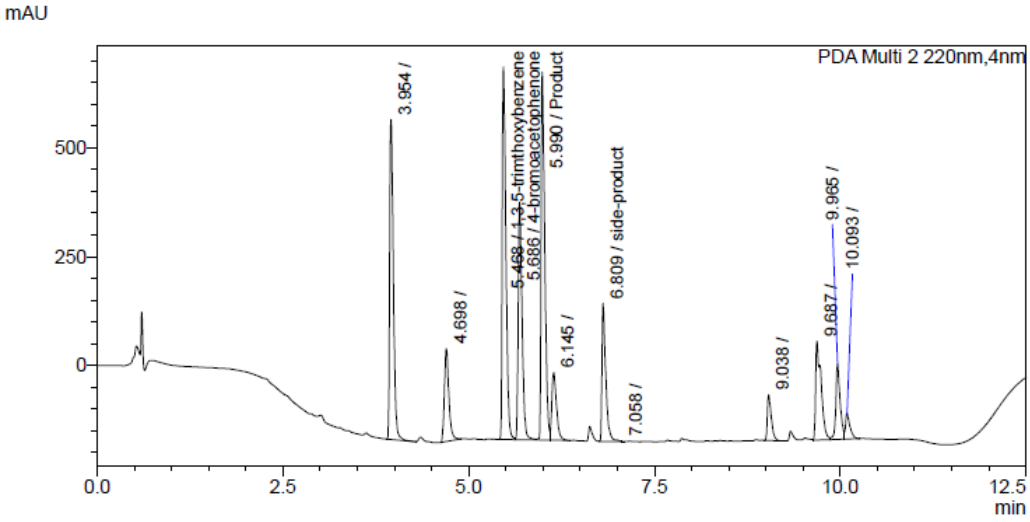

Figure A151. Representative UPLC trace for Heck arylation (^{DMP}DAB–Pd–MAH/P(*t*Bu)$_3$)

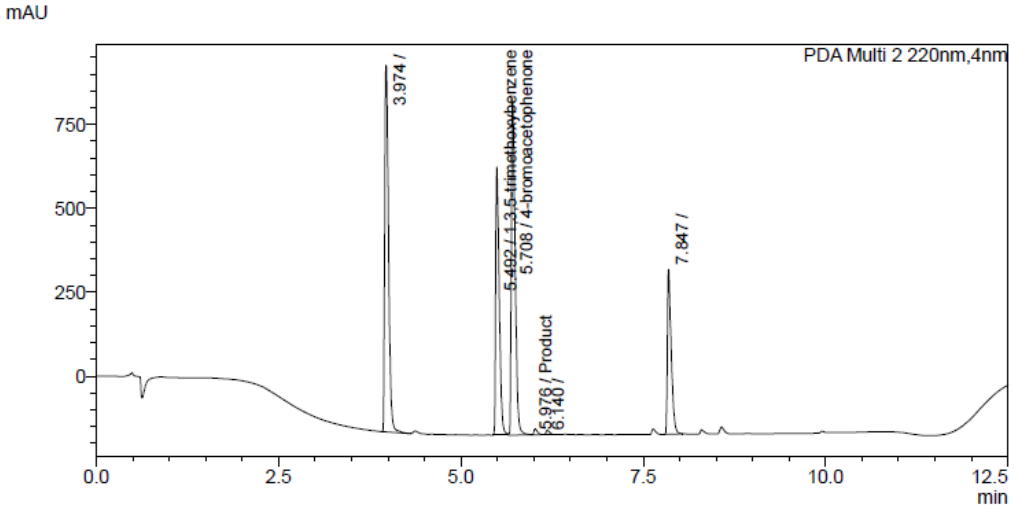

Figure A152. Representative UPLC trace for Heck arylation (Pd_2dba_3•$CHCl_3$/$P(Cy)_3$)

Table A19. HPLC peak areas for the screen of the Heck arylation.

Peak Area				
		4-bromoacetophenone	(E)-3-(4-acetylphenyl)-2-methyl acrylic acid methyl ester	1,3,5-trimethoxybenzene
$Pd(OAc)_2$	P(Cy)3	3697354	0	2713253
	Xphos	3133597	1010419	2705608
	P(*o*-tol)3	4054456	0	2665803
	cataCXium A	3648619	0	2750180
	dppp	5046162*	613668	2780601
	P(*t*Bu)3	3877056	0	2863547
$[Pd(allyl)Cl]_2$	P(Cy)3	3990226	0	2714838
	Xphos	4011877	0	2712272
	P(*o*-tol)3	3372182	1386149	2593248
	cataCXium A	3615156	0	2716009
	dppp	4262695*	0	2754042
	P(*t*Bu)3	289680	4093293	2804407
Pd_2dba_3•$CHCl_3$	P(Cy)3	3652851	5205	2726519
	Xphos	3269325	983800	2707691
	P(*o*-tol)3	2154853	2455809	2721192
	cataCXium A	3575334	0	2700032
	dppp	5268009*	0	2695499
	P(*t*Bu)3	175305	4021632	2785341
^{DMP}DAB–Pd–MAH	P(Cy)3	3934671	0	2821811
	Xphos	4098690	0	2776081
	P(*o*-tol)3	3695598*	1178678	2804769
	cataCXium A	3835483	0	2899726
	dppp	6550918*	0	2797375
	P(*t*Bu)3	1977407	2894277	2934081

*: The peak overlaps with other peaks.

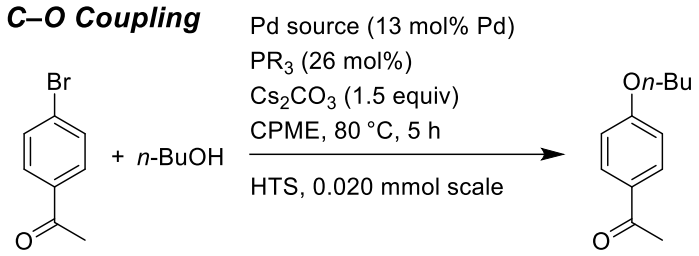

Table A20. LC gradient profile 1 in C–O coupling.

Time (min)	Mobile Phase A %	Mobile Phase B %	Flow Rate (mL/min)	Injection Volume (µL)
initial	90	10	0.5	2
1	90	10		
6.5	10	90		
8	10	90		
8.1	90	10		
10	90	10		

Table A21. LC gradient profile 2 in C–O coupling.

Time (min)	Mobile Phase A %	Mobile Phase B %	Flow Rate (mL/min)	Injection Volume (µL)
initial	90	10	0.5	2
1	90	10		
3	10	90		
4	10	90		
4.01	90	10		
5	90	10		

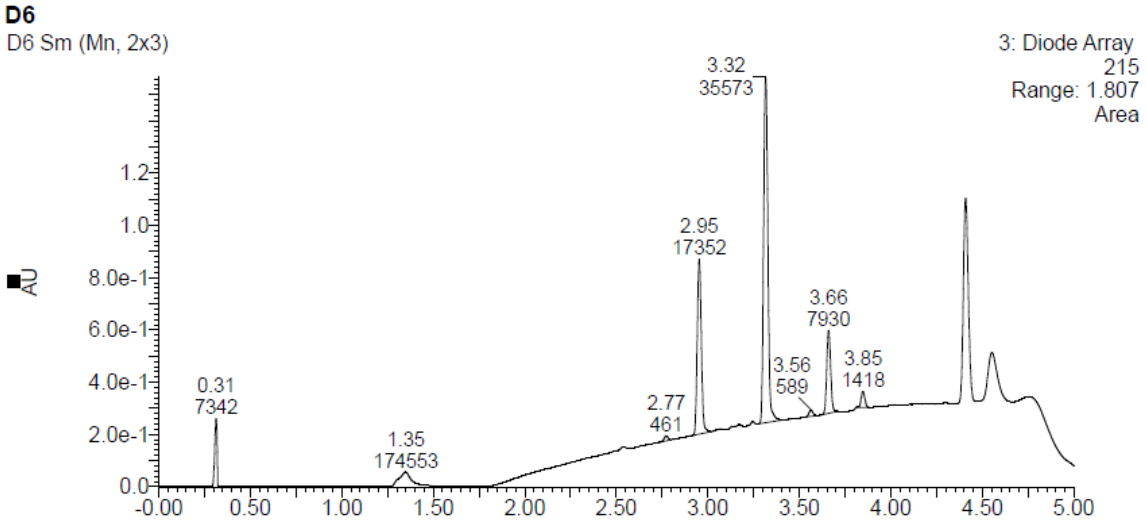

Figure A153. Representative LC-MS trace for C–O coupling ([DMP]DAB–Pd–MAH/BippyPhos)

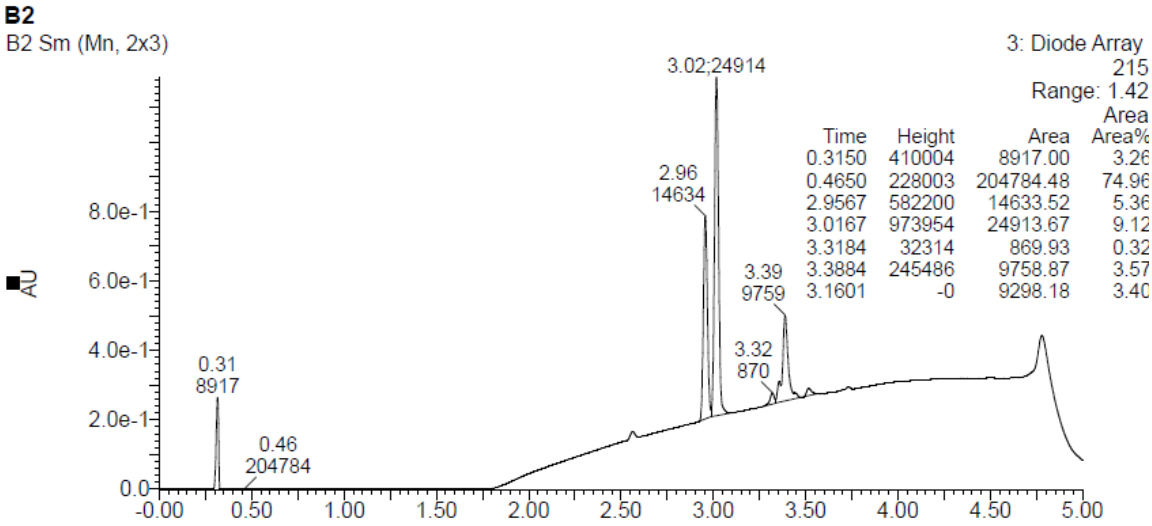

Figure A154. Representative LC-MS trace for C–O coupling ([Pd(allyl)Cl]$_2$/XPhos)

Table A22. HPLC peak areas for the screen of the C–O coupling**.**

Peak Area				
		4-bromoacetophenone	1-(4-*n*-Butoxyphenyl)ethanone	1,3,5-trimethoxybenzene
$Pd(OAc)_2$	BrettPhos	0	16394	9937
	Xphos	0	4796	16462
	*t*BuXPhos	3431	3294	3249
	*t*BuBrettPhos	8133	24288	17588
	Me_4*t*BuXPhos	0	21140	15193
	BippyPhos	0	33879	16345
$[Pd(allyl)Cl]_2$	BrettPhos	0	24797	15639
	Xphos	24914	870	14634
	*t*BuXPhos	17478	7831	18873
	*t*BuBrettPhos	9261	9856	18759
	Me_4*t*BuXPhos	11568	12345	18724
	BippyPhos	16455	12421	16929
Pd_2dba_3•$CHCl_3$	BrettPhos	0	26791	15385
	Xphos	2122	4430	15765
	*t*BuXPhos	6607	20584	14592
	*t*BuBrettPhos	4168	23313	16532
	Me_4*t*BuXPhos	3077	15562	15412
	BippyPhos	0	28533	15741
^{DMP}DAB–Pd–MAH	BrettPhos	3675	21248	12767
	Xphos	12303	3776	15751
	*t*BuXPhos	18218	15658	15632
	*t*BuBrettPhos	9388	19751	15729
	Me_4*t*BuXPhos	14421	13669	15527
	BippyPhos	0	35573	17352

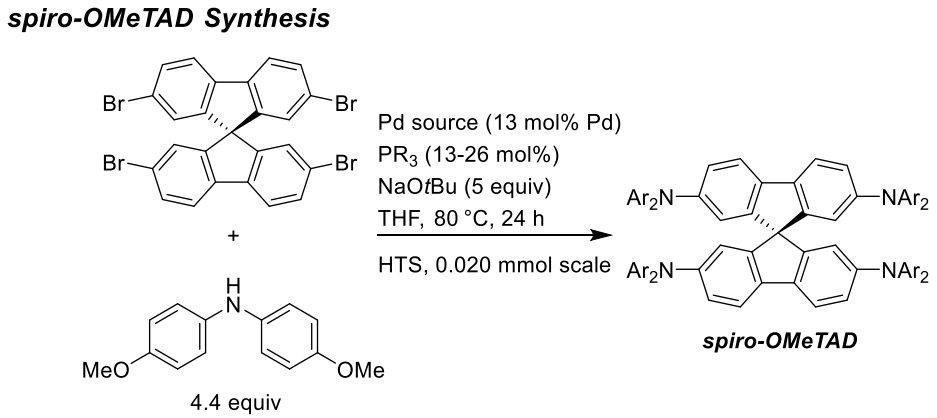

Table A23. UPLC gradient profile in the synthesis of *spiro*-OMeTAD.

Time (min)	Mobile Phase B (ACN) %	Flow Rate (mL/min)	Injection Volume (µL)
0.01	30	0.8	2
0.01-10	30-95		
10-13.4	95		
13.4-13.5	95-30		

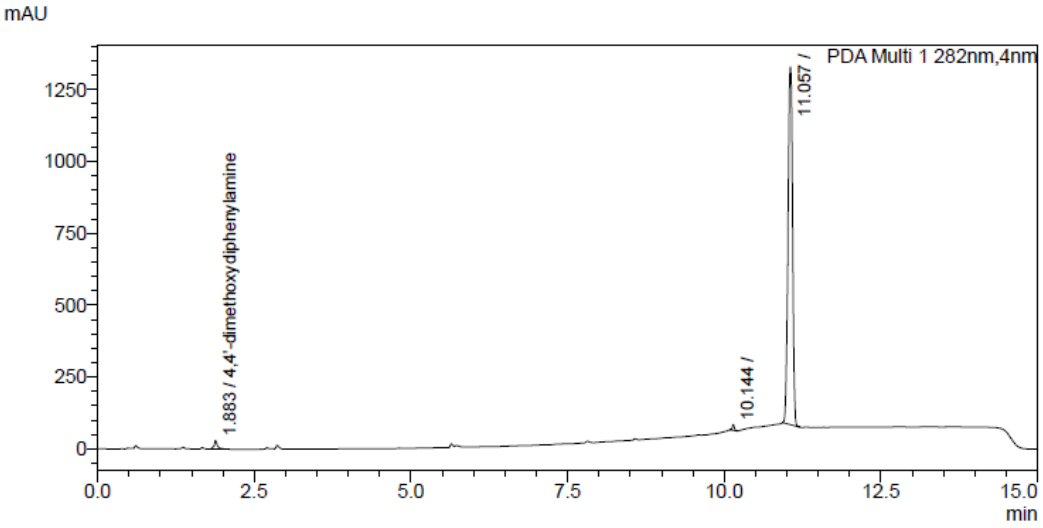

Figure A155. Representative UPLC trace for synthesis of *spiro*-OMeTAD at 282 nm (^{DMP}DAB–Pd–MAH/XPhos)

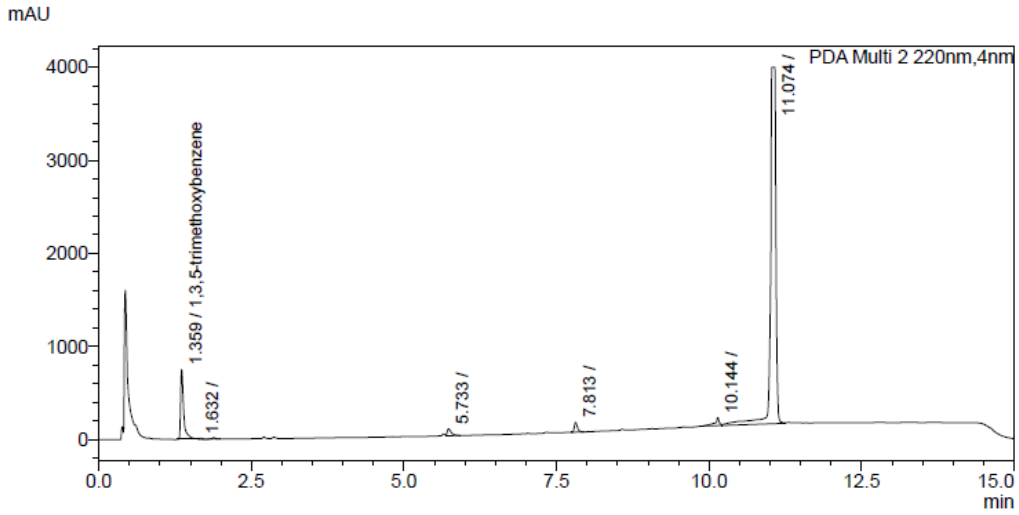

Figure A156. Representative UPLC trace for synthesis of *spiro*-OMeTAD at 220 nm (^{DMP}DAB–Pd–MAH/XPhos)

Table A24. HPLC peak areas for the screen of the synthesis of spiro-OMeTAD.

Peak Area				
		4,4'-dimethoxydiphenylamine	Spiro-OMeTAD	1,3,5-trimethoxybenzene
^{DMP}DAB–Pd–MAH	BrettPhos	7284590	3866889	3648099
	Xphos	116877	9326234	2570339
	*t*BuXPhos	3145161	4339269	2431577
	Sphos	349246	7523095	2457494
	RuPhos	1396243	7727987	2609098
	XantPhos	1739682	8708891	2588164

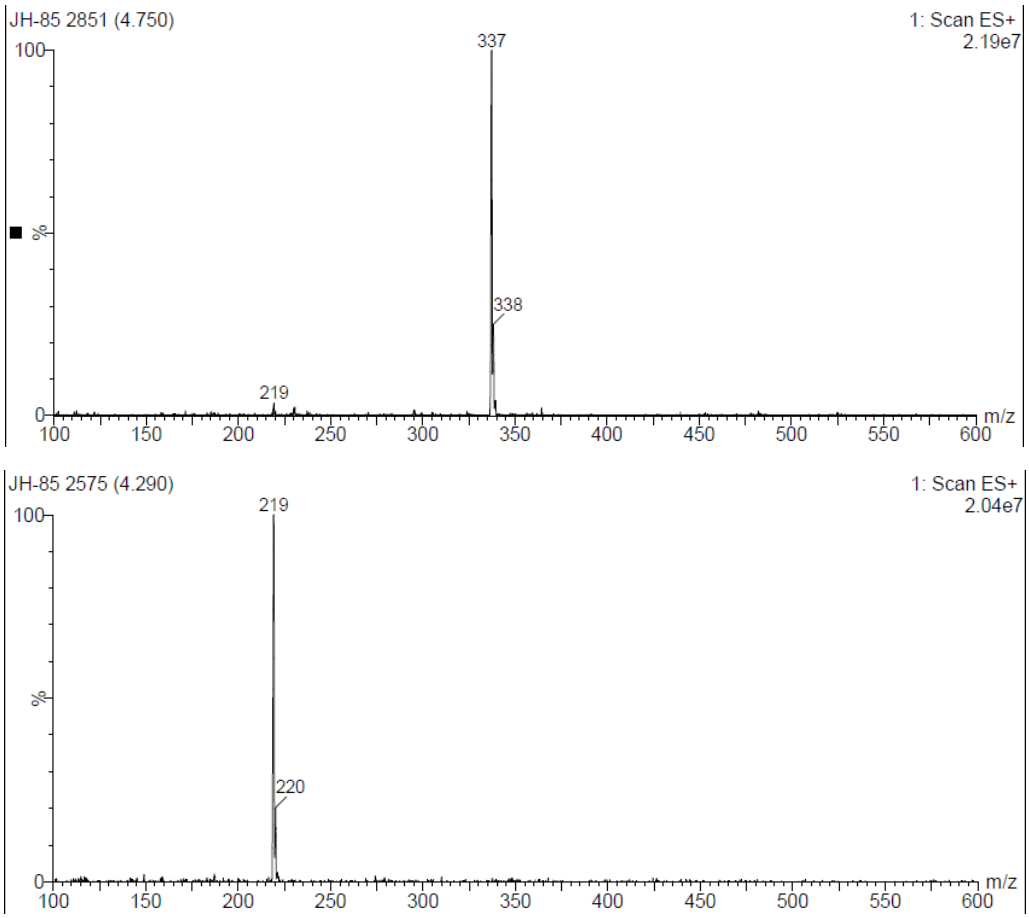

Figure A157. MS (ESI) data from LCMS of isolated (*E*)-3-(4-acetylphenyl)-2-methyl acrylic acid methyl ester confirming presence of bis(arylation) product (minor, top) and mono(arylation) product (major, bottom).

Appendix References

(1) Fuchs, S.; Berl, V.; Lepoittevin, J.-P. A Highly Stereoselective Divergent Synthesis of Bicyclic Models of Photoreactive Sesquiterpene Lactones. *Eur. J. Org. Chem.* **2007**, *2007* (7), 1145–1152. https://doi.org/10.1002/ejoc.200600611.

(2) Trost, B. M.; Van Vranken, D. L.; Bingel, C. A Modular Approach for Ligand Design for Asymmetric Allylic Alkylations via Enantioselective Palladium-Catalyzed Ionizations. *J. Am. Chem. Soc.* **1992**, *114* (24), 9327–9343. https://doi.org/10.1021/ja00050a013.

(3) Koch, G.; Lloyd-Jones, G. C.; Loiseleur, O.; Pfaltz, A.; Prétôt, R.; Schaffner, S.; Schnider, P.; von Matt, P. Synthesis of Chiral (Phosphinoaryl)oxazolines, a Versatile Class of Ligands for Asymmetric Catalysis. *Recl. Trav. Chim. Pays-Bas* **1995**, *114* (4–5), 206–210. https://doi.org/10.1002/recl.19951140413.

(4) Wang, D.; Zheng, Y.; Yang, M.; Zhang, F.; Mao, F.; Yu, J.; Xia, X. Room-Temperature Cu-Catalyzed N-Arylation of Aliphatic Amines in Neat Water. *Org. Biomol. Chem.* **2017**, *15* (38), 8009–8012. https://doi.org/10.1039/C7OB02126G.

(5) DeAngelis, A. J.; Gildner, P. G.; Chow, R.; Colacot, T. J. Generating Active "L-Pd(0)" via Neutral or Cationic π-Allylpalladium Complexes Featuring Biaryl/Bipyrazolylphosphines: Synthetic, Mechanistic, and Structure–Activity Studies in Challenging Cross-Coupling Reactions. *J. Org. Chem.* **2015**, *80* (13), 6794–6813. https://doi.org/10.1021/acs.joc.5b01005.

(6) Jiang, Y.; Wang, Q.-Q.; Liang, S.; Hu, L.-M.; Little, R. D.; Zeng, C.-C. Electrochemical Oxidative Amination of Sodium Sulfinates: Synthesis of Sulfonamides Mediated by NH_4I as a Redox Catalyst. *J. Org. Chem.* **2016**, *81* (11), 4713–4719. https://doi.org/10.1021/acs.joc.6b00615.

(7) Ueda, S.; Su, M.; Buchwald, S. L. Completely N^1-Selective Palladium-Catalyzed Arylation of Unsymmetric Imidazoles: Application to the Synthesis of Nilotinib. *J. Am. Chem. Soc.* **2012**, *134* (1), 700–706. https://doi.org/10.1021/ja2102373.

(8) Littke, A. F.; Fu, G. C. A Versatile Catalyst for Heck Reactions of Aryl Chlorides and Aryl Bromides under Mild Conditions. *J. Am. Chem. Soc.* **2001**, *123* (29), 6989–7000. https://doi.org/10.1021/ja010988c.

(9) Gowrisankar, S.; Sergeev, A. G.; Anbarasan, P.; Spannenberg, A.; Neumann, H.; Beller, M. A General and Efficient Catalyst for Palladium-Catalyzed C−O Coupling Reactions of Aryl Halides with Primary Alcohols. *J. Am. Chem. Soc.* **2010**, *132* (33), 11592–11598. https://doi.org/10.1021/ja103248d.

(10) Abate, A.; Hollman, D. J.; Teuscher, J.; Pathak, S.; Avolio, R.; D'Errico, G.; Vitiello, G.; Fantacci, S.; Snaith, H. J. Protic Ionic Liquids as p-Dopant for Organic Hole Transporting Materials and Their Application in High Efficiency Hybrid Solar Cells. *J. Am. Chem. Soc.* **2013**, *135* (36), 13538–13548. https://doi.org/10.1021/ja406230f.

(11) Zhang, E.; Tang, J.; Li, S.; Wu, P.; Moses, J. E.; Sharpless, K. B. Chemoselective Synthesis of Polysubstituted Pyridines from Heteroaryl Fluorosulfates. *Chem. – Eur. J.* **2016**, *22* (16), 5692–5697. https://doi.org/10.1002/chem.201600167.

(12) Takahashi, R.; Kubota, K.; Ito, H. Air- and Moisture-Stable Xantphos-Ligated Palladium Dialkyl Complex as a Precatalyst for Cross-Coupling Reactions. *Chem. Commun.* **2020**, *56* (3), 407–410. https://doi.org/10.1039/C9CC06946A.